Floor Acceleration Demands in Reinforced-Concrete Buildings with Nominal Torsion

A Thesis Submitted

in Partial Fulfilment of the Requirements

for the Degree of

DOCTOR OF PHILOSOPHY

by

Ankur Jain

(2019CEZ0004)

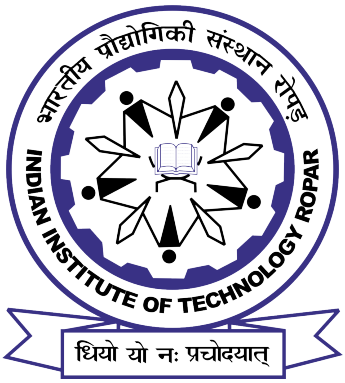

DEPARTMENT OF CIVIL ENGINEERING

INDIAN INSTITUTE OF TECHNOLOGY ROPAR

February, 2025

Ankur Jain: *Floor Acceleration Demands in Reinforced-Concrete Buildings with Nominal Torsion*

Copyright ©2025, Indian Institute of Technology Ropar

All Rights Reserved

To my esteemed parents, whose boundless love, wisdom, and sacrifices have been the foundation of all my pursuits, and to my cherished wife, whose unwavering support, patience, and encouragement have been my guiding light.

Declaration of Originality

I hereby declare that the work which is being presented in the thesis entitled **Floor Acceleration Demands in Reinforced-Concrete Buildings with Nominal Torsion** has been solely authored by me. The thesis presents the result of my own independent investigation/research conducted during the time period from July 2019 to February 2025, under the supervision of **Dr. Mitesh Surana**, Assistant Professor, Indian Institute of Technology Ropar. To the best of my knowledge, it is an original work, both in terms of research content and narrative, and has not been submitted or accepted elsewhere, in part or in full, for the award of any degree, diploma, fellowship, associateship, or similar title of any university or institution. Further, due credit has been attributed to the relevant state-of-the-art and collaborations (if any) with appropriate citations and acknowledgments, in line with established ethical norms and practices. I also declare that any idea/data/fact/source stated in my thesis has not been fabricated/ falsified/ misrepresented. All the principles of academic honesty and integrity have been followed. I fully understand that if the thesis is found to be unoriginal, fabricated, or plagiarized, the Institute reserves the right to withdraw the thesis from its archive and revoke the associated Degree conferred. Additionally, the Institute also reserves the right to appraise all concerned sections of society of the matter for their information and necessary action (if any). If accepted, I hereby consent for my thesis to be available online in the Institute's Open Access repository, inter-library loan, and the title & abstract to be made available to outside organizations.

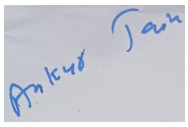

Signature

Name: Ankur Jain

Entry Number: 2019CEZ0004

Program: Doctor of Philosophy

Department: Civil Engineering, Indian Institute of Technology Ropar,

Rupnagar, Punjab 140001

Date: 24-02-2025

Acknowledgements

I would like to begin by expressing my deepest gratitude to the individuals whose constant support, encouragement, and guidance have been instrumental in the completion of this thesis. First and foremost, I extend my heartfelt thanks to my supervisor, **Dr. Mitesh Surana**, Assistant Professor, Department of Civil Engineering, Indian Institute of Technology Ropar. His profound knowledge, insightful guidance, and constructive feedback have been invaluable throughout this research journey. His ability to inspire and motivate me at every stage has been exceptional. I sincerely appreciate my former supervisor, **Dr. Amarnath Roy Choudhary**, Assistant Professor at Indian Institute of Technology Kanpur, for his invaluable insights during our brief time together.

I am grateful for the financial support from the **Ministry of Education, Government of India** and the **Anusandhan National Research Foundation, Department of Science and Technology, Government of India**, which enabled this research. My sincere thanks also go to the **seven anonymous reviewers** for their insightful suggestions that enhanced my work.

My heartfelt gratitude goes to my family for their unwavering support. My parents, **Shri Mahesh Kumar Jain** and **Smt. Sukhvati Jain**, has been a constant source of strength.as I am thankful to my father-in-law, **Shri Jaikumar Jain**, and mother-in-law, **Smt. Sushma Jain**, for their warm support. I am incredibly grateful to my wife, **Payal Ankur Jain**, whose love, patience, and belief in me have been my guiding force. I also acknowledge the support of my sisters, **Jyotsna Jain** and **Dr. Bhavana Jain**.

I would also like to acknowledge my friends **Ankur Singh**, **Ashish Kumar Chaudhary**, **Abdin Bedada Huluka**, **Aaditya Bhamidipati**, **Dharmil Baldev**, **Manisha Das**, **Niraj Janardhan Sahare**, **Pankaj Kundu**, **Sachchidanand Kushwaha**, **Shubham Jain**, and **Zimmy Singh Naorem**, for their invaluable friendship, camaraderie, and support. Finally, I sincerely thank all well-wishers, named or unnamed, whose support was vital to the completion of this thesis.

Certificate

This is to certify that the thesis entitled **Floor Acceleration Demands in Reinforced-Concrete Buildings with Nominal Torsion**, submitted by **Ankur Jain (2019CEZ0004)** for the award of the degree of **Doctor of Philosophy** of Indian Institute of Technology Ropar, is a record of bonafide research work carried out under my guidance and supervision. To the best of my knowledge and belief, the work presented in this thesis is original and has not been submitted, either in part or full, for the award of any other degree, diploma, fellowship, associateship or similar title of any university or institution.

In my opinion, the thesis has reached the standard fulfilling the requirements of the regulations relating to the Degree.

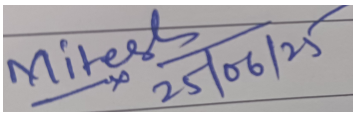

Signature of the Supervisor

Name: Dr. Mitesh Surana

Department: Civil Engineering

Indian Institute of Technology Ropar

Rupnagar, Punjab 140001

Date: 24-02-2025

Lay Summary

Earthquake induces shaking of a building in all six directions, thereby affecting both the building and its contents (e.g., air conditioning units and piping systems, etc.). Understanding movements caused by the shaking of buildings during earthquakes is vital for ensuring the seismic safety of both the building and its contents. The coupling between the translation and twisting motion of a building can complicate the prediction of the building's response under earthquakes. Thus, this research examines how buildings behave during earthquakes, particularly when the building undergoes coupled translational-twisting motions.

The main aim of this study is to explore how the coupling between the translational and twisting motion impacts the shaking experienced on different floors in buildings. Specifically, the research investigates 24 buildings, with and without undergoing significant twisting motions. Earthquake conditions are replicated by simulating building response under 14,400 different earthquake scenarios, and the effects of coupled translational and twisting motions induced in the buildings are studied.

One of the key findings of the study is that current building regulations may significantly underestimate the amount of shaking experienced by the building under earthquakes, especially at the extreme ends of the building, where the effects of coupled translational and twisting motion are the most intense. This finding suggests that buildings experiencing significant twisting motions can put the contents at greater risk during earthquakes than previously recognized. The study indicates that areas farther from the building's center experience significantly stronger shaking than those prescribed in the current building regulations. To address this issue, the research proposes multiple new equations for predicting the expected level of shaking experienced by the building at its extreme ends, under earthquakes. The proposed equations provide better estimates of the acceleration demands on contents in buildings undergoing coupled translational and twisting motions, under earthquakes. By utilizing the proposed equations alongside existing building regulations, engineers and designers can ensure that contents are better protected in the event of an earthquake.

Abstract

Accurately estimating floor acceleration demands is essential to ensure the seismic safety of secondary systems and building contents. The floor acceleration demands can vary significantly among different building types, reflecting a complex interplay of various influencing factors. The research work presented in this thesis investigates the impact of nominal torsion on floor acceleration demands in buildings. To achieve the aforementioned objective, 24 reinforced-concrete moment-resisting frame buildings are analyzed, 16 torsionally irregular and eight torsionally regular, exhibiting varying degrees of torsional irregularity and diverse plan shapes. These buildings are subjected to 14,400 linear and non-linear dynamic time history analyses using a suite of 20 far-field ground motion records, with and without considering rotational ground motions.

It is observed that current seismic code provisions significantly underestimate the peak floor acceleration demands for rigid secondary systems for both elastic and moderately inelastic torsionally irregular buildings. Among the investigated buildings, the median peak floor acceleration demands are underestimated by up to 137%, at the flexible edge. Likewise, for flexible secondary systems, existing code provisions can substantially miscalculate the median total acceleration amplification, underestimating it by as much as 539%. Both the degree of torsional irregularity and inelasticity significantly influence the amplification of the peak floor acceleration and the total acceleration. The total acceleration amplification further depends on the tuning ratio between the building and the secondary system. The rotational ground motions have a notable influence on both peak floor acceleration and total acceleration amplification, especially at the stiff edge (up to 53% and 54%, respectively), regardless of the extent of torsional irregularity and level of inelasticity (ductility demand) in the building.

The relationships between torsional amplification factors and torsional irregularity indices are examined for rigid, flexible, and very flexible secondary systems. For rigid and flexible secondary systems, torsional amplification factors are observed to be well-correlated with floor displacement-based torsional irregularity indices. In contrast, for very flexible secondary systems, these factors tend to

remain almost constant and independent of the characteristics of both the building and the secondary systems. Novel predictive equations are proposed to estimate torsional amplification factors for buildings with and without nominal torsion. These proposals are validated against multiple application examples, demonstrating that the proposed equations, when used alongside the latest code provisions, provide more accurate estimates of floor acceleration demands in buildings, also accounting for the effects of rotational ground motions.

Keywords: Floor response spectra; Peak floor acceleration; Secondary systems; Seismic design; Torsional irregularity.

List of Publications

Refereed journals

1. **Jain A** and Surana M. In-plan distribution of peak floor acceleration demands in torsionally irregular buildings, ***Journal of Building Engineering***, 90, 109360, 2024. DOI: https://doi.org/10.1016/j.jobe.2024.109360

2. **Jain A** and Surana M. Peak floor acceleration demands in torsionally irregular buildings, ***Earthquake Engineering and Structural Dynamics***, 53(3), 2024. DOI: https://doi.org/10.1002/eqe.4056

3. **Jain A** and Surana M. Floor-displacement based torsional amplification factors for seismic design of acceleration-sensitive non-structural component in torsionally irregular buildings, ***Engineering Structures***, 254, 2022. DOI: https://doi.org/10.1016/j.engstruct.2022.113871

4. **Jain A** and Surana M. Floor acceleration amplification factors for buildings with nominal torsion, ***Bulletin of Earthquake Engineering***. (Under review)

5. **Jain A** and Surana M. Effects of rotational ground motions on amplification of floor acceleration demands in inelastic regular reinforced-concrete buildings, ***Soil Dynamics and Earthquake Engineering***. (Manuscript under preparation)

Conference proceedings

1. **Jain A** and Surana M. Effects of building torsion on seismic demand of acceleration-sensitive non-structural components, ***18th World Conference on Earthquake Engineering (WCEE 2024)***, Milan, Italy, 2024.

2. **Jain A** and Surana M. Effect of the damping ratio of non-structural components on floor acceleration demands in torsionally irregular buildings, ***8th ECCOMAS Thematic Conference on Computational Methods in Structural Dynamics and Earthquake Engineering***

(COMPYDYN 2021 Vol. II), M. Papadrakakis and M. Fragiadakis (Ed.) Athens, Greece, pp. 4660-4669, 2021. DOI: https://doi.org/10.7712/120121.8815.19158

3. **Jain A** and Surana M. Effect of supporting structure's torsion on floor acceleration demands in buildings on slopes, ***Recent Advances in Earthquake Engineering***, Virtual Conference on Disaster Risk Reduction – Civil Engineering for a Disaster Resilient Society, India, 2021. DOI: https://doi.org/10.1007/978-981-16-4617-1

Contents

Declaration iv

Acknowledgements v

Certificate vi

Lay Summary vii

Abstract viii

List of Publications x

List of Figures xxi

List of Tables xlv

Nomenclature xlvii

1 Introduction 1

1.1 Background 1

1.2 Seismic performance of secondary systems 2

1.3 Classification of secondary systems 3

1.4 Building code provisions 8

1.4.1 Nominal torsion in buildings 9

1.4.2 Floor accelerations in buildings 10

1.5 Research gaps 11

1.6 Research objectives 13

1.7 Scope of the research work and methodology 13

1.7.1 Scope of the research . . . 13
1.7.2 Research methodology . . . 14
1.8 Organization of thesis . . . 16

2 Literature Review 21

2.1 Background . . . 21
2.2 Estimation of floor acceleration demands . . . 22
2.2.1 Approaches for estimating floor acceleration demands . . . 22
2.2.1.1 Coupled approach . . . 23
2.2.1.2 De-coupled approach . . . 24
2.3 Factors influencing peak floor acceleration . . . 27
2.3.1 Fundamental period of the building . . . 27
2.3.2 Relative height of the floor . . . 28
2.3.3 Building inelasticity . . . 31
2.3.4 Presence of infill walls . . . 32
2.3.5 Ground motion characteristics . . . 33
2.4 Factors influencing floor response spectra . . . 34
2.4.1 Modal period of the building . . . 35
2.4.2 Relative height of the floor . . . 36
2.4.3 Building inelasticity . . . 37
2.4.4 Presence of infill walls . . . 38
2.4.5 Presence of torsional irregularity in buildings . . . 39
2.4.6 Ground motion characteristics . . . 40
2.4.7 Inelasticity of the secondary system . . . 41
2.4.8 Damping ratio of the secondary system . . . 42
2.5 Method for the estimation of FRS . . . 43

2.5.1 SDOF-based methods 43
2.5.2 MDOF-based methods 44
2.5.3 Direct methods 44
2.5.4 Code-based methods 45
2.6 Summary 45

3 Building Archetypes, Modeling, and Analyses 49
3.1 Introduction 49
3.2 Selection of building archetypes 49
3.3 Modeling and design of the buildings 51
3.3.1 Dynamic characteristics of the buildings 53
3.4 Torsional irregularity indices of the buildings 54
3.5 Non-linear modeling and analysis 58
3.5.1 Ground motion selection 60
3.5.2 Time history analyses 62
3.6 Summary 66

4 Peak Floor Acceleration 67
4.1 Introduction 67
4.2 Peak floor acceleration demands 67
4.3 Influence of rotational ground motions 78
4.4 Summary 82

5 Floor Response Spectra 85
5.1 Introduction 85
5.2 Characteristics of the floor response spectra 86
5.2.1 Component amplification factor 89

5.2.2 Total amplification factor 98

5.2.3 Spectral amplification factors 107

5.3 Influence of the rotational ground motions on spectral amplification factors 118

5.4 Summary 123

6 Torsional Amplification Factors **127**

6.1 Introduction 127

6.2 Torsional amplification factors 127

6.2.1 Torsional amplification factors for the rigid secondary systems 128

6.2.1.1 Influence of rotational ground motions on torsional amplification factors of the rigid secondary systems . 131

6.2.2 Torsional amplification factors for the flexible secondary systems 137

6.2.2.1 Influence of rotational ground motions on torsional amplification factor for flexible secondary systems . . 144

6.2.3 Torsional amplification factors for the very flexible secondary systems 150

6.2.3.1 Influence of rotational ground motions on torsional amplification factor for very flexible secondary systems 152

6.3 Relationships between torsional amplification factor and different torsional irregularity indices 154

6.3.1 Torsional amplification factors for the rigid secondary systems 155

6.3.1.1 At the extreme edges 155

6.3.1.2 Across the building plan 158

6.3.2 Torsional amplification factors for the flexible secondary systems at the extreme edges 161

6.4 Proposed recommendations 164

6.4.1 Recommendations to estimate the torsional amplification factors for rigid, flexible, and very flexible secondary systems . 164

6.4.1.1 Point a' of the multi-linear curve 165

6.4.1.2 Segments a'–d', d'–e', and e'–h' of the multi-linear curve 167

6.4.1.3 Segments h'–i' of the multi-linear curve 168

6.4.2 Recommendations to estimate the torsional amplification factors for rigid secondary systems across the building plan . . 168

6.5 Summary 169

7 Validation of the Proposed Recommendations 175

7.1 Introduction 175

7.2 Selection of building archetypes 175

7.3 Modeling, analysis, and design of the buildings 178

7.3.1 Dynamic characteristics of the investigated buildings 179

7.3.2 Torsional irregularity indices of the buildings 181

7.3.3 Ground motion selection and time history analyses 182

7.4 Validation of the proposed model 184

7.4.1 Torsional amplification factors using the proposed model . . . 186

7.4.1.1 Proposed TAFs for rigid secondary systems 186

7.4.1.2 Proposed TAFs for flexible secondary systems 188

7.4.1.2.1 Group 1 buildings 189

7.4.1.2.2 Group 2 buildings 192

7.4.1.3 Proposed TAFs for very flexible secondary systems . 194

7.4.2 Efficacy of the proposed equations for existing seismic design codes 195

7.4.2.1 For rigid secondary systems 195

7.4.2.2 For flexible secondary systems . . . 201
7.4.2.2.1 Group 1 buildings . . . 201
7.4.2.2.2 Group 2 building . . . 204
7.5 Summary . . . 208

8 Conclusions and Recommendations for Future Work 213
8.1 Conclusions . . . 213
8.2 Recommendations for future work . . . 220

References 223

A Peak Floor Acceleration 241
A.1 Peak floor acceleration response . . . 241
A.2 In-plan distribution of the peak floor acceleration response . . . 244

B Floor Response Spectra 255
B.1 Component amplification factor . . . 255
B.2 Total amplification factor . . . 264
B.3 Spectral amplification factor . . . 274

C Torsional Amplification Factors 285
C.1 Torsional amplification factors for the rigid secondary systems . . . 285
C.1.1 At the extreme edges . . . 285
C.1.2 Across the floor plan . . . 288
C.2 Torsional amplification factors for the rigid, flexible, and very flexible secondary systems . . . 298
C.3 Regression analysis parameters . . . 307
C.3.1 For rigid secondary systems . . . 307

C.3.2 For flexible secondary systems 310

List of Figures

1.1 Dislodgement of water tank appendages from the rooftops of both unfinished and finished reinforced-concrete frame buildings in Bhuj [1]. 4

1.2 Damage observed in residential building at Deorali [2]: (a) Extensive cracking in infill walls and damage to the reinforced-concrete column, (b) exposed mild steel reinforcement in the damaged reinforced-concrete column, and (c) out-of-plane collapse of the infill wall. 4

1.3 Cost comparison of the structure, secondary systems, and contents in buildings with various occupancies [3, 4]. 5

1.4 Classification of secondary systems. 6

1.5 Possible failure modes of acceleration-sensitive secondary systems. Note: a_{eq} is the acceleration due to earthquake forces, μ is the coefficient of friction, g is the acceleration due to gravity, α is the angle at which the secondary system is lifted, ω is the angular frequency, and r_d is the half of the diagonal length of the rigid block. 6

1.6 Various forms of plan irregularities in buildings [5]. 9

1.7 Variations of the PFA/PGA, a_p, and a_t in different building codes. . . 12

1.8 Schematic illustration of SE and FE in a multi-story building. 15

1.9 Outline of the methodology used in this thesis. 17

2.1 Typical layout showing the concept and definition of FRS 35

3.1 Typical plan layouts, section sizes, stiffness eccentricity, and strength eccentricity details of the WTI and ETI buildings. The stiffness and strength eccentricities shown in the building plan correspond to the first-floor level of the 4-story building with extreme torsional irregularity. 'FF_{ij}' and 'SF_{ij}' refer to the flexible and stiff frames located at the 'i^{th}' frame and 'j^{th}' floor level, respectively, within the building. 52

3.2 Typical three-dimensional (3D) elevation of the 4-story buildings investigated in the present thesis. 53

3.3 Locations of the CR, CS, and CM for the buildings with torsional and extreme torsional irregularities. 57

3.4 Variations of the torsional irregularity indices of seismic design codes for the investigated buildings (obtained using the mode superposition method). 59

3.5 Variations of the torsional irregularity indices obtained using the ELF method [6]. 60

3.6 Representative view of the distributed plasticity approach (fiber model) applied to a column. 61

3.7 Comparison of the 5%-damped pseudo-spectral acceleration response spectra of the selected ground motions with the target spectrum. . . . 62

3.8 Schematic diagram illustrating the concept of strength ratio (SR). S_{dy} - spectral displacement at yielding, and S_{du} - spectral displacement at the ultimate point. 63

3.9 Comparison of the response spectra for the horizontal and rotational components of the ground motions selected in this study. 65

4.1 PFA/PGA at various locations on the floor plan of the 'E4T', 'W4T', and 'N4T' buildings. 69

4.2 PFA/PGA at various locations on the floor plan of the 'E8T', 'W8T', and 'N8T' buildings. 69

4.3 In-plan distribution of PFA/PGA at different floors of the 'E4T' building. 72

4.4 In-plan distribution of PFA/PGA at different floors of the 'E8T' building. 72

4.5 In-plan distribution of PFA/PGA at different floors of the 'W4T' building. 73

4.6 In-plan distribution of PFA/PGA at different floors of the 'W8T' building. 74

4.7 In-plan distribution of PFA/PGA at different floors of the 'N4T' building. 75

4.8 In-plan distribution of PFA/PGA at different floors of the 'N8T' building. 76

4.9 Overestimation/underestimation of the PFA/PGA distributions at the center of rigidity, extreme stiff edge, and extreme flexible edge with respect to code provisions. 77

5.1 Floor response spectra for the 'E4T' building estimated using bi-directional time history analyses. Dashed vertical lines indicate the elastic modal periods in the direction under consideration. 86

5.2 Floor response spectra for the 'E8T' building estimated using bi-directional time history analyses. Dashed vertical lines indicate the elastic modal periods in the direction under consideration. 87

5.3 Floor response spectra for the 'W4T' building estimated using bi-directional time history analyses. Dashed vertical lines indicate the elastic modal periods in the direction under consideration. 88

5.4 Floor response spectra for the 'W8T' building estimated using bi-directional time history analyses. Dashed vertical lines indicate the elastic modal periods in the direction under consideration. 88

5.5 Floor response spectra for the 'N4T' building estimated using bi-directional time history analyses. Dashed vertical lines indicate the elastic modal periods in the direction under consideration. 90

5.6 Floor response spectra for the 'N8T' building estimated using bi-directional time history analyses. Dashed vertical lines indicate the elastic modal periods in the direction under consideration. 90

5.7 Component amplification factors for the 'E4T' building obtained using bi-directional time history analyses. Dashed vertical lines indicate the elastic modal periods in the direction under consideration. 91

5.8 Component amplification factors for the 'E8T' building obtained using bi-directional time history analyses. Dashed vertical lines indicate the elastic modal periods in the direction under consideration. 92

5.9 Component amplification factors for the 'W4T' building obtained using bi-directional time history analyses. Dashed vertical lines indicate the elastic modal periods in the direction under consideration. 95

5.10 Component amplification factors for the 'W8T' building obtained using bi-directional time history analyses. Dashed vertical lines indicate the elastic modal periods in the direction under consideration. 96

5.11 Component amplification factors for the 'N4T' building obtained using bi-directional time history analyses. Dashed vertical lines indicate the elastic modal periods in the direction under consideration. 98

5.12 Component amplification factors for the 'N8T' building obtained using bi-directional time history analyses. Dashed vertical lines indicate the elastic modal periods in the direction under consideration. 99

5.13 Total amplification factors for the 'W4T' building obtained using bi-directional time history analyses. Dashed vertical lines indicate the elastic modal periods in the direction under consideration. 103

5.14 Total amplification factors for the 'W8T' building obtained using bi-directional time history analyses. Dashed vertical lines indicate the elastic modal periods in the direction under consideration. 104

5.15 Total amplification factors for the 'N4T' building obtained using bi-directional time history analyses. Dashed vertical lines indicate the elastic modal periods in the direction under consideration. 105

5.16 Total amplification factors for the 'N8T' building obtained using bi-directional time history analyses. Dashed vertical lines indicate the elastic modal periods in the direction under consideration. 106

5.17 Total amplification factors for the 'E4T' building obtained using bi-directional time history analyses. Dashed vertical lines indicate the elastic modal periods in the direction under consideration. 107

5.18 Total amplification factors for the 'E8T' building obtained using bi-directional time history analyses. Dashed vertical lines indicate the elastic modal periods in the direction under consideration. 108

5.19 Spectral amplification factors for the 'E4T' building, with and without the rotational ground motions. Dashed vertical lines indicate the elastic modal periods in the direction under consideration. 109

5.20 Spectral amplification factors for the 'E8T' building, with and without the rotational ground motions. Dashed vertical lines indicate the elastic modal periods in the direction under consideration. 110

5.21 Spectral amplification factors for the 'W4T' building, with and without the rotational ground motions. Dashed vertical lines indicate the elastic modal periods in the direction under consideration. 114

5.22 Spectral amplification factors for the 'W8T' building, with and without the rotational ground motions. Dashed vertical lines indicate the elastic modal periods in the direction under consideration. 115

5.23 Spectral amplification factors for the 'N4T' building, with and without the rotational ground motions. Dashed vertical lines indicate the elastic modal periods in the direction under consideration. 116

5.24 Spectral amplification factors for the 'N8T' building, with and without the rotational ground motions. Dashed vertical lines indicate the elastic modal periods in the direction under consideration. 117

5.25 Effective period ratio for the inelastic buildings investigated in this study. 117

6.1 Variations of torsional amplification factor for the rigid secondary systems along the height of the 'E4T', 'W4T', and 'N4T' buildings. . 131

6.2 Variations of torsional amplification factor for the rigid secondary systems along the height of the 'E8T', 'W8T', and 'N8T' buildings. . 132

6.3 In-plan distribution of torsional amplification factor for rigid secondary systems at different floors of the 'E4T' building. 132

6.4 In-plan distribution of torsional amplification factor for rigid secondary systems at different floors of the 'E8T' building. 133

6.5 In-plan distribution of torsional amplification factor for rigid secondary systems at different floors of the 'W4T' building. 133

6.6 In-plan distribution of torsional amplification factor for rigid secondary systems at different floors of the 'W8T' building. 134

6.7 In-plan distribution of torsional amplification factor for rigid secondary systems at different floors of the 'N4T' building. 134

6.8 In-plan distribution of torsional amplification factor for rigid secondary systems at different floors of the 'N8T' building. 135

6.9 Torsional amplification factors for the 'E4T' building estimated using time history analyses with and without rotational ground motions. Dashed vertical lines indicate the elastic modal periods in the direction under consideration. 141

6.10 Torsional amplification factors for the 'E8T' building estimated using time history analyses with and without rotational ground motions. Dashed vertical lines indicate the elastic modal periods in the direction under consideration. 142

6.11 Torsional amplification factors for the 'W4T' building estimated using time history analyses with and without rotational ground motions. Dashed vertical lines indicate the elastic modal periods in the direction under consideration. 143

6.12 Torsional amplification factors for the 'W8T' building estimated using time history analyses with and without rotational ground motions. Dashed vertical lines indicate the elastic modal periods in the direction under consideration. 144

6.13 Torsional amplification factors for the 'N4T' building estimated using time history analyses with and without rotational ground motions. Dashed vertical lines indicate the elastic modal periods in the direction under consideration. 145

6.14 Torsional amplification factors for the 'N8T' building estimated using time history analyses with and without rotational ground motions. Dashed vertical lines indicate the elastic modal periods in the direction under consideration. 146

6.15 Comparison of the estimated torsional amplification factors for very flexible secondary systems (TAF_{VF} at $T_s = 3T_1$) at the FE for the 4- and 8-storied T-shaped buildings, with and without the rotational ground motions. 152

6.16 Comparison of the estimated torsional amplification factors for very flexible secondary systems (TAF_{VF} at $T_s = 3T_1$) at the SE for the 4- and 8-storied T-shaped buildings, with and without the rotational ground motions. 153

6.17 Comparison of the estimated torsional amplification factors for very flexible secondary systems (TAF_{VF} at $T_s = 4T_1$) at the FE for the 4- and 8-storied T-shaped buildings, with and without the rotational ground motions. 153

6.18 Comparison of the estimated torsional amplification factors for very flexible secondary systems (TAF_{VF} at $T_s = 4\,T_1$) at the SE for the 4- and 8-storied T-shaped buildings, with and without the rotational ground motions. 154

6.19 Torsional amplification factors for rigid secondary systems (TAF_R) at the flexible edges of the ETI and WTI buildings plotted with their elastic displacement ratios ($\Delta_{max}/\Delta_{avg}$). 156

6.20 Torsional amplification factors for rigid secondary systems (TAF_R) at the flexible edges of the ETI and WTI buildings plotted with their elastic displacement ratios ($\Delta_{max}/\Delta_{min}$). 157

6.21 Scatter plot showing the results of the Breusch-Pagan test conducted on 160 datasets comprising of TAF_R and torsional irregularity indices, from the analyzed ETI and WTI buildings. 157

6.22 Torsional amplification factors for the flexible frames of all investigated buildings. 160

6.23 Scatter plot showing results of (a) the Breusch-Pagan test and (b) the regression analysis. 161

6.24 Scatter plot showing the results of the Breusch-Pagan test conducted on 160 datasets from the investigated ETI and WTI buildings. 162

6.25 Scatter plots showing the maximum TAF_F values versus the corresponding displacement ratio ($\Delta_{max}/\Delta_{avg}$) for various ETI and WTI buildings. 162

6.26 Scatter plots showing the maximum TAF_F values versus the corresponding displacement ratio ($\Delta_{max}/\Delta_{min}$) for various ETI and WTI buildings. 163

6.27 Proposed model for the estimation of torsional amplification factors for rigid, flexible, and very flexible secondary systems. 166

7.1 Typical plan layouts, section sizes, and stiffness eccentricity details of the buildings considered for validation of the proposed equations. The stiffness eccentricities shown in the building plan correspond to the first-floor level of the 3-story building. 176

7.2 Typical plan, elevations (along-slope), section sizes, and eccentricity details of the considered step-back buildings. 177

7.3 Variations of the torsional irregularity indices of seismic design codes for the Group 1 buildings (obtained using the mode superposition method). 182

7.4 Variations of the torsional irregularity indices of seismic design codes for the Group 2 buildings (obtained using the mode superposition method). Here, the horizontal dotted lines in the plots show the base floor levels of the respective buildings. 183

7.5 Comparisons of the estimated TAF_R from time history analyses with and without rotational ground motions with those obtained from the proposed equations, along the height of 'E3E', 'E3P', 'E6E', and 'E6P' buildings. 186

7.6 Comparisons of the estimated in-plan distribution of TAF_R from time history analyses with those obtained from the proposed equations, along the height of 'E3E', 'E3P', 'E6E', and 'E6P' buildings. 187

7.7 Comparisons of the torsional amplification factors for the 'E3E' and 'E6E' buildings, estimated from time history analyses with and without rotational ground motions and those predicted by the proposed equations. 189

7.8 Comparisons of the torsional amplification factors for the 'E3P' and 'E6P' buildings, estimated from time history analyses with and without rotational ground motions and those predicted by the proposed equations. 190

7.9 Comparisons of the torsional amplification factors for the '2SB' building, estimated from time history analyses with and without rotational ground motions and those predicted by the proposed equations. 191

7.10 Comparisons of the torsional amplification factors for the '4SB' building, estimated from time history analyses with and without rotational ground motions and those predicted by the proposed equations. 192

7.11 Comparisons of the torsional amplification factors for the '8SB' building, estimated from time history analyses with and without rotational ground motions and those predicted by the proposed equations. 193

7.12 Comparisons of the PFA/PGA at the SE, estimated from time history analyses with and without considering rotational ground motions, as well as from building codes, with and without applying the proposed equations, for the 'E3E,' 'E3P,' 'E6E,' and 'E6P' buildings. 197

7.13 Comparisons of the PFA/PGA at the FE, estimated from time history analyses with and without considering rotational ground motions, as well as from building codes, with and without applying the proposed equations, for the 'E3E,' 'E3P,' 'E6E,' and 'E6P' buildings. 198

7.14 Comparisons of the in-plan distribution of the PFA/PGA, as estimated from the bi-directional time history analyses and from building codes with and without applying the proposed equations, for the 'E3E,' 'E3P,' 'E6E,' and 'E6P' buildings (Elastic). The curves corresponding to ASCE 7 are not visible in some plots (g, h, j, and k) as they are overlapped with EC 8 curves. 199

7.15 Comparison of the in-plan distribution of the PFA/PGA, as estimated from the bi-directional time history analyses and from building codes with and without applying the proposed equations, for the 'E3E,' 'E3P,' 'E6E,' and 'E6P' buildings (SR = 2). 200

7.16 Comparisons of total amplification (a_t) estimated from time history analyses with and without considering rotational ground motions, as well as from building codes, with and without applying the proposed equations, for the 'E3E' and 'E6E' buildings. 203

7.17 Comparisons of total amplification (a_t) estimated from time history analyses with and without considering rotational ground motions, as well as from building codes, with and without applying the proposed equations, for the 'E3P' and 'E6P' buildings. 204

7.18 Comparisons of total amplification (a_t) estimated from time history analyses with and without considering rotational ground motions, as well as from building codes, with and without applying the proposed equations, for the '2SB' building. 208

7.19 Comparisons of total amplification (a_t) estimated from time history analyses with and without considering rotational ground motions, as well as from building codes, with and without applying the proposed equations, for the '4SB' building. 209

7.20 Comparisons of total amplification (a_t) estimated from time history analyses with and without considering rotational ground motions, as well as from building codes, with and without applying the proposed equations, for the '8SB' building. 210

A.1 PFA/PGA at various locations on the floor plan of the 'E4U', 'W4U', and 'N4U' buildings. 241

A.2 PFA/PGA at various locations on the floor plan of the 'E8U', 'W8U', and 'N8U' buildings. 242

A.3 PFA/PGA at various locations on the floor plan of the 'E4S', 'W4S', and 'N4S' buildings. 242

A.4 PFA/PGA at various locations on the floor plan of the 'E8S', 'W8S', and 'N8S' buildings. 243

A.5 PFA/PGA at various locations on the floor plan of the 'E4R', 'W4R', and 'N4R' buildings. 243

A.6 PFA/PGA at various locations on the floor plan of the 'E8R', 'W8R', and 'N8R' buildings. 244

A.7 In-plan distribution of PFA/PGA at different floors of the 'E4U' building. 245

A.8 In-plan distribution of PFA/PGA at different floors of the 'E8U' building. 245

A.9 In-plan distribution of PFA/PGA at different floors of the 'W4U' building. 246

A.10 In-plan distribution of PFA/PGA at different floors of the 'W8U' building. 246

A.11 In-plan distribution of PFA/PGA at different floors of the 'N4U' building. 247

A.12 In-plan distribution of PFA/PGA at different floors of the 'N8U' building. 247

A.13 In-plan distribution of PFA/PGA at different floors of the 'E4S' building. 248

A.14 In-plan distribution of PFA/PGA at different floors of the 'E8S' building. 248

A.15 In-plan distribution of PFA/PGA at different floors of the 'W4S' building. 249

A.16 In-plan distribution of PFA/PGA at different floors of the 'W8S' building. 249

A.17 In-plan distribution of PFA/PGA at different floors of the 'N4S' building. 250

A.18 In-plan distribution of PFA/PGA at different floors of the 'N8S' building. 250

A.19 In-plan distribution of PFA/PGA at different floors of the 'E4R' building. 251

A.20 In-plan distribution of PFA/PGA at different floors of the 'E8R' building. 251

A.21 In-plan distribution of PFA/PGA at different floors of the 'W4R' building. 252

A.22 In-plan distribution of PFA/PGA at different floors of the 'W8R' building. 252

A.23 In-plan distribution of PFA/PGA at different floors of the 'N4R' building. 253

A.24 In-plan distribution of PFA/PGA at different floors of the 'N8R' building. 253

B.1 Component amplification factors for the 'E4U' building obtained using bi-directional time history analyses. Dashed vertical lines indicate the elastic modal periods in the direction under consideration. 255

B.2 Component amplification factors for the 'E8U' building obtained using bi-directional time history analyses. Dashed vertical lines indicate the elastic modal periods in the direction under consideration. 256

B.3 Component amplification factors for the 'W4U' building obtained using bi-directional time history analyses. Dashed vertical lines indicate the elastic modal periods in the direction under consideration. 256

B.4 Component amplification factors for the 'W8U' building obtained using bi-directional time history analyses. Dashed vertical lines indicate the elastic modal periods in the direction under consideration. 257

B.5 Component amplification factors for the 'N4U' building obtained using bi-directional time history analyses. Dashed vertical lines indicate the elastic modal periods in the direction under consideration. 257

B.6 Component amplification factors for the 'N8U' building obtained using bi-directional time history analyses. Dashed vertical lines indicate the elastic modal periods in the direction under consideration. 258

B.7 Component amplification factors for the 'E4S' building obtained using bi-directional time history analyses. Dashed vertical lines indicate the elastic modal periods in the direction under consideration. 258

B.8 Component amplification factors for the 'E8S' building obtained using bi-directional time history analyses. Dashed vertical lines indicate the elastic modal periods in the direction under consideration. 259

B.9 Component amplification factors for the 'W4S' building obtained using bi-directional time history analyses. Dashed vertical lines indicate the elastic modal periods in the direction under consideration. 259

B.10 Component amplification factors for the 'W8S' building obtained using bi-directional time history analyses. Dashed vertical lines indicate the elastic modal periods in the direction under consideration. 260

B.11 Component amplification factors for the 'N4S' building obtained using bi-directional time history analyses. Dashed vertical lines indicate the elastic modal periods in the direction under consideration. 260

B.12 Component amplification factors for the 'N8S' building obtained using bi-directional time history analyses. Dashed vertical lines indicate the elastic modal periods in the direction under consideration. 261

B.13 Component amplification factors for the 'E4R' building obtained using bi-directional time history analyses. Dashed vertical lines indicate the elastic modal periods in the direction under consideration. 261

B.14 Component amplification factors for the 'E8R' building obtained using bi-directional time history analyses. Dashed vertical lines indicate the elastic modal periods in the direction under consideration. 262

B.15 Component amplification factors for the 'W4R' building obtained using bi-directional time history analyses. Dashed vertical lines indicate the elastic modal periods in the direction under consideration. 262

B.16 Component amplification factors for the 'W8R' building obtained using bi-directional time history analyses. Dashed vertical lines indicate the elastic modal periods in the direction under consideration. 263

B.17 Component amplification factors for the 'N4R' building obtained using bi-directional time history analyses. Dashed vertical lines indicate the elastic modal periods in the direction under consideration. 263

B.18 Component amplification factors for the 'N8R' building obtained using bi-directional time history analyses. Dashed vertical lines indicate the elastic modal periods in the direction under consideration. 264

B.19 Total amplification factors for the 'E4U' building obtained using bi-directional time history analyses. Dashed vertical lines indicate the elastic modal periods in the direction under consideration. 265

B.20 Total amplification factors for the 'E8U' building obtained using bi-directional time history analyses. Dashed vertical lines indicate the elastic modal periods in the direction under consideration. 265

B.21 Total amplification factors for the 'W4U' building obtained using bi-directional time history analyses. Dashed vertical lines indicate the elastic modal periods in the direction under consideration. 266

B.22 Total amplification factors for the 'W8U' building obtained using bi-directional time history analyses. Dashed vertical lines indicate the elastic modal periods in the direction under consideration. 266

B.23 Total amplification factors for the 'N4U' building obtained using bi-directional time history analyses. Dashed vertical lines indicate the elastic modal periods in the direction under consideration. 267

B.24 Total amplification factors for the 'N8U' building obtained using bi-directional time history analyses. Dashed vertical lines indicate the elastic modal periods in the direction under consideration. 267

B.25 Total amplification factors for the 'E4S' building obtained using bi-directional time history analyses. Dashed vertical lines indicate the elastic modal periods in the direction under consideration. 268

B.26 Total amplification factors for the 'E8S' building obtained using bi-directional time history analyses. Dashed vertical lines indicate the elastic modal periods in the direction under consideration. 268

B.27 Total amplification factors for the 'W4S' building obtained using bi-directional time history analyses. Dashed vertical lines indicate the elastic modal periods in the direction under consideration. 269

B.28 Total amplification factors for the 'W8S' building obtained using bi-directional time history analyses. Dashed vertical lines indicate the elastic modal periods in the direction under consideration. 269

B.29 Total amplification factors for the 'N4S' building obtained using bi-directional time history analyses. Dashed vertical lines indicate the elastic modal periods in the direction under consideration. 270

B.30 Total amplification factors for the 'N8S' building obtained using bi-directional time history analyses. Dashed vertical lines indicate the elastic modal periods in the direction under consideration. 270

B.31 Total amplification factors for the 'E4R' building obtained using bi-directional time history analyses. Dashed vertical lines indicate the elastic modal periods in the direction under consideration. 271

B.32 Total amplification factors for the 'E8R' building obtained using bi-directional time history analyses. Dashed vertical lines indicate the elastic modal periods in the direction under consideration. 271

B.33 Total amplification factors for the 'W4R' building obtained using bi-directional time history analyses. Dashed vertical lines indicate the elastic modal periods in the direction under consideration. 272

B.34 Total amplification factors for the 'W8R' building obtained using bi-directional time history analyses. Dashed vertical lines indicate the elastic modal periods in the direction under consideration. 272

B.35 Total amplification factors for the 'N4R' building obtained using bi-directional time history analyses. Dashed vertical lines indicate the elastic modal periods in the direction under consideration. 273

B.36 Total amplification factors for the 'N8R' building obtained using bi-directional time history analyses. Dashed vertical lines indicate the elastic modal periods in the direction under consideration. 273

B.37 Spectral amplification factors for the 'E4U' building, with and without the rotational ground motions. Dashed vertical lines indicate the elastic modal periods in the direction under consideration. 274

B.38 Spectral amplification factors for the 'E8U' building, with and without the rotational ground motions. Dashed vertical lines indicate the elastic modal periods in the direction under consideration. 275

B.39 Spectral amplification factors for the 'W4U' building, with and without the rotational ground motions. Dashed vertical lines indicate the elastic modal periods in the direction under consideration. 275

B.40 Spectral amplification factors for the 'W8U' building, with and without the rotational ground motions. Dashed vertical lines indicate the elastic modal periods in the direction under consideration. 276

B.41 Spectral amplification factors for the 'N4U' building, with and without the rotational ground motions. Dashed vertical lines indicate the elastic modal periods in the direction under consideration. 276

B.42 Spectral amplification factors for the 'N8U' building, with and without the rotational ground motions. Dashed vertical lines indicate the elastic modal periods in the direction under consideration. 277

B.43 Spectral amplification factors for the 'E4S' building, with and without the rotational ground motions. Dashed vertical lines indicate the elastic modal periods in the direction under consideration. 277

B.44 Spectral amplification factors for the 'E8S' building, with and without the rotational ground motions. Dashed vertical lines indicate the elastic modal periods in the direction under consideration. 278

B.45 Spectral amplification factors for the 'W4S' building, with and without the rotational ground motions. Dashed vertical lines indicate the elastic modal periods in the direction under consideration. 278

B.46 Spectral amplification factors for the 'W8S' building, with and without the rotational ground motions. Dashed vertical lines indicate the elastic modal periods in the direction under consideration. 279

B.47 Spectral amplification factors for the 'N4S' building, with and without the rotational ground motions. Dashed vertical lines indicate the elastic modal periods in the direction under consideration. 279

B.48 Spectral amplification factors for the 'N8S' building, with and without the rotational ground motions. Dashed vertical lines indicate the elastic modal periods in the direction under consideration. 280

B.49 Spectral amplification factors for the 'E4R' building, with and without the rotational ground motions. Dashed vertical lines indicate the elastic modal periods in the direction under consideration. 280

B.50 Spectral amplification factors for the 'E8R' building, with and without the rotational ground motions. Dashed vertical lines indicate the elastic modal periods in the direction under consideration. 281

B.51 Spectral amplification factors for the 'W4R' building, with and without the rotational ground motions. Dashed vertical lines indicate the elastic modal periods in the direction under consideration. 281

B.52 Spectral amplification factors for the 'W8R' building, with and without the rotational ground motions. Dashed vertical lines indicate the elastic modal periods in the direction under consideration. 282

B.53 Spectral amplification factors for the 'N4R' building, with and without the rotational ground motions. Dashed vertical lines indicate the elastic modal periods in the direction under consideration. 282

B.54 Spectral amplification factors for the 'N8R' building, with and without the rotational ground motions. Dashed vertical lines indicate the elastic modal periods in the direction under consideration. 283

C.1 Variations of torsional amplification factor for the rigid secondary systems along the height of the 'E4U', 'W4U', and 'N4U' buildings. . 285

C.2 Variations of torsional amplification factor for the rigid secondary systems along the height of the 'E8U', 'W8U', and 'N8U' buildings. . 286

C.3 Variations of torsional amplification factor for the rigid secondary systems along the height of the 'E4S', 'W4S', and 'N4S' buildings. . . 286

C.4 Variations of torsional amplification factor for the rigid secondary systems along the height of the 'E8S', 'W8S', and 'N8S' buildings. . . 287

C.5 Variations of torsional amplification factor for the rigid secondary systems along the height of the 'E4R', 'W4R', and 'N4R' buildings. . 287

C.6 Variations of torsional amplification factor for the rigid secondary systems along the height of the 'E8R', 'W8R', and 'N8R' buildings. . 288

C.7 In-plan distribution of torsional amplification factor for rigid secondary systems at different floors of the 'E4U' building. 289

C.8 In-plan distribution of torsional amplification factor for rigid secondary systems at different floors of the 'E8U' building. 289

C.9 In-plan distribution of torsional amplification factor for rigid secondary systems at different floors of the 'W4U' building. 290

C.10 In-plan distribution of torsional amplification factor for rigid secondary systems at different floors of the 'W8U' building. 290

C.11 In-plan distribution of torsional amplification factor for rigid secondary systems at different floors of the 'N4U' building. 291

C.12 In-plan distribution of torsional amplification factor for rigid secondary systems at different floors of the 'N8U' building. 291

C.13 In-plan distribution of torsional amplification factor for rigid secondary systems at different floors of the 'E4S' building. 292

C.14 In-plan distribution of torsional amplification factor for rigid secondary systems at different floors of the 'E8S' building. 292

C.15 In-plan distribution of torsional amplification factor for rigid secondary systems at different floors of the 'W4S' building. 293

C.16 In-plan distribution of torsional amplification factor for rigid secondary systems at different floors of the 'W8S' building. 293

C.17 In-plan distribution of torsional amplification factor for rigid secondary systems at different floors of the 'N4S' building. 294

C.18 In-plan distribution of torsional amplification factor for rigid secondary systems at different floors of the 'N8S' building. 294

C.19 In-plan distribution of torsional amplification factor for rigid secondary systems at different floors of the 'E4R' building. 295

C.20 In-plan distribution of torsional amplification factor for rigid secondary systems at different floors of the 'E8R' building. 295

C.21 In-plan distribution of torsional amplification factor for rigid secondary systems at different floors of the 'W4R' building. 296

C.22 In-plan distribution of torsional amplification factor for rigid secondary systems at different floors of the 'W8R' building. 296

C.23 In-plan distribution of torsional amplification factor for rigid secondary systems at different floors of the 'N4R' building. 297

C.24 In-plan distribution of torsional amplification factor for rigid secondary systems at different floors of the 'N8R' building. 297

C.25 Torsional amplification factors for the 'E4U' building estimated using time history analyses with and without rotational ground motions. Dashed vertical lines indicate the elastic modal periods in the direction under consideration. 298

C.26 Torsional amplification factors for the 'E8U' building estimated using time history analyses with and without rotational ground motions. Dashed vertical lines indicate the elastic modal periods in the direction under consideration. 299

C.27 Torsional amplification factors for the 'W4U' building estimated using time history analyses with and without rotational ground motions. Dashed vertical lines indicate the elastic modal periods in the direction under consideration. 299

C.28 Torsional amplification factors for the 'W8U' building estimated using time history analyses with and without rotational ground motions. Dashed vertical lines indicate the elastic modal periods in the direction under consideration. 300

C.29 Torsional amplification factors for the 'N4U' building estimated using time history analyses with and without rotational ground motions. Dashed vertical lines indicate the elastic modal periods in the direction under consideration. 300

C.30 Torsional amplification factors for the 'N8U' building estimated using time history analyses with and without rotational ground motions. Dashed vertical lines indicate the elastic modal periods in the direction under consideration. 301

C.31 Torsional amplification factors for the 'E4S' building estimated using time history analyses with and without rotational ground motions. Dashed vertical lines indicate the elastic modal periods in the direction under consideration. 301

C.32 Torsional amplification factors for the 'E8S' building estimated using time history analyses with and without rotational ground motions. Dashed vertical lines indicate the elastic modal periods in the direction under consideration. 302

C.33 Torsional amplification factors for the 'W4S' building estimated using time history analyses with and without rotational ground motions. Dashed vertical lines indicate the elastic modal periods in the direction under consideration. 302

C.34 Torsional amplification factors for the 'W8S' building estimated using time history analyses with and without rotational ground motions. Dashed vertical lines indicate the elastic modal periods in the direction under consideration. 303

C.35 Torsional amplification factors for the 'N4S' building estimated using time history analyses with and without rotational ground motions. Dashed vertical lines indicate the elastic modal periods in the direction under consideration. 303

C.36 Torsional amplification factors for the 'N8S' building estimated using time history analyses with and without rotational ground motions. Dashed vertical lines indicate the elastic modal periods in the direction under consideration. 304

C.37 Torsional amplification factors for the 'E4R' building estimated using time history analyses with and without rotational ground motions. Dashed vertical lines indicate the elastic modal periods in the direction under consideration. 304

C.38 Torsional amplification factors for the 'E8R' building estimated using time history analyses with and without rotational ground motions. Dashed vertical lines indicate the elastic modal periods in the direction under consideration. 305

C.39 Torsional amplification factors for the 'W4R' building estimated using time history analyses with and without rotational ground motions. Dashed vertical lines indicate the elastic modal periods in the direction under consideration. 305

C.40 Torsional amplification factors for the 'W8R' building estimated using time history analyses with and without rotational ground motions. Dashed vertical lines indicate the elastic modal periods in the direction under consideration. 306

C.41 Torsional amplification factors for the 'N4R' building estimated using time history analyses with and without rotational ground motions. Dashed vertical lines indicate the elastic modal periods in the direction under consideration. 306

C.42 Torsional amplification factors for the 'N8R' building estimated using time history analyses with and without rotational ground motions. Dashed vertical lines indicate the elastic modal periods in the direction under consideration. 307

List of Tables

1.1 Classification of commonly used secondary systems [4]. 7

3.1 Dynamic characteristics of the investigated buildings. 55

3.2 A suite of 20 far field ground motion records used in this study. . . . 64

4.1 Median PFA/PGA for the investigated buildings. 71

4.2 Median increase (%) in PFA/PGA due to rotational ground motions. 79

5.1 Median peak component amplification factor for the 4-story buildings. 93

5.2 Median peak component amplification factor for the 8-story buildings. 94

5.3 Median peak total amplification factor for the 4-story buildings. . . . 100

5.4 Median peak total amplification factor for the 8-story buildings. . . . 101

5.5 Median peak spectral amplification factor for the 4-story buildings. . 111

5.6 Median peak spectral amplification factor for the 8-story buildings. . 112

5.7 Median peak increase (%) in spectral amplification factor due to rotational ground motions for the 4-story buildings. 119

5.8 Median peak increase (%) in spectral amplification factor due to rotational ground motions for the 8-story buildings. 121

6.1 Median torsional amplification factor for rigid secondary systems in 4- and 8-storied buildings. 130

6.2 Median increase (%) in torsional amplification factor for rigid secondary systems due to rotational ground motion. 136

6.3 Median peak torsional amplification factor for flexible secondary systems in the 4-story buildings. 139

6.4 Median peak torsional amplification factor for flexible secondary systems in the 8-story buildings. 140

6.5 Median peak increase (%) in torsional amplification factor for flexible secondary systems due to rotational ground motions in the 4-story buildings. 148

6.6 Median peak increase (%) in torsional amplification factor for flexible secondary systems due to rotational ground motions in the 8-story buildings. 149

6.7 Values of the tuning ratio for the proposed model (Figure 6.27). . . . 166

6.8 Proposed values of the exponents α and β to estimate the torsional amplification factor for rigid secondary systems. 167

6.9 Proposed values of the exponents δ and θ to estimate the torsional amplification factor for flexible secondary systems. 167

6.10 Proposed values of the exponent 'γ' to estimate the torsional amplification factor for rigid secondary systems across the floor plan. 169

7.1 Dynamic characteristics of the Group 1 buildings. 179

7.2 Dynamic characteristics of the Group 2 buildings. 180

7.3 A suite of 20 far field ground motion records used for Group 1 buildings. 184

7.4 A suite of 20 far field ground motion records used for Group 2 buildings. 185

C.1 Regression analysis parameters for $\Delta_{max}/\Delta_{avg}$ versus torsional amplification factor for rigid secondary systems at the FE. 308

C.2 Regression analysis parameters for $\Delta_{max}/\Delta_{min}$ versus torsional amplification factor for rigid secondary systems at the FE. 309

C.3 Regression analysis parameters for $\Delta_{max}/\Delta_{avg}$ versus peak torsional amplification factor for flexible secondary systems at the FE. 310

C.4 Regression analysis parameters for $\Delta_{max}/\Delta_{min}$ versus peak torsional amplification factor for flexible secondary systems at the FE. 311

Nomenclature

2D	Two-dimensional
3D	Three-dimensional
α_{eq}	Acceleration due to earthquake force
α_{mx}	Modal mass participation in the X-direction
α_{my}	Modal mass participation in the Y-direction
α	Angle at which the secondary system is lifted
Δ_{avg}	Average displacement at the floor level of interest
Δ_{max}	Maximum displacement at the floor level of interest
Δ_{min}	Minimum displacement at the floor level of interest
μ	Coefficient of friction
ω	Angular frequency
θ_{mz}	Modal mass participation corresponding to the rotational mode of vibration about Z-direction
ξ_s	Damping of the secondary system
a_p	Component amplification factor
a_t	Total amplification factor
b	Width of the component
cR_1	Hardening control factor 1
cR_2	Hardening control factor 2
e_{CR}	Stiffness eccentricity

e_{CS} Strength eccentricity

F_{eq} Horizontal seismic force

g Acceleration due to gravity

H Total height of the building

h Height of the component

M_w Moment magnitude of earthquake

r_d Half of the diagonal length of the rigid block

R_{rup} Closest distance to the rupture surface

R_X Rotational component of the ground motion about X-axis

R_Y Rotational component of the ground motion about Y-axis

R_Z Rotational component of the ground motion about Z-axis

R Response modification factor

r Torsional radius

R_0 Initial slope of the transition curve

R^2 Coefficient of determination

S_{ad} Design spectral acceleration

S_{ay} Spectral acceleration at yielding

$S_a(T_1,5\%)$ 5%-Damped spectral acceleration at the fundamental period (T_1)

S_{du} Spectral displacement at the ultimate point

S_{dy} Spectral displacement at yielding

T_{eff} Effective (inelastic) period of the building

T_s Period of vibration of the secondary system

T_s/T_1 Tuning ratio

T_1 Fundamental period of the building

V_p Primary wave velocity

$V_{s,\ 30}$ Average shear-wave velocity from the surface to a depth of 30 m

W Weight of the component

Z Height of the floor measured from the base

Z/H Relative height

AC Air conditioning

CM Center of mass

COV Coefficient of variation

CR Center of rigidity

CS Center of strength

CSMIP California Strong Motion Instrumentation Program

DAF Dynamic amplification factor

DMF Damping modification factor

ELF Equivalent lateral force

ETI Extreme torsional irregularity

FE Flexible edge

FF_{ij} Flexible frame 'i' at 'j^{th}' floor

FM Fundamental mode

FRS Floor response spectra

FSA Floor spectral acceleration

GRS Ground response spectra

$H_{1/2}$ Horizontal component of the ground motion

HM Higher mode

HVAC Heating, ventilation, and air conditioning

MCE Maximum considered earthquake

MDOF Multiple-degree-of-freedom-system

MPA Modal pushover analysis

MRF Moment resisting frame

NEHRP National Earthquake Hazard Reduction Programme

NTI No torsional irregularity

OGS Open ground story

OLS Ordinary least squares

PBD Performance-based design

PCA Peak component acceleration

PFA Peak floor acceleration

PGA Peak ground acceleration

PGA_X Peak ground acceleration of the ground motion in X-direction

PGA_Y Peak ground acceleration of the ground motion in Y-direction

PGV Peak ground velocity

RC Reinforced-concrete

RCMRF Reinforced-concrete moment resisting frame

RSN Record sequence number

SB Step-back

SDOF Single-degree-of-freedom-system

SE Stiff edge

SF_{ij} Stiff frame 'i' at 'j^{th}' floor

SH Shear waves with horizontal particle motion

SMRF Special moment resisting frame

SR Strength ratio

SRL Surface rupture length

SRSS Square root of sum of squares

SSP Single station procedure

SV Shear waves with vertical particle motion

TAF Torsional amplification factor

$TAF_{F,max}$ Peak torsional amplification factor for the flexible secondary systems

TAF_{FM} Torsional amplification factors for flexible secondary systems tuned within the building's fundamental mode region

TAF_{F} Torsional amplification factor for the flexible secondary systems

TAF_{HM} Torsional amplification factors for flexible secondary systems tuned within the building's higher mode region

TAF_{R} Torsional amplification factor for the rigid secondary systems

TAF_{TZ} Torsional amplification factors for flexible secondary systems tuned within the transition zone between the building's fundamental and higher mode regions

TAF_{VF} Torsional amplification factor for the very flexible secondary systems

UI Uniform infills

WTI With torsional irregularity

Chapter 1

Introduction

1.1 Background

A building is constructed by interconnecting structural members such as beams, columns, slabs, and shear walls. Slabs act as horizontal elements (e.g., floors and roofs) that evenly distribute the loads to the beams; beams act as horizontal members that provide support to the building's weight and transfer it to the columns; columns act as vertical members supporting the beams and transferring the load to the foundation. Shear walls also act as vertical structural elements that provide additional stiffness to prevent excessive lateral displacement of the building and strength to resist lateral forces, mainly caused by earthquakes or wind. All these structural elements work in synchronization to create a structurally sound and stable building capable of withstanding different types of loading.

Besides the aforementioned structural elements, buildings (often referred to as supporting structures) also include secondary systems and contents. The term "*secondary systems and contents*" in a building refers to those systems/elements that are neither a part of the gravity load-resisting system nor a part of the lateral load-resisting system but offer functionality to buildings. Typical examples of secondary systems in buildings include light fixtures, electrical equipment, gas pipes, wastewater pipes, bookshelves, suspended ceilings, parapets, furniture, tanks, ducts, and elevators, among many others. Secondary systems are essential for the overall functionality of a building, as they include both contents critical to everyday operations and components that may directly impact the safety of occupants in the event of an emergency. The failure of these systems can result in significant economic losses, operational disruptions, and even life-threatening situations, as evidenced during past earthquakes [1, 2, 7–12]. Therefore, understanding the response of secondary systems and contents under different loading scenarios is

equally important.

Recent earthquakes and their destructive impact on buildings and their contents [1, 2, 7–10] have underscored the necessity for robust seismic design methodologies to ensure the satisfactory performance of both the building and secondary systems. In this context, the peak floor acceleration (PFA, which represents the maximum acceleration experienced at a given floor of the building during an earthquake) serves as a crucial parameter to estimate seismic demands for rigid secondary systems. In contrast, the floor response spectra (FRS) serve as a critical input to estimate seismic demands in relatively flexible secondary systems. Both the shape and amplitude of PFA and FRS (at different floors) are influenced by multiple factors, e.g., the dynamic characteristics of the building, the intensity of the earthquake, the structural configuration, and the dynamic properties and characteristics of the secondary systems, etc.

The presence of nominal torsion in buildings affects the dynamic behavior and characteristics of the buildings and, eventually, the PFA and FRS. Torsion in buildings occurs when a building's center of mass (CM) does not coincide with its center of rigidity (CR), causing uneven distribution of floor acceleration and displacement demands during seismic events [13–15]. This offset between CM and CR leads to increased/decreased acceleration or displacement demands at floors, also affecting secondary systems and contents attached to those floors. Current seismic design standards [6, 16, 17] lack specific provisions for addressing the effects of nominal and accidental torsion in the context of the design of secondary systems. This research gap highlights the immediate need for the development of procedures to account for the effects of building torsion in the seismic design of secondary systems. Accordingly, the present research work in this thesis has focused on understanding and predicting the effects of nominal building torsion in estimating the PFA and FRS demands in buildings.

1.2 Seismic performance of secondary systems

The secondary systems in a building usually experience accelerations that can be significantly larger than the peak ground acceleration (PGA) experienced by the building itself, mainly due to dynamic amplification effects. It had been reported

[7, 18–21] that many buildings lost functionality solely due to damage in secondary systems, even though the structural performance of most buildings during these events was deemed satisfactory. Significant damage to secondary systems has been observed in major seismic events, including the 2010 Darfield earthquake [7], the 2010 Chile earthquake [22], the 2012 Emilia earthquake [9], and the 2016 Central Italy earthquake [10]. Recently, the 2001 Bhuj earthquake [1] and the 2011 Sikkim earthquake [11, 12, 23] underscored the seismic vulnerability of secondary systems in the Indian housing stock. During the 2001 Bhuj earthquake and the 2011 Sikkim earthquake, widespread damage was observed in secondary systems, including dislodgement of water tanks (Figure 1.1) [24, 25], destruction of partition walls (Figure 1.2), and failure of suspended ceilings. These failures caused significant operational disruptions in critical facilities, such as hospitals and administrative buildings, even though, in many cases, the structural performance of these buildings was generally satisfactory.

Ensuring the seismic safety and operational continuity of secondary systems during seismic events is paramount, particularly in lifeline structures such as hospitals, where failure of these systems can lead to life-threatening injuries, casualties, and significant delays in post-earthquake recovery efforts. Further, secondary systems constitute a substantial portion of a building's overall cost, with their contributions up to 92% of the total cost in hospitals, according to Taghavi and Miranda [26]. Additionally, Murty et al. [4] reported that these systems could account for up to 80% of the total building cost in residential buildings in India (Figure 1.3). Consequently, severe damage to these systems during seismic events can also result in extensive economic losses and operational disruptions, especially in business environments where continuity is critical. Therefore, the evaluation of existing seismic design provisions and the development of new guidelines to ensure the seismic resilience of secondary systems is an essential step in earthquake engineering.

1.3 Classification of secondary systems

The secondary systems and contents exhibit widely varying characteristics that are often classified based on their functionality, sensitivity, and flexibility (Figure 1.4).

Functionality-wise, secondary systems are typically categorized as architectural, electrical, and mechanical components [18], each serving distinct roles in the routine operation of the building. Architectural components include elements like false ceilings, facades, and furniture, which contribute to the aesthetics of the building. Electrical components cover items such as air conditioning (AC) units, light fixtures, and electrical wiring, which are essential for providing power and lighting throughout



Figure 1.1: Dislodgement of water tank appendages from the rooftops of both unfinished and finished reinforced-concrete frame buildings in Bhuj [1].



(a) (b) (c)

Figure 1.2: Damage observed in residential building at Deorali [2]: (a) Extensive cracking in infill walls and damage to the reinforced-concrete column, (b) exposed mild steel reinforcement in the damaged reinforced-concrete column, and (c) out-of-plane collapse of the infill wall.

the building. Mechanical components are items like industrial equipment and elevators, which are crucial for the mechanical operations within the building.

Based on the sensitivity of their seismic response, secondary systems are categorized as acceleration-sensitive, displacement-sensitive, or combined acceleration- and displacement-sensitive [4]. Acceleration-sensitive systems, such as furniture, tanks, and bookshelves, are governed by floor acceleration and may fail due to rocking, sliding, or overturning (Figure 1.5). Displacement-sensitive systems, like masonry walls and parapets, are affected by relative deformations at their support points. Some systems, such as elevators and piping, exhibit both acceleration and displacement sensitivity. A list of common secondary systems based on these classifications is provided in Table 1.1.

Based on flexibility, secondary systems are classified as rigid, flexible, or very flexible. Rigid systems—typically acceleration-sensitive due to their short natural periods ($T_s \leq 0.06$; [27])—tend to move with the supporting structure and experience seismic forces approximately proportional to the floor acceleration (e.g., heavy furniture, tanks), as illustrated in Figure 1.5. In contrast, flexible systems (e.g., suspended ceilings, partitions) with longer natural periods ($T_s > 0.06$; [27]) tend to vibrate independently of the supporting structure and are often more affected by displacement-sensitive mechanisms, resulting in amplified seismic responses. Very

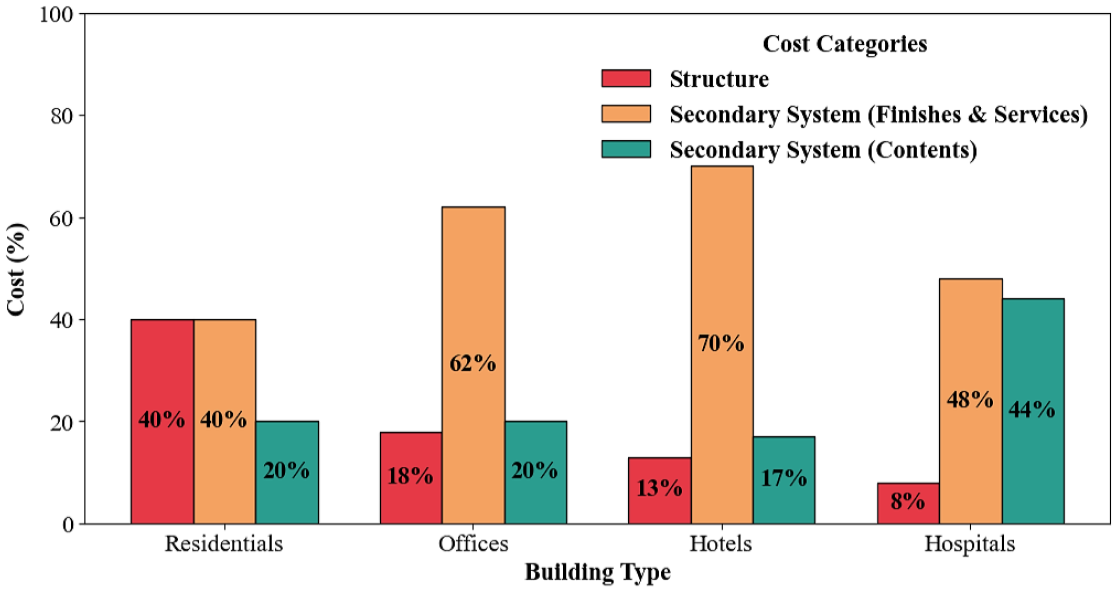

Figure 1.3: Cost comparison of the structure, secondary systems, and contents in buildings with various occupancies [3, 4].

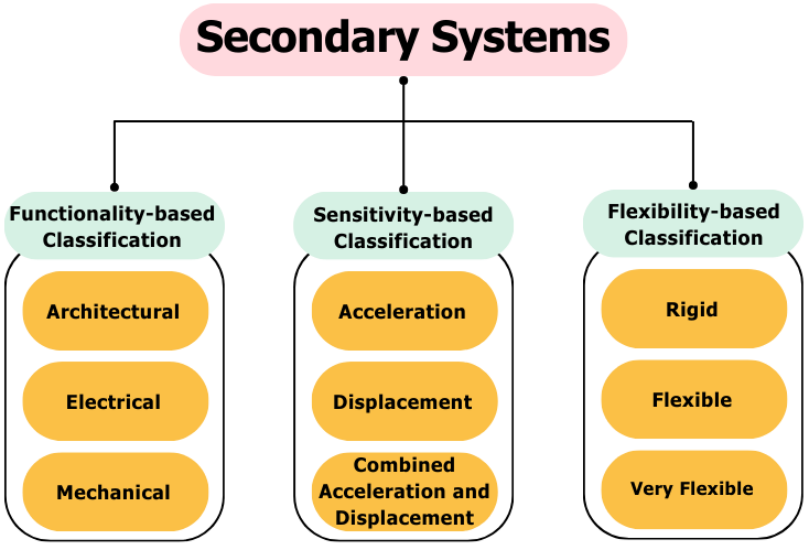

Figure 1.4: Classification of secondary systems.

flexible systems (e.g., HVAC ductwork, piping) undergo significant deformation but can dissipate energy, though they are more prone to damage. These classifications are essential for understanding seismic behavior and designing effective mitigation strategies.

In this thesis, the emphasis is placed on the seismic safety and design considerations specifically related to the light-weight acceleration-sensitive secondary systems in torsionally regular and irregular reinforced-concrete moment-resisting frame (RCMRF) buildings.

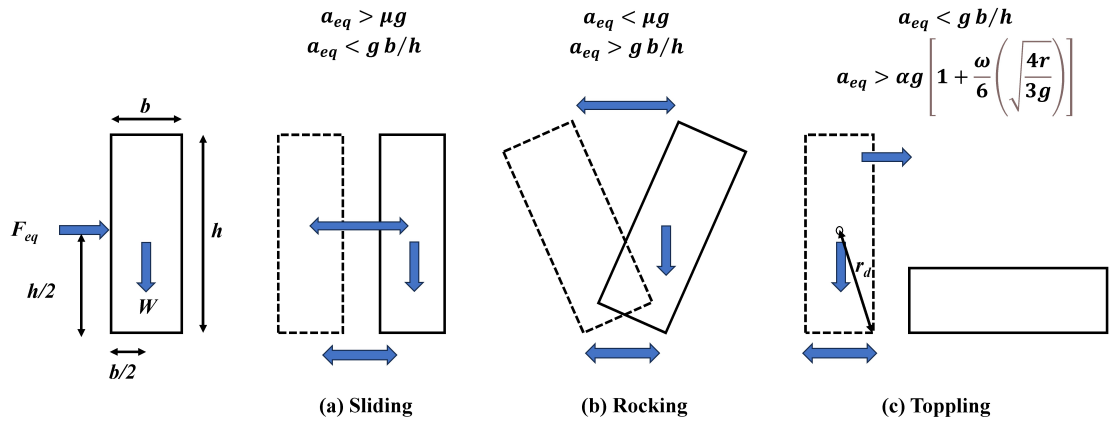

Figure 1.5: Possible failure modes of acceleration-sensitive secondary systems. Note: a_{eq} is the acceleration due to earthquake forces, μ is the coefficient of friction, g is the acceleration due to gravity, α is the angle at which the secondary system is lifted, ω is the angular frequency, and r_d is the half of the diagonal length of the rigid block.

Table 1.1: Classification of commonly used secondary systems [4].

Functionality-based classification	**Sub-class**	**Secondary system**	**Sensitivity-based classification**		
			Acceleration	**Displacement**	**Combined**
Architectural	Furniture	a. Storage shelves	✓	×	×
		b. Multi-level material stacks			
	False ceilings	a. Directly stuck to or hung from the roof	✓	×	×
		b. Suspended integrated ceiling system	S	P	✓
	Openings	a. Doors and windows	S	P	✓
		b. Large-panel glass panes with frames (as windows or infill walling material)			
		c. Other partitions			
	Partitions not held snugly between lateral load-resisting members		S	P	✓
	Stairs		P	S	✓
	Vertical projections	Parapets	✓	×	×
	Exterior or interior facades	Tiles (ceramic, stone, glass, or other)	S	P	✓
		a. Pasted on the surface			
		b. Bolted to the surface			
		c. Hung from hooks bolted to the surface			
	Exterior structural glazing systems		S	P	✓
Electrical	Appliances	a. Refrigerators	✓	×	×
		b. Washing machines			
		c. Gas cylinders			
		d. TVs			
		e. Diesel generators			
		f. Water pumps (small)			
		g. Window ACs			
		h. Wall-mounted ACs			
	Vertical projections	Antennas communication towers on rooftops	✓	×	×
	From both interior and exterior of the building	a. Power cables & wires	×	✓	×
		b. Telecom wires			
Mechanical	Vertical projections	a. Chimneys & Stacks	✓	×	×
		b. Water tanks (small)			
		c. Hoardings anchored on rooftops			
	Horizontal projections	a. Sunshades	✓	×	×
		b. Canopies and marquees			
		c. Hoardings anchored to the vertical face	S	P	✓
	From both interior and exterior of the building	a. Water supply pipes	×	✓	×
		b. Gas pipes			
		c. Sewage pipes			
		d. Rainwater conduits			
		e. Elevators			
		f. Fire hydrant equipment			
		g. AC ducts			
	Within the building	a. Pressurized fluid pipes	S	P	✓
		b. Fire hydrant piping network			
		c. Miscellaneous fluid pipelines			
	Storage vessels and water heaters	a. Flat bottom containers and vessels	✓	×	×
		b. Structurally supported vessels			
	Other mechanical equipments	a. Boilers and furnaces	✓	×	×
		b. General manufacturing and process machinery			
		c. HVAC equipment			

1.4 Building code provisions

Major national building codes [5, 6, 16] are vital for upholding the safety and structural reliability of buildings, offering comprehensive guidelines for their design, construction, and maintenance. These codes encompass essential material specifications, structural design, and detailing requirements for different buildings. These building codes advocate the construction of regular and symmetric buildings in seismic-prone regions. A regular building is characterized by its uniformity and symmetry in design and layout, which helps to ensure an even distribution of mass, stiffness, and strength throughout the structure. These buildings typically have symmetrical floor plans and elevations, meaning the shape and size of each floor are consistent, and the overall geometry is simple, often rectangular or square, without significant projections. The design allows for a continuous load path, meaning that loads are transferred smoothly from the upper parts of the building down to the foundation. Regular buildings also feature uniformity in elevation, with consistent floor heights and structural elements, contributing to predictable and stable behavior during seismic events. However, the practical constraints lead to building design that deviates from the ideal regular and symmetric buildings, resulting in irregular buildings.

Irregular buildings exhibit more complex behavior, especially during seismic events. The irregularities in the buildings can manifest in various forms, including plan and elevation irregularities. Plan irregularity refers to asymmetries or deviations from regular geometric shapes in the horizontal layout of a building. This can include torsional irregularity, re-entrant corners, floor slabs having excessive cut-outs or openings, out-of-plane offsets in vertical elements, and a non-parallel lateral force system, as depicted in Figure 1.6. Elevation irregularity, on the other hand, involves variations in terms of mass, stiffness, strength, or any combination of them in two or more successive stories along the building height. The presence of these irregularities can lead to an uneven distribution of seismic forces and displacement demands. While adherence to building codes can help mitigate different irregularities, torsional irregularity is intrinsic to buildings and may persist despite meticulous design efforts. This thesis exclusively focuses on buildings

with torsional irregularities (Figure 1.6(a)), aiming to provide a comprehensive understanding of their impact on acceleration-sensitive secondary systems as well as potential solutions to account for their effects in the seismic design of secondary systems.

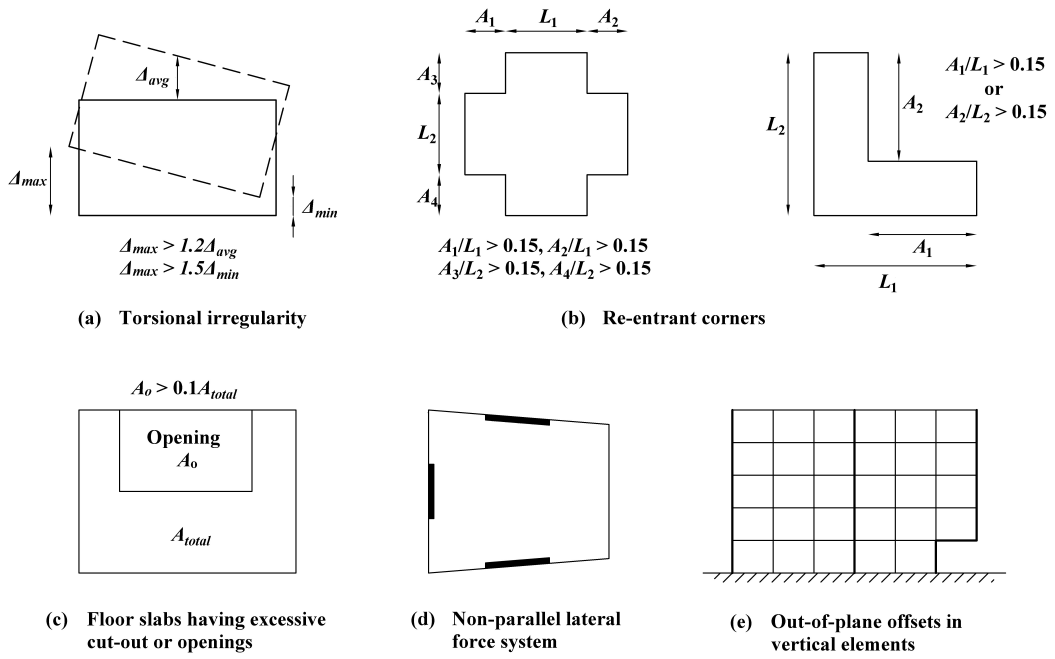

Figure 1.6: Various forms of plan irregularities in buildings [5].

1.4.1 Nominal torsion in buildings

Torsion refers to the twisting or rotational deformation that occurs in a building when it is exposed to seismic motions. Torsional effects are particularly significant in building design, especially in irregular buildings or those with complex configurations. Torsionally irregular buildings are among the most common building typologies encountered in the urban housing stock [28–30]. Several reasons contribute to nominal torsion in buildings, e.g., irregular plan shape, asymmetric stiffness and or strength distribution of the lateral load-resisting elements, uneven mass distribution in the floor plan, and any combination of the features as mentioned above. Many times, torsion can be observed even in perfectly symmetric buildings, either due to accidental reasons (i.e., variations between assumed and actual distribution of mass and/or stiffness) or significant rotational ground motion (R_Z) itself. Consequently, torsionally irregular buildings possess a non-coincident CR and CM, resulting in lateral translational-torsional coupling in the structural response. The offset between the CR and CM is referred to as static floor eccentricity (e_{CR}).

To date, it is still unknown how the building torsion affects the PFA and FRS and how it can be incorporated into seismic codes. With the increased use of services, architectural elements, and utilities in buildings sensitive to floor accelerations, it becomes essential to investigate the effect of nominal torsion on the PFA and FRS demands.

Seismic design codes [5, 6, 16, 27] define the criterion for classifying a building to be torsionally irregular. For example, EC 8 [16] defines a building to be torsionally irregular if the ratio between the static floor eccentricity (e_{CR}) to the torsional radius (r) exceeds a value of 0.30. ASCE 7 [6] and IS 1893 [5] describe the floor displacement-based indices to define the torsional irregularity in the buildings. According to ASCE 7 [6], when the ratio between the maximum to average edge displacements ($\Delta_{max}/\Delta_{avg}$) at a given floor exceeds 1.20, the building is said to be torsionally irregular (Figure 1.6(a)). Furthermore, ASCE 7-16 [27], an earlier version of ASCE 7, also defines extreme torsional irregularity in buildings. According to this definition, when the ($\Delta_{max}/\Delta_{avg}$) at a given floor exceeds 1.40, a building is classified as having extreme torsional irregularity. IS 1893 [5] defines a building to be torsionally irregular when the ratio between the maximum to minimum edge displacements ($\Delta_{max}/\Delta_{min}$) at a given floor exceeds 1.50. Later, this provision was amended in IS 1893 (Amendment 2) [31], and the torsional irregularity is said to exist in a building if the ratio $\Delta_{max}/\Delta_{avg}$ exceeds 1.20 at any floor level. In addition, EC 8 [16] defines torsional irregularity in buildings based on the relationship between the natural periods corresponding to the translational and rotational modes of vibration. Specifically, a building is classified to be torsionally irregular if the natural period corresponding to the fundamental rotational mode exceeds that of the first two translational modes along each principal plan direction. This criterion also serves as a key indicator for identifying buildings where torsional effects play a significant role in structural response, underscoring the need to address torsional irregularity in seismic design.

1.4.2 Floor accelerations in buildings

Current seismic design codes [6, 16, 17] provide various equations for estimating the floor accelerations and seismic forces required for the seismic design of secondary

systems. These include the estimation of the in-structure amplification factor (PFA/PGA), component amplification factor (a_p), and normalized floor response spectra with respect to PGA (a_t). The PFA/PGA ratio, as specified in several modern design codes, quantifies the amplification of ground motion along the building height. The PFA/PGA ratios from various contemporary codes are illustrated in Figure 1.7(a). Presently, ASCE 7-16, EC 8, and IS 16700 adopt a linearly increasing distribution of PFA/PGA with relative height (Z/H; here, Z and H define the height of the floor measured from the base, and the total height of the building, respectively), based on the assumption that the fundamental mode of vibration primarily governs the building's response. In the recent update to ASCE 7-16, ASCE 7 [6] incorporates the fundamental period of vibration and provides a more comprehensive consideration of the whiplash effect induced by higher modes in its formulation.

The parameter a_p describes the effect of the frequency tuning between the secondary system and the building. EC 8 defines this value as a function of the tuning ratio (T_s/T_1; here, T_s and T_1 represent the period of the secondary system and the fundamental period of the building, respectively), with a peak value of 2.2 (Figure 1.7(b)). In contrast, the other building codes, ASCE 7 and IS 16700 [17], consider it to be a constant value (based on the peak in FRS) equal to 2.8 and 2.5, respectively. The parameter a_t combines both of these amplification effects, i.e., PFA amplification along the building height and amplification due to frequency tuning between the secondary system and building, resulting in the corresponding maximum values equal to 4 (governed by an upper bound), 5.5, and 5 in ASCE 7, EC 8 and IS 16700, respectively (Figure 1.7(c)). These parameters can be used to determine expected accelerations and seismic force demands on secondary systems, provided the input PGA is known.

1.5 Research gaps

The seismic design of the secondary system is critical for ensuring building resilience during seismic events. Even in the modern seismic design codes, many factors are overlooked or inadequately addressed due to insufficient research or other limitations. One notable omission in current national building codes is the inclusion of the effects

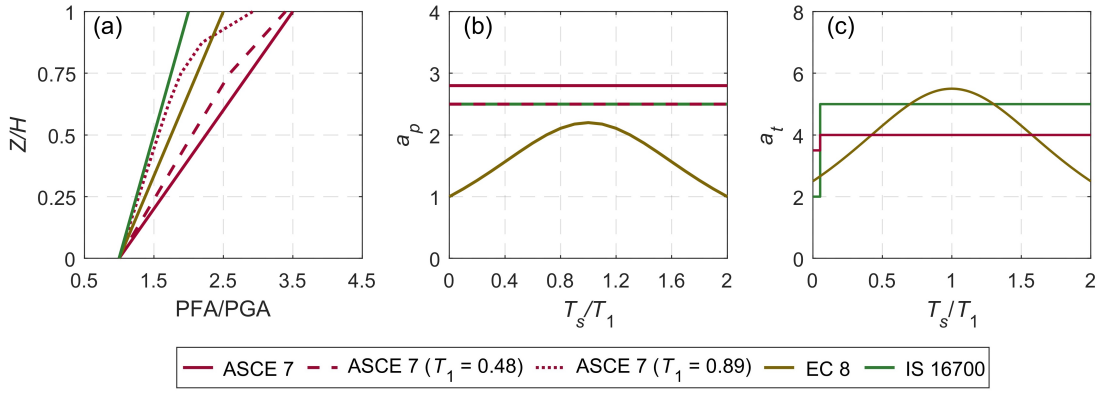

Figure 1.7: Variations of the PFA/PGA, a_p, and a_t in different building codes.

of nominal building torsion in estimating floor acceleration demands for the seismic design of secondary systems in buildings. This oversight underscores the need for further investigation and incorporation of relevant provisions into future building code revisions to enhance the seismic safety of secondary systems. The identified research gaps in the building codes are described below:

- The existing seismic design methods do not consider the effects of plan and elevation irregularities in the building in estimating seismic force demands on the secondary systems;

- The existing seismic design methods do not consider the effects of torsional characteristics of the building in estimating seismic force demands on the secondary systems;

- The simplified methods that can be used in design practice to estimate the effect of the damping ratio of secondary systems on torsional amplification are not yet available;

- The existing seismic design methods for computing seismic force demands on the secondary systems for their seismic design do not account for the floor diaphragm flexibility.

Addressing these research gaps presents a significant opportunity to advance the field by developing design recommendations to enhance the seismic design provisions for secondary systems in buildings.

1.6 Research objectives

Based on the identified research gaps in the previous section, the objectives of the research work conducted in this thesis are formulated, and they are as follows:

- To investigate and understand the in-plan distribution of PFA demands in buildings with nominal torsion under their elastic and inelastic response;
- To investigate and understand the FRS in buildings with nominal torsion under their elastic and inelastic response;
- To investigate and understand the influence of rotational ground motions on the floor acceleration response (in terms of both PFA and FRS) of buildings with and without nominal torsion;
- To develop design recommendations for estimating floor acceleration amplification in buildings with and without nominal torsion.

1.7 Scope of the research work and methodology

1.7.1 Scope of the research

The Seismic design of the secondary system is critical for ensuring building resilience during seismic events. However, the current building codes [5, 6, 16] do not address the effects of nominal building torsion in computing seismic force demands on secondary systems. The lack of this specific consideration in the seismic design of secondary systems can pose a potential threat to the safety of attached secondary systems in buildings with nominal torsion. Additionally, the existing literature to date needs to include comprehensive studies that specifically examine the effects of nominal building torsion on floor acceleration demands and, hence, seismic force demands on the light-weight acceleration-sensitive secondary systems. Addressing this research gap presents an important opportunity to advance the field by developing design recommendations to enhance the seismic design provisions of acceleration-sensitive secondary systems in such buildings. Thus, the scope of this research focuses on mid-rise ductile RCMRF buildings with nominal torsion, considering their elastic and inelastic responses.

The findings of this study led to the development of practice-oriented models, which are then validated using application example buildings (not used in developing the recommendations) to ensure their practical applicability. Furthermore, the research aims to develop simplified design guidelines that can be applied in conjunction with existing building code provisions to predict the floor accelerations, accounting for the effects of nominal torsion in buildings. This study focuses exclusively on RC bare-frame buildings, deliberately excluding the influence of infill walls to isolate the fundamental dynamic behavior of the structural system and to manage modeling complexity within the scope of the current work.

1.7.2 Research methodology

In the present work, a group of 24 RCMRF buildings located on plain ground is considered. The selected buildings exhibit varying degrees of torsional irregularity and feature different plan shapes, including T, U, rectangular, and square configurations. The considered buildings are 4-story and 8-story tall. All these buildings have been designed following provisions of the relevant Indian standards (IS 456 [32], IS 1893 [5], IS 13920 [33]) and have been studied in detail. Further, the multi-directional non-linear time history analyses (simultaneous application of two horizontal components of ground motions, with and without rotational ground motion) are conducted on these buildings using ground motions recorded in the far field. The secondary system is assumed to remain elastic, with its mass being very small relative to the building's mass (e.g., less than 0.1%; [34–36]). Consequently, dynamic interaction effects between the building and the secondary system are ignored. To evaluate the floor acceleration demands on the light-weight acceleration-sensitive secondary systems, the '*Floor Response Spectrum*' method has been used.

In these buildings, the flexural failure mode of beams and columns has been considered. Shear failure of both beams and columns is not anticipated in special moment-resisting frame (SMRF) buildings [37] designed and detailed using the capacity design principle, and therefore, it has been neglected. The buildings are assumed to be on a rock site, and hence, the effects of soil and foundation flexibility on the seismic response of buildings have been excluded from this study. PFA and

FRS are obtained at different floors of each investigated building and at various locations on the floor plan, including the CR (refer Section 3.4), the center of strength (CS; refer Section 3.4), the flexible edge (FE), and the stiff edge (SE), for a 5% damping ratio (ξ_S) in the secondary system. The extreme edge positioned farther from the CR, which experiences larger displacement, is defined as the FE, while the one closer to the CR, with smaller displacement, is categorized as the SE [38] (Figure 1.8). To examine the in-plan distribution of PFA demands, additional PFAs are computed at various locations across both flexible and stiff frames. The frames near the FE, or those situated between the CR and the FE, are classified as flexible frames, with the FE itself included in this category. In contrast, stiff frames refer to those near the SE or positioned between the CR and the SE, encompassing the SE as well.

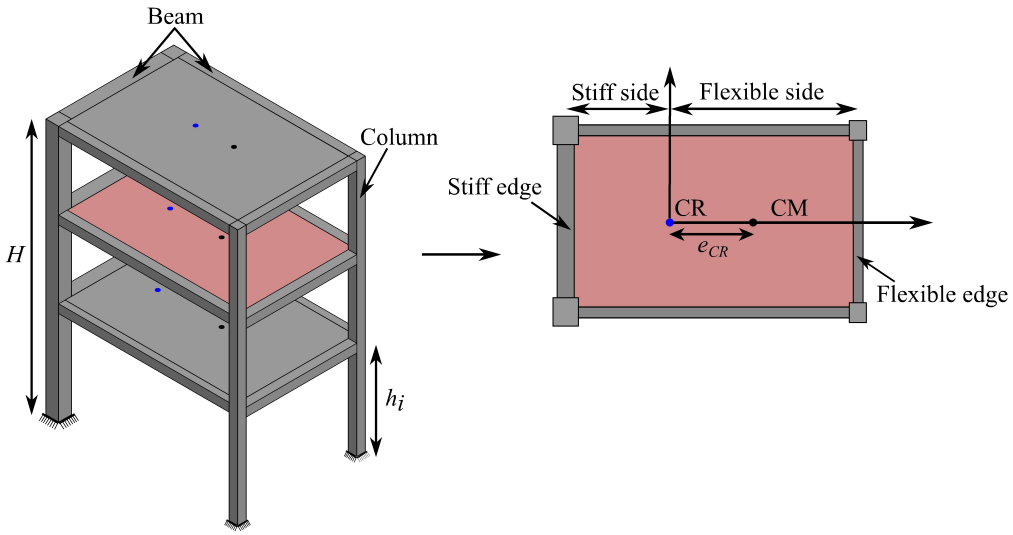

Figure 1.8: Schematic illustration of SE and FE in a multi-story building.

The floor torsional amplification factor (TAF), defined as the ratio between the floor spectral ordinate at the flexible or stiff frames to the floor spectral ordinate at the CR or CS, is estimated as a function of the tuning ratio (i.e., the ratio between the period of the secondary system, T_s, and the fundamental period of the building, T_1). Three different types of TAF are estimated: (i) TAF_R, representing the TAF for an infinitely rigid secondary system; (ii) TAF_F, which represents the peak torsional amplification factor within the influence zone of different vibrational modes of the building, and (iii) TAF_{VF}, representing the TAF for a very flexible secondary system. The correlations of the peak TAFs for the rigid and flexible

secondary systems with their floor displacement-based torsional irregularity indices (i.e., ($\Delta_{max}/\Delta_{avg}$) and ($\Delta_{max}/\Delta_{min}$)) are investigated.

Simplified recommendations are proposed to predict the TAFs as a function of tuning ratio, provided any one of the above-described floor displacement-based torsional irregularity indices for the building of interest is known. The proposed recommendations are applied and further validated on example buildings situated on plain ground and on hill slopes, all exhibiting torsional irregularities. These example structures are distinct from those used in the development of the proposed model. The brief methodology used in this thesis is outlined in Figure 1.9.

1.8 Organization of thesis

This thesis is organized into eight chapters, each addressing different aspects of secondary systems in buildings, their seismic performance, and their implications for seismic design provisions and building codes. It begins by establishing the background, reviewing existing literature, and outlining the need for the study. Subsequent chapters focus on the methodology, including the selection of building archetypes, modeling approaches, and ground motion selection. The study examines the PFA and FRS, the effects of torsional irregularity, building inelasticity, and the influence of rotational ground motions. The findings contribute to the development of improved seismic design recommendations, which are validated through multiple application examples. The thesis concludes with a summary of key contributions, limitations, and future research directions aimed at enhancing the seismic resilience of secondary systems in torsionally irregular buildings.

Chapter 1 provides the background information necessary for understanding the importance of secondary systems in buildings. It begins with a general overview of buildings, the role of secondary systems in maintaining building functionality, and their classification. The chapter also highlights the economic implications of secondary systems. A review of the performance of secondary systems during past earthquakes is presented. Furthermore, existing guidelines in building codes for torsional irregularity and floor acceleration demands, their limitations, and the need for the current research are discussed. The chapter concludes with the research objectives, the scope of the work, and an overview of the thesis structure.

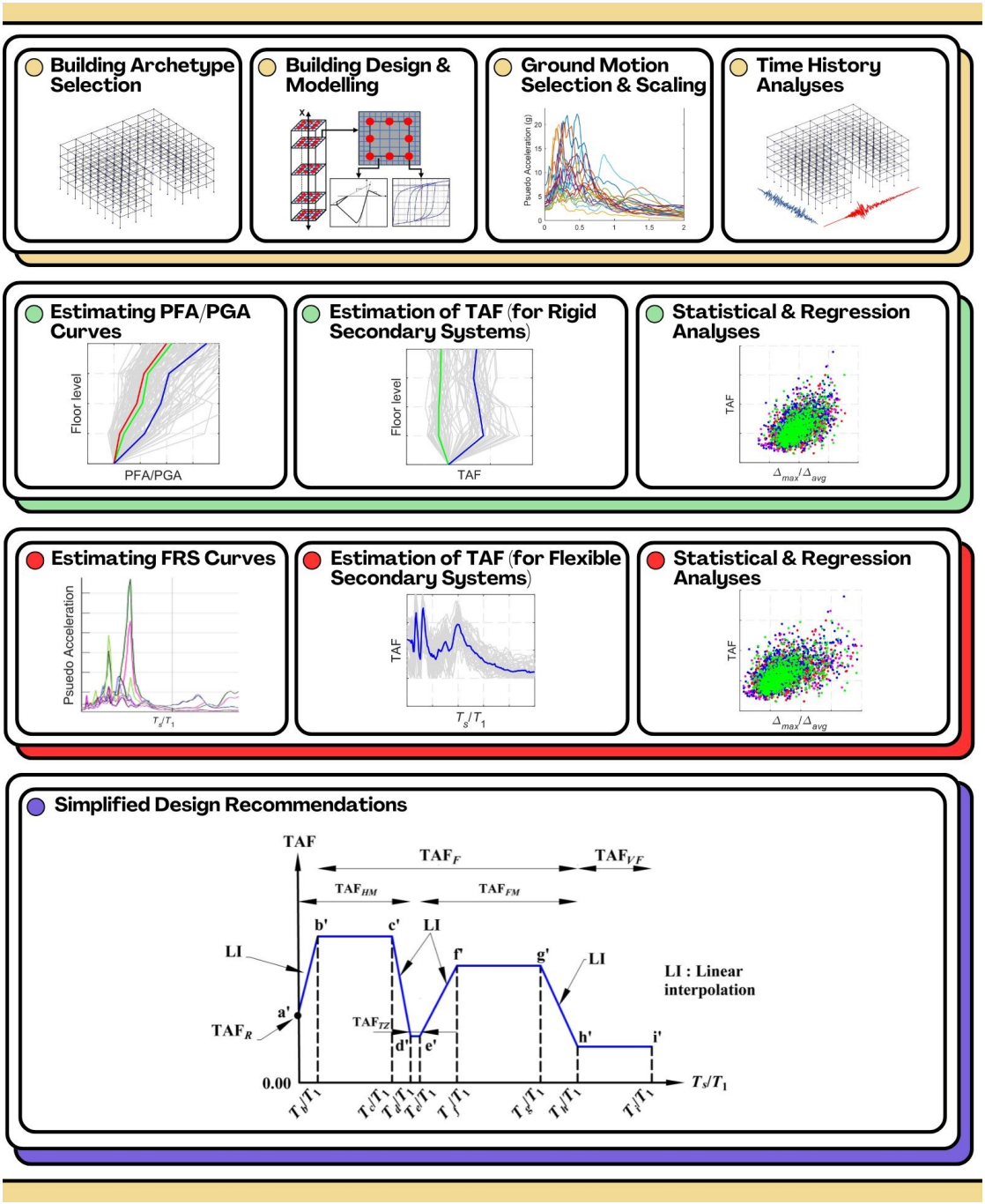

Figure 1.9: Outline of the methodology used in this thesis.

Chapter 2 presents a comprehensive state-of-the-art on the estimation of floor acceleration demands through shake table tests, instrumented building responses, analytical methods (coupled and de-coupled approaches), and numerical simulations. The chapter further examines various factors influencing the PFA and FRS demands, including relative height of the floor, lateral load-resisting systems, modal periods, building inelasticity, ground motion characteristics, and rotational ground motions. The chapter concludes with a summary of the literature, emphasizing the need for

a comprehensive analysis of the floor acceleration response in buildings with and without nominal torsion, including rotational ground motions.

Chapter 3 outlines the selection of building archetypes, focusing on plan irregularities. The chapter details both linear and non-linear modeling approaches, including the design details of structural elements, material properties, and reinforcement details. The chapter also describes the development of finite element models, detailing assumptions, material models for concrete and steel, and other key aspects of simulation. The dynamic and torsional characteristics of the building are examined using various building codes. The details of ground motions used in this study are presented along with the record selection criteria and their spectral characteristics. By integrating these elements, Chapter 3 provides the foundation for further analyses, enabling a detailed investigation of the floor acceleration response of the considered buildings.

Chapter 4 addresses the assessment of PFA demands and their impact on rigid secondary systems under earthquakes. It begins by analyzing the in-structural amplification factor, exploring how PFA demands vary across different building configurations, including factors such as building height, structural irregularities, and building inelasticity. This analysis highlights the significant amplification of PFA due to nominal torsion in buildings. Additionally, the chapter presents a comparative evaluation of the computed PFA values with code-based predictions. This comparison identifies instances where code provisions underestimate PFA demands, particularly in buildings with nominal torsion, highlighting the need for improved accuracy in design methods. The chapter also investigates the influence of rotational ground motions on PFA demands, exploring their contribution to raising PFA demands and their interplay with building height, structural irregularities, and building inelasticity.

Chapter 5 focuses on the evaluation of FRS and its implications for flexible and very flexible secondary systems in buildings under earthquakes. The chapter begins by analyzing the normalized floor acceleration response, including parameters such as a_p, a_t and spectral amplification factor, providing an in-depth examination of how these demands are influenced by building attributes such as building height,

structural irregularities, and building inelasticity. In addition, the chapter presents a comparative analysis of the computed a_p and a_t values from the investigated buildings against the values prescribed in the building codes. This analysis highlights cases where code-based models fall short and underestimate the acceleration demands in buildings with nominal torsion, thereby underscoring the need for more accurate provisions in current seismic design codes. Further, the chapter explores the influence of rotational ground motions on FRS, exploring its contribution to raising FRS demands and its interplay with building height, structural irregularities, and building inelasticity.

Chapter 6 focuses on estimating the TAF for rigid, flexible, and very flexible secondary systems at different floors in the investigated buildings. It also investigates the influence of rotational ground motions on the estimated TAFs. Additionally, the chapter explores the relationships between the estimated TAFs (TAF_R, TAF_F, and TAF_{VF}) and various torsional irregularity indices of the building codes. Overall, the chapter concludes with a method that accounts for the effects of nominal torsion and rotational ground motions on floor acceleration demands in buildings.

Chapter 7 presents application examples of the developed method in this study for different building types and suites of ground motions, distinct from those used for its development. Furthermore, it demonstrates how incorporating the proposed method improves seismic force prediction for light-weight acceleration-sensitive secondary systems using existing building code provisions.

Chapter 8 summarizes the key findings of the research, highlighting the main contributions of the research work to estimate floor acceleration demands in buildings with nominal torsion. The chapter critically examines the limitations of the current study, providing insights into areas where further investigation could enhance the understanding of floor acceleration demands in buildings with nominal torsion. Additionally, it discusses the potential for refining design recommendations in building codes to improve the seismic resilience of secondary systems and proposes directions for future research that could lead to more robust and effective seismic design practices.

Chapter 2

Literature Review

2.1 Background

The seismic safety of secondary systems plays a critical role in the overall functionality and safety of buildings; however, it has received less attention compared to building design procedures. Recent state-of-the-art reviews on secondary systems [18, 39, 40] emphasized the significance of the floor response of buildings in evaluating the seismic performance of secondary systems. Many recent earthquake events [7–10] have highlighted that even when the structural framework of a building performs well, secondary systems often experience significant damage, leading to operational disruptions and economic losses, as also discussed earlier in Chapter 1. This fact warrants the need for a more comprehensive understanding of the provisions related to the seismic safety of secondary systems in buildings.

The growing recognition of the importance of secondary systems has led researchers to investigate various aspects that affect their dynamic response, which is significantly affected by the characteristics of both the building and the secondary system itself. The building-specific characteristics that affect the seismic response of the secondary system include height (e.g., [41, 42]), modal periods (e.g., [43, 44]), strength (or ductility demand) (e.g., [45, 46]), lateral load-resisting system (e.g., [43]), floor diaphragm flexibility, and presence of elevation or plan irregularities (e.g., [45, 47]). On the other hand, the known characteristics specific to secondary systems that in turn affect their seismic response include the period of vibration (e.g., [46, 48]), damping ratio (e.g., [48, 49]), inelasticity of the secondary system, and the vertical location (e.g., [50, 51]) within the building. These insights obtained from earlier studies have driven the development of methodologies to estimate PFA and FRS, to better estimate seismic demands for rigid and flexible secondary systems in buildings, respectively.

2.2 Estimation of floor acceleration demands

The seismic design of secondary systems using floor response traces back to the 1970s [49, 52–60]. Since then, researchers have developed various methods to accurately estimate floor acceleration demands in buildings, which are critical for the effective seismic design of secondary systems. The methods to estimate the floor acceleration demands in buildings can be broadly categorized into four major categories: (i) Shake table tests, (ii) Instrumented building response, (iii) Analytical techniques, and (iv) Numerical simulations. Each of these methods contributes to unique insights into the floor acceleration response of buildings under seismic excitations.

Shake table tests [61–67] are employed to simulate seismic events and study the real-time behavior of the building and its attachments/secondary systems. Shake tables replicate ground motions, allowing researchers to understand the behavior of both primary systems and secondary systems under seismic loading. The shake table test provides direct empirical data on floor acceleration responses, making them invaluable for validating theoretical models and enhancing seismic design strategies. However, the applicability of shake table tests is limited by constraints on building height and weight. In contrast, instrumented building response [68–70] mainly rely on recorded data from actual buildings equipped with accelerometers and sensors, capturing floor accelerations during real earthquakes and providing empirical evidence of how secondary systems respond under earthquake excitations.

Analytical methods [52–60, 71–74] rely on simplified assumptions and apply the fundamental principles of structural dynamics (e.g., modal combination of floor response of buildings in each of the vibration modes) to theoretically estimate floor acceleration demands. Numerical simulations [49, 75–83], utilize advanced computational techniques to model and simulate building behavior under earthquakes and allow for detailed predictions of floor accelerations accounting for the characteristics of the building, secondary system, and ground motions.

2.2.1 Approaches for estimating floor acceleration demands

The estimation of floor acceleration demands is essential for assessing the performance of secondary systems within buildings. The approaches to estimating

the floor acceleration demands can be broadly categorized into two major categories: (i) the coupled approach [54–57, 59, 60, 78, 79], and (ii) the de-coupled approach [52, 53, 71–77, 82].

2.2.1.1 Coupled approach

The coupled approach involves modeling both the primary and the secondary systems together in a fully integrated system. In this method, the dynamic interaction between the primary system and the secondary system is explicitly considered. The coupled approach captures the complex feedback mechanisms between the building's movements and the accelerations experienced by secondary components. While this method offers higher precision in estimating floor acceleration demands, it can be computationally intensive, especially for large-scale structures.

Sackman et al. [54] employed an analytical approach utilizing perturbation techniques to estimate the dynamic characteristics of a combined primary and secondary system, consisting of a multi-degree-of-freedom (MDOF) primary system and a light-weight single-degree-of-freedom (SDOF) secondary system. They derived closed-form expressions for key modal properties, factoring in dynamic behavior, tuning effects, and dynamic interactions, enabling mode-superposition to evaluate the secondary system's response to excitations. Kiureghian et al. [55] introduced an analytical mode-superposition approach to evaluate FRS in systems where a light-weight secondary system is attached to a primary system subjected to stochastic excitations. This method builds upon the modal properties of the combined equipment-structure system, as formulated by Sackman et al. [54], and considers both power spectral density and response spectrum inputs to accurately capture the system's dynamic response.

Igusa and Kiureghian [56, 57] conducted a comprehensive analytical investigation into the dynamic interaction of secondary systems in buildings. Firstly, they [56] focused on a two-dimensional equipment-structure system, deriving closed-form expressions for its modal properties using perturbation theory. Their analysis, based on the characteristics of individual subsystems, identified dynamic interaction as a critical factor influencing the system's response and established

criteria to quantify its impact. In another study [57], they introduced an efficient method for evaluating MDOF secondary systems while accounting for dynamic interaction effects. This approach, combining modal synthesis, perturbation theory, and random vibration principles, enabled the synthesis of the composite primary-secondary system's modal properties. For seismic inputs defined by ground response spectra (GRS), the response of secondary systems can be directly estimated, greatly simplifying the analysis without the need for detailed time history simulations.

Suarez and Singh [59, 60] developed an analytical method using mode synthesis to determine the modal properties of a combined SDOF primary and secondary system. They derived eigenvalues through an inelastic characteristic equation and provided closed-form expressions for the eigenvectors. This approach enables the calculation of FRS while accounting for dynamic interaction between the primary and secondary systems.

Pan et al. [78] introduced an improved modal pushover analysis (MPA) method to refine the previous MPA procedure [84, 85] for more accurate FRS estimation in MDOF systems with prominent higher-mode effects, while also considering complex dynamic interactions. Their method involves formulating multiple equivalent SDOF systems while accounting for the impact of the fundamental mode on the yielding of higher modes (inelastic deformations that occur in higher modes) during the process of deriving these equivalent SDOF systems. The final FRS is derived by combining the results from inelastic dynamic analyses of each equivalent SDOF system using the Square Root of the Sum of Squares (SRSS) method. Further, Pan et al. [79] introduced a novel simplified procedure for estimating FRS that incorporates a direct multi-mode technique and considers coupling effects to establish equivalent modal systems. By integrating the capacity spectrum method with ductility-based FRS for each modal system, the methodology enhanced the overall estimation of FRS.

2.2.1.2 De-coupled approach

The de-coupled approach, commonly referred to as the '*Floor Response Spectrum*' method, simplifies seismic analysis by treating secondary systems as independent from the primary system, provided the secondary system's mass is negligible

compared to that of the primary system, typically less than 0.1% [34–36]. In this method, floor acceleration demands are estimated based solely on the response of the primary system. The approach involves first determining the seismic response of the primary system and then using the resulting floor accelerations to evaluate the dynamic response of the secondary systems.

Duff [52], employing an analytical approach, derived FRS directly from GRS using a simplified deterministic method. This work involved the development of both an analytical framework and a streamlined graphical technique for the direct generation of FRS from GRS. Peters et al. [53] proposed an analytical method for determining FRS through modal analysis of a primary system with an interaction-free SDOF system attached. Their findings demonstrate that the FRS can be evaluated based on the dynamic behavior of specific two-degree-of-freedom systems, particularly in resonance conditions where traditional superimposition rules may be questionable.

Lin and Mahin [49] conducted a numerical study to assess the impact of inelastic deformations in the supporting structure on the response of secondary systems. They introduced an amplification factor, defined as the ratio of the FRS for an inelastic structure to that for an elastic structure, to quantify these effects. Through a statistical evaluation of results generated from ten earthquake ground motions, they formulated design guidelines for predicting this amplification factor. Singh et al. [58] developed an analytical approach based on the mode acceleration method and principles of random vibration to directly generate FRS. This approach is particularly effective for rigid structural systems and for floors situated near the base, where high-frequency modes significantly influence the floor acceleration response.

Yasui et al. [71], utilizing an analytical approach, developed a direct method for generating FRS from design response spectra, focusing solely on the modal characteristics of the primary system. Vukobratović and Fajfar [75] conducted a numerical study that examined the impact of various parameters on FRS. They modeled both the primary and secondary systems as SDOF systems. Based on their findings, they proposed a simplified method for generating FRS for inelastic structures directly from the design response spectrum, extending Yasui et al.'s [71]

method originally developed for elastic structures. This new approach allows for the estimation of approximate floor acceleration spectra as a function of the input acceleration spectra and the dynamic characteristics of both the primary and the secondary systems. Subsequently, Vukobratović and Fajfar [76] further refined this method by adapting it to MDOF systems, expanding its applicability in seismic design. Later, they further simplified their approach [77] and included the option to account for the inelastic response of the secondary system by increasing its damping ratio, making the methodology even more versatile.

Sullivan et al. [80] performed a comprehensive numerical analysis on FRS for both elastic and inelastic SDOF systems, identifying critical factors that shape and intensify floor acceleration demands. They proposed predictive equations for FRS, introducing an apparent dynamic amplification factor (DAF) supported by an empirical formulation that incorporates the period and inelasticity of the primary system, as well as the elastic damping ratio of the secondary system. Further, Calvi and Sullivan [81] extended the methodology to elastic MDOF systems. They introduced a simplified modal combination approach for predicting FRS in upper stories while accounting for the limited filtering effect of input ground motion in lower stories. Jiang et al. [72] introduced a direct spectra-to-spectra method for generating FRS using GRS and modal properties of the primary system, such as natural frequencies, modal damping, and mode shapes. They also proposed a new modal combination rule, FRS-CQC, based on random vibration theory to account for correlations between structural modal responses and equipment-structure interactions.

In the present thesis, the '*Floor Response Spectrum*' method is employed, as the secondary systems are assumed to have a negligible mass, i.e., less than 0.1% of the building's total mass [34–36]. This assumption allows for the decoupling of secondary systems from the dynamic behavior of the primary system, simplifying the analysis by focusing on the seismic demand imposed on these systems without significantly affecting the overall structural response.

2.3 Factors influencing peak floor acceleration

PFA is a key parameter in the seismic design of secondary systems, representing the maximum acceleration experienced by building floors during seismic events. Its accurate estimation is crucial for evaluating the seismic vulnerability of rigid secondary systems, which are particularly susceptible to elevated floor-level accelerations. In the current building codes [6, 16, 17], the expressions to estimate PFA as a function of PGA are defined. This ratio (PFA/PGA), referred to as the in-structure amplification factor, quantifies the amplification of ground motion from the building's base to the upper floors, thereby providing a measure of the dynamic amplification effects experienced within the building. The PFA/PGA values recommended by various contemporary design standards, including ASCE 7 [6], EC 8 [16], and IS 16700 [17], are shown in Figure 1.7(a).

The comparison of PFA/PGA ratios across different codes underscores the variability in the estimated amplification, pointing to the necessity for a more holistic approach that considers multiple factors influencing seismic response just beyond the fundamental mode. These factors include the building's fundamental period (T_1), the relative height of the floor, the degree of inelastic behavior, the presence of infill walls, and the characteristics of the ground motion. Detailed discussions on these factors and their influence on PFA are provided in the subsequent sections.

2.3.1 Fundamental period of the building

The fundamental period of a building is a key parameter in determining its seismic response, as it reflects the flexibility of a structure. ASCE 7 [6] typically utilizes this period for estimating the distribution of PFA along the building's height. However, studies [68, 70, 86–88] suggest that relying solely on the fundamental period may lead to inaccurate estimations.

Miranda and Taghavi [73, 89] observed during their study that a building's fundamental period significantly impacts the PFA demands. They [73] developed a simplified method to estimate PFA distributions along a building's height based on the dynamic characteristics of the first three modes of vibration. Their approach utilized an equivalent continuum model comprising a flexural beam and a

shear beam interconnected by axially rigid links, capturing the building's dynamic behavior. However, the method's applicability was limited to linear elastic buildings, restricting its accuracy in accounting for inelastic effects and inelastic seismic responses commonly encountered in real structures. Medina et al. [41] investigated stiff and flexible building frames and observed that PFA/PGA primarily depends on the fundamental period of the building.

Fathali and Lizundia [68] conducted an analysis of PFAs recorded at 16 instrumented stations of the California Strong Motion Instrumentation Program (CSMIP), focusing on tall buildings of up to 54 stories. Their findings revealed that the amplification of PFA exhibits an inverse relationship with the building's fundamental period. They observed that the ASCE 7-05 [90] equations to estimate the PFA/PGA are a good fit for short-period buildings ($T_1 < 0.50\ s$), whereas they are significantly conservative for medium-period ($0.50\ s \leq T_1 < 1.50\ s$) and long-period buildings ($T_1 \geq 1.50\ s$). Furthermore, they suggested improvements to the ASCE 7-05 equations to estimate the PFA/PGA by incorporating the fundamental period of the building.

Wieser et al. [86] and Surana et al. [50] observed that with an increase in the fundamental period of the building, the PFA/PGA at the roof level decreases. Additionally, the PFA/PGA at the roof level may even be lower than unity for buildings with $T_1 > 2.50\ s$. Wieser et al. [86] reported that for elastically responding buildings with $1.00\ s < T_1 < 4.00\ s$, ASCE 7-10 [91] could overestimate PFA/PGA by a factor of up to 4.00. They further proposed improved equations incorporating the effect of the building's fundamental period to evaluate the PFA/PGA.

2.3.2 Relative height of the floor

The relative height of the floor has been a focal point in understanding the seismic demands on secondary systems because it directly influences the performance and safety of these systems during an earthquake. As buildings sway and deform under seismic forces, the distribution of accelerations can significantly differ between floors, leading to varied responses in secondary systems. Several studies have offered insights into how these demands deviate from standard code provisions and vary across different structural systems and heights.

Jayamon et al. [92] carried out a comprehensive study on the seismic performance of secondary systems connected to wood shear wall structures. Their findings revealed that contrary to the acceleration distribution predicted by ASCE 7-10 [91] design guidelines, the highest floor accelerations often occurred at the first-floor level in the wood-frame models analyzed. This result highlighted a deviation from the expected pattern of acceleration demands along the building height. Chaudhuri and Hutchinson [82] conducted numerical analyses on eight 2D steel MRF buildings, typical of West Coast U.S. structures, to examine PFA variations across building heights. Through inelastic time history analyses with thirty-two ground motions, they observed an S-shaped PFA distribution. At the lower floors, the response was dominated by shear behavior due to fundamental-mode effects, whereas higher modes significantly influenced the upper floors, leading to flexurally dominated behavior. The middle floors displayed a blend of shear and flexural responses. Their findings emphasized the crucial role of higher modes in shaping PFA distributions across building heights.

Reinoso and Miranda [74] found that in high-rise buildings, PFA demands tend to remain nearly uniform and close to the PGA for up to 90% of the building's height. However, at the uppermost levels, the influence of higher modes can cause significant amplifications, resulting in average PFA/PGA values reaching approximately 2.0 at the roof level. To address these amplified demands, they proposed a simplified method for estimating lateral acceleration distributions in high-rise buildings during seismic events. This method employed a continuous model that combined the characteristics of both flexural and shear cantilever beams, providing an effective approach to capture the building's dynamic response.

Singh et al. [93] and Lucchini et al. [94] observed the "*whiplashing effect*" of higher modes, a phenomenon that significantly amplifies floor accelerations near the upper levels of multi-story buildings. This effect is attributed to higher mode contributions, which are not accounted for by a distribution based solely on the fundamental mode. Singh et al. [93] proposed a straightforward method to account for this effect by incorporating the fundamental period into the equation used to evaluate the PFA/PGA ratio. Subsequently, both the NIST [95] and ASCE 7 [6] guidelines incorporated the fundamental period of the building into the PFA/PGA

calculation to better account for this effect. To highlight this consideration, two additional curves for ASCE 7 are shown in Figure 1.7, corresponding to fundamental periods of 0.48 s and 0.89 s, respectively. These curves illustrate how accounting for the whiplashing effect modifies the PFA/PGA estimates, especially at higher floors.

Petrone et al. [87] conducted a comprehensive analysis of five RCMRFs, each with a floor-to-floor height of 3 meters and ranging from 1 to 10 stories. Their findings indicate that existing code provisions [16, 91] for estimating PFA/PGA ratios generally produce conservative estimates, thereby providing an adequate margin of safety in seismic design. The study further suggested that a linear distribution, increasing from a ratio of 1 at the base to 2 at the top, would more accurately align with their analytical results. Surana et al. [50] conducted a detailed numerical investigation into PFA demands in RC frame buildings, emphasizing the effect of building height on floor acceleration. Their findings highlighted that PFA demand is predominantly influenced by the relative height, with a noticeable trend of decreasing PFA at the roof level as the building's period of vibration increases. To improve the accuracy of PFA estimations, they proposed a new model that incorporates relative height as a significant factor, offering a refined approach to predict floor acceleration demands across various structural heights and dynamic characteristics.

Uma et al. [83] conducted a detailed numerical study to investigate the seismic response of 3- and 10-stories RCMRF and steel eccentrically braced frames. Through inelastic dynamic analyses, they observed that the amplification of PFA/PGA ratios along the building height was notably lower than the levels specified in New Zealand's seismic code [96], which recommends an amplification factor of 3 at the roof level. Anajafi and Medina [70] evaluated the accuracy of ASCE 7-16 provisions for estimating equivalent static force demands using floor motion data from 59 instrumented buildings. Their analysis revealed that the PFA/PGA ratio is influenced by the placement of the secondary system within the building's height, indicating that the acceleration demands vary significantly along the vertical axis of the structure. Shang et al. [88] observed that the assumption of the linear distribution of the PFA/PGA along the building height in the seismic design codes, i.e., ASCE 7-16 and EC 8, might result in significant underestimation or

overestimation. The findings from these studies collectively emphasize the critical importance of accounting for location-specific effects when assessing seismic demands on secondary systems.

2.3.3 Building inelasticity

Buildings are designed to respond inelastically during strong earthquakes, and hence, the inelastic energy dissipation in the building significantly influences the PFA demands. The inelastic behavior of buildings alters their dynamic characteristics and, hence, the distribution and magnitude of PFA. Several studies have explored how inelastic building response can alter PFA demands during seismic events, thereby underscoring the importance of incorporating building inelasticity into design practices.

Rodriguez et al. [97] conducted a detailed investigation into the PFA demands in buildings with structural walls, identifying a clear inverse relationship between building inelasticity and PFA demands. Their findings indicated that as the level of inelasticity within the building increases, the amplification in PFA demands tends to decrease, highlighting the impact of inelastic behavior on floor acceleration demands. Chaudhuri and Hutchinson [98] further corroborated the relationship between inelasticity and reduced floor accelerations through their analysis of steel MRF buildings. They observed that as the inelasticity of a building increases, the influence of higher modes becomes more prominent, generally leading to a reduction in PFA/PGA ratios. However, they noted some exceptions where this trend did not hold, suggesting that the interaction between higher modes and inelastic behavior can vary depending on specific structural characteristics.

Taghavi and Miranda [89] found that while linear structures can amplify ground motion, inelastic structures might exhibit lower floor accelerations than ground accelerations, particularly in taller buildings with longer periods. Wang et al. [69] analyzed the seismic response of two multi-story RC instrumented buildings subjected to strong earthquakes. They noted that the ASCE 7-05 provisions often overestimated PFA demands, especially when the buildings experienced pronounced inelastic behavior. Petrone et al. [87] contributed further insights through the analysis of five RC buildings designed according to EC 8 [16]. Their findings

indicated that ASCE 7-10 [91] and EC 8 underestimated PFA/PGA ratios in elastic buildings, particularly at the upper stories, reflecting a lack of sensitivity to the amplification effects associated with higher modes. Conversely, ASCE 7-10 was found to overestimate these values for inelastic buildings.

Lucchini et al. [94] underscored the limitations of current code-compliant models, noting that failure to consider inelasticity led to the overestimation of PFA. Similarly, Weiser et al. [86] examined inelasticity effects in steel MRF buildings and observed that PFA amplification diminishes as both the vibration period lengthens and inelasticity increases. They proposed simplified expressions to compute PFA amplification along the building's height, using the effective period (T_{eff}) to capture the influence of inelasticity.

Surana et al. [50] found that the amplification of PFA demands along a building's height is influenced by the degree of inelasticity. The importance of accounting for inelasticity was also emphasized by the NIST [95], which recommended the use of the response modification factor (R) to better capture the impact of building ductility in reducing floor acceleration demands. Anajafi and Medina [70] assessed the accuracy of the ASCE 7-16 equations for estimating equivalent static force demands, utilizing floor motion records from 59 instrumented buildings. Their findings revealed that for earthquakes with PGA values less than 50% of the design PGA (close to elastic response), the ASCE 7-16 provisions overestimate the PFA/PGA ratio by as much as a factor of 1.8.

2.3.4 Presence of infill walls

The presence of infill walls significantly influences PFA demands during seismic events by interacting with the structural components, contributing to the overall stiffness and strength of the frame, and altering the dynamic response of the structure. Mollaioli et al. [99] investigated PFA demands in RC frames of varying heights—specifically 4, 6, and 8 stories—both with and without infill walls. Their analysis revealed that the impact of infill walls on PFA demands diminished with the increase in the number of stories, highlighting the relationship between structural height and the effectiveness of infill in moderating acceleration responses. Lucchini et al. [94] revealed that the presence of infill walls can significantly alter the PFA

distribution profile throughout the height of the building.

Blasi et al. [100] investigated the influence of infill walls on the dynamic response of buildings, with a particular emphasis on how variations in the elastic modulus of infill panels affect PFA throughout the height of the building. Their research revealed that modifications in the stiffness of infill walls could considerably impact the PFA distribution, thereby affecting the acceleration demands imposed on secondary systems at different levels. Furthermore, they noted that infill walls generally mitigate irregularities in elevation, resulting in a more uniform PFA distribution across the building's height.

Surana et al. [44] investigated the dynamic response of RC frames, comparing uniformly infilled (UI) frames with unreinforced masonry walls and open ground stories (OGS). They found that the PFA/PGA ratio was significantly higher in UI frames than in OGS buildings. This difference is attributed to the longer vibration period of the OGS buildings. Additionally, the study revealed that the PFA/PGA ratio increases almost linearly in UI frames, with a noticeable increase at the roof level while remaining nearly constant in OGS buildings.

2.3.5 Ground motion characteristics

Few studies have investigated the effects of various ground motion characteristics on PFA estimation and the resulting demands on buildings during seismic events. Bozorgnia et al. [101] conducted an in-depth investigation into the influence of near-fault ground motions, which are typified by large velocity pulses and high-energy content. Their research demonstrated that such ground motions can induce substantial floor accelerations, especially in low- to mid-rise buildings. The study underscored the necessity of incorporating both PGA and velocity-based intensity measures, such as peak ground velocity (PGV), to more accurately estimate floor accelerations under near-fault conditions.

Fardis [102] further highlighted the limitations of using a single intensity measure like PGA for PFA estimation. His research underscored the importance of considering additional parameters such as ground motion duration, spectral acceleration, and peak ground velocity (PGV), especially when dealing with irregular buildings where PFA patterns may be less predictable. Poudel et al. [103]

investigated the influence of the rotational ground motions on the PFA demands. The study analyzed three special SMRF buildings subjected to far field ground motions. Their findings revealed that the rotational ground motion resulted in a substantial increase in PFA/PGA values, with an approximate rise of 7% at the CM and up to 33% at the corners of the roof levels.

2.4 Factors influencing floor response spectra

The FRS represents the peak dynamic response of SDOF oscillators, with varying natural frequencies and for a given damping ratio, situated at specific floors of a building. These oscillators are subjected to the building's floor acceleration resulting from seismic excitation. It accounts for the amplification and modification of seismic energy as it propagates through the building, influenced by the building's natural frequencies, damping ratio, and mode shapes. FRS plays a vital role in designing and ensuring the seismic safety of flexible and very flexible secondary systems, where floor-level accelerations can exhibit significant variability.

The interaction between the building's dynamic properties and ground motion selectively amplifies or attenuates vibrational frequencies due to the filtering effects of the primary system. The structure typically attenuates frequencies that deviate from its natural frequencies while amplifying those that are in resonance, thereby modifying the incoming ground motion [80, 104]. Figure 2.1 illustrates the transformation of base-level ground motion into FRS. As a result, extensive research has been undertaken to analyze the critical factors influencing the response of secondary systems by estimating FRS based on the fundamental principles of structural dynamics. The primary factors affecting FRS encompass the building's modal period, the relative height of the floor, the inelastic behavior of the building, the presence of infill walls, torsional irregularities, ground motion characteristics, inelasticity of the secondary systems, and the damping ratio of secondary systems. The subsequent sections provide a detailed discussion of studies addressing these factors.

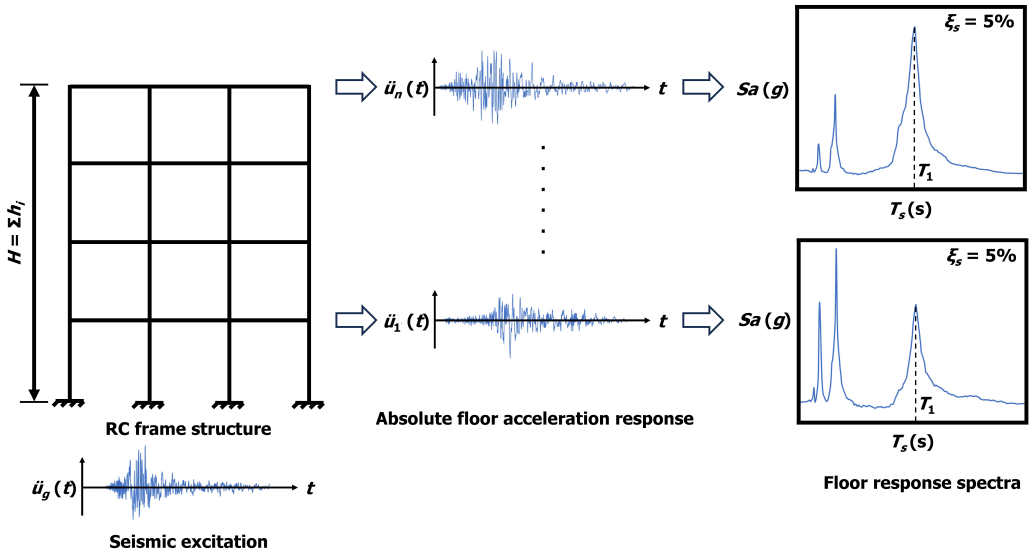

Figure 2.1: Typical layout showing the concept and definition of FRS

2.4.1 Modal period of the building

The modal periods of a building significantly influence the characteristics of the FRS, as they govern the dynamic interaction between the building and the ground motion. The fundamental period, along with higher modal periods, dictates the amplification and distribution of seismic energy across different floors, affecting both the magnitude and shape of the FRS.

Many studies have noted sharp peaks in the floor acceleration spectrum when the period of vibration of secondary systems aligns with that of the building [41, 42, 75–77, 86, 94, 105, 106]. This effect is also evident for higher modes in buildings where these modes significantly contribute to the seismic response. Sankaranarayanan and Medina [107] found that the reduction in peak acceleration demands in the short-period range ($T_s/T_1 \leq 0.50$) is influenced by the fundamental period of the primary building, where T_s represents the vibration period of the secondary system.

Chaudhuri and Villaverde [108] noted that the amplification effect of building inelasticity on the peak acceleration response of a linear secondary system is most pronounced when the building is subjected to narrow-band excitation with a dominant period close to the fundamental period. Mollaioli et al. [99] observed that the maximum amplification of seismic demands in secondary systems occurs when these systems are in tune with the primary system's first (T_1) or second (T_2)

modal periods.

Petrone et al. [87] conducted a comparison of floor response predictions for both elastic and inelastic buildings through time history analyses against the provisions outlined in EC 8. Their findings indicated that EC 8 tends to exaggerate acceleration demands for secondary systems with periods near the fundamental period of the building, while it substantially underestimates demands related to higher modes of vibration. Petrone et al. [106] addressed the peaks in FRS associated with higher modes by refining the EC 8 spectral shape. They introduced a piecewise formulation that incorporates a flat plateau to account for peaks corresponding to both fundamental and higher modes. They advocated using a normalized period ratio (T_s/T_1; also known as tuning ratio) to express the amplification factor.

2.4.2 Relative height of the floor

The relative height of the floor is important in understanding the distribution of seismic demands across different floors. As seismic waves propagate through a building, the interaction between the ground motion and the building's dynamic properties, including stiffness, damping ratio, and modal participation, leads to variations in floor-level accelerations.

Sankaranarayanan and Medina [42] studied peak acceleration demands for secondary systems on various inelastic MRF structures exposed to 40 far field ground motions. Their findings indicate that floor acceleration demands are highly sensitive to the floor's location within the building, with upper levels typically experiencing greater acceleration amplification. This trend underscores the significance of height-dependent variation in floor acceleration demands, an important factor for seismic design considerations. Similarly, Mollaioli et al. [99] conducted a detailed assessment of floor acceleration demands on RC frames, focusing on the relative height of the floor. They observed that the amplification of acceleration demands is more pronounced at higher floors. Comparable trends are observed in the studies by Vukobratović and Fajfar [76], Berto et al. [51], Uma et al. [83], Wieser et al. [86], Petrone et al. [87, 106], Landge and Ingle [109], and Shang et al. [88], each reinforcing the pattern of acceleration amplification at elevated floors, which is critical for seismic response predictions of secondary systems.

2.4.3 Building inelasticity

Building inelasticity plays a significant role in shaping the FRS by altering the dynamic response of a building during seismic events. When a building transitions into the inelastic range, energy dissipation mechanisms such as hysteretic damping and plastic deformation come into play, reducing the amplification of floor accelerations compared to an elastic response [70]. Various research efforts [41, 49, 86, 94, 97, 98, 108, 110, 111] have demonstrated that inelastic behavior in buildings can lead to a reduction in floor acceleration responses, particularly for secondary systems with periods aligned with the building's fundamental period.

Lin and Mahin [49] introduced an amplification factor model to assess the impact of inelastic responses in supporting structures. However, Oropeza et al. [105] identified that this model [49] might overestimate inelastic effects for buildings with higher fundamental periods. They addressed this by proposing an improved amplification factor derived from inelastic time history analyses. Sankaranarayanan [112] and Medina et al. [41, 113] introduced an acceleration response modification factor to quantify the impact of a supporting structure's inelastic behavior. This factor serves as the reciprocal of the amplification factor originally defined by Lin and Mahin [49] and is utilized in generating the FRS while accounting for the effects of building inelasticity. Villaverde [114] proposed an approximate method for determining the inelastic seismic response of secondary systems attached to inelastic supporting structures, taking into account the geometric characteristics, masses, and target ductility of the structure.

Sankaranarayanan [112] noted that the building inelasticity led to a reduction in FRS values when the period of the secondary system closely aligned with the building's modal periods [78], with a more significant reduction near the fundamental period than at higher modal periods. Sankaranarayanan and Medina [107] demonstrated that inelasticity in the structure significantly amplifies acceleration demands, particularly for secondary systems located on lower floors with vibration periods less than half of the building's fundamental period. Chaudhuri and Hutchinson [98] observed that increased inelasticity in buildings results in greater participation of higher modes of vibration.

Vukobratović and Fajfar [75, 76] investigated the influence of inelasticity on the FRS for SDOF and MDOF systems. Their findings revealed that inelastic primary systems produce lower peak FRS values associated with the first mode compared to their elastic counterparts. Lucchini et al. [94] and Angelis et al. [115] found that building inelasticity has a notably greater influence on the FRS in buildings with infill walls, as the walls interact with the structural frame and induce complex dynamic responses. Zhai et al. [111] developed a predictive model to estimate the mean amplification factor for near-fault pulse-like ground motions, effectively accounting for the inelastic effects of the primary system. This model considers the periods of both the primary and secondary systems, as well as the ductility of the primary system. Petrone et al. [87] compared the floor response of elastic and inelastic buildings obtained from time history analyses. They emphasized the need to incorporate ductility demand in FRS evaluations.

2.4.4 Presence of infill walls

The presence of infill walls significantly alters the global response of buildings under seismic loading, affecting both the distribution and peak values of spectral accelerations across all stories. Infill walls contribute to both the stiffness and the strength of the frame, which can modify the seismic demand on the building, and consequently, the FRS [44, 100, 116–118].

Asgarian and McClure [116] examined the impact of infill walls on FRS. Their findings indicate that buildings with infill walls experience increased acceleration demands on secondary systems located on the upper floors. This increase is attributed to the added stiffness from the infill walls, which amplifies the floor accelerations at higher levels. Blasi et al. [100] also observed that infill walls contribute to the amplification of FRS. Surana [118] analyzed a set of mid-rise bare and uniformly infilled RC frame buildings under various earthquake intensities to evaluate their FRS. The findings confirmed that the presence of infill walls significantly impacts FRS and should be accounted for in seismic design.

2.4.5 Presence of torsional irregularity in buildings

The presence of torsional irregularity in buildings introduces significant complexities in the seismic response, directly affecting the FRS. Torsional irregularity arises from an uneven distribution of stiffness, mass, or strength, causing the building to twist about its vertical axis during seismic excitation. As a result, floor-level accelerations can be amplified/de-amplified, leading to a non-uniform distribution of seismic demands across the floor plan.

Yang and Huang [119] showed that the torsional amplification of acceleration demands on the secondary system depends on the modal participation factors for the rotational modes of vibration of the building. Agrawal and Datta [120] observed that with an increase in the floor eccentricity in the building, the acceleration response of the secondary system gets amplified when they are tuned to structural modes of vibration. Qu et al. [121] found that torsional effects can increase the acceleration demands on secondary systems situated at the periphery of the floor plan. Aldeka et al. [47] studied the response of a secondary system attached to elastically responding plan irregular RC buildings. They observed torsional amplification effects to be more pronounced at the FE in high-rise buildings than the low-rise buildings.

Aldeka et al. [122] reported that with an increase in the magnitude of the floor eccentricity in the building, the acceleration response of the secondary system attached at the FE increases significantly. In contrast, the acceleration response of the secondary system was not much affected while attached to the CR. Surana et al. [117] studied the floor acceleration response in multi-story step-back and split-foundation buildings. They reported that the code provisions of EC 8 and FEMA P750 underestimate the floor acceleration demands in this special class of irregular buildings, as the existing models in both EC 8 and FEMA P750 do not include the effects of nominal building torsion in the estimation of the floor acceleration demands.

Torsional response and diaphragm flexibility of the primary system have a significant influence on the shape and peak values of the FRS according to Anajafi and Medina [123]. They observed that the torsional response can amplify the acceleration demands on the secondary systems located around the edge of the floor

plan. This study showed that typical buildings exhibited torsional behavior and diaphragm flexibility that may increase the force demands on the secondary system by a factor of up to 2.0. Ruggieri and Vukobratović [124] investigated acceleration demands in low-rise RC buildings with torsional irregularities, evaluating FRS to develop empirical formulas for torsional amplification effects. They considered eight archetype buildings with varying floor eccentricities designed by offsetting the CR from the CM. Their findings showed that, in elastic models, acceleration demands depend on the position of secondary systems and the static eccentricity, whereas in inelastic models, additional considerations of building ductility and yield strength are required. Furthermore, they observed that FRS peaks at the FE increased relative to the CM with greater static eccentricity.

2.4.6 Ground motion characteristics

The characteristics of ground motion play a critical role in shaping the FRS and the seismic demands experienced on various floors of a building. Parameters such as intensity, frequency content, duration, and pulse-like features govern the interaction between the input motion and the building's dynamic properties, significantly influencing the amplification and distribution of floor-level accelerations. Aldeka et al. [47, 122] examined the seismic response of secondary systems mounted on irregular RC buildings and found that the acceleration of these systems increases as the PGA value rises, as long as the primary system remains within the elastic range. When the PGA value exceeds the structure's elastic limit, resulting in damage and inelastic behavior, the periods of vibration increase due to reduced stiffness. This indicates that the maximum component acceleration amplification factor occurs at the structure's elastic seismic capacity.

Calvi and Sullivan [81] investigated MDOF structures responding within the elastic range. They proposed a simplified modal combination approach for estimating acceleration spectra on upper floors, considering the limited filtering of ground motion input that occurs on lower floors. Zhai et al. [111] found that near-fault pulse-like ground motions can significantly amplify floor accelerations, with the increase in amplification reaching up to 17% in buildings with longer fundamental periods.

Lucchini et al. [125] conducted a detailed analysis on a 6-storied RC frame to create a probabilistic model for assessing seismic demand on secondary systems. Their findings indicated that peak spectral accelerations within the impact zone of a natural mode are influenced by earthquake intensity. However, they also observed that the variation in peak spectral accelerations along the building's height remains relatively constant, regardless of increases in earthquake intensity. Surana et al. [126] performed analyses on RC frame building models, conducting a total of 1,289 non-linear dynamic simulations to evaluate floor responses across varying levels of inelasticity. Their results demonstrated that floor response correlates more effectively with the GRS than with PGA or PFA.

Few studies [103, 127, 128] have comprehensively investigated the influence of the rotational ground motions. Poudel et al. [103] identified a notable influence of the rotational ground motions on the floor accelerations, particularly in torsionally rigid structures with shorter periods corresponding to the rotational mode of vibration ($\leq 0.50\ s$). The study highlighted that a_t is significantly amplified at the corners of the structure compared to the CM. Additionally, it was observed that the inclusion of rotational ground motions can result in an acceleration increase of up to 82% at periods associated with the building's fundamental mode region.

2.4.7 Inelasticity of the secondary system

Seismic design codes often use component response modification factors to account for the inelastic behavior of secondary systems. For instance, ASCE 7-16 incorporates a factor ranging from 1.0 to 12.0 to reflect different secondary system characteristics, and EC 8 employs a similar approach. Typically, these factors are derived from engineering judgment rather than experimental or numerical analysis.

Villaverde [114] introduced strength reduction factors to represent the inelastic behavior of secondary systems and their supporting structures, while Chaudhuri and Villaverde [108] evaluated the seismic responses of inelastic secondary systems supported by MRFs. They [108] observed that the deformation demands on inelastic secondary systems attached to inelastic buildings typically fall below the selected response modification factor. However, this does not apply when the secondary systems are tuned to higher modes of the supporting building, particularly if the

natural period of these modes is under about 0.2 seconds.

Vukobratović and Fajfar [77] recommended incorporating the inelastic behavior of secondary systems by adjusting their damping ratio when developing FRS for ductile secondary systems. Anajafi et al. [129] developed inelastic FRS for several code-compliant buildings while accounting for varying degrees of secondary system inelasticity. Their results demonstrated that secondary system inelasticity notably decreased peak FRS values near the building's modal periods in elastic structures. Moreover, it markedly lessened the impact of the tuning period ratio, the damping ratio, and the properties of both the building and ground motion on the FRS.

2.4.8 Damping ratio of the secondary system

Damping ratio of the secondary system significantly affects the seismic performance of secondary systems in buildings. A lower damping ratio results in sharper FRS peaks, particularly for systems with periods similar to that of the primary system, while a higher damping ratio generally reduces FRS values [42, 76, 77, 122].

Astroza et al. [130] and Aragaw and Calvi [131] have shown that the viscous damping ratios for secondary systems generally span from 0.5% to 20% [131], with most falling within the lower range of 1% to 2% [130]. The low damping ratios highlight the need for accurate modeling to ensure their safety and functionality during earthquakes. Sankaranarayanan and Medina [42] observed that an increase in the damping ratio of secondary systems could significantly reduce their acceleration response. Similar observations are made by Vukobratović and Fajfar [76, 77]. Pan et al. [78] observed that the damping ratio of secondary systems significantly affects floor acceleration amplification, particularly in the short and fundamental period ranges.

Anajafi and Medina [43] conducted a thorough investigation into how the damping ratio of secondary systems affects FRS. They defined the damping modification factor (DMF) as the ratio of the FRS at a given damping ratio to the FRS at a standard 5% damping ratio, allowing for a direct comparison of FRS values across different damping levels. Their study revealed that a reduction in the secondary system's damping ratio from 5% to 1% could lead to an increase in floor acceleration demands by up to 116%, particularly when the secondary system is

tuned to the structural modes of vibration. Based on their numerical analysis, they proposed empirical equations to predict the DMF based on the secondary system's damping ratio and tuning period. Kazantzi et al. [48] proposed a probabilistic model that incorporates the mean and lognormal standard deviation of the DMF, utilizing recorded floor acceleration data to enhance the prediction accuracy of FRS values across different damping ratios.

Surana et al. [46] observed that the DMFs for the elastic FRS are influenced by the secondary system's damping ratio, the tuning ratio, modal periods, and the inelasticity level of the building structure. Considering these factors, they proposed a multi-linear model to compute DMFs for the elastic FRS. Studies by Sankaranarayanan and Medina [42] and Surana et al. [46] emphasized the significant impact of the secondary system's damping ratio on design floor acceleration demands in regular and symmetric buildings exhibiting pure translational responses.

2.5 Method for the estimation of FRS

Researchers have employed a range of methodologies to develop FRS, leveraging approaches such as SDOF-based methods, MDOF-based methods, direct generation techniques, and code-based methods. Each approach offers unique advantages, from simplifying calculations to enhancing precision, depending on the complexity of the structural system and the required level of detail in the analysis.

2.5.1 SDOF-based methods

The SDOF-based method [52, 71, 72, 75–77, 80, 81] estimates the FRS by modeling the secondary system as an SDOF oscillator subjected to the floor acceleration of the primary SDOF system. This method employs a component amplification factor (a_p), defined as the ratio of the maximum acceleration of the secondary system to the peak floor acceleration at its mounting point. The a_p accounts for the amplification effects caused by the dynamic properties of the secondary system, including its natural frequency and damping characteristics. This approach captures the interaction between the ground motion, the primary system's dynamic response, and the secondary system's behavior under seismic loading.

2.5.2 MDOF-based methods

The SDOF-based methods are limited in capturing the complex seismic responses of the MDOF primary systems. To address this, recent research [78, 79, 81, 131, 132] has introduced methods for generating FRS based on MDOF primary systems using modal superposition techniques and an SDOF secondary system. This approach incorporates the contributions of multiple vibration modes, effectively overcoming the shortcomings of the SDOF-based methods, which fail to account for the higher-mode effects in MDOF primary systems. By combining the responses in individual modes, the FRS more accurately reflects the dynamic behavior of the building across various levels.

2.5.3 Direct methods

Direct method differs from other approaches as it uses a predefined function to estimate FRS. The spectral amplification factor facilitates the direct generation of FRS from the GRS or the design response spectrum by employing the spectral amplification factor [133]. This factor is quantitatively defined as the ratio of the FRS to the GRS, thereby providing a means to translate ground motion characteristics into floor motion characteristics. In recent years, various amplification factor functions [86, 117, 126] have been developed to improve the accuracy of FRS generation. Wieser et al. [86] introduced an empirical multi-linear envelope spectral acceleration amplification function that takes into account several critical factors, including the T_s/T_1, Z/H, and the influence of higher modes. Surana et al. [117, 126] proposed floor amplification functions that enable the direct estimation of FRS at any specified height based on the GRS. This approach relies on an understanding of the first two mode shapes, the modal periods of the building, and the strength ratio of the building.

Additionally, direct methods also focused on the total amplification (a_t), expressed as the ratio of FRS to PGA, which is equivalent to the product of a_p and PFA/PGA. This enables a streamlined, one-step calculation of floor spectral values by applying the a_p directly to a specified PGA level. Singh et al. [93] developed equations for estimating FRS/PGA that consider the effects of potential resonance with higher modes. Medina [134] established distinct FRS/PGA values

for flexible and rigid secondary systems through inelastic dynamic analyses of 2D shear-wall structures with heights of 3, 9, and 15 stories. For elastic secondary systems exhibiting a 5% damping ratio, Medina [134] recommends FRS/PGA values of 3 or 12 for flexible systems situated near the bottom or top of the structure, while suggesting values of 2 or 4 for rigid systems. Hou et al. [135] proposed a model for estimating a_p using a shake table test in low-rise steel concentrically braced frames. Petrone et al. [106] developed a method for estimating FRS/PGA values that integrates the building's fundamental period and considers higher mode effects. This approach provides conservative FRS predictions across a wide range of periods, especially those close to the fundamental period. Fathali and Lizundia [68] conducted a study on instrumented buildings and introduced a multi-segment a_p spectrum to derive FRS values from PFA measurements. Their proposed a_p values ranged from 1.0 to 2.5.

2.5.4 Code-based methods

Different seismic design codes [6, 16, 17, 27] have proposed various methods for estimating PFA from PGA. For rigid secondary systems with periods shorter than 0.06 seconds and flexible secondary systems with periods longer than 0.06 seconds [6], ASCE 7-16 and IS 16700 recommend a_p values ranging from 1.0 to 2.5. However, ASCE 7 has slightly increased this range to between 1.0 and 2.8. In the case of EC 8, the a_p values depend on both T_s and T_1, specifically the ratio T_s/T_1, with a peak value of 2.2 at the roof. Figure 1.7(b) and 1.7(c) show the a_p and a_t, respectively, as recommended in ASCE 7, EC 8, and IS 16700.

2.6 Summary

The seismic design of secondary systems has been extensively studied since the 1970s, leading to the development of diverse methodologies for estimating floor acceleration demands. These methods for seismic design of secondary systems can be broadly categorized into shake table tests, instrumented building responses, analytical techniques, and numerical simulations. Shake table tests provide real-time insights, while instrumented buildings offer empirical data from actual earthquake events. Analytical and numerical approaches enable the theoretical and computational

evaluation of floor acceleration demands, respectively. The estimation of floor acceleration demands can follow either a coupled approach, where primary and secondary systems are modeled together to account for dynamic interaction, or a decoupled approach, where secondary systems are analyzed independently of the primary system. Coupled methods, while computationally intensive, provide higher precision and are necessary for heavy secondary systems, whereas decoupled methods, suitable for light-weight secondary systems, offer simplified yet practical solutions for seismic design.

Research has highlighted the critical role of PFA in the seismic design of rigid secondary systems, emphasizing the need to consider the fundamental period, the relative height of the floor, building inelasticity, ground motion characteristics, and the presence of infill walls. Contemporary seismic design codes provide guidelines for PFA estimation, but variations in recommendations suggest the need for more comprehensive approaches that integrate multiple influencing factors.

FRS serves as a vital tool for assessing the seismic performance of flexible and very flexible secondary systems. Studies show that the building's modal period and its dynamic interaction with seismic frequencies significantly influence the FRS profile. Additionally, the variation of FRS at different relative heights of the floor, often amplified at upper floors, and the role of inelastic behavior in reducing seismic demands on secondary systems are critical considerations. The influence of ground motion characteristics and structural features, such as infill walls, on FRS and floor accelerations further underscores the complexities involved in the seismic design of flexible secondary systems. Advanced studies highlight the importance of incorporating damping ratio, inelasticity, and resonance effects into seismic design methods of secondary systems.

This comprehensive review underscores the progress in understanding and estimating floor acceleration demands. However, it also identifies critical gaps in the existing literature and building codes, particularly regarding the effects of nominal torsion on floor acceleration demands. Torsional effects, which arise due to uneven stiffness, mass, or strength distribution, can significantly amplify floor accelerations and create non-uniform seismic demands on secondary systems. The absence of

detailed investigations into these effects highlights the need for further research to develop more accurate and holistic methods that account for the diverse factors influencing the dynamic response of buildings and secondary systems.

Chapter 3

Building Archetypes, Modeling, and Analyses

3.1 Introduction

This chapter outlines the selection, modeling, analysis, and design of low- to mid-rise RCMRF building archetypes resting on firm ground conditions. The selected building archetypes reflect a wide range of irregular plan buildings, often observed in the existing housing stock in India. In these buildings, nominal torsion is introduced to facilitate a detailed examination of their impact on floor acceleration response. This approach aims to provide a comprehensive understanding of the floor acceleration response of torsionally irregular building archetypes.

3.2 Selection of building archetypes

The housing stock in India comprises a diverse array of building types, each presenting distinct challenges for their seismic analysis and design, particularly given the country's varied seismotectonic and topographic setup. Low-rise buildings up to four stories are prevalent in both rural and urban areas and often utilize load-bearing masonry walls. These structures generally exhibit a shorter natural period (usually in the acceleration-controlled range of the response spectra), rendering them susceptible to high-frequency seismic waves, especially in seismically active regions (such as the Himalayan foothills and northeast India), which fall under seismic Zones IV and V.

Mid-rise buildings from five to ten stories employ RCMRFs often combined with infill walls or sometimes with shear wall systems. These structural systems have moderate flexibility and exhibit a moderate natural period (usually in the velocity-controlled range of the response spectra). The earthquake behavior of these

buildings has been extensively studied (after the 2001 Bhuj earthquake [1]), which underscored the need for robust design standards for such structures. With the growing demand for urban buildings, nowadays, mid-rise buildings are also emerging in suburban areas, emphasizing the need for comprehensive analysis to ensure their seismic resilience. High-rise buildings, typically exceeding ten stories, are becoming increasingly common in metropolitan cities (e.g., Mumbai, Delhi, Kolkata, Chennai, and Hyderabad). These structures often incorporate advanced structural systems, including RC shear walls, braced frames, and outriggers, to effectively manage the significant seismic forces and displacements experienced during earthquakes.

The 2001 Bhuj earthquake [1] and the 2011 Sikkim earthquake [11, 12, 23] revealed significant vulnerabilities of low- and mid-rise buildings in India, particularly emphasizing the need for improved safety measures for secondary systems. These events underscore how inadequately designed secondary systems can lead to severe damage or even collapse, highlighting the importance of incorporating seismic design considerations for these systems to enhance overall building resilience during earthquakes. In light of India's diverse seismic zones, the Indian Standards for Earthquake Resistant Design (IS 1893) [5] play a pivotal role in guiding the analysis and design of buildings. However, challenges persist in adapting global best practices to meet the specific needs and conditions of urban centers across India.

The present work aims to study the impact of the nominal building torsion on the floor acceleration response of buildings. To achieve this objective, an extensive range of torsionally irregular RCMRF buildings with varied plan shapes is selected. These buildings include 16 torsionally irregular and eight regular buildings, encompassing a total of 24 buildings. The nominal torsion in these 16 buildings is introduced in two different ways. The first way includes the selection of square and rectangular plan shape (regular shape) buildings (Figures 3.1(a)-(b)) with an asymmetric distribution of the lateral load-resisting elements, whereas the second way to cause torsion in the buildings includes the selection U- and T-plan shape (irregular shape) buildings (Figures 3.1(c)-(d)) with asymmetric distribution of the lateral load-resisting elements. The individual building frames are classified as flexible frames (FF_{ij}) or stiff frames (SF_{ij}), (where 'i' denotes the frame's position relative to the extreme flexible or stiff edge, and 'j' represents the floor level in the

building), depending on their locations with respect to the CR in the floor plan. These buildings are 4- and 8-storied, representative of low- and mid-rise housing stock in urban areas.

The lateral load-resisting elements are arranged in the building plan to result in three different extents of torsional irregularities: (i) extreme torsional irregularity (ETI), i.e., $\Delta_{max}/\Delta_{avg} \geq 1.4$, (ii) with torsional irregularity (WTI), i.e., $1.4 > \Delta_{max}/\Delta_{avg} \geq 1.2$, and (iii) no torsional irregularity (NTI), i.e., $\Delta_{max}/\Delta_{avg} < 1.2$. The story height is constant for all stories and is considered as 3.3 m. The considered buildings are abbreviated using three features: (i) extent of nominal torsion (ETI, WTI, and NTI), (ii) number of stories (4 and 8), and (iii) plan shape (Rectangular–R, Square–S, T, and U). For example, the abbreviation 'E4R' represents a rectangular plan 4-story building with extreme torsional irregularity. The three-dimensional (3D) elevation views of the selected building archetypes are illustrated in Figure 3.2.

3.3 Modeling and design of the buildings

The structural models for the selected group of buildings are developed and designed using ETABS [136], adhering to the Indian Standards (IS 875 Part 1 & 2, 1987 [137, 138]) for load application and in accordance with the strong-column–weak-beam philosophy and capacity shear, which is fundamental to capacity design. The dead load intensities on the floors range from 11.40 to 13.50 kN/m^2, and on the roof, they range from 8.50 to 9.60 kN/m^2. For all buildings, live loads are consistently applied as 3.00 kN/m^2 on the floors and 1.50 kN/m^2 on the roof. These buildings are designed as the Special MRFs, following the Indian Standards [5, 32, 33], considering them situated at the rock/stiff site class for the Indian Seismic Zone V (Peak ground acceleration, PGA=0.36g). The load combinations used in the structural design are as per IS 1893, Clause 6.3.4 [5], ensuring adequate consideration of gravity and seismic effects in accordance with code requirements. The beams and columns are made of M40 grade concrete, whereas steel reinforcement of Fe550 grade is used. The typical cross-sectional dimensions, obtained through iterative design and code compliance checks using ETABS, are presented in Figure 3.1 for the ETI and WTI buildings. For the NTI buildings, the typical cross-sectional dimensions of the beams and columns are adopted as 0.30 m × 0.40 m and 0.40 m × 0.40 m, respectively. The

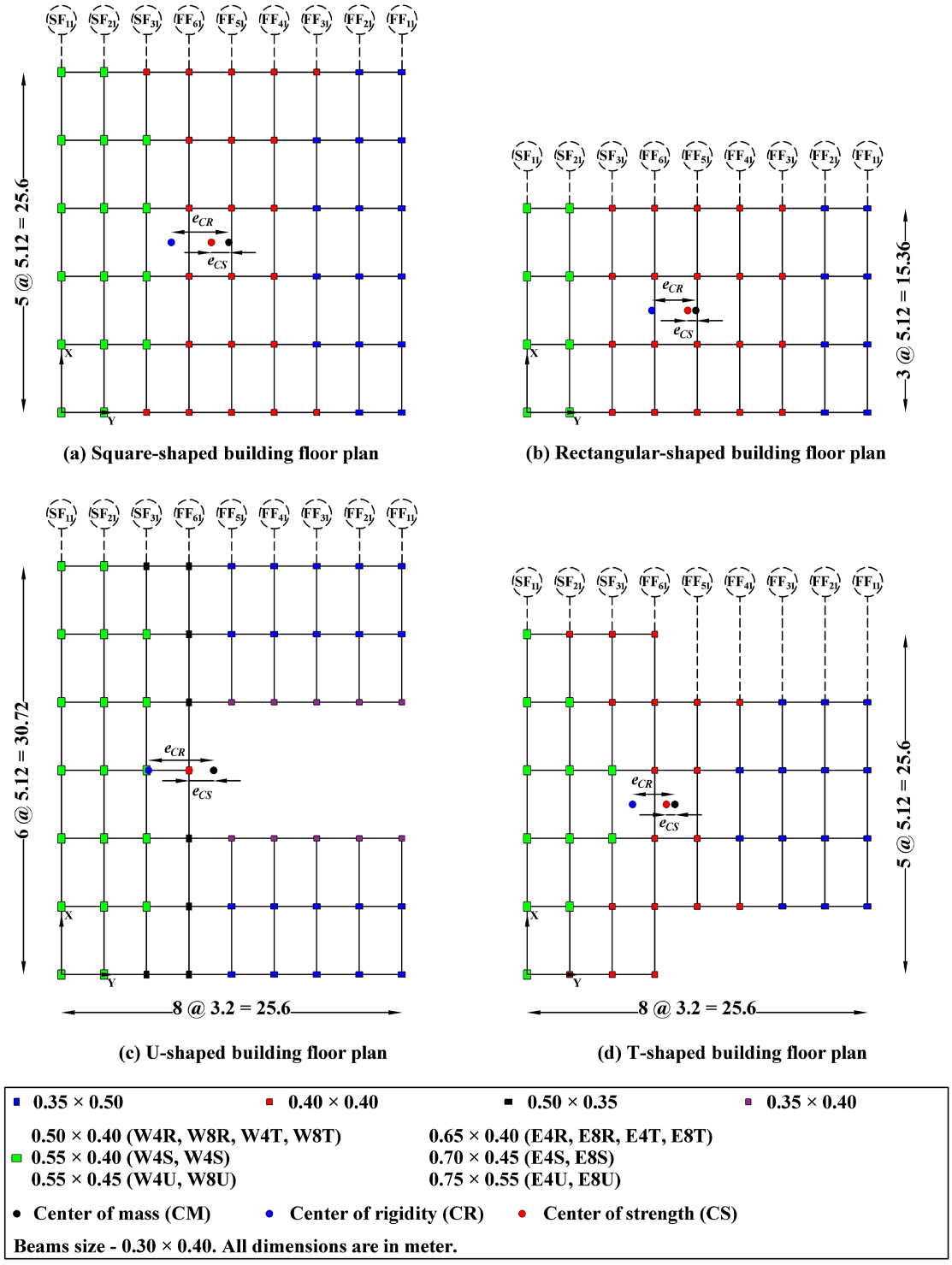

Figure 3.1: Typical plan layouts, section sizes, stiffness eccentricity, and strength eccentricity details of the WTI and ETI buildings. The stiffness and strength eccentricities shown in the building plan correspond to the first-floor level of the 4-story building with extreme torsional irregularity. 'FF_{ij}' and 'SF_{ij}' refer to the flexible and stiff frames located at the 'i^{th}' frame and 'j^{th}' floor level, respectively, within the building.

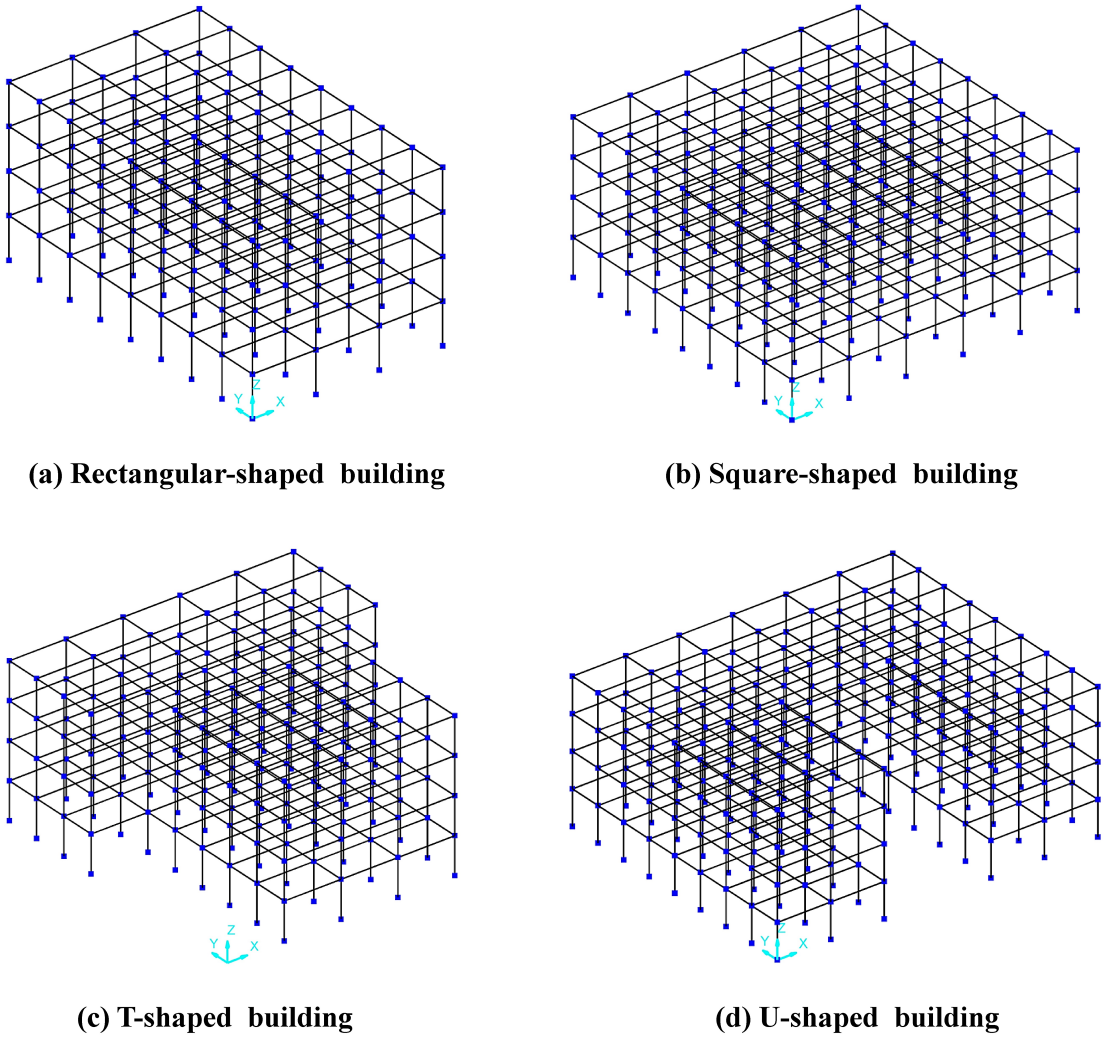

(a) Rectangular-shaped building **(b) Square-shaped building**

(c) T-shaped building **(d) U-shaped building**

Figure 3.2: Typical three-dimensional (3D) elevation of the 4-story buildings investigated in the present thesis.

longitudinal reinforcement in beams varied from 0.28% to 1.64% at the top face and from 0.28% to 1.17% at the bottom face, while the reinforcement in columns ranged from 0.95% to 3.95%. The spacing of transverse reinforcement in both beams and columns does not exceed 100 mm in the end regions; thus, the considered buildings confirm the ductile detailing provisions of IS 13920 [33].

3.3.1 Dynamic characteristics of the buildings

Earlier studies [41, 42, 45, 49] showed that the floor response of the buildings is significantly affected by their dynamic characteristics; thus, modal analysis is performed in OPENSEES [139] for all the buildings to obtain their dynamic characteristics. The dynamic characteristics (i.e., periods and modal mass participation factors) as obtained from the 3D modal analysis for the first three

modes of vibration are summarized in Table 3.1. The modal responses are combined using the SRSS method, appropriate for buildings with well-separated natural modes [5]. It is to be noted that the ratio between the first translational to the first rotational mode period is greater than unity (the term 'first' mode is defined as the mode with the highest modal mass participation) in the X-direction of excitation for all the investigated buildings. Thus, these buildings are expected to behave as torsionally rigid buildings in the X-direction.

In these investigated buildings, the modal mass participation corresponding to the first mode ranges between 68.16-84.90%, implying that the fundamental vibrational mode dominates the seismic response of these buildings. The torsional irregularity results in translational-torsional coupling of modes in the X-direction (shown by grey cells, Table 3.1). The significant modal mass participation in translational (X-direction) and rotational modes (R_Z) indicates translational-torsional coupling between these modes. Even in plan-regular buildings, minor asymmetries in stiffness or mass distribution can lead to non-negligible coupling, influencing both modal characteristics and dynamic response. The extent of torsional coupling varied from 2.49-13.13%, 0.90-4.77%, and 0.01-0.17% (in the X-direction) for ETI, WTI, and NTI buildings, respectively. Among all these buildings, U-shaped buildings exhibited the highest translational-torsional coupling of modes, whereas rectangular-shaped buildings exhibited the lowest. Further, for a given plan shape of the building, the translational-torsional coupling of modes is observed to be higher for 4-story buildings than for their 8-story counterparts. This indicates that building torsion can have a more severe impact on shorter-height buildings, highlighting the increased vulnerability of these buildings to torsional effects.

3.4 Torsional irregularity indices of the buildings

Seismic design codes [5, 6, 16, 27] define the torsional irregularity in the buildings using different indices. ASCE 7 [6], ASCE 7-16 [27], and IS 1893 [5] define the torsional irregularity in the buildings using the elastic floor displacement-based indices. According to ASCE 7-16, if the ratio $\Delta_{max}/\Delta_{avg}$ exceeds 1.20 (or 1.40) at any floor level, the building is said to be torsionally irregular (or extreme torsionally

Table 3.1: Dynamic characteristics of the investigated buildings.

Mode	Period	Modal Mass Participation			Period	Modal Mass Participation			Period	Modal Mass Participation		
	(s)	α_{mx}[a]	α_{my}[b]	θ_{mz}[c]	(s)	α_{mx}[a]	α_{my}[b]	θ_{mz}[c]	(s)	α_{mx}[a]	α_{my}[b]	θ_{mz}[c]
	N4R				**W4R**				**E4R**			
1	0.76	83.34	-	-	0.75	80.62	-	02.59	0.73	75.11	-	07.80
2	0.67	-	-	84.16	0.64	02.36	-	80.98	0.60	-	84.19	-
3	0.64	-	84.90	-	0.61	-	84.35	-	0.60	06.89	-	74.65
	N8R				**W8R**				**E8R**			
1	1.57	81.15	-	00.01	1.56	80.03	-	00.90	1.52	78.02	-	02.49
2	1.37	00.01	-	81.81	1.34	00.83	-	80.53	1.28	02.19	-	78.16
3	1.31	-	81.94	-	1.27	-	81.67	-	1.24	-	81.43	-
	N4S				**W4S**				**E4S**			
1	0.75	83.71	-	-	0.73	78.60	-	04.55	0.70	72.29	-	10.30
2	0.65	-	-	84.58	0.61	-	84.13	-	0.60	-	83.51	-
3	0.65	-	84.87	-	0.61	04.11	-	78.98	0.57	08.99	-	72.14
	N8S				**W8S**				**E8S**			
1	1.56	81.20	-	-	1.51	79.33	-	01.48	1.48	76.77	-	03.41
2	1.34	-	-	81.79	1.27	01.36	-	79.66	1.22	-	80.98	-
3	1.33	-	81.70	-	1.26	-	81.24	-	1.22	02.96	-	77.09
	N4T				**W4T**				**E4T**			
1	0.77	83.57	-	00.07	0.75	79.08	-	04.29	0.73	71.72	-	11.22
2	0.67	00.07	-	84.27	0.65	04.03	-	79.48	0.61	-	83.91	-
3	0.66	-	84.90	-	0.62	-	84.14	-	0.61	10.18	-	71.73
	N8T				**W8T**				**E8T**			
1	1.56	81.20	-	00.08	1.54	79.35	-	01.62	1.5	76.40	-	04.09
2	1.37	00.08	-	81.55	1.32	01.55	-	79.57	1.27	03.74	-	76.59
3	1.33	-	81.78	-	1.27	-	81.25	-	1.25	-	81.16	-
	N4U				**W4U**				**E4U**			
1	0.75	83.22	-	00.13	0.72	77.80	-	04.77	0.68	68.16	-	13.13
2	0.64	00.14	-	84.39	0.59	-	83.85	-	0.56	-	82.32	-
3	0.63	-	84.84	-	0.59	04.35	-	78.63	0.54	11.33	-	68.74
	N8U				**W8U**				**E8U**			
1	1.57	80.76	-	00.17	1.52	78.42	-	01.96	1.46	74.65	-	04.53
2	1.31	00.19	-	81.46	1.23	01.86	-	78.95	1.17	-	80.32	-
3	1.29	-	81.66	-	1.22	-	81.08	-	1.17	03.93	-	75.54

Grey cells show the translational-torsional coupling of modes in the X-direction. [a]Modal mass participation in the X-direction (%); [b]Modal mass participation in the Y-direction (%); [c]Modal mass participation corresponding to the rotational mode of vibration (%).

irregular). However, it shall be noted that in the latest version of ASCE 7, the definition of extreme torsional irregularity in buildings is omitted. IS 1893 defines a building as torsionally irregular if the ratio $\Delta_{max}/\Delta_{min}$ (where Δ_{min} is the minimum edge displacement at a building floor in the direction under consideration) exceeds 1.50 at any floor level. Later, this provision was amended in IS 1893 (Amendment no. 2) [31], and the torsional irregularity is said to exist in a building if the ratio

$\Delta_{max}/\Delta_{avg}$ exceeds 1.20 at any floor level. In contrast, EC 8 defines a building as torsionally irregular if the ratio e_{CR}/r (where e_{CR} is the static stiffness eccentricity, and r is the torsional radius) exceeds a value of 0.30.

Past studies [13–15] have shown that the location of the CR [140] and CS are equally crucial for understanding a building's torsional response, with the CR being more important for the elastic torsional response and the CS for the inelastic torsional response. It is worth noting that the location of the inelastic CR and CS for a building changes with the progression of yielding of structural elements and from ground motion to ground motion. Thus, the determination of the inelastic CR and CS is not straightforward. In the existing literature [14, 15], different definitions of CR are defined, which are differentiated into either CRs of all floors or CR of a single floor in a multi-story building. The '*All floor CR*' can be defined as the set of points, with one point on each floor, such that when a lateral load pattern is applied through these points, no rotation occurs in any of the floors. On the other hand, the '*Single floor CR*' is defined as the point on a floor such that applying a lateral load passing through that point does not induce any rotation in that particular floor, while the other floors in the building may experience rotation [14]. In this study, the '*Single floor CR*' definition has been used, and CRs and torsional radius of all buildings are estimated using the method available in Bisch et al. [141].

The CS refers to the center of yield strengths of the resisting elements [13]. It represents the centroid of the distribution of yield strengths among the lateral load-resisting elements at any floor level within the building. In this study, the CSs at different floor levels are estimated using the equations proposed by Sadek and Tso [13]. In these equations, the lateral force capacity of all the vertical elements is considered to determine the coordinates of CS. As the study aims to develop a simple procedure that can be used to estimate floor acceleration demands accounting for the effect of torsion in buildings without complexity; thus, the elastic CR and the elastic CS are used throughout this study. The investigated buildings exhibit close proximity between the CR and CS in the upper half of the WTI buildings (Figure 3.3). However, in the lower half of the WTI buildings and throughout the height of the ETI buildings, the positions of the CR and CS are more offset, with the maximum offset reaching 11.9% of the plan dimension for the building labeled

'E8U'.

Accordingly, the present work estimates three different torsional irregularity indices in the investigated buildings, namely: (i) e_{CR}/r, (ii) $\Delta_{max}/\Delta_{avg}$, and (iii) $\Delta_{max}/\Delta_{min}$. The floor displacements, Δ_{max}, Δ_{min}, and Δ_{avg}, are computed from the three-dimensional building model using the mode superposition method with the response spectrum defined in IS 1893 (Figure 3.4). Furthermore, the displacement parameters (Δ_{max} and Δ_{avg}) have also been estimated using the Equivalent Lateral Force (ELF) method, as prescribed in ASCE 7, with results shown in Figure 3.5. The ELF method, a simplified approach to seismic design, applies lateral forces equivalent to the estimated seismic demand, considering the building's fundamental mode of vibration to approximate the distribution of seismic forces. All these indices are illustrated in Figures 3.4(c)-(h) along with their specified limits as recommended in different building codes [5, 6, 16, 27]. Additionally, the normalized strength eccentricity (e_{CS}), with respect to the building width (b), is presented in Figures

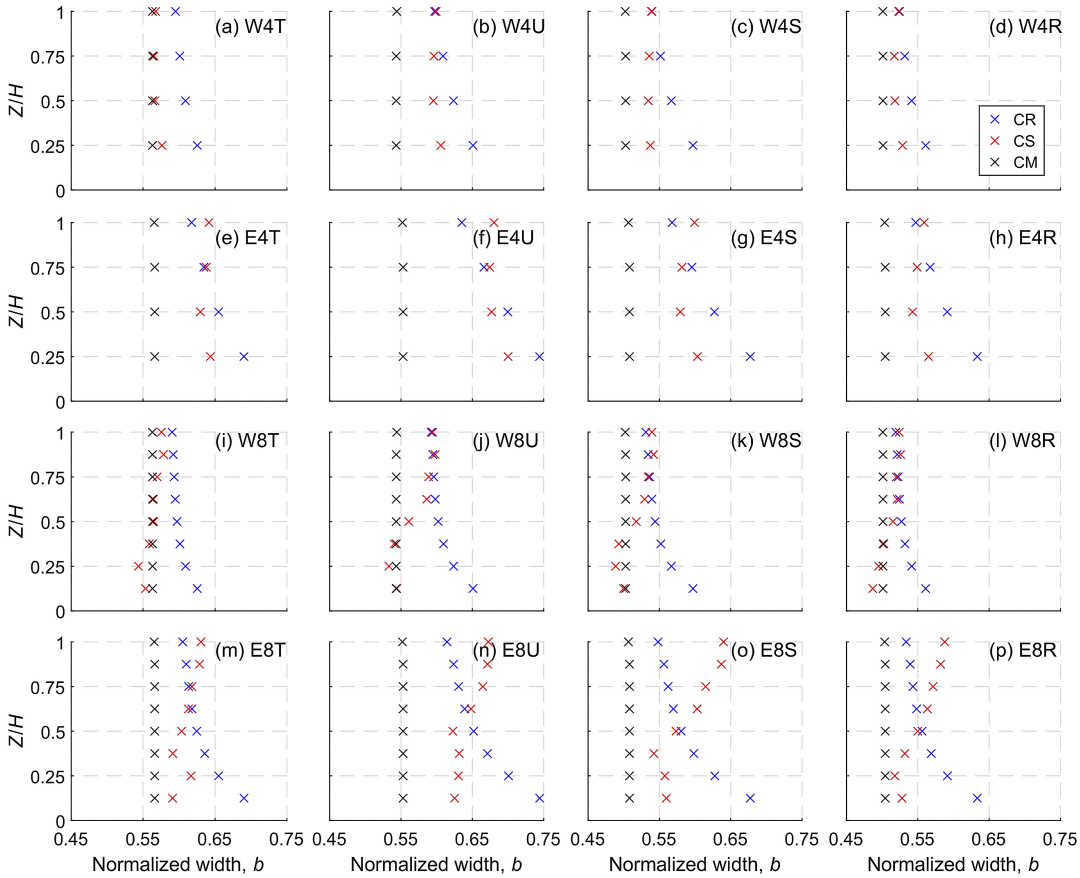

Figure 3.3: Locations of the CR, CS, and CM for the buildings with torsional and extreme torsional irregularities.

3.4(a)-(b) for all investigated building models. The e_{CS} is defined as the distance between the center of mass (CM) and the center of strength (CS).

In the investigated buildings, the maximum displacement ratios are observed at the first-floor level, reflecting significant torsional effects, and these values gradually reduce as the floor level increases (Figures 3.4-3.5). The torsional irregularity indices derived from both methods, i.e., mode superposition using the response spectrum and the ELF method, are similar. Consequently, the mode superposition using the response spectrum method has been adopted in this research for estimating torsional irregularity in the buildings. Among the selected buildings, 16 out of 24 buildings are found to be torsionally irregular, according to ASCE 7 and IS 1893 criteria, while the other eight buildings are torsionally regular. Interestingly, some buildings that are classified as torsionally irregular according to ASCE 7 (Figures 3.4(e)-(f)) and IS 1893 (Figures 3.4(g)-(h)), specifically the WTI buildings, are not considered torsionally irregular by EC 8 (Figures 3.4(c)-(d)). Thus, only six buildings, specifically the ETI buildings, have an e_{CR}/r ratio exceeding 0.30, meeting the criteria for torsional irregularity according to EC 8. Notably, T-shaped buildings (E4T and E8T) are classified as regular according to EC 8 (Figures 3.4(c)-(d)). This discussion highlights that the definitions of torsional irregularity in ASCE 7 and IS 1893 are more stringent compared to those in EC 8.

3.5 Non-linear modeling and analysis

For the present study, three-dimensional non-linear numerical models are developed using OPENSEES [139] based on the design details of these buildings. The distributed plasticity approach, also known as the fiber model (Figure 3.6), is utilized to model the inelastic behavior of RC frame members, enabling a comprehensive representation of the distribution of plasticity along the length of both beams and columns. This method effectively captures complex response phenomena such as rebar yielding and material degradation, making it particularly adept for accurately assessing the seismic performance of the buildings under consideration.

The beams and columns are modeled using "*ForceBeamColumn*" elements with five Gauss-Lobatto integration points [142], and floor slabs are modeled as rigid diaphragms. The confined and unconfined concrete material models are assigned

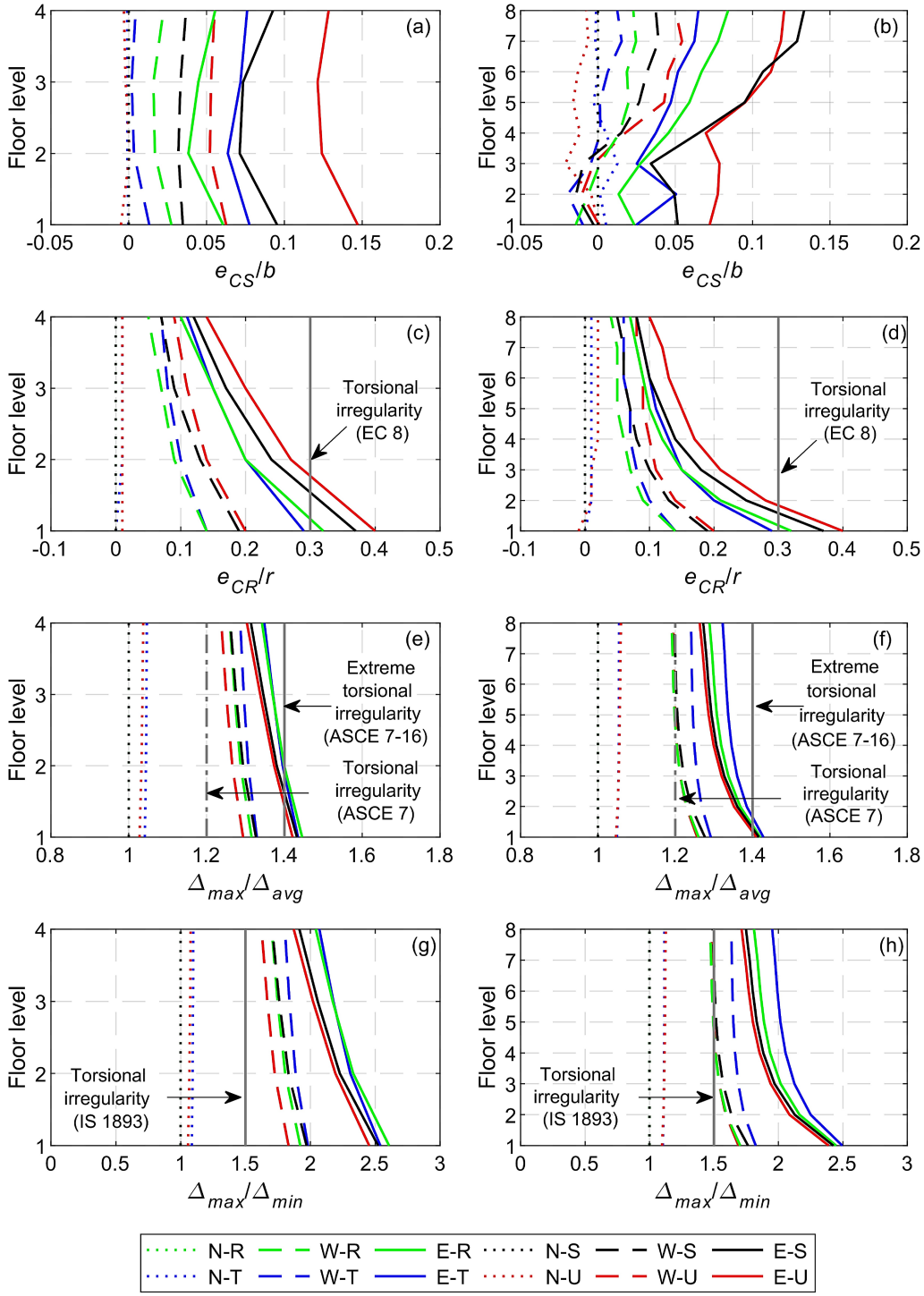

Figure 3.4: Variations of the torsional irregularity indices of seismic design codes for the investigated buildings (obtained using the mode superposition method).

for the core concrete and cover concrete regions, respectively. The "*Concrete02*" uniaxial material model available in OPENSEES is used to model the non-linear behavior of concrete fibers. The material properties of confined and unconfined concrete are computed using the model proposed by Mander et al. [143] and Karthik and Mander [144]. The concrete material parameters include the cube compressive

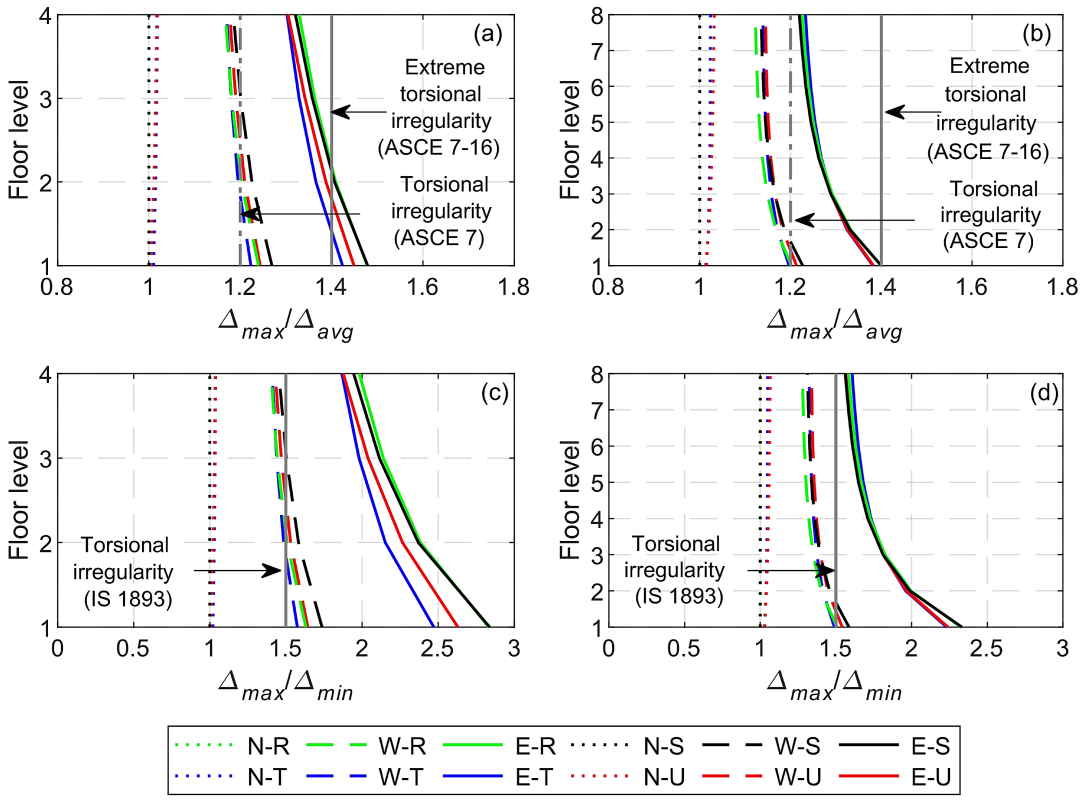

Figure 3.5: Variations of the torsional irregularity indices obtained using the ELF method [6].

strength of 40 MPa and unconfined concrete peak strain of 0.0025. The concrete elastic modulus is estimated by OPENSEES [139] based on the concrete properties and does not need to be specified as an input parameter. The non-linear behavior of steel reinforcing bars is modeled using the "*Steel02*" uniaxial material model available in OPENSEES, based on the uniaxial Giuffre-Menegotto-Pinto steel [145] material object with isotropic strain hardening. Steel reinforcement is characterized by its yield strength of 550 MPa and initial elastic modulus of 2×10^5 MPa. The transition of the steel model from elastic to plastic behavior is governed by the constants R_o, cR_1, and cR_2, which are set to 18.5, 0.9250, and 0.15, respectively [145]. The flexure failure mode of beams and columns has been considered, as shear failure is not expected to occur in the bare SMRF buildings [37] designed and detailed using the capacity design principle.

3.5.1 Ground motion selection

The objective of the present research work in this thesis is to investigate the impact of nominal building torsion on the floor acceleration response of buildings.

Accordingly, multi-directional non-linear dynamic analyses are conducted on the developed numerical building models using a far field ground motion record suite selected as per the criteria recommended in FEMA P695 [37], and those are summarized in Table 3.2. The selected ground motion record suite consists of 20 pairs of recorded seismic ground motions. These selected ground motions represent the design response spectrum for Seismic Zone V (PGA = $0.36g$) of IS 1893, which defines the target spectrum of ground motions for the site of interest. The comparison of the 5%-damped pseudo-spectral acceleration response spectra (geometric mean of two horizontal components) of the selected ground motions with the target spectrum is illustrated in Figure 3.7. The characteristics of the selected suite of ground motion records include their moment magnitudes ranging between M_w 6.53 to M_w 7.62, with a suite mean of M_w 7.10, and the PGA (geometric mean) ranging between $0.13g$ to $0.78g$, with a suite mean of $0.39g$. All the ground motions were recorded on NEHRP site classes C and D. The additional details comprising of related to the selected set of ground motions are available in Table 3.2. The ground motions are scaled in amplitude to result in a targeted SR (an indirect measure of

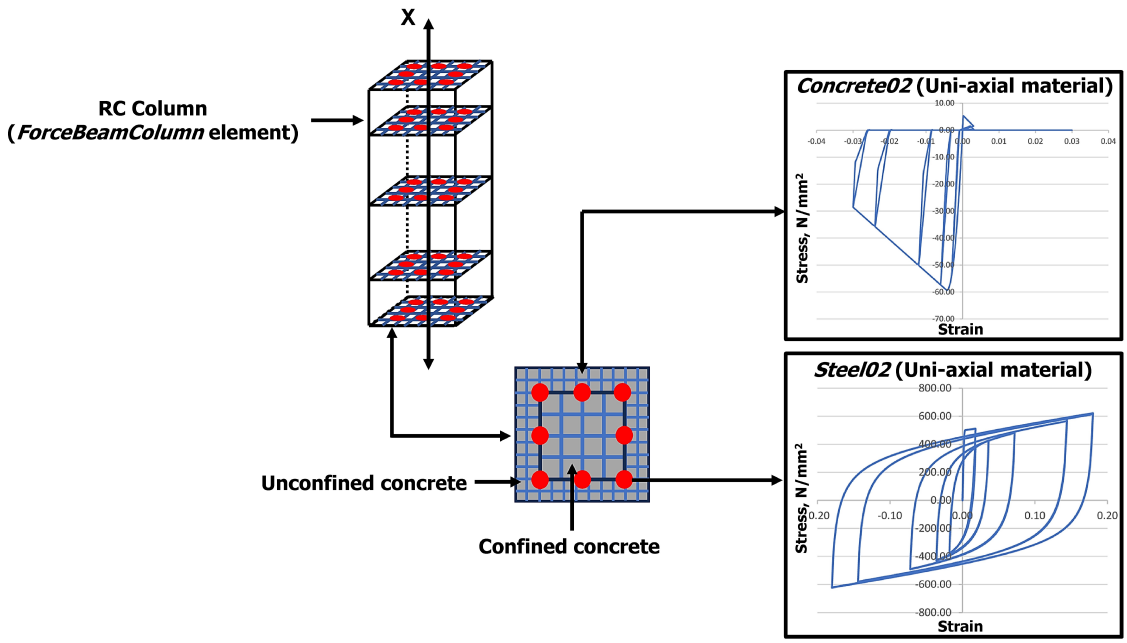

Figure 3.6: Representative view of the distributed plasticity approach (fiber model) applied to a column.

the ductility demand in the building, refer to Figure 3.8) as per Equation 3.1:

$$\text{SR} = \frac{S_a(T_1, 5\%)}{S_{ay}} \tag{3.1}$$

where $S_a(T_1,\ 5\%)$ is the 5%-damped spectral acceleration at the fundamental building period (in the X-direction) for the ground motion of interest, and S_{ay} is the spectral acceleration at the yielding of the building, which is obtained from the non-linear static analysis of the building. Alternatively, S_{ay} can be computed as the product of design spectral acceleration, S_{ad} and the overstrength ratio of the building [6].

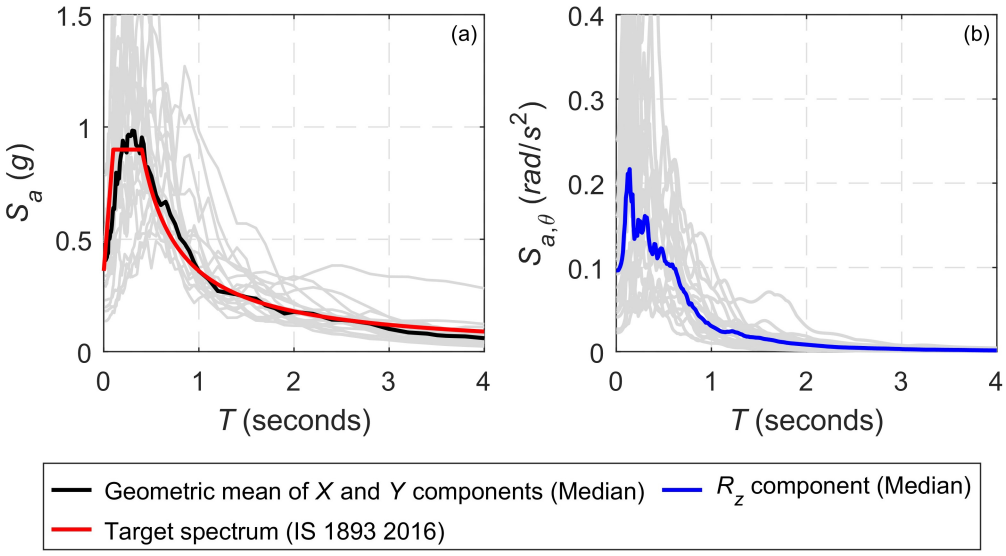

Figure 3.7: Comparison of the 5%-damped pseudo-spectral acceleration response spectra of the selected ground motions with the target spectrum.

3.5.2 Time history analyses

Time history analysis is a sophisticated method employed in the seismic performance assessment of buildings. By subjecting a building to earthquake ground motions, this approach allows for a detailed examination of the building's dynamic response, capturing its inelastic behavior and enabling a more accurate prediction of its performance under seismic loading conditions. This study conducted multi-directional time history analyses on all the selected buildings for five different SRs. These analyzed cases include elastic and inelastic buildings with SRs of 1, 2, 3, and 4. The building response is expected to remain predominantly elastic for SR significantly less than unity since S_{ay} is obtained from the non-linear static

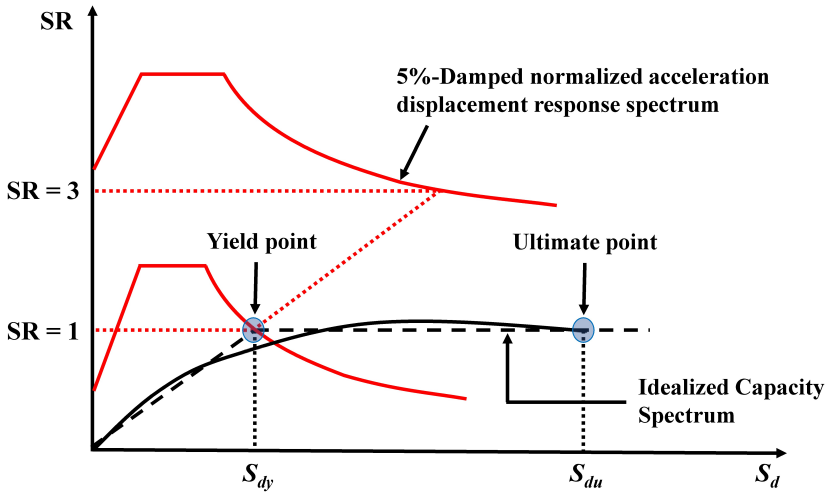

Figure 3.8: Schematic diagram illustrating the concept of strength ratio (SR). S_{dy} - spectral displacement at yielding, and S_{du} - spectral displacement at the ultimate point.

analysis of the building, and it is defined as the spectral acceleration corresponding to the yielding of significant members in the building. At SR = 2, the ground motions correspond to the Maximum Considered Earthquake (MCE) level, where a moderately inelastic response is anticipated. At SR = 4, the ground motions represent shaking significantly exceeding the MCE level, leading to a highly inelastic response. This classification enables a systematic evaluation of structural and floor acceleration demands across different seismic performance levels/ductility demands. The amplitude scaling factors for the analyzed cases range between 0.23-5.26.

The investigations are carried out with and without incorporating the rotational (R_Z) ground motions. The rotational ground motions are derived using the Single Station Procedure (SSP), as formulated by Basu et al. [146]. This method utilizes three translational acceleration records of a single station alongside essential parameters, including station-specific primary wave velocity (V_P), shear wave velocity ($V_{S,\,30}$), focal depth, and surface rupture length (SRL). The V_P is estimated in accordance with the guideline established by Suwal and Kuwano [147], while the SRL is evaluated using the equations proposed by Wells and Coppersmith [148]. The values of these parameters for the ground motions employed in this study are presented in Table 3.2. The method assumes a homogeneous elastic half-space for the soil medium and establishes a principal plane, an imaginary vertical plane that connects the recording station with the earthquake's epicenter, along which primary

and secondary waves propagate. Torsional acceleration is computed from the SH component (horizontally polarized shear wave), which is derived as the resultant of the measured accelerations in directions orthogonal to the principal plane. The translational acceleration records are decomposed into body waves: primary waves (compressional), SV waves (shear waves with vertical particle motion), and SH waves (shear waves with horizontal particle motion). The method accounts for the reflections and refractions of these waves, enabling the calculation of their resultant displacement fields, which are then utilized to extract the rotational components of motion (R_X, R_Y, and R_Z).

Table 3.2: A suite of 20 far field ground motion records used in this study.

RSN[a]	Event name	Year	Station name	M_w[b]	R_{rup}[c] (km)	$V_{s,\,30}$[d] (m/sec)	V_p[e] (m/sec)	PGA_X (g)	PGA_Y (g)	Depth (km)	SRL[f] (km)
169	Imperial Valley-06	1979	Delta	6.53	22	242	419	0.24	0.35	10.00	19
174	Imperial Valley-06	1979	El Centro Ar. #11	6.53	13	196	340	0.37	0.38	10.00	19
570	Taiwan SMART1(45)	1986	SMART1 C00	7.30	56	309	535	0.12	0.15	15.80	55
580	Taiwan SMART1(45)	1986	SMART1 O06	7.30	54	293	508	0.17	0.19	15.80	55
725[g]	Superstition Hills-02	1987	Poe Road (temp)	6.54	11	317	548	0.48	0.29	09.00	19
752	Loma Prieta	1989	Capitola	6.93	15	289	500	0.52	0.45	17.50	36
767	Loma Prieta	1989	Gilroy Array #3	6.93	13	350	606	0.56	0.37	17.50	36
953	Northridge-01	1994	Beverly Hills-M.	6.69	17	356	616	0.45	0.50	17.50	23
960	Northridge-01	1994	Can. Count.-WLC	6.69	12	327	564	0.41	0.47	17.50	23
1111	Kobe_ Japan	1995	Nishi-Akashi	6.90	07	609	1055	0.49	0.47	17.90	36
1116	Kobe_ Japan	1995	Shin-Osaka	6.90	19	256	443	0.23	0.23	17.90	36
1158	Kocaeli_ Turkey	1999	Duzce	7.51	15	282	488	0.31	0.36	15.90	102
1244	Chi-Chi_ Taiwan	1999	CHY101	7.62	10	259	448	0.34	0.40	06.80	109
1485	Chi-Chi_ Taiwan	1999	TCU045	7.62	26	705	1220	0.48	0.51	06.80	109
1602	Duzce_ Turkey	1999	Bolu	7.14	12	294	508	0.75	0.82	11.00	54
1633	Manjil_ Iran	1990	Abbar	7.37	13	724	1254	0.53	0.50	19.00	80
3748	Cape Mendocino	1992	Fortuna Fire Sta.	7.01	19	388	672	0.38	0.27	09.60	36
3749	Cape Mendocino	1992	Fortuna Fire Sta.	7.01	20	355	615	0.33	0.28	09.60	36
3754	Landers	1992	Indio-Jackson Rd.	7.28	49	292	506	0.31	0.13	07.00	69
5985	El Mayor-Cucapah	2010	El Centro Diff. Ar.	7.20	23	202	350	0.55	0.51	10.00	60
5992	El Mayor-Cucapah	2010	El Centro Ar. #11	7.20	16	196	340	0.44	0.59	10.00	60

[a]Record sequence number; [b]Moment magnitude; [c]The closest distance to the rupture surface; [d]Average shear-wave velocity from the surface to a depth of 30 m; [e]Primary wave velocity; [f]Surface rupture length [148]. [g]Replaced by RSN 3748 for analyses involving the rotational component of the ground motion due to the unavailability of the vertical component, which is essential for estimating the rotational component.

Figure 3.9 presents the comparison of the geometric mean response spectra of two horizontal components of ground motions with their corresponding rotational component of the ground motion. The ordinates of these plots are to be read on the

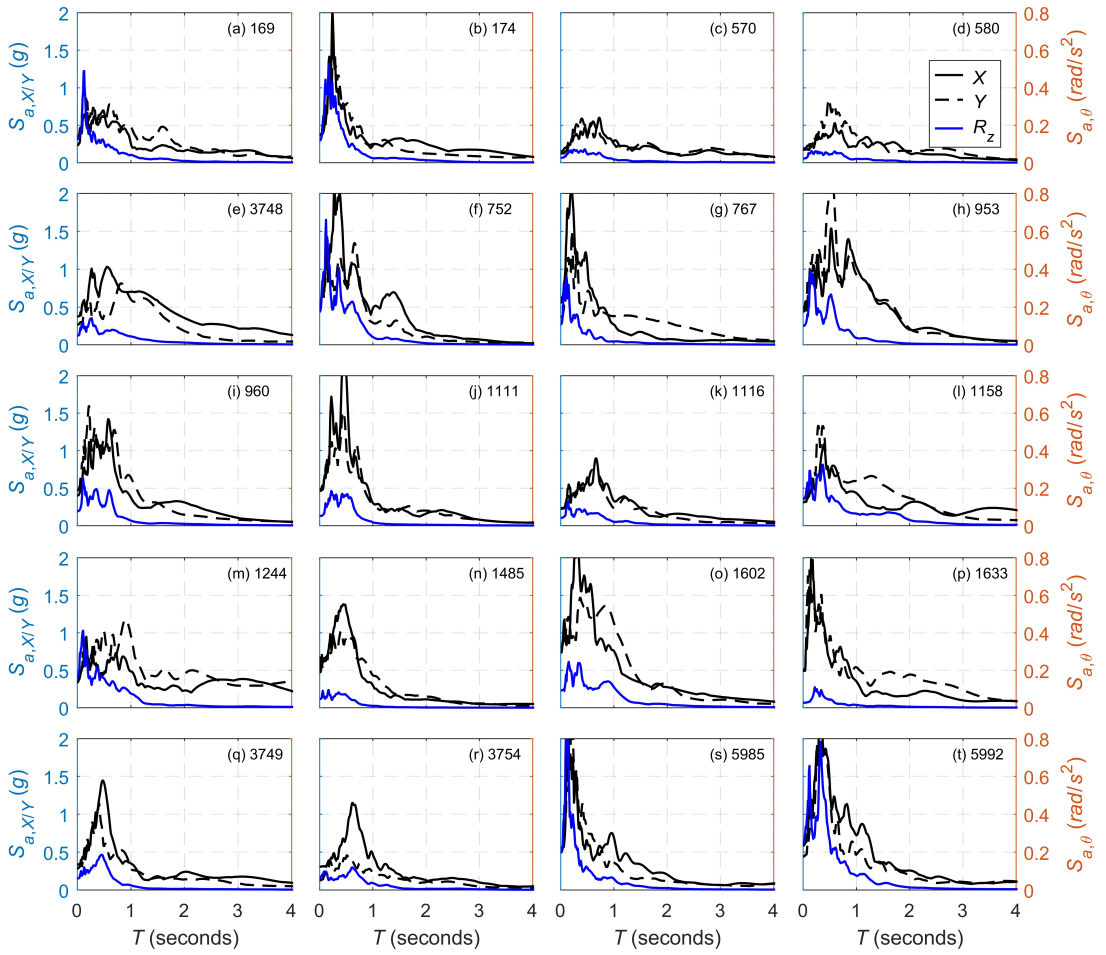

Figure 3.9: Comparison of the response spectra for the horizontal and rotational components of the ground motions selected in this study.

left side for the horizontal component of the ground motions and on the right side for the rotational component of the ground motions. It can be observed that rotational ground motions are significantly small (between 0.56 – 7.15%) compared to the horizontal component of ground motions corresponding to the same earthquake.

To conduct the non-linear time history analyses, when only the two horizontal translational components are considered, the analyses are divided into two groups: Set 1 and Set 2. In Set 1, the H_1 component of the ground motion is applied in the X-direction, while the H_2 component is applied in the Y-direction. In Set 2, this is reversed, with H_2 applied in the X-direction and H_1 in the Y-direction. For each building and SRs, 40 cases of bi-directional time history analyses are conducted for each building under consideration for the specific SR of interest. In contrast, when rotational ground motion is incorporated in addition to the two horizontal components, it is applied in two orientations: first, with a clockwise

rotation about the vertical axis along with the horizontal components, and then with an anti-clockwise rotation about the vertical axis along with the horizontal components. This approach results in a comprehensive set of 80 multi-directional time history analyses for each building and SRs, ensuring a thorough assessment of their seismic response. Mass and stiffness proportional Rayleigh damping equal to 2.5% is assigned [27]. The periods equal to $1.5\,T_1$ and the period that results in at least 95% cumulative mass participation in either of the directions of the building define the Rayleigh damping [27].

3.6 Summary

This chapter presents the selection, modeling, and analysis of low- to mid-rise RCMRF building archetypes utilized in this study. The selection process prioritizes plan-irregular configurations, with a particular focus on torsionally irregular buildings commonly found in the Indian building stock. The chapter then advances into the modeling approach, which integrates both linear and non-linear methodologies for the analysis of the selected building archetypes. It elaborates on typical design details while providing an in-depth representation of torsional irregularities using various torsional irregularity indices recommended in building codes. The dynamic characteristics of these plan-irregular buildings are examined through the development of detailed finite element models. The chapter addresses the selection of ground motions and explores the SSP employed to derive rotational ground motions. Lastly, the response spectra of horizontal and rotational ground motions are compared.

Chapter 4

Peak Floor Acceleration

4.1 Introduction

This chapter presents the results of a numerical study on estimating PFA demands and their amplification due to varying extents of nominal torsion in the building. It also examines the effects of inelasticity (ductility demands) and the influence of the rotational ground motions on torsionally irregular RCMRF buildings, as described in Chapter 3. These buildings are analyzed in their elastic and inelastic states using time history analyses for five different levels of ductility demands in buildings. In total, 14,400 linear and non-linear dynamic time history analyses are conducted on the considered buildings, subjected to a suite of far field ground motion records, discussed in Chapter 3. This chapter aims to evaluate the distribution of the PFA demands across the building's floor plan and along the height, compare them with the existing code provisions, and offer insights into amplification in PFA demands (both qualitatively and quantitatively) due to building torsion subjected to the lateral translational ground motions alone, and combined lateral translational and rotational ground motions.

4.2 Peak floor acceleration demands

To date, seismic design codes [6, 16, 17, 27] provide simplified expressions to estimate the in-structure amplification factor (defined as the ratio between the PFA and PGA) and subsequently the PFA demands in the buildings. These expressions assume a linearly increasing distribution of PFA/PGA along the building height, based on the premise that the fundamental vibrational mode governs the building's response. However, this assumption is reasonable only for low-rise buildings that exhibit purely translational responses under earthquake excitations. This PFA/PGA indicates how much the ground motion is amplified at various floors within a building during

an earthquake. Thus, the accurate estimation of PFA is vital for evaluating the seismic vulnerability of rigid secondary systems that are sensitive to accelerations transmitted by the building at their point of attachment.

To investigate the PFA demands in the considered buildings, the absolute floor acceleration time histories in the X-direction at each floor level are extracted across the FF_{ij} and SF_{ij} frames distributed in the building's floor plan, including at the CR and the CS, for the analyzed levels of the SRs (i.e., the elastic case and the inelastic cases with SR of 1, 2, 3, and 4). A total of 3,16,800 PFAs and PFA/PGA (distributed across different nodes and floor levels of the buildings) are estimated and compared with provisions of seismic design codes [6, 16, 17]. For the investigated buildings, it is observed that the positions of the SE and the FE do not switch over at different floors while determined using the mode-superposition method. Further, the PFA demands estimated with respect to the CR are observed to be, in general, conservative compared to the CS, as observed in Figures 4.1–4.2. Therefore, from here onwards, all the discussions are conducted for the PFA/PGA at the CR on the floor plan. Grey lines in plots show the PFA/PGA from a given ground motion, and colored lines show their median and the corresponding design codes' predicted values.

It is worth noting that PFA/PGA estimation in ASCE 7 depends on the building characteristics (i.e., T_1 and level of inelasticity) and the floor level of interest. In contrast, EC 8 and IS 16700 recommend PFA/PGA only, dependent on the floor level of interest. The variation of PFA/PGA at the critical locations such as extreme edges, i.e., FF_{1j} (FE) and SF_{1j} (SE) frames along with the CR provides insights into the influence of nominal torsion across the floor plan on PFA demands. To maintain conciseness, plots of 4- and 8-story T-shaped ETI, WTI, and NTI buildings are presented in this Chapter. The plots of the PFA/PGA responses for other building configurations are included in the Appendix A (Figures A.1–A.24).

Figures 4.1 and 4.2 illustrate the height-wise variation of the PFA/PGA at the CS, the CR, the SE, and the FE alongside comparisons with corresponding code-predicted values. Additionally, Figures 4.3–4.8 depict the in-plan distribution of the PFA/PGA across various floor levels, accompanied by the respective

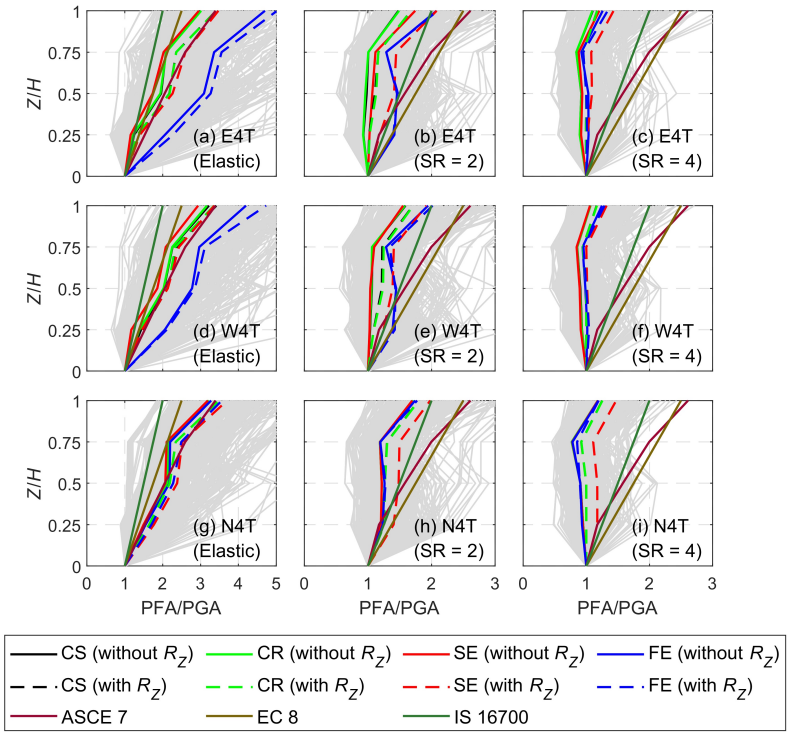

Figure 4.1: PFA/PGA at various locations on the floor plan of the 'E4T', 'W4T', and 'N4T' buildings.

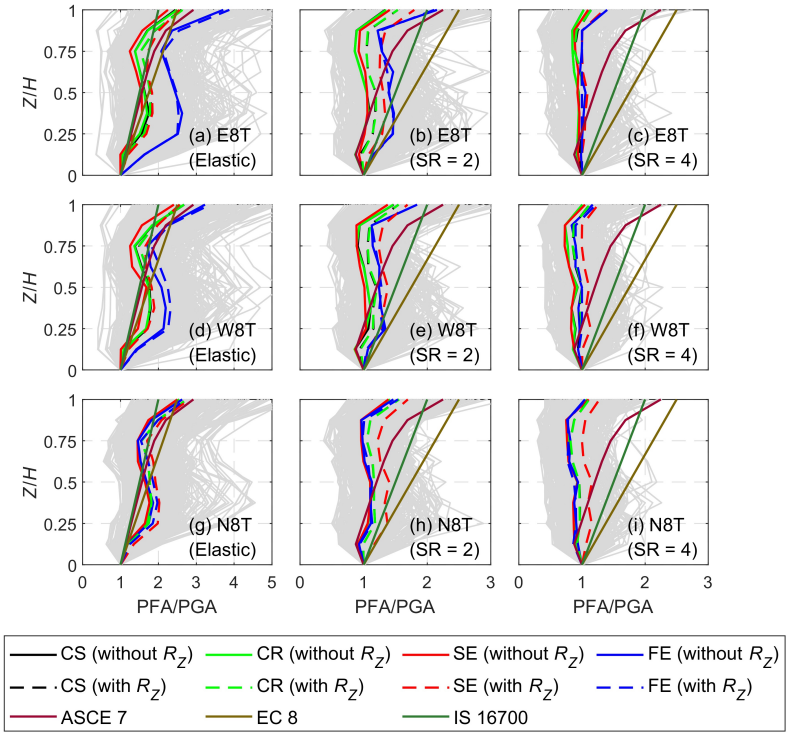

Figure 4.2: PFA/PGA at various locations on the floor plan of the 'E8T', 'W8T', and 'N8T' buildings.

code-predicted values. Table 4.1 provides a summary of the median PFA/PGA values at two critical locations height-wise, i.e., Z/H=0.25 (at a lower floor, where

torsional effects are maximum), and Z/H=1.00 (at the roof, where the amplification effects are maximum) for all building configurations, encompassing both elastic and inelastic cases. The PFA/PGA values obtained from bi-directional time history analyses (X and Y) and tri-directional time history analyses (X, Y, and R_Z) are presented in figures for a comprehensive evaluation.

At the lower floor level (Z/H=0.25) of 4-story buildings exhibiting elastic response, the median PFA/PGA at the CR for ETI, WTI, and NTI buildings are measured as 1.26, 1.39 (Figure 4.1(d)), and 1.52 (Figure 4.1(g)), respectively. These values are comparable to the corresponding values at the SE (1.23, 1.21, and 1.50 (Figures 4.1(g), 4.7(a)), respectively). However, at the FE, the median PFA/PGA values are significantly larger, reaching 2.06 for ETI (Figures 4.1(a), 4.3(a)) and WTI (Figures 4.1(d), 4.5(a)) buildings and 1.55 for the NTI (Figures 4.1(g), 4.7(a)) building. At the roof level (Z/H=1.00), the median PFA/PGA increases substantially across all critical locations due to amplified inertial effects at higher elevations, where the building's dynamic response is more pronounced. At the CR, these values are 3.37, 3.27, and 3.24 for ETI, WTI, and NTI buildings, respectively, which are quite comparable with the corresponding values of 3.40, 3.15, and 3.23 at the SE, while the FE experiences the largest median in-structural amplification ratios, reaching to 4.92, 4.23, and 3.28 (Figures 4.1(g), 4.7(d)) for ETI, WTI, and NTI buildings, respectively. The significantly increased PFA/PGA responses at the FE of ETI and WTI buildings can be attributed to the torsional amplification of accelerations, which has pronounced effects at the extreme edges of the building.

For the 8-story buildings exhibiting elastic response, the median PFA/PGA at Z/H=0.25 are generally higher compared to their 4-story counterparts due to increased participation of higher modes in relatively taller buildings, which contributes primarily in the bottom half of the building. At the CR, the median PFA/PGA are 1.58, 1.73, and 1.69 (Figure 4.2(g)) for ETI, WTI, and NTI buildings, respectively. These values marginally exceed the corresponding SE values of 1.42, 1.47, and 1.69 for ETI, WTI, and NTI buildings but consistently remain lower than the FE values measured as 2.51 (Figures 4.2(a), 4.4(a)), 2.25, and 1.74 (Figures 4.2(g), 4.8(a)), respectively. The higher median PFA/PGA at the FE underscores

Table 4.1: Median PFA/PGA for the investigated buildings.

Building	4-Story						8-Story					
	$Z/H = 0.25$			$Z/H = 1.00$			$Z/H = 0.25$			$Z/H = 1.00$		
	FE	CR	SE	FE	CR	SE	FE	CR	SE	FE	CR	SE
Elastic												
E-T	2.06	1.22	1.15	4.70	3.01	2.96	2.51	1.50	1.37	3.71	2.49	2.25
E-U	1.90	1.23	1.23	4.92	3.37	3.40	2.46	1.58	1.42	3.73	2.68	2.37
E-S	2.04	1.16	1.16	4.54	3.17	3.17	2.42	1.56	1.37	3.72	2.57	2.30
E-R	2.05	1.26	1.12	4.65	3.13	3.01	2.46	1.53	1.39	3.74	2.58	2.28
W-T	2.06	1.39	1.17	4.20	3.17	2.94	2.14	1.67	1.46	3.23	2.68	2.41
W-U	2.01	1.32	1.21	4.23	3.27	3.15	2.25	1.73	1.47	3.25	2.67	2.34
W-S	1.92	1.27	1.16	4.09	3.18	2.87	2.15	1.65	1.38	3.20	2.54	2.13
W-R	1.86	1.33	1.15	4.00	3.19	2.73	1.97	1.69	1.47	3.09	2.60	2.31
N-T	1.55	1.52	1.50	3.28	3.22	3.19	1.74	1.69	1.64	2.63	2.55	2.50
N-U	1.42	1.40	1.39	3.28	3.17	3.09	1.70	1.65	1.62	2.58	2.50	2.47
N-S	1.50	1.50	1.50	3.08	3.08	3.08	1.70	1.69	1.69	2.54	2.54	2.53
N-R	1.52	1.51	1.50	3.25	3.24	3.23	1.64	1.63	1.62	2.51	2.48	2.45
SR = 2												
E-T	1.42	0.92	1.02	2.08	1.49	1.74	1.46	0.99	1.02	2.15	1.35	1.41
E-U	1.25	0.92	1.00	2.12	1.77	1.92	1.50	0.98	0.99	2.17	1.44	1.59
E-S	1.36	1.01	1.04	1.99	1.70	1.89	1.42	0.94	1.00	2.00	1.42	1.50
E-R	1.51	1.01	1.01	2.16	1.72	1.89	1.45	0.98	0.99	2.16	1.35	1.49
W-T	1.39	1.03	1.03	1.95	1.58	1.55	1.34	1.04	1.04	1.84	1.47	1.38
W-U	1.30	0.99	1.03	1.96	1.62	1.80	1.38	1.06	0.98	2.02	1.51	1.42
W-S	1.32	0.98	0.99	1.96	1.67	1.73	1.41	1.11	1.01	1.94	1.51	1.44
W-R	1.36	1.01	0.98	2.00	1.67	1.61	1.28	1.06	1.00	1.90	1.49	1.38
N-T	1.23	1.21	1.20	1.74	1.72	1.70	1.11	1.07	1.06	1.47	1.41	1.39
N-U	1.15	1.13	1.11	1.69	1.64	1.61	1.08	1.08	1.09	1.49	1.48	1.49
N-S	1.17	1.15	1.16	1.60	1.60	1.63	1.14	1.13	1.12	1.47	1.47	1.45
N-R	1.17	1.16	1.15	1.75	1.72	1.68	1.12	1.10	1.09	1.51	1.46	1.42
SR = 4												
E-T	1.04	0.90	0.92	1.26	1.10	1.21	1.01	0.94	0.95	1.40	1.03	1.10
E-U	1.04	0.94	0.96	1.32	1.19	1.31	0.98	0.93	0.99	1.40	1.01	1.14
E-S	1.05	0.94	0.96	1.27	1.12	1.25	1.01	0.94	0.97	1.34	1.05	1.16
E-R	1.10	0.89	0.92	1.49	1.13	1.28	1.03	0.90	0.94	1.36	1.02	1.14
W-T	1.02	0.93	0.91	1.25	1.07	1.06	0.96	0.89	0.83	1.17	1.01	1.05
W-U	1.02	0.92	0.89	1.23	1.13	1.14	1.00	0.90	0.82	1.25	1.11	1.13
W-S	1.06	0.92	0.93	1.35	1.13	1.16	0.98	0.94	0.92	1.19	1.11	1.12
W-R	1.04	0.89	0.89	1.29	1.13	1.12	0.92	0.86	0.84	1.23	1.01	1.05
N-T	0.93	0.95	0.95	1.19	1.18	1.19	0.91	0.89	0.87	1.05	1.08	1.11
N-U	0.94	0.94	0.94	1.12	1.12	1.13	0.95	0.92	0.92	1.11	1.13	1.13
N-S	0.89	0.90	0.89	1.09	1.09	1.09	0.91	0.90	0.90	1.07	1.07	1.07
N-R	0.97	0.95	0.94	1.11	1.09	1.09	0.91	0.88	0.84	1.06	1.05	1.06

Note: Median values are color-coded using a gradient across all buildings: light red for the lowest median values, yellow for mid-range values, and green for the highest median values.

the vulnerability of rigid secondary systems at FEs in taller buildings due to mode coupling and the localization of higher mode effects. Interestingly, at the roof

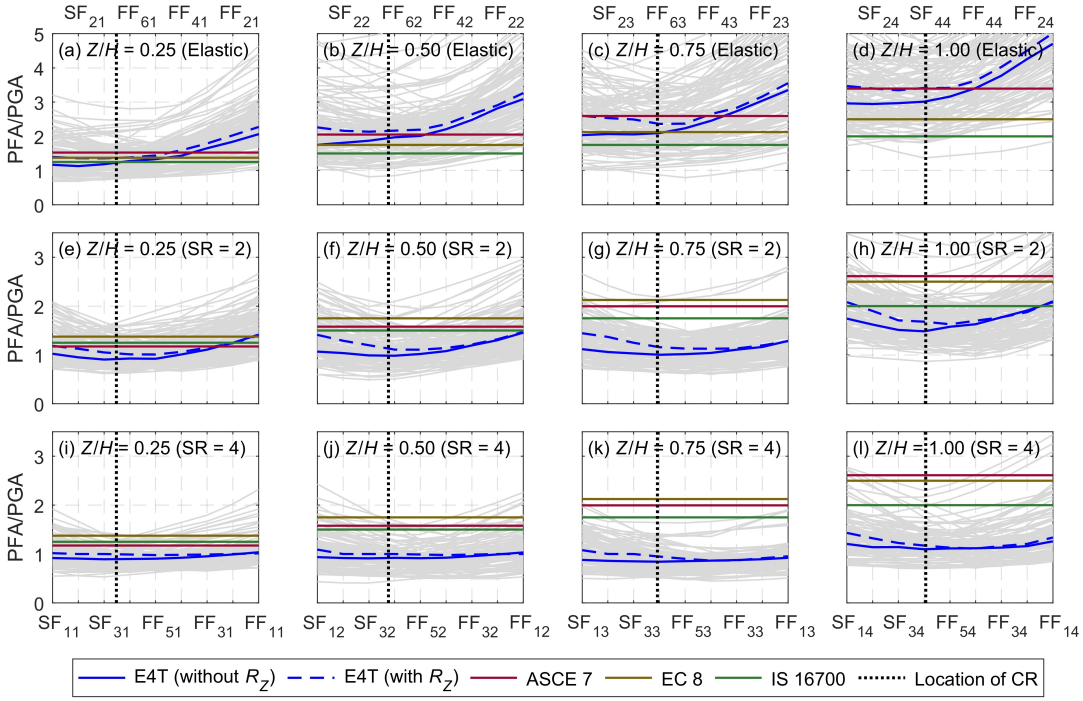

Figure 4.3: In-plan distribution of PFA/PGA at different floors of the 'E4T' building.

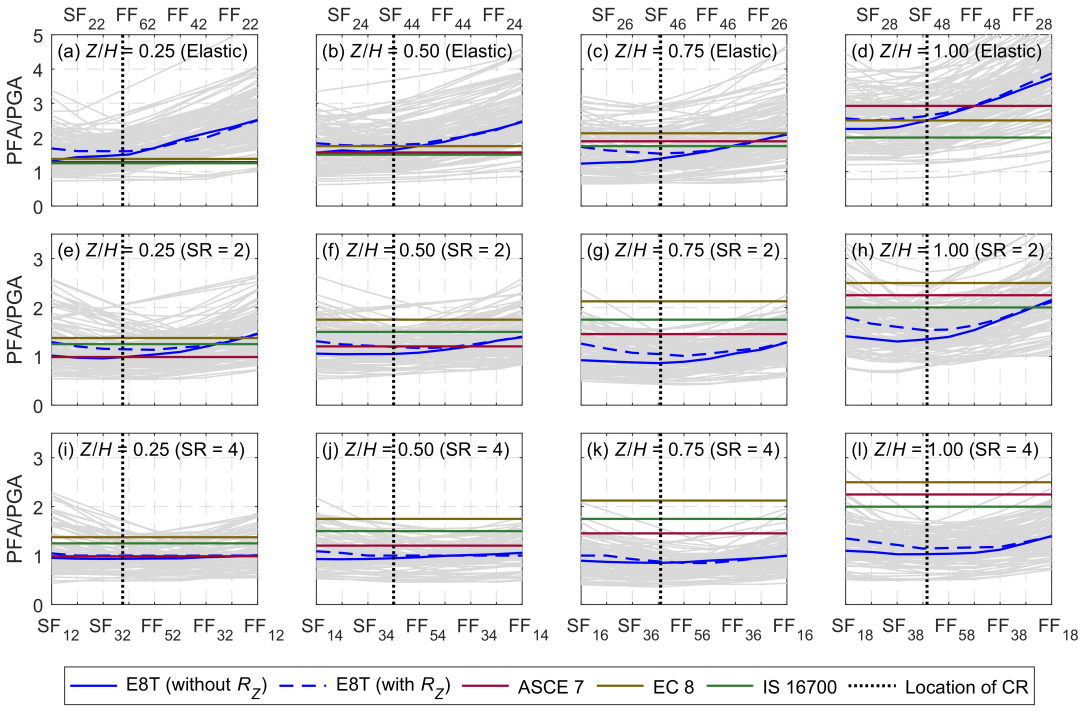

Figure 4.4: In-plan distribution of PFA/PGA at different floors of the 'E8T' building.

level (Z/H=1.00), the median PFA/PGA for the 8-story buildings is lower than their 4-story counterparts. At the CR, the median PFA/PGA decreased to 2.68, 2.68 (Figures 4.2(d)), and 2.55 (Figures 4.2(g)) for ETI, WTI, and NTI buildings,

respectively. A similar trend is observed at the SE, with in-structure amplification ratios of 2.37, 2.41 (Figures 4.2(d), 4.6(d)), and 2.53, respectively. However, the FE still experiences the largest in-structure amplification ratios of 3.74, 3.25, and 2.63 (Figures 4.2(g), 4.8(d)) for ETI, WTI, and NTI buildings. This decrease in the median PFA/PGA at Z/H=1.00 for 8-story buildings can be primarily attributed to their increased flexibility in comparison to the 4-story building.

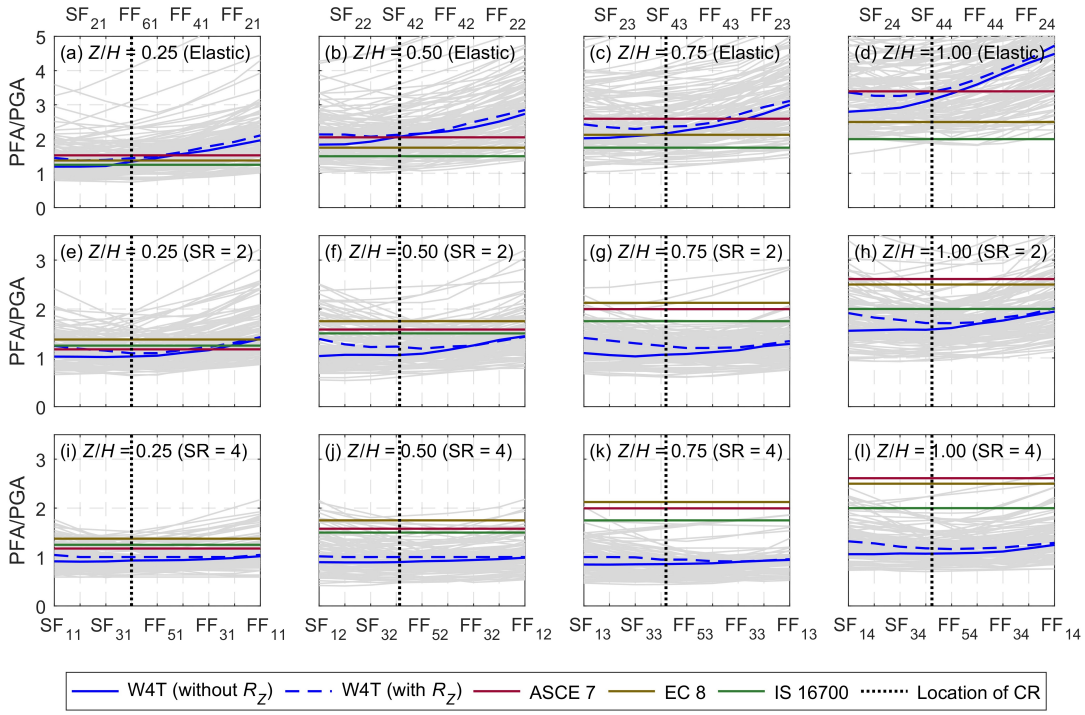

Figure 4.5: In-plan distribution of PFA/PGA at different floors of the 'W4T' building.

It is worth noting that across the floor plan, the most critical values of PFA/PGA usually occur at one of the extreme edges of the floor, i.e., FE (i.e., FF_{1j}) in ETI and WTI buildings, whereas at the SE in NTI buildings. Figure 4.9 presents the overestimation (shown by a light green shaded region) and underestimation (shown by a light red shaded region) between the median PFA/PGA and the corresponding code predicted values for all the analyzed buildings under their elastic and inelastic responses (SRs equal to 1, 2, 3, and 4). In the case of buildings exhibiting elastic response, ASCE 7 consistently tends to underestimate the median PFA/PGA. Specifically, for stiff frames (SF_{1j} to SF_{4j}), these underestimations reach a maximum of 32% for ASCE 7 (Figure 4.9(a)), 34% for EC 8 (Figure 4.9(b)), and 68% for IS 16700 (Figure 4.9(c)), across all the examined buildings.

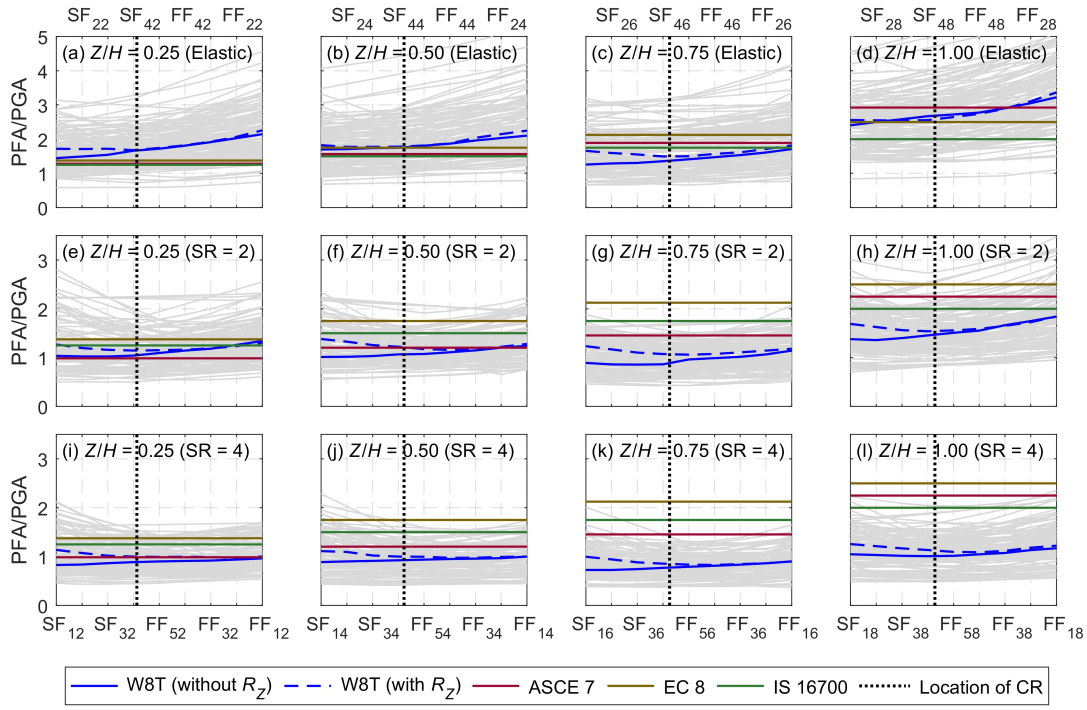

Figure 4.6: In-plan distribution of PFA/PGA at different floors of the 'W8T' building.

Across all building types, ASCE 7, EC 8, and IS 16700 underestimated the median PFA/PGA, even at the CR up to 23% (Figure 4.2(d)), 28% (Figure 4.1(d)), and 60% (Figure 4.1(d)), respectively. For the flexible frames (FF_{1j} to FF_{6j}), these underestimation trends gradually intensify, reaching up to 96% for ASCE 7 (Figures 4.2(a) and 4.9(a)), 90% for EC 8 (Figures 4.1(a) and 4.9(b)), and 137% for IS 16700 (Figures4.1(a) and 4.9(c)).

For buildings exhibiting moderately inelastic response (SR = 2), the median PFA/PGA values reveal distinct trends influenced by torsional irregularity and inelastic energy dissipation. At the lower floor level (Z/H=0.25) of the 4-story buildings, the median PFA/PGA values at the CR and the SE for ETI, WTI, and NTI buildings remain closely aligned, with values near unity, specifically 1.01, 1.03 (Figures 4.1(e)), 1.21 (Figure 4.1(h)), and 1.04, 1.03 (Figures 4.1(e) and 4.5(e)), 1.20 (Figures 4.1(h) and 4.7(e)), respectively. However, at the FE, the values, though reduced compared to their elastic counterpart, still experience relatively larger values compared to the CR and the SE, reaching 1.51 for ETI, 1.39 (Figures 4.1(e) and 4.5(e)) for WTI, and 1.23 (Figures 4.1(h) and 4.7(e)) for NTI buildings. These elevated values at the FE highlight an important fact that, despite inelastic

energy dissipation in buildings, torsional amplification continues to dominate at the FE. At the roof level (Z/H=1.00), the median PFA/PGA values increase notably across all critical locations due to larger inertial effects at higher elevations. The values at the CR and the SE for ETI, WTI, and NTI buildings are 1.77, 1.67, 1.72 (Figures 4.1(h)), and 1.92, 1.80, 1.70 (Figures 4.1(h) and4.7(h)), respectively. However, the FE experiences the highest in-structure amplification ratio, with values reaching 2.16 for ETI, 2.00 for WTI, and 1.75 for NTI buildings. This confirms that torsional irregularity continues to concentrate accelerations at FEs even in buildings exhibiting moderately inelastic response.

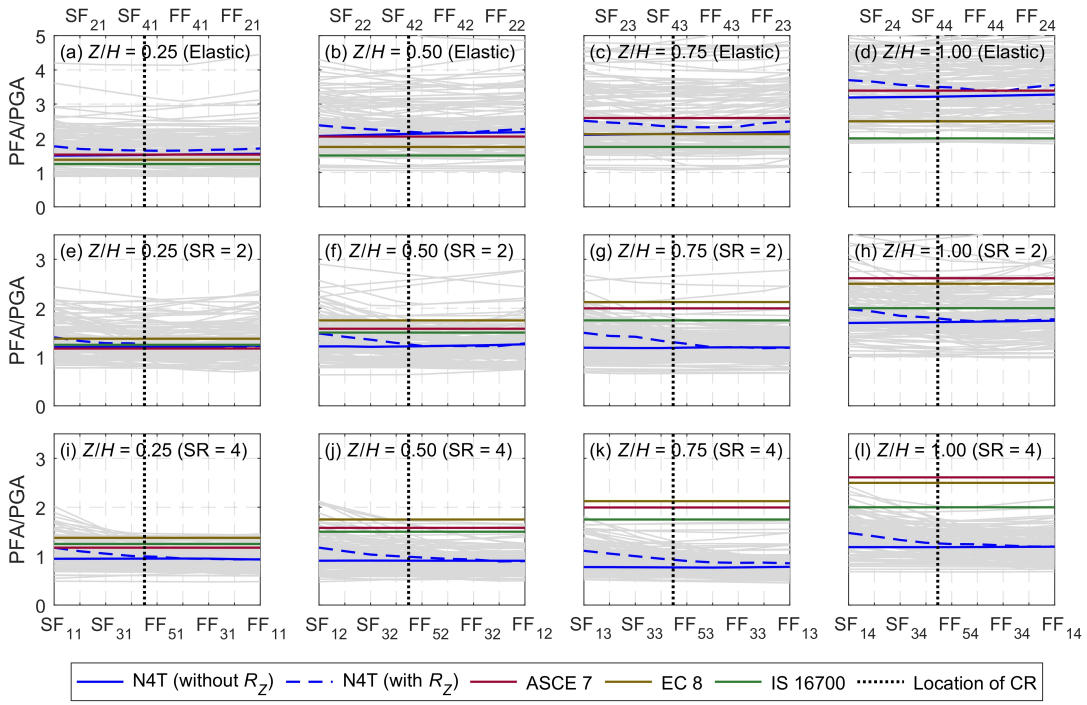

Figure 4.7: In-plan distribution of PFA/PGA at different floors of the 'N4T' building.

For 8-story buildings exhibiting moderately inelastic response (SR = 2) at Z/H=0.25, the median PFA/PGA values at the CR and the SE for ETI, WTI, and NTI buildings are 0.99 (Figures 4.2(b)), 1.11, 1.13, and 1.02 (Figures 4.2(b), 4.4(e)), 1.04 (Figures 4.2(e), 4.8(e)), 1.12, respectively. In contrast, the FE exhibits higher values, reaching 1.50 for ETI, 1.41 for WTI, and 1.14 for NTI buildings. At the roof level (Z/H=1.00), the median PFA/PGA values for 8-story buildings are notably smaller compared to the 4-story counterparts. The median PFA/PGA values at the CR and SE for ETI, WTI, and NTI buildings are 1.44, 1.51, and

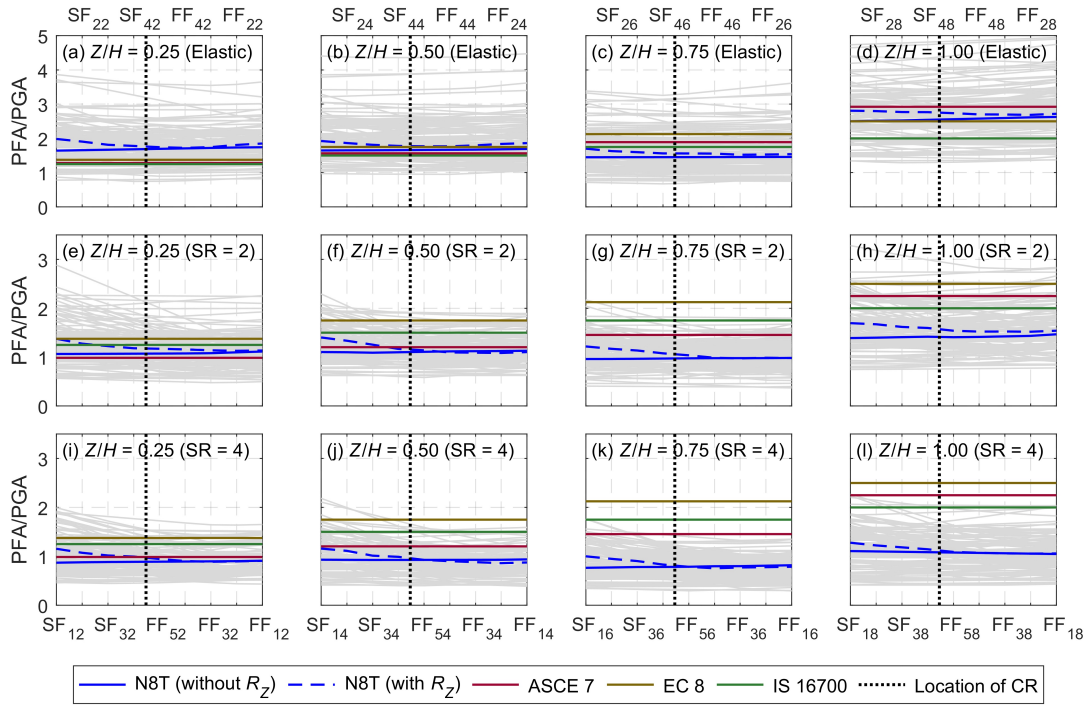

Figure 4.8: In-plan distribution of PFA/PGA at different floors of the 'N8T' building.

1.48 at the CR and 1.59, 1.44, and 1.49 at the SE, respectively. The FE still experiences the largest accelerations, with values reaching 2.17 for ETI, 2.02 for WTI, and 1.51 for NTI buildings. Among the investigated codes, the provisions of EC 8 and IS 16700 provide a reasonable estimate of the median PFA/PGA for the 8-story buildings at the CR and the SE, whereas the ASCE model underpredicted the median PFA/PGA for the 8-story buildings, even at the CR up to 12% (Figure 4.9(g)), and the SE up to 8% (Figure 4.9(g)). In addition, provisions of all codes underpredicted the PFA/PGA at the FE. This underestimation at the FE can be up to 54% (Figures 4.2(b), 4.4(e), 4.9(g)), 12% (Figure 4.9(h)), and 23% (Figure 4.9(i)) for ASCE 7, EC 8, and IS 16700, respectively.

In buildings exhibiting highly inelastic response (SR = 4), the median PFA/PGA significantly reduces to 1.10 (Figures 4.1(c), 4.4(i)) at Z/H=0.25 and 1.49 (Figures 4.1(c), 4.4(l)) at Z/H=1.00 across all 4- and 8-story buildings. In this specific case, the provisions of all codes provided reasonable estimates of the PFA/PGA at all the locations on the floor plan of 4-story buildings. It is primarily due to the fact that in this specific case of buildings exhibiting highly inelastic response, the beneficial effect of the building inelasticity on the PFA/PGA demands

(i.e., reduction) supersedes the negative effect (i.e., increase) of the building torsion, particularly for EC 8 and IS 16700 (as these codes do not consider the effect of building inelasticity in the PFA/PGA estimation). In contrast, for 8-story buildings exhibiting highly inelastic response (SR = 4), only ASCE underestimated the PFA/PGA at the CR up to 10% (Figure 4.9(m)), at the SE up to 8% (Figure 4.9(m) and at the FE up to 20% (Figure 4.9(m)).

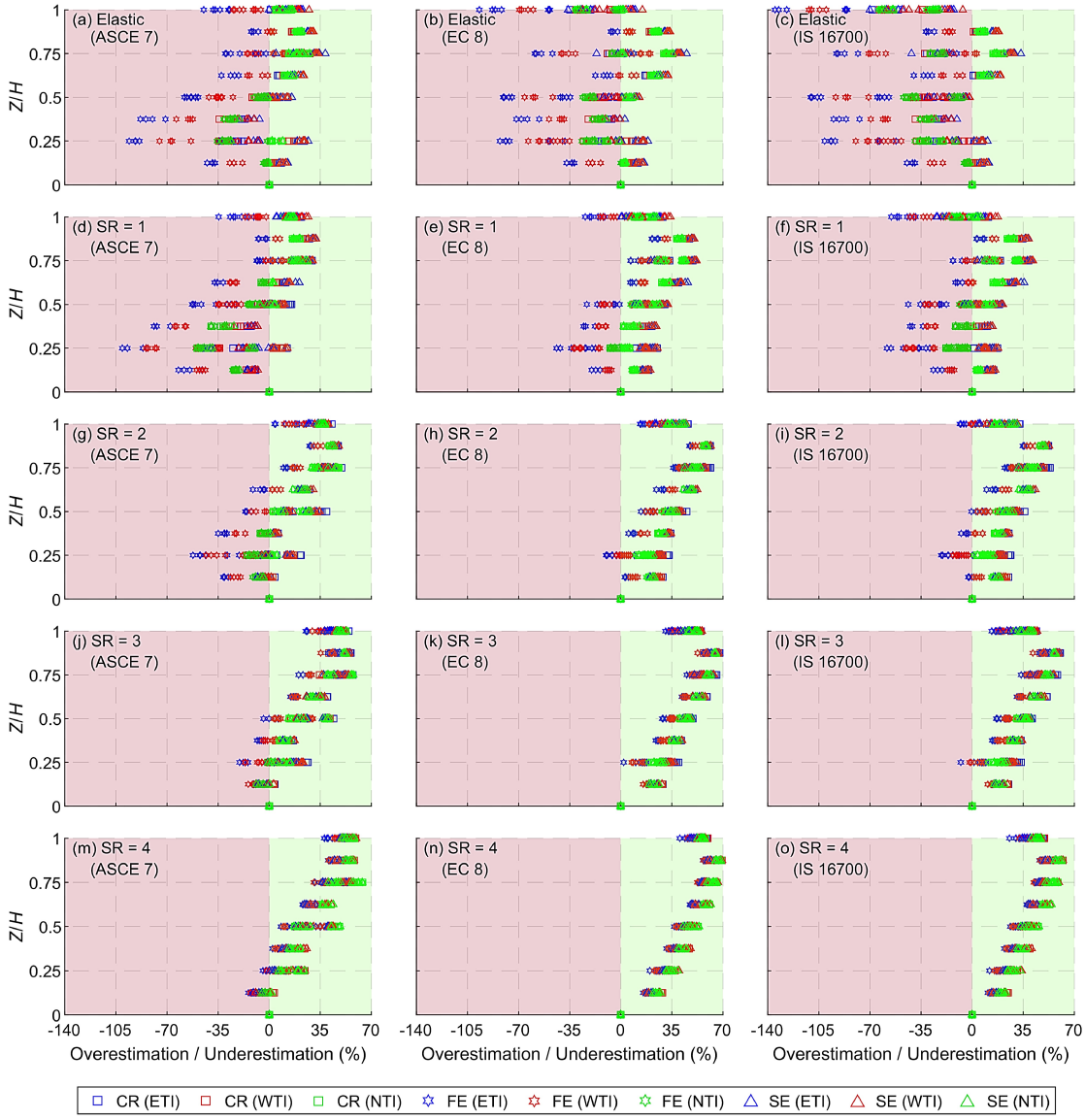

Figure 4.9: Overestimation/underestimation of the PFA/PGA distributions at the center of rigidity, extreme stiff edge, and extreme flexible edge with respect to code provisions.

These underestimations in PFA demands (Figure 4.9) using code models can be primarily attributed to the absence of parameters in the code's PFA prediction equations to take care of possible acceleration amplification due to building torsion.

Further, ASCE 7 uses the relative height (Z/H), the fundamental period of the building, and the level of the building's inelastic response (ductility demand) in estimating PFA demands, whereas EC 8 and IS 16700 estimate PFA demands as a function of the relative height (Z/H) without taking into care the fundamental period and inelasticity of the building. As PFA demand prediction in ASCE 7 is a function of the building inelasticity; hence, ASCE 7 underestimated PFA demands by larger magnitudes compared to EC 8 and IS 16700 (where beneficial effects of building inelasticity on PFA demands are counterbalanced by the building torsion), particularly under inelastic response of buildings (i.e., SRs = 1, 2, 3, and 4). In addition to this, EC 8 and IS 16700 amplify this PFA/PGA underestimation further (especially more for shorter period buildings), as these codes do not include building-specific parameters, i.e., the fundamental period of the building in the estimation of the PFA/PGA.

4.3 Influence of rotational ground motions

The effects of the rotational ground motions on the median PFA/PGA demands for the investigated buildings are depicted along the height and across the floor plan, using dashed lines, in Figures 4.1–4.2 and Figures 4.3-4.8, respectively. Table 4.2 summarizes the influence of the rotational ground motions on PFA demands in the investigated buildings. The effects of rotational ground motions on PFA demands are summarized in percentages using the median estimate at two different relative heights, i.e., at $Z/H = 0.25$ and 1.00, for all the investigated buildings.

To illustrate the detailed influence of the rotational ground motions, the median PFA/PGA demands for a suite of ground motion records are discussed. This broader assessment highlights general trends and ensures that the findings are representative, accounting for record-to-record variability in the inferences. Table 4.2 presents the median increase in PFA/PGA due to the rotational ground motions. The median values are visually represented using a gradient color profile, where green indicates the maximum value, light red represents the minimum value, and yellow corresponds to the intermediate value at different edges of the building (Table 4.2). In the following discussions, the overall median influence of the rotational ground motions on PFA/PGA responses across all the investigated buildings is presented.

Table 4.2: Median increase (%) in PFA/PGA due to rotational ground motions.

Building	4-Story						8-Story					
	$Z/H = 0.25$			$Z/H = 1.00$			$Z/H = 0.25$			$Z/H = 1.00$		
	FE	CR	SE	FE	CR	SE	FE	CR	SE	FE	CR	SE
Elastic												
E-T	10	9	21	7	13	17	0	8	23	4	6	14
E-U	4	6	16	-1	4	20	1	4	24	1	5	25
E-S	4	17	25	7	12	20	-4	8	21	-1	4	17
E-R	7	7	28	3	11	19	-1	8	23	-1	4	15
W-T	2	4	24	13	6	15	6	0	18	4	-3	6
W-U	5	10	22	14	14	21	1	2	23	7	4	13
W-S	7	14	29	11	8	24	4	2	28	7	5	24
W-R	5	9	20	11	6	23	9	2	19	1	4	10
N-T	10	8	18	9	8	16	6	3	21	3	8	12
N-U	17	16	24	15	11	20	8	5	18	8	10	12
N-S	11	6	14	17	15	23	4	2	17	3	6	13
N-R	8	6	15	9	9	17	10	7	24	8	11	17
SR = 2												
E-T	-1	11	16	1	13	19	0	15	27	-2	14	27
E-U	-1	9	14	4	5	17	-8	19	36	0	15	14
E-S	-3	7	25	1	5	16	1	21	36	5	8	25
E-R	0	5	30	3	4	14	2	12	29	-3	10	20
W-T	3	6	21	4	8	23	-3	10	22	0	6	23
W-U	0	7	18	-1	14	18	1	11	33	0	13	22
W-S	3	10	25	6	5	24	-3	5	22	1	8	22
W-R	5	8	27	2	6	23	0	7	25	-3	5	26
N-T	3	11	23	3	5	15	2	10	29	5	10	22
N-U	2	5	21	5	9	27	7	9	26	7	8	17
N-S	0	5	18	10	9	22	0	5	25	3	6	19
N-R	-1	2	16	1	3	18	-1	8	28	1	8	23
SR = 4												
E-T	-2	11	11	6	7	19	-1	7	10	0	11	23
E-U	-4	6	5	4	9	21	2	8	1	3	10	12
E-S	3	7	5	8	9	24	-1	6	6	3	6	20
E-R	0	12	11	-1	7	17	-2	11	12	2	10	20
W-T	3	8	14	3	9	25	4	12	37	4	12	20
W-U	0	9	13	4	9	26	0	12	29	2	6	14
W-S	-3	9	11	-1	7	25	2	6	13	6	6	19
W-R	-1	12	21	3	4	22	5	13	36	3	11	25
N-T	0	7	26	3	11	29	0	9	33	1	3	15
N-U	6	7	12	2	7	24	-1	8	28	-2	1	18
N-S	6	12	23	6	10	31	3	11	32	-4	3	20
N-R	1	5	14	3	11	32	0	9	43	4	11	31

Note: Negative median values represent decrease due to R_Z. Median values are color-coded using a gradient across all buildings: light red for the lowest median values, yellow for mid-range values, and green for the highest median values.

In the case of the elastic 4-story buildings, rotational ground motions resulted in an increase in the median PFA/PGA at the SE, up to 31%, 36%, and 28% for the ETI, WTI, and NTI buildings, respectively. Conversely, at the FE, the median PFA/PGA increase is relatively lower, reaching only up to 10%, 14%, and 21%, while at the CR, the increase in the median PFA/PGA is 20%, 15%, and 17%. In the 8-story buildings exhibiting elastic response, the increase in median PFA/PGA due to the rotational ground motions persists, with the maximum increase in the median PFA/PGA reaching up to 47%, 38%, and 34% for the ETI, WTI, and NTI buildings, respectively. At the FE, the increase in the median PFA/PGA reduced to 9%, 14%, and 21%, while at the CR, it is reduced to 13%, 15%, and 21% for the ETI, WTI, and NTI buildings, respectively.

For buildings exhibiting moderately inelastic response (SR = 2), the median PFA/PGA increases due to rotational ground motions; however, it shows a mixed trend when compared to elastic cases. In the 4-story buildings, the SE experiences the highest increase in the median PFA/PGA due to rotational ground motions, reaching 34%, 37%, and 43% for the ETI, WTI, and NTI buildings, respectively. The CR exhibits median PFA/PGA increase of 22%, 17%, and 20% due to rotational ground motions, while the FE records significantly lower median PFA/PGA increase of only 4%, 6%, and 14% for the ETI, WTI, and NTI buildings, respectively. In contrast, for the 8-story buildings exhibiting moderately inelastic response (SR = 2), the SE continues to record the highest median PFA/PGA increase due to rotational ground motions with values increasing to 47%, 53%, and 40% for the ETI, WTI, and NTI buildings, respectively. At the CR, the median PFA/PGA increase due to rotational ground motions reaches 29%, 20%, and 17%, while at the FE, it remains minimal at 9%, 9%, and 7% for the ETI, WTI, and NTI buildings, respectively. These findings indicate that the effects of the rotational ground motions are significant, particularly at the SE and the CR, even for moderately inelastic systems, where inelastic energy dissipation takes place in the building.

For 4-story buildings exhibiting highly inelastic response (SR = 4), the SE continues to experience notable median PFA/PGA increase due to the rotational ground motions, with values of 25%, 29%, and 42% for the ETI, WTI, and NTI buildings, respectively. In contrast, the CR shows the median PFA/PGA of 15%,

19%, and 24% for the ETI, WTI, and NTI buildings, while the FE records the lowest levels, at 8%, 4%, and 18%, due to rotational ground motions. In the 8-story buildings exhibiting highly inelastic response (SR = 4), the SE retains its position as the most affected location, with median PFA/PGA increase due to rotational ground motions reaching 24%, 47%, and 45% for the ETI, WTI, and NTI buildings, respectively. At the CR, the increase in the median PFA/PGA reaches 13%, 26%, and 23%, while the FE shows the smallest values, recorded at 7%, 7%, and 8%, due to rotational ground motions.

These results highlight that as building inelasticity increases, the rotational ground motions continue to exert a significant influence at all locations. This is further evident in Table 4.2, where it is clearly visible that the maximum median increase in the PFA/PGA due to rotational ground motions occurs at the SE (highlighted by green color cells). While the CR and the FE experience relatively smaller increases in the median PFA/PGA due to rotational ground motions. When comparing the increase in the median PFA/PGA for 4- and 8-story buildings, the SE in 8-story buildings shows a slightly higher increase in WTI (29% vs. 47%) but a lower increase in NTI (28% vs. 34%). These variations underscore the nuanced influence of building height on the median increase in PFA/PGA due to rotational ground motions.

Among the analyzed cases, 69% exhibited an increase in the PFA/PGA due to the rotational ground motions, while 31% showed a reduction in the PFA/PGA responses. For buildings exhibiting both elastic and inelastic response, the SE consistently experiences the highest increase in the PFA/PGA due to rotational ground motions. The effects of rotational ground motions are more comparable for 4-story and 8-story buildings (up to 43% and 53%, respectively). In general, the building's inelastic response tends to amplify the effect of rotational ground motions, with the effect increasing from 20% (for 'W8R', at the SE) in buildings exhibiting elastic response to 47% (for 'W8R', at the SE) in the buildings exhibiting highly inelastic response. The reduction in the median PFA/PGA due to rotational ground motions reached only 8% (for 'E8R' and 'E8U' buildings at the FE). Interestingly, NTI buildings, despite their lack of presence of nominal torsion (specifically square and rectangular shape), still showed a significant increase, up to 45% (for 'N8R', at

the SE) due to rotational ground motions.

From the presented results, it is clear that both increases and decreases can occur in the median PFA/PGA responses due to rotational ground motions. These effects may arise from either the clockwise or anti-clockwise application of rotational ground motions. It is further important that sometimes both clockwise and anti-clockwise application of the rotational ground motions results in an increase or decrease in the PFA/PGA responses. This behavior is likely governed by the phase relationship between the translational and rotational motions of a building under earthquake excitation. As a result, the critical orientation of the rotational ground motions cannot be determined beforehand. These observations demonstrate the potential of the rotational ground motions to substantially elevate the PFA demands, which can have critical implications on the seismic design of rigid secondary systems.

4.4 Summary

This chapter focuses on the estimation of peak floor accelerations (PFAs) in torsionally regular and irregular buildings, emphasizing the amplification in PFA demands along the building height and across the floor plan due to varying degrees of nominal torsion and inelastic behavior of the building, and also due to rotational ground motions. Utilizing the building models and ground motion records detailed in Chapter 3, a total of 14,400 linear and non-linear time history analyses are conducted across five ductility demand levels, with and without considering the rotational ground motions. Absolute floor acceleration time histories are extracted at various locations across the floor plan, including the CR and the CS, under both elastic and inelastic responses of buildings. A total of 3,16,800 PFAs and PFA/PGA ratios are calculated and compared with provisions of ASCE 7, EC 8, and IS 16700, revealing discrepancies that underline the necessity for improved predictive models for estimating PFA demands in buildings with nominal torsion. Based on the extensive numerical investigations presented in this Chapter, the following are key observations and findings:

- Existing seismic design code provisions consistently underestimated the PFA/PGA in buildings with nominal torsion, especially in buildings exhibiting

elastic and moderately inelastic response, for the flexible as well as stiff frames. The maximum underestimation of the PFA/PGA has been observed under the elastic response of buildings for the extreme flexible frames, with its magnitude reaching up to 96%, 90%, and 137% for ASCE 7, EC 8, and IS 16700, respectively. The underestimations in the PFA/PGA from the ASCE 7 provisions can be attributed to the absence of parameter in code equations to take care of torsional amplification, whereas, in the case of EC 8 and IS 16700, it can be jointly attributed to the absence of building parameters, i.e., the extent of torsion, and the fundamental period.

- Under the elastic response of buildings, nominal torsion increases the PFA/PGA demands at the FE while slightly decreasing them at the SE, compared to the CR. The building inelasticity tends to further reduce the PFA/PGA demands at both the FE and the SE compared to their elastic counterparts. These observations suggest that the floor plan location and building inelasticity-dependent PFA/PGA demand prediction models shall be used in buildings with nominal torsion.

- As the inelastic response of the building increases, the detrimental impact of torsional amplification of the PFA/PGA is mitigated by the beneficial effects of the building's inelasticity. As a result, the EC 8 and IS 16700 provide reasonable estimates of PFA/PGA in highly inelastic torsionally irregular buildings. In contrast, ASCE 7 explicitly incorporates the effect of building inelasticity in the code prediction equation and hence provides non-conservative estimates of the PFA/PGA, even for buildings exhibiting highly inelastic response with nominal torsion.

- The rotational ground motions can significantly increase (or decrease) the PFA/PGA responses across all torsional irregularity categories (ETI, WTI, and NTI) and building inelasticity levels, with the SE consistently experiencing the highest increase. The increasing or decreasing effects on PFA/PFA demands due to rotational ground motions do not correlate with the degree of torsional irregularity in the building.

- Among analyzed cases, in 69% of cases, the rotational ground motions induced

an increase in the PFA/PGA, with the median increase reaching up to 53% (at the SE). Conversely, in 31% of cases, a decrease in the PFA/PGA is observed due to rotational ground motions, with reductions limited to 8% (at the FE). Even in NTI buildings with no nominal torsion (specifically square and rectangular shapes), the rotational ground motions caused a significant increase in the median PFA/PGA, reaching up to 45%.

- Building inelasticity significantly amplified the effects of rotational ground motions, with the median PFA/PGA increasing from 20% in buildings exhibiting elastic response to 47% ('W8R' at the SE) in buildings exhibiting highly inelastic response. Even in NTI buildings, the effects of rotational ground motions on the median PFA/PGA are evident, and the building inelasticity amplified the effects of rotational ground motions from 25% in the buildings exhibiting elastic response to 45% in the buildings exhibiting highly inelastic response (for 'N8R' building). This observation highlights the greater vulnerability of rigid secondary systems, even in inelastic NTI buildings, due to rotational ground motions.

- The median increase in PFA/PGA demands due to rotational ground motions is most significant at the SE, with a maximum increase of up to 53% observed in the 'W8U' building. In comparison, the median increase at the CR and FE is 29% and 21%, respectively. On the other hand, the median reduction in PFA/PGA demands due to rotational ground motions is limited to FE, with a reduction of approximately 8%.

Chapter 5

Floor Response Spectra

5.1 Introduction

This chapter focuses on understanding the characteristics of FRS in buildings with nominal torsion. The absolute acceleration time histories at the various locations on the floor plan are estimated, and subsequently, FRS are generated for the investigated RCMRF buildings under their elastic and inelastic responses. The determination of FRS helps in understanding the acceleration demands on the light-weight, flexible, and very flexible acceleration-sensitive secondary systems subjected to the floor motions. FRS are determined by conducting time history analyses, with and without including the effects of the rotational ground motions. In order to generalize the seismic demands on the light-weight secondary systems and to make a fair comparison with the existing seismic design provisions, the derived FRS are normalized using two different intensity measures, i.e., PFA and PGA. Some recent studies [71, 72, 86, 117, 126] have shown that FRS are amplified GRS, and hence better correlated to the GRS. Accordingly, the derived FRS are also normalized with the input GRS in the direction under consideration.

The first way of normalization of the FRS by PFA results in the *'Component amplification factor'* (a_p), which describes amplification in seismic demands relative to the PFA (mainly underscoring the amplification effects associated with tuning between the primary and the secondary system). In contrast, the normalization of the FRS by PGA results in the *'Total amplification factor'* (a_t), which combines the amplification of the PGA along the building height (discussed in Chapter 4) and amplification due to tuning between the primary and the secondary system (discussed herein). The normalization of the FRS by GRS results in spectral amplification factors (SAFs), which demonstrate the spectral amplification effects at a given floor level of interest with respect to the ground spectral ordinate.

5.2 Characteristics of the floor response spectra

To understand the characteristics of the FRS, the 5%-damped FRS are obtained at critical locations in the floor plan, i.e., the FE, the CR, the CS, and the SE. The FRS shown in grey color lines are the individual ground motion responses, those shown in colored lines are the median responses (Figures 5.1–5.6), and their important characteristics are discussed. Each ordinate of the FRS represents the 5%-damped peak acceleration response of the SDOF secondary system attached at the floor level of interest in the building as a function of the period of the secondary system. To understand these FRS, the observed peaks in FRS can be subdivided into two categories: (i) the peaks in the FRS due to frequency tuning between the building and secondary system, and (ii) the peaks in the FRS which were also in the GRS (as FRS are amplified GRS).

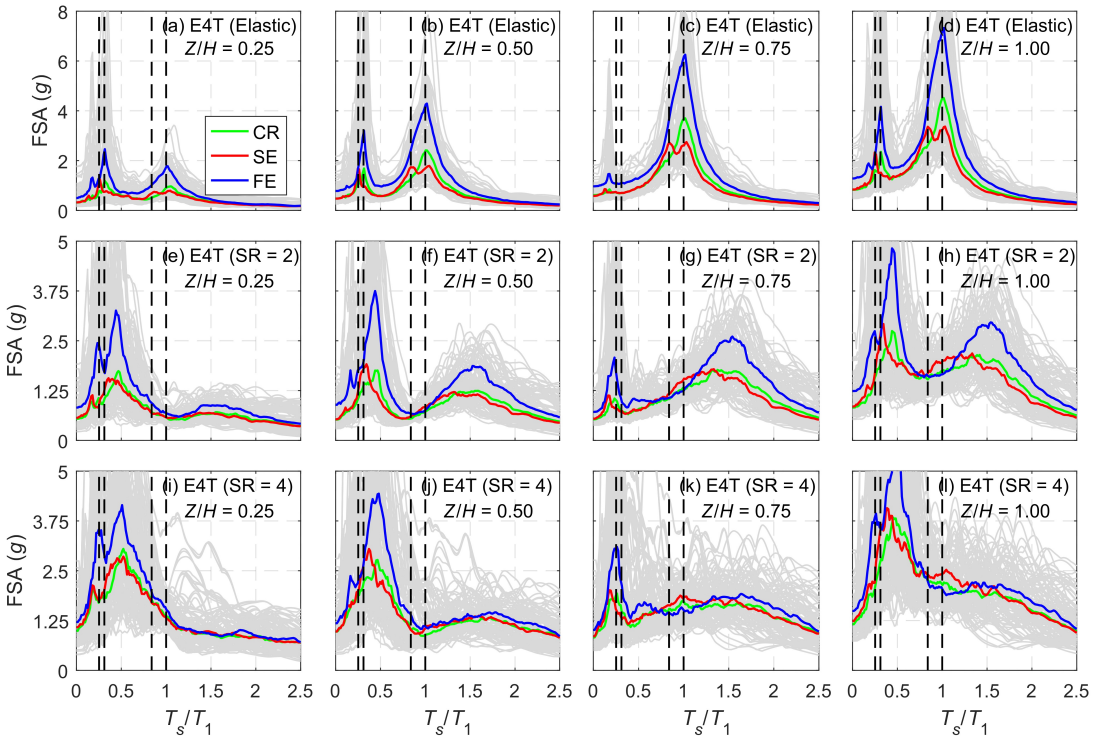

Figure 5.1: Floor response spectra for the 'E4T' building estimated using bi-directional time history analyses. Dashed vertical lines indicate the elastic modal periods in the direction under consideration.

The first and foremost important characteristic of the FRS is that they exhibit multiple sharp peaks (Figures 5.1–5.6) when the secondary system is tuned within the building's fundamental or higher mode regions (the dashed line in the figures

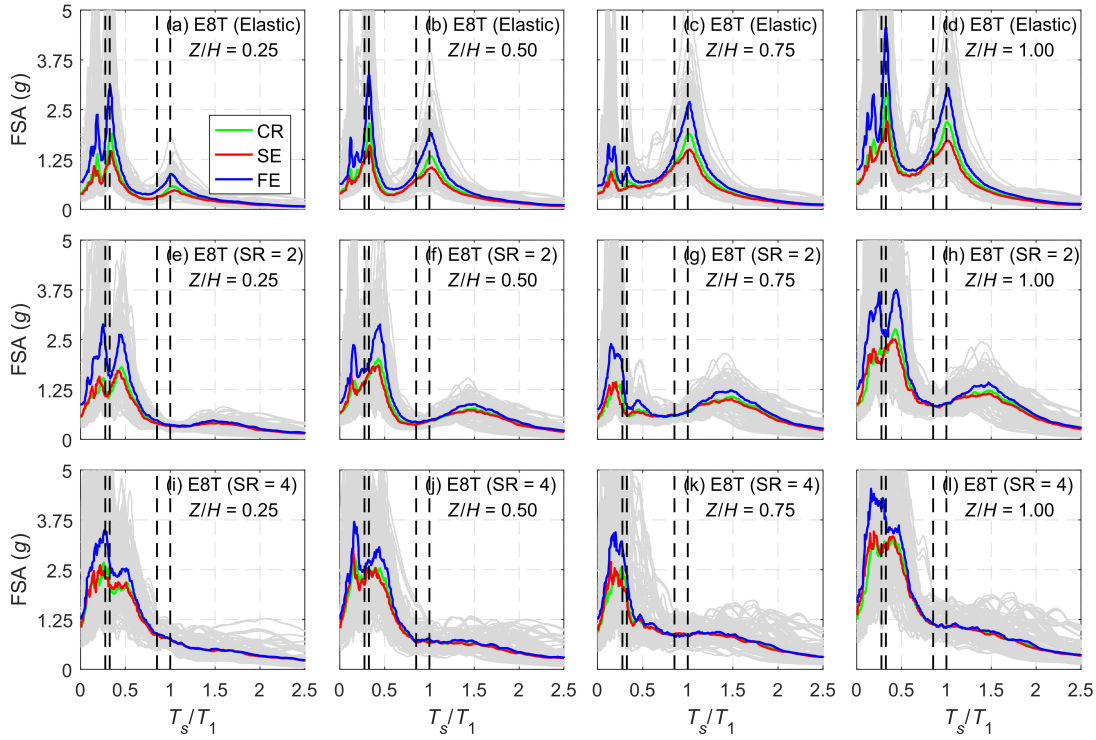

Figure 5.2: Floor response spectra for the 'E8T' building estimated using bi-directional time history analyses. Dashed vertical lines indicate the elastic modal periods in the direction under consideration.

represents the first few modes of vibration of the building, in the direction under consideration). These FRS exhibit significant record-to-record variability (Figures 5.1–5.6), which can be attributed to the variations in the frequency content of different ground motions. It is further important to highlight that most of the light-weight acceleration-sensitive secondary systems have their natural periods in the short-period range, where the secondary systems are expected to be tuned within the building's higher mode region, and a substantial amplification in the acceleration demands on secondary systems can be expected.

The other interesting observation in FRS is about the existence of closely spaced dual peaks in ETI buildings at the SE (Figures 5.1(a)-(d)). These closely spaced dual peaks are more pronounced for the 4-story buildings and relatively insignificant (not distinctly visible) for 8-story buildings (Figures 5.2(a)-(d)). Between these closely spaced dual peaks (Figures 5.1(a)-(d)), the one corresponds to case when the secondary system is in tune with the building's fundamental mode of vibration (where a large mass participated in translation, along with a relatively low mass participated in the building rotation, Table 3.1), whereas, the other corresponds to

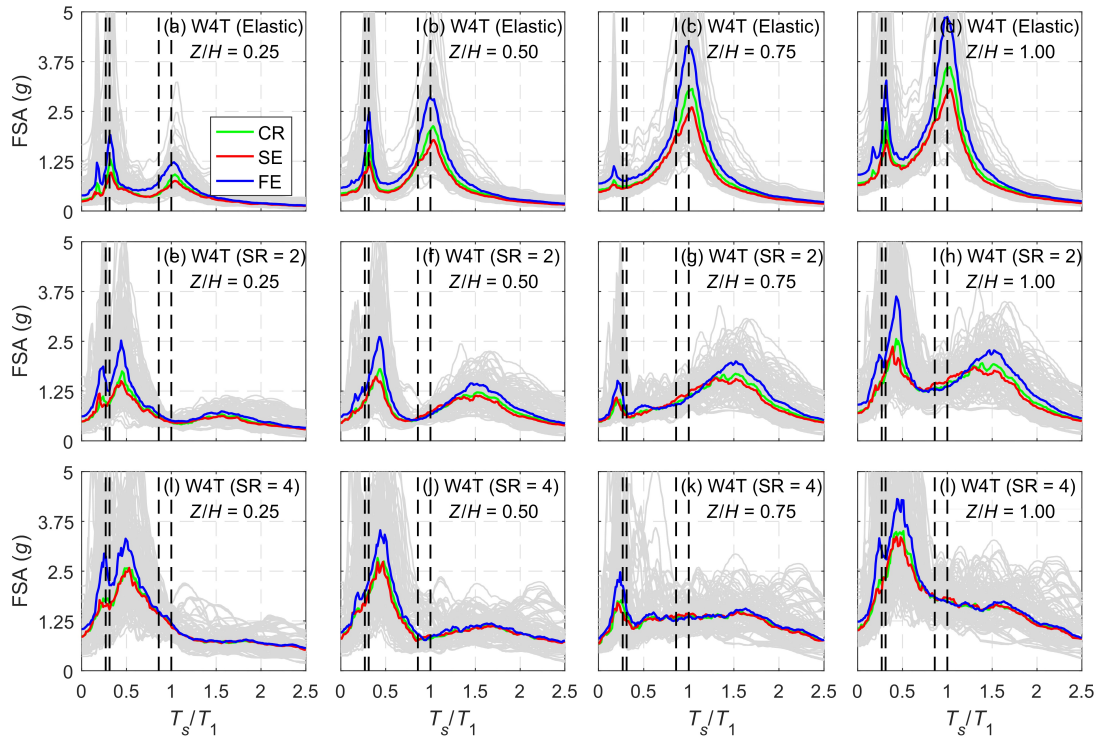

Figure 5.3: Floor response spectra for the 'W4T' building estimated using bi-directional time history analyses. Dashed vertical lines indicate the elastic modal periods in the direction under consideration.

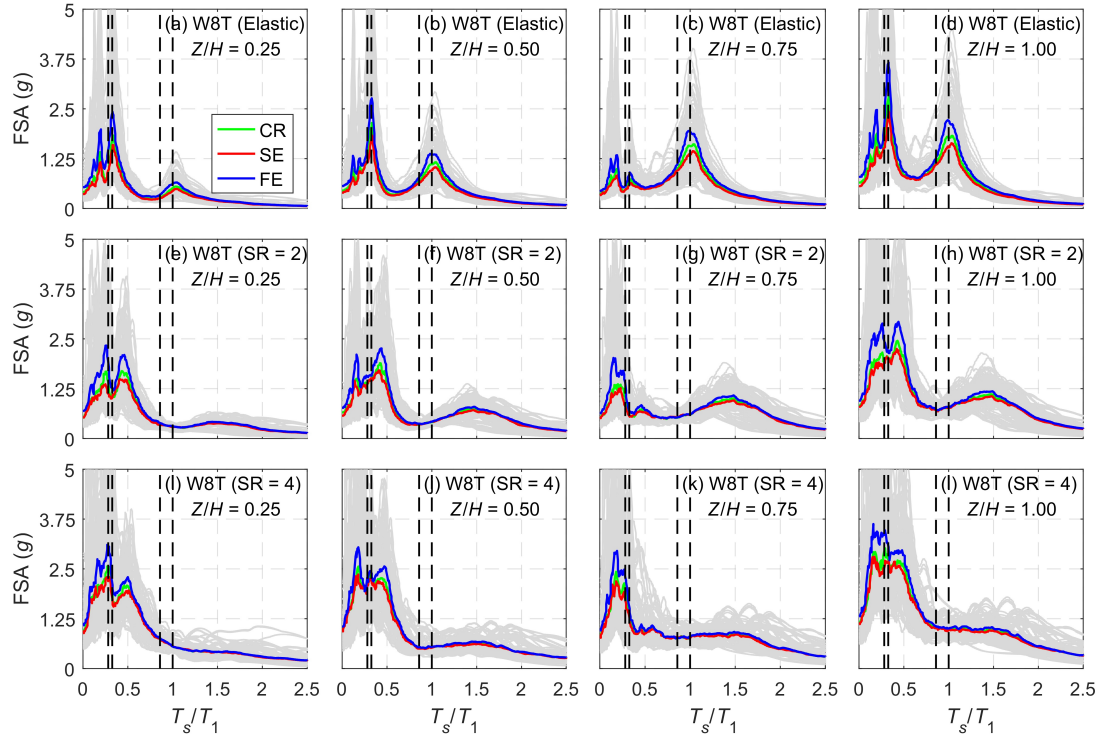

Figure 5.4: Floor response spectra for the 'W8T' building estimated using bi-directional time history analyses. Dashed vertical lines indicate the elastic modal periods in the direction under consideration.

the case when secondary system is in tune with the rotational mode of vibration (where a large mass participated in the building rotation, along with a relatively low mass participated in the translation, Table 3.1). This effect gradually reduces for WTI and NTI buildings (Figures 5.3–5.6), and such closely spaced dual peaks are not visible. This observation can be attributed to reduced mode coupling effects in WTI and NTI buildings.

As the building inelasticity increases, the spectral response associated with the acceleration demands when the secondary system is tuned within the building's fundamental mode region decreases significantly due to energy dissipation, material damping, and stiffness degradation caused by cracking. However, when the secondary system is tuned within the building's higher mode region, the acceleration demands show an increase in the response, as they are less affected by inelastic energy dissipation mechanisms such as yielding and hysteretic damping, which primarily influence the secondary system tuned within the building's fundamental mode region. Furthermore, in ETI buildings (Figures 5.1–5.2), the response at the FE is the highest, followed by the CR and then the SE. As the nominal torsion in the building decreases, the differences in the floor acceleration response between the FE, CR, and SE diminish significantly and eventually converge in NTI buildings (Figures 5.5–5.6).

5.2.1 Component amplification factor

Figures 5.7–5.12 present the FRS normalized by PFA, representing the component amplification factor (a_p). The a_p is obtained at critical locations in the floor plan, i.e., the FE, CR, CS, and SE (individual ground motion results shown by grey color), and their median responses (shown by colored lines) are derived (Figures 5.7–5.12; Tables 5.1–5.2). Similar results are also obtained for the other investigated buildings (the remaining 18), with the corresponding plots summarized in Appendix B (Figures B.1–B.18). The obtained median peak values of a_p in this study are compared with the seismic design code provisions of IS 16700, ASCE 7, and EC 8.

ASCE 7 and IS 16700 specify the maximum a_p values of 2.8 and 2.5, respectively, (independent of the tuning ratio, T_s/T_1, and the floor level), while EC 8 defines a_p as a function of the tuning ratio (T_s/T_1) and the relative height (Z/H), with

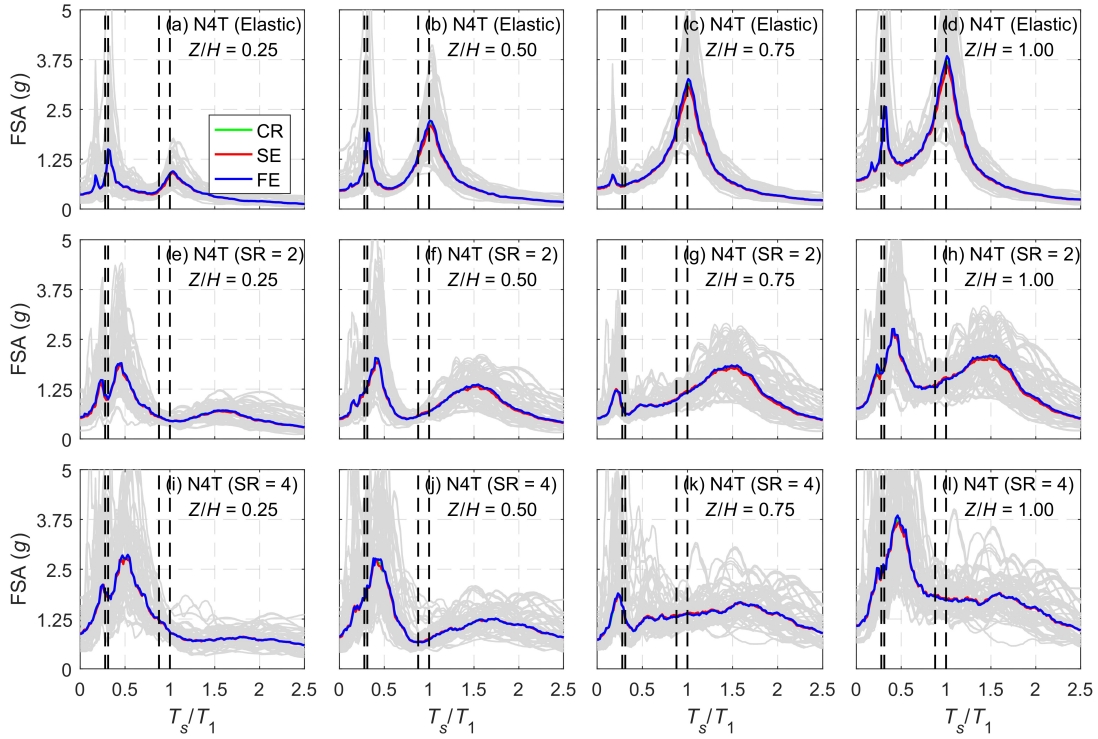

Figure 5.5: Floor response spectra for the 'N4T' building estimated using bi-directional time history analyses. Dashed vertical lines indicate the elastic modal periods in the direction under consideration.

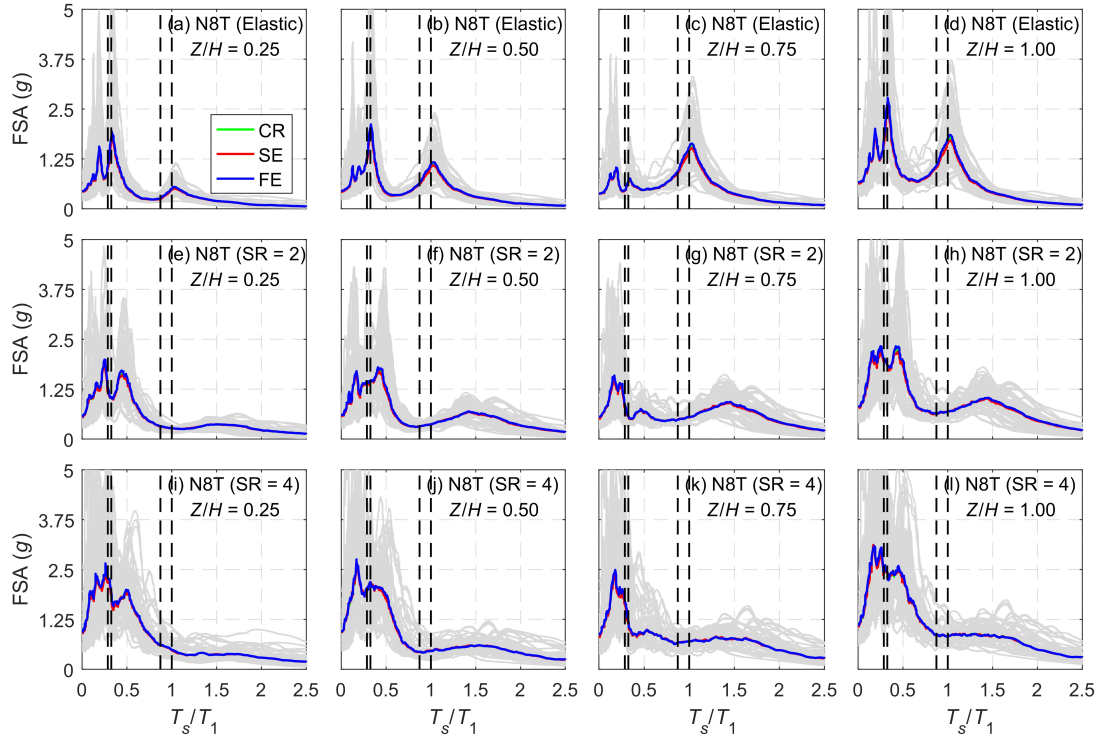

Figure 5.6: Floor response spectra for the 'N8T' building estimated using bi-directional time history analyses. Dashed vertical lines indicate the elastic modal periods in the direction under consideration.

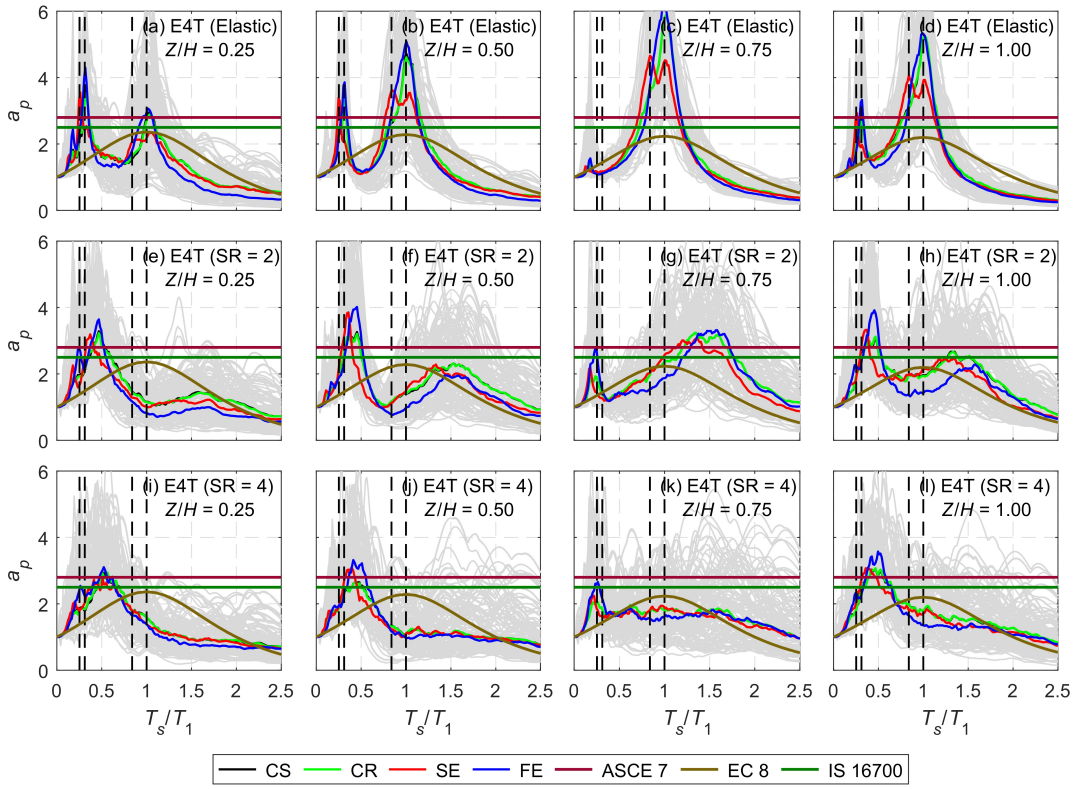

Figure 5.7: Component amplification factors for the 'E4T' building obtained using bi-directional time history analyses. Dashed vertical lines indicate the elastic modal periods in the direction under consideration.

a peak value of 2.36 at $Z/H = 0.25$, which decreases to 2.20 at $Z/H = 1.00$. The variations of the a_p values across different tuning ratios suggest sharp peaks when the secondary system is tuned within the building's fundamental and higher mode regions. This observation highlights that significant dynamic amplifications in acceleration demands are expected in cases when the secondary system is tuned to the building's modes of vibration.

For 4-story buildings exhibiting elastic response, the median peak a_p at the CR corresponding to the case when the secondary system is tuned within the building's fundamental mode region are 6.19, 6.36, and 6.07 for ETI, WTI, and NTI, respectively. These values notably exceed the corresponding median peak a_p values at the SE, which are 4.66, 5.59, and 6.06, and are less but comparable to those at the FE, measured as 6.45, 6.39, and 6.14. When the secondary system is tuned within the building's higher mode region, the median peak a_p values reduce significantly to 3.66, 4.21, and 4.27 at the CR; 3.68, 3.66, and 4.26 at the SE; and 4.66, 4.56, and 4.27 at the FE, with the most significant values observed at the FE.

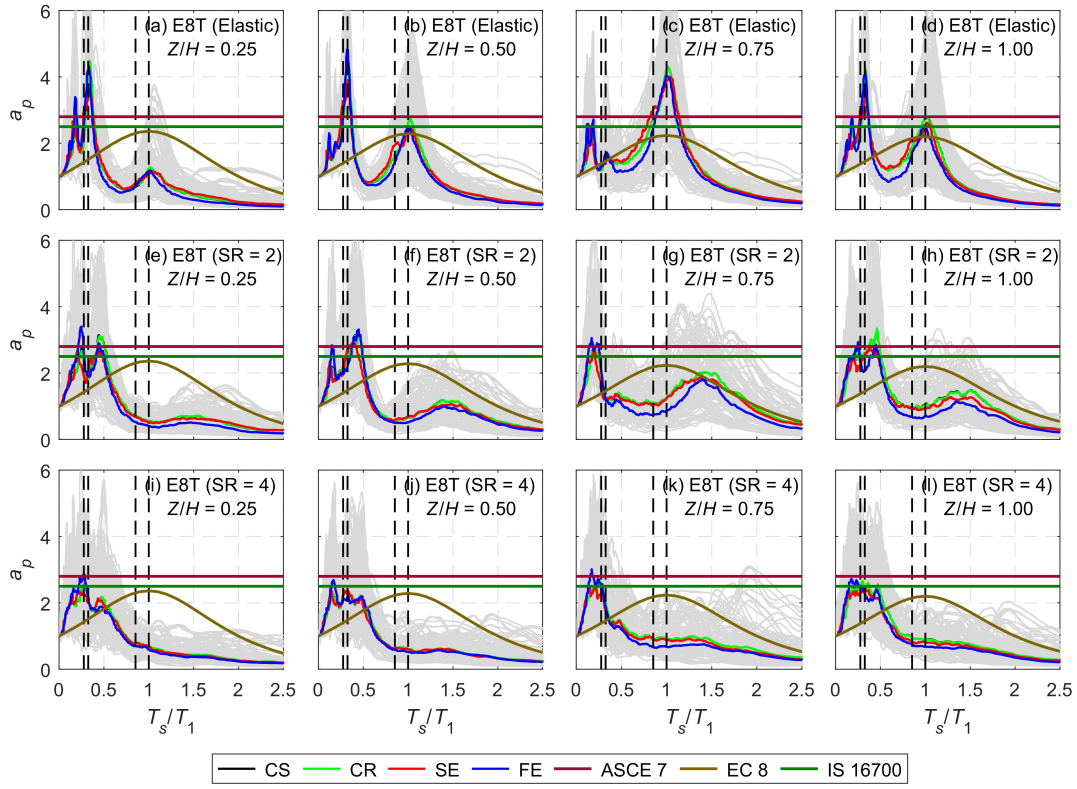

Figure 5.8: Component amplification factors for the 'E8T' building obtained using bi-directional time history analyses. Dashed vertical lines indicate the elastic modal periods in the direction under consideration.

For 8-story buildings exhibiting elastic response, the median peak a_p corresponding to the case when the secondary system is tuned within the building's fundamental mode region is significantly reduced due to the increased flexibility of these buildings compared to their 4-story counterparts. At the CR, the median peak a_p is observed as 4.63, 4.22, and 4.23 for ETI, WTI, and NTI, respectively. These values are more than those obtained at the SE (4.06, 4.15, and 4.21) and at the FE (4.08, 4.15, and 4.34). However, when the secondary system is tuned within the building's higher mode region, the median peak a_p increases significantly up to 47% compared to the 4-story counterpart, reaching 5.22, 5.42, and 5.24 at the CR; 4.41, 5.02, and 5.22 at the SE; and 5.35, 5.42, and 5.33 at the FE. The most pronounced component amplification, when the secondary system is tuned within the building's higher mode region, occurs at the FE, with the median peak a_p values surpassing their counterparts in 4-story buildings.

The code-prescribed limits for a_p as defined by ASCE 7, EC 8, and IS 16700, significantly underestimate the observed peak a_p at the CR, SE, and FE in both

Table 5.1: Median peak component amplification factor for the 4-story buildings.

Building	$Z/H = 0.25$						$Z/H = 1.00$					
	FM			HM			FM			HM		
	FE	CR	SE	FE	CR	SE	FE	CR	SE	FE	CR	SE
Elastic												
E4T	3.06	2.89	2.37	4.30	3.54	3.55	5.34	5.24	4.07	3.33	2.72	2.93
E4U	3.18	2.95	2.43	4.08	3.14	3.17	5.37	5.24	4.23	2.97	2.41	2.24
E4S	3.37	3.27	2.44	4.66	3.59	3.24	5.66	5.41	4.11	3.42	2.67	2.48
E4R	3.02	3.00	2.41	4.29	3.66	3.68	5.42	5.47	4.08	3.37	2.78	2.90
W4T	2.76	2.75	2.77	4.56	4.21	3.63	5.15	5.14	4.73	3.56	3.31	2.85
W4U	3.17	3.32	2.90	4.38	4.09	3.66	5.32	5.67	4.96	3.41	3.19	2.73
W4S	3.07	3.16	2.75	4.34	3.82	3.15	5.68	5.60	5.02	3.36	2.97	2.44
W4R	2.91	2.80	2.89	4.29	4.18	3.61	5.12	5.20	4.79	3.20	3.15	2.63
N4T	2.52	2.49	2.48	4.24	4.24	4.23	5.28	5.17	5.07	3.49	3.50	3.49
N4U	2.58	2.51	2.48	4.15	4.13	4.09	5.44	5.34	5.27	3.46	3.47	3.47
N4S	2.67	2.67	2.67	4.05	4.05	4.05	5.43	5.43	5.43	3.49	3.49	3.49
N4R	2.58	2.58	2.59	4.27	4.27	4.26	5.30	5.29	5.28	3.50	3.50	3.49
SR = 2												
E4T	2.01	2.46	2.05	3.64	3.23	3.19	2.28	2.67	2.47	3.92	3.12	3.33
E4U	1.83	2.04	1.90	3.78	2.85	3.10	2.57	2.55	2.66	3.79	2.66	2.90
E4S	1.88	2.25	1.92	3.77	2.86	3.07	2.56	2.69	2.65	3.86	2.98	3.03
E4R	1.88	2.44	1.99	3.78	3.26	3.08	2.50	2.64	2.63	3.87	3.08	3.35
W4T	2.04	2.48	2.26	3.75	3.53	3.02	2.38	2.58	2.57	3.83	3.62	3.09
W4U	1.77	2.25	2.13	3.65	3.43	3.06	2.51	2.54	2.45	3.87	3.41	3.07
W4S	1.85	2.30	2.13	3.93	3.48	3.01	2.57	2.67	2.69	3.95	3.50	3.13
W4R	2.10	2.36	2.22	3.80	3.71	3.03	2.46	2.66	2.66	3.79	3.78	3.00
N4T	2.18	2.18	2.17	3.89	3.83	3.80	2.79	2.77	2.73	3.99	3.99	3.99
N4U	2.22	2.25	2.26	4.02	3.94	3.71	2.75	2.71	2.65	3.89	3.82	3.81
N4S	2.22	2.21	2.19	3.84	3.86	3.85	2.78	2.77	2.74	3.85	3.83	3.84
N4R	2.18	2.23	2.28	3.94	4.01	3.93	2.70	2.76	2.74	4.11	4.07	4.02
SR = 4												
E4T	2.82	2.71	2.62	3.11	2.94	2.78	2.58	2.66	2.35	3.58	3.07	3.09
E4U	2.33	2.33	2.15	2.86	2.48	2.56	2.29	2.33	2.16	3.41	2.75	3.03
E4S	2.52	2.51	2.22	3.04	2.77	2.73	2.36	2.53	2.21	3.58	3.00	3.14
E4R	2.47	2.76	2.37	3.36	3.05	2.87	2.41	2.82	2.32	3.66	3.45	3.26
W4T	2.81	2.83	2.66	3.17	3.12	2.94	2.76	2.86	2.73	3.63	3.38	3.29
W4U	2.50	2.77	2.64	3.08	3.09	2.82	2.42	2.51	2.41	3.37	3.41	3.23
W4S	2.72	2.85	2.62	3.32	3.17	2.84	2.55	2.67	2.50	3.50	3.40	3.26
W4R	2.74	2.91	2.68	3.18	3.27	2.99	2.58	2.79	2.62	3.40	3.35	3.30
N4T	3.11	3.08	3.05	3.52	3.48	3.48	2.88	2.85	2.83	3.56	3.55	3.52
N4U	2.98	3.07	3.04	3.60	3.60	3.55	2.75	2.71	2.67	3.93	3.80	3.77
N4S	3.21	3.16	3.11	3.44	3.47	3.51	2.84	2.81	2.77	3.56	3.58	3.55
N4R	2.99	3.03	3.02	3.54	3.49	3.47	2.91	2.90	2.90	3.74	3.71	3.67

Note: Median values are color-coded using a gradient for the secondary systems tuned within the building's fundamental and higher mode regions across all buildings: light red (lowest) to green (highest) for the secondary systems tuned within the building's fundamental mode region and light blue (lowest) to sky blue (highest) for higher mode region, with intermediate values in yellow and purple, respectively.

Table 5.2: Median peak component amplification factor for the 8-story buildings.

Building	$Z/H = 0.25$						$Z/H = 1.00$					
	FM			HM			FM			HM		
	FE	CR	SE	FE	CR	SE	FE	CR	SE	FE	CR	SE
Elastic												
E8T	1.18	1.27	1.15	4.33	4.49	3.63	2.54	2.80	2.62	4.17	4.28	3.49
E8U	0.99	1.10	1.16	4.67	4.43	3.69	2.26	2.61	2.38	4.48	4.31	3.55
E8S	1.20	1.37	1.24	4.25	4.38	3.53	2.51	2.74	2.61	4.33	4.29	3.41
E8R	1.04	1.16	1.08	4.41	4.62	3.70	2.37	2.70	2.57	4.24	4.29	3.37
W8T	1.08	1.20	1.18	4.43	4.65	4.39	2.54	2.73	2.66	4.34	4.42	3.96
W8U	1.03	1.10	1.15	4.34	4.52	4.27	2.35	2.56	2.59	4.18	4.18	4.22
W8S	1.08	1.20	1.16	4.44	4.57	4.29	2.56	2.68	2.86	4.22	4.24	3.95
W8R	1.07	1.12	1.08	4.72	4.79	4.54	2.35	2.45	2.49	4.28	4.28	3.89
N8T	1.12	1.13	1.14	4.81	4.67	4.64	2.42	2.37	2.35	4.21	4.18	4.14
N8U	1.11	1.11	1.11	4.75	4.71	4.63	2.48	2.40	2.38	4.21	4.18	4.15
N8S	1.12	1.12	1.12	4.60	4.60	4.61	2.40	2.41	2.41	4.24	4.24	4.24
N8R	1.12	1.13	1.13	4.64	4.61	4.60	2.45	2.45	2.45	4.20	4.20	4.20
SR = 2												
E8T	1.37	1.68	1.57	3.40	3.11	2.76	1.22	1.53	1.34	2.93	3.34	2.75
E8U	1.30	1.48	1.38	3.32	2.83	2.91	1.19	1.47	1.19	2.94	3.06	2.93
E8S	1.26	1.52	1.31	3.33	2.95	2.92	1.15	1.45	1.19	3.01	3.18	2.78
E8R	1.42	1.72	1.51	3.26	3.12	2.76	1.25	1.57	1.31	3.06	3.33	2.78
W8T	1.51	1.57	1.64	3.25	3.21	3.24	1.38	1.49	1.48	3.26	3.44	3.03
W8U	1.45	1.53	1.50	3.25	3.10	3.04	1.24	1.37	1.40	3.00	3.26	2.98
W8S	1.32	1.51	1.46	3.33	3.12	2.95	1.28	1.39	1.35	2.91	3.13	2.78
W8R	1.51	1.55	1.68	3.30	3.14	3.12	1.35	1.46	1.45	3.09	3.24	2.99
N8T	1.61	1.66	1.64	3.15	3.19	3.14	1.63	1.60	1.58	3.15	3.08	3.15
N8U	1.56	1.57	1.57	3.16	3.10	3.07	1.54	1.50	1.46	3.22	3.22	3.10
N8S	1.51	1.53	1.55	3.21	3.19	3.19	1.56	1.53	1.53	3.28	3.29	3.32
N8R	1.58	1.63	1.60	3.10	3.13	3.12	1.54	1.56	1.55	3.21	3.20	3.22
SR = 4												
E8T	1.52	1.64	1.54	2.86	2.53	2.36	1.40	1.70	1.39	2.71	2.66	2.44
E8U	1.42	1.55	1.48	2.84	2.48	2.41	1.37	1.49	1.24	2.65	2.73	2.51
E8S	1.52	1.52	1.38	2.80	2.46	2.51	1.36	1.47	1.33	2.72	2.66	2.44
E8R	1.53	1.59	1.54	3.08	2.68	2.66	1.46	1.75	1.43	2.84	2.66	2.52
W8T	1.69	1.67	1.68	2.88	2.74	2.62	1.58	1.68	1.62	2.76	2.85	2.67
W8U	1.50	1.54	1.51	2.86	2.72	2.59	1.38	1.45	1.44	2.61	2.67	2.54
W8S	1.56	1.64	1.59	2.91	2.76	2.59	1.29	1.44	1.37	2.66	2.63	2.51
W8R	1.68	1.73	1.71	2.93	2.74	2.56	1.57	1.78	1.57	2.79	2.82	2.55
N8T	1.78	1.79	1.81	2.67	2.62	2.62	1.77	1.79	1.73	2.90	2.89	2.83
N8U	1.78	1.77	1.77	2.72	2.72	2.70	1.65	1.61	1.56	2.84	2.83	2.83
N8S	1.67	1.68	1.69	2.59	2.59	2.56	1.69	1.70	1.72	2.84	2.81	2.79
N8R	1.76	1.77	1.78	2.88	2.86	2.84	1.80	1.85	1.80	2.97	2.96	3.00

Note: Median values are color-coded using a gradient for the secondary systems tuned within the building's fundamental and higher mode regions across all buildings: light red (lowest) to green (highest) for the secondary systems tuned within the building's fundamental mode region and light blue (lowest) to sky blue (highest) for higher mode region, with intermediate values in yellow and purple, respectively.

4-story and 8-story buildings exhibiting elastic response. In 4-story buildings, the median peak a_p, corresponding to the cases when the secondary system is tuned within the building's fundamental and higher mode region, exceeds the code limits up to 189% and 112%, respectively. These values change to 107% and 146% for 8-story buildings, thereby underscoring the codes' inability to accurately predict a_p values. The extent of nominal torsion does not appear to have a substantial impact on the peak a_p, and the differences in response among the CR, SE, and FE are notably reduced as the extent of nominal torsion decreases. For instance, in the case of NTI buildings, the responses at the CR, SE, and FE converge, indicating minimal variation across these locations.

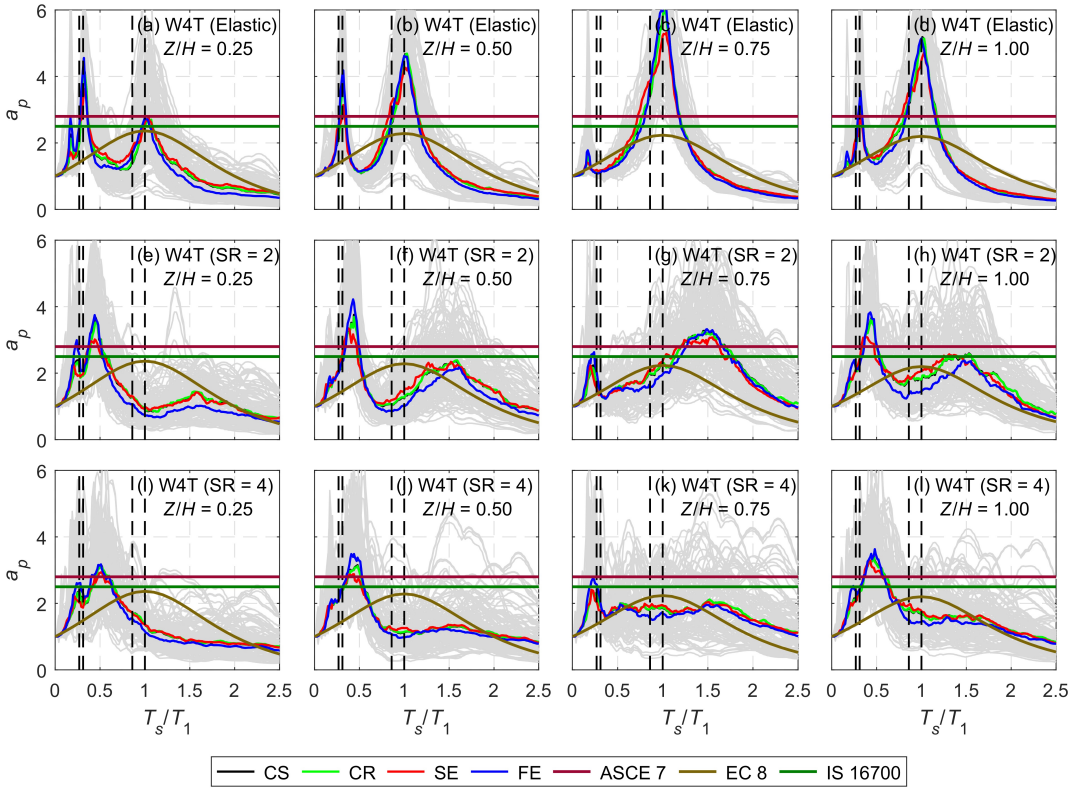

Figure 5.9: Component amplification factors for the 'W4T' building obtained using bi-directional time history analyses. Dashed vertical lines indicate the elastic modal periods in the direction under consideration.

For 4-story buildings exhibiting moderately inelastic response (SR = 2), the median peak a_p decreases significantly compared to their elastic counterparts, which can be primarily attributed to the inelastic energy dissipation in the building. The median peak a_p at the CR corresponding to the case when the secondary system is tuned within the building's fundamental mode region is 3.24, 3.37, and 3.62 for

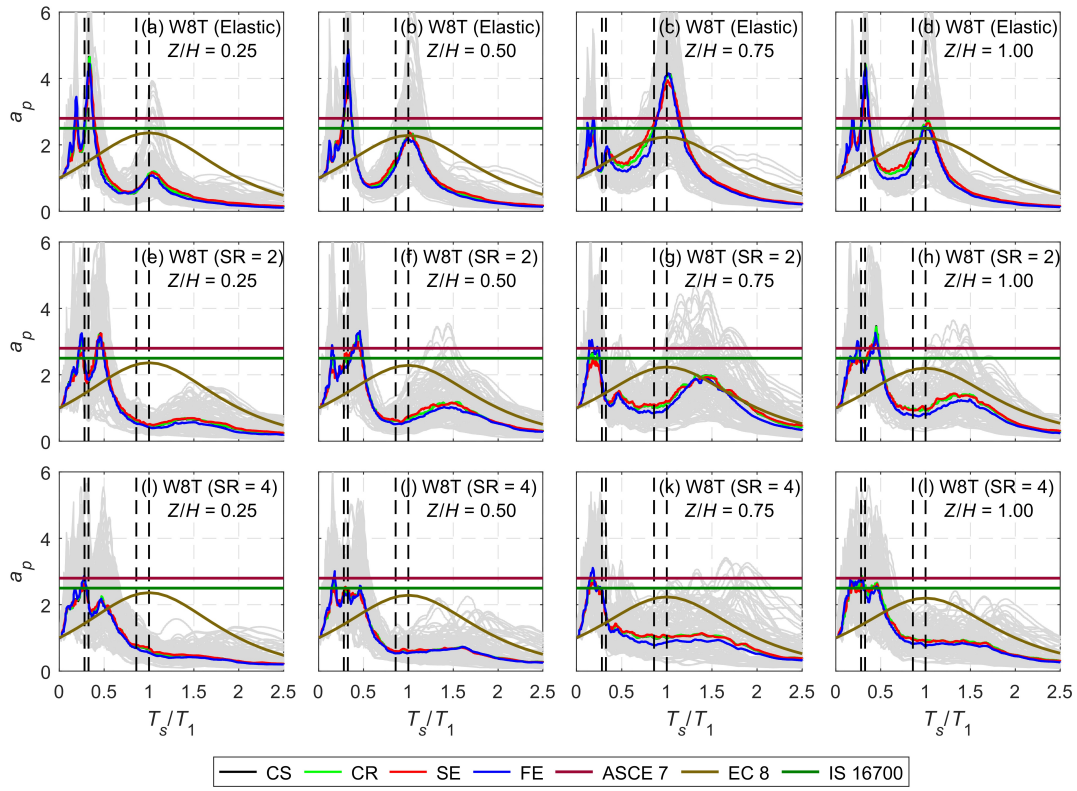

Figure 5.10: Component amplification factors for the 'W8T' building obtained using bi-directional time history analyses. Dashed vertical lines indicate the elastic modal periods in the direction under consideration.

ETI, WTI, and NTI, respectively. These values are comparable to the median peak a_p values at the SE (3.26, 3.37, and 3.59) but slightly lower than those at the FE, which are 3.57, 3.46, and 3.74. When the secondary system is tuned within the building's higher mode region, the median peak a_p values reduce to 3.31, 3.78, and 4.27 at the CR; 3.86, 3.36, and 4.16 at the SE; and 4.17, 4.22, and 4.26 at the FE, with the most pronounced values observed at the FE.

For 8-story buildings exhibiting moderately inelastic response (SR = 2), the median peak a_p at the CR corresponding to the case when the secondary system is tuned within the building's fundamental mode region are 2.19, 2.08, and 2.03 for ETI, WTI, and NTI, respectively, which are higher than those observed at the SE (1.92, 2.05, and 2.00) and the FE (1.90, 1.99, and 2.03). However, when the secondary system is tuned within the building's higher mode region, the median peak a_p increases significantly (in comparison to the fundamental mode region), reaching 3.72, 3.69, and 3.64 at the CR; 3.28, 3.47, and 3.63 at the SE; and 3.79, 3.84, and 3.76 at the FE.

It is interesting to note that the reduction in peak a_p is higher for the cases when the secondary system is tuned within the building's fundamental mode region, as the building dissipates a larger amount of energy through the fundamental mode of vibration. Thus, for buildings exhibiting moderately inelastic response, the reduction in peak a_p has mitigated underestimation by building codes to some extent. However, the code-prescribed values still underestimate the median peak a_p at all critical locations across 4-story and 8-story buildings up to 91%.

For 4-story buildings exhibiting highly inelastic response (SR = 4), the observed median peak a_p decreases further compared to their elastic and moderately inelastic counterparts. The median peak a_p at the CR corresponding to the case when the secondary system is tuned within the building's fundamental mode region are 2.82, 2.91, and 3.16 for ETI, WTI, and NTI buildings, respectively. These values are higher than those at the SE (2.62, 2.73, and 3.11) but comparable to those at the FE (2.82, 2.81, and 3.21). When the secondary system is tuned within the building's higher mode region, the median peak a_p values reach 3.45, 3.41, and 3.80 for ETI, WTI, and NTI buildings, respectively, indicating considerable component amplification. Similar trends are observed at the SE (3.40, 3.30, and 3.77) and the FE (3.85, 3.90, and 3.93), with the highest component amplification consistently occurring at the FE.

For 8-story buildings exhibiting highly inelastic response (SR = 4), the median peak a_p values remained comparable to their moderately inelastic counterparts. The median peak a_p at the CR corresponding to the case when the secondary system is tuned within the building's fundamental mode region are 2.05, 2.16, and 2.25 for ETI, WTI, and NTI buildings, respectively, which are higher than those obtained at the SE (1.72, 1.98, and 2.26) and the FE (1.82, 2.11, and 2.23). When the secondary system is tuned within the building's higher mode region, the median peak a_p values reduce (compared to elastic and moderately inelastic counterparts) 3.10, 3.27, and 3.65 at the CR, while at the SE, they are 2.94, 3.10, and 3.61. Further, at the FE, these values are obtained as 3.28, 3.41, and 3.67. Despite these reductions due to the beneficial effects of the building's inelasticity, significant component amplification effects persist, especially at the FE. Thus, for buildings exhibiting highly inelastic response, the code-prescribed values continue to underestimate the median peak a_p

at all critical locations across both 4-story and 8-story buildings by up to 76%, with the exception of the case when the secondary system is tuned within the building's fundamental mode region in 8-story buildings, where the codes provide an accurate prediction of the a_p.

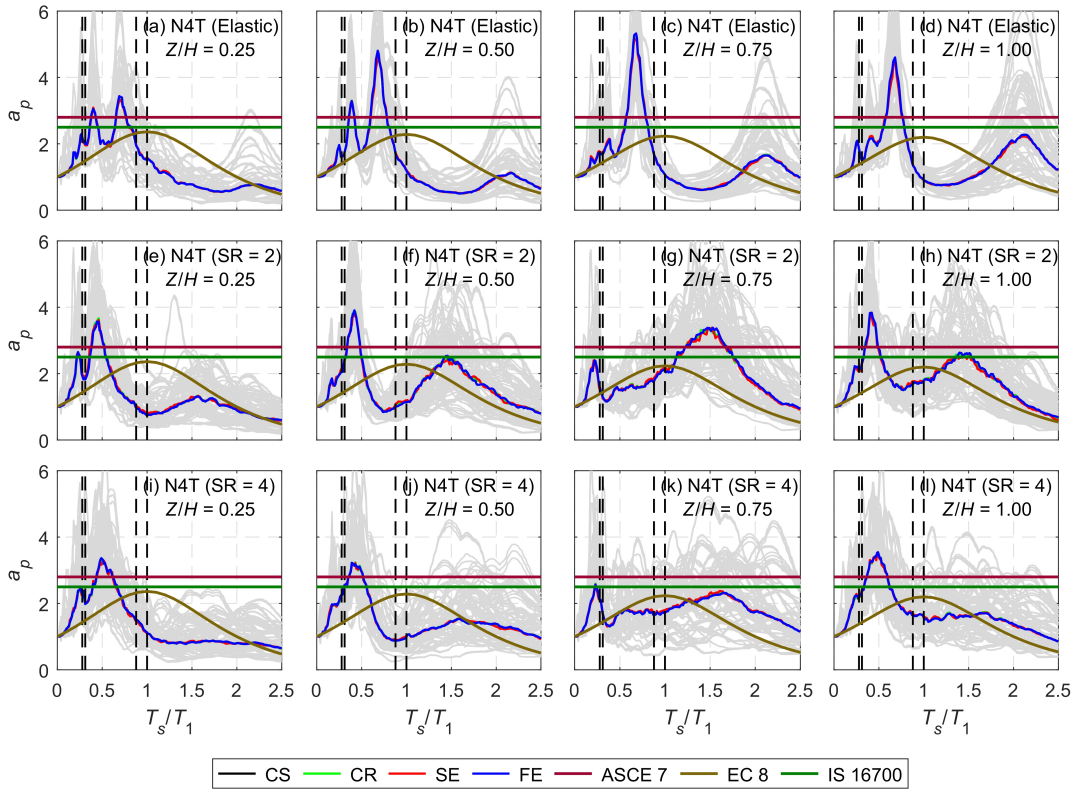

Figure 5.11: Component amplification factors for the 'N4T' building obtained using bi-directional time history analyses. Dashed vertical lines indicate the elastic modal periods in the direction under consideration.

5.2.2 Total amplification factor

Figures 5.17–5.16 (Tables 5.3–5.4) present the FRS normalized by PGA, resulting total amplification factor (a_t). The a_t represents the combined effects of floor amplification (PFA/PGA) and component amplification (a_p) in the code models and depends on the characteristics (spectral shape) of the ground motion and its amplification by the building. The obtained peak values of a_t are compared with the provisions of IS 16700, ASCE 7, and EC 8. The values of a_t in all the considered seismic design codes are dependent on Z/H, with maximum values reaching 4, 5.5, and 5 in ASCE 7, EC 8, and IS 16700, respectively. The variations in the a_t values across different tuning ratios exhibit sharp peaks when the secondary system is tuned within the building's fundamental and higher mode regions, indicating substantial

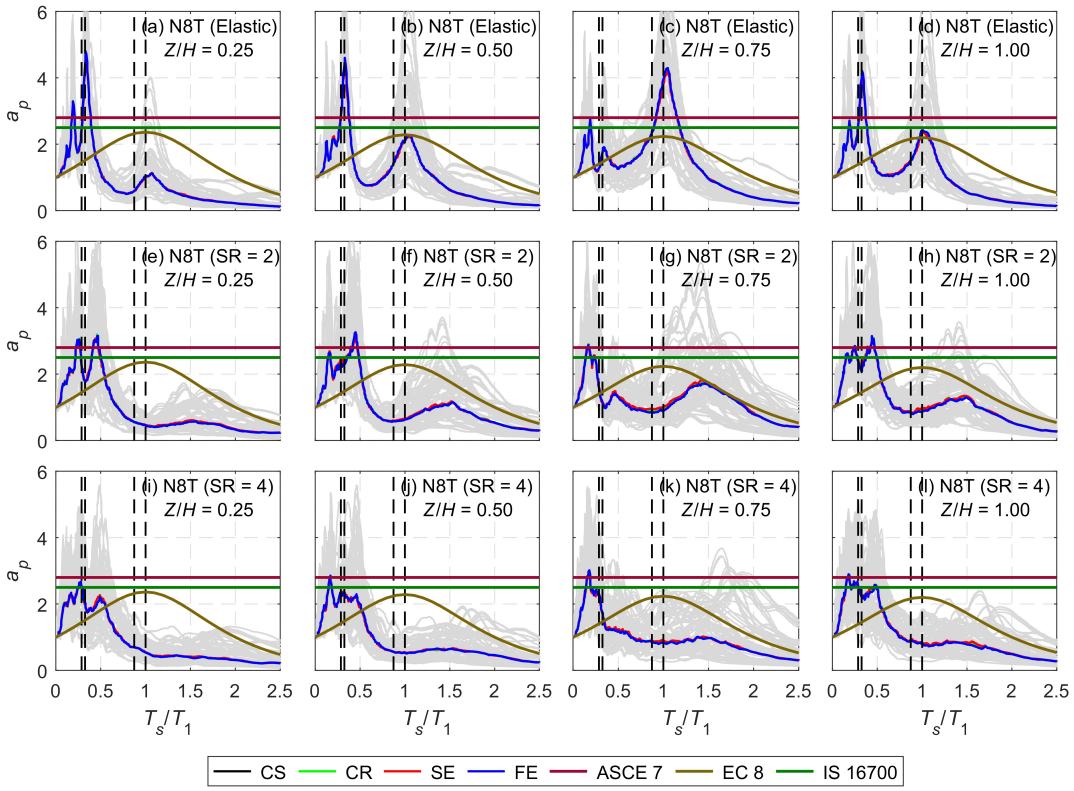

Figure 5.12: Component amplification factors for the 'N8T' building obtained using bi-directional time history analyses. Dashed vertical lines indicate the elastic modal periods in the direction under consideration.

dynamic amplification of acceleration demands for tuned secondary systems.

For 4-story buildings exhibiting elastic response, the median peak a_t values at the CR when the secondary system is tuned within the building's fundamental mode region are 16.86, 16.62, and 16.26 for ETI, WTI, and NTI, respectively. These values at the CR exceed those at the SE, which are 14.10, 13.71, and 16.20, but are lower than the corresponding values at the FE, measured as 25.55, 21.16, and 16.32. In contrast, when the secondary system is tuned within the building's higher mode region, the median peak a_t at the CR are 10.05, 11.08, and 11.03 for ETI, WTI, and NTI, respectively, which reduce to 8.99, 8.99, and 10.84 at the SE, and increase to 16.44, 15.87, and 11.28 at the FE.

For 8-story buildings exhibiting elastic response, the median peak a_t reduces significantly, compared to their 4-story counterparts. The median peak a_t values at the CR, when the secondary system is tuned within the building's fundamental mode region, are 7.49, 6.78, and 6.33 for ETI, WTI, and NTI, respectively. These values are slightly higher than those at the SE, recorded as 6.21, 5.90, and 6.26, and lower

Table 5.3: Median peak total amplification factor for the 4-story buildings.

Building	$Z/H = 0.25$						$Z/H = 1.00$					
	FM			HM			FM			HM		
	FE	CR	SE	FE	CR	SE	FE	CR	SE	FE	CR	SE
Elastic												
E4T	5.61	3.42	2.54	8.70	4.29	4.40	24.03	15.05	11.30	14.95	8.32	8.18
E4U	5.51	3.37	2.77	8.51	4.09	4.14	25.55	16.86	14.10	16.25	9.13	8.61
E4S	5.84	3.58	2.67	9.07	4.46	3.88	24.17	16.72	13.06	16.44	10.05	8.32
E4R	5.59	3.52	2.60	8.32	4.71	4.19	23.40	15.59	11.65	14.90	9.36	8.99
W4T	5.22	3.91	3.26	8.49	5.89	4.41	21.16	16.07	12.98	14.11	9.95	7.69
W4U	4.98	3.85	3.20	8.59	5.85	4.58	20.41	16.27	13.71	15.87	11.08	8.99
W4S	5.02	3.84	3.09	7.82	5.15	3.78	20.80	16.62	13.51	13.44	9.73	6.78
W4R	5.04	3.86	3.14	7.51	5.34	4.07	21.05	16.39	13.40	12.57	9.78	7.33
N4T	3.97	3.85	3.78	6.42	6.31	6.25	15.33	14.70	14.31	11.28	11.03	10.84
N4U	3.97	3.85	3.76	6.29	6.21	6.13	16.25	15.45	14.87	10.80	10.49	10.24
N4S	3.96	3.96	3.96	6.15	6.15	6.15	15.73	15.73	15.73	10.45	10.45	10.46
N4R	3.95	3.93	3.91	6.55	6.52	6.49	16.32	16.26	16.20	10.60	10.57	10.54
SR = 2												
E4T	3.00	2.21	2.00	5.42	2.93	3.57	4.56	3.66	4.40	7.99	4.80	5.90
E4U	2.45	1.96	1.87	4.49	2.65	3.15	5.38	4.47	5.12	7.61	4.39	5.78
E4S	2.60	2.12	1.96	4.86	2.86	3.41	5.07	4.55	4.85	7.52	4.92	6.04
E4R	2.83	2.38	2.03	5.49	3.17	3.81	5.30	4.05	4.94	8.07	5.20	6.38
W4T	3.03	2.60	2.38	5.78	3.82	3.10	4.30	3.74	3.75	8.47	5.67	5.11
W4U	2.68	2.41	2.17	5.04	3.37	3.20	4.69	4.13	4.48	7.46	5.26	5.17
W4S	2.78	2.47	2.21	4.96	3.55	3.17	4.76	4.06	4.50	7.27	5.52	5.73
W4R	2.92	2.60	2.29	5.78	3.81	3.06	4.30	3.90	4.03	8.36	5.66	5.14
N4T	2.90	2.88	2.84	4.58	4.50	4.53	4.49	4.43	4.37	6.90	6.88	6.85
N4U	2.79	2.73	2.68	4.83	4.73	4.64	4.38	4.26	4.06	6.96	6.93	6.49
N4S	2.73	2.72	2.72	4.42	4.44	4.47	4.10	4.11	4.12	6.32	6.37	6.37
N4R	2.87	2.80	2.75	5.10	4.92	4.75	4.00	4.00	3.94	7.27	7.14	7.13
SR = 4												
E4T	2.86	2.47	2.31	3.18	2.57	2.39	3.57	3.01	2.96	4.61	3.34	3.82
E4U	2.46	2.11	2.01	3.25	2.33	2.61	3.08	2.82	2.88	4.78	3.29	4.01
E4S	2.53	2.18	2.11	3.14	2.58	2.62	3.05	2.75	2.80	4.67	3.44	3.84
E4R	3.08	2.41	2.24	3.70	2.67	2.73	3.86	3.12	2.90	5.73	4.03	4.21
W4T	2.88	2.63	2.50	3.18	2.84	2.67	3.47	3.05	2.91	4.48	3.69	3.61
W4U	2.64	2.48	2.34	3.21	2.63	2.51	3.12	2.86	2.77	4.19	3.66	3.66
W4S	3.00	2.54	2.38	3.65	2.88	2.57	3.44	3.09	2.95	5.02	3.97	3.88
W4R	3.03	2.54	2.40	3.42	2.93	2.67	3.62	3.18	2.97	4.85	3.86	3.81
N4T	2.71	2.71	2.69	3.15	3.13	3.15	3.38	3.36	3.35	4.46	4.39	4.33
N4U	2.88	2.76	2.69	3.42	3.37	3.12	3.20	3.09	2.97	4.95	4.78	4.61
N4S	2.80	2.79	2.78	3.05	3.03	3.01	3.17	3.17	3.17	4.14	4.12	4.11
N4R	2.72	2.71	2.69	3.29	3.21	3.17	3.49	3.48	3.41	4.48	4.40	4.33

Note: Median values are color-coded using a gradient for the secondary systems tuned within the building's fundamental and higher mode regions across all buildings: light red (lowest) to green (highest) for the secondary systems tuned within the building's fundamental mode region and light blue (lowest) to sky blue (highest) for higher mode region, with intermediate values in yellow and purple, respectively.

than those at the FE, measured as 9.78, 7.87, and 6.52. When the secondary system is tuned within the building's higher mode region, the median peak a_t increases to 11.37, 10.33, and 9.96 at the CR. These values exceed those at the SE (8.76, 9.00,

Table 5.4: Median peak total amplification factor for the 8-story buildings.

Building	$Z/H = 0.25$						$Z/H = 1.00$					
	FM			HM			FM			HM		
	FE	CR	SE	FE	CR	SE	FE	CR	SE	FE	CR	SE
Elastic												
E8T	2.93	2.10	1.60	9.99	6.02	4.72	9.78	7.49	6.21	14.71	9.51	7.28
E8U	2.41	1.71	1.46	10.33	6.62	5.25	9.00	7.13	5.98	16.33	11.37	8.76
E8S	2.60	1.96	1.67	10.02	6.20	4.73	8.78	7.09	6.05	14.99	10.60	7.84
E8R	2.47	1.85	1.57	9.70	6.28	4.69	8.18	6.66	5.55	14.00	9.61	7.17
W8T	2.35	1.93	1.76	8.55	6.39	5.38	7.78	6.53	5.82	12.44	9.73	7.97
W8U	2.06	1.77	1.65	8.31	6.59	5.67	7.40	6.15	5.58	12.62	10.33	9.00
W8S	2.24	1.85	1.65	8.45	6.61	5.50	7.87	6.78	5.90	11.69	9.50	8.00
W8R	2.04	1.77	1.64	8.28	6.84	5.85	6.76	6.00	5.33	11.71	9.73	8.16
N8T	1.90	1.84	1.81	7.43	7.17	6.96	6.52	6.27	6.08	10.21	9.78	9.46
N8U	1.85	1.81	1.77	7.29	7.06	6.86	6.44	6.15	5.92	10.39	9.96	9.63
N8S	1.84	1.84	1.84	7.13	7.13	7.12	6.26	6.26	6.26	9.71	9.70	9.69
N8R	1.86	1.84	1.82	6.93	6.84	6.75	6.40	6.33	6.26	9.69	9.59	9.49
SR = 2												
E8T	1.91	1.61	1.45	5.00	2.76	2.74	2.56	2.18	2.02	6.14	4.27	4.27
E8U	1.76	1.38	1.34	5.02	2.54	2.90	2.45	2.07	1.94	6.74	4.30	4.43
E8S	1.73	1.46	1.35	4.64	2.77	2.99	2.45	2.10	1.92	6.38	4.52	4.46
E8R	1.86	1.59	1.40	4.91	2.84	2.75	2.57	2.13	2.04	6.21	4.09	4.20
W8T	1.86	1.73	1.58	4.31	3.02	2.87	2.45	2.17	2.05	5.40	4.19	3.92
W8U	1.80	1.57	1.45	4.48	3.04	2.81	2.32	2.07	1.93	5.69	4.32	4.01
W8S	1.76	1.57	1.43	4.57	3.69	3.20	2.41	2.13	1.94	5.55	4.41	4.13
W8R	1.88	1.71	1.55	4.22	2.97	2.65	2.47	2.18	2.02	5.47	4.34	3.90
N8T	1.79	1.78	1.73	3.24	3.13	3.04	2.27	2.24	2.19	4.28	4.09	4.04
N8U	1.82	1.83	1.82	3.26	3.22	3.21	2.35	2.26	2.18	4.69	4.53	4.33
N8S	1.86	1.85	1.84	3.22	3.20	3.21	2.18	2.18	2.18	4.45	4.45	4.45
N8R	1.82	1.80	1.75	3.32	3.23	3.11	2.25	2.17	2.15	4.62	4.48	4.37
SR = 4												
E8T	1.47	1.35	1.32	2.88	2.21	2.17	1.83	1.50	1.42	3.77	2.77	2.69
E8U	1.45	1.25	1.25	2.83	2.17	2.29	1.77	1.57	1.50	3.69	2.85	2.87
E8S	1.42	1.28	1.22	2.84	2.12	2.44	1.66	1.50	1.48	3.64	2.86	3.07
E8R	1.61	1.41	1.25	3.10	2.28	2.16	1.91	1.62	1.49	3.97	2.76	2.86
W8T	1.41	1.31	1.28	2.75	2.33	2.17	1.78	1.61	1.48	3.29	2.70	2.62
W8U	1.50	1.36	1.31	2.74	2.35	2.26	1.76	1.52	1.42	3.41	2.93	2.86
W8S	1.43	1.32	1.29	2.73	2.36	2.24	1.54	1.50	1.41	3.46	2.75	2.70
W8R	1.50	1.42	1.37	2.85	2.37	2.12	1.82	1.61	1.48	3.50	2.82	2.68
N8T	1.37	1.35	1.32	2.43	2.36	2.27	1.64	1.60	1.57	2.98	2.99	2.95
N8U	1.45	1.41	1.38	2.47	2.48	2.46	1.68	1.64	1.60	3.09	3.05	3.05
N8S	1.46	1.45	1.45	2.44	2.45	2.45	1.79	1.79	1.78	2.94	2.96	2.95
N8R	1.42	1.38	1.35	2.51	2.42	2.40	1.73	1.71	1.71	3.19	3.08	3.03

Note: Median values are color-coded using a gradient for the secondary systems tuned within the building's fundamental and higher mode regions across all buildings: light red (lowest) to green (highest) for the secondary systems tuned within the building's fundamental mode region and light blue (lowest) to sky blue (highest) for higher mode region, with intermediate values in yellow and purple, respectively.

and 9.69) but remain lower than those at the FE (16.33, 12.62, and 10.39).

The significantly higher median peak a_t observed for relatively short-period

4-story buildings (Figures 5.17–5.16) suggests that for these buildings, where the predominant ground motion period is closer to the fundamental period of the building (T_1), current code models may substantially underestimate floor accelerations in buildings exhibiting elastic response. The median peak a_t values for the case when the secondary system is tuned within the building's fundamental mode region of the 4-story buildings exhibiting elastic response significantly exceed the maximum values prescribed by the codes, with underestimations up to 539%, 365%, and 411% by ASCE 7, EC 8, and IS 16700, respectively, particularly at the FE. For 8-story buildings exhibiting elastic response, while the median peak a_t values decrease, they still exceed the code-prescribed limits, with maximum underestimations of 308%, 197%, and 227%. These trends confirm that current code models significantly underestimate the median peak a_t values under tuned response cases, especially at critical locations like CR, SE, and FE. While the extent of nominal torsion appears to significantly influence the peak response at the FE, the differences in response between the CR, the SE, and the FE diminish as the nominal torsion in the building decreases. For example, in the case of NTI buildings (Figure 5.15), the responses at the CR, SE, and FE almost converge, showing minimal variation across these locations.

Under moderately inelastic conditions (SR = 2), the median peak a_t values reduce significantly due to inelastic energy dissipation in the building. For 4-story buildings, the median peak a_t values at the CR, when the secondary system is tuned within the building's fundamental mode region, are 4.55, 4.13, and 4.43 for ETI, WTI, and NTI buildings, respectively. At the SE, the median peak a_t values are 5.12, 4.50, and 4.37, and at the FE, they are 5.38, 4.76, and 4.49. In contrast, when the secondary system is tuned within the building's higher mode region, the median peak a_t at the CR is 5.20, 5.67, and 7.14 for ETI, WTI, and NTI buildings, respectively. At the SE, the median peak a_t values are 6.38, 5.73, and 7.13, and at the FE, they are 8.07, 8.47, and 7.27. The median peak a_t values showed a reduction compared to their elastic counterparts, although the median peak a_t values when the secondary system is tuned within the building's higher mode region remain significantly amplified at the FE. Compared with the code provisions, the ASCE 7 underestimates the median peak a_t for the case when the secondary system is tuned

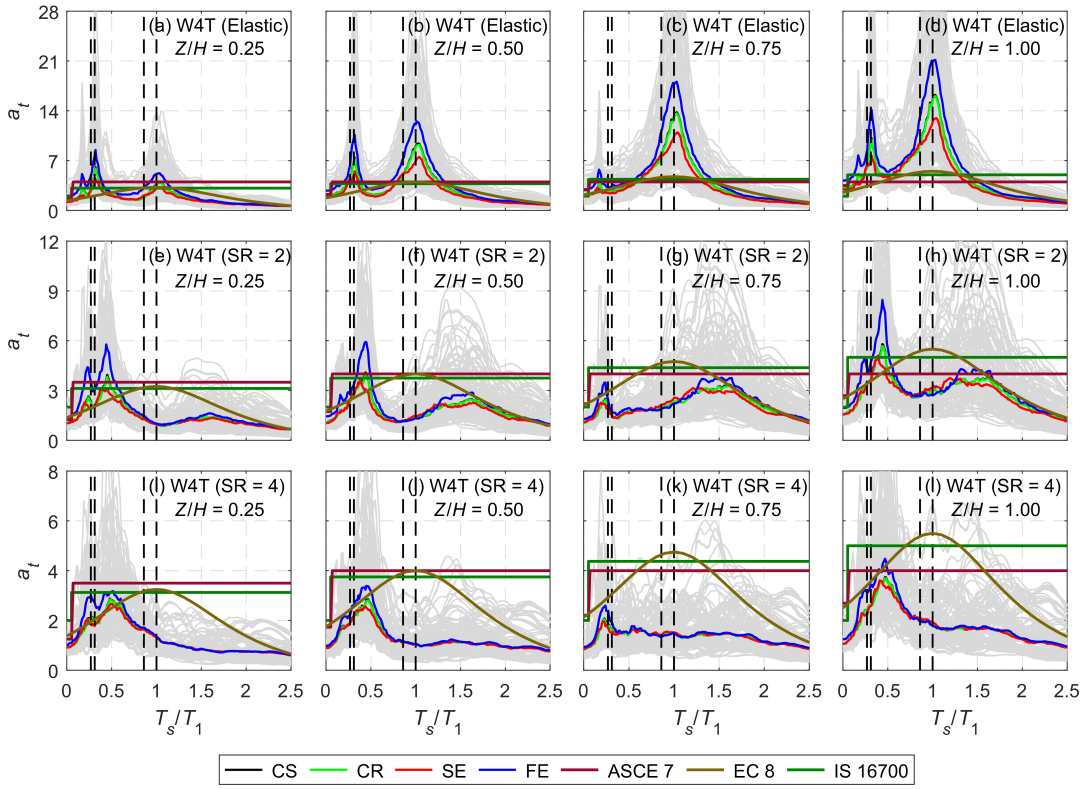

Figure 5.13: Total amplification factors for the 'W4T' building obtained using bi-directional time history analyses. Dashed vertical lines indicate the elastic modal periods in the direction under consideration.

within the building's fundamental mode region by up to 35%. IS 16700 and EC 8 provide more accurate predictions for the case when the secondary system is tuned within the building's fundamental mode region, particularly at the CR and SE. However, all codes underestimated the median peak a_t values for the case when the secondary system is tuned within the building's higher mode region, with maximum underestimation reaching up to 112%.

For 8-story buildings exhibiting moderately inelastic response (SR = 2), the median peak a_t values at the CR, when the secondary system is tuned within the building's fundamental mode region, are 2.18, 2.18, and 2.26 for ETI, WTI, and NTI buildings, respectively. At the SE, the median peak a_t are 2.04, 2.05, and 2.19, and at the FE, they are 2.57, 2.47, and 2.35. These values represent a significant reduction compared to their elastic counterparts. In contrast, when the secondary system is tuned within the building's higher mode region, the median peak a_t values at the CR are 4.52, 4.41, and 4.53 for ETI, WTI, and NTI buildings, respectively. At the SE, the median peak a_t values are 4.46, 4.13, and 4.45, while the FE exhibits

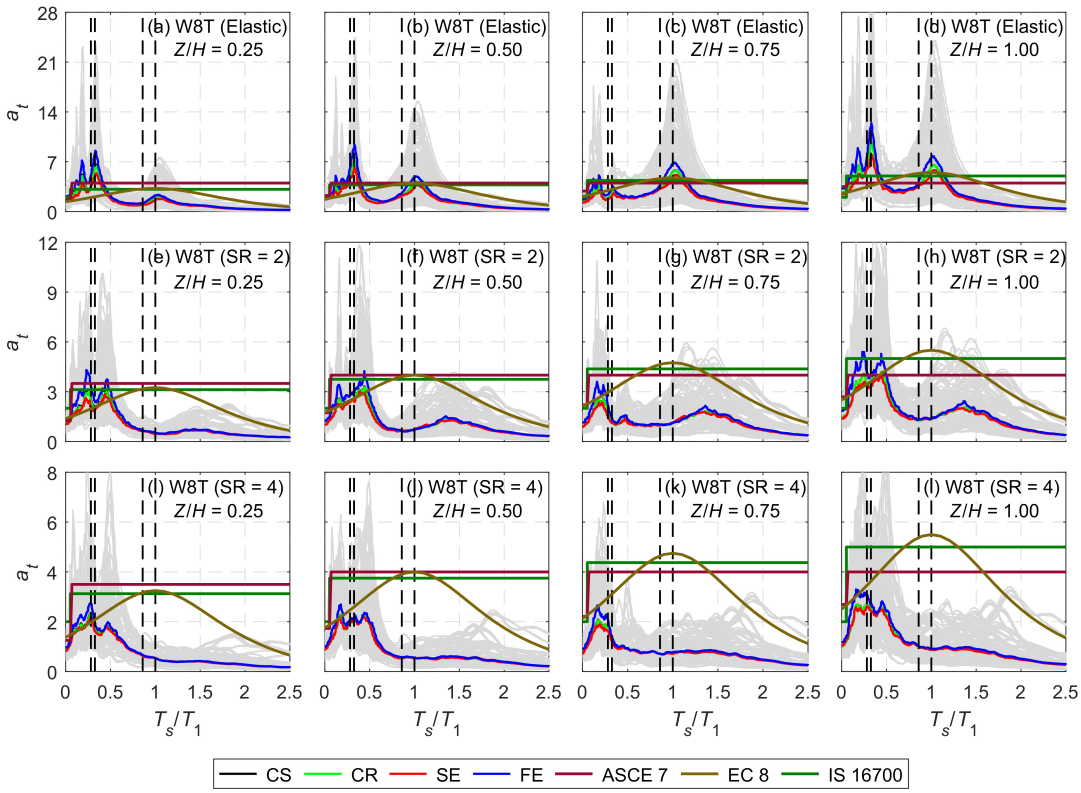

Figure 5.14: Total amplification factors for the 'W8T' building obtained using bi-directional time history analyses. Dashed vertical lines indicate the elastic modal periods in the direction under consideration.

relatively higher values of 6.74, 5.69, and 4.69. While all code models accurately predict the median peak a_t values when the secondary system is tuned within the building's fundamental mode region for 8-story buildings, they underestimate the median peak a_t values when the secondary system is tuned within the building's higher mode region. ASCE 7 model significantly underestimated the median peak a_t when the secondary system is tuned within the building's higher mode region, with observed values exceeding the ASCE limit by up to 69%. In contrast, IS 16700 and EC 8 show relatively better agreement at the CR and SE but still fall short at the FE by 35%.

For 4-story buildings exhibiting highly inelastic response (SR = 4), the median peak a_t values at the CR, when the secondary system is tuned within the building's fundamental mode region, are 3.12, 3.18, and 3.48 for ETI, WTI, and NTI buildings, respectively. These values show a significant decline compared to their elastic counterparts, which exhibited values of 16.86, 16.62, and 16.26, respectively. This significant reduction underscores the pronounced damping effect and inelastic energy

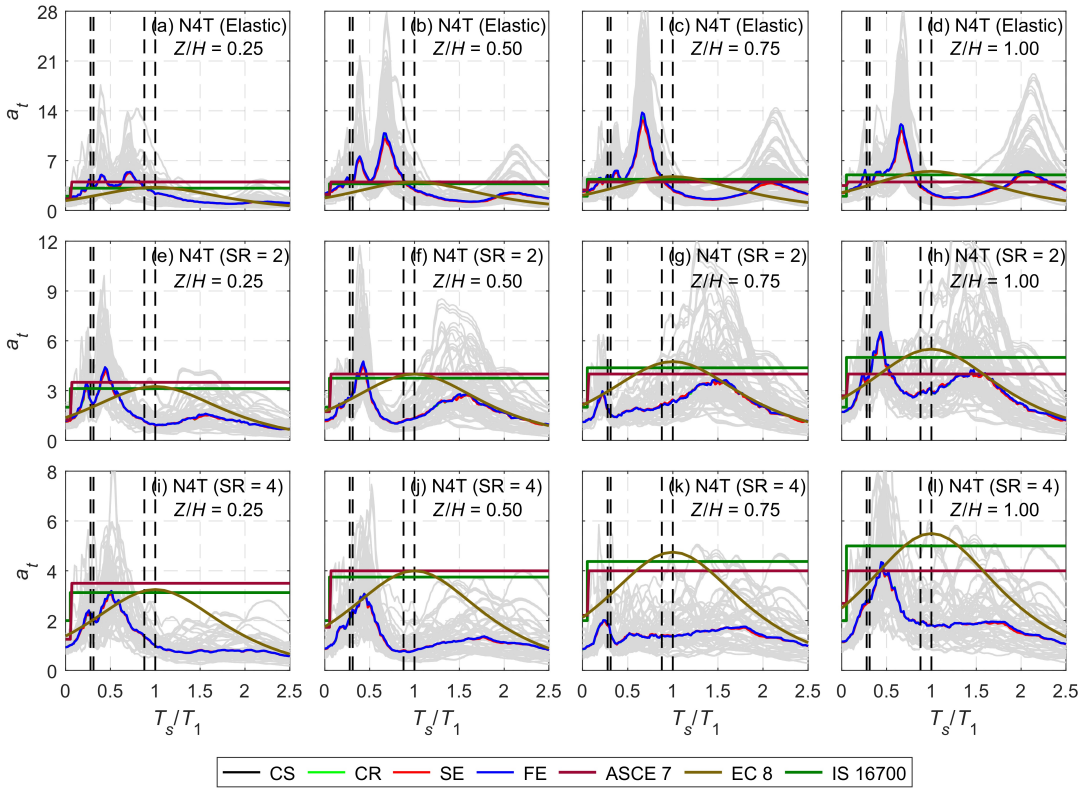

Figure 5.15: Total amplification factors for the 'N4T' building obtained using bi-directional time history analyses. Dashed vertical lines indicate the elastic modal periods in the direction under consideration.

dissipation in the building. A similar pattern is evident at other critical locations, with the median peak a_t values decreasing to 3.86, 3.62, and 3.49 at the FE and 2.96, 2.97, and 3.41 at the SE. These reductions further validate the mitigating influence of inelasticity on a_t. The median peak a_t values at the CR, when the secondary system is tuned within the building's higher mode region, are 4.03, 3.97, and 4.78 for ETI, WTI, and NTI buildings, respectively, whereas, at the SE, these values are 4.21, 3.88, and 4.61, which increase to 5.73, 5.02, and 4.95 at the FE. These reductions in a_t values highlight the substantial decrease in dynamic amplification in buildings exhibiting highly inelastic response.

For 8-story buildings exhibiting highly inelastic response (SR = 4), the median peak a_t values at the CR, when the secondary system is tuned within the building's fundamental mode region, are 1.62, 1.61, and 1.79 for ETI, WTI, and NTI buildings, respectively. Similar trends are observed at the SE, where the values are 1.50, 1.48, and 1.78, and at the FE, with values of 1.91, 1.82, and 1.79. The median peak a_t values at the CR, when the secondary system is tuned within the building's higher

mode region, are 2.86, 2.93, and 3.08 for ETI, WTI, and NTI buildings, respectively. At the SE, they increase to 3.07, 2.86, and 3.05, while the FE exhibits the highest values at 3.97, 3.50, and 3.19. These results demonstrate the mitigating effect of inelasticity on dynamic amplification across all critical locations.

When compared with code-prescribed values, the observed median peak a_t for 4-story buildings exhibiting highly inelastic response aligns well with the ASCE 7, IS 16700, and EC 8 predictions when the secondary system is tuned within the building's fundamental mode region at all floor locations. However, when the secondary system is tuned within the building's higher mode region, the IS 16700 and EC 8 predictions remain reasonably accurate, and the ASCE 7 model underestimates the median peak a_t values at the FE up to 43%. In the case of 8-story buildings, the code models provide accurate predictions of the median peak a_t when the secondary system is tuned within the building's fundamental mode region across all critical locations, while EC 8 underestimates the median peak a_t values at the SE, CR, and FE up to 59%.

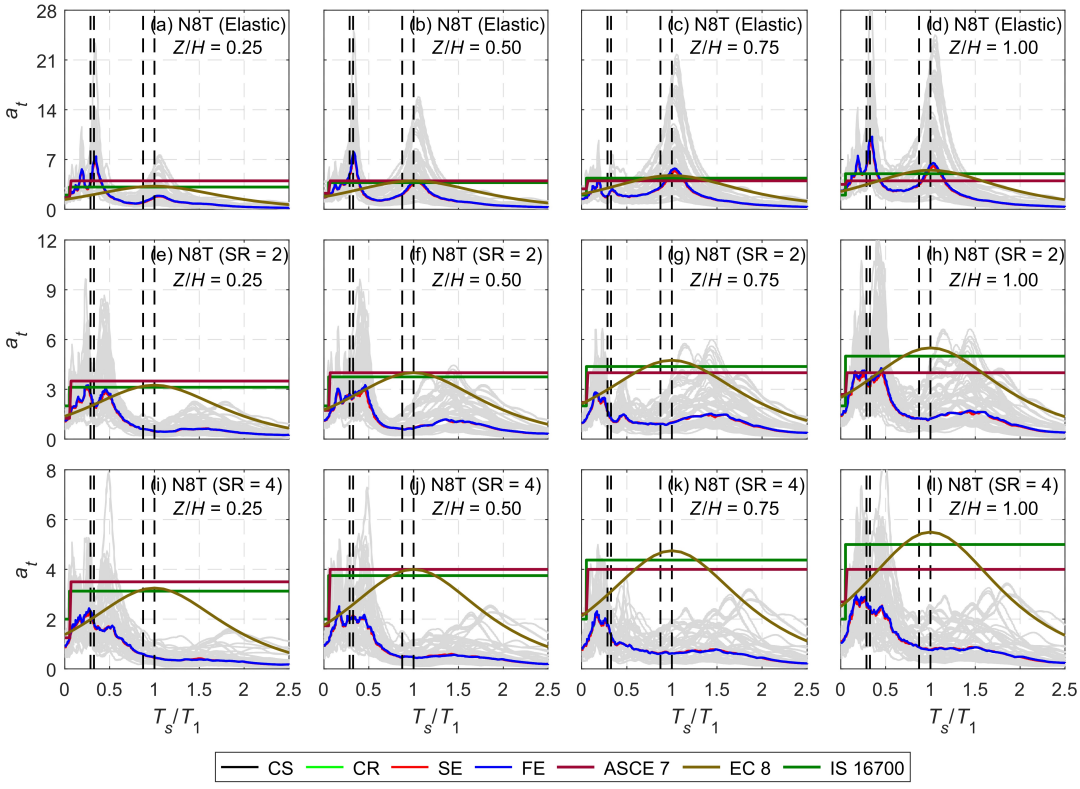

Figure 5.16: Total amplification factors for the 'N8T' building obtained using bi-directional time history analyses. Dashed vertical lines indicate the elastic modal periods in the direction under consideration.

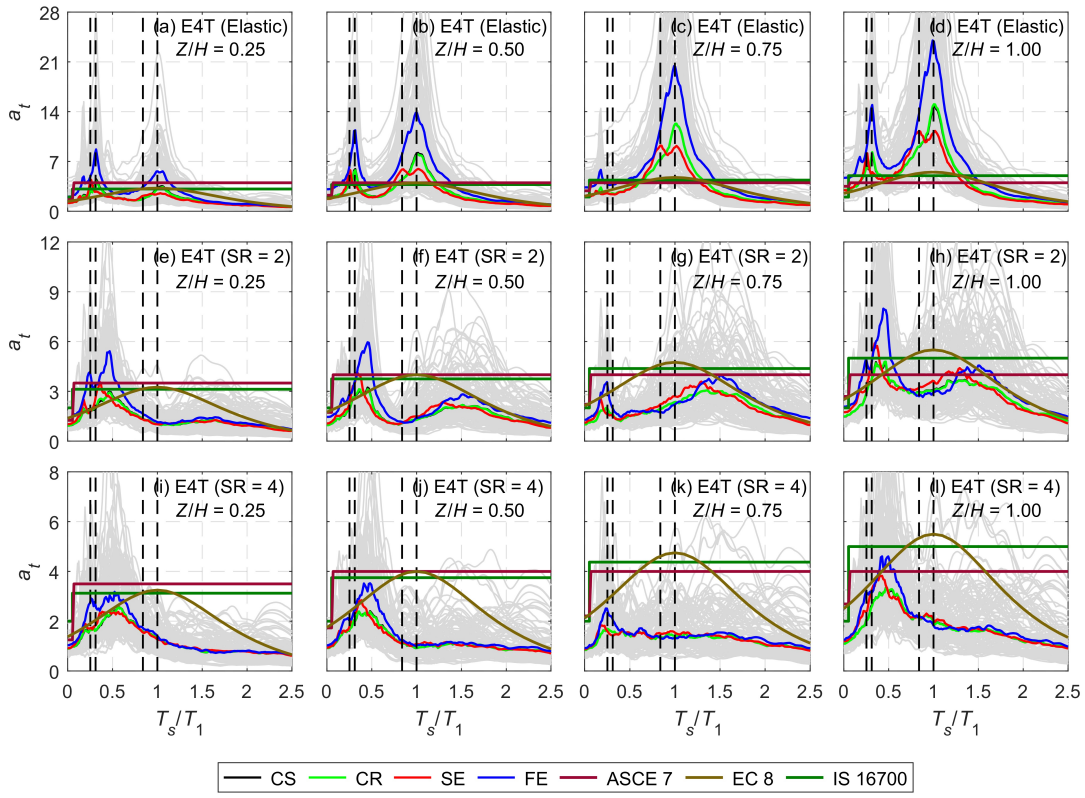

Figure 5.17: Total amplification factors for the 'E4T' building obtained using bi-directional time history analyses. Dashed vertical lines indicate the elastic modal periods in the direction under consideration.

5.2.3 Spectral amplification factors

Past studies [71, 72, 86, 117, 126] have shown that FRS are amplified GRS, and determination of the FRS from the GRS results in the least coefficient of variation (COV) as compared to the PFA or PGA used in the current codes. Accordingly, the FRS normalized by GRS, representing the spectral amplification factors (SAF), is computed as a function of the tuning ratio (T_s/T_1) and presented in Figures 5.19–5.24 and Tables 5.5–5.6. It can be observed from Figures 5.19–5.24 that the peaks in SAF curves are relatively less prominent compared to a_p and a_t curves when the secondary system is tuned within the building's higher mode region. The main reason for this lies in the shapes of the GRS, which have their peak typically in the short-period range (i.e., towards higher modes of vibration of buildings). When the FRS is normalized with the corresponding GRS, this effect is eliminated, suppressing the peaks corresponding to the case when the secondary system is tuned within the building's higher mode region.

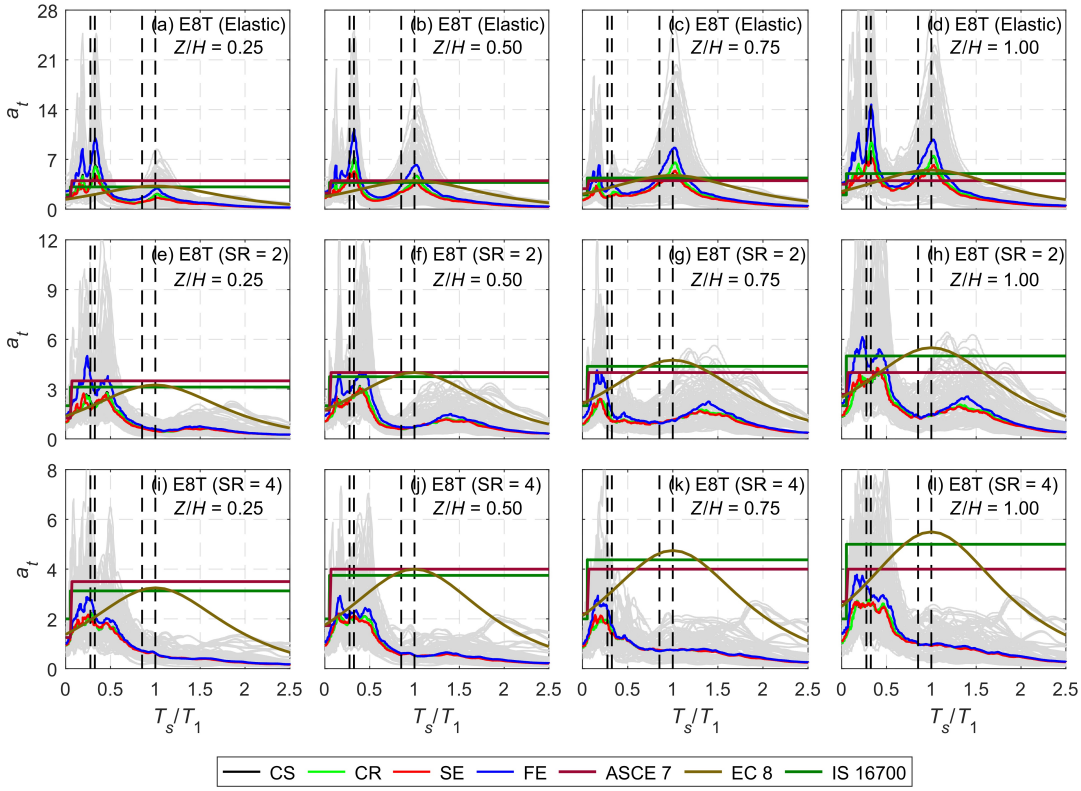

Figure 5.18: Total amplification factors for the 'E8T' building obtained using bi-directional time history analyses. Dashed vertical lines indicate the elastic modal periods in the direction under consideration.

For 4-story buildings exhibiting elastic response, the median peak SAF values at the CR corresponding to the case when the secondary system is tuned within the building's fundamental mode region are 10.55, 10.66, and 10.55 for ETI, WTI, and NTI, respectively. These values at the CR are higher than those at the SE, where they are 7.55, 8.89, and 10.02, but lower than the corresponding values at the FE, which are 15.29, 13.79, and 10.50. In contrast, the median peak SAF values at the CR corresponding to the case, when the secondary system is tuned within the building's higher mode region, are 4.29, 4.90, and 4.93, and at the SE, they reach 4.26, 3.75, and 5.24. At the FE, these values increase to 7.14, 6.91, and 5.28.

For 8-story buildings exhibiting elastic response, the median peak SAF values at the CR corresponding to the case when the secondary system is tuned within the building's fundamental mode region are 10.38, 10.35, and 10.51 for ETI, WTI, and NTI, respectively. These values are slightly higher than those at the SE, where they are 8.51, 9.14, and 10.32, but lower than the values at the FE, which are 14.19, 11.92, and 10.73. In contrast, the median peak SAF values at the CR corresponding

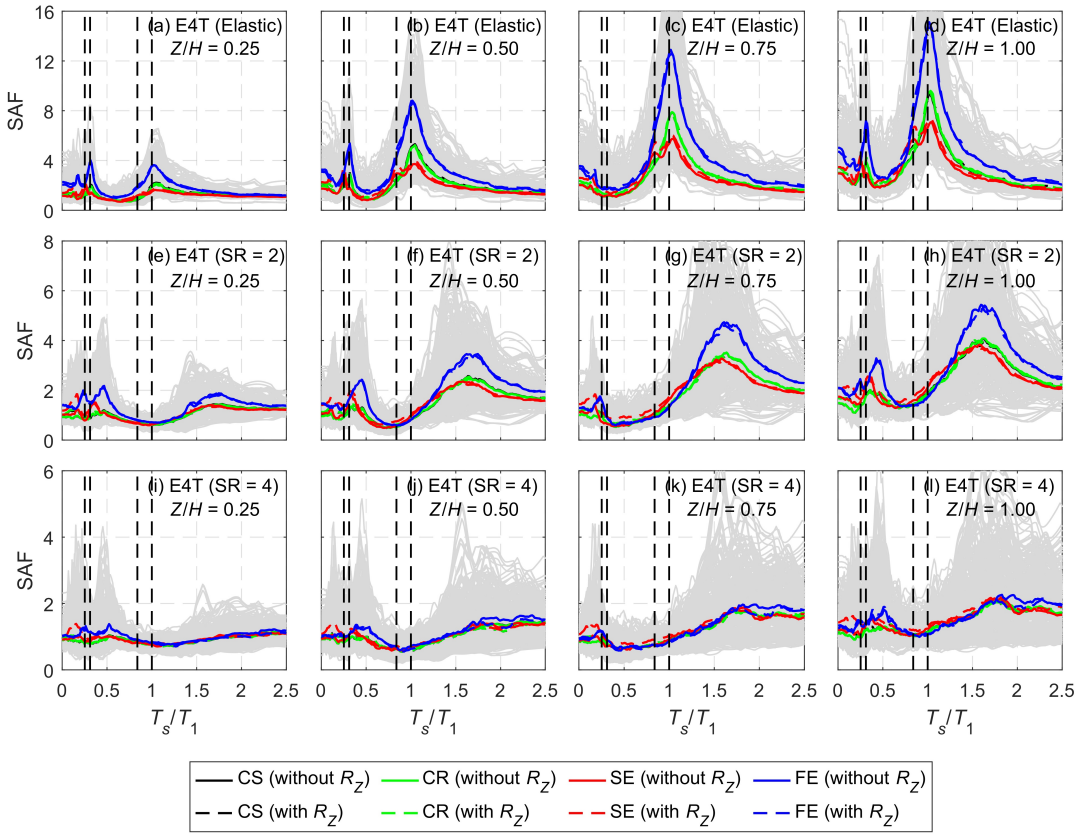

Figure 5.19: Spectral amplification factors for the 'E4T' building, with and without the rotational ground motions. Dashed vertical lines indicate the elastic modal periods in the direction under consideration.

to the case, when the secondary system is tuned within the building's higher mode region, are 4.84, 4.90, and 4.77 at the CR. These values are higher than those at the SE (3.70, 4.22, and 4.72) but still lower than the values at the FE (6.73, 6.19, and 4.96).

A comparison of these SAF values reveals that the extent of nominal torsion significantly influences the SAF values. As the nominal torsion increases, a notable increase in SAF is observed, particularly at the FE. Moreover, the difference in SAF values across the FE, SE, and CR becomes smaller with decreasing nominal torsion. For example, in the ETI buildings, the peak median SAF values at the FE, CR, and SE are 15.29, 10.55, and 7.55, respectively, while in the NTI buildings, these values are 10.50, 10.55, and 10.02. Further, as the tuning ratio (T_s/T_1) exceeds unity, the SAF begins to decrease at the FE, the CR, and the SE, and the differences between the three curves also diminish significantly. This phenomenon occurs because the building is less effectively excited at frequencies below its natural frequency. Hence,

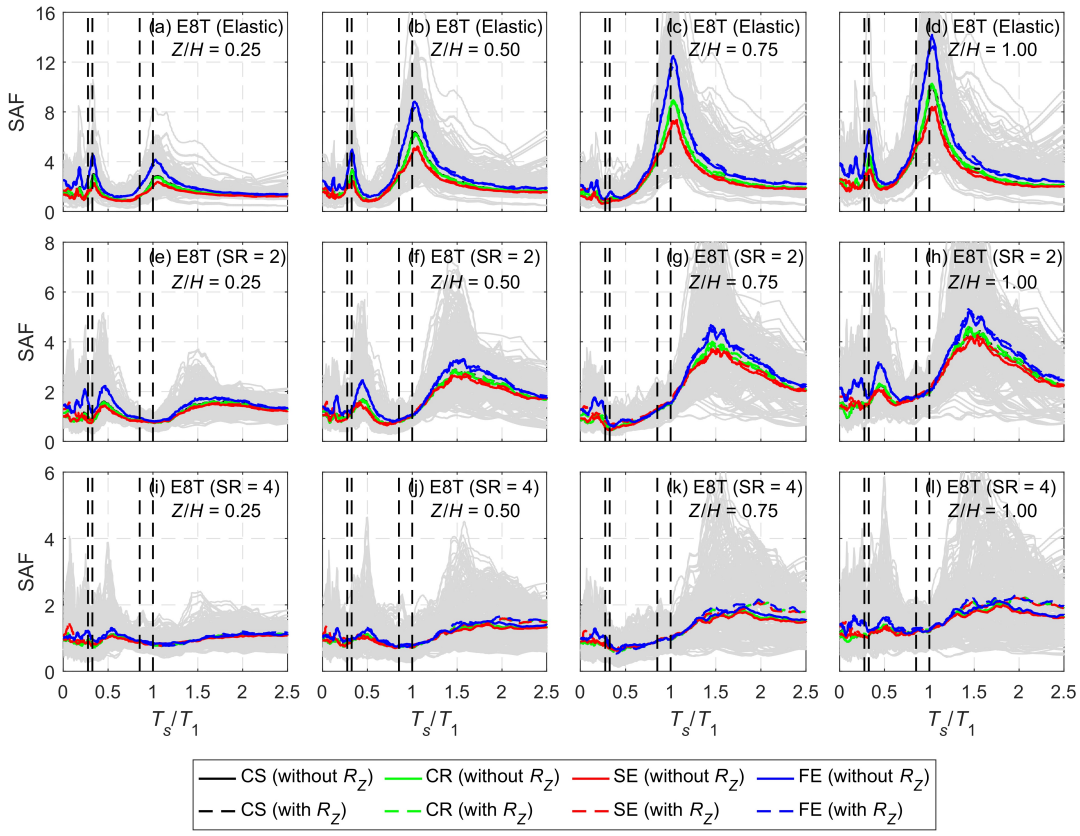

Figure 5.20: Spectral amplification factors for the 'E8T' building, with and without the rotational ground motions. Dashed vertical lines indicate the elastic modal periods in the direction under consideration.

for the secondary systems with tuning ratio, i.e., $T_s/T_1 \geq 2.0$, the responses at the FE, CR, and SE of the building tend to converge, implying that the corresponding FRS approaches GRS (Figures 5.19–5.24). This observation is in agreement with the earlier studies on regular buildings [44, 72, 75, 76, 126].

Under 4-story moderately inelastic conditions (SR = 2), the observed peak median SAF values for the secondary system tuned within the building's fundamental mode region exhibit a noticeable reduction compared to their elastic counterparts due to the dissipation of a significant portion of the input energy through hysteretic behavior and material damping. Further, the peak median SAF shifts rightwards, implying the elongation in the building's period, and the resulting peak median SAF occurs when the secondary system is in tune with the elongated building's period (Figures 5.19(e)-(h)–5.24(e)-(h)). The median peak SAF values at the CR, corresponding to the case when the secondary system is tuned within the building's fundamental mode region, are 4.61, 4.75, and 4.92 for the ETI, WTI,

Table 5.5: Median peak spectral amplification factor for the 4-story buildings.

Building	$Z/H = 0.25$						$Z/H = 1.00$					
	FM			HM			FM			HM		
	FE	CR	SE	FE	CR	SE	FE	CR	SE	FE	CR	SE
Elastic												
E4T	3.65	2.06	1.63	4.02	1.95	1.86	15.12	9.60	7.07	7.09	3.88	3.93
E4U	3.22	1.98	1.68	3.71	1.83	1.82	14.62	9.67	7.47	7.14	4.02	4.26
E4S	3.55	2.17	1.67	3.86	1.94	1.88	14.24	9.90	7.55	7.03	4.29	3.96
E4R	3.63	2.19	1.62	3.79	2.03	1.74	15.29	10.55	7.34	6.72	4.05	3.73
W4T	3.32	2.53	2.11	4.05	2.76	1.94	13.22	10.31	8.73	6.91	4.90	3.56
W4U	3.23	2.47	2.07	3.76	2.49	1.98	13.79	10.66	8.89	6.62	4.73	3.75
W4S	3.27	2.44	1.93	3.61	2.35	1.73	13.18	10.48	8.38	6.25	4.36	3.41
W4R	3.06	2.44	2.00	3.74	2.65	1.88	12.35	10.33	8.34	6.32	4.81	3.48
N4T	2.75	2.70	2.67	2.94	2.89	2.85	10.48	10.12	9.79	5.10	4.94	4.83
N4U	2.74	2.68	2.60	2.94	2.89	2.86	10.50	10.13	9.83	5.25	5.12	5.05
N4S	2.68	2.68	2.68	2.75	2.75	2.75	9.83	9.83	9.83	5.08	5.08	5.08
N4R	2.68	2.68	2.67	2.94	2.92	2.91	10.07	10.04	10.02	5.28	5.26	5.24
SR = 2												
E4T	1.88	1.44	1.41	2.18	1.15	1.49	5.44	4.09	3.84	3.29	1.93	2.56
E4U	1.72	1.41	1.36	1.96	1.19	1.42	5.54	4.11	3.82	3.36	1.92	2.61
E4S	1.79	1.47	1.41	2.00	1.17	1.50	5.44	4.37	3.77	3.24	2.03	2.62
E4R	2.02	1.56	1.46	2.31	1.32	1.48	6.07	4.61	4.19	3.53	2.19	2.58
W4T	1.91	1.71	1.56	2.17	1.50	1.27	5.65	4.58	4.34	3.15	2.28	2.05
W4U	1.91	1.63	1.57	2.00	1.36	1.35	5.51	4.58	4.30	3.06	2.29	2.31
W4S	1.95	1.69	1.60	2.10	1.39	1.39	5.67	4.75	4.43	3.13	2.29	2.24
W4R	1.94	1.70	1.59	2.19	1.54	1.24	5.18	4.60	4.19	3.20	2.36	2.15
N4T	2.02	1.99	1.95	2.01	1.98	1.93	6.17	6.02	5.90	2.86	2.76	2.73
N4U	1.86	1.85	1.79	1.98	1.93	1.87	5.68	5.38	5.12	2.91	2.80	2.77
N4S	1.86	1.89	1.86	1.91	1.89	1.88	5.29	5.47	5.37	2.75	2.80	2.82
N4R	1.85	1.89	1.80	2.06	2.01	1.98	5.62	5.84	5.42	2.90	2.86	2.82
SR = 4												
E4T	1.22	1.14	1.12	1.38	1.02	1.03	2.26	2.10	2.18	1.81	1.31	1.54
E4U	1.17	1.10	1.08	1.28	1.04	1.18	2.63	2.27	2.19	1.93	1.54	1.89
E4S	1.15	1.11	1.11	1.33	1.03	1.10	2.52	2.26	2.17	1.86	1.46	1.65
E4R	1.24	1.19	1.16	1.53	1.06	1.11	2.90	2.75	2.66	2.20	1.58	1.79
W4T	1.23	1.21	1.20	1.43	1.13	1.05	2.25	2.22	2.14	1.84	1.52	1.42
W4U	1.21	1.18	1.16	1.27	1.06	1.03	2.41	2.29	2.29	1.93	1.48	1.52
W4S	1.22	1.21	1.20	1.46	1.16	1.07	2.81	2.63	2.53	1.94	1.63	1.53
W4R	1.27	1.23	1.20	1.41	1.10	1.06	2.27	2.22	2.24	1.95	1.58	1.54
N4T	1.40	1.39	1.38	1.35	1.34	1.32	2.74	2.72	2.72	1.83	1.79	1.75
N4U	1.23	1.36	1.23	1.26	1.32	1.26	2.76	3.23	2.56	1.78	1.86	1.71
N4S	1.30	1.34	1.30	1.20	1.21	1.21	2.40	2.49	2.40	1.62	1.62	1.63
N4R	1.23	1.33	1.22	1.33	1.36	1.29	2.50	2.99	2.48	1.82	1.95	1.80

Note: Median values are color-coded using a gradient for the secondary systems tuned within the building's fundamental and higher mode regions across all buildings: light red (lowest) to green (highest) for the secondary systems tuned within the building's fundamental mode region and light blue (lowest) to sky blue (highest) for higher mode region, with intermediate values in yellow and purple, respectively.

and NTI buildings, respectively. Similarly, at the SE, these values are 4.19, 4.43, and 5.90, while at the FE, they are relatively higher, recorded as 6.07, 5.67, and

Table 5.6: Median peak spectral amplification factor for the 8-story buildings.

Building	$Z/H = 0.25$						$Z/H = 1.00$					
	FM			HM			FM			HM		
	FE	CR	SE	FE	CR	SE	FE	CR	SE	FE	CR	SE
Elastic												
E8T	4.16	2.73	2.37	4.51	2.91	2.27	14.19	10.27	8.41	6.60	4.53	3.38
E8U	3.43	2.52	2.16	4.34	2.73	2.23	12.10	9.78	8.51	6.73	4.64	3.70
E8S	3.60	2.72	2.28	4.38	2.83	2.12	11.97	9.68	8.02	6.43	4.68	3.41
E8R	3.81	2.88	2.37	4.62	3.03	2.26	12.82	10.38	8.45	6.68	4.84	3.47
W8T	3.57	2.98	2.67	4.33	3.38	2.79	11.92	10.00	8.90	6.19	4.78	3.92
W8U	3.36	2.84	2.56	3.99	3.21	2.82	11.73	9.95	8.86	5.91	4.90	4.22
W8S	3.40	2.88	2.52	3.98	3.22	2.63	11.33	9.85	8.75	5.74	4.73	3.94
W8R	3.52	3.04	2.65	4.11	3.36	2.77	11.68	10.35	9.14	5.85	4.82	4.12
N8T	3.28	3.17	3.07	3.46	3.28	3.16	10.73	10.38	10.11	4.96	4.72	4.58
N8U	3.02	2.91	2.85	3.35	3.23	3.12	10.49	9.95	9.55	4.95	4.71	4.51
N8S	3.17	3.17	3.17	3.27	3.26	3.26	10.32	10.32	10.32	4.71	4.70	4.70
N8R	3.05	3.02	2.98	3.32	3.28	3.24	10.30	10.19	10.08	4.82	4.77	4.72
SR = 2												
E8T	1.77	1.58	1.51	2.23	1.58	1.42	5.20	4.55	4.21	3.10	2.30	2.08
E8U	1.69	1.50	1.42	2.06	1.44	1.33	5.27	4.35	3.91	3.06	2.24	2.03
E8S	1.76	1.52	1.45	2.11	1.47	1.36	5.08	4.46	4.13	3.06	2.28	2.00
E8R	1.81	1.64	1.56	2.20	1.52	1.37	5.18	4.56	4.36	3.14	2.31	2.03
W8T	1.77	1.71	1.67	2.11	1.71	1.58	5.10	4.59	4.48	2.79	2.35	2.16
W8U	1.71	1.59	1.53	2.01	1.64	1.53	5.31	4.44	4.21	2.88	2.40	2.12
W8S	1.75	1.65	1.60	1.96	1.68	1.47	4.69	4.43	4.11	2.78	2.33	2.09
W8R	1.86	1.77	1.69	2.07	1.71	1.57	5.14	4.77	4.73	2.81	2.40	2.15
N8T	1.81	1.79	1.77	1.87	1.80	1.74	4.87	4.69	4.58	2.48	2.35	2.28
N8U	1.68	1.68	1.65	1.85	1.77	1.74	4.92	4.73	4.71	2.53	2.44	2.35
N8S	1.78	1.78	1.78	1.79	1.79	1.79	4.77	4.78	4.81	2.48	2.48	2.49
N8R	1.84	1.92	1.83	1.84	1.82	1.74	4.80	5.00	4.83	2.47	2.46	2.37
SR = 4												
E8T	1.14	1.11	1.09	1.24	1.11	1.08	2.12	2.05	1.99	1.61	1.41	1.31
E8U	1.11	1.08	1.06	1.25	1.06	1.04	1.99	1.93	1.88	1.72	1.46	1.44
E8S	1.12	1.09	1.08	1.26	1.11	1.08	2.18	2.10	2.04	1.76	1.53	1.39
E8R	1.25	1.17	1.15	1.38	1.18	1.10	2.56	2.47	2.37	1.69	1.47	1.37
W8T	1.18	1.17	1.16	1.27	1.20	1.14	2.53	2.40	2.33	1.55	1.38	1.31
W8U	1.15	1.15	1.13	1.26	1.14	1.11	2.23	2.08	2.02	1.62	1.48	1.39
W8S	1.21	1.18	1.15	1.29	1.17	1.12	2.01	1.95	1.89	1.66	1.46	1.41
W8R	1.21	1.20	1.20	1.29	1.21	1.14	2.58	2.47	2.36	1.62	1.46	1.37
N8T	1.20	1.20	1.20	1.22	1.19	1.18	2.50	2.47	2.48	1.50	1.47	1.45
N8U	1.19	1.19	1.20	1.25	1.24	1.23	2.50	2.47	2.46	1.53	1.47	1.45
N8S	1.21	1.21	1.21	1.23	1.23	1.23	2.48	2.48	2.47	1.45	1.44	1.45
N8R	1.22	1.40	1.26	1.23	1.28	1.20	2.22	2.81	2.31	1.53	1.60	1.49

Note: Median values are color-coded using a gradient for the secondary systems tuned within the building's fundamental and higher mode regions across all buildings: light red (lowest) to green (highest) for the secondary systems tuned within the building's fundamental mode region and light blue (lowest) to sky blue (highest) for higher mode region, with intermediate values in yellow and purple, respectively.

6.17. This decreasing trend in SAF values compared to their elastic counterparts is also evident when the secondary system is tuned within the building's higher mode

region at all locations. At the CR, these SAF values are 2.19, 2.36, and 2.68 for the ETI, WTI, and NTI buildings, respectively, whereas at the SE, the corresponding values are 2.62, 2.31, and 2.82, while at the FE, they are 3.53, 3.20, and 2.91.

For 8-story buildings exhibiting moderately inelastic response (SR = 2), the median peak SAF values at the CR corresponding to cases when the secondary system is tuned within the building's fundamental mode region reduce compared to their elastic counterparts and are observed as 4.56, 4.77, and 5.08 for the ETI, WTI, and NTI buildings, respectively. Similar reductions are observed at the SE, where the SAF values are 4.36, 4.73, and 4.83, and at the FE, with values of 5.27, 5.31, and 4.92. The median peak SAF values at the CR corresponding to the case when the secondary system is tuned within the building's higher mode region are 2.31, 2.40, and 2.48 for the ETI, WTI, and NTI buildings, respectively. The SE also exhibits reductions, with SAF values of 2.08, 2.16, and 2.49, while the FE shows values of 3.14, 2.88, and 2.53.

With increasing inelasticity (ductility demand) in buildings, the spectral peak becomes diffused, spanning multiple periods of vibration (e.g., Figures 5.19(e)-(l)). This diffusion occurs as the peak spectral amplification remains nearly constant but extends over a wider range of periods, resulting in the flattening of the SAF curves corresponding to the cases when the secondary system is tuned within the building's fundamental mode region.

For 4-story buildings exhibiting highly inelastic response (SR = 4), the peak median SAF values at the CR corresponding to cases when the secondary system is tuned within the building's fundamental mode region are significantly reduced compared to their elastic counterparts and observed as 2.75, 2.63, and 2.63 for ETI, WTI, and NTI buildings, respectively. Similar trends also occur at the SE and FE, where buildings exhibiting highly inelastic response record the reduction in SAF values when the secondary system is tuned within the building's fundamental mode region, and these SAF values are 2.66, 2.53, and 2.72 at the SE and 2.90, 2.81, and 2.76 at the FE, respectively, for ETI, WTI, and NTI buildings. The reductions in the median peak SAF are also observed when the secondary system is tuned within the building's higher mode region. However, these reductions are relatively less

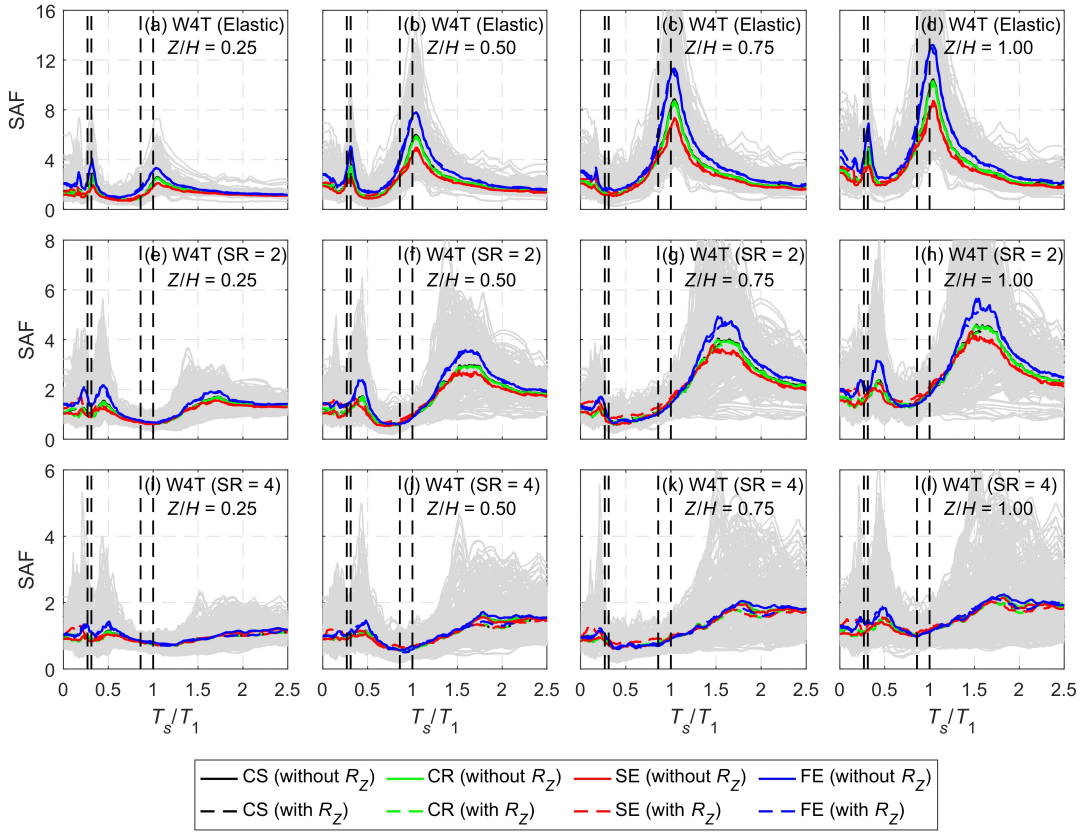

Figure 5.21: Spectral amplification factors for the 'W4T' building, with and without the rotational ground motions. Dashed vertical lines indicate the elastic modal periods in the direction under consideration.

pronounced compared to when the secondary system is tuned within the building's fundamental mode region. This is because the building primarily dissipates energy through the fundamental mode. For example, at the FE, elastic SAF values of 7.14, 6.91, and 5.28 drop to 2.20, 1.95, and 1.83 for buildings exhibiting highly inelastic response. Similarly, at the SE, the values decrease to 1.89, 1.54, and 1.80, while at the CR, they reduce to 1.58, 1.63, and 1.81.

For 8-story buildings exhibiting highly inelastic response (SR = 4), the peak median SAF values at the CR corresponding to cases when the secondary system is tuned within the building's fundamental mode region are significantly reduced compared to their elastic counterparts and observed as 2.47, 2.47, and 2.71 for ETI, WTI, and NTI buildings, respectively. Similar reductions are also observed at the SE, where these values reach 2.37, 2.36, and 2.48, and the FE, where they are 2.56, 2.58, and 2.50. The peak median SAF values at the CR corresponding to the case when the secondary system is tuned within the building's higher mode region are

1.53, 1.48, and 1.52, while at the SE, they are 1.44, 1.41, and 1.49. At the FE, these SAF values are recorded as 1.76, 1.66, and 1.53. It is also evident that for buildings exhibiting highly inelastic response, the difference in SAF values across various locations in the floor plan and for different levels of torsional irregularity starts diminishing, implying the mitigating effect of the building's inelasticity on the torsional floor acceleration response.

As the structure transitions into the inelastic state, the progressive yielding and subsequent damage to the individual structural elements lead to a reduction in the overall stiffness of the building. This stiffness degradation causes an elongation in the building's fundamental period, denoted as the *'effective period'* (T_{eff}). Estimating T_{eff} for the building models after the seismic event is crucial because the inelastic behavior and damage experienced during an earthquake significantly alter the dynamic properties of the building. T_{eff} for the investigated building models is estimated by performing *eigenvalue analyses* on the building's damaged state after

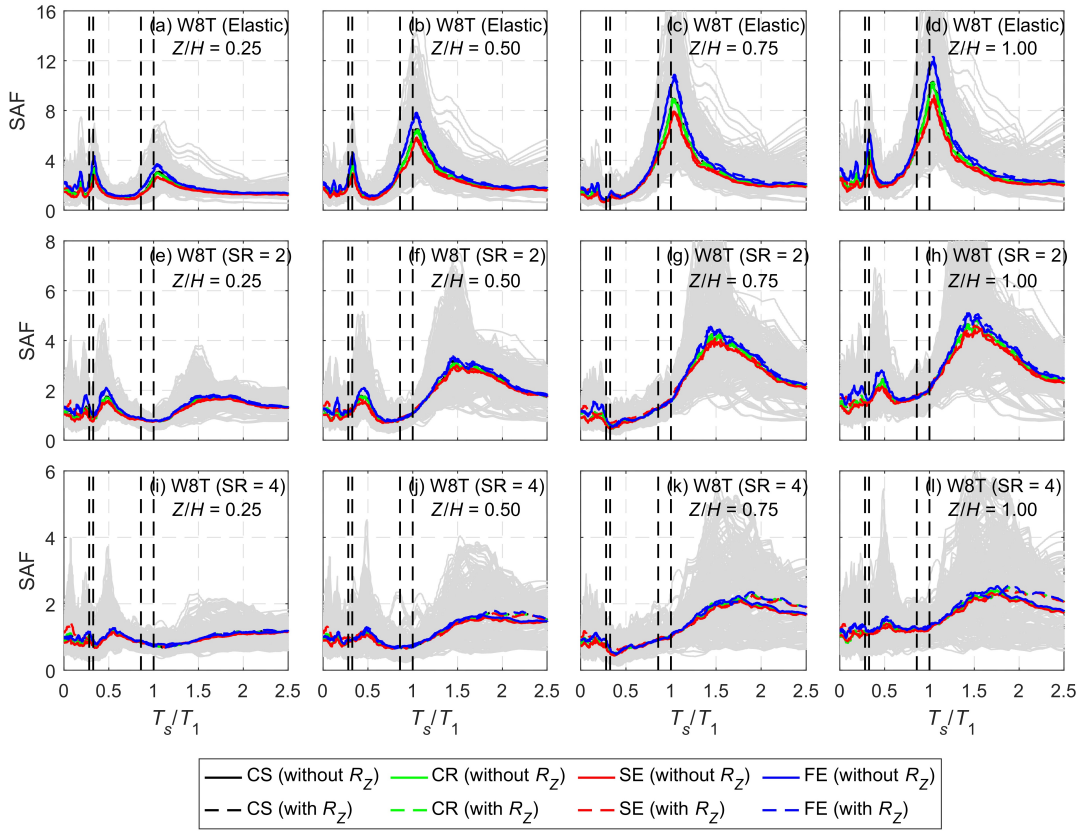

Figure 5.22: Spectral amplification factors for the 'W8T' building, with and without the rotational ground motions. Dashed vertical lines indicate the elastic modal periods in the direction under consideration.

application of the earthquake ground motion, taking into account the stiffness degradation and damage that occurred during the seismic event. The obtained median T_{eff}, normalized with T_1, ranges from 1.38 (for SR=1) to 1.66 (for SR = 4; Figure 5.25) for all the analyzed buildings. This indicates a significant elongation of T_1 as the building transitions from elastic to highly inelastic states. From the obtained estimates of T_{eff}, it is further observed that T_{eff} remains consistent across varying levels of torsional irregularity, indicating that the relationship between period elongation and inelasticity is not significantly influenced by the extent of torsional irregularity in the building. These findings are utilized later to develop a model to predict torsional amplification in the floor response of torsionally irregular buildings exhibiting elastic and inelastic response.

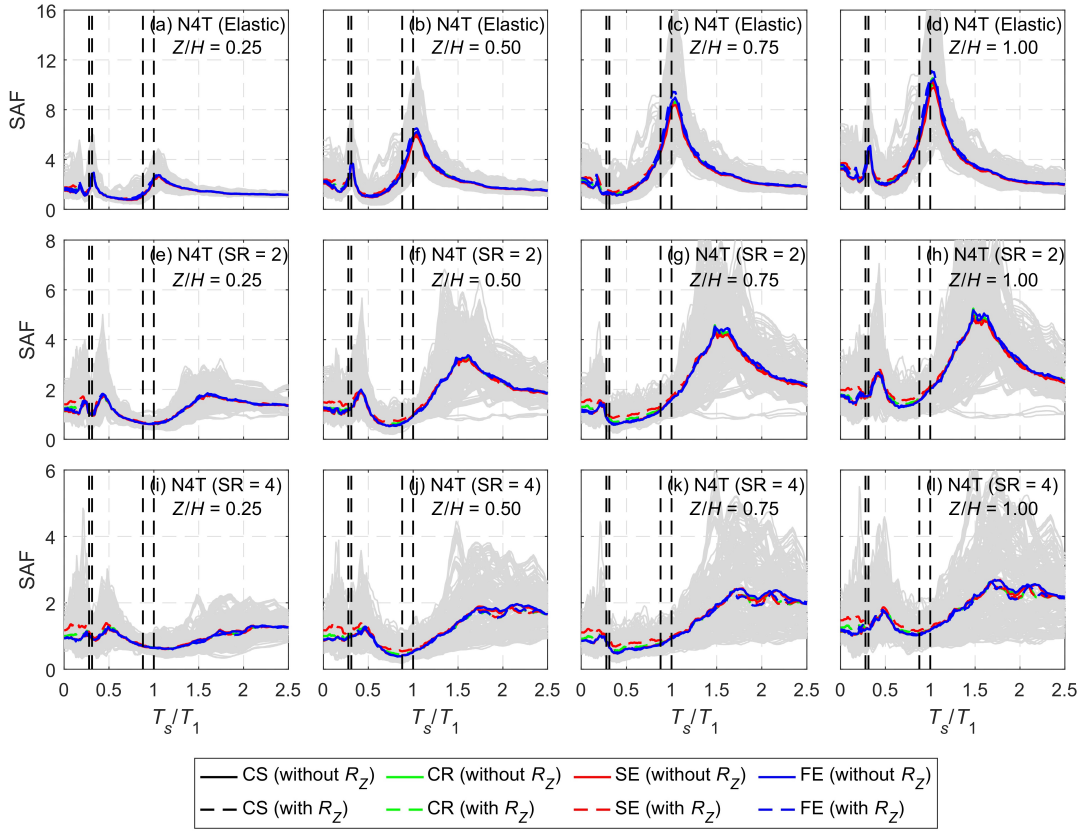

Figure 5.23: Spectral amplification factors for the 'N4T' building, with and without the rotational ground motions. Dashed vertical lines indicate the elastic modal periods in the direction under consideration.

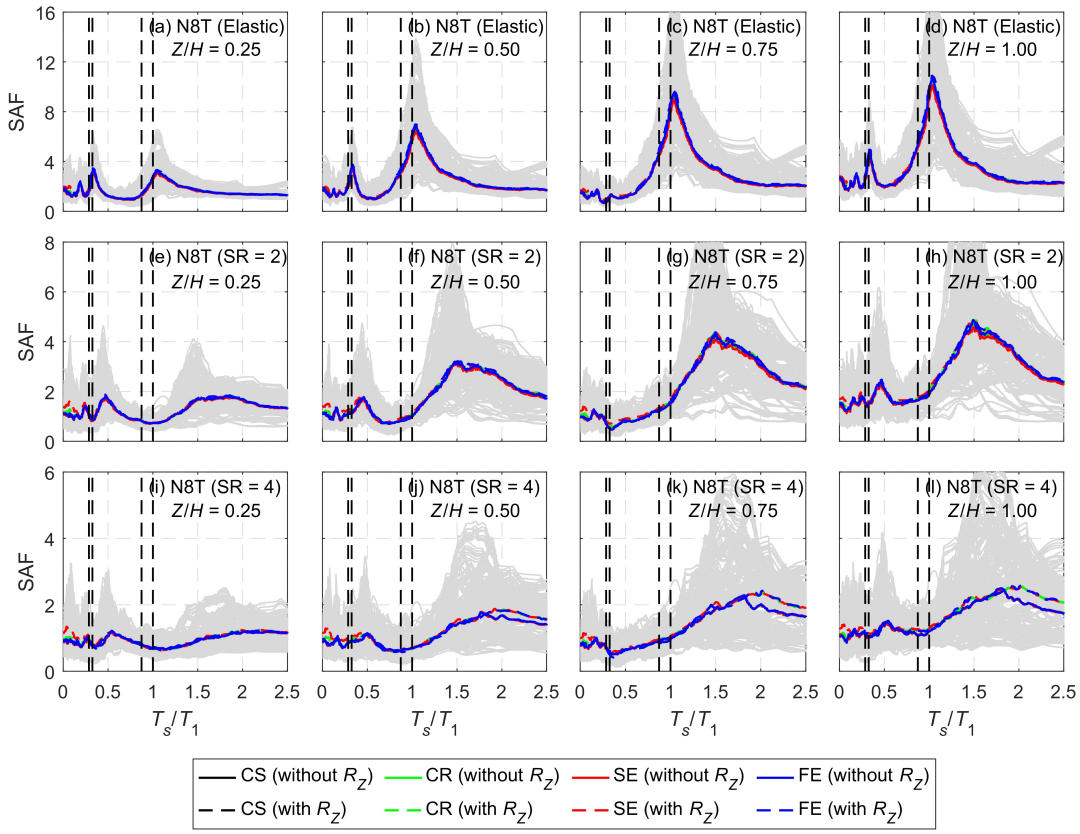

Figure 5.24: Spectral amplification factors for the 'N8T' building, with and without the rotational ground motions. Dashed vertical lines indicate the elastic modal periods in the direction under consideration.

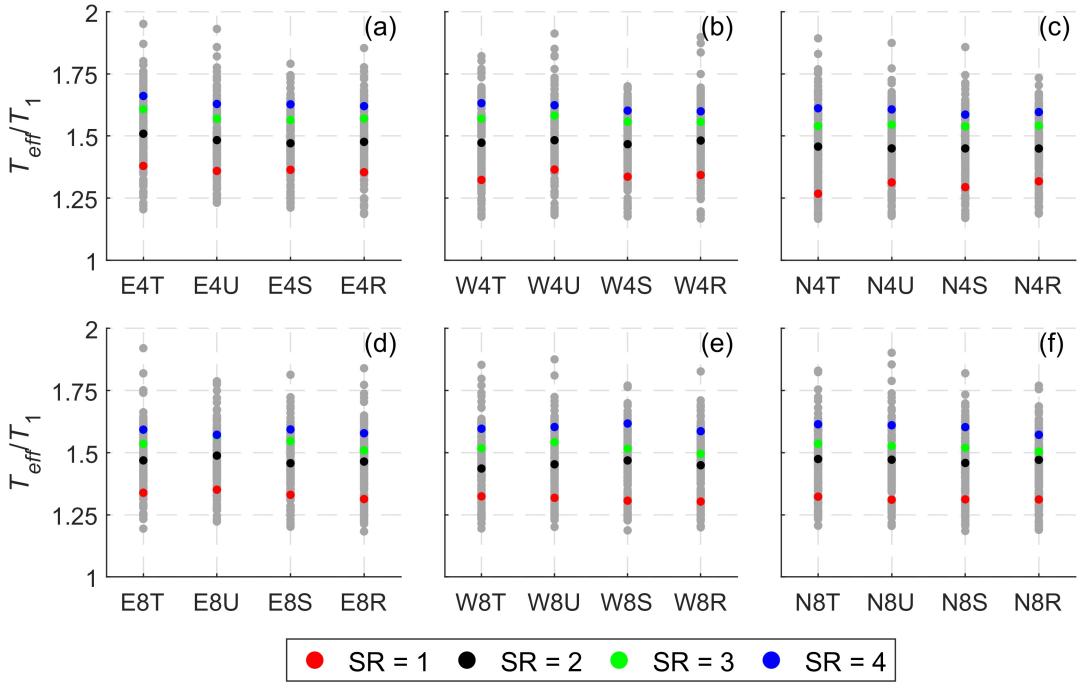

Figure 5.25: Effective period ratio for the inelastic buildings investigated in this study.

5.3 Influence of the rotational ground motions on spectral amplification factors

This section discusses the impact of rotational ground motions on the floor acceleration response of the investigated buildings. Tables 5.7–5.8 summarize the influence of the rotational ground motions on SAF in terms of the median percentage increase in acceleration demands at different locations on the floor plan for the cases when the secondary system is tuned within the building's fundamental and higher mode regions. The influence of the rotational ground motions on the median SAF for the 4- and 8-story T-shape buildings is shown in Figures 5.19–5.24.

To illustrate the influence of rotational ground motions on the floor acceleration response, the discussions are conducted with respect to the increase in median SAF response considering a suite of ground motion records. This analysis highlights the overall trends and ensures the findings are applicable to different types of seismic events. Tables 5.7–5.8 present the median increase in SAF induced by the rotational ground motions across all the investigated buildings.

The influence of rotational ground motions on SAF varies significantly depending on the fact that whether the secondary system is tuned within the building's fundamental or higher mode regions. For 4-story buildings exhibiting elastic response, the influence of rotational ground motions on the median SAF values is most pronounced at the SE. For the case when the secondary system is tuned within the building's fundamental mode region, rotational ground motions increased median SAF values by up to 10%, 8%, and 6% at the SE, 4%, 3%, and 6% at the CR, and 1%, 3%, and 8% at the FE for ETI, WTI, and NTI buildings, respectively. For the case when the secondary system is tuned within the building's higher mode region, the median SAFs due to rotational ground motions increase even to a greater extent than the fundamental mode case, reaching 54%, 51%, and 26% at the SE, 15%, 10%, and 13% at the CR, and 10%, 11%, and 29% at the FE for the ETI, WTI, and NTI buildings, respectively.

For 8-story buildings exhibiting elastic response, a mild reduction in the increase of the median SAF values is observed due to rotational ground motions compared to

Table 5.7: Median peak increase (%) in spectral amplification factor due to rotational ground motions for the 4-story buildings.

Building	$Z/H = 0.25$						$Z/H = 1.00$					
	FM			HM			FM			HM		
	FE	CR	SE	FE	CR	SE	FE	CR	SE	FE	CR	SE
Elastic												
E4T	-1	4	9	4	5	20	-3	-1	5	6	10	14
E4U	-1	-3	-2	-2	-1	34	-4	-1	0	0	2	28
E4S	-2	1	3	0	4	19	0	0	4	0	2	23
E4R	0	2	10	8	6	30	-4	-4	0	10	10	27
W4T	0	0	-1	-8	-9	6	-2	-3	-5	-4	-7	7
W4U	-2	-2	2	-3	1	2	-1	-2	2	0	2	8
W4S	1	0	8	5	6	18	1	1	1	5	9	23
W4R	3	3	7	-6	-5	4	1	-2	3	0	-3	4
N4T	2	0	-1	-2	-1	3	6	4	6	0	0	3
N4U	2	1	3	-4	-5	-4	4	4	4	-2	-4	-1
N4S	1	2	4	1	1	0	8	6	5	-2	-6	0
N4R	1	2	2	-6	-6	-5	5	5	6	-5	-8	-1
SR = 2												
E4T	-3	0	-4	-4	19	26	-3	-2	-2	-3	5	5
E4U	-1	-4	-3	-6	23	30	1	1	-2	-6	11	12
E4S	-2	-1	-2	-1	24	35	0	-2	3	-6	0	6
E4R	-4	1	1	-2	4	31	-4	-3	-2	2	1	7
W4T	1	-2	1	1	1	32	-4	-2	-5	-1	4	12
W4U	-4	-3	-2	-3	2	31	-3	-3	-1	-3	1	9
W4S	-4	-1	-1	-3	8	31	-3	-2	-2	1	3	6
W4R	-2	-1	-1	1	-1	35	-1	-3	4	1	3	8
N4T	-2	-2	-2	1	4	7	-2	-6	0	2	2	9
N4U	-5	-6	-4	-9	-11	-5	-12	-14	-13	-7	-8	-2
N4S	-5	-5	-4	-8	-11	-3	-11	-12	-11	-10	-10	-4
N4R	-8	-7	-7	-14	-13	-7	-20	-19	-16	-8	-6	-1
SR = 4												
E4T	-4	-3	-2	-3	3	36	-5	-4	-1	5	6	7
E4U	-8	-3	-2	-1	23	33	-15	-4	3	3	2	4
E4S	-5	-3	-2	-4	8	29	-10	-2	5	12	0	15
E4R	-2	-4	-2	3	0	27	-12	-14	-9	-5	-2	1
W4T	-4	-4	-4	-5	0	24	-5	-9	-5	3	5	11
W4U	-6	-5	-4	1	1	28	-4	-4	-5	-4	2	6
W4S	1	0	1	-3	1	31	-8	-12	-6	3	2	12
W4R	-3	-3	-2	5	8	31	9	5	3	6	8	9
N4T	1	0	-1	2	7	10	-2	-2	-5	2	2	8
N4U	-5	-4	-4	-5	-7	5	-21	-19	-19	-1	-2	4
N4S	-5	-4	-5	1	3	12	0	0	0	3	5	12
N4R	-4	-4	-4	-7	-6	3	-15	-14	-14	-1	0	6

Note: Negative median values represent decrease due to R_Z. Median values are color-coded using a gradient for the secondary systems tuned within the building's fundamental and higher mode regions across all buildings: light red (lowest) to green (highest) for the secondary systems tuned within the building's fundamental mode region and light blue (lowest) to sky blue (highest) for higher mode region, with intermediate values in yellow and purple, respectively.

their 4-story counterparts. For the case when the secondary system is tuned within the building's fundamental mode region, rotational ground motions increased the median SAF values at the SE up to 5%, 5%, and 7% for the ETI, WTI, and NTI buildings, respectively. At the FE, these increases in the median SAF values due to rotational ground motions are recorded as 3%, 6%, and 8%, while at the CR, these values are measured as 3%, 5%, and 8%, for the ETI, WTI, and NTI buildings, respectively. For the case when the secondary system is tuned within the building's higher mode region, the median SAFs due to the rotational ground motions are increased substantially, reaching 42%, 33%, and 17% at the SE, 6%, 7%, and 8% at the CR, and 4%, 5%, and 8% at the FE for the ETI, WTI, and NTI buildings, respectively.

For 4-story buildings exhibiting moderately inelastic response (SR = 2), when the secondary system is tuned within the building's fundamental mode region, the rotational ground motions increased median SAF values at the SE by up to 3%, 4%, and 1% for ETI, WTI, and NTI buildings, respectively. At the FE, it increased median SAF values by 2% and 1% for ETI and WTI buildings, with no increase observed for NTI buildings. Whereas, at the CR, the peak median increase is about 1% for ETI buildings, while WTI buildings showed no change, and NTI buildings experienced even a minor (2%) decrease. For the case when the secondary system is tuned within the building's higher mode region, the median SAFs due to rotational ground motions are increased than the fundamental mode case, with the increase reaching 46%, 46%, and 14% at the SE and 42%, 13%, and 9% at the CR for the ETI, WTI, and NTI buildings, respectively. At FE, the increase in the median SAF values due to rotational ground motions reaches 4%, 2%, and 6% for the ETI, WTI, and NTI buildings, respectively.

For 8-story buildings exhibiting moderately inelastic response (SR = 2), when the secondary system is tuned within the building's fundamental mode region, the rotational ground motion increased the median SAF values up to 8%, 6%, and 7% at the SE, 11%, 12%, and 6% at the FE, and 9%, 7%, and 7% at the CR for the ETI, WTI, and NTI buildings, respectively. For the case when the secondary system is tuned within the building's higher mode region, the median SAFs due to rotational ground motions are increased even to a greater extent than the fundamental mode

Table 5.8: Median peak increase (%) in spectral amplification factor due to rotational ground motions for the 8-story buildings.

Building	$Z/H = 0.25$						$Z/H = 1.00$					
	FM			HM			FM			HM		
	FE	CR	SE	FE	CR	SE	FE	CR	SE	FE	CR	SE
Elastic												
E8T	-3	2	0	2	0	1	-6	-2	-1	0	1	4
E8U	2	2	2	2	1	0	0	0	-2	0	1	5
E8S	3	3	1	-5	-3	-4	1	1	3	-5	-4	1
E8R	0	-1	0	-2	3	2	0	0	2	-2	-2	8
W8T	4	1	1	-4	-4	-1	3	3	4	-6	-3	3
W8U	3	3	4	2	2	1	3	3	4	1	1	3
W8S	4	3	5	3	2	4	5	5	5	2	1	5
W8R	1	2	3	-2	-5	-2	1	1	3	0	-3	0
N8T	1	0	0	2	0	3	2	0	0	0	0	3
N8U	7	5	5	4	1	3	5	5	5	4	0	3
N8S	1	0	-1	3	-1	1	2	1	1	0	-1	5
N8R	7	5	4	3	0	3	4	3	4	2	0	4
SR = 2												
E8T	-1	2	3	1	-1	12	2	1	1	3	3	0
E8U	4	0	2	-1	-3	24	5	5	2	3	1	7
E8S	6	5	2	2	0	25	11	9	6	7	1	10
E8R	3	2	2	1	3	20	2	4	1	4	1	4
W8T	3	3	3	-4	3	3	-1	5	3	0	4	1
W8U	5	4	3	3	1	8	-2	3	2	4	2	9
W8S	4	5	4	12	6	11	12	5	6	7	6	7
W8R	2	2	3	0	1	2	3	5	2	-2	2	4
N8T	1	2	2	-4	-2	3	-1	4	6	-4	1	4
N8U	6	5	5	-3	-1	3	6	7	2	-1	-1	2
N8S	0	1	0	1	0	3	5	5	5	-1	-1	1
N8R	0	-1	2	-4	-3	2	3	4	4	-2	1	3
SR = 4												
E8T	5	5	4	6	5	36	8	9	11	4	0	18
E8U	0	2	2	-2	9	31	3	-1	5	0	1	8
E8S	6	4	5	0	2	39	-5	-4	1	-3	-4	21
E8R	-2	0	0	0	-4	30	2	4	7	6	1	13
W8T	3	3	1	3	0	29	0	5	4	4	6	8
W8U	1	-2	-1	4	1	28	-4	2	7	5	4	4
W8S	-2	-1	0	-2	-3	27	13	15	17	-5	0	3
W8R	11	9	5	3	0	27	7	9	12	4	4	8
N8T	3	4	4	-2	0	16	3	4	3	2	3	3
N8U	4	4	3	-1	-1	19	6	6	5	1	3	5
N8S	6	6	6	-3	-3	22	9	9	10	5	4	7
N8R	2	0	-2	-4	-3	16	12	12	11	0	3	3

Note: Negative median values represent decrease due to R_Z. Median values are color-coded using a gradient for the secondary systems tuned within the building's fundamental and higher mode regions across all buildings: light red (lowest) to green (highest) for the secondary systems tuned within the building's fundamental mode region and light blue (lowest) to sky blue (highest) for higher mode region, with intermediate values in yellow and purple, respectively.

case, with the increase reaching 42%, 53%, and 24% at the SE, 19%, 9%, and 7% at the CR, and 8%, 12%, and 5% at the FE for the ETI, WTI, and NTI buildings, respectively.

For 4-story buildings exhibiting highly inelastic response (SR = 4), when the secondary system is tuned within the building's fundamental mode region, the rotational ground motions increased median SAF values at the SE by up to 5% for ETI and 3% for WTI buildings, with no increase observed for NTI buildings. At the FE, median SAF values decreased by 2% for ETI buildings but increased by 9% and 1% for WTI and NTI buildings, respectively. At the CR, the median SAF values decreased by 1% for ETI buildings, increased by 6% for WTI buildings, and showed no change for NTI buildings. When the secondary system is tuned within the building's higher mode region, the median SAFs due to rotational ground motions increase and reach 36%, 34%, and 26% at the SE; 25%, 12%, and 9% at the CR; and 12%, 7%, and 4% at the FE for ETI, WTI, and NTI buildings, respectively.

For 8-story buildings exhibiting highly inelastic response (SR = 4), even a further increase in the peak median SAF is observed at all critical locations—SE, CR, and FE—when compared to their elastic and moderately inelastic counterparts. For the case when the secondary system is tuned within the building's fundamental mode region, the rotational ground motions increased the median SAF values at the SE up to 17%, 17%, and 16% for the ETI, WTI, and NTI buildings, respectively. At the FE, these increases in the median SAF values due to rotational ground motions are recorded as 13%, 15%, and 13%, while at the CR, these values are measured as 14%, 16%, and 17%, for the ETI, WTI, and NTI buildings, respectively. For the case when the secondary system is tuned within the building's higher mode region, the median SAFs due to rotational ground motions are increased even to a greater extent than the fundamental mode case, with the increase at the SE reaching 43%, 47%, and 32%, and 9%, 7%, and 8%, at the CR for the ETI, WTI, and NTI buildings, respectively. At FE, these increases in the median SAF values due to the rotational ground motions reach 7%, 12%, and 5% for the ETI, WTI, and NTI buildings, respectively.

The presented results in this section highlight that the rotational ground

motions exert maximum acceleration increase effects at the SE, followed by the CR and the FE. The observed trends indicate that the effects of rotational ground motions on the median SAF are significant and dominant even for NTI buildings. Under the elastic response of the buildings, the maximum effects on the median SAF due to rotational ground motions are observed to be 16% (for 'N8S' building), and 32% (for 'N8U' and 'N8R' buildings) at the SE, for the cases when the secondary system is tuned within the building's fundamental and higher mode regions, respectively. As building inelasticity increases, the influence of the rotational ground motions becomes even more pronounced at all critical locations, with the maximum influence at the SE, where the median SAF increases up to 47% (for the 'W8R' building). This trend is clearly demonstrated in Tables 5.7–5.8, where the maximum median increase consistently occurs at the SE (shown by highlighted green and sky blue cells), while the CR and the FE experience a relatively lower median increase in the SAF values due rotational ground motions, its effects at these locations remain noteworthy for all buildings analyzed in this study.

5.4 Summary

This chapter focuses on understanding the characteristics of the FRS and explores the estimation of a_p, a_t, and SAF at the FE, the SE, and the CR in buildings with nominal torsion. The a_p and a_t values are compared with their corresponding code-predicted values to assess the validity of the current code models for predicting acceleration demands in buildings with nominal torsion. A total of 14,400 linear and non-linear time history analyses are performed, and absolute floor acceleration time histories are extracted at the FE, the SE, and the CR under both elastic and inelastic building responses, with and without considering rotational ground motions. The a_p and a_t values are further assessed against the provisions of ASCE 7, EC 8, and IS 16700, highlighting discrepancies that underscore the need for improved predictive models to estimate floor accelerations in buildings with nominal torsion. Additionally, spectral amplification factors are examined, and the impact of rotational ground motions on the floor acceleration demands is quantified. Based on the comprehensive numerical investigations conducted in this Chapter, the following are key observations and findings:

- The FRS in extreme torsionally irregular buildings exhibits two closely spaced (dual) peaks at the SE, with the effect being most pronounced in 4-story ETI buildings and gradually diminishing for WTI and NTI buildings due to the reduced contribution from translational-rotational coupling in the modes of vibration of such buildings. Out of these two peaks, one corresponds to the building's fundamental mode, where a large mass participates primarily in translational motion with a small rotational coupling, while the other peak is associated with the building's rotational mode of vibration, where a significant mass participates in rotational motion, with a small translational coupling.

- Existing seismic design code provisions consistently underestimate a_p in both torsionally regular and irregular buildings. The highest underestimation occurs under the elastic response at the FE, reaching 130%, 189%, and 158% for ASCE 7, EC 8, and IS 16700, respectively. In buildings exhibiting highly inelastic response, the underestimation decreases to 40%, 76%, and 57% for ASCE 7, EC 8, and IS 16700, respectively.

- Existing seismic design code provisions also underestimate a_t in both torsionally regular and irregular buildings. The highest underestimation occurs under the elastic response at the FE, reaching 539%, 411%, and 365% for ASCE 7, EC 8, and IS 16700, respectively. For buildings exhibiting highly inelastic response, EC 8 and IS 16700 provide accurate estimations of a_t, whereas ASCE 7 continues to underestimate a_t up to 47%.

- The maximum SAF for the secondary systems tuned within the building's fundamental mode region occurs at the FE for the 4-story buildings exhibiting elastic response, with values of 15.29, 13.79, and 10.50 for ETI, WTI, and NTI buildings, respectively. For the secondary systems tuned within the building's higher mode region, the SAF values are 7.14, 6.91, and 5.28 for ETI, WTI, and NTI buildings, respectively. However, for buildings exhibiting highly inelastic response, there is a significant decrease in SAF values, with values of 2.90, 2.81, and 2.76 at the FE for the secondary systems tuned within the building's fundamental mode region and 2.20, 1.95, and 1.83 for the secondary systems tuned within the building's higher mode region, respectively, for ETI, WTI,

and NTI buildings.

- The extent of nominal torsion has a significant impact on the median SAF. As the nominal torsion decreases, there is a noticeable reduction in SAF, particularly at the FE, and the differences in the SAF values between the FE, SE, and CR become almost negligible. For instance, in the case of the ETI building, the peak median SAF values for the secondary systems tuned within the building's fundamental mode region at the FE, SE, and CR are 15.29, 7.55, and 10.54, respectively. In contrast, for the NTI building, the peak median SAF values at the SE, FE, and CR are nearly comparable, with values of 10.50, 10.02, and 10.55, respectively.

- The inelastic buildings exhibited elongation in the fundamental period of the building. The effective (elongated) period remains relatively constant across different levels of nominal torsion in buildings, suggesting that the relationship between period elongation and inelasticity is not affected by the extent of nominal torsion in the building.

- The rotational ground motions can notably increase SAF values across all torsional irregularity categories (ETI, WTI, and NTI) and levels of building inelasticity, with the SE consistently showing the highest increase in SAF. Further, the increase or decrease in SAF values due to rotational ground motions is not correlated with the extent of nominal torsion in the building.

- The effects of rotational ground motions are more pronounced for the inelastic buildings. Due to the rotational ground motions, the median SAFs are increased up to 30% and 47% for buildings exhibiting elastic and highly inelastic response, respectively.

- The effect of rotational ground motions is the most severe at the SE, followed by the CR and the FE. For the case when the secondary system is tuned within the building's higher mode region, the rotational ground motions increase SAF values up to 54% at the SE, 42% at the CR, and 29% at the FE.

Chapter 6

Torsional Amplification Factors

6.1 Introduction

This chapter focuses on estimating torsional amplification factors (TAFs) for the rigid, flexible, and very flexible light-weight secondary systems in buildings exhibiting elastic and inelastic response with nominal torsion along their height. The primary objective of this Chapter is to estimate the TAFs and to examine their correlations with the floor displacement-based torsional irregularity indices of the seismic design codes. By establishing these correlations, this study addresses the limitations of the existing code-based predictions and proposes practice-oriented equations for the estimation of TAFs for seismic design of the light-weight acceleration-sensitive secondary systems in buildings with nominal torsion. The applicability of the equations proposed herein is demonstrated later in Chapter 7.

6.2 Torsional amplification factors

The TAFs are calculated as the ratio of the 5%-damped floor acceleration response at the FE or SE to that at the CR. The CR serves as a reference point, where lateral forces induce only translational motion without torsional effects. This ensures that the estimated amplification accurately captures the nominal torsion influence at different locations in the building, independent of the rigid body translation. Throughout this thesis, the TAFs are finally expressed as a function of the tuning ratio (T_s/T_1), where T_s is the period of the secondary system, and T_1 is the fundamental period of the building, to describe that how the tuning between the building and secondary system affects them. In this Chapter, the characteristics of the TAFs are thoroughly analyzed across all examined cases to provide a deeper understanding of them.

In this thesis, three different types of TAFs are described based on the

classification of the light-weight acceleration-sensitive secondary system: (i) the TAF at T_s/T_1=0, representing the TAFs corresponding to the rigid secondary systems (TAF_R), (ii) the TAF in the influence zones of different modes of vibration, corresponding to the flexible secondary systems (TAF_F), and (iii) the TAF outside the influence zones of different modes of vibration, corresponding to the very flexible secondary systems (TAF_{VF}). Each of these TAFs is further discussed in detail subsequently in this Chapter.

6.2.1 Torsional amplification factors for the rigid secondary systems

To investigate the torsional amplification of PFA/PGA, the ratios of the PFA/PGA for any frame of interest (i.e., SF_{1j} to FF_{1j}) are normalized by those obtained at the CR (or at the CS) for the given building, ground motion, floor level, and SR of interest. The derived ratio is termed as the TAF_R. The estimated TAF_R for 4- and 8-story T-shape ETI, WTI, and NTI buildings are presented along the height in Figures 6.1–6.2 and across the plan in Figures 6.3–6.8. The location of CR is delineated by dotted vertical lines. Grey lines show the TAF from a given ground motion, and colored lines show the respective medians. These plots correspond to the buildings' elastic and inelastic (SR = 2 and 4) responses. Similar plots exist for other buildings, and those are provided in the Appendix C (Figures C.1–C.24).

Table 6.1 present the median TAF_R at two different relative heights, $Z/H = 0.25$ and 1.00 for the 4- and 8-story buildings exhibiting elastic and inelastic response (SR = 2 and 4). The first important observation that can be made from Figures 6.1–6.2 is that the TAFs (i.e., at the FE and SE) obtained with respect to the CR ($TAF_{SE/CR}$ or $TAF_{FE/CR}$) or the CS ($TAF_{SE/CS}$ or $TAF_{FE/CS}$) are more or less comparable throughout the building height, with maximum differences in their median values up to only 6%, among all the investigated cases. This observation can be attributed to relatively smaller differences (Figure 3.3) between the locations of the CR and CS at any given floor level of interest among all the analyzed cases. Hence, from here onwards, all the discussions are reported on TAFs estimated with respect to the CR.

The shaded region in the Figures 6.1–6.2 represents the band of median TAF_R,

illustrating how TAF_R increases with building's nominal torsion (row-wise, e.g., compare row 1 and row 2) and reduces with the building inelasticity (column-wise). The maximum values of median TAF_R under the elastic response of the buildings are observed at the FE (FF_{11}) as 1.76 (Figures 6.1(a), 6.3(a)), 1.43, and 1.03 for ETI, WTI, and NTI buildings, respectively. Interestingly, among all the investigated buildings, the maximum value of median TAF_R is observed for the 'E4T' building (Figures 6.1(a), 6.3(a)), though it is not torsionally irregular according to EC 8 (i.e., it is torsionally regular), as the e/r for this building is less than 0.30. The other interesting observation about the TAF_R is that they are observed to be close to unity at the SE and stiff frames under the elastic response of the buildings, with their maximum median values equal to 1.00, 0.95 (Figure 6.2(d)), and 1.00 for ETI, WTI, and NTI buildings, respectively, implying their relative insensitivity to nominal torsion in buildings.

With the increase in the inelasticity of the buildings, the TAF_R at the FE (or the flexible frames) reduces and increases marginally at the SE (or stiff frames). For buildings exhibiting highly inelastic response (SR = 4), the maximum median TAF_R at the FE reached up to 1.44, 1.25, and 1.02 for ETI, WTI, and NTI buildings, whereas, at the SE, reached up to 1.12, 1.00, and 1.00 for ETI, WTI, and NTI buildings, respectively. For a given building, the inelasticity reduced TAFs by up to 29% for the flexible frames (FF_{1j} to FF_{6j}) and increased up to 21% for stiff frames (SF_{1j} to SF_{4j}) for the investigated SRs.

These findings indicate that the torsional amplification of the PFA in buildings with nominal torsion depends upon (i) the extent of nominal torsion at a given floor level, (ii) the location of the frame with respect to the CR at the floor level (significant towards flexible frames and only marginal towards stiff frames), and (iii) the degree of inelastic response exhibited by the building. Hence, it is important to include the effects of the aforementioned parameters in the seismic building codes to accurately estimate PFA demands in buildings with nominal torsion.

Table 6.1: Median torsional amplification factor for rigid secondary systems in 4- and 8-storied buildings.

Building	4-Story				8-Story			
	$Z/H = 0.25$		$Z/H = 1.00$		$Z/H = 0.25$		$Z/H = 1.00$	
	FE	SE	FE	SE	FE	SE	FE	SE
Elastic								
E-T	1.76	0.99	1.56	0.98	1.62	0.89	1.51	0.93
E-U	1.52	1.00	1.47	0.97	1.58	0.92	1.43	0.90
E-S	1.58	0.99	1.45	0.98	1.57	0.88	1.44	0.88
E-R	1.67	0.96	1.47	0.95	1.56	0.89	1.38	0.89
W-T	1.41	0.88	1.33	0.91	1.32	0.87	1.29	0.91
W-U	1.43	0.90	1.28	0.93	1.28	0.88	1.25	0.90
W-S	1.42	0.91	1.28	0.91	1.28	0.84	1.24	0.88
W-R	1.34	0.85	1.27	0.89	1.27	0.87	1.19	0.89
N-T	1.01	0.99	1.02	0.99	1.03	0.98	1.03	0.98
N-U	1.01	0.99	1.02	0.98	1.03	0.98	1.03	0.97
N-S	1.00	1.00	1.00	1.00	1.00	1.00	1.00	1.00
N-R	1.00	1.00	1.00	1.00	1.01	0.99	1.01	0.99
SR = 2								
E-T	1.56	1.11	1.32	1.13	1.48	1.01	1.52	1.07
E-U	1.28	1.08	1.23	1.10	1.42	1.06	1.46	1.05
E-S	1.44	1.11	1.21	1.14	1.49	1.05	1.42	1.13
E-R	1.53	1.10	1.27	1.12	1.48	1.03	1.51	1.10
W-T	1.38	0.99	1.28	0.99	1.25	0.95	1.23	0.95
W-U	1.37	1.01	1.18	1.05	1.27	0.96	1.29	0.96
W-S	1.34	0.99	1.19	1.03	1.29	0.94	1.28	0.97
W-R	1.37	0.99	1.23	0.99	1.24	0.95	1.23	0.96
N-T	1.01	1.00	1.01	1.00	1.03	0.98	1.03	0.99
N-U	1.01	0.99	1.02	0.99	1.00	1.00	1.01	1.00
N-S	1.00	1.01	1.00	1.00	1.00	1.00	1.00	1.01
N-R	1.01	1.00	1.00	1.00	1.03	1.00	1.03	0.99
SR = 4								
E-T	1.19	1.04	1.21	1.05	1.11	1.02	1.31	1.03
E-U	1.08	1.03	1.12	1.11	1.10	1.03	1.33	1.08
E-S	1.15	1.01	1.12	1.11	1.10	1.04	1.29	1.11
E-R	1.25	1.05	1.30	1.12	1.21	1.03	1.34	1.11
W-T	1.18	0.99	1.16	0.99	1.14	0.97	1.15	0.98
W-U	1.15	1.00	1.13	1.01	1.13	0.99	1.20	1.00
W-S	1.13	1.00	1.17	1.00	1.07	0.99	1.19	0.99
W-R	1.16	0.98	1.19	1.01	1.15	0.95	1.19	0.99
N-T	1.01	1.00	1.01	1.00	1.02	0.99	1.02	0.99
N-U	1.00	1.00	1.00	1.00	1.00	1.00	1.00	1.00
N-S	1.00	1.00	1.00	1.00	1.00	1.00	1.00	1.00
N-R	1.01	0.99	1.00	1.00	1.02	0.98	1.03	0.98

Note: Median values are color-coded using a gradient across all buildings: light red for the lowest median values, yellow for mid-range values, and green for the highest median values.

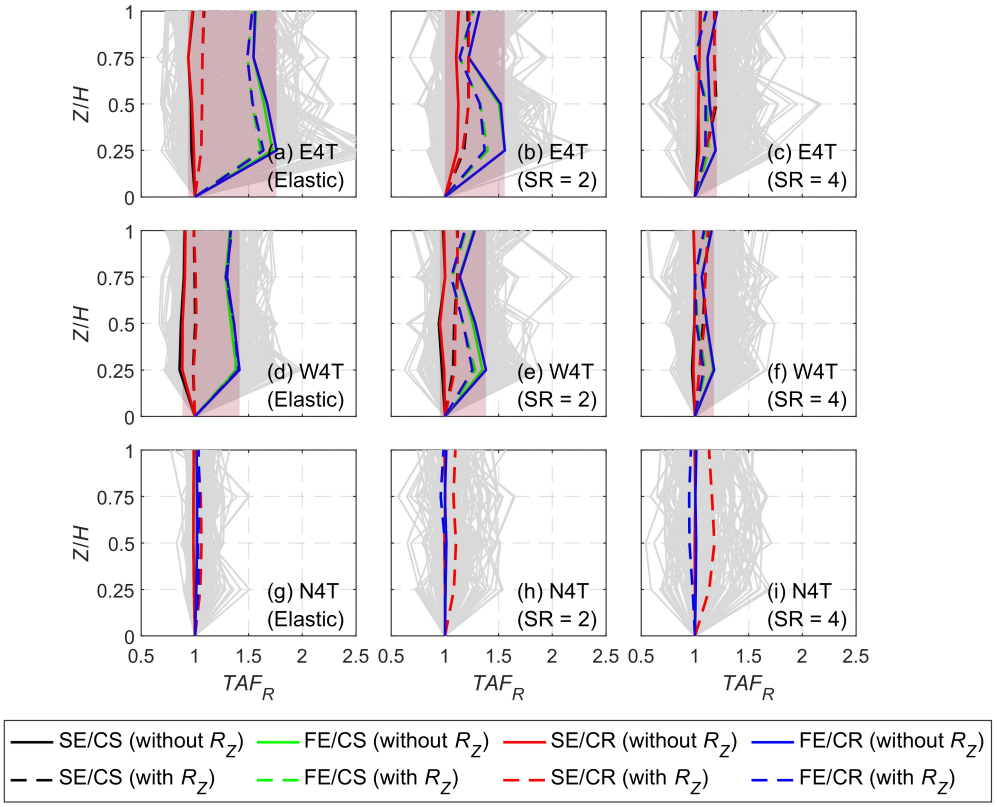

Figure 6.1: Variations of torsional amplification factor for the rigid secondary systems along the height of the 'E4T', 'W4T', and 'N4T' buildings.

6.2.1.1 Influence of rotational ground motions on torsional amplification factors of the rigid secondary systems

The influence of rotational ground motions on the median TAF_R of the analyzed buildings is depicted using dashed lines along the building height (Figures 6.1–6.2), and also across the floor plan (Figures 6.3–6.8). Table 6.2 provides the median percentage increase in the TAF_R due to rotational ground motions, across elastic and inelastic response cases (SR = 2 and 4), at two different relative heights, Z/H = 0.25 and 1.00.

To comprehensively understand the influence of rotational ground motions, it is essential to evaluate the median TAF_R across a suite of ground motion records. This broader evaluation provides a more generalized perspective, capturing overall trends, and also accounts for the record-to-record variability. Table 6.2 presents the median increase in TAF_R induced by rotational ground motions. These median values are visually represented using a gradient color scale, where green denotes the highest values, light red indicates the lowest, and yellow represents intermediate values. The

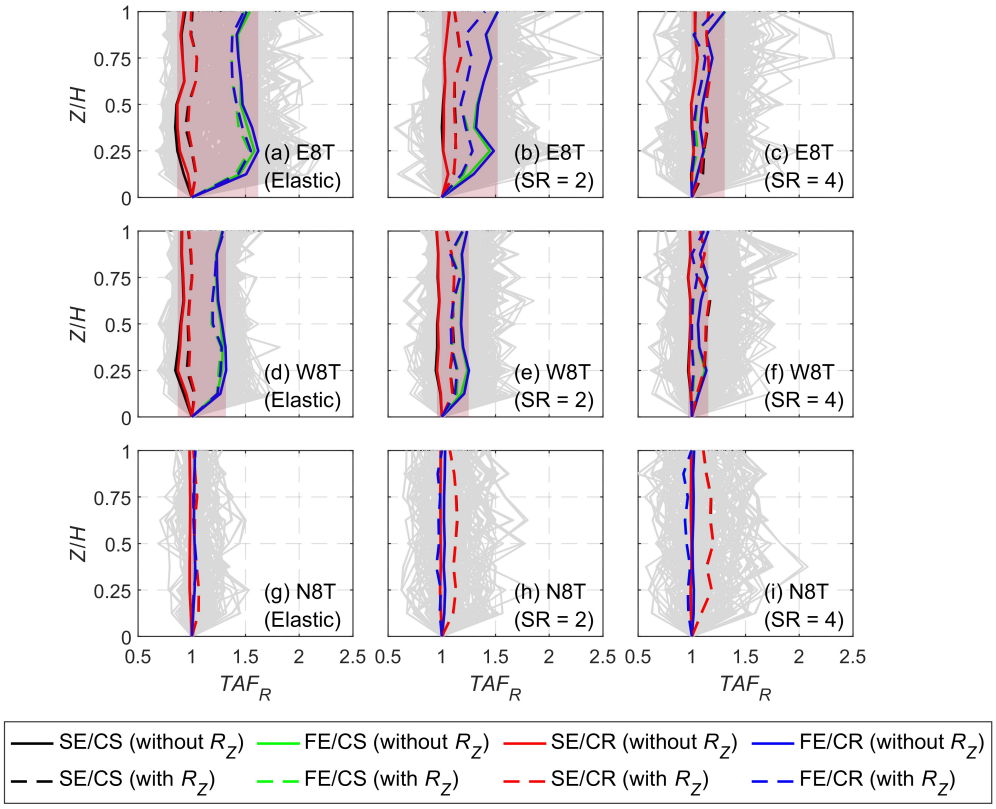

Figure 6.2: Variations of torsional amplification factor for the rigid secondary systems along the height of the 'E8T', 'W8T', and 'N8T' buildings.

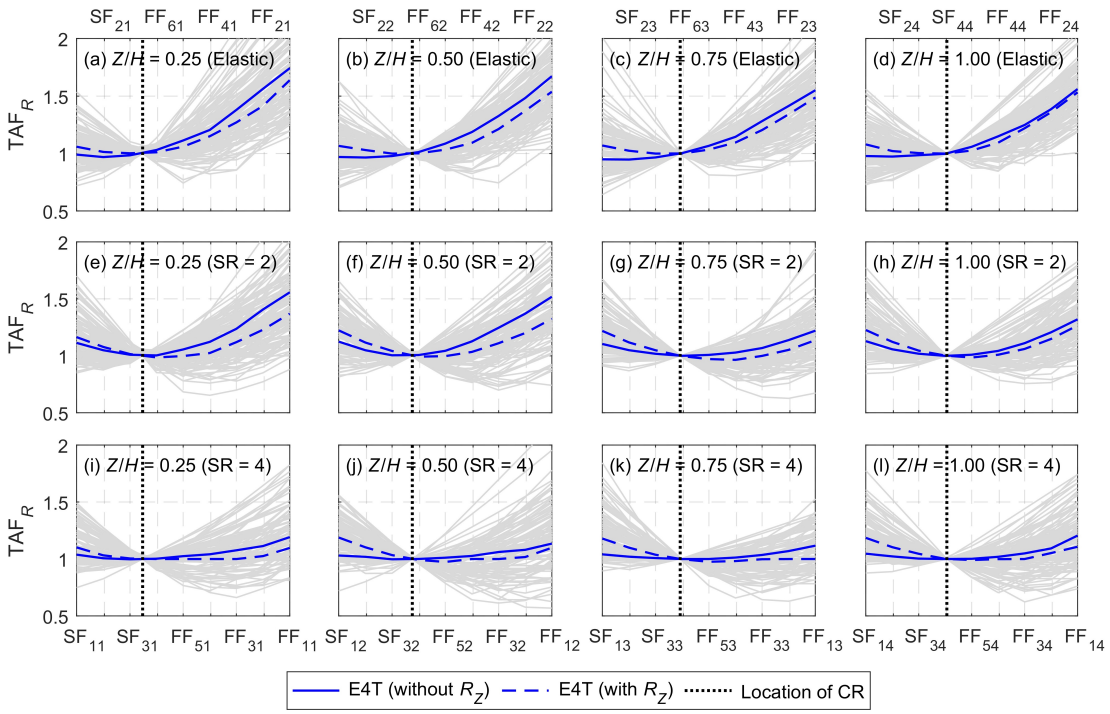

Figure 6.3: In-plan distribution of torsional amplification factor for rigid secondary systems at different floors of the 'E4T' building.

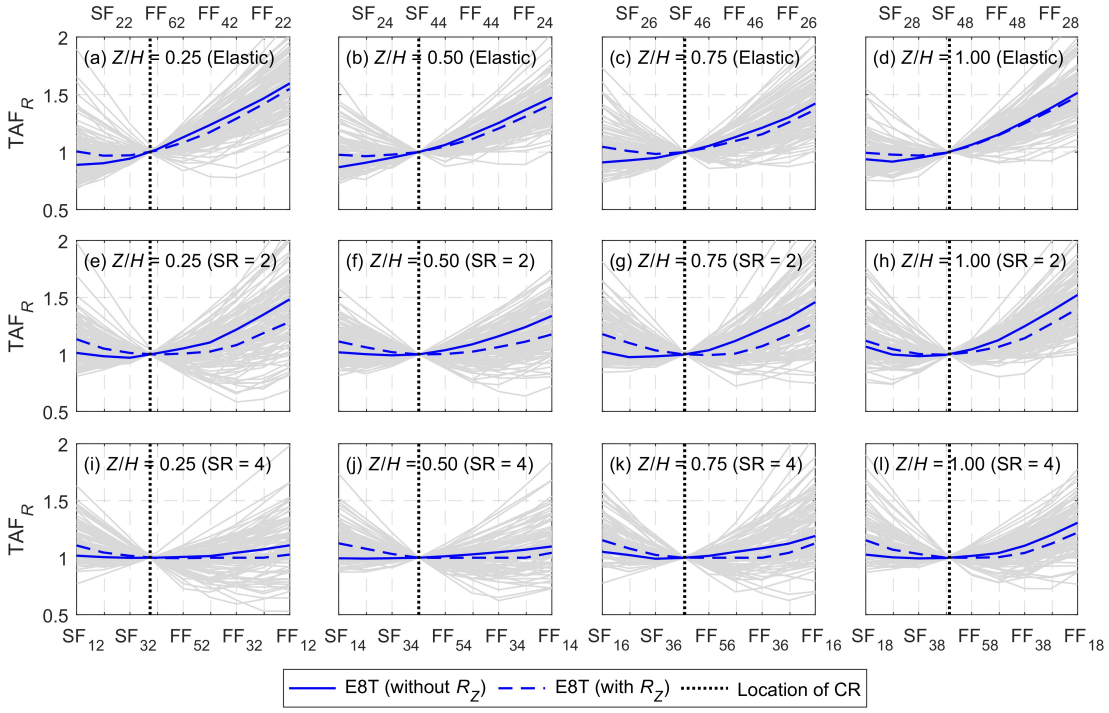

Figure 6.4: In-plan distribution of torsional amplification factor for rigid secondary systems at different floors of the 'E8T' building.

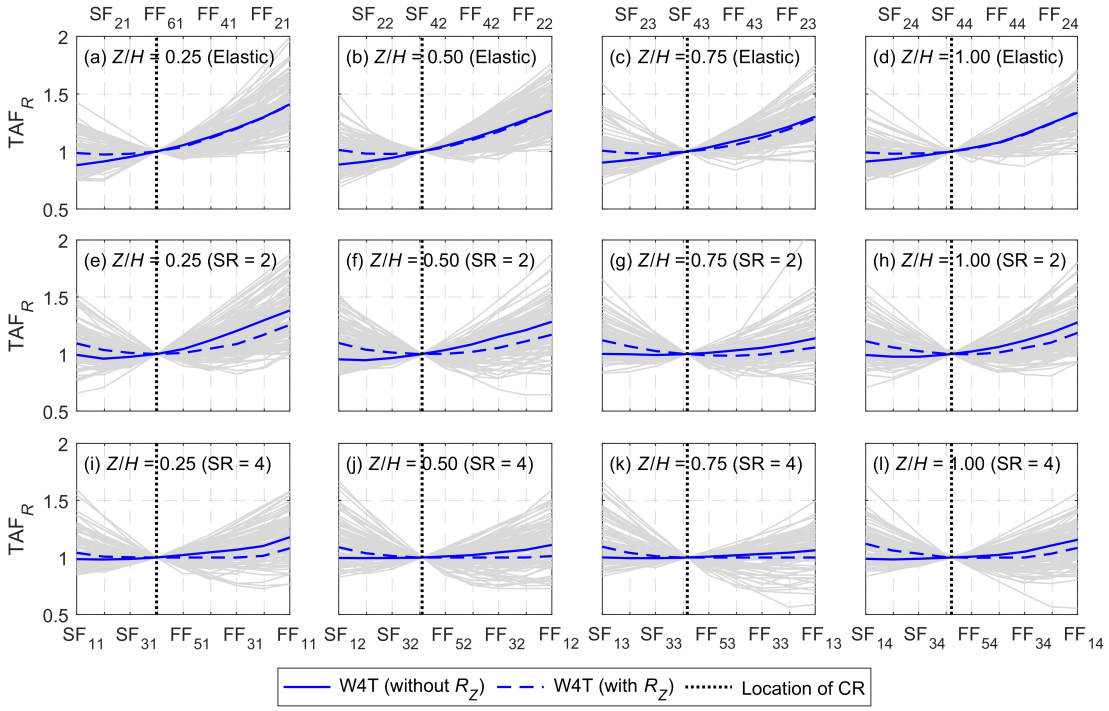

Figure 6.5: In-plan distribution of torsional amplification factor for rigid secondary systems at different floors of the 'W4T' building.

following discussion focuses on the median influence of rotational ground motions on TAF_R across all investigated buildings, ensuring a comprehensive interpretation of its effects.

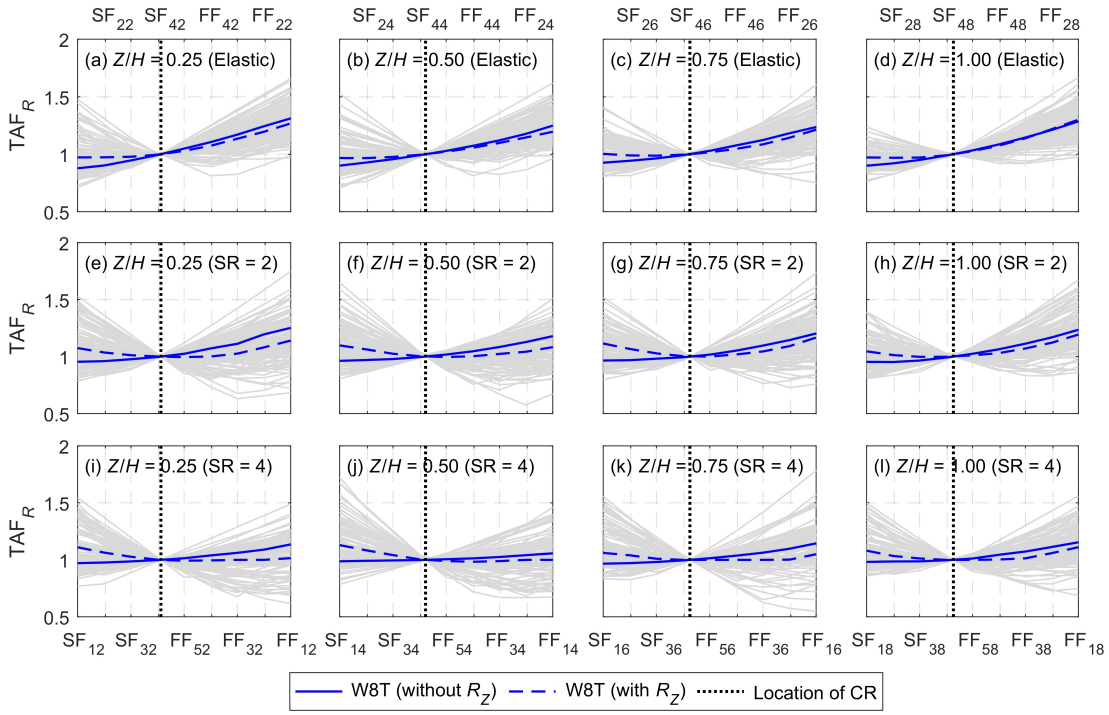

Figure 6.6: In-plan distribution of torsional amplification factor for rigid secondary systems at different floors of the 'W8T' building.

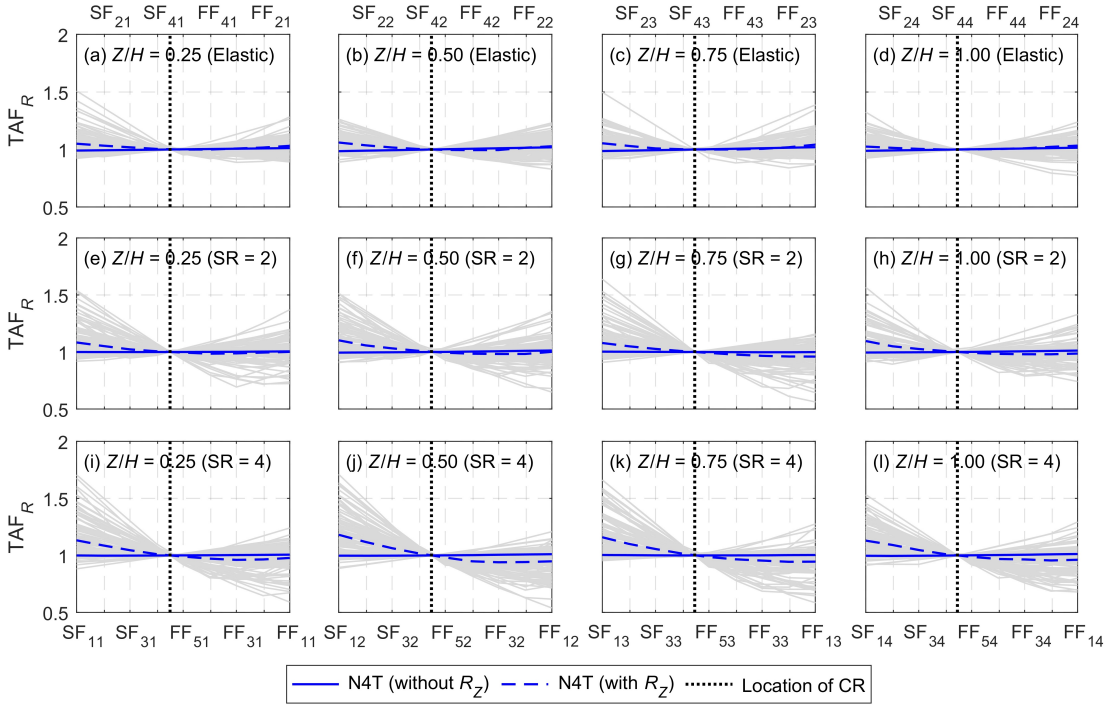

Figure 6.7: In-plan distribution of torsional amplification factor for rigid secondary systems at different floors of the 'N4T' building.

For 4-story buildings exhibiting elastic response, the rotational ground motions result in the highest median TAF_R increase at the SE, with values of 14%, 18%, and 8% for ETI, WTI, and NTI buildings, respectively. In contrast, the FE

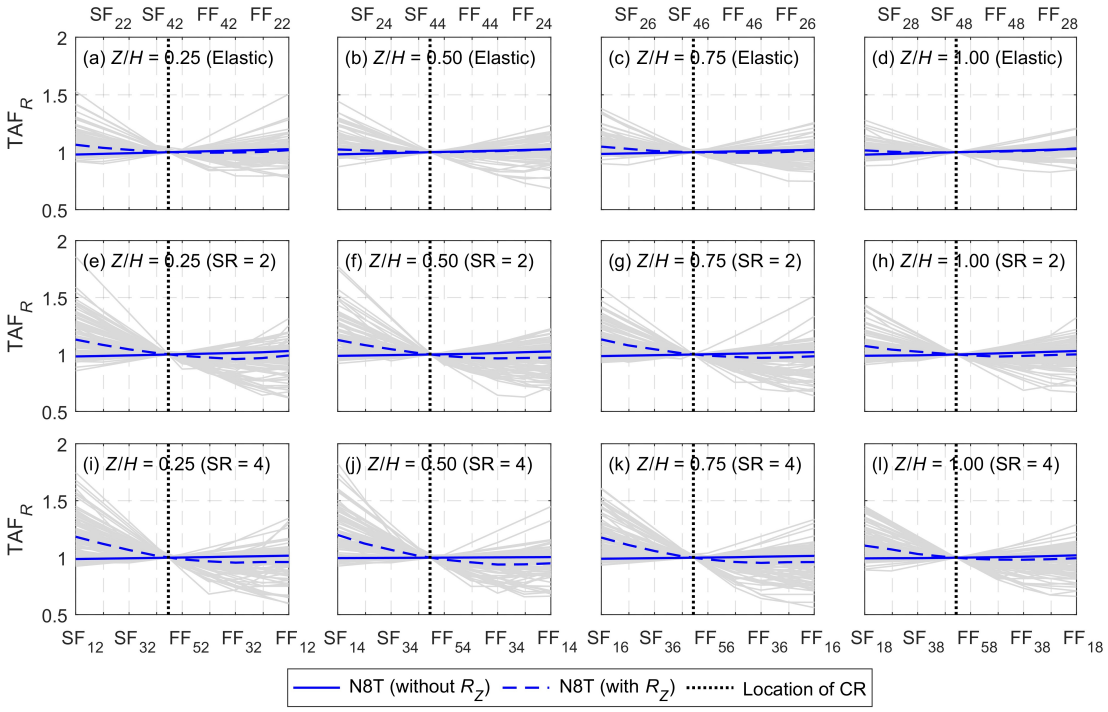

Figure 6.8: In-plan distribution of torsional amplification factor for rigid secondary systems at different floors of the 'N8T' building.

experiences a decrease of 8% in ETI buildings but shows a slight increase of about 2% and 4% in WTI and NTI buildings, respectively. A similar trend is observed in 8-story buildings exhibiting elastic response, where the overall median TAF_R increase remained comparable to that of the 4-story buildings. The SE continues to exhibit the highest median TAF_R increase, reaching 15%, 15%, and 9% for ETI, WTI, and NTI buildings, while the FE shows a decrease of 7% in ETI buildings, but an increase of about 3% in both WTI and NTI buildings.

For buildings exhibiting moderately inelastic response (SR = 2), the increase in median TAF_R due to the rotational ground motions at the SE remains comparable to the elastic case, with values of 16%, 18%, and 15% for ETI, WTI, and NTI buildings, respectively. However, at the FE, the decrease in the median TAF_R is observed for ETI, WTI, and NTI buildings, with values of 14%, 10%, and 5%, respectively. In 8-story buildings exhibiting moderately inelastic response (SR = 2), the SE continues to experience the highest increase in the median TAF_R, reaching 20%, 19%, and 18%, whereas the FE records decrease in the median TAF_R of 15%, 11%, and 7% for ETI, WTI, and NTI buildings, respectively.

For 4-story buildings exhibiting highly inelastic response (SR = 4), the increase

Table 6.2: Median increase (%) in torsional amplification factor for rigid secondary systems due to rotational ground motion.

Building	4-Story				8-Story			
	$Z/H = 0.25$		$Z/H = 1.00$		$Z/H = 0.25$		$Z/H = 1.00$	
	FE	SE	FE	SE	FE	SE	FE	SE
Elastic								
E-T	-7	7	-2	10	-4	13	-2	7
E-U	-3	6	-6	8	-6	11	-2	14
E-S	-5	10	-3	7	-5	13	-3	11
E-R	-4	7	-3	12	-5	13	0	8
W-T	-1	12	1	9	-4	12	1	7
W-U	-2	15	1	11	-2	10	1	7
W-S	-3	15	1	12	0	15	1	10
W-R	2	18	0	10	-5	13	3	10
N-T	2	6	1	4	-1	9	0	4
N-U	3	7	4	6	1	7	2	5
N-S	4	8	3	6	0	9	1	4
N-R	2	8	2	6	0	9	0	4
SR = 2								
E-T	-12	5	-4	9	-13	12	-8	5
E-U	-7	2	-4	9	-13	8	-9	7
E-S	-14	4	-5	8	-13	11	-5	5
E-R	-10	3	-2	7	-9	14	-6	5
W-T	-9	10	-7	12	-9	13	-3	10
W-U	-9	11	-4	8	-6	15	-5	9
W-S	-4	13	-4	12	-8	16	-4	7
W-R	-5	12	-7	13	-7	16	-2	9
N-T	-3	9	-2	10	-4	15	-3	9
N-U	0	13	-3	12	-2	15	0	8
N-S	0	12	-1	13	-2	16	0	9
N-R	0	10	-1	10	-3	16	-2	10
SR = 4								
E-T	-8	6	-8	13	-7	9	-7	12
E-U	-7	4	-8	12	-6	7	-10	6
E-S	-4	5	-3	10	-8	8	-6	7
E-R	-5	4	-8	8	-6	9	-1	11
W-T	-8	6	-6	13	-11	14	-4	10
W-U	-6	6	-7	13	-11	9	-5	8
W-S	0	8	-5	14	-6	7	-2	10
W-R	-3	9	-8	17	-8	20	-5	13
N-T	-2	13	-4	13	-5	20	-2	11
N-U	0	7	-2	11	-3	16	-1	9
N-S	-2	13	-3	16	-3	20	-1	13
N-R	-1	10	-2	16	-3	23	-3	15

Note: Negative median values represent decrease due to R_Z. Median values are color-coded using a gradient across all buildings: light red for the lowest median values, yellow for mid-range values, and green for the highest median values.

in median TAF_R at the SE remains consistent with the elastic case, with values of 15%, 18%, and 18% for ETI, WTI, and NTI buildings, respectively. Conversely, the FE exhibits a decrease in the median TAF_R response, with values of 13%, 12%, and 6% for ETI, WTI, and NTI buildings, respectively. A similar pattern is observed in 8-story buildings exhibiting highly inelastic response (SR = 4), where the SE continues to experience the highest increase in the median TAF_R, reaching 18%, 27%, and 24%, while the FE exhibits a further decrease in the median TAF_R reaching about 13%, 14%, and 9% for ETI, WTI, and NTI buildings, respectively.

Overall, the maximum median increase in TAF_R due to rotational ground motions reaches 27% at the SE, while the FE experiences a significantly lower increase of about 4% only. The results highlight that the SE consistently undergoes the highest median TAF_R increase across all building types and inelasticity levels, whereas the FE generally shows a minimal increase and even a decrease in most cases (e.g., up to 15% for 'E8U' building). Both the 4- and 8-story buildings showed a similar and comparable trend of increase in TAF_R due to rotational ground motions. Notably, NTI buildings, despite having no torsional irregularity, still show the median TAF_R increase of 24% (for 'N8R' building) at the SE, due to rotational ground motions. Further, the extent of nominal torsion does not have much effect on the median TAF_R increase due to rotational ground motions.

6.2.2 Torsional amplification factors for the flexible secondary systems

To examine the TAFs for the flexible secondary systems, the SAF at the FE and SE is normalized by the SAF at the CR (or the CS) for each building, ground motion, floor level, and SR of interest. This normalized ratio, referred to as TAF_F, is estimated for 4- and 8-story T-shaped ETI, WTI, and NTI buildings. The results considering both elastic and inelastic responses (with SRs = 2 and 4) are presented in Figures 6.9–6.14. Similar plots are obtained for other cases but reported in the Appendix C (Figures C.25–C.42). The median values for the elastic and inelastic cases (SR = 2 and 4) are presented in Tables 6.3–6.4. Grey lines show the torsional amplification spectrum for a given ground motion for the secondary system's damping ratio of 5%, and colored lines show the respective medians.

For 4-story buildings exhibiting elastic response, the maximum values of the median TAF_F corresponding to the case when the secondary system is tuned within the building's fundamental mode region are measured at the FE, as 2.06 (Figure 6.9(b)), 1.69 (Figure 6.11(a)), and 1.08 for ETI, WTI, and NTI buildings, respectively. However, at the SE, these median TAF_F reduce to 1.38, 1.16, and 1.00 for ETI, WTI, and NTI buildings, respectively. For the case when the secondary system is tuned within the building's higher mode region, the median TAF_F increases compared to the fundamental mode region and reaches 2.33 (Figure 6.9(a)), 1.83 (Figure 6.11(a)), and 1.04 at the FE, and 1.51, 1.26, and 1.02 at the SE, for ETI, WTI, and NTI buildings respectively.

For 8-story buildings exhibiting elastic response, a reduction in the median TAF_F is observed compared to their 4-story counterparts. The maximum value of the median TAF_F corresponding to the case, when the secondary system is tuned within the building's fundamental mode region, are measured as 1.61, 1.37, and 1.08 for ETI, WTI, and NTI buildings, respectively, at the FE. However, at the SE, these median TAF_F reduce to 1.18, 1.04, and 1.00 for ETI, WTI, and NTI buildings, respectively. For the case when the secondary system is tuned within the building's higher mode region, the median TAF_F increases to 1.98 (Figure 6.10(a)), 1.54, and 1.08 at the FE, and 1.32, 1.04, and 1.00 at the SE, for ETI, WTI, and NTI buildings respectively. These results highlight that the median TAF_F is generally higher when secondary systems are tuned within the building's higher mode region. Additionally, the median TAF_F is the highest for ETI buildings and the lowest for NTI buildings. Moreover, the median TAF_F is higher for 4-story buildings and relatively lower for 8-story buildings.

For 4-story buildings exhibiting moderately inelastic response (SR = 2), the maximum values of the median TAF_F decreases corresponding to the case when the secondary system is tuned within the building's fundamental mode region, compared to the elastic counterpart. The median TAF_F values at the FE are obtained as 1.51 (Figure 6.9(b)), 1.29 (Figure 6.11(a)), and 1.05 for ETI, WTI, and NTI buildings, respectively. At the SE, the median TAF_F further decreases to 1.25, 1.18, and 1.03 for ETI, WTI, and NTI buildings, respectively. For the case when the secondary system is tuned within the building's higher mode region, the

Table 6.3: Median peak torsional amplification factor for flexible secondary systems in the 4-story buildings.

Building	$Z/H = 0.25$				$Z/H = 1.00$			
	FM		HM		FM		HM	
	FE	SE	FE	SE	FE	SE	FE	SE
Elastic								
E4T	2.01	1.26	2.33	1.41	1.85	1.24	1.89	1.36
E4U	1.87	1.31	2.25	1.31	1.70	1.38	1.90	1.27
E4S	1.84	1.28	2.10	1.42	1.70	1.35	1.78	1.40
E4R	1.91	1.34	2.17	1.51	1.73	1.22	1.77	1.46
W4T	1.69	1.07	1.83	1.12	1.44	1.03	1.59	1.06
W4U	1.57	1.11	1.70	1.15	1.44	1.10	1.49	1.12
W4S	1.64	1.16	1.78	1.26	1.42	1.06	1.47	1.14
W4R	1.53	1.06	1.73	1.08	1.32	1.02	1.47	1.08
N4T	1.05	1.00	1.02	1.00	1.05	1.00	1.02	1.00
N4U	1.08	1.00	1.02	1.02	1.06	1.00	1.03	1.01
N4S	1.00	1.00	1.00	1.00	1.00	1.00	1.00	1.00
N4R	1.00	1.00	1.01	1.00	1.00	1.00	1.00	1.00
SR = 2								
E4T	1.31	1.14	2.30	1.44	1.35	1.22	1.79	1.40
E4U	1.26	1.15	2.11	1.31	1.33	1.23	1.73	1.35
E4S	1.23	1.14	2.07	1.44	1.28	1.23	1.60	1.46
E4R	1.32	1.18	2.10	1.51	1.33	1.23	1.79	1.48
W4T	1.17	1.05	1.76	1.16	1.20	1.08	1.58	1.10
W4U	1.19	1.12	1.72	1.26	1.24	1.13	1.47	1.20
W4S	1.16	1.09	1.74	1.29	1.19	1.13	1.53	1.17
W4R	1.17	1.06	1.72	1.24	1.16	1.10	1.58	1.14
N4T	1.02	1.01	1.02	1.02	1.03	1.01	1.03	1.01
N4U	1.03	1.01	1.04	1.02	1.05	1.01	1.04	1.02
N4S	1.00	1.00	1.00	1.02	1.00	1.00	1.01	1.01
N4R	1.01	1.00	1.04	1.01	1.01	1.01	1.03	1.01
SR = 4								
E4T	1.23	1.04	1.59	1.18	1.17	1.09	1.49	1.26
E4U	1.13	1.04	1.54	1.16	1.13	1.12	1.42	1.29
E4S	1.14	1.03	1.52	1.17	1.09	1.12	1.36	1.25
E4R	1.25	1.05	1.90	1.25	1.18	1.13	1.78	1.34
W4T	1.13	1.01	1.41	1.04	1.11	1.03	1.47	1.04
W4U	1.12	1.03	1.42	1.09	1.07	1.09	1.35	1.08
W4S	1.12	1.03	1.58	1.14	1.09	1.06	1.51	1.10
W4R	1.14	1.03	1.49	1.05	1.10	1.05	1.45	1.08
N4T	1.01	1.00	1.03	1.01	1.01	1.00	1.02	1.01
N4U	1.02	1.01	1.02	1.01	1.03	1.01	1.03	1.00
N4S	1.00	1.00	1.01	1.01	1.00	1.00	1.01	1.01
N4R	1.01	1.00	1.03	1.01	1.01	1.01	1.03	1.00

Note: Median values are color-coded using a gradient for both fundamental and higher modes across all buildings: light red (lowest) to green (highest) for secondary systems tuned within the building's fundamental mode region and light blue (lowest) to sky blue (highest) for higher mode region, with intermediate values in yellow and purple, respectively.

Table 6.4: Median peak torsional amplification factor for flexible secondary systems in the 8-story buildings.

Building	$Z/H = 0.25$				$Z/H = 1.00$			
	FM		HM		FM		HM	
	FE	SE	FE	SE	FE	SE	FE	SE
Elastic								
E8T	1.59	1.03	1.98	1.25	1.41	1.06	1.81	1.10
E8U	1.58	1.11	1.93	1.27	1.45	1.14	1.74	1.22
E8S	1.53	1.04	1.91	1.29	1.33	1.06	1.73	1.24
E8R	1.50	1.01	1.83	1.22	1.32	1.07	1.69	1.09
W8T	1.32	0.99	1.52	1.00	1.25	1.01	1.44	0.99
W8U	1.37	1.03	1.52	0.99	1.27	1.03	1.43	1.00
W8S	1.30	0.99	1.45	1.01	1.20	1.03	1.44	0.99
W8R	1.23	0.99	1.42	1.01	1.17	1.00	1.38	0.99
N8T	1.05	1.00	1.06	0.99	1.05	1.00	1.05	0.99
N8U	1.06	1.00	1.08	0.99	1.07	1.00	1.06	1.00
N8S	1.00	1.00	1.00	1.00	1.00	1.00	1.00	1.00
N8R	1.02	1.00	1.02	1.00	1.01	1.00	1.02	1.00
SR = 2								
E8T	1.24	1.01	1.93	1.28	1.17	1.02	1.99	1.36
E8U	1.24	1.05	1.93	1.29	1.19	1.05	1.78	1.41
E8S	1.20	1.03	1.80	1.38	1.15	1.05	1.85	1.53
E8R	1.25	1.02	1.89	1.30	1.19	1.04	2.00	1.51
W8T	1.12	1.00	1.51	1.02	1.12	1.00	1.46	1.02
W8U	1.14	1.02	1.50	1.07	1.15	1.02	1.41	1.06
W8S	1.12	1.00	1.53	1.04	1.09	1.01	1.56	1.11
W8R	1.13	1.00	1.46	1.01	1.11	1.03	1.52	1.06
N8T	1.02	1.01	1.05	1.00	1.03	1.01	1.04	1.00
N8U	1.02	1.01	1.04	1.02	1.04	1.00	1.04	1.02
N8S	1.00	1.00	1.01	1.01	1.00	1.00	1.02	1.01
N8R	1.02	1.01	1.05	1.01	1.02	1.02	1.07	1.00
SR = 4								
E8T	1.10	1.01	1.42	1.11	1.09	1.01	1.60	1.21
E8U	1.10	1.01	1.37	1.10	1.11	1.03	1.57	1.31
E8S	1.11	1.01	1.33	1.14	1.08	1.02	1.46	1.35
E8R	1.13	1.02	1.48	1.18	1.11	1.02	1.75	1.41
W8T	1.05	1.00	1.21	1.01	1.08	1.00	1.39	1.06
W8U	1.09	1.01	1.27	1.05	1.08	1.01	1.42	1.06
W8S	1.05	1.00	1.23	1.03	1.04	1.00	1.46	1.13
W8R	1.07	1.00	1.26	1.02	1.07	1.00	1.50	1.09
N8T	1.02	1.01	1.04	1.00	1.02	1.01	1.04	1.00
N8U	1.01	1.01	1.02	1.02	1.02	1.00	1.03	1.03
N8S	1.00	1.00	1.01	1.01	1.00	1.00	1.01	1.01
N8R	1.01	1.02	1.05	1.01	1.02	1.02	1.08	1.01

Note: Median values are color-coded using a gradient for both fundamental and higher modes across all buildings: light red (lowest) to green (highest) for secondary systems tuned within the building's fundamental mode region and light blue (lowest) to sky blue (highest) for higher mode region, with intermediate values in yellow and purple, respectively.

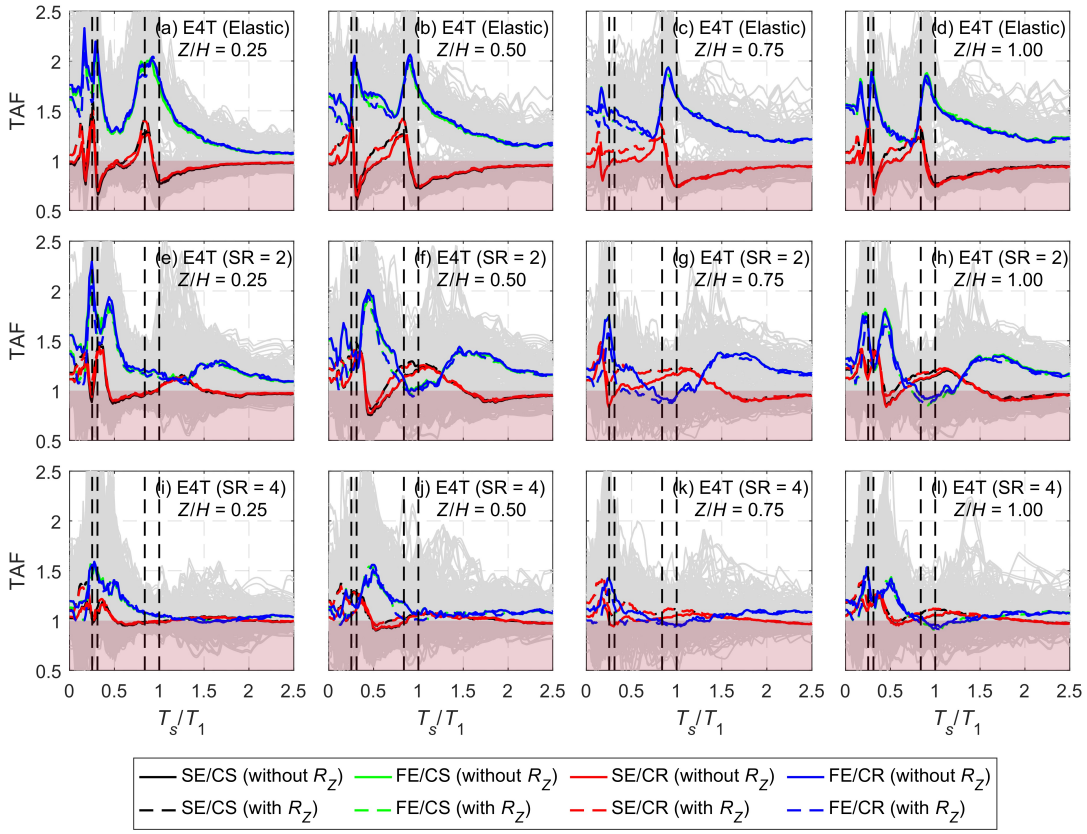

Figure 6.9: Torsional amplification factors for the 'E4T' building estimated using time history analyses with and without rotational ground motions. Dashed vertical lines indicate the elastic modal periods in the direction under consideration.

median TAF_F experiences a minor reduction and remains relatively similar to their elastic counterparts, with values of 2.30 (Figure 6.9(a)), 1.76 (Figure 6.11(a)), and 1.05 at the FE, and 1.51, 1.29, and 1.02 at the SE for ETI, WTI, and NTI buildings, respectively.

For 8-story buildings exhibiting moderately inelastic response (SR = 2), the maximum value of the median TAF_F corresponding to the case, when the secondary system is tuned within the building's fundamental mode region is lower than both their 4-story as well as elastic counterparts, with values of 1.33, 1.19, and 1.04 for ETI, WTI, and NTI buildings, respectively, at the FE. At the SE, the median TAF_F further reduces to 1.10, 1.05, and 1.02 for ETI, WTI, and NTI buildings, respectively. For the case when the secondary system is tuned within the building's higher mode region, the median TAF_F decreases to 2.12, 1.56, and 1.08 at the FE, and 1.57, 1.13, and 1.02 at the SE for ETI, WTI, and NTI buildings, respectively.

For 4-story buildings exhibiting highly inelastic response (SR = 4), the median

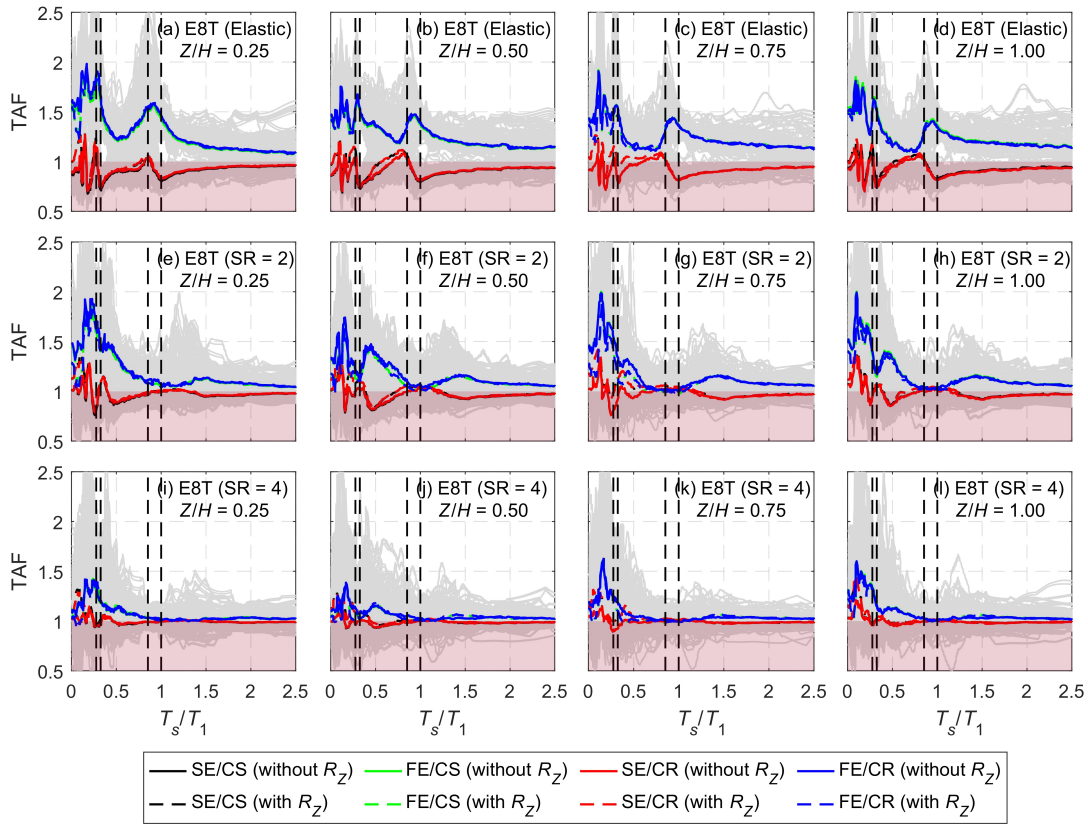

Figure 6.10: Torsional amplification factors for the 'E8T' building estimated using time history analyses with and without rotational ground motions. Dashed vertical lines indicate the elastic modal periods in the direction under consideration.

values of TAF_F corresponding to the case, when the secondary system is tuned within the building's fundamental mode region significantly decrease compared to its elastic counterparts, with values of 1.37, 1.15, and 1.03 for ETI, WTI, and NTI buildings, respectively, at the FE. At the SE, the median TAF_F values further decrease to 1.13, 1.09, and 1.02 for ETI, WTI, and NTI buildings, respectively. A reduction in the median TAF_F compared to their elastic counterpart is also observed for the case when the secondary system is tuned within the building's higher mode region, with values of 1.90, 1.58, and 1.04 at the FE, and 1.46, 1.18, and 1.01 at the SE for ETI, WTI, and NTI buildings, respectively.

For 8-story buildings exhibiting highly inelastic response (SR = 4), the median TAF_F values corresponding to the case, when the secondary system is tuned within the building's fundamental mode region, further reduce to 1.15, 1.10, and 1.03 for ETI, WTI, and NTI buildings, respectively, at the FE. At the SE, the median TAF_F values reduce further to 1.03 for all three building types. For the case when

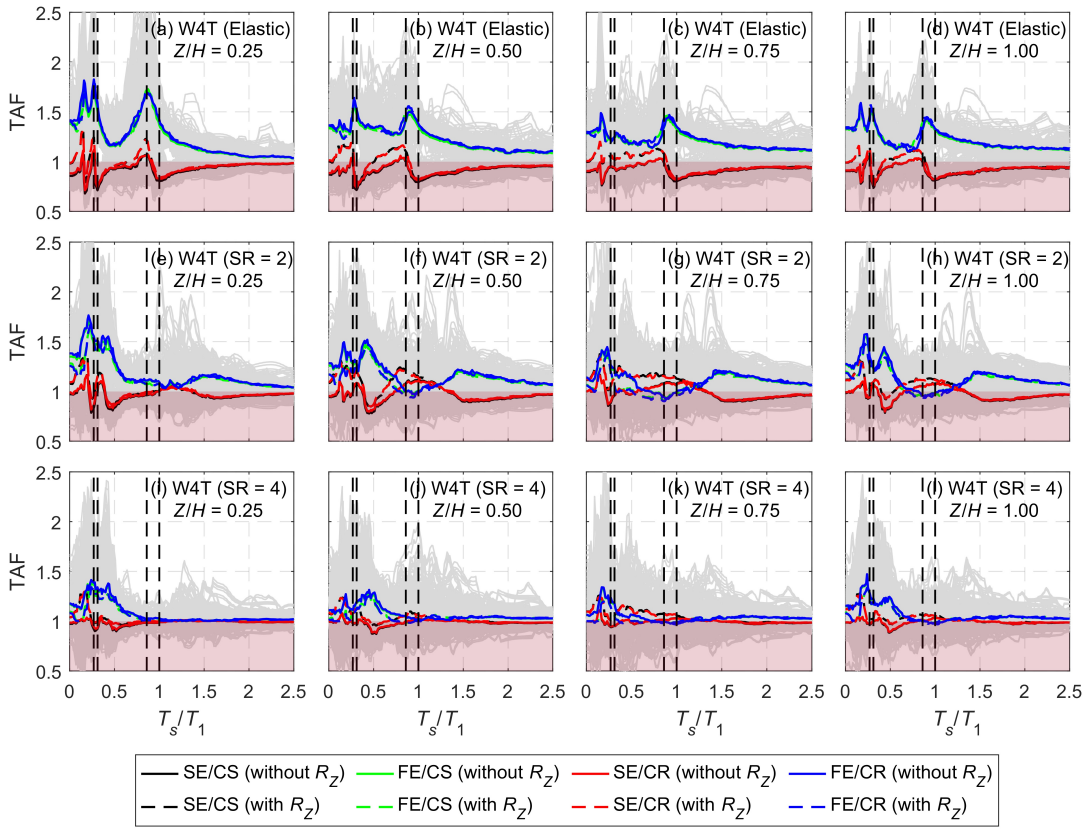

Figure 6.11: Torsional amplification factors for the 'W4T' building estimated using time history analyses with and without rotational ground motions. Dashed vertical lines indicate the elastic modal periods in the direction under consideration.

the secondary system is tuned within the building's higher mode region, the median TAF_F values decrease to 1.91, 1.50, and 1.10 at the FE, and 1.41, 1.13, and 1.03 at the SE for ETI, WTI, and NTI buildings, respectively.

Overall, the presented results reveal that notable differences exist between the median TAF_F values at the FE and the SE, with the median TAF_F consistently and significantly higher at the FE across all building types and inelasticity levels examined herein. Among the building types, ETI buildings show the highest median TAF_F values, followed by WTI, while NTI buildings consistently have the lowest median TAF_F. These median TAF_F decreases as building inelasticity increases, with a notable reduction in the median TAF_F when the secondary system is tuned within the building's fundamental mode region, as buildings transition from elastic to moderately and highly inelastic states, mainly due to inelastic energy dissipation, through the building's fundamental mode. Further, the median TAF_F are higher for 4-story buildings and also higher for the case when the secondary system is

tuned within the building's higher mode region compared to those obtained when the secondary system is tuned within the building's fundamental mode region. These trends suggest that nominal torsional effects are even more severe for shorter periods. As most of the light-weight acceleration-sensitive secondary systems have their periods in the vicinity of higher modes of buildings (in short-period range), it is essential to include amplification of acceleration demands due to nominal torsion.

6.2.2.1 Influence of rotational ground motions on torsional amplification factor for flexible secondary systems

This section analyzes the impact of rotational ground motions on the estimated TAF_F. Figures 6.9–6.14 compare the median TAF_F for 4- and 8-story T-shaped buildings with and without rotational ground motions. The discussion focuses on the increase in the median peak TAF_F due to rotational ground motions, considering a suite of ground motion records. This broader analysis helps in identifying and understanding overall trends and ensuring the inclusion of the record-to-record

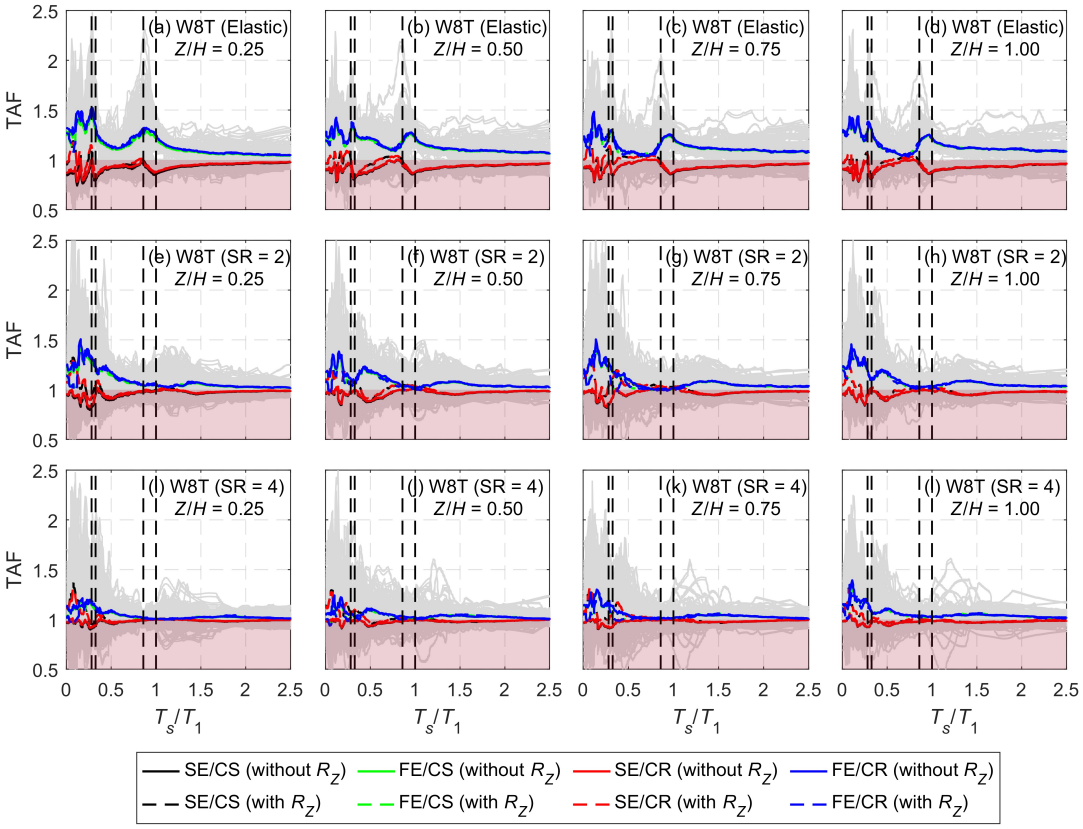

Figure 6.12: Torsional amplification factors for the 'W8T' building estimated using time history analyses with and without rotational ground motions. Dashed vertical lines indicate the elastic modal periods in the direction under consideration.

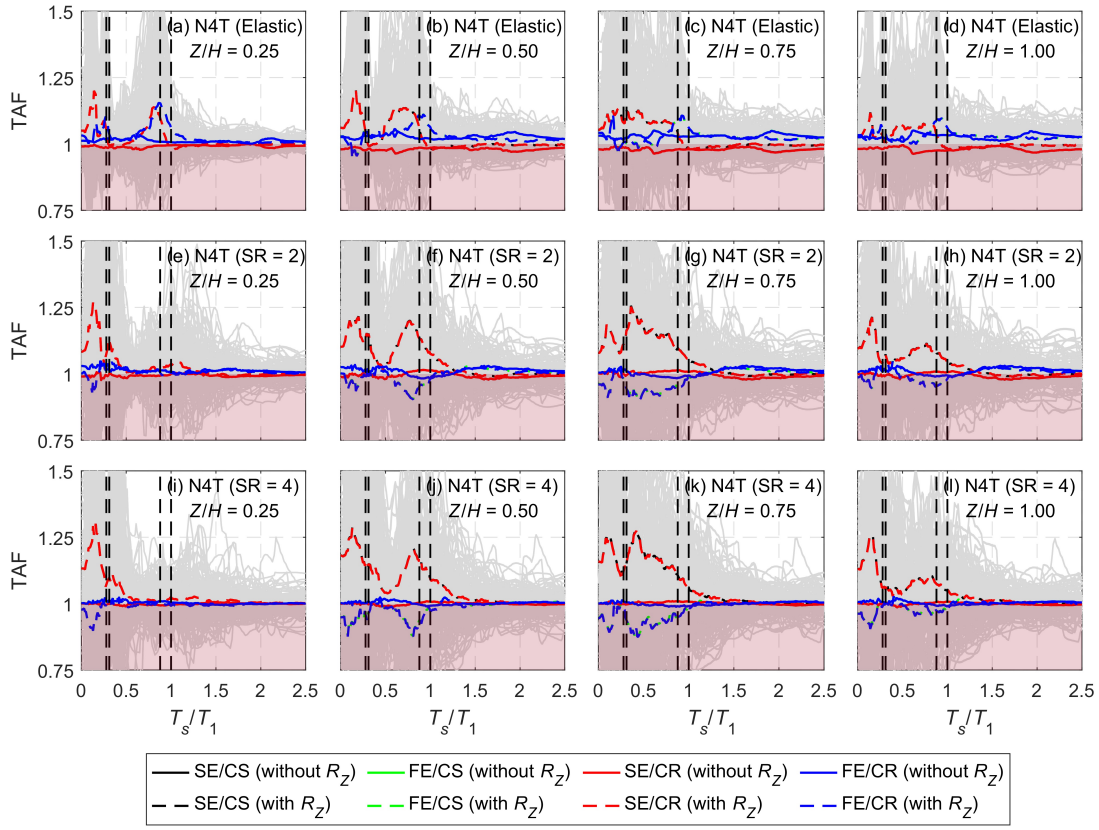

Figure 6.13: Torsional amplification factors for the 'N4T' building estimated using time history analyses with and without rotational ground motions. Dashed vertical lines indicate the elastic modal periods in the direction under consideration.

variability in the inferences. Tables 6.5–6.6 summarize the percentage increase in the median peak TAF_F for both buildings exhibiting elastic and inelastic response (SR = 2 and 4), at two different relative heights, $Z/H = 0.25$ and 1.

For 4-story buildings exhibiting elastic response, when the secondary system is tuned within the building's fundamental mode region, the rotational ground motions increase the median peak TAF_F values at the SE up to 14%, 18%, and 20% for ETI, WTI, and NTI buildings, respectively. Though, at the FE, the increase in the median peak TAF_F values are limited to 2%, 5%, and 15%. When the secondary system is tuned within the building's higher mode region, the median peak TAF_F increases at the SE and reaches up to 21%, 25%, and 27%, while at the FE, a reduction of 12% is observed for ETI buildings, whereas, both WTI and NTI buildings experience an increase of 2% and 10%, respectively.

For 8-story buildings exhibiting elastic response, the increase in the median peak TAF_F due to rotational ground motions is relatively lower compared to the 4-story

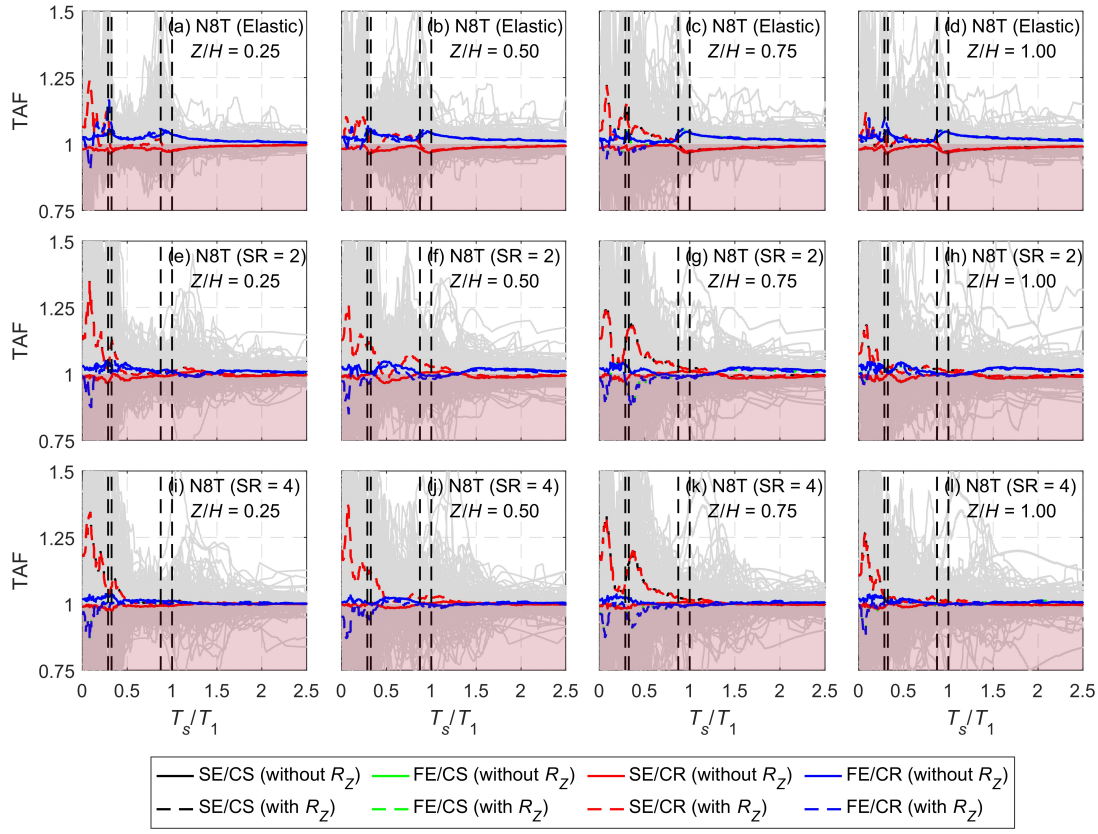

Figure 6.14: Torsional amplification factors for the 'N8T' building estimated using time history analyses with and without rotational ground motions. Dashed vertical lines indicate the elastic modal periods in the direction under consideration.

buildings, when the secondary system is tuned within the building's fundamental mode region. For this case, the rotational ground motions increase the median peak TAF_F values at the SE only up to 6%, 10%, and 9%, and at the FE only up to 2%, 3%, and 4% for the ETI, WTI, and NTI buildings, respectively. In contrast, when the secondary system is tuned within the building's higher mode region, the median peak TAF_F increases significantly, reaching 20%, 31%, and 30% at the SE, but it is limited to only about 1%, 3%, and 15% at the FE, for the ETI, WTI, and NTI buildings, respectively.

For 4-story buildings exhibiting moderately inelastic response (SR = 2), the median peak TAF_F due to rotational ground motions increases compared to their elastic counterparts. When the secondary system is tuned within the building's fundamental mode region, the median peak TAF_F values at the SE increase up to 5%, 13%, and 24% for ETI, WTI, and NTI buildings, respectively. In contrast, at the FE, reductions of about 8% and 6% are observed for ETI and WTI buildings,

while NTI buildings showed a slight increase of about 1%. When the secondary system is tuned within the building's higher mode region, the increase in median peak TAF_F values becomes more pronounced, reaching 9%, 19%, and 30% at the SE, for ETI, WTI, and NTI buildings, respectively. At the FE, the median peak TAF_F values decrease up to 20% and 10% for ETI and WTI buildings, while NTI buildings experience an increase of about 5%.

For 8-story buildings exhibiting moderately inelastic response (SR = 2), when the secondary system is tuned within the building's fundamental mode region, the rotational ground motions increase the median peak TAF_F values at the SE by 5%, 6%, and 11% for ETI, WTI, and NTI buildings, respectively. At the FE, the median peak TAF_F values increase by 1% for both ETI and NTI buildings, while a reduction of about 3% is observed for WTI buildings. When the secondary system is tuned within the building's higher mode region, the increase in the median peak TAF_F at the SE becomes even more significant, reaching up to 18%, 36%, and 41% for ETI, WTI, and NTI buildings, respectively. However, at the FE, the median peak TAF_F values decrease up to 23% and 15% for ETI and WTI buildings, while NTI buildings experience an increase of about 3%.

For 4-story buildings exhibiting highly inelastic response (SR = 4), the median peak TAF_F values further increase due to rotational ground motions compared to the elastic case. When the secondary system is tuned within the building's fundamental mode region, the median peak TAF_F values at the SE increase up to 6%, 10%, and 19% for ETI, WTI, and NTI buildings, respectively. At the FE, these values increase to 3% and 2% for ETI and NTI buildings, while a reduction of about 5% is observed for WTI buildings. When the secondary system is tuned within the building's higher mode region, the increase in the median peak TAF_F becomes more pronounced, reaching up to 20%, 31%, and 30% at the SE. At the FE, increases of about 9% and 2% are recorded for ETI and NTI buildings, while a reduction of 9% is observed for WTI buildings.

A similar trend is observed in 8-story buildings exhibiting highly inelastic response (SR = 4), where the median peak TAF_F increase due to rotational ground motions remains higher compared to their elastic counterparts. When the secondary

Table 6.5: Median peak increase (%) in torsional amplification factor for flexible secondary systems due to rotational ground motions in the 4-story buildings.

Building	$Z/H = 0.25$				$Z/H = 1.00$			
	FM		HM		FM		HM	
	FE	SE	FE	SE	FE	SE	FE	SE
Elastic								
E4T	2	11	-7	7	-2	9	-2	4
E4U	0	0	-3	3	-2	3	-8	7
E4S	0	7	-3	5	-3	8	-6	6
E4R	2	9	-7	6	-1	12	-3	5
W4T	2	15	-2	17	1	8	-1	10
W4U	3	17	-3	16	0	15	-2	11
W4S	-1	11	-5	15	1	15	1	15
W4R	5	15	-2	25	3	9	0	7
N4T	12	14	8	20	4	8	4	12
N4U	15	17	10	22	7	11	8	11
N4S	13	19	10	24	5	12	7	16
N4R	11	16	6	27	5	9	5	15
SR = 2								
E4T	-2	-2	-11	-1	-2	1	-5	2
E4U	-1	-1	-15	1	0	1	-8	4
E4S	-1	-2	-10	-2	-1	3	-2	5
E4R	-2	-2	-5	0	-2	2	-5	3
W4T	-1	1	-5	15	-1	4	-6	18
W4U	-1	-2	-4	9	-1	3	-4	10
W4S	0	0	-4	15	-1	5	-5	19
W4R	-1	0	-5	18	-1	6	-5	18
N4T	0	4	0	26	0	10	2	21
N4U	0	3	3	26	0	10	1	23
N4S	1	5	5	30	0	12	3	26
N4R	0	4	0	28	0	10	0	26
SR = 4								
E4T	0	-1	-1	14	-1	3	4	11
E4U	-3	-2	-13	7	-3	3	-4	5
E4S	3	-1	-3	13	-1	4	3	12
E4R	-2	-1	-7	12	-4	4	-5	11
W4T	-3	0	-5	25	-4	4	-9	22
W4U	-1	-1	-6	20	0	3	-3	20
W4S	0	0	-4	20	-2	5	-6	22
W4R	0	-1	-2	31	-1	6	-4	23
N4T	0	2	0	30	1	10	1	25
N4U	-1	1	0	20	-1	7	0	20
N4S	0	2	2	28	2	10	1	28
N4R	-1	1	-1	24	0	8	-2	24

Note: Negative median values represent decrease due to R_Z. Median values are color-coded using a gradient for both fundamental and higher modes across all buildings: light red (lowest) to green (highest) for secondary systems tuned within the building's fundamental mode region and light blue (lowest) to sky blue (highest) for higher mode region, with intermediate values in yellow and purple, respectively.

Table 6.6: Median peak increase (%) in torsional amplification factor for flexible secondary systems due to rotational ground motions in the 8-story buildings.

Building	$Z/H = 0.25$				$Z/H = 1.00$			
	FM		HM		FM		HM	
	FE	SE	FE	SE	FE	SE	FE	SE
Elastic								
E8T	0	3	-2	3	1	2	-3	12
E8U	0	2	-2	5	0	1	-1	14
E8S	0	4	-2	6	1	4	-3	10
E8R	0	6	1	7	0	2	-3	13
W8T	0	2	1	18	-1	3	-1	9
W8U	3	10	-2	21	2	6	-2	10
W8S	2	7	2	20	1	4	-3	12
W8R	1	0	2	18	0	2	1	9
N8T	1	2	11	25	1	3	5	12
N8U	4	4	15	26	1	3	10	12
N8S	2	5	12	30	2	4	7	17
N8R	1	3	10	28	1	3	5	16
SR = 2								
E8T	-2	1	-5	2	-2	2	-15	2
E8U	-1	0	-7	3	0	3	-4	0
E8S	0	1	-3	4	-1	2	-11	-1
E8R	-1	2	-4	7	-2	2	-7	0
W8T	-1	1	-6	27	-3	2	-3	23
W8U	-2	1	-7	18	-1	3	-3	18
W8S	0	1	-4	23	0	2	-8	16
W8R	-2	2	-3	34	-1	1	-6	24
N8T	0	1	0	35	0	2	0	18
N8U	0	2	2	32	0	3	2	15
N8S	0	2	2	38	1	4	0	21
N8R	-1	2	0	41	-1	2	-3	21
SR = 4								
E8T	0	0	1	17	0	1	-3	22
E8U	0	0	3	13	-3	1	-7	12
E8S	-2	0	8	14	0	1	-1	17
E8R	2	-1	2	17	2	1	0	10
W8T	1	1	-1	30	-1	1	-7	23
W8U	-2	-1	-3	22	-2	1	-7	23
W8S	0	0	-1	27	0	1	-8	20
W8R	1	1	-1	36	-1	1	-8	23
N8T	0	1	-2	35	0	2	0	26
N8U	0	0	1	34	0	2	0	23
N8S	1	1	1	35	0	2	1	29
N8R	-1	0	-3	38	0	1	-5	34

Note: Negative median values represent decrease due to R_Z. Median values are color-coded using a gradient for both fundamental and higher modes across all buildings: light red (lowest) to green (highest) for secondary systems tuned within the building's fundamental mode region and light blue (lowest) to sky blue (highest) for higher mode region, with intermediate values in yellow and purple, respectively.

system is tuned within the building's fundamental mode region, the rotational ground motions increase the median peak TAF_F values at the SE by 2%, 5%, and 11% for ETI, WTI, and NTI buildings, respectively. At the FE, these increases in the median peak TAF_F are 4%, 2%, and 1% for ETI, WTI, and NTI buildings, respectively. The impact of rotational ground motions becomes significantly greater when the secondary system is tuned within the building's higher mode region, resulting in the median peak TAF_F increases of 25%, 38%, and 44% at the SE for ETI, WTI, and NTI buildings, respectively. At the FE, an increase of about 8% is observed for ETI buildings, while NTI buildings show an increase of only 1%, but WTI buildings experience a 15% reduction in the median peak TAF_F, due to rotational ground motions.

From the above discussions, it is observed that the NTI buildings are most affected by the rotational ground motions, with the median peak TAF_F values increasing up to 44% (for SR = 4 in the 'N8R' building). Further, the impact of rotational ground motions is most significant at the SE, where the median peak response rises up to 44% (for SR = 4 in the N8R building), while the maximum increase in the median peak TAF_F at the FE is recorded only about 15% (in the elastic case for the 'N4U' and 'N8U' buildings). Overall, the effects of rotational ground motions are observed to be inversely related to the extent of the nominal torsion present in the building, especially at the SE. For instance, the median peak TAF_F values increase up to 13%, 34%, and 44% for 'E8R', 'W8R', and 'N8R' buildings, respectively, highlighting the greater impact of rotational ground motions on buildings with reduced nominal torsion.

6.2.3 Torsional amplification factors for the very flexible secondary systems

Very flexible secondary systems are systems that have a period significantly higher as compared to the fundamental period of the building. In this study, the parameter tuning ratio (T_s/T_1) is utilized to classify the very flexible secondary systems. The secondary systems with $T_s/T_1 \geq 1.50$ for buildings exhibiting elastic response, and $T_s/T_1 \geq 2.00$ for inelastic response (due to period elongation effects, as discussed in Chapter 5) are classified as the very flexible secondary systems. As shown earlier

in Figures 6.9–6.14, the TAF starts to decline away from the fundamental mode region ($T_s/T_1 > 1.00$) and at very long periods. Hence, to analyze the TAF_{VF} (at very long periods), the maximum median TAF_{VF} among all the analyzed buildings corresponding to $T_s = 3T_1$ are discussed here. Figures 6.15–6.18 illustrate the TAF_{VF} at $T_s = 3T_1$ and $4T_1$ at both the FE, and the SE, considering 4- and 8-story T-shaped buildings exhibiting elastic and inelastic response.

For the 4-story buildings exhibiting elastic response, the maximum median TAF_{VF} at the FE reaches 1.21, 1.12, and 1.02 for ETI, WTI, and NTI buildings, respectively. At the SE, however, it remains consistently equal to 1.00 across all examined cases. Similarly, for 8-story buildings exhibiting elastic response, no significant reduction in the median TAF_{VF} is observed, with their median peak values reaching 1.13, 1.08, and 1.02 for ETI, WTI, and NTI buildings, while at the SE, it remained 1.00. In the case of 4-story buildings exhibiting highly inelastic response (SR = 4), the maximum median TAF_{VF} values at the FE decrease to 1.08, 1.06, and 1.02 for ETI, WTI, and NTI buildings, respectively, compared to their elastic counterparts, whereas no change is observed at the SE. For 8-story buildings exhibiting highly inelastic response (SR = 4), the maximum median TAF_{VF} values further reduce to 1.04, 1.02, and 1.01 for ETI, WTI, and NTI buildings, respectively, while remaining at 1.00, at the SE across all analyzed cases.

From these results, it is noted that the TAF_{VF} corresponding to very long periods shows minor torsional amplification effects, which approached unity with a further increase in inelasticity and T_s/T_1. These observations can be attributed to the insignificant dynamic interaction effects between the secondary system and the building at sufficiently longer periods. When the natural period of the secondary system significantly diverges from the dominant vibration periods of the building, the coupling between their dynamic responses weakens. This results in smaller torsional amplification effects as the system transitions from a resonance-dominated response to a phase where torsional and translational motions are less coupled. It is observed that the maximum median TAF_{VF} values at very long periods decrease from 1.21 in the elastic case to 1.08 in the highly inelastic case at the FE. Additionally, at longer periods, the extent of nominal torsion has no significant impact, as the median TAF_{VF} values range from 1.21 in ETI buildings to 1.02 in NTI buildings at

the FE. Moreover, the effect of the number of stories on TAF_{VF} is also negligible, with the maximum median TAF_{VF} decreasing from 1.21 (4-story buildings) to 1.13 (8-story buildings). Furthermore, the SE consistently exhibits a median TAF_{VF} of 1.00, indicating no influence of the nominal torsion at very long periods at the SE. Collectively, these findings suggest that for a very long period, the FRS approaches the GRS, even for buildings exhibiting nominal torsion.

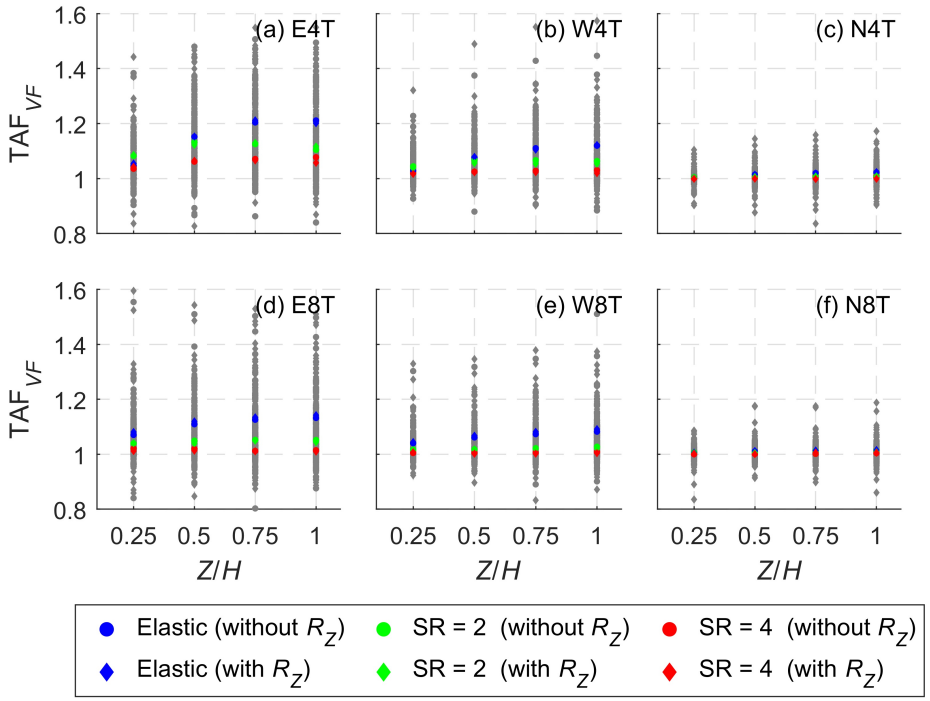

Figure 6.15: Comparison of the estimated torsional amplification factors for very flexible secondary systems (TAF_{VF} at $T_s = 3T_1$) at the FE for the 4- and 8-storied T-shaped buildings, with and without the rotational ground motions.

6.2.3.1 Influence of rotational ground motions on torsional amplification factor for very flexible secondary systems

This section examines the impact of rotational ground motions on the estimated TAF_{VF}. The maximum median TAF_{VF} response at $3T_1$ obtained from the time history analyses with rotational ground motions are further discussed and compared with the values obtained without considering rotational ground motions to examine its impact. The comparison of results with and without rotational ground motions indicates insignificant differences in the maximum median TAF_{VF} values. For 4-story buildings exhibiting elastic response, the median TAF_{VF} at the FE remains at 1.21, 1.12, and 1.02 for ETI, WTI, and NTI buildings, respectively, comparable to the values obtained without rotational ground motion. Similarly, at the SE, the median

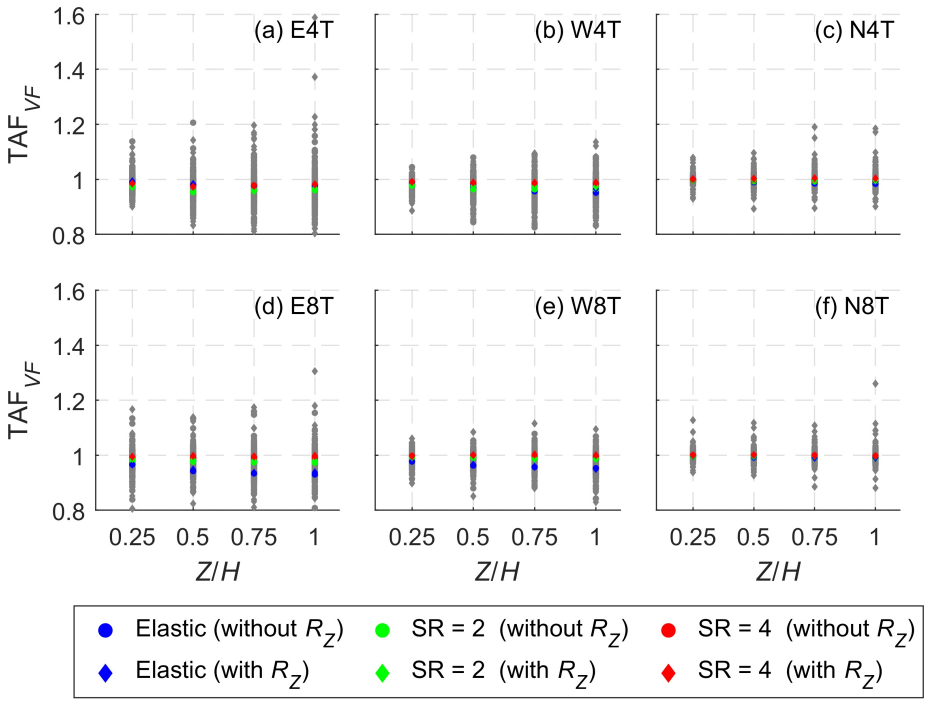

Figure 6.16: Comparison of the estimated torsional amplification factors for very flexible secondary systems (TAF_{VF} at $T_s = 3T_1$) at the SE for the 4- and 8-storied T-shaped buildings, with and without the rotational ground motions.

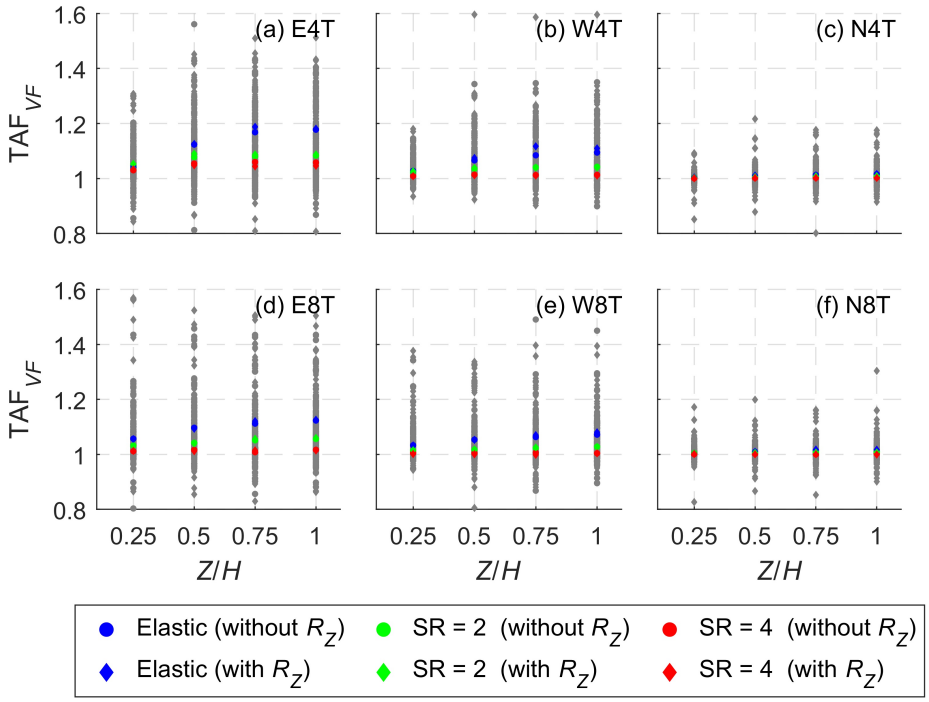

Figure 6.17: Comparison of the estimated torsional amplification factors for very flexible secondary systems (TAF_{VF} at $T_s = 4T_1$) at the FE for the 4- and 8-storied T-shaped buildings, with and without the rotational ground motions.

TAF_{VF} consistently remains at 1.00, showing no amplification. The trend is also observed in 8-story buildings exhibiting elastic response, where the median TAF_{VF}

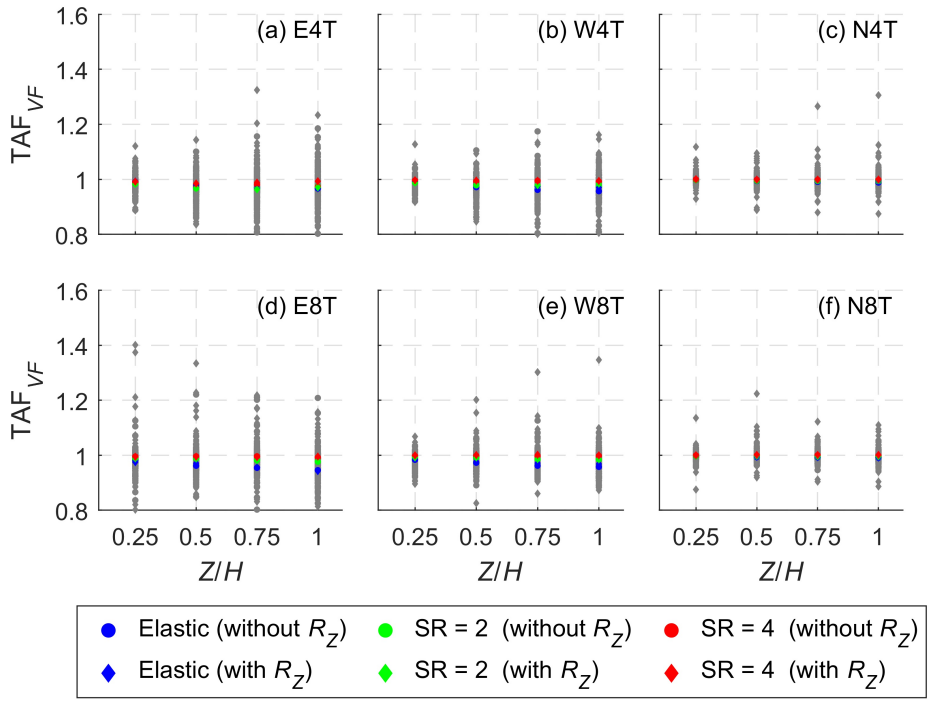

Figure 6.18: Comparison of the estimated torsional amplification factors for very flexible secondary systems (TAF_{VF} at $T_s = 4\,T_1$) at the SE for the 4- and 8-storied T-shaped buildings, with and without the rotational ground motions.

values of 1.14, 1.09, and 1.02 remain unchanged at the FE, while the SE continues to exhibit a stable value of 1.00. In 4-story buildings exhibiting highly inelastic response (SR = 4), the maximum median TAF_{VF} at the FE remains consistent with the elastic case, with values of 1.08, 1.05, and 1.01, while no variation is observed at the SE. Likewise, in 8-story buildings exhibiting highly inelastic response, the values remain nearly identical, with 1.05, 1.02, and 1.01 at the FE and 1.00 at the SE in all cases. These findings confirm that TAF_{VF} are not influenced by the rotational ground motions.

6.3 Relationships between torsional amplification factor and different torsional irregularity indices

Based on the findings presented in this Chapter, it is evident that TAFs play a crucial role in predicting acceleration demands in buildings with nominal torsion, making their consideration essential in the seismic design of the light-weight acceleration-sensitive secondary systems. To understand the correlation between

elastic floor displacement-based torsional irregularity indices and the obtained TAFs, linear regression analyses are performed separately for the TAFs corresponding to rigid and flexible secondary systems. In these regression analyses, the TAF is considered the dependent variable, while the floor displacement ratio serves as the independent variable. To capture the inherent record-to-record variability in the elastic floor displacement-based torsional irregularity indices ($\Delta_{max}/\Delta_{avg}$ and $\Delta_{max}/\Delta_{min}$), the elastic floor displacements are obtained from the bi-directional linear dynamic time history analyses. The elastic floor displacements Δ_{min} and Δ_{max} are obtained as the absolute maximum floor displacements obtained from the displacement histories at the SE and the FE, respectively, at a given floor, whereas, Δ_{max} is obtained as the average of the absolute maximum floor displacements at the SE, and the FE, of the floor under consideration.

Given that the maximum median TAF_R and TAF_F for NTI buildings are limited to 1.03 (1.28 with R_Z) and 1.10 (1.46 with R_Z), respectively, they are excluded from the regression analyses and taken into consideration by imposing the lower bound limit on the proposed TAFs. During the analysis phase of regression, a critical consideration is the assumption of homoscedasticity, which assumes constant variance of the errors. However, if this assumption is violated and the variability of the residuals changes with variations in the independent variable(s), it is referred to as heteroskedasticity. This condition can significantly impact the accuracy and reliability of the regression analysis. To assess the presence of heteroskedasticity, the Breusch-Pagan test [149] is performed on the datasets, following which Ordinary least squares (OLS) regression [150] is conducted. Further, the results of the regression analyses conducted for TAF_R and TAF_F are discussed in the following sections.

6.3.1 Torsional amplification factors for the rigid secondary systems

6.3.1.1 At the extreme edges

A very simple model function is chosen for the regression analysis, i.e., $y = x^a$, where 'x' and 'y' are the torsional irregularity index and TAF (TAF_R or TAF_F), respectively, whereas 'a' represents the exponent obtained from the regression

analysis. The obtained TAF_R at the FE for ETI and WTI buildings at various floor levels is plotted in Figures 6.19–6.20 alongside their corresponding elastic floor displacement-based torsional irregularity indices ($\Delta_{max}/\Delta_{avg}$ and $\Delta_{max}/\Delta_{min}$), for different elastic and inelastic response cases. For a total of 16 ETI and WTI buildings, considering all elastic and inelastic cases, 80 Breusch-Pagan tests are performed separately for the two independent variables ($\Delta_{max}/\Delta_{avg}$ and $\Delta_{max}/\Delta_{min}$), bringing the total number of tests to 160. Among these 160 tests, heteroskedasticity was identified in only 22 instances, signified by a p-value less than 0.05 (refer to Figure 6.21). Hence, these instances are excluded from further analysis. In most cases (138 out of 160 tests), the assumption of homoscedasticity holds, as indicated by a p-value greater than or equal to 0.05. This implies relatively consistent variances across the datasets.

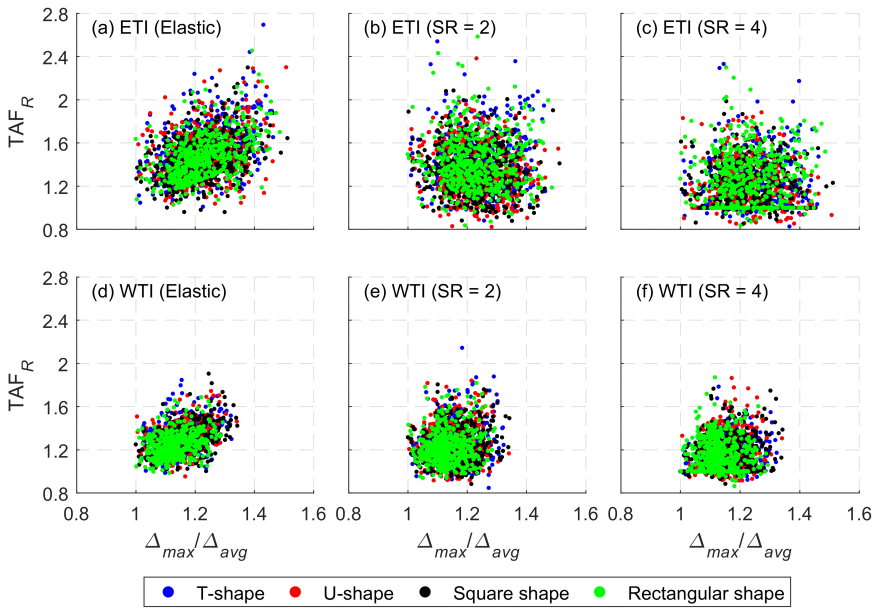

Figure 6.19: Torsional amplification factors for rigid secondary systems (TAF_R) at the flexible edges of the ETI and WTI buildings plotted with their elastic displacement ratios ($\Delta_{max}/\Delta_{avg}$).

Consequently, the OLS regression method is applied to the remaining 138 datasets. Notably, the residuals are found to be normally distributed in all cases. The estimated values of exponent 'a' for the elastic case and different SR values lie in the range 1.14 to 1.97 (in the case of $\Delta_{max}/\Delta_{avg}$ versus TAF_R) and 0.47 to 0.85 (in the case of $\Delta_{max}/\Delta_{min}$ versus TAF_R). The analyses revealed a remarkably significant relationship, as evidenced by higher t-values and all

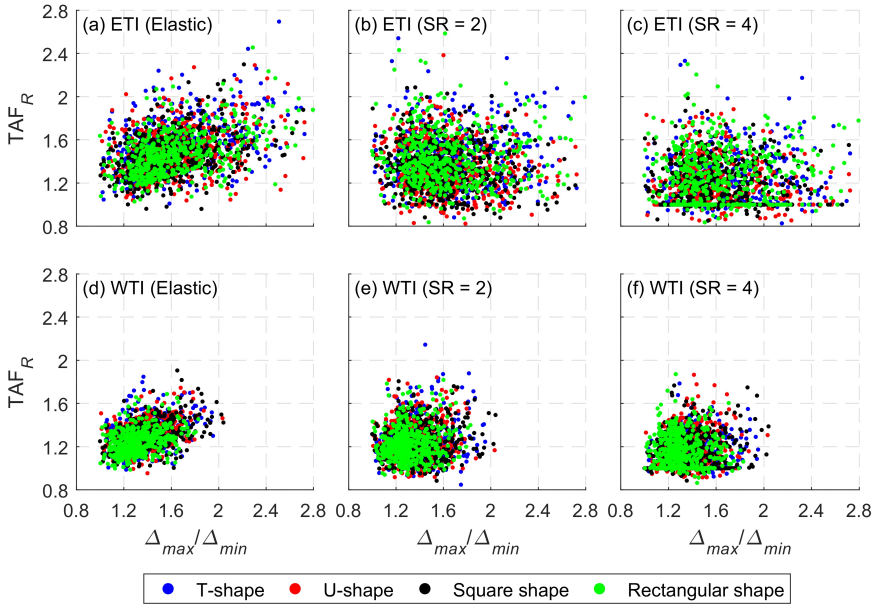

Figure 6.20: Torsional amplification factors for rigid secondary systems (TAF_R) at the flexible edges of the ETI and WTI buildings plotted with their elastic displacement ratios ($\Delta_{max}/\Delta_{min}$).

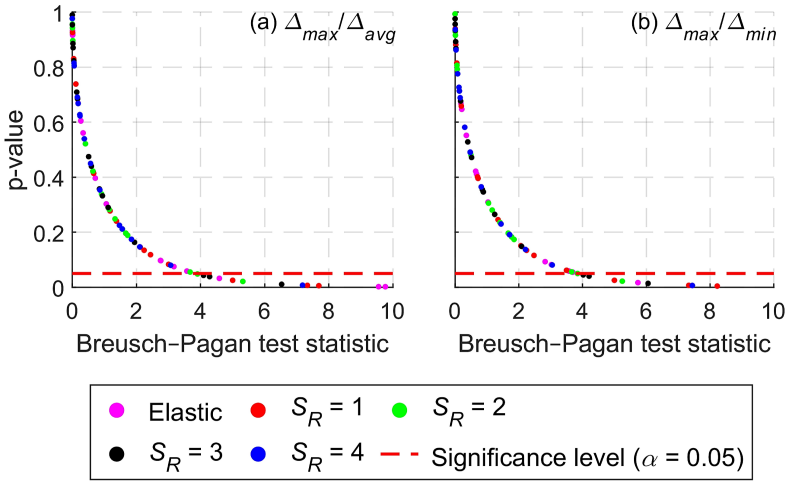

Figure 6.21: Scatter plot showing the results of the Breusch-Pagan test conducted on 160 datasets comprising of TAF_R and torsional irregularity indices, from the analyzed ETI and WTI buildings.

corresponding p-values ($\Pr(>|t|)$) being approximately equal to zero. The coefficient of determination (R^2) values are consistently high, with a range between 0.51 to 0.89 (in the case of $\Delta_{max}/\Delta_{avg}$ versus TAF_R) and 0.48 to 0.88 (in the case of $\Delta_{max}/\Delta_{min}$ versus TAF_R), suggesting that the changes in the SR can explain a significant proportion of the variation in the exponent 'a'. Moreover, the F-statistic results demonstrated the regression model's overall significance, with extremely low associated p-values approximately equal to zero. The conducted regression analyses

and estimated exponent 'a' also indicated that the torsional amplification occurs at the FE, and with an increase in the inelasticity of the building, TAF_R at the FE reduces significantly. These findings collectively emphasize the strong correlation that exists between TAF_R at FE and torsional irregularity indices, $\Delta_{max}/\Delta_{avg}$ and $\Delta_{max}/\Delta_{min}$. For more detailed information on the obtained regression parameters, Tables C.1 and C.2 can be referred to in the Appendix C.

In contrast, at the SE, a de-amplification of in-structure acceleration is observed under the elastic response of buildings, which turned into an amplification of in-structure acceleration under the inelastic response. Among the investigated buildings, the maximum value of TAF_R is as high as 1.73 and 1.64 with and without considering rotational ground motions, respectively, even at the SE; however, the median TAF_R among all the investigated buildings at the SE does not exceed 1.28 and 1.12 with and without rotational ground motions, respectively. The linear regression between the TAF_R at the SE and the elastic floor displacement-based torsional irregularity indices do not exhibit any relationships for buildings exhibiting elastic and inelastic response. Overall, the regression analyses showed that the building's torsional and strength characteristics-dependent TAF_R should be used to estimate PFA demands at the FE, whereas a constant TAF_R, independent of the building characteristics at the SE, is sufficient.

6.3.1.2 Across the building plan

Since the existing torsional irregularity indices ($\Delta_{max}/\Delta_{avg}$ and $\Delta_{max}/\Delta_{min}$) are determined from floor displacements at the extreme edges, they cannot be applied to locations in between these edges. Thus, in cases where the TAF_R between the extreme edges is to be studied, the relationship between TAF_R and the displacement ratio is investigated. This ratio is defined as the ratio of the maximum elastic displacement of the flexible frame 'FF_i' ($\Delta_{FF,\,ij}$) to that at the CR ($\Delta_{CR,\,j}$) both obtained at the 'j^{th}' floor, is investigated. The rationale for choosing and investigating the relationships between the elastic displacement ratio, $\Delta_{FF,\,ij}/\Delta_{CR,\,j}$ and the torsional amplification of the PFA are based on the guidelines outlined in different seismic design codes [5, 6, 16] that advocate the use of the displacement ratio of $\Delta_{max}/\Delta_{avg}$ as an indicator of torsional irregularity (or an indirect measure

of the floor rotation due to building nominal torsion). Further, the CR is the point on the floor plan that exhibits pure translation response; hence, it is taken as the reference point for the normalization of both acceleration and displacement floor response of the buildings with nominal torsion.

Accordingly, the estimated TAF_Rs for the flexible frames for all buildings and floors are plotted in Figure 6.22, with the elastic displacement ratio ($\Delta_{FF,\,ij}/\Delta_{CR,\,j}$) for the investigated elastic and inelastic response cases. The displacement histories of elastic floor displacement, $\Delta_{FF,\,ij}$(t) and $\Delta_{CR,\,j}$(t), for all the frames, floors, and buildings are estimated from the bi-directional linear dynamic time history analyses. The elastic floor displacements, $\Delta_{FF,\,ij}$ and $\Delta_{CR,\,j}$ for each ground motion are estimated as the absolute maximum floor displacements obtained from the displacement histories for the given frame at the floor level of interest. Hence, the effects of aleatoric (record-to-record) variability are explicitly taken into account in estimating the elastic floor displacements. It is to be noted that even for the flexible frames, the possibility of torsional acceleration de-amplification cannot be overlooked entirely (Figure 6.22). Among all the investigated buildings, the lowest torsional de-amplification factors are obtained as 0.66 for the flexible frames and 0.48 for the stiff frames (not shown here). Conversely, the highest TAF_Rs are obtained as 2.79 and 1.66 for the flexible and the stiff frames, respectively. It is to be noted that the objective of the study is to develop design recommendations to take care of the torsional amplification in acceleration demands; hence, torsional de-amplification factors are ignored.

To achieve this, a basic model function is selected with its functional form as $y = x^b$, where 'y' refers to TAF_Rs, and 'x' refers to $\Delta_{FF,\,ij}/\Delta_{CR,\,j}$, whereas '$b$' signifies the exponent obtained from the regression analysis. In the regression analyses, the TAF_Rs and the displacement ratio $\Delta_{FF,\,ij}/\Delta_{CR,\,j}$ is treated as the dependent variable and the independent (predictor) variables. To ensure the statistical analyses' accuracy, the Breusch-Pagan test [149]) is conducted to detect the heteroskedasticity in the TAF_Rs and displacement ratio pairs obtained from the dynamic time history analyses at each stiff and flexible frame, totaling 720 tests. In 72% of cases, the assumption of homoscedasticity holds, as indicated by a p-value of 0.05 or higher, as shown in Figure 6.23(a). A p-value equal to or greater than 0.05 indicates relatively

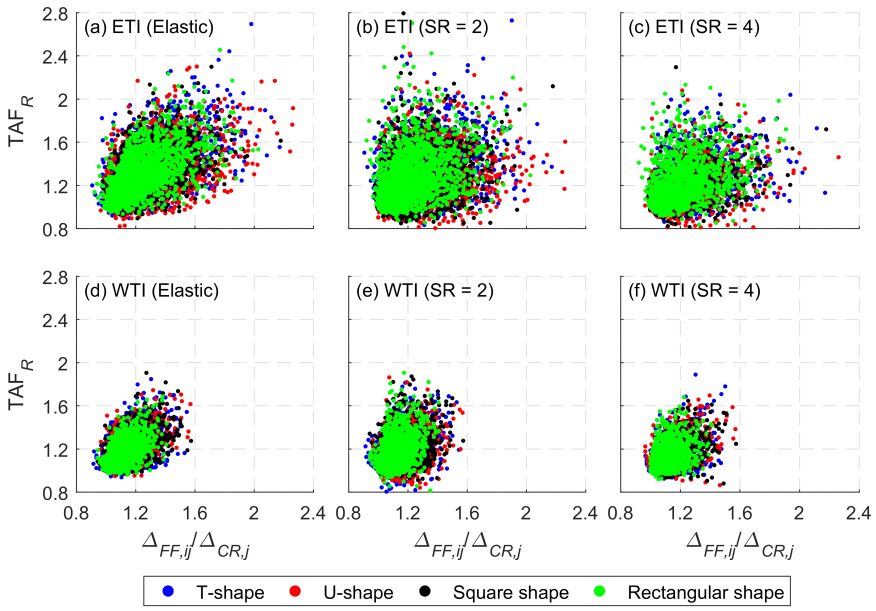

Figure 6.22: Torsional amplification factors for the flexible frames of all investigated buildings.

consistent variances among the datasets. Conversely, samples with a p-value below 0.05 suggest the presence of heteroskedasticity and are thus excluded from further analysis. Consequently, the OLS method is used for linear regression analyses. It is important to note that the residuals are found to follow a normal distribution in all cases. The values of the exponent 'b' range from 0.48 to 1.56 for the elastic case and various SR values as illustrated in Figure 6.23(b). The analysis showed a notably significant relationship in the case of flexible frames, as evidenced by the very low standard error (less than 0.03) and all corresponding p-values (Pr(>|t|)) being approximately equal to zero. Furthermore, the coefficient of determination (R^2) consistently indicates strong correlations, ranging from 0.47 to 0.89. Furthermore, the F-statistic results establish the overall significance of the regression model, with exceedingly low associated p-values, approximately equal to zero. These regression analyses, along with the derived exponent 'b', emphasize the presence of torsional amplification effects across these frames. Moreover, as the building's inelasticity increases, there is a noticeable decrease in TAF_Rs. Collectively, these findings highlight a robust correlation between TAF_Rs and torsional irregularity indices. The regression analyses emphasize that torsional amplification occurs for the flexible frames, and as the building SR increases, TAF_Rs significantly decrease for the flexible frames. These observations of the statistical and regression analyses are utilized

in developing the simplified model for the prediction of TAF_Rs in the subsequent section.

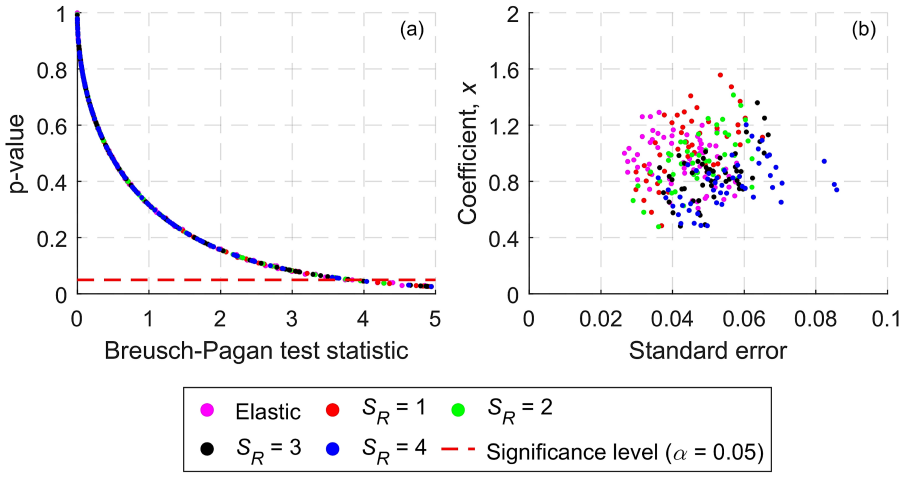

Figure 6.23: Scatter plot showing results of (a) the Breusch-Pagan test and (b) the regression analysis.

6.3.2 Torsional amplification factors for the flexible secondary systems at the extreme edges

Similar to the regression analyses conducted in Section 6.3.1.1 for rigid secondary systems, a simple model function is adopted, where the peak TAF_F ($TAF_{F,\ max}$), corresponding to the case when the secondary system is tuned within the fundamental mode region, is considered the dependent variable, while the torsional irregularity index serves as the independent variable. The chosen model function for the regression is $y = x^c$, where 'x' denotes the torsional irregularity index and 'y' represents the $TAF_{F,\ max}$, with 'c' being the exponent derived from the regression analyses. The $TAF_{F,\ max}$, corresponding to the fundamental mode region, is used for the regression analyses due to its consistent and dominant influence on the structural response, providing a reliable and stable basis for developing a generalized model. The $TAF_{F,\ max}$ corresponding to the higher mode region tends to exhibit larger values. However, these peaks do not correspond to a single dominant mode, leading to significant variability across different buildings and reducing the reliability of direct regression analyses. The peak TAF_F ($TAF_{F,\ max}$) values estimated corresponding to the case when the secondary system is tuned within the building's fundamental mode region at the FE are plotted in Figures 6.25–6.26 with their elastic floor displacement-based torsional irregularity indices

($\Delta_{max}/\Delta_{avg}$ and $\Delta_{max}/\Delta_{min}$).

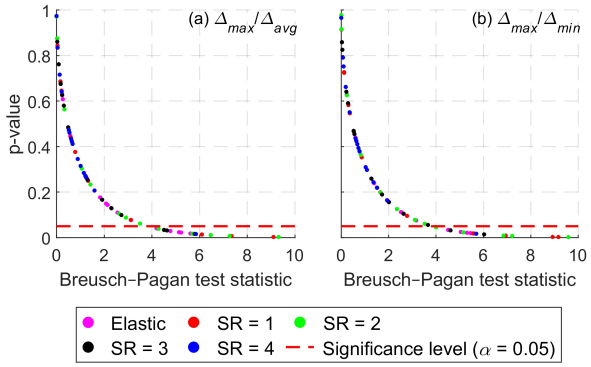

Figure 6.24: Scatter plot showing the results of the Breusch-Pagan test conducted on 160 datasets from the investigated ETI and WTI buildings.

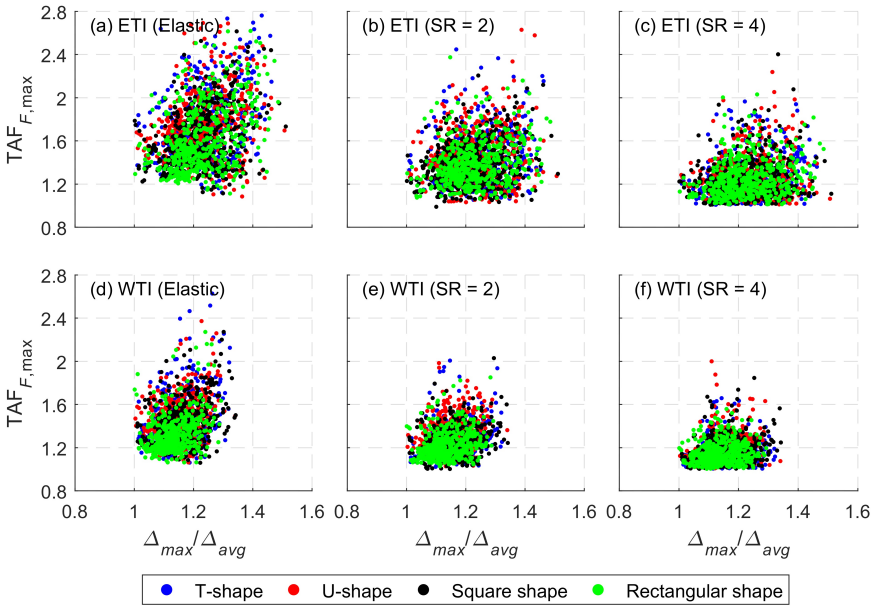

Figure 6.25: Scatter plots showing the maximum TAF_F values versus the corresponding displacement ratio ($\Delta_{max}/\Delta_{avg}$) for various ETI and WTI buildings.

Before conducting the regression analyses, the presence of heteroskedasticity is tested using the Breusch-Pagan test [149]. This test is applied individually to 16 ETI and WTI buildings for each elastic case and different SRs, resulting in a total of 80 tests. The test was performed separately for the two independent variables ($\Delta_{max}/\Delta_{avg}$ and $\Delta_{max}/\Delta_{min}$), bringing the total number of tests to 160. heteroskedasticity was identified in only 44 instances, as indicated by p-values below 0.05 (Figure 6.24), and these cases were subsequently excluded from further analysis. In the remaining 116 tests, p-values of 0.05 or higher confirmed the assumption of homoscedasticity, indicating relatively uniform variances across the datasets.

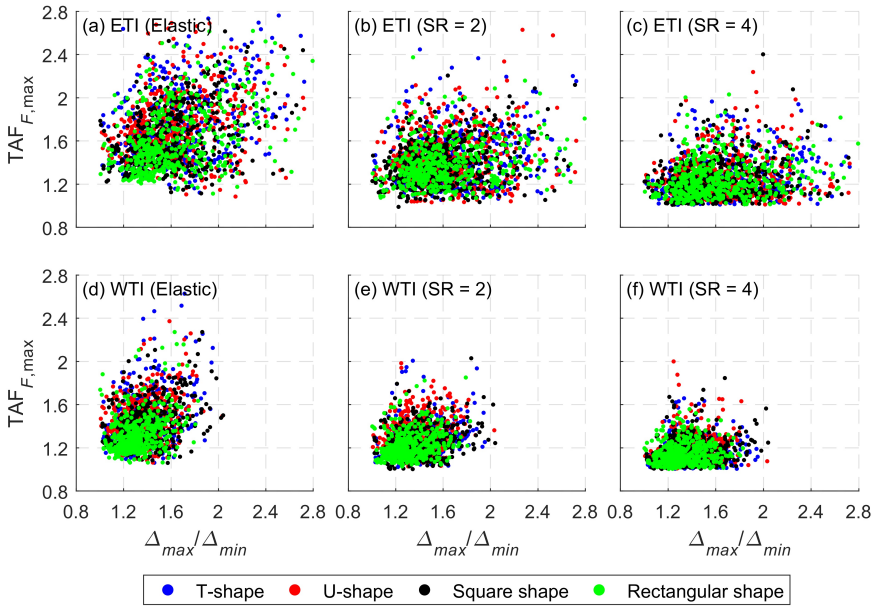

Figure 6.26: Scatter plots showing the maximum TAF_F values versus the corresponding displacement ratio ($\Delta_{max}/\Delta_{min}$) for various ETI and WTI buildings.

As a result, the OLS regression method was applied to the remaining 116 datasets. In all cases, the residuals followed a normal distribution, confirming the appropriateness of OLS for the analysis. The estimated values of exponent 'c' for the elastic case and different SR values lie in the range 0.50 to 2.62 (in the case of $\Delta_{max}/\Delta_{avg}$ versus $TAF_{F,\ max}$) and 0.23 to 1.16 (in the case of $\Delta_{max}/\Delta_{min}$ versus $TAF_{F,\ max}$). The analysis revealed a highly significant relationship, as indicated by elevated t-values and p-values (Pr(>|t|)) consistently at or near zero. The coefficient of determination (R^2) values remained high, ranging from 0.50 to 0.93 (for $\Delta_{max}/\Delta_{avg}$ versus $TAF_{F,\ max}$) and from 0.48 to 0.91 (for $\Delta_{max}/\Delta_{min}$ versus $TAF_{F,\ max}$), suggesting that variations in SR account for a substantial portion of the changes in the exponent 'c'. Furthermore, the F-statistic results confirmed the overall significance of the regression model, with extremely low p-values approaching zero. The regression analyses and estimated exponent 'c' also indicated that torsional amplification predominantly occurs at the FE, and as the building's inelasticity increases, $TAF_{F,\ max}$ at the FE decreases significantly. These findings highlight a strong correlation between $TAF_{F,\ max}$ at the FE and the torsional irregularity indices $\Delta_{max}/\Delta_{avg}$ and $\Delta_{max}/\Delta_{min}$, reinforcing their relevance in assessing torsional amplification effects in seismic design of the light-weight acceleration-sensitive secondary systems. For detailed information on the obtained

regression parameters, refer to Tables C.3 and C.4 in Appendix C, which provide regression parameters, for both buildings exhibiting elastic and inelastic response (SR = 2 and 4).

6.4 Proposed recommendations

6.4.1 Recommendations to estimate the torsional amplification factors for rigid, flexible, and very flexible secondary systems

This section introduces practice-oriented design recommendations to predict the TAFs for estimating floor acceleration demands in buildings with nominal torsion. Based on the results of the regression analyses, Equations 6.1–6.5 are proposed considering the torsional irregularity indices, $\Delta_{max}/\Delta_{avg}$ and $\Delta_{max}/\Delta_{min}$, respectively. These equations are derived considering TAFs at the FE; hence, when applied at locations other than the FE on the floor plan, they are expected to provide conservative estimates of the TAFs. The $\Delta_{max}/\Delta_{avg}$ and $\Delta_{max}/\Delta_{min}$ can be computed using an elastic three-dimensional building model with the mode superposition method using the response spectrum. For any given case (i.e., the floor level, the extent of nominal torsion, and the SR), marginal variations in the estimated TAF_Rs are expected while calculated using Equation 6.1. These marginal differences could be attributed to the aleatoric uncertainties in estimating the torsional irregularity indices of seismic design codes using ground motion records.

$$\text{TAF}_R = \begin{cases} 1.30, & \text{for SE} \\ \left(\dfrac{\Delta_{max}}{\Delta_{avg}}\right)^{\alpha}, & \text{for FE} \\ \left(\dfrac{\Delta_{max}}{\Delta_{min}}\right)^{\beta}, & \text{for FE} \end{cases} \tag{6.1}$$

$$\text{TAF}_{HM} = 1.25 \times \text{TAF}_{FM} \qquad \frac{T_b}{T_1} \leq \frac{T_s}{T_1} \leq \frac{T_c}{T_1} \tag{6.2}$$

$$\text{TAF}_{TZ} = \begin{cases} 1.20 \leq \left(\dfrac{\Delta_{max}}{\Delta_{avg}}\right)^{\delta} \leq 1.50, \\ 1.20 \leq \left(\dfrac{\Delta_{max}}{\Delta_{min}}\right)^{\theta} \leq 1.50 \end{cases} \qquad \frac{T_d}{T_1} \leq \frac{T_s}{T_1} \leq \frac{T_e}{T_1} \tag{6.3}$$

$$\text{TAF}_{FM} = \begin{cases} \left(\dfrac{\Delta_{max}}{\Delta_{avg}}\right)^{\delta} \geq 1.20, \\ \left(\dfrac{\Delta_{max}}{\Delta_{min}}\right)^{\theta} \geq 1.20 \end{cases} \qquad \frac{T_f}{T_1} \leq \frac{T_s}{T_1} \leq \frac{T_g}{T_1} \tag{6.4}$$

$$\text{TAF}_{VF} = 1.20 \qquad \frac{T_h}{T_1} \leq \frac{T_s}{T_1} \tag{6.5}$$

Figure 6.27 presents the multi-linear model, corresponding to the proposed equations, for estimating TAFs for rigid, flexible, and very flexible secondary systems. The T_s/T_1 values must be adjusted for elastic and different inelasticity level, hence, the T_s/T_1 values depicted in Figure 6.27 are to be obtained from Table 6.7, corresponding to a specific SR value, to account for the period shift (elongation) induced by the building inelasticity. It shall be noted that, as discussed earlier, the building dissipates a larger amount of energy through the fundamental mode of vibration. Hence, period elongation effects are only considered in the fundamental mode region. The proposed multi-linear curve is divided into five segments for the estimation of TAFs, corresponding to different values of T_s/T_1. These segments are denoted as a' (TAF_R), a'–d' (TAF_{HM}), d'–e' (TAF_{TZ}), e'–h' (TAF_{FM}), and h'–i' (TAF_{VF}). The values between these segments are to be interpolated linearly (a'–b', c'–d', e'–f' , g'–h'), as indicated in Figure 6.27. Each segment is further discussed in this section.

6.4.1.1 Point a' of the multi-linear curve

Point a' defines the TAF for the infinitely rigid secondary systems within the multi-linear curve. At the FE, the equation for TAF_R is dependent on torsional irregularity indices ($\Delta_{max}/\Delta_{avg}$ and $\Delta_{max}/\Delta_{min}$). Thus, values of TAF_R can be estimated as per the proposed Equation 6.1 for $\Delta_{max}/\Delta_{avg}$ and $\Delta_{max}/\Delta_{min}$, at T_s/T_1 = 0.

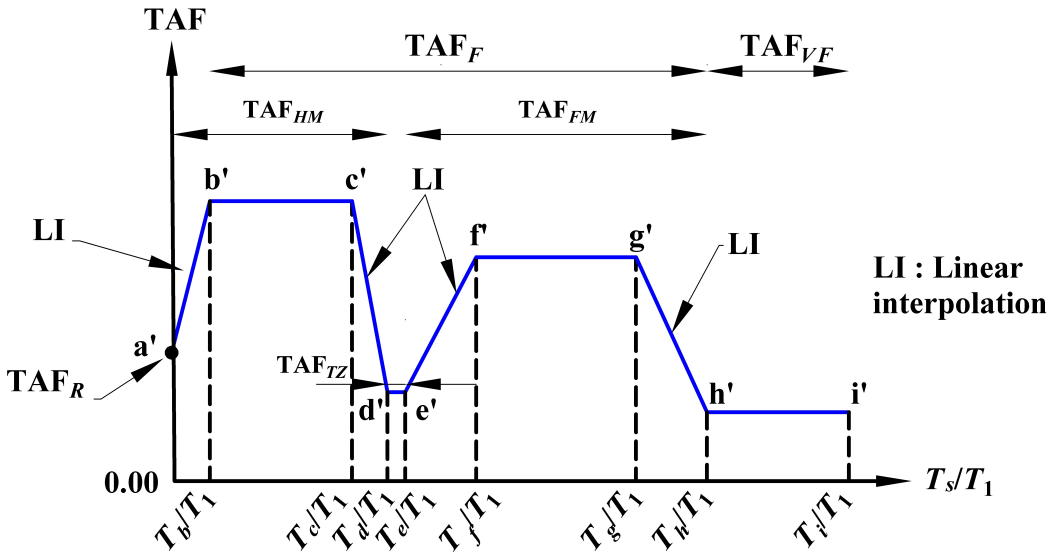

Figure 6.27: Proposed model for the estimation of torsional amplification factors for rigid, flexible, and very flexible secondary systems.

The exponents α and β can be determined from Table 6.8 for a given SR of interest. If the SR of a building under investigation falls between the values listed in Table 6.8, linear interpolation is permitted. In cases where the SR is unknown, it is recommended to use the exponents α and β corresponding to the elastic case. In contrast, as discussed in Section 6.2, torsional de-amplification is observed at the SE under an elastic response, while a marginal amplification of TAF_R up to 1.12 occurs under an inelastic response. Furthermore, due to the influence of rotational ground motions, the maximum median increase in TAF_R at the SE remains relatively consistent for both buildings exhibiting elastic and inelastic response, reaching a peak of up to 27%, with a corresponding TAF_R value of 1.28. Therefore, for estimating TAF_R at the SE, a conservative value of 1.30, independent of the building's torsional and strength characteristics, is recommended.

Table 6.7: Values of the tuning ratio for the proposed model (Figure 6.27).

SR	T_b/T_1	T_c/T_1	T_d/T_1	T_e/T_1	T_f/T_1	T_g/T_1	T_h/T_1
Elastic	0.10	0.50	0.60	0.65	0.85	1.30	1.50
1	0.10	0.50	0.60	0.88	1.15	1.76	2.02
2	0.10	0.50	0.60	0.94	1.23	1.89	2.18
3	0.10	0.50	0.60	1.00	1.32	2.01	2.32
4	0.10	0.50	0.60	1.07	1.40	2.15	2.48

Table 6.8: Proposed values of the exponents α and β to estimate the torsional amplification factor for rigid secondary systems.

Exponent	SR				
	Elastic	1	2	3	4
α	1.75	1.65	1.55	1.45	1.35
β	0.80	0.75	0.70	0.65	0.60

Table 6.9: Proposed values of the exponents δ and θ to estimate the torsional amplification factor for flexible secondary systems.

Exponent	SR				
	Elastic	1	2	3	4
δ	2.00	1.80	1.20	1.00	0.80
θ	0.85	0.75	0.50	0.40	0.35

6.4.1.2 Segments a'–d', d'–e', and e'–h' of the multi-linear curve

Segments a'–d', d'–e', and e'–h' of the multi-linear curve represents the region corresponding to the flexible secondary systems. The segment a'–d' corresponds to the torsional amplification factor when the secondary system is tuned to the building's higher modes (TAF_{HM}), while segment e'–h' ($T_e/T_1 \leq T_s/T_1 \leq T_h/T_1$) represents the torsional amplification factor when the secondary system is tuned to the building's fundamental mode (TAF_{FM}). The TAF_F for this segment is expressed in terms of $(\Delta_{max}/\Delta_{avg})^{\delta}$ and $(\Delta_{max}/\Delta_{min})^{\theta}$ as shown in Equations 6.2–6.4, with the values of δ and θ provided in Table 6.9. Based on the analyses of the obtained TAF_F from the NTI buildings, torsional amplification can be expected under rotational ground motions. Hence, the lower bound limit of 1.20, respectively, is applied to the TAF_F values in view of the applicability of the proposed equations for the regular buildings.

The segment a'–d' ($T_a/T_1 \leq T_s/T_1 \leq T_d/T_1$) characterizes the TAF_F corresponding to higher modes. Within this range, the TAF_F is expressed as 1.25 times that of the fundamental mode, reflecting the trends observed in the analyzed building data. Similarly, the segment d'–e' ($T_d/T_1 \leq T_s/T_1$ T_e/T_1) represents the torsional amplification factor in transition zone (TAF_{TZ}) of the fundamental and higher modes. In this range, the TAF_F is defined similarly to the fundamental mode TAF_F, but the upper limit is constrained to 1.50 to better reflect the characteristics of the torsional amplification spectrum.

6.4.1.3 Segments h'–i' of the multi-linear curve

The segment h'–i' ($T_h/T_1 \leq T_s/T_1 \leq T_i/T_1$) represents the TAF for very long periods (TAF_{VF}). A constant value of 1.20 is proposed for this segment (Equation 6.5), acknowledging that the TAF_{VF} at very long periods declines sharply and approaches unity, as discussed earlier in Section 6.2.3.

6.4.2 Recommendations to estimate the torsional amplification factors for rigid secondary systems across the building plan

Based on the observations summarized in Sections 6.2.1 and 6.3.1.2, which investigated TAF_Rs and analyzed the relationships between the TAF_Rs and the elastic displacement ratio ($\Delta_{FF,\,ij}/\Delta_{CR,\,j}$), the practice-oriented equations (Equations 6.6–6.7) are proposed. As shown in Figures 6.3–6.8 and discussed subsequently, the torsional de-amplification of PFA occurs for the stiff frames during the elastic response of the building, which turned into marginal torsional amplification of PFA under inelastic response, with the corresponding maximum (median) value not exceeding 1.28 and 1.12 among all the analyzed cases with and without considering rotational ground motion, respectively. Hence, for the extreme stiff frame, Equation 6.6 prescribes a constant value of TAF_Rs equal to 1.30 regardless of the extent of nominal torsion, floor level, and the SR of the building. For other stiff frames (i.e., those located away from extreme stiff frames) and up to the CR, the TAF_Rs can be obtained using a linear interpolation while taking TAF_R equal to 1, at the CR. In contrast, the TAF_Rs for the flexible frames can be estimated using Equation 6.7. The equations proposed for estimating the values of TAF_Rs for PFA in buildings with nominal torsion are:

$$\text{TAF}_R = \begin{cases} 1.30, & \text{at the extreme stiff frames of all floors.} \\ 1.00, & \text{at the center of rigidity of all floors.} \\ \text{linear interpolation,} & \text{for other stiff frames in between the extreme stiff frame and center of rigidity.} \end{cases} \tag{6.6}$$

$$\text{TAF}_R = \left(\frac{\Delta_{FF,\,ij}}{\Delta_{CR,\,j}}\right)^{\gamma}, \quad \text{for the } i^{\text{th}} \text{ flexible frame at } j^{\text{th}} \text{ floor.} \tag{6.7}$$

To estimate TAF_Rs for the flexible frames, the displacement ratio $\Delta_{FF,\,ij}/\Delta_{CR,\,j}$ of the building can be estimated using an elastic analysis of a three-dimensional building, with the mode superposition method using the response spectrum analysis. The exponents γ in Equation 6.7 can be estimated using Table 6.10 for SR up to 4. For SR values in between those listed in Table 6.10, linear interpolation may be used. For the cases where SR is not known in advance, the exponent γ corresponding to the elastic case can be used to conservatively estimate TAF_Rs.

Table 6.10: Proposed values of the exponent 'γ' to estimate the torsional amplification factor for rigid secondary systems across the floor plan.

Exponent	**SR**				
	Elastic	**1**	**2**	**3**	**4**
γ	1.10	1.00	0.90	0.80	0.70

6.5 Summary

This chapter presents a detailed evaluation of TAFs for the light-weight acceleration-sensitive secondary systems in buildings with nominal torsion, considering their elastic and inelastic behavior. The characteristics of TAFs are examined based on their flexibility-based classification, i.e., for the rigid (TAF_R), flexible (TAF_F), and very flexible (TAF_{VF}) secondary systems. Detailed regression analyses are conducted between the obtained TAFs and floor displacement-based torsional irregularity indices from seismic design codes. Based on the conducted regression analyses, practice-oriented equations are proposed to improve the estimation of TAFs, explicitly incorporating the effects of nominal building torsion

and rotational ground motions in the seismic design of acceleration-sensitive secondary systems. The findings presented in this Chapter are summarized, and they are as follows:

- TAF_R are the highest for ETI buildings, followed by WTI and NTI buildings. The maximum (median) TAF_R at the FE occurs under the elastic response of the buildings, and the corresponding values for ETI, WTI, and NTI buildings are 1.76, 1.43, and 1.03, respectively. On the other hand, the maximum (median) TAF_R at the SE occurs under the inelastic response of the buildings, and the corresponding values for ETI, WTI, and NTI buildings are 1.12, 1.00, and 1.00, respectively. These magnitudes of TAF_R suggest their dependency on a building's nominal torsion and strength characteristics. Further, ignoring them, especially at the FE, can significantly underestimate the in-structure acceleration demands for rigid secondary systems.

- For buildings responding elastically, the effects of torsional amplification for rigid secondary systems are more pronounced in the flexible frames, while torsional de-amplification effects are more significant in the stiff frames. The building's inelastic response helps in reducing torsional amplification for rigid secondary systems in flexible frames (up to 29%) while increasing it in stiff frames (up to 21%), compared to their elastic counterparts. Hence, the TAF_R are found to be dependent on the extent of nominal torsion in the building, the location of the frame from the center of rigidity, as well as the extent of inelastic action expected in the building under earthquake excitation.

- TAF_F is the highest for ETI buildings and the lowest for NTI buildings. The maximum (median) TAF_F at the FE occurs during the buildings' elastic response, with values reaching up to 2.06, 1.69, and 1.08 for ETI, WTI, and NTI buildings, respectively, when the secondary system is tuned within the building's fundamental mode region, and 2.33, 1.83, and 1.04 when the secondary system is tuned within the building's higher mode region. Conversely, the maximum (median) TAF_F at the SE are limited to 1.38, 1.16, and 1.00 for the case when the secondary system is tuned within the building's fundamental mode region, and 1.51, 1.26, and 1.02, when the secondary system

is tuned within the building's higher mode region, corresponding to ETI, WTI, and NTI buildings, respectively. These values highlight that torsional amplification effects are more pronounced at the FE and also at short periods (in the vicinity of higher modes). Hence, the TAF_F prediction model shall account for these effects.

- TAF_F also varies marginally with the building height. For 4-story buildings exhibiting elastic response, the peak median TAF_F values reach 2.06 when the secondary system is tuned within the building's fundamental mode region, which further increases to 2.33 when the secondary system is tuned within the building's higher mode region. However, in elastic 8-story buildings, these values reduce to 1.61 and 1.98 when the secondary system is tuned within the building's fundamental and higher mode regions, respectively. This observation further strengthens the finding that TAF_F values are higher at short periods.

- The building inelasticity significantly reduces TAF_F. For 4-story buildings exhibiting elastic response, the maximum median TAF_F at the FE for the case, when the secondary system is tuned within the building's fundamental mode region, is 2.06, 1.69, and 1.08 for ETI, WTI, and NTI buildings, respectively. However, in 4-story buildings exhibiting highly inelastic response, these values decrease to 1.37, 1.15, and 1.03, respectively, highlighting the mitigating effect of the building's inelasticity on TAF_F. Hence, the building inelasticity dependent TAF_F shall be used in the seismic design of flexible secondary systems.

- At very long periods, torsional amplification tends to approach unity due to the reduced degree of dynamic interaction between the secondary system and the building. Furthermore, the presence of nominal torsion has a negligible impact at very long periods or very flexible systems, with the median TAF_{VF} values ranging from 1.21 in ETI buildings to 1.02 in NTI buildings, at the FE. The TAF_{VF} at the SE remained unaffected, consistently exhibiting the median TAF_{VF} of 1.00, among all analyzed cases. Further, the building inelasticity reduced the maximum median TAF_{VF} at the FE, though the reduction is

insignificant. However, at the SE, the median TAF_{VF} remains constant at 1.00, indicating no significant effect of the building inelasticity. Hence, for all practical purposes, TAF_{VF} can be assumed to be independent of the extent of nominal torsion and building inelasticity.

- The rotational ground motions have a greater impact on TAF_R at the SE compared to the FE. The median TAF_R increase at the SE remains relatively consistent, reaching a maximum of 27%, while at the FE, it varies, with a maximum increase limited only up to 4%, and many times even decreases, up to 15%.

- The impact of rotational ground motions on the median peak TAF_F varies with structural configuration and inelasticity levels. The increase in the median peak TAF_F due to rotational ground motions is more significant when the secondary system is tuned within the building's higher mode region, reaching up to 44%, in contrast to 24% when the secondary system is tuned within the building's fundamental mode region. This observation can be attributed to relatively richer high-frequency content in the rotational ground motions.

- The maximum median peak TAF_F increase due to rotational ground motions at the SE elevated from 14% in the elastic case to 19% in the highly inelastic case, while at the FE, it decreases from 15% to -1%, when the secondary system is tuned within the building's fundamental mode region. In contrast, when the secondary system is tuned within the building's higher mode region, the SE experiences a more pronounced effect, with the maximum increase rising from 14% (elastic) to 44% (highly inelastic), whereas at the FE, it decreases from 15% to 1%. These results indicate that the building's inelasticity influences TAF_F by amplifying the effects of rotational ground motions at the SE while reducing effects at the FE, with a stronger impact observed in the higher modes region.

- The inclusion of rotational ground motions has no significant impact on TAF_{VF} values. Both buildings exhibiting elastic and highly inelastic responses show consistent trends, with no noticeable amplification at the SE and the FE. These

findings indicate that rotational ground motions do not influence TAF_{VF} across different buildings and inelasticity levels.

- The TAF_R showed a strong correlation with the elastic floor displacement-based indices of the seismic design codes (i.e., $\Delta_{max}/\Delta_{avg}$ and $\Delta_{max}/\Delta_{min}$). This fact implies that the torsional irregularity indices of seismic design codes can be used as a proxy to incorporate the effects of the building's nominal torsion in estimating the in-structure acceleration amplification.

- The torsional amplification factors at the FE show a strong relationship with the torsional irregularity indices ($\Delta_{max}/\Delta_{avg}$ and ($\Delta_{max}/\Delta_{min}$) for both TAFs corresponding to rigid and flexible secondary systems. The findings lead to the proposal of the practice-oriented building's torsional and strength characteristics dependent TAFs. Further, the lower bound limits applied in these TAFs take care of the possible increase in the acceleration demands due to rotational ground motions.

- The in-plan distribution of TAFs within the building exhibited a robust relationship with the elastic displacement ratio (i.e., $\Delta_{FF,\,ij}/\Delta_{CR,\,j}$). It is observed that for the flexible frames, the acceleration amplification due to the building's nominal torsion is approximately proportional to the displacement amplification due to the building's nominal torsion.

Chapter 7

Validation of the Proposed Recommendations

7.1 Introduction

This chapter outlines the validation of the TAF prediction models proposed in Chapter 6 to account for the effects of nominal building torsion on floor acceleration demands for the rigid, flexible, and very flexible secondary systems. To assess the efficacy of the proposed recommendations, low- to mid-rise RCMRF building archetypes resting on both plain and sloped terrain conditions are considered. The selected building typologies encompass a wide range of plan irregular and combined plan and elevation irregular buildings commonly observed in the existing housing stock in India. To ensure a comprehensive evaluation, a total of 1,400 time history analyses are conducted, capturing a diverse set of seismic scenarios, inelastic responses, and building configurations.

7.2 Selection of building archetypes

To validate the efficacy of the proposed models, they are tested on two groups of RCMRF buildings. The first group, referred to as Group 1, consists of four buildings with extreme torsional irregularities. The buildings selected are of E- and Plus-shaped plan layouts, which are inherently irregular (Figure 7.1). These buildings feature an asymmetric distribution of the lateral load-resisting elements. The group includes both 3-story and 6-story buildings, which are representative of low- to mid-rise housing stock in urban areas. The lateral load-resisting elements are arranged in the building plan to result in extreme torsional irregularity (ETI), i.e., $\Delta_{max}/\Delta_{avg} \geq 1.4$. The story height is constant for all stories and is considered as 3.2 m. The E- and Plus-shaped buildings are abbreviated in a manner

consistent with that used for the investigated buildings, discussed in Chapter 3. The typical cross-section sizes of the beams and columns for the Group 1 buildings are summarized in Figure 7.1.

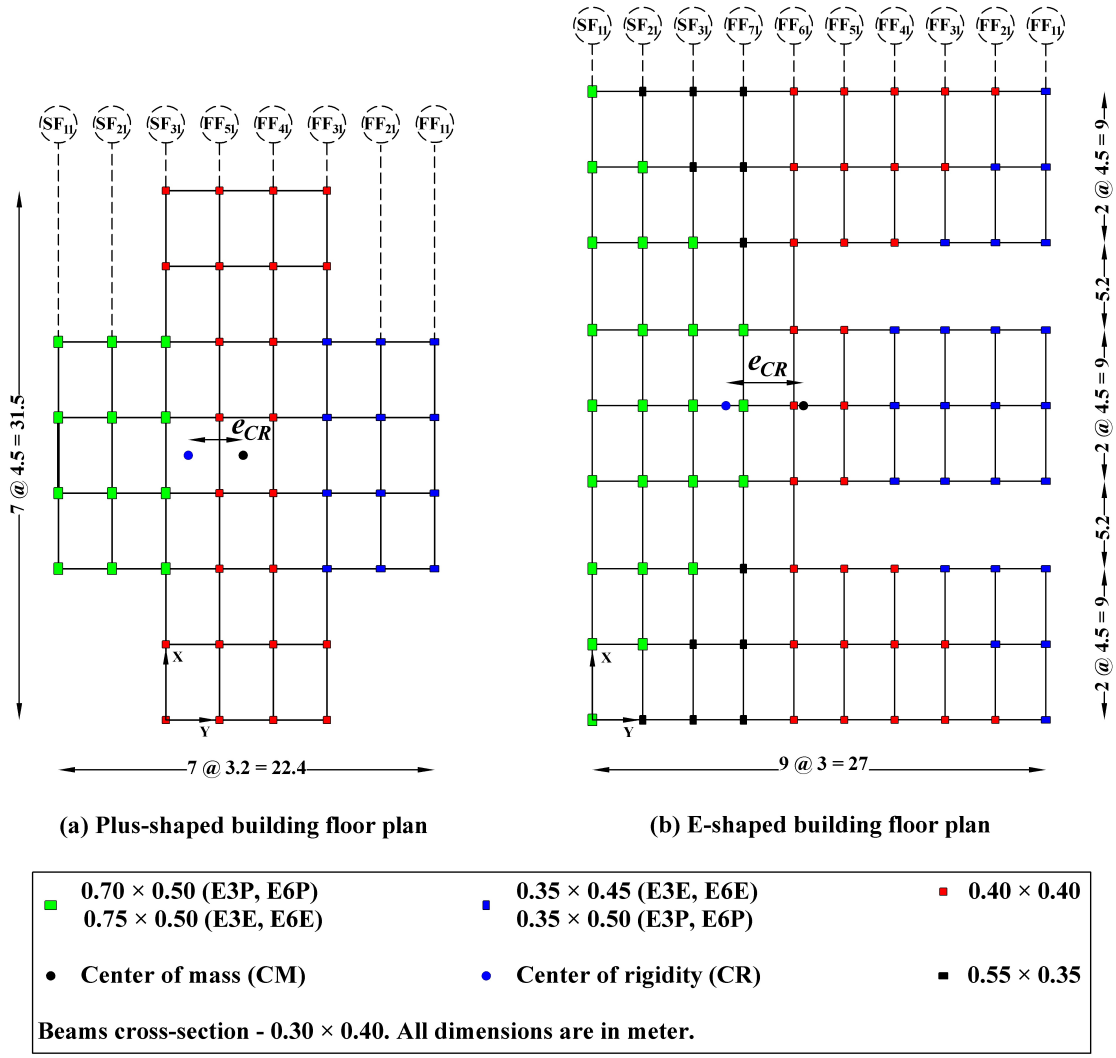

Figure 7.1: Typical plan layouts, section sizes, and stiffness eccentricity details of the buildings considered for validation of the proposed equations. The stiffness eccentricities shown in the building plan correspond to the first-floor level of the 3-story building.

The second group, termed Group 2, consists of three step-back buildings (i.e., buildings resting on sloping ground) exhibiting both plan and elevation irregularities. Based on the particulars collected from the field surveys in an earlier study [151, 152], an archetypal building plan (Figure 7.2) is chosen to represent the variety of characteristics of RC step-back buildings observed in hilly regions of India. Three different buildings with 2-, 4-, and 8-stories (here onwards referred to as '2SB', '4SB', and '8SB') above the topmost foundation level are considered. It is to be noted that

in the case of step-back buildings, defining the number of stories for a given building is not straightforward (e.g., since in a given building, the number of stories can be different while measured on the uphill side and downhill side, respectively). Thus, consistent with earlier studies [117, 152], the number of stories above the topmost foundation level indicates the number of stories in the step-back buildings.

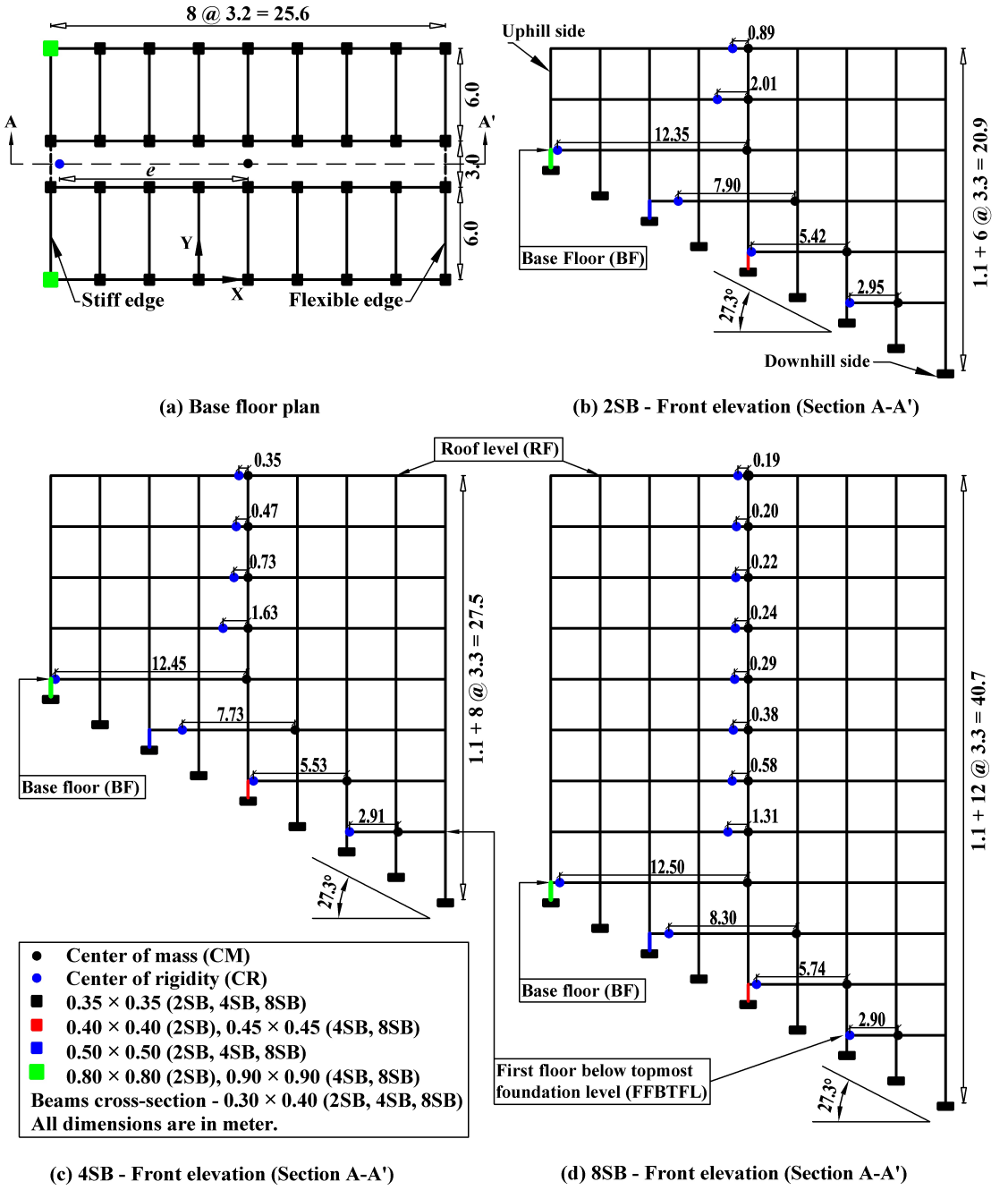

Figure 7.2: Typical plan, elevations (along-slope), section sizes, and eccentricity details of the considered step-back buildings.

The chosen set of low- to mid-rise step-back RC frame buildings represents existing (prevalent) housing stock in the Indian Himalayan region, characterized by

the presence of moderate to steep slopes [117]. One of the key reasons for including step-back buildings in this thesis is their wide variation in floor eccentricities (the distance between the CM and CR) along the building height. This variation leads to significant differences in torsional responses across different floors. Additionally, all three step-back buildings are classified as ETI since their torsional irregularity index ($\Delta_{max}/\Delta_{avg}$) exceeds 1.40. These three buildings rest on sloping ground, with a ground slope of 2:1 (Horizontal: Vertical), which typically represents one of the most prominent ground slope conditions observed in hilly regions of India. The number of stories below the topmost foundation level is identical, and their number is governed by the ground slope. The story height is set constant for all stories and considered as 3.30 m. These buildings are further characterized by the ground-supported short columns of heights equal to 1.10 m and 2.75 m in the successive stories (Figures 7.2((b)-(d))), resting on the slope.

7.3 Modeling, analysis, and design of the buildings

The structural models for the selected groups of buildings are developed and designed using ETABS [136], adhering to the Indian Standards [137, 138] for load application. The methodology described in Chapter 3 is considered for these buildings' seismic analysis and design. For Group 1 buildings, the longitudinal reinforcement in beams varied from 0.28% to 1.17% and 0.28% to 0.84% at the top and bottom faces, respectively, whereas the longitudinal reinforcement in columns ranged between 0.95% and 2.55%. In contrast, Group 2 buildings exhibited a variation in the beam reinforcement from 0.28% to 1.83% at the top face and 0.28% to 1.31% at the bottom face, with column reinforcement ranging between 2.01% and 3.93%. The spacing of transverse reinforcement in both beams and columns does not exceed 100 mm in the end regions; thus, the considered buildings confirm the ductile detailing provisions of IS 13920 [33].

For the present study, three-dimensional non-linear numerical models are developed using OPENSEES [139] based on the design details of Group 1 and Group 2 buildings. For Group 1 buildings, only the flexural failure mode of beams

and columns has been considered, as shear failure is not expected to occur in SMRF buildings [37] designed and detailed using the capacity design principle. However, in the case of Group 2 buildings, which are located on a slope and have short columns, the shear failure of short columns can be expected and has been modelled using the *LimitState material model* [61, 153–155] available in OPENSEES.

7.3.1 Dynamic characteristics of the investigated buildings

The modal analysis is performed in OPENSEES for all the buildings to obtain their dynamic characteristics. The dynamic characteristics (i.e., periods and modal mass participation factors) for Group 1 buildings, as obtained from the 3D modal analysis for the first three modes of vibration, are summarized in Table 7.1. In contrast, the buildings on hill slopes have complex dynamic behavior, with distinct modes of vibrations for portions above and below the topmost foundation level. Hence, for Group 2 buildings, the dynamic characteristics of the first 15 modes of vibration are presented in Table 7.2. It is to be noted that the ratio between the first translational to the first rotational mode period is greater than unity (the term 'first' mode is defined as the mode with the highest modal mass participation) in the X-direction of excitation for all Group 1 and Group 2 buildings. Thus, these buildings are expected to behave as torsionally rigid buildings.

Table 7.1: Dynamic characteristics of the Group 1 buildings.

Mode	Period (s)	Modal Mass Participation (%)			Period (s)	Modal Mass Participation (%)		
		α_{mx}[a]	α_{my}[b]	θ_{mz}[c]		α_{mx}[a]	α_{my}[b]	θ_{mz}[c]
	E3E				**E3P**			
1	0.44	60.53	-	23.69	0.45	64.51	-	20.31
2	0.38	-	85.24	-	0.40	-	84.69	-
3	0.36	21.11	-	60.83	0.38	18.23	-	63.99
	E6E				**E6P**			
1	0.97	70.26	-	10.52	0.97	73.06	-	08.30
2	0.82	-	82.09	-	0.85	-	81.62	-
3	0.81	09.42	-	71.14	0.84	07.45	-	73.10

Grey cells show the translational-torsional coupling of modes in the X-direction. [a]Modal mass participation in the X-direction (%); [b]Modal mass participation in the Y-direction (%); [c]Modal mass participation corresponding to the rotational mode of vibration (%).

In the case of Group 1 buildings, the modal mass participation corresponding to the first mode ranges between 60.53-73.06%, implying that the fundamental vibrational mode dominates the seismic response of these buildings. The torsional

Table 7.2: Dynamic characteristics of the Group 2 buildings.

Mode	Period	Modal Mass Participation			Period	Modal Mass Participation			Period	Modal Mass Participation		
	(s)	α_{mx}[a]	α_{my}[b]	θ_{mz}[c]	(s)	α_{mx}[a]	α_{my}[b]	θ_{mz}[c]	(s)	α_{mx}[a]	α_{my}[b]	θ_{mz}[c]
	2SB				4SB				8SB			
1	0.48	35.57	-	00.01	0.92	49.40	-	00.35	1.78	57.43	-	03.41
2	0.39	01.41	-	38.53	0.73	00.57		51.42	1.45	00.63	-	60.04
3	0.35	-	36.56	-	0.63	00.00	50.42	-	1.23	00.00	60.22	00.01
4	0.19	32.32	-	21.49	0.28	06.16	-	00.04	0.58	08.25	-	00.03
5	0.15	06.60	-	00.01	0.23	00.36	-	05.05	0.47	00.05	-	07.81
6	0.13	00.14	-	01.02	0.20	-	05.31	-	0.40	-	07.68	-
7	0.13	00.10	-	04.71	0.19	21.59	-	17.54	0.32	02.93	-	00.03
8	0.12	-	04.75	-	0.14	03.71	-	00.06	0.27	00.04	-	02.81
9	0.12	-	35.41	-	0.12	00.01	-	02.32	0.23	-	02.69	
10	0.10	01.98	-	01.43	0.12	-	06.18	-	0.21	01.38	-	00.06
11	0.10	-	01.64	-	0.12	00.16	-	01.80	0.18	00.21	-	00.99
12	0.09	00.02	-	-	0.11	-	23.62	-	0.16	-	01.34	-
13	0.09	-	00.00	-	0.11	00.00	-	00.01	0.15	09.36	-	10.16
14	0.08	00.91	-	00.21	0.11	-	00.01	-	0.15	05.50	-	01.38
15	0.08	-	-	-	0.10	00.05	-	00.01	0.14	-	00.00	-

Grey cells show the translational-torsional coupling of modes in the X-direction. [a]Modal mass participation in the X-direction (across-slope); [b]Modal mass participation in the Y-direction (along-slope); [c]Modal mass participation corresponding to the rotational mode of vibration (%).

irregularity in the investigated buildings results in translational-torsional coupling of modes in the X-direction (shown by grey cells, Table 7.1). The extent of torsional coupling varied from 8.30-23.69% in the X-direction. For a given plan shape, the translational-torsional coupling of modes is observed to be higher in 3-story buildings compared to their 6-story counterparts, consistent with the findings for the investigated buildings in Chapter 3. This indicates that torsional effects have a more significant impact on shorter buildings, highlighting their increased vulnerability to torsional motion.

In the case of Group 2 buildings, it is observed that the step-back buildings have significantly different dynamic behavior as compared to the ordinary buildings resting on plain ground (Group 1). The first mode (defined as the mode with the highest modal mass participation in the direction under consideration) of step-back buildings corresponds to vibration of the building mass (significant proportion) above the topmost foundation level only (in all the directions, i.e., across-slope (X), along-slope (Y), and rotation (R_z)). As a result, almost comparable mass participates in the first three modes (e.g., 35.57%, 38.53%, and 36.56% corresponding

to 'Mode 1', 'Mode 2' and 'Mode 3', respectively, in '2SB' building) for all the buildings, and also a higher modal mass participation factor is achieved in all the directions (along-slope, across-slope, and rotation), in the building (i.e. '8SB') with the most number of stories above the topmost foundation level.

In contrast, consistent with the observations of an earlier study [117], the building mass below the topmost foundation level vibrates in multiple higher vibration modes (i.e. 'Mode j', where, j≥4 for the investigated cases, and also varies from building-to-building, Table 7.2). The other important observation associated with the dynamic behavior of step-back buildings lies in the fact that due to non-coincident CM and CR at all floors, the translational and rotational modes are coupled in the across-slope direction (shown by grey cells in Table 7.2). The ratio between the first translational to the first rotational mode period is greater than unity (the term 'first' mode is defined as the mode with the highest modal mass participation, 'Mode 1' and 'Mode 2' are the first translational and the first rotational modes, respectively) in the across-slope direction for all the buildings; thus, these buildings are expected to behave as torsionally rigid buildings.

7.3.2 Torsional irregularity indices of the buildings

The torsional irregularity indices for Group 1 and Group 2 buildings are presented in Figures 7.3 and 7.4, alongside their specified limits as recommended by building codes [5, 6, 27], illustrating the ratios $\Delta_{max}/\Delta_{avg}$ and $\Delta_{max}/\Delta_{min}$ at different floor levels. The floor displacements—Δ_{max} and Δ_{min}, are computed using a three-dimensional building model through the mode superposition method, with the response spectrum defined in IS 1893 [5].

The Group 1 buildings show the highest displacement ratios at the first-floor level, indicating significant torsional effects. These values gradually decrease with increasing floor level (Figure 7.3). However, in the Group 2 buildings, the maximum displacement ratios are observed at the fourth-floor level, which also has the maximum stiffness eccentricity. It is evident that for each of the step-back buildings, the maximum torsional effects are observed to exist at the base floor level (Figure 7.4), and the torsional effects reduce while moving either upwards or downwards from the base floor level. The plots further show that the displacement-based

index $\Delta_{max}/\Delta_{min}$ exceeds the threshold of 1.50, whereas $\Delta_{max}/\Delta_{avg}$ exceeds the threshold of 1.40, indicating the torsional irregularity and the extreme torsional irregularity in all three step-back buildings, as per the provisions of IS 1893 and ASCE 7, respectively. In all the step-back buildings, the extent of torsion is almost comparable at the bottommost floor level. Still, the torsional effects at the roof level are observed to be significantly different. The highest torsional effects at the roof level are observed in the '2SB' building, and the least torsional effects at the roof level are observed in the '8SB' building. This fact underlines an important observation that for a given plan shape and slope, with an increase in the number of stories above the topmost foundation level, the torsional effects at the roof level in step-back buildings reduce.

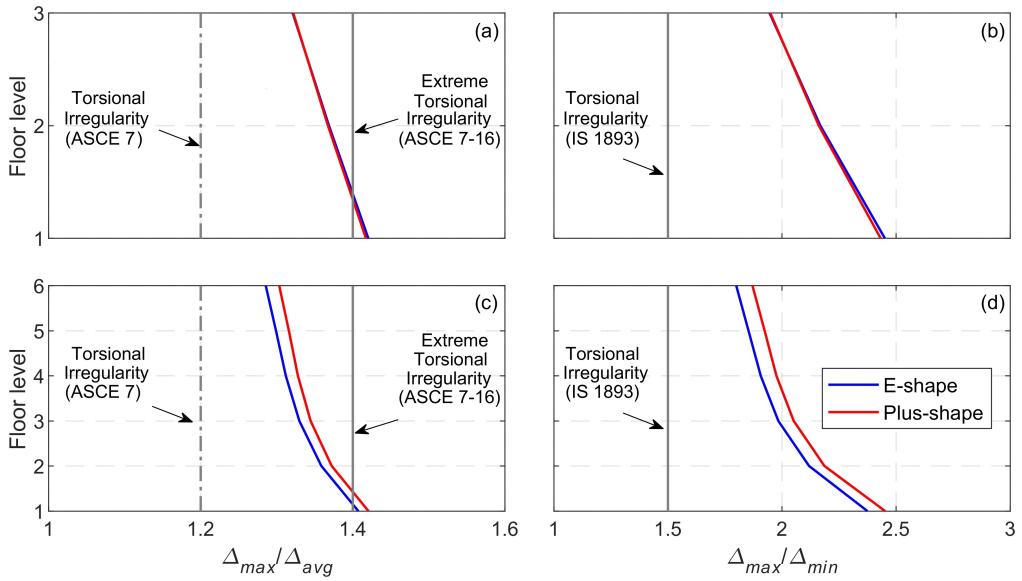

Figure 7.3: Variations of the torsional irregularity indices of seismic design codes for the Group 1 buildings (obtained using the mode superposition method).

7.3.3 Ground motion selection and time history analyses

Time history analyses are conducted for the selected building groups, both with and without considering rotational ground motions. The far field ground motion suite for Group 1 buildings is presented in Table 7.3, while a different suite is used for Group 2 buildings, as shown in Table 7.4. These ground motions are selected based on the criteria recommended in FEMA P695 [37]. Each ground motion record suite consists of 20 pairs of recorded seismic ground motions, with moment magnitudes ranging from M_w 6.50 to M_w 7.62 and a suite mean of M_w 7.08 for both groups. For

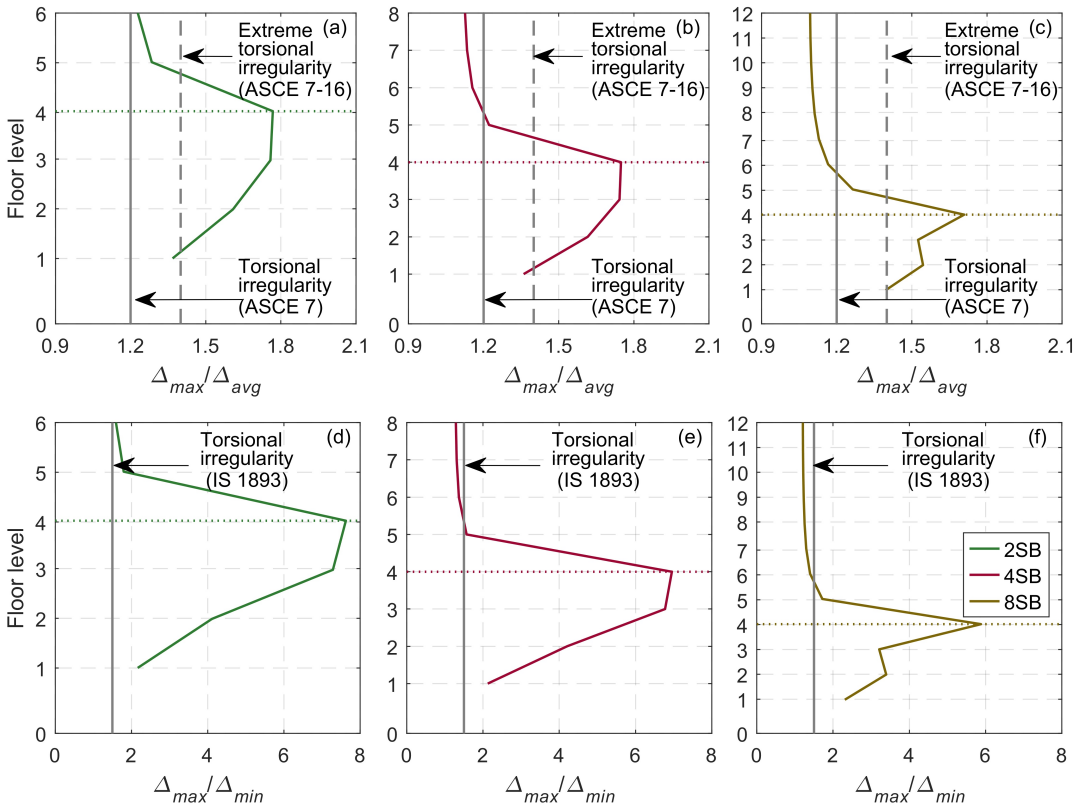

Figure 7.4: Variations of the torsional irregularity indices of seismic design codes for the Group 2 buildings (obtained using the mode superposition method). Here, the horizontal dotted lines in the plots show the base floor levels of the respective buildings.

Group 1 buildings, the geometric mean of PGA ranges from $0.14g$ to $1.84g$, with a suite mean of $0.40g$, while for Group 2 buildings, it ranges from $0.14g$ to $0.78g$, with a suite mean of $0.35g$. All ground motions were recorded on NEHRP site classes C and D. Additional details on the selected ground motions are provided in Tables 7.3 and 7.4. The ground motions are amplitude-scaled to achieve the targeted SR, as defined in Equation 3.1.

To validate the proposed model, this study performed multi-directional time history analyses on all Group 1 and Group 2 buildings for five different SRs. The analyzed cases encompass buildings exhibiting both elastic and inelastic responses with SRs of 1, 2, 3, and 4. The amplitude scaling factors for the analyzed cases range between 0.26-5.20. It is to be noted that SR = 1 does not correspond to the elastic case since, Say, is obtained from the non-linear static analysis of the building, and it is defined as the spectral acceleration corresponding to the yielding of significant members in the building. The analyses are performed both with and

Table 7.3: A suite of 20 far field ground motion records used for Group 1 buildings.

RSN[a]	Event name	Year	Station name	M_w[b]	R_{rup}[c] (km)	$V_{s,\,30}$[d] (m/sec)	V_p[e] (m/sec)	PGA_X (g)	PGA_Y (g)	Depth (km)	SRL[f] (km)
125	Friuli_ Italy-01	1976	Tolmezzo	6.50	16	505	875	0.36	0.32	10.00	18
313	Corinth_ Greece	1981	Corinth	6.60	10	361	626	0.24	0.30	33.00	22
721	Superstition Hills-02	1987	El Centro Imp. Co.	6.54	18	192	333	0.36	0.26	09.00	19
768	Loma Prieta	1989	Gilroy Array #4	6.93	14	222	384	0.42	0.22	17.50	36
776	Loma Prieta	1989	Holl.-South & Pine	6.93	28	282	489	0.37	0.18	17.50	36
963	Northridge-01	1994	Castaic-Old Rge Rt.	6.69	21	450	780	0.57	0.52	17.50	25
1012	Northridge-01	1994	LA 00	6.69	19	706	1223	0.27	0.38	17.50	25
1101	Kobe_ Japan	1995	Amagasaki	6.90	11	256	443	0.28	0.33	17.90	35
1186	Chi-Chi_ Taiwan	1999	CHY014	7.62	34	348	602	0.26	0.23	06.80	109
1198	Chi-Chi_ Taiwan	1999	CHY029	7.62	11	545	944	0.29	0.24	06.80	109
3676	Taiwan SMART1(45)	1986	SMART1 M06	7.30	55	308	534	0.13	0.16	15.00	66
3746	Cape Mendocino	1992	Cen. Beach_Naval	7.01	18	459	795	0.32	0.48	09.60	41
4223	Niigata_ Japan	2004	NIGH06	6.63	32	493	854	0.36	0.42	15.80	23
4846	Chuetsu-oki_ Japan	2007	Joetsu Yana. Pad.	6.80	31	606	1049	0.33	0.28	10.00	30
4868	Chuetsu-oki_ Japan	2007	Yam. Tak. Nagaoka	6.80	28	655	1135	0.36	0.33	10.00	30
5478	Iwate_ Japan	2008	AKT023	6.90	17	556	963	0.38	0.37	34.75	39
5482	Iwate_ Japan	2008	AKTH04	6.90	18	459	795	1.36	2.50	34.75	39
5829	El Mayor-Cucapah_ Mexico	2010	RIITO	7.20	14	242	419	0.40	0.38	10.00	56
5837	El Mayor-Cucapah_ Mexico	2010	El Centro-I.&Ross	7.20	20	229	397	0.38	0.37	10.00	56
6923	Darfield_ New Zealand	2010	Kaiapoi North Sch.	7.00	31	255	442	0.36	0.30	10.00	41

[a]Record sequence number; [b]Moment magnitude; [c]The closest distance to the rupture surface; [d]Average shear-wave velocity from the surface to a depth of 30 m; [e]Primary wave velocity; [f]Surface rupture length [148].

without rotational ground motions. Additionally, the time history analyses are conducted following the same methodology as discussed in Chapter 3. Mass and stiffness proportional Rayleigh damping of 2.5% is assigned, following ASCE 7-16 guidelines. The Rayleigh damping is defined based on periods equal to $1.5\,T_1$ and the period corresponding to at least 95% cumulative mass participation in either direction of the building.

7.4 Validation of the proposed model

The linear and non-linear dynamic time history analyses are conducted on Group 1 and Group 2 buildings, and the absolute floor acceleration time histories are extracted at different locations on the floor plan. Further, using these absolute floor acceleration time histories, PFA/PGA and FRS are obtained, following which the total amplification (a_t) and torsional amplification factors (TAFs) are estimated. The proposals made in Chapter 6 are validated by applying them to the obtained TAFs and at for Group 1 and Group 2 buildings. This validation process involves

comparing the median peak TAFs predicted by the proposed model with those derived from time history analyses, with and without rotational ground motions. The accuracy of the proposed equations is evaluated based on their ability to estimate the median for Group 1 and Group 2 buildings. These analyses further highlight the strengths and potential limitations of the proposed model when applied within the framework of existing building code formulations, providing insights into its practical applicability for seismic design and assessment of the light-weight acceleration-sensitive secondary systems.

Table 7.4: A suite of 20 far field ground motion records used for Group 2 buildings.

RSN[a]	Event name	Year	Station name	M_w[b]	R_{rup}[c] (km)	$V_{s,\,30}$[d] (m/sec)	V_p[e] (m/sec)	PGA_X (g)	PGA_Y (g)	Depth (km)	SRL[f] (km)
169	Imperial Valley-06	1979	Delta	6.53	22	242	419	0.24	0.35	10.00	19
174	Imperial Valley-06	1979	El Centro Array #11	6.53	13	196	340	0.37	0.38	10.00	19
576	Taiwan SMART1(45)	1986	SMART1 M07	7.30	55	328	567	0.16	0.16	15.80	66
725[g]	Superstition Hills-02	1987	Poe Road (temp)	6.54	11	317	548	0.48	0.29	09.00	19
768	Loma Prieta	1989	Gilroy Array #4	6.93	14	222	384	0.42	0.22	17.50	36
777	Loma Prieta	1989	Hollister City Hall	6.93	28	199	344	0.25	0.22	17.50	36
953	Northridge-01	1994	Bev. Hills-14145 Mul.	6.69	17	356	616	0.45	0.50	17.50	23
960	Northridge-01	1994	Can. Country-WLC	6.69	12	326	564	0.41	0.47	17.50	23
1101	Kobe_ Japan	1995	Amagasaki	6.90	11	256	443	0.28	0.33	17.90	35
1147	Kocaeli_ Turkey	1999	Ambarli	7.51	70	175	303	0.25	0.19	15.00	92
1158	Kocaeli_ Turkey	1999	Duzce	7.51	15	282	488	0.31	0.36	15.90	102
1182	Chi-Chi_ Taiwan	1999	CHY006	7.62	10	438	759	0.36	0.36	06.80	109
1198	Chi-Chi_ Taiwan	1999	CHY029	7.62	11	545	944	0.29	0.24	06.80	109
1602	Duzce_ Turkey	1999	Bolu	7.14	12	294	508	0.75	0.82	11.00	54
1633	Manjil_ Iran	1990	Abbar	7.37	13	724	1254	0.53	0.50	19.00	80
3676	Taiwan SMART1(45)	1986	SMART1 M06	7.30	55	308	534	0.13	0.16	15.00	66
3746	Cape Mendocino	1992	Cen. Beach_Naval	7.01	18	459	795	0.32	0.48	09.60	41
3748	Cape Mendocino	1992	Fortuna Fire Sta.	7.01	19	388	672	0.38	0.27	09.60	36
3749	Cape Mendocino	1992	Fortuna Fire Station	7.01	20	355	615	0.33	0.28	09.60	36
5829	El Mayor-Cucapah_ Mexico	2010	RIITO	7.20	14	242	419	0.40	0.38	10.00	56
5837	El Mayor-Cucapah_ Mexico	2010	El Centro-I.&Ross	7.20	20	229	397	0.38	0.37	10.00	56

[a]Record sequence number; [b]Moment magnitude; [c]The closest distance to the rupture surface; [d]Average shear-wave velocity from the surface to a depth of 30 m; [e]Primary wave velocity; [f]Surface rupture length [148]. [g]Replaced by RSN 3748 for analyses involving the rotational component of the ground motion, due to the unavailability of the vertical component, which is essential for estimating the rotational component.

7.4.1 Torsional amplification factors using the proposed model

7.4.1.1 Proposed TAFs for rigid secondary systems

Figure 7.5 illustrates the variation in TAF_R at the SE and the FE along the height of 3- and 6-story, E- and Plus-shaped buildings. The results include TAF_R values estimated from time history analyses with and without rotational ground motions, along with their comparisons with those predicted using the proposed model for both elastic and inelastic responses (SR = 2 and 4). The discussions in this section are limited to the maximum TAF_R values obtained and predicted (based on $\Delta_{max}/\Delta_{avg}$) for different buildings, locations on the floor plan, and building inelasticity.

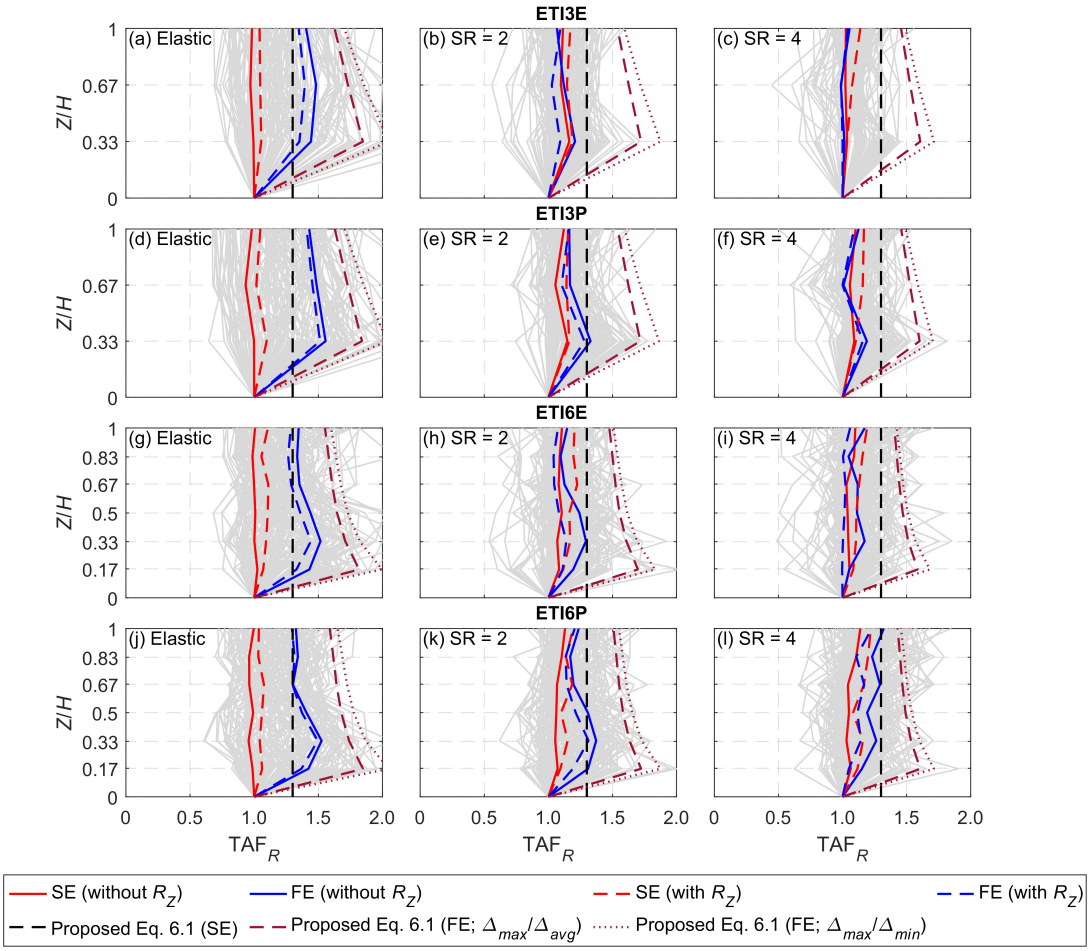

Figure 7.5: Comparisons of the estimated TAF_R from time history analyses with and without rotational ground motions with those obtained from the proposed equations, along the height of 'E3E', 'E3P', 'E6E', and 'E6P' buildings.

For buildings exhibiting elastic response, the maximum median TAF_R values are

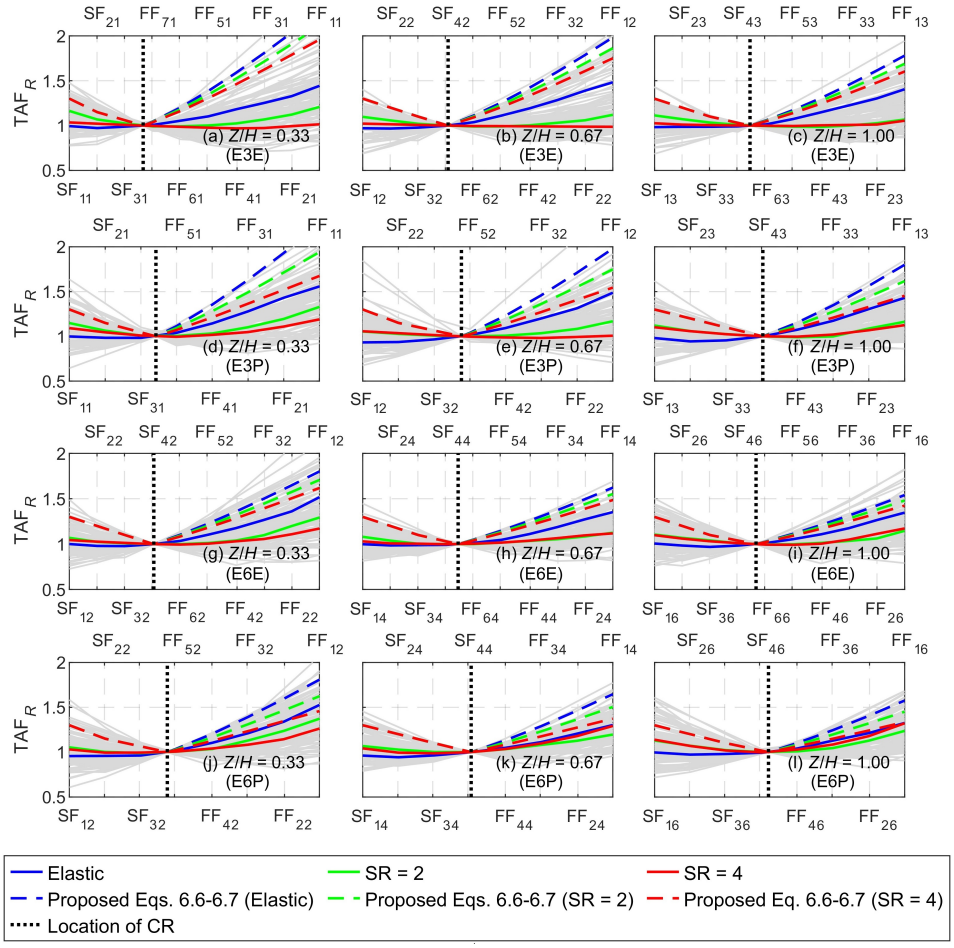

Figure 7.6: Comparisons of the estimated in-plan distribution of TAF_R from time history analyses with those obtained from the proposed equations, along the height of 'E3E', 'E3P', 'E6E', and 'E6P' buildings.

observed to be 1.56 (Figures 7.5(d) and 7.6(d)) and 1.53 (Figures 7.5(j), 7.6(j)), at the FE (extreme flexible frame, FF_{1j}), for 3- and 6-story buildings, respectively. In contrast, at the SE (extreme stiff frame, SF_{1j}), the maximum median TAF_R values are 1.10 (Figure 7.5(d)) and 1.11 (Figure 7.5(g)), for 3- and 6-story buildings, respectively. The proposed model predicts conservative TAF_R values of 1.84 and 1.74 at the FE and 1.30 at the SE for the respective cases.

For buildings exhibiting moderately inelastic response (SR = 2), the maximum median TAF_R decreases due to the inelastic energy dissipation. The maximum median TAF_R values are observed to be 1.33 (Figures 7.5(e) and 7.6(d)) and 1.37 (Figures 7.5(k) and 7.6(j)) at the FE for 3- and 6-story buildings, respectively. In contrast, at the SE (extreme stiff frame, SF_{1j}), the maximum median TAF_R values increase slightly, and they are 1.19 (Figure 7.5(b)) and 1.22 (Figure 7.5(h)) for 3-

and 6-story buildings, respectively. The proposed model predicts conservative TAF_R values of 1.72 and 1.63 at the FE and 1.30 at the SE for the respective cases.

For buildings exhibiting highly inelastic response (SR = 4), the maximum median TAF_R values are observed to be 1.19 (Figures 7.5(f) and 7.6(d)) and 1.32 (Figures 7.5(l) and 7.6(l)), at the FE, for 3- and 6-story buildings, respectively. In contrast, at the SE (extreme stiff frame, SF_{1j}), the maximum median TAF_R values increase slightly and they are 1.17 (Figure 7.5(f)) and 1.22 (Figure 7.5(l)), for 3- and 6-story buildings, respectively. The proposed model predicts conservative TAF_R values of 1.60 and 1.43 at the FE and 1.30 at the SE for the respective cases.

The TAF_R predicted using the proposed model (Equations 6.1, 6.6 , and 6.7) is consistently observed to be conservative compared to the TAF_R estimated from time history analyses across all floor levels and buildings (Figures 7.5 and 7.6). The TAF_R predicted using $\Delta_{max}/\Delta_{min}$ tends to be slightly more conservative than those obtained using $\Delta_{max}/\Delta_{avg}$ across all buildings, floor levels, and SR values of interest. The observed conservatism in predicting TAF_R for PFA demands in buildings with nominal torsion remains acceptable, given the inherent building-to-building variability, modeling assumptions, and the associated uncertainties in structural analysis and design. Thus, the elastic floor displacement ratios (i.e., $\Delta_{max}/\Delta_{avg}$, $\Delta_{max}/\Delta_{min}$, and $\Delta_{FF,\,ij}/\Delta_{CR,\,j}$) are able to reasonably predict the TAF_R accurately.

7.4.1.2 Proposed TAFs for flexible secondary systems

Figures 7.7—7.11 present the comparisons of TAFs estimated from time history analyses, with and without rotational ground motions, with those predicted by the proposed equations (Equations 6.2–6.4) for Group 1 and Group 2 buildings. These TAFs are plotted against the tuning ratio to assess the accuracy of the proposed model. These plots illustrate the variations of TAFs at the first/second and roof levels for both buildings exhibiting elastic and inelastic response (SR = 2 and 4). The discussions in this section are limited to the maximum TAF_F values obtained and predicted (based on $\Delta_{max}/\Delta_{avg}$) for different buildings, locations on the floor plan, and building inelasticity.

7.4.1.2.1 Group 1 buildings Figures 7.7—7.8 present the TAFs obtained from time history analyses, both with and without rotational ground motions, alongside those predicted by the proposed equations for E- and Plus-shaped buildings. For buildings exhibiting elastic response, the maximum median TAF_F values when the secondary system is tuned within the building's fundamental mode region are 1.99 (Figure 7.8(a)) and 1.75 (Figure 7.7(c)) at the FE for 3- and 6-story buildings, respectively. In contrast, at the SE, the maximum median TAF_F values are 1.40 and 1.44 for both 3- and 6-story buildings. The proposed model predicts slightly higher TAF_F values of 2.01 and 1.85 at both the FE and the SE for the 3- and 6-story buildings, respectively. For the case when the secondary system is tuned within the building's higher mode region, the maximum median TAF_F values observed are 2.09 (Figure 7.8(a)) and 1.94 (Figure 7.7(c)) at the FE for 3- and 6-story buildings, respectively. At the SE, the maximum median TAF_F observed are 1.44 and 1.37 for 3- and 6-story buildings, respectively. The proposed model predicts TAF_F values of 2.51 and 2.31 for 3- and 6-story buildings, respectively, at both the FE and SE.

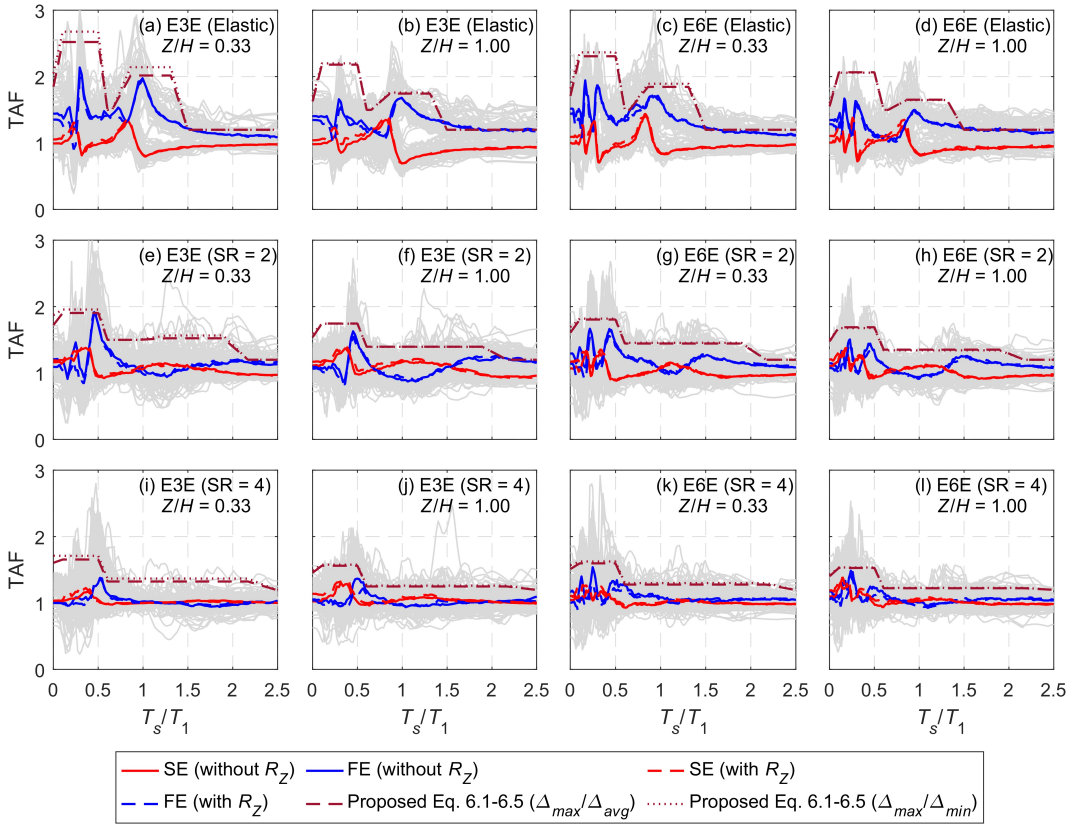

Figure 7.7: Comparisons of the torsional amplification factors for the 'E3E' and 'E6E' buildings, estimated from time history analyses with and without rotational ground motions and those predicted by the proposed equations.

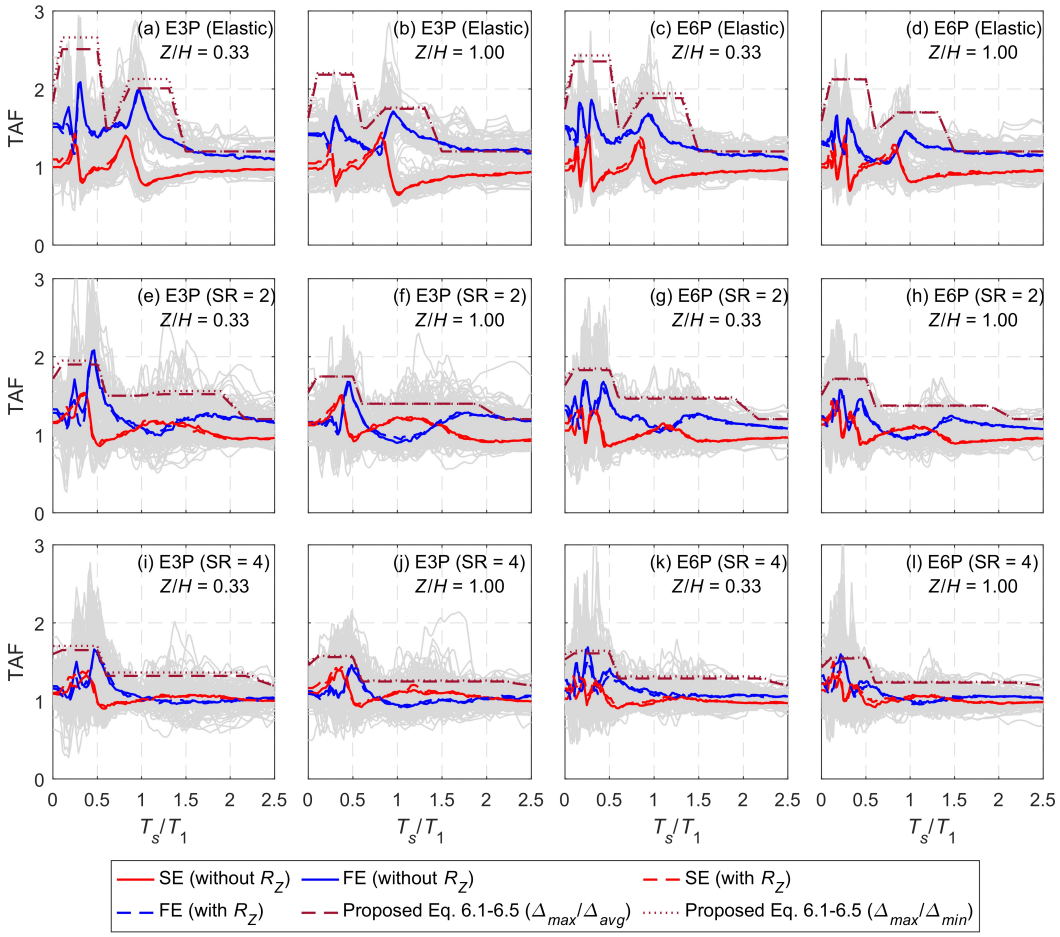

Figure 7.8: Comparisons of the torsional amplification factors for the 'E3P' and 'E6P' buildings, estimated from time history analyses with and without rotational ground motions and those predicted by the proposed equations.

For buildings exhibiting moderately inelastic response (SR = 2), the maximum median TAF_F values when the secondary system is tuned within the building's fundamental mode region are 1.38 (Figure 7.8(e)) and 1.30 (Figure 7.7(g)) at the FE, for 3- and 6-story buildings, respectively. In contrast, at the SE, the maximum median TAF_F values are 1.21 and 1.16 for 3- and 6-story buildings, respectively. The proposed model predicts slightly higher TAF_F values of 1.52 and 1.44 at both the FE and the SE for the 3- and 6-story buildings, respectively. For the case when the secondary system is tuned within the building's higher mode region, the maximum median TAF_F values observed are 2.08 (Figure 7.8(e)) and 1.67 (Figure 7.7(g)) at the FE, for 3- and 6-story buildings, respectively. At the SE, the corresponding maximum median TAF_F values are 1.54 and 1.35 for 3- and 6-story buildings. The proposed model predicts TAF_F values of 1.90 and 1.81 for 3- and 6-story buildings, respectively, at both the FE and SE.

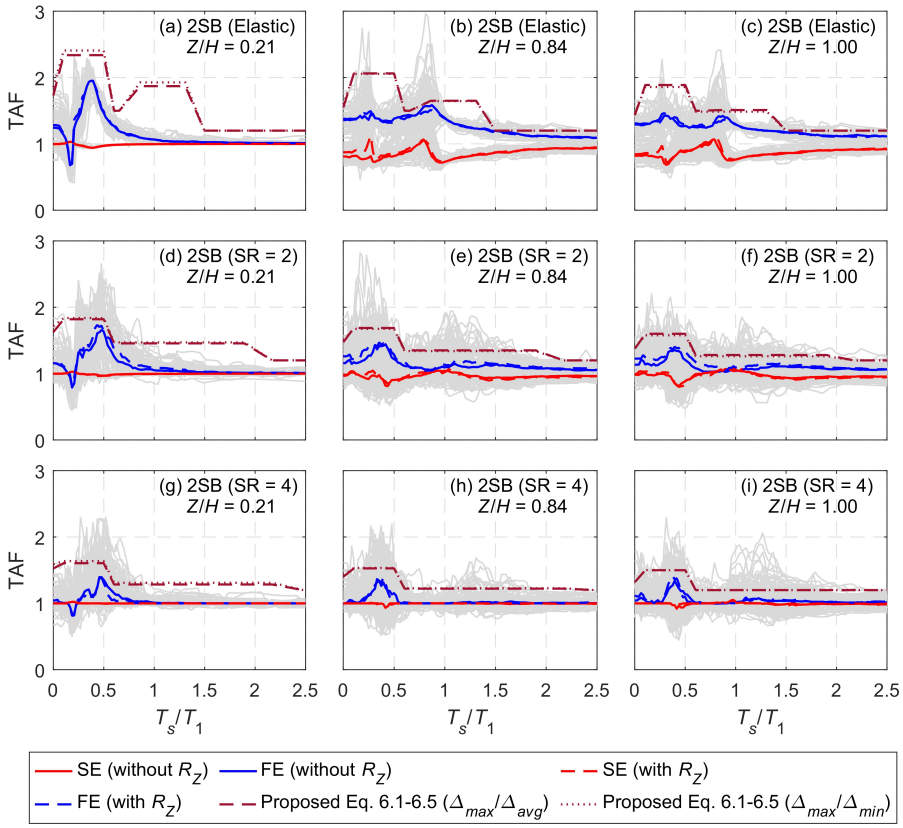

Figure 7.9: Comparisons of the torsional amplification factors for the '2SB' building, estimated from time history analyses with and without rotational ground motions and those predicted by the proposed equations.

For buildings exhibiting highly inelastic response (SR = 4), the maximum median TAF_F values when the secondary system is tuned within the building's fundamental mode region are 1.37 (Figure 7.8(i)) and 1.28 (Figure 7.8(k)) at the FE, for 3- and 6-story buildings, respectively. In contrast, at the SE, the maximum median TAF_F values are 1.09 and 1.06 for 3- and 6-story buildings, respectively. The proposed model predicts slightly higher TAF_F values of 1.32 and 1.29 at both the FE and the SE for the 3- and 6-story buildings, respectively. For the case when the secondary system is tuned within the building's higher mode region, the maximum median TAF_F values observed are 1.66 (Figure 7.8(i)) and 1.69 (Figure 7.8(k)) at the FE, for 3- and 6-story buildings, respectively. At the SE, the corresponding maximum median TAF_F values are 1.39 and 1.32 for 3- and 6-story buildings. The proposed model predicts TAF_F values of 1.65 and 1.61 for 3- and 6-story buildings, respectively, at both the FE and SE.

7.4.1.2.2 Group 2 buildings Figures 7.9—7.11 present the TAFs obtained from time history analyses, both with and without rotational ground motions, alongside those predicted by the proposed equations for '2SB', '4SB', and '8SB' buildings.

For buildings exhibiting elastic response, the maximum median TAF_F values when the secondary system is tuned within the building's fundamental mode region are 1.58 (Figure 7.9(b)), 1.34 (Figure 7.10(b)), and 1.22 (Figure 7.11(b)) at the FE, for '2SB', '4SB', and '8SB' buildings, respectively. At the SE, the corresponding maximum median TAF_F values are 1.07, 1.09, and 1.05 for '2SB', '4SB', and '8SB' buildings, respectively. The proposed model predicts reasonably accurate TAF_F values of 1.65, 1.33, and 1.22 for '2SB', '4SB', and '8SB' buildings, respectively, at both the FE and SE. For the case when the secondary system is tuned within the building's higher mode region, the maximum median TAF_F values observed are 1.50 (Figure 7.9(b)), 1.71 (Figure 7.10(b)) and 1.29 (Figure 7.11(b)) at the FE, for '2SB',

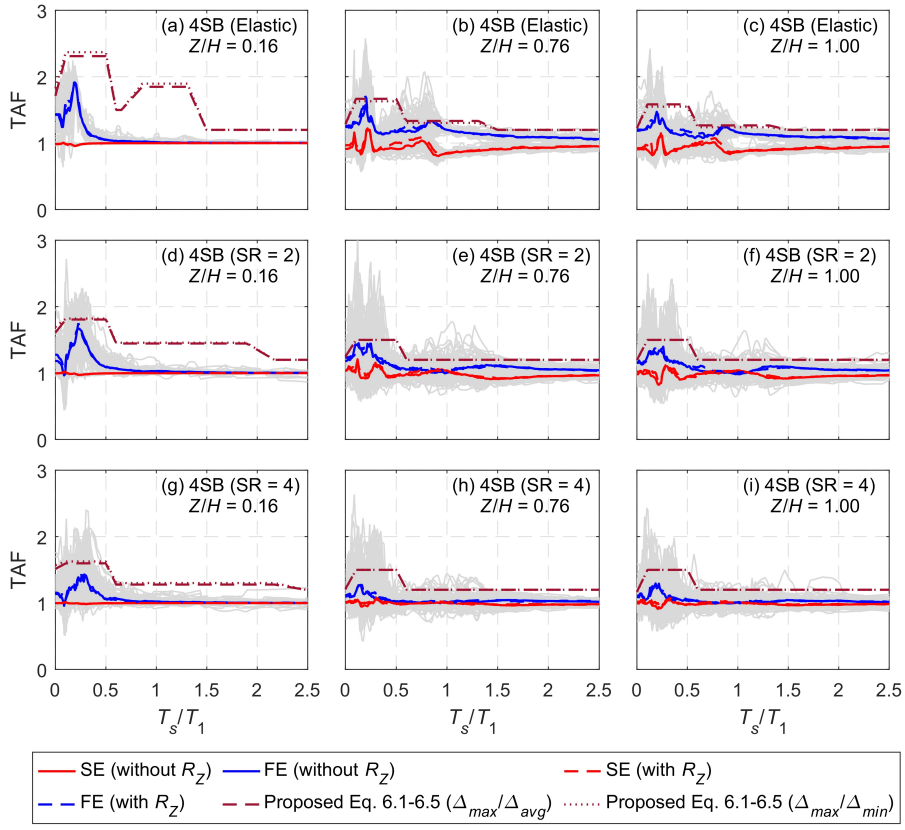

Figure 7.10: Comparisons of the torsional amplification factors for the '4SB' building, estimated from time history analyses with and without rotational ground motions and those predicted by the proposed equations.

'4SB', and '8SB' buildings, respectively. At the SE, the corresponding maximum median TAF_F values are 1.12, 1.22, and 1.17 for '2SB', '4SB', and '8SB' buildings, respectively. The proposed model predicts TAF_F values of 2.06, 1.67, and 1.52 at both the FE and SE for '2SB', '4SB', and '8SB' buildings, respectively.

For buildings exhibiting moderately inelastic response (SR = 2), the maximum median TAF_F values when the secondary system is tuned within the building's fundamental mode region are 1.33 (Figure 7.9(d)), 1.12 (Figure 7.10(e)) and 1.07 (Figure 7.11(f)) at the FE, for '2SB', '4SB', and '8SB' buildings, respectively. At the SE, the corresponding maximum median TAF_F values are 1.00, 1.06, and 1.01 for '2SB', '4SB', and '8SB' buildings, respectively. The proposed model predicts reasonably conservative TAF_F values of 1.46, 1.20, and 1.20 for '2SB', '4SB', and '8SB' buildings, respectively, at both the FE and SE. For the case when the secondary system is tuned within the building's higher mode region, the maximum median TAF_F values are 1.73 (Figure 7.9(d)), 1.45 (Figure 7.10(e)), and 1.34 (Figure

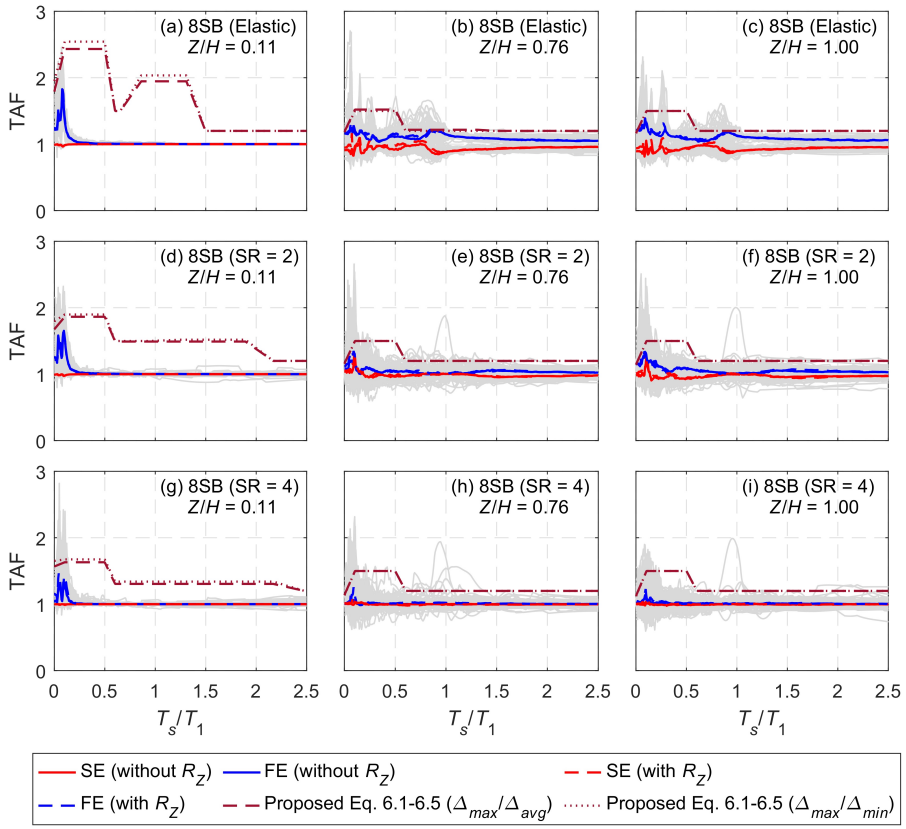

Figure 7.11: Comparisons of the torsional amplification factors for the '8SB' building, estimated from time history analyses with and without rotational ground motions and those predicted by the proposed equations.

7.11(f)) at the FE, for '2SB', '4SB', and '8SB' buildings, respectively. At the SE, the corresponding maximum median TAF_F values are 1.03, 1.21, and 1.24 for '2SB', '4SB', and '8SB' buildings, respectively. The proposed model predicts TAF_F values of 1.82, 1.50, and 1.50 at both the FE and SE for '2SB', '4SB', and '8SB' buildings, respectively.

For buildings exhibiting highly inelastic response (SR = 4), the maximum median TAF_F values when the secondary system is tuned within the building's fundamental mode region are 1.13 (Figure 7.9(g)), 1.07 (Figure 7.10(g)) and 1.03 (Figure 7.11(h)) at the FE, for '2SB', '4SB', and '8SB' buildings, respectively. At the SE, the corresponding maximum median TAF_F values are 1.00, 1.00, and 1.00 for '2SB', '4SB', and '8SB' buildings. The proposed model predicts reasonably conservative TAF_F values of 1.28, 1.28, and 1.20 for '2SB', '4SB', and '8SB' buildings, respectively, at both the FE and SE. For the case when the secondary system is tuned within the building's higher mode region, the maximum median TAF_F values are 1.40 (Figure 7.9(g)), 1.46 (Figure 7.10(g)), and 1.26 (Figure 7.11(h)) at the FE, for '2SB', '4SB', and '8SB' buildings, respectively. At the SE, the corresponding maximum median TAF_F values are 1.03, 1.01, and 1.08 for '2SB', '4SB', and '8SB' buildings, respectively. The proposed model predicts TAF_F values of 1.60, 1.60, and 1.50 at both the FE and SE for '2SB', '4SB', and '8SB' buildings, respectively.

The TAF_F values predicted using the proposed model (Equations 6.2-–6.4) consistently show a reasonably conservative trend when compared to those derived from time history analyses. This conservatism is observed across all floor levels and building configurations, as illustrated in Figures 7.7 - 7.11.

7.4.1.3 Proposed TAFs for very flexible secondary systems

As discussed earlier in Chapter 5, the torsional amplification factor for very flexible secondary systems (TAF_{VF}) tends to approach unity as the secondary system period (T_s) moves beyond the fundamental mode region. To evaluate the TAF_{VF} behavior in this long-period range, the maximum median TAF_{VF} corresponding to $T_s = 3\,T_1$ is examined for all analyzed buildings, with and without rotational ground motion.

For Group 1 buildings (Figures 7.7–7.8), the results indicate that for buildings exhibiting elastic response, the maximum median TAF_{VF} reaches 1.16 at the FE

and 0.98 at the SE in 3-story buildings, while in 6-story buildings, it remains at 1.16 at the FE and 0.99 at the SE. In buildings exhibiting moderately inelastic response (SR = 2), the TAF_{VF} remains unchanged for 3-story buildings, with values of 1.16 at the FE and 0.99 at the SE, whereas, for 6-story buildings, a slight reduction is observed, with TAF_{VF} decreasing to 1.07 at the FE, while remaining at 0.99 at the SE. In buildings exhibiting highly inelastic response (SR = 4), a further decrease in TAF_{VF} is observed. In 3-story buildings, the TAF_{VF} reduces to 1.07 at the FE and slightly increases to 1.01 at the SE, while in 6-story buildings, it continues to decline and reaches 1.05 at the FE and 1.00 at the SE.

For Group 2 buildings (Figures 7.9–7.11), under their elastic response, the maximum median TAF_{VF} values at the FE and the SE are 1.10 and 1.00, respectively, for '2SB' buildings, 1.07 and 1.00 for '4SB' buildings, and 1.05 and 1.00 for '8SB' buildings. In buildings exhibiting moderately inelastic response (SR = 2), a minor change in TAF_{VF} is observed, with values of 1.06, 1.03, and 1.02 at the FE for '2SB', '4SB', and '8SB' buildings, respectively, while at the SE, the TAF_{VF} remains at 1.00 in all cases. In buildings exhibiting highly inelastic response (SR = 4), the maximum median TAF_{VF} values at the FE are recorded as 1.01 for 2SB, 1.01 for 4SB, and 1.01 for '8SB' buildings, while at the SE, the TAF_{VF} remains constant at 1.00.

The TAF_{VF} predicted using the proposed model (Equation 6.5) is consistently conservative when compared to the estimated TAF_{VF} obtained from time history analyses, both with and without considering rotational ground motion, across all floor levels and building types, as shown in Figures 7.7–7.11. Notably, the maximum TAF_{VF} for all Group 1 and Group 2 buildings is 1.16, against a model-predicted value of 1.20, highlighting the accuracy of the proposals.

7.4.2 Efficacy of the proposed equations for existing seismic design codes

7.4.2.1 For rigid secondary systems

To evaluate the effectiveness of the proposed equations for existing seismic design codes [6, 16, 17], the PFA/PGA values at the SE and the FE of the buildings

are derived from time history analyses, both with and without rotational ground motions. The percentage of underestimation and overestimation relative to the seismic design code provisions (with and without applying the proposed TAFs) is then assessed (Figures 7.12–7.13). Additionally, the in-plan distribution of PFA/PGA across all stiff and flexible frames (Figures 7.14–7.15) is also obtained from bi-directional time history analyses. The percentage differences are evaluated against the values derived from the seismic design code provisions, both with and without the application of the proposed TAFs, to highlight the efficacy of the proposed recommendations. The TAF_R are conservative while computed using $\Delta_{max}/\Delta_{min}$ compared to those obtained using $\Delta_{max}/\Delta_{avg}$. Hence, for comparison purposes (at the extreme edges), the PFA/PGA corresponding to the FE are estimated using $\Delta_{max}/\Delta_{avg}$.

As discussed in Chapter 4, under the elastic response, the provisions of existing seismic design codes [6, 16, 17] underestimated the PFA/PGA at the SE up to 6% (Figures 7.12(d) and 7.14(f)), 48% (Figures 7.12(d) and 7.14(f)) and 85% (Figures 7.12(d) and 7.14(f)), while using ASCE 7, EC 8, and IS 16700, respectively. After applying the proposed TAF_R (estimated using Equation 6.1), the underestimation at the SE reduced to 23% for EC 8 (Figure 7.12(d)) and 54% for IS 16700 (Figure 7.12(d)), while ASCE 7 provided accurate estimates of PFA/PGA. Similarly, when Equation 6.6 is used to estimate the proposed TAF_R across all stiff frames within the building plan, the final PFA/PGA values derived from EC 8 and IS 16700 remained underestimated by up to 50% and 88%, respectively (Figure 7.14(f)), across all stiff frames. In contrast, ASCE 7 continues to predict accurate PFA/PGA estimates. For buildings exhibiting inelastic response (SR = 2 and 4), PFA/PGA demands reduce at the SE, and both EC 8 and IS 16700 codes provide conservative estimates of the PFA/PGA, even without the application of the proposed TAF_R. In contrast, ASCE 7 underpredicted PFA/PGA demands at the first-floor level (specifically for 6-story buildings, Figures 7.12(h) and (k)), which vanished after the application of the proposed TAFs at the SE.

The existing seismic code provisions underestimate the PFA/PGA at the FE, especially for the elastic response of both E-shape and Plus-shape buildings at all floor levels. At the FE, under the elastic response of the buildings, the extent of

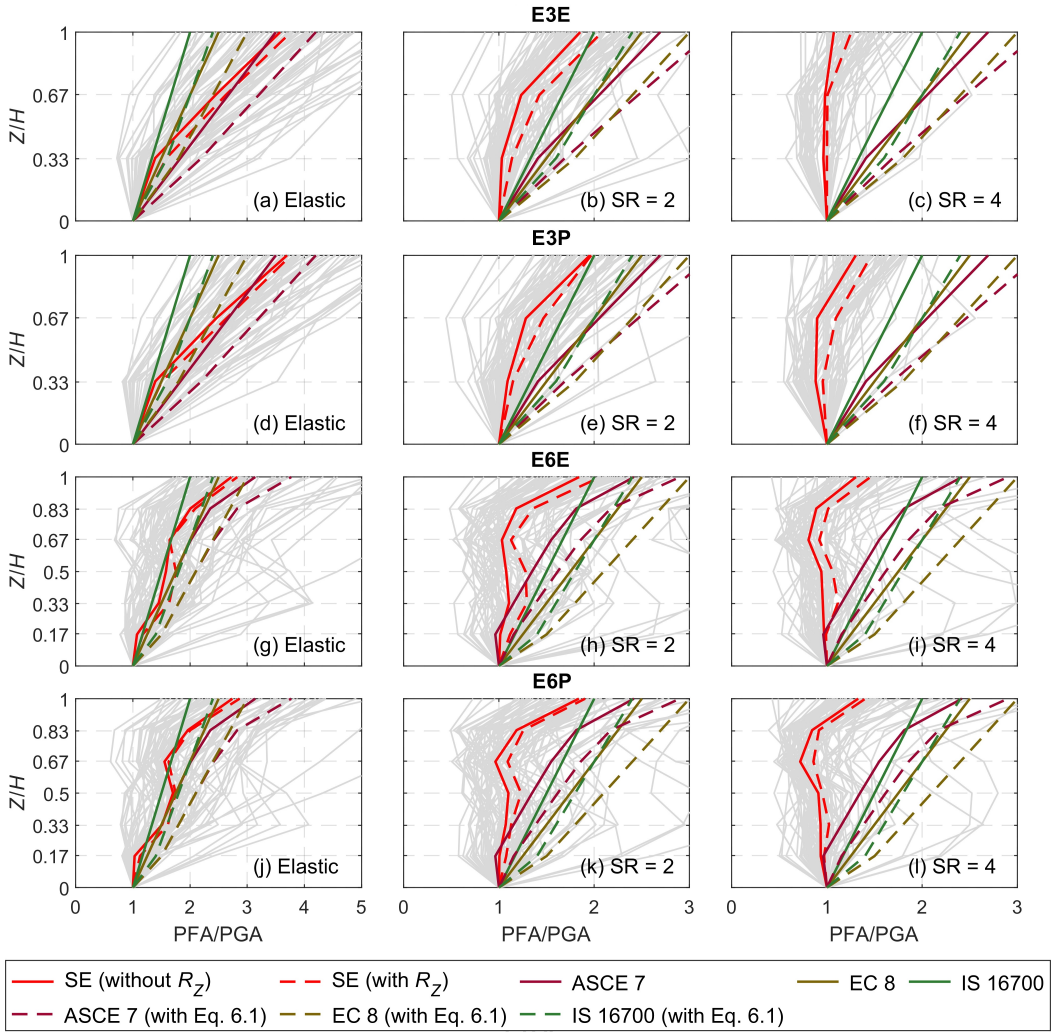

Figure 7.12: Comparisons of the PFA/PGA at the SE, estimated from time history analyses with and without considering rotational ground motions, as well as from building codes, with and without applying the proposed equations, for the 'E3E,' 'E3P,' 'E6E,' and 'E6P' buildings.

underestimation in PFA/PGA values was observed to be as high as 56% (Figures 7.13(j) and 7.14(j)), 114% (Figures 7.13(d) and 7.14(f)), and 168% (Figures 7.13(d) and 7.14(f)) while using the provisions of ASCE 7, EC 8, and IS 16700, respectively. Upon applying the proposed TAF_R estimated using Equation 6.1, the PFA/PGA values obtained from EC 8 and IS 16700 remained underestimated by up to 38% (Figure 7.13(d)) and 72% (Figure 7.13(d)), respectively, at the FE. Likewise, when Equation 6.7 is employed to estimate the TAF_R and subsequently applied alongside code models to determine the PFA/PGA values across the flexible frames, the underestimation persists, reaching up to 43% for EC 8 and 79% for IS 16700 (Figure 7.14(c)). In contrast, ASCE 7 provides accurate PFA/PGA estimates, both at

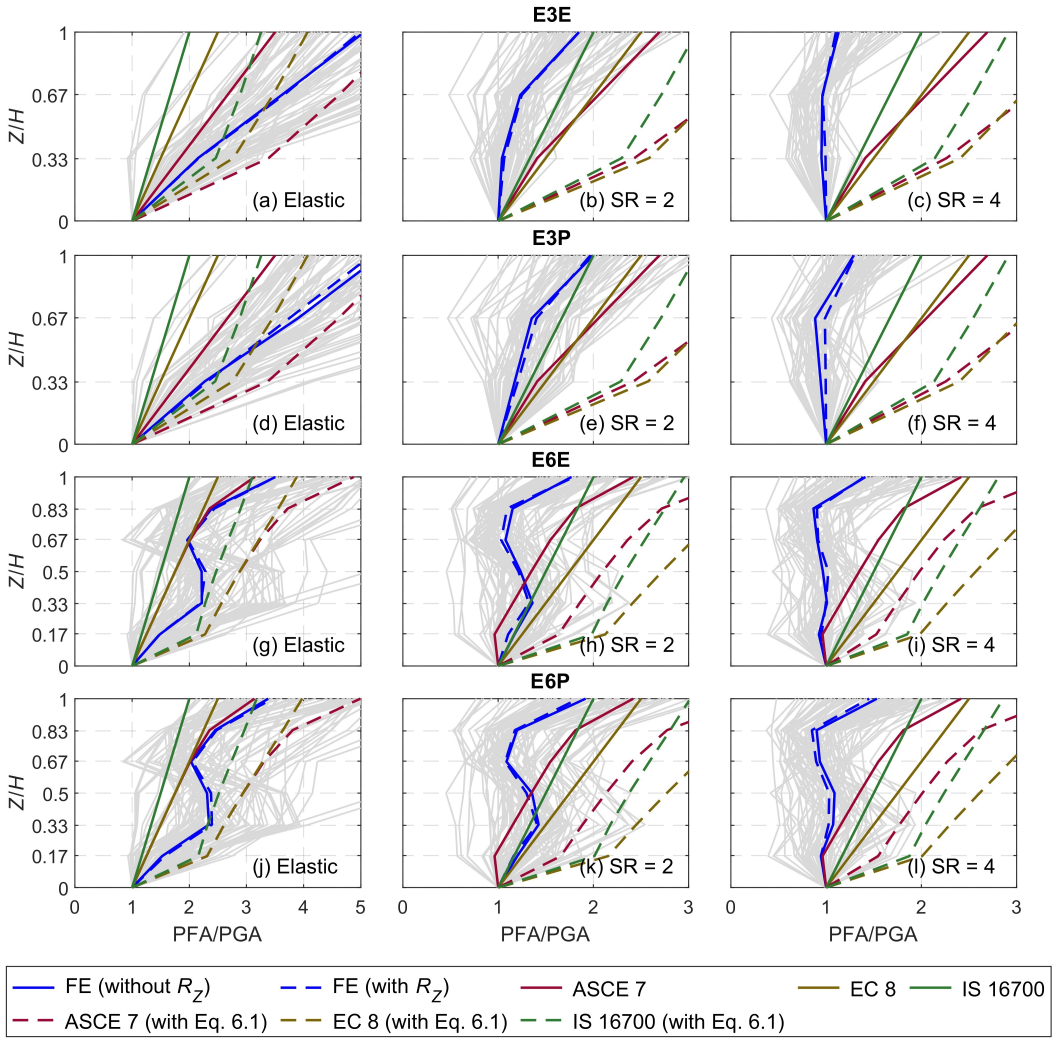

Figure 7.13: Comparisons of the PFA/PGA at the FE, estimated from time history analyses with and without considering rotational ground motions, as well as from building codes, with and without applying the proposed equations, for the 'E3E,' 'E3P,' 'E6E,' and 'E6P' buildings.

the extreme FE and across all flexible frames. The underprediction in PFA/PGA demands is higher for 3-story buildings compared to the 6-story buildings, as the provisions of both EC 8 and IS 16700 codes do not consider the influence of T_1 in predicting PFA/PGA demands.

For buildings exhibiting moderately inelastic response (SR = 2), the extent of the underestimation in PFA/PGA has been observed up to 25% and 7% (Figure 7.13(k), 7.15(j)) from ASCE 7 and IS 16700, respectively, while EC 8 provided a reasonable estimate of the PFA/PGA demands. After applying the proposed TAF_R at the FE, all code models provide reasonably conservative estimates of PFA/PGA. For buildings exhibiting highly inelastic response (SR = 4), the extent

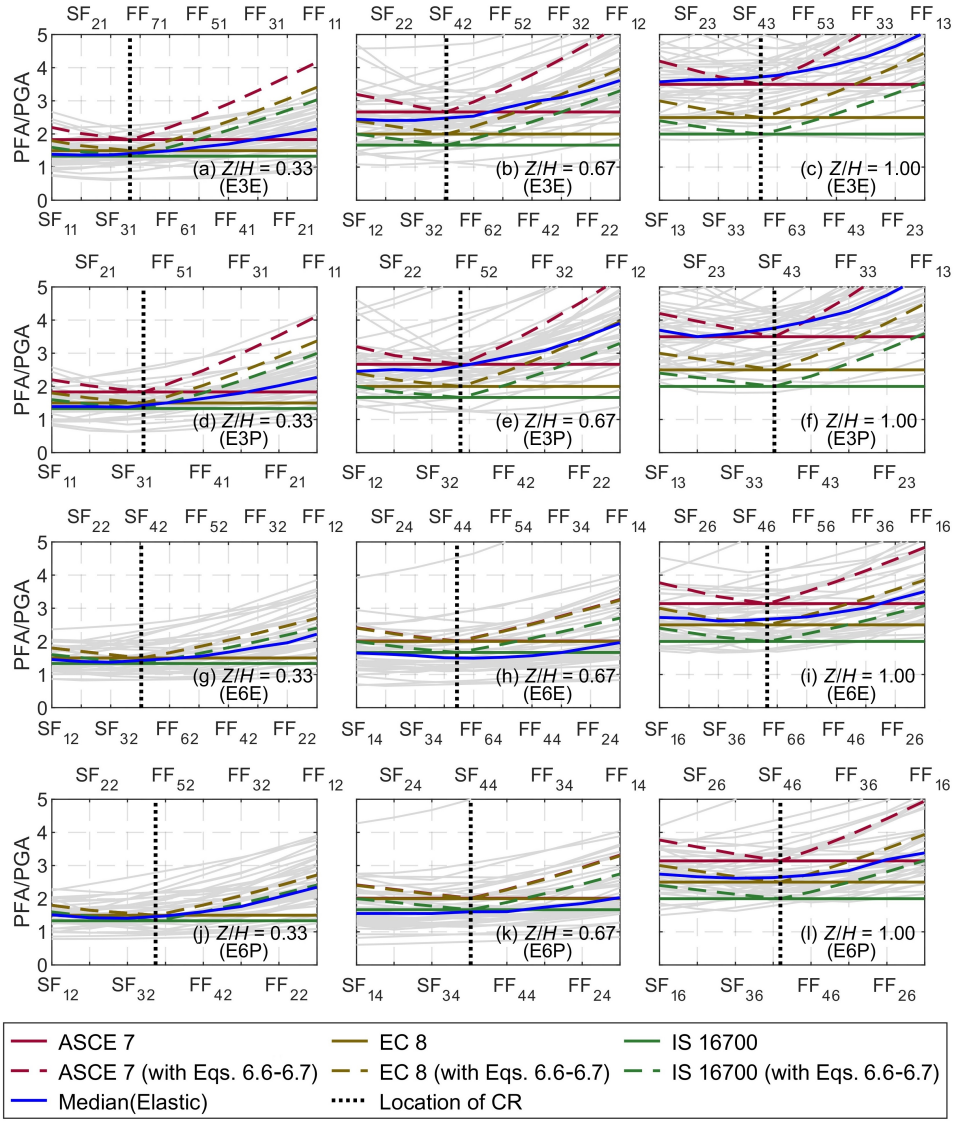

Figure 7.14: Comparisons of the in-plan distribution of the PFA/PGA, as estimated from the bi-directional time history analyses and from building codes with and without applying the proposed equations, for the 'E3E,' 'E3P,' 'E6E,' and 'E6P' buildings (Elastic). The curves corresponding to ASCE 7 are not visible in some plots (g, h, j, and k) as they are overlapped with EC 8 curves.

of the underestimation in PFA/PGA vanished (Figure 7.13), and all codes provided conservative estimates of PFA/PGA.

It is worth noting that after the application of the proposed TAF_R, ASCE 7 provided reasonably accurate estimates of the PFA/PGA at the SE and the FE for buildings exhibiting both elastic and inelastic response. On the other hand, both EC 8 and IS 16700 codes underestimated PFA/PGA, especially at the FE and the SE in the buildings exhibiting elastic response. This underestimation is reduced with an increase in SR as the building's inelasticity overcomes the detrimental effects

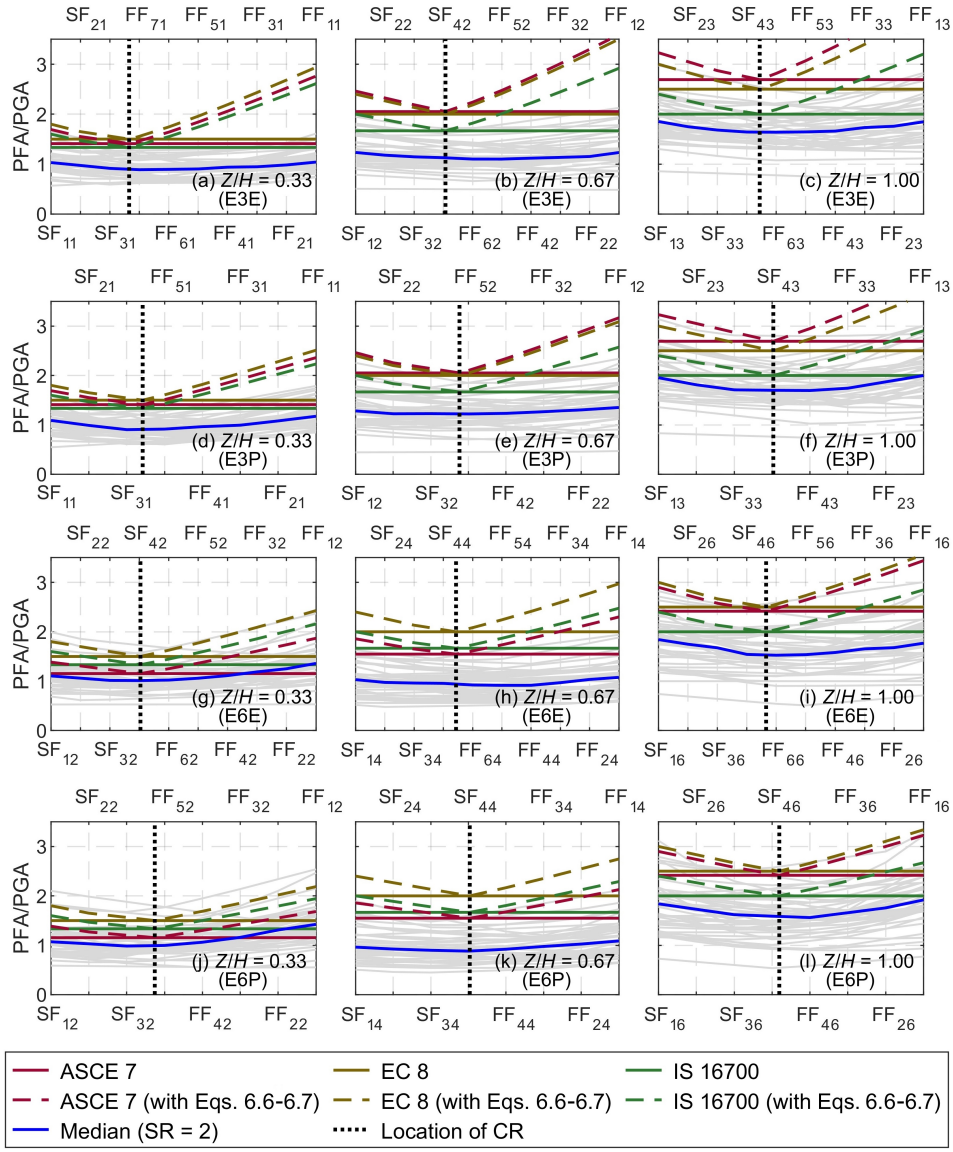

Figure 7.15: Comparison of the in-plan distribution of the PFA/PGA, as estimated from the bi-directional time history analyses and from building codes with and without applying the proposed equations, for the 'E3E,' 'E3P,' 'E6E,' and 'E6P' buildings (SR = 2).

of the building's nominal torsion. Overall, the underestimation in estimating the PFA/PGA demands, particularly while using EC 8 and IS 16700 codes, could be primarily attributed to the lack of inclusion of the building-specific characteristics (specifically T_1) in these codes [87, 88]. The presented discussions highlighted the ease in the applicability of the proposed equations and subsequent improvements in seismic code predictions (particularly while proposed TAF_R applied along with ASCE 7 provisions) and the need to improve PFA/PGA models in EC 8 and IS 16700.

7.4.2.2 For flexible secondary systems

The total amplification (a_t) at the FE and the SE, estimated from time history analyses with and without rotational ground motions, is presented in Figures 7.16-–7.17 for Group 1 buildings and Figures 7.18-–7.20 for Group 2 buildings. These plots compare the total amplification predicted by building codes, both with and without the application of the proposed equations (Equations 6.1–6.5). The variations in the median peak a_t values across different tuning ratios show pronounced peaks when the secondary system is tuned within the building's fundamental or higher mode regions. This behavior highlights significant dynamic amplification of acceleration demands for secondary systems at these tuned frequencies.

7.4.2.2.1 Group 1 buildings For 3-story buildings exhibiting elastic response, the response from the time history analyses shows a significant underestimation in the median peak a_t predicted using existing seismic design provisions. When the secondary system is tuned within the building's fundamental mode region, the extent of underestimation in code predictions reached up to 710%, 489%, and 548% at the FE (Figure 7.17(b)), and 363%, 237%, and 271% at the SE (Figure 7.17(b)), based on the provisions of ASCE 7, EC 8, and IS 16700, respectively. However, applying the proposed TAF_F in conjunction with the code models, the underestimation in predicting median peak a_t is reduced to 364%, 265%, and 271% at the FE, and 163%, 97%, and 111% at the SE, for ASCE 7, EC 8, and IS 16700, respectively. For the secondary systems tuned within the building's higher mode region, the underestimation is lower but still substantial, reaching 151%, 83%, and 101% at the FE (Figure 7.17(b)) and 85%, 34%, and 48% at the SE (Figure 7.17(b)) for ASCE 7, EC 8, and IS 16700, respectively. With the application of the proposed TAF_F in conjunction with the code models, the underestimation in predicting the median peak at the FE is reduced to 20% for ASCE 7 and 34% for EC 8, while IS 16700 provides accurate predictions. At the SE, all code models accurately predict the response when the proposed TAF_F is applied.

For 6-story buildings exhibiting elastic response, when the secondary system is tuned within the building's fundamental mode region, the extent of underestimation

in code-based predictions reaches up to 199%, 118%, and 139% at the FE (Figure 7.17(d)), and 99%, 45%, and 60% at the SE (Figure 7.17(d)), based on the provisions of ASCE 7, EC 8, and IS 16700, respectively. However, incorporating the proposed TAF_F alongside the code models significantly reduces these underestimations, bringing them down to 76%, 28%, and 41% at the FE for ASCE 7, EC 8, and IS 16700, respectively. At the SE, all codes provided conservative estimates, except for ASCE 7, which continued to exhibit an underestimation of up to 17%. When the secondary system is tuned within the building's higher mode region, the underestimation becomes even more significant, with values reaching 263%, 307%, and 191% at the FE (Figure 7.17(d)), and 187%, 234%, and 130% at the SE (Figure 7.17(d)) for ASCE 7, EC 8, and IS 16700, respectively. However, upon applying the proposed TAF_F to these code equations, the underestimation at the FE is reduced to 71%, 92%, and 37%, and at the SE to 35%, 57%, and 8% for ASCE 7, EC 8, and IS 16700, respectively.

For 3-story buildings exhibiting moderately inelastic response (SR = 2), when the secondary system is tuned within the building's fundamental mode region, the underestimation is observed to be 73%, 86%, and 38% at the FE (Figure 7.17(f)), and 68%, 34%, and 34% at the SE (Figure 7.17(f)), based on the provisions of ASCE 7, EC 8, and IS 16700, respectively. However, with the application of the proposed TAF_F to these code models, the underestimation at the FE is reduced to 23% and 81%, while at the SE, it decreases to 20% and 23% for ASCE 7 and EC 8, respectively. In contrast, IS 16700 provided accurate predictions. For secondary systems tuned within the building's higher mode region, although underestimation was reduced, it remained significant, reaching 59%, 16%, and 28% at the FE (Figure 7.17(f)), for ASCE 7, EC 8, and IS 16700, respectively. At the SE, underestimation is 31% for ASCE 7 and 5% for IS 16700 (Figure 7.17(f)). However, after applying the proposed TAF_F, all building codes provided conservative predictions of the median peak a_t both the FE and the SE.

For 6-story buildings exhibiting moderately inelastic response (SR = 2), the code models have accurately predicted the median peak a_t for the secondary systems tuned within the building's fundamental mode region at the FE and the SE. However, when the secondary system is tuned within the building's higher mode

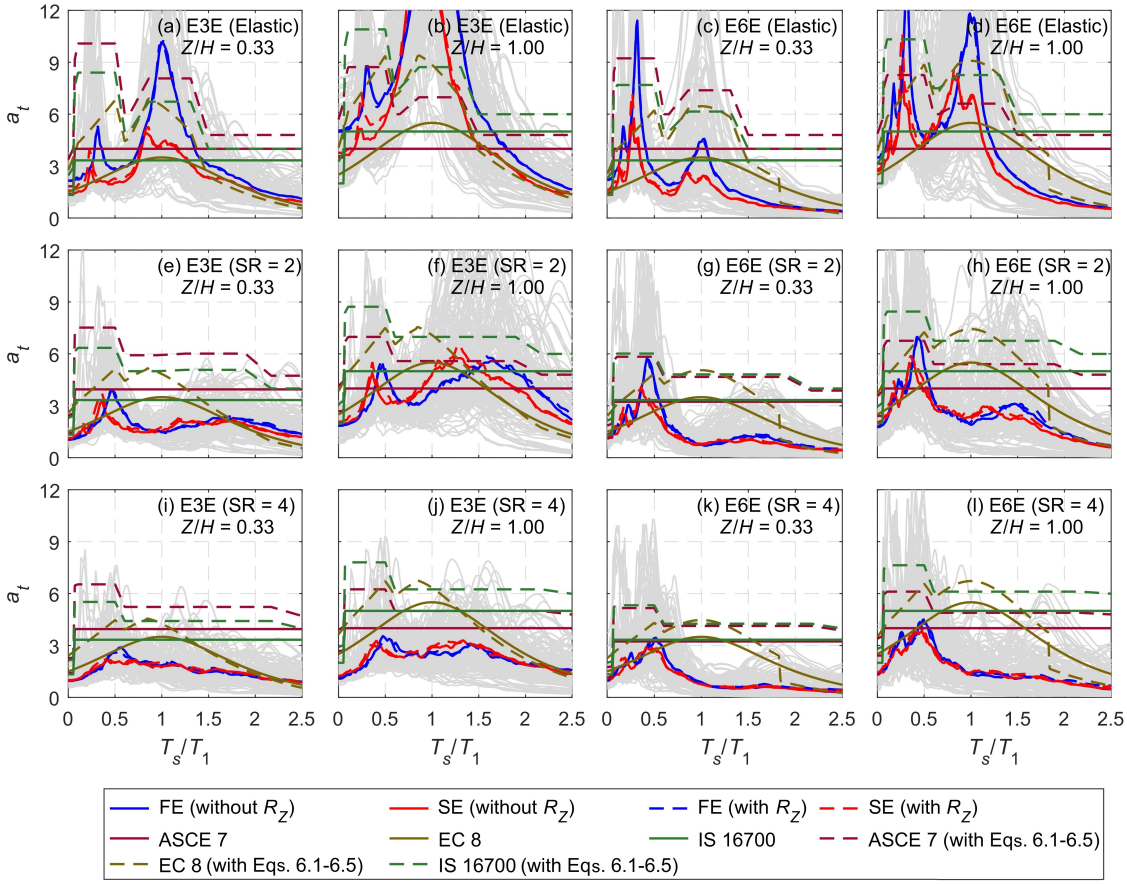

Figure 7.16: Comparisons of total amplification (a_t) estimated from time history analyses with and without considering rotational ground motions, as well as from building codes, with and without applying the proposed equations, for the 'E3E' and 'E6E' buildings.

region, underestimations of 98%, 44%, and 58% at the FE, and 36%, 42%, and 9% at the SE are observed for ASCE 7, EC 8, and IS 16700, respectively (Figure 7.17(h)). After applying the proposed TAF_F in conjunction with the building codes, a minor underestimation of 13% is observed at the FE for both ASCE 7 and EC 8, while IS 16700 provides accurate predictions. However, at the SE, no further underestimation occurs when the proposed TAF_F is incorporated into the building codes.

For 3-story buildings exhibiting highly inelastic response (SR = 4), no underestimation is observed across all building codes when secondary systems are tuned to the building's fundamental mode regions, except for a minor 7% underestimation in ASCE 7, when secondary systems are tuned within the building's higher mode region. However, upon applying the proposed TAF_F in conjunction with the building codes, this underestimation is eliminated. For 6-story buildings

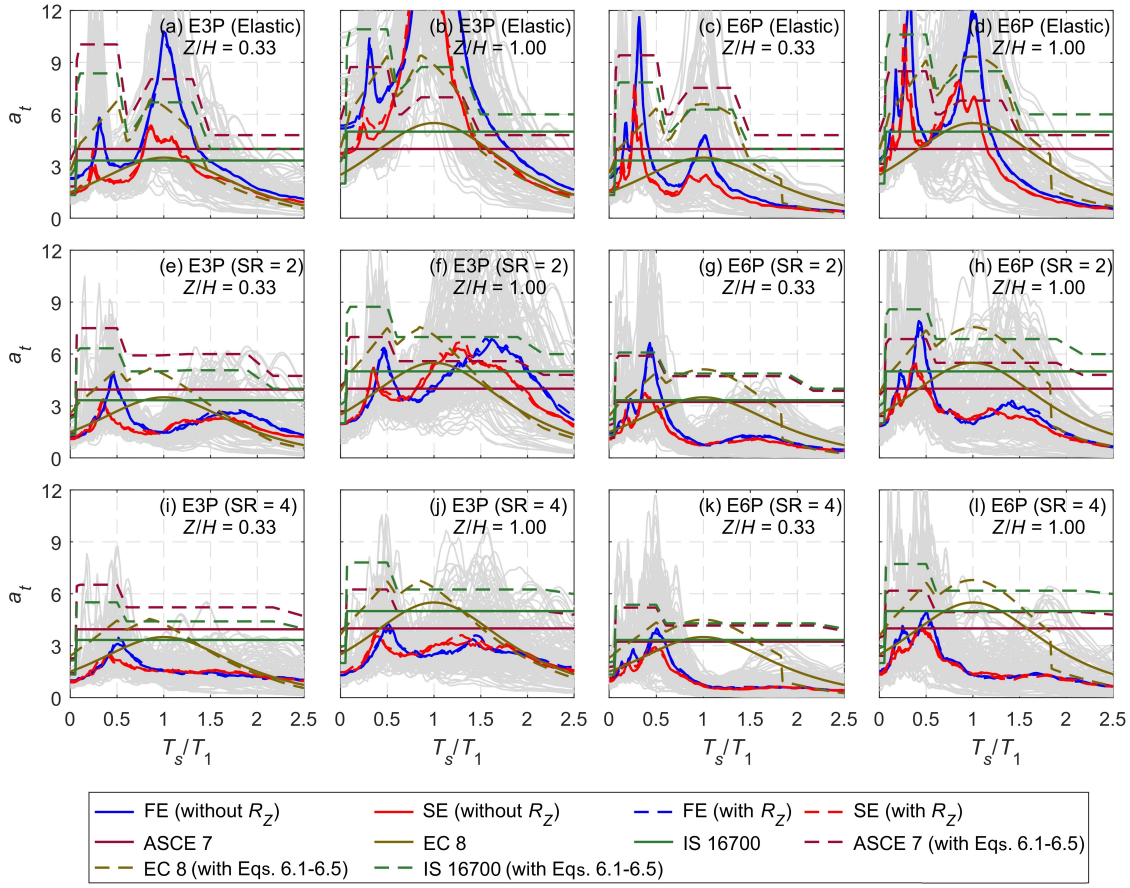

Figure 7.17: Comparisons of total amplification (a_t) estimated from time history analyses with and without considering rotational ground motions, as well as from building codes, with and without applying the proposed equations, for the 'E3P' and 'E6P' buildings.

exhibiting highly inelastic response (SR = 4), all building codes accurately predict the median peak a_t when the secondary system is tuned within the building's fundamental mode region. However, when the secondary system is tuned within the building's higher mode region, only ASCE 7 underestimates the median peak a_t by 25% at the FE (Figure 7.17(l)), while EC 8 and IS 16700 provide accurate predictions. At the SE, all codes yield conservative estimates. Upon applying the proposed TAF_F, the underestimation in ASCE 7 is also eliminated.

7.4.2.2.2 Group 2 building For '2SB' building exhibiting elastic response, when secondary systems are tuned within the building's fundamental mode region, underestimation reached up to 768%, 532%, and 595% at the FE (Figure 7.18(c)), and 416%, 275%, and 113% at the SE (Figure 7.18(c)), for ASCE 7, EC 8, and IS 16700, respectively. Upon the application of the proposed TAF_F, these

underestimations reduce to 475%, 318%, and 360% at the FE, and 241%, 148%, and 173% at the SE for ASCE 7, EC 8, and IS 16700, respectively. For secondary systems tuned within the building's higher mode region, underestimation remained substantial but was comparatively lower, reaching 196%, 231%, and 137% at the FE (Figure 7.18(c)), and 69%, 78%, and 35% at the SE (Figure 7.18(c)) for the same codes. With the proposed TAF_F, these underestimations reduce to 57%, 72%, and 25% at the FE for ASCE 7, EC 8, and IS 16700, respectively. However, at SE, all the code models are predicted accurately with the proposed TAF_F.

For '4SB' buildings exhibiting elastic response, underestimation for secondary systems tuned within the building's fundamental mode region is 408%, 270%, and 307% at the FE (Figure 7.19(c)), and 293%, 185%, and 214% at the SE (Figure 7.19(c)), based on ASCE 7, EC 8, and IS 16700. With the proposed TAF_F, the underestimations reduced but are still significant, reaching 301%, 192%, and 221% at the FE, and 210%, 125%, and 149% at the SE for ASCE 7, EC 8, and IS 16700, respectively (Figure 7.19(c)). When the secondary systems tuned within the building's higher mode region, the underestimation was even more pronounced, rising to 272%, 168%, and 197% at the FE (Figure 7.19(c)), and 170%, 97%, and 116% at the SE (Figure 7.19(c)). Upon applying the proposed TAF_F, the underestimation is reduced to 135%, 168%, and 88% at the FE, and 71%, 95%, and 36% at the SE (Figure 7.19(c)).

For '8SB' buildings exhibiting elastic response, the secondary systems tuned within the building's fundamental mode region resulted in underestimations of 105%, 49%, and 64% at the FE (Figure 7.20(c)), and 64%, 19%, and 31% at the SE (Figure 7.20(c)) under ASCE 7, EC 8, and IS 16700. With the proposed TAF_F, the underestimations are reduced to 71%, 24%, and 37% at the FE, respectively, for ASCE 7, EC 8, and IS 16700. At the SE, though EC 8 predicted accurately, the underestimation reduced to 37% and 10% for ASCE 7 and IS 16700, respectively (Figure 7.20(c)). When the secondary systems tuned within the building's higher mode region, the extent of underestimation increased significantly, reaching 246%, 292%, and 177% at the FE (Figure 7.20(c)), and 185%, 214%, and 128% at the SE (Figure 7.20(c)). After the application of the proposed TAF_F, these underestimations reduced to 138%, 157%, and 90% at the FE, and 90%, 109%,

and 52% at the SE (Figure 7.20(c)) for ASCE 7, EC 8, and IS 16700, respectively.

For buildings exhibiting moderately inelastic response (SR = 2), the '2SB' building exhibits significant underestimation in code predictions when secondary systems are tuned within the building's fundamental mode region. The underestimation reaches up to 48%, 70%, and 19% at the FE (Figure 7.18(f)) for ASCE 7, EC 8, and IS 16700, respectively. Similarly, at the SE, underestimations of up to 28%, 34%, and 2% are observed for ASCE 7, EC 8, and IS 16700, respectively (Figure 7.18(f)). With the application of the proposed TAF_F, IS 16700 provides accurate predictions. However, ASCE 7 and EC 8 still exhibit underestimations up to 18% and 43% at the FE, respectively. At the SE, the underestimation in ASCE 7 and IS 16700 is eliminated, while EC 8 continues to show an underestimation of up to 18%. For secondary systems tuned within the building's higher mode region, underestimation remains substantial but comparatively lower, reaching 43%, 47%, and 14% at the FE for ASCE 7, EC 8, and IS 16700, respectively. However, no underestimation is observed at the SE. With the proposed TAF_F applied alongside the building codes, all code models provide accurate predictions at the FE.

For '4SB' building exhibiting moderately inelastic response (SR = 2), underestimation for secondary systems tuned within the building's fundamental mode region is 31%, 30%, and 5% at the FE (Figure 7.19(f)), for ASCE 7, EC 8, and IS 16700, respectively. At the SE, ASCE 7 and EC 8 exhibited minor underpredictions of 10% and 5%, while IS 16700 provided accurate predictions. With the proposed TAF_F, underestimation at the FE is reduced to 10% for ASCE 7 and EC 8, while IS 16700 predicts accurately. However, at the SE, all code models provide accurate predictions with the proposed TAF_F. When the secondary systems are tuned within the building's higher mode region, the underestimation became more pronounced, reaching 71%, 62%, and 37% at the FE (Figure 7.19(f)) and 36%, 35%, and 8% at the SE (Figure 7.19(f)) for ASCE 7, EC 8, and IS 16700, respectively. Applying the proposed TAF_F at the FE, IS 16700 predicts accurately; however, ASCE 7 and EC 8 are underestimated by 14% and 11%, respectively. At the SE, all code models are predicted accurately with the proposed TAF_F.

For '8SB' building exhibiting moderately inelastic response (SR = 2), no

underestimation is observed for secondary systems tuned within the building's fundamental mode region at either the FE or SE (Figure 7.20(f)). However, when the secondary systems are tuned within the building's higher mode region, underestimation at the FE reaches 9% for ASCE 7 and 45% for EC 8 (Figure 7.20(f)), while at the SE, EC 8 exhibits underestimation of up to 34%. With the application of the proposed TAF_F in conjunction with the code models, these underestimations are completely eliminated at both the FE and SE. For '2SB' and '8SB' buildings exhibiting highly inelastic response (SR = 4) (Figures 7.18(i) and 7.20(i)), the code models show no underestimation for secondary systems tuned within either the building's fundamental or higher mode regions at both the FE and SE. In contrast, for '4SB' buildings exhibiting highly inelastic response (SR = 4), underestimation is observed only for secondary systems tuned within the building's higher mode region, reaching 2% for ASCE 7 and 11% for EC 8 at the FE, while no underestimation occurs at the SE (Figure 7.19(i)). However, with the application of the proposed TAF_F in conjunction with the code models, these underestimations are eliminated.

The underestimation of floor acceleration demands in seismic design codes [6, 16, 17] can be attributed to the amplification of floor accelerations due to the torsional response of buildings, which is not adequately addressed in current provisions. Applying the proposed TAF_F to these codes significantly improves the accuracy of floor acceleration predictions as they account for the effect of nominal building torsion. However, despite this improvement, underestimation persists, particularly when the secondary systems are tuned within the building's fundamental or higher mode regions. This discrepancy arises from the inability of code provisions to fully capture higher-mode effects, which are known to substantially amplify floor accelerations in mid-rise and high-rise buildings [106]. Additionally, existing code provisions do not adequately account for the spectral shape of ground motions, which typically peak in the short-period range, further contributing to the observed underestimation of floor acceleration demands. Consequently, refining seismic design equations to incorporate higher-mode contributions is essential for achieving more accurate predictions of floor accelerations in buildings with torsional irregularities.

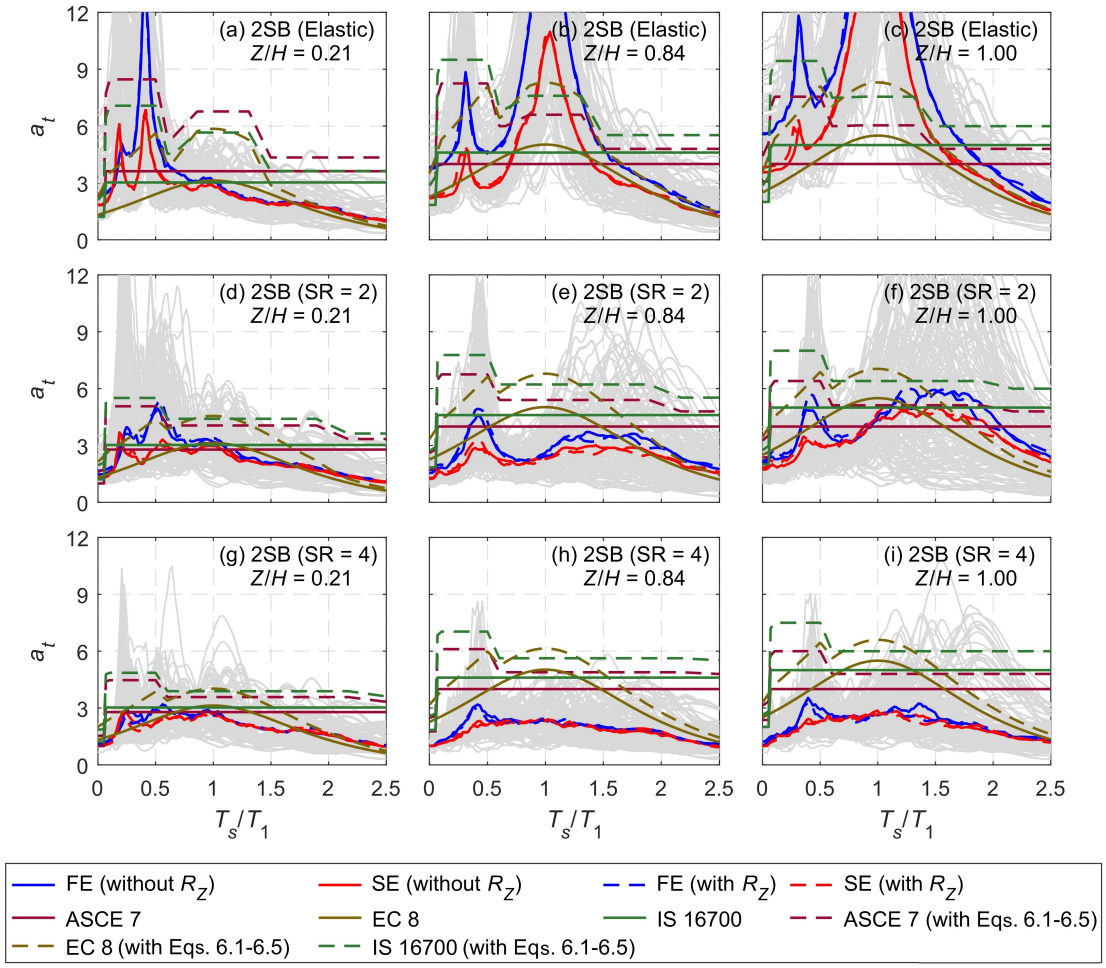

Figure 7.18: Comparisons of total amplification (a_t) estimated from time history analyses with and without considering rotational ground motions, as well as from building codes, with and without applying the proposed equations, for the '2SB' building.

7.5 Summary

This chapter presented the validation of the proposed TAF prediction models, assessing their effectiveness in capturing the influence of nominal building torsion on floor acceleration demands for rigid, flexible, and very flexible secondary systems. The validation is carried out through extensive time history analyses on a diverse set of low- to mid-rise RCMRF building archetypes, including both plan irregular and combined plan and elevation irregular buildings. Two distinct groups of buildings were considered. Group 1 comprised four E- and Plus-shaped buildings with ETI configuration ($\Delta_{max}/\Delta_{avg} > 1.4$), characterized by asymmetric lateral load-resisting elements. These included 3- and 6-story buildings representing low- to mid-rise urban housing stock in India. Group 2 included step-back buildings

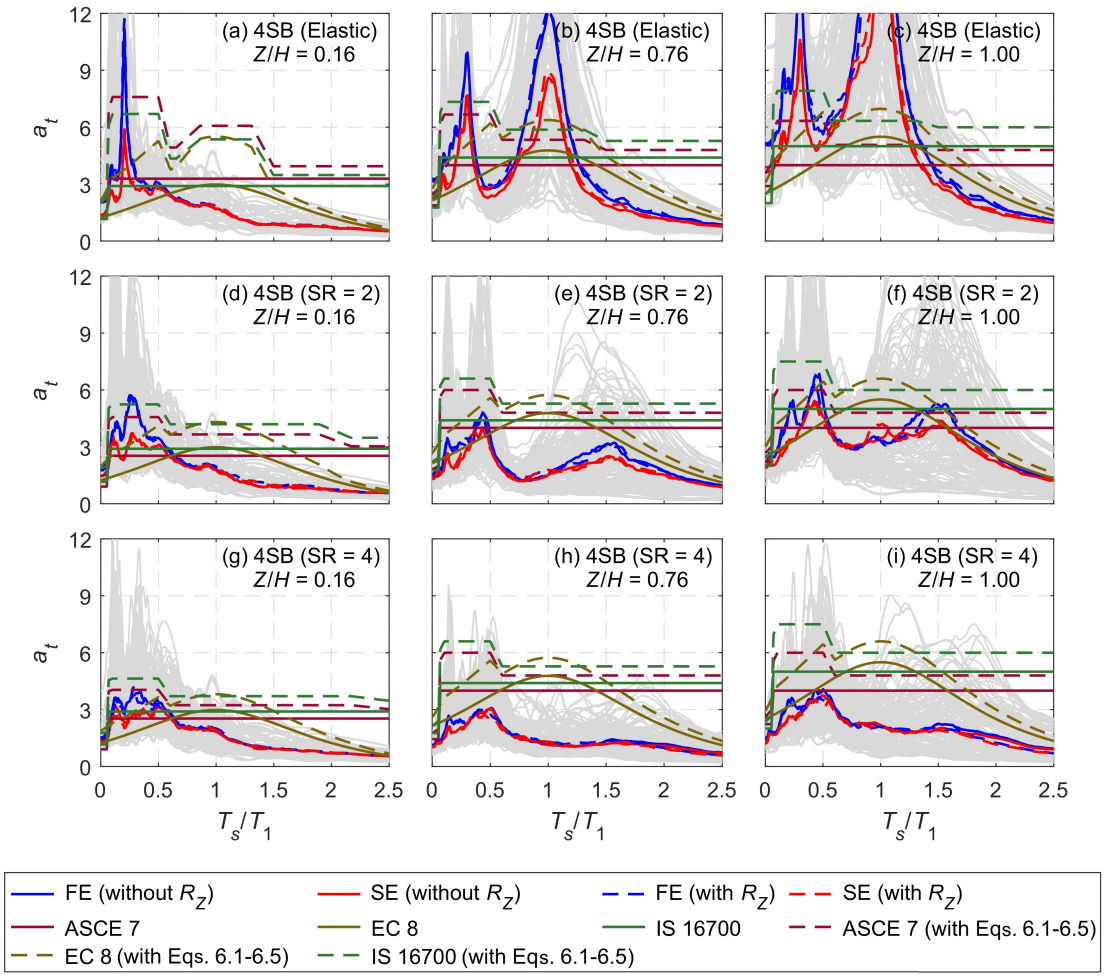

Figure 7.19: Comparisons of total amplification (a_t) estimated from time history analyses with and without considering rotational ground motions, as well as from building codes, with and without applying the proposed equations, for the '4SB' building.

situated on sloping ground, exhibiting both plan and elevation irregularities. Three representative step-back buildings with 2, 4, and 8 stories above the topmost foundation level are selected to reflect the common construction typologies in hilly regions of India. All step-back buildings are classified as ETI. A total of 1,400 time history analyses are conducted to evaluate the proposed models under a wide range of seismic scenarios, structural configurations, and inelastic responses. The results demonstrated that the proposed models effectively capture torsional amplification effects across different building types. The findings from this validation provide strong support for the applicability of the proposed models in predicting torsional amplification effects in buildings with nominal torsion, reinforcing their practical relevance for seismic design and assessment of the light-weight acceleration-sensitive

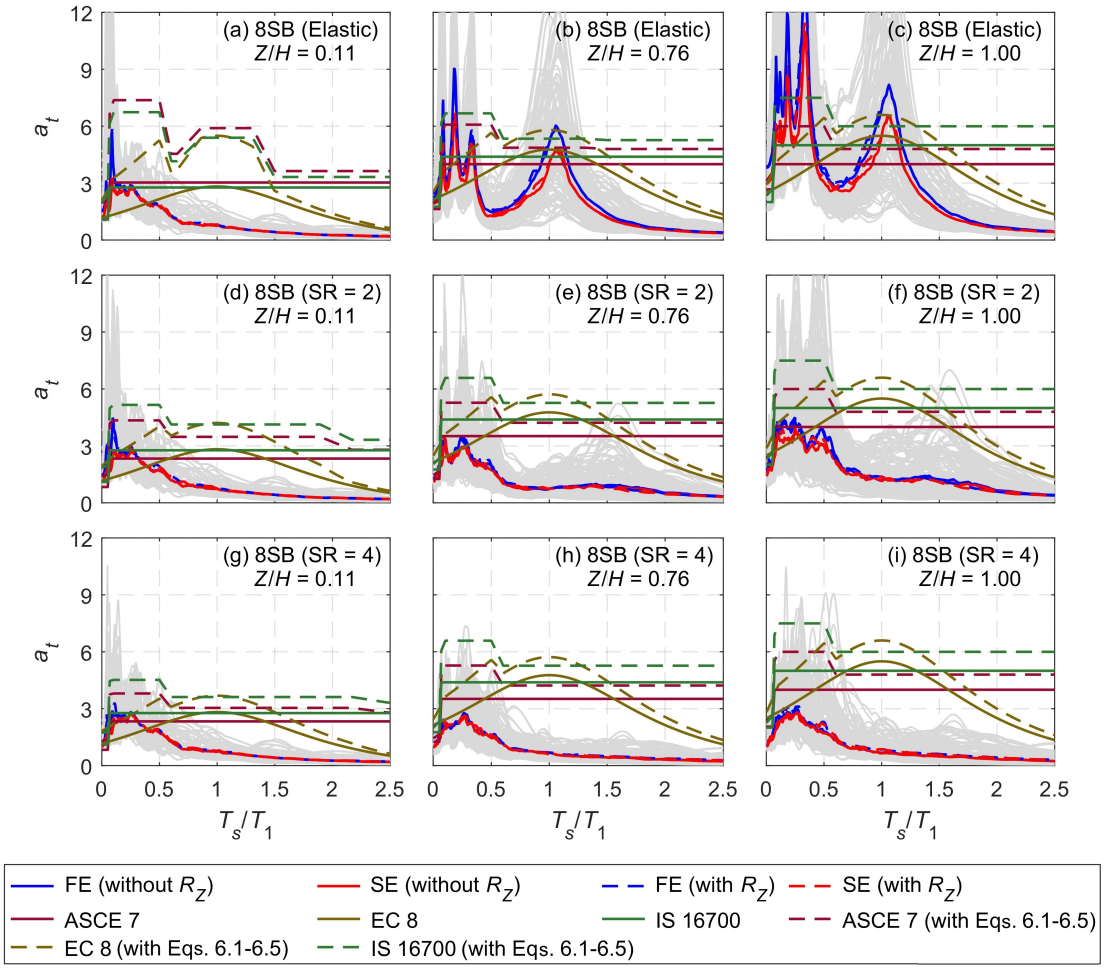

Figure 7.20: Comparisons of total amplification (a_t) estimated from time history analyses with and without considering rotational ground motions, as well as from building codes, with and without applying the proposed equations, for the '8SB' building.

secondary systems. The key insights gained from this validation study are summarized below.

- A comparison of the obtained median TAFs for rigid, flexible, and very flexible secondary systems with those predicted using the proposed model demonstrates that the model provides reasonably accurate TAF predictions, eliminating the need for computationally challenging and time-intensive time history analyses. It confirms that the elastic displacement ratios ($\Delta_{max}/\Delta_{avg}$, $\Delta_{max}/\Delta_{min}$, and $\Delta_{FF,\,ij}/\Delta_{CR,\,j}$) can effectively estimate the required TAFs with sufficient accuracy.

- The proposed model, while applied in conjunction with the existing provisions of seismic design codes, increased the accuracy of the code proposals

for predicting PFA/PGA demands across the floor plan. When applied with ASCE 7 provisions, PFA/PGA demands are reasonably well-predicted, even for buildings with nominal torsion. However, in particular, the underestimation of PFA/PGA demands for buildings exhibiting elastic response is seen mainly for EC 8 and IS 16700. This observation can be attributed to the lack of building-specific characteristics (specifically T_1) in predicting PFA/PGA using EC 8 and IS 16700. The study suggests a need to refine the existing seismic design provisions of EC 8 and IS 16700 to achieve more precise estimates of the PFA/PGA demands.

- The proposed model also improves the accuracy of total amplification predictions when combined with seismic design codes. However, while the application of TAF_F enhances prediction accuracy, underestimation persists specifically when the secondary system is tuned within the building's fundamental mode region of a short-period building and when the secondary system is tuned within the building's higher mode region for long-period buildings. This limitation stems from the inability of existing code provisions to take into account the spectral shape of the ground motions (in predicting floor acceleration demands), which typically have their peak in the short-period range.

- TAF predicted using both $\Delta_{max}/\Delta_{min}$ and $\Delta_{max}/\Delta_{avg}$ are conservative across all buildings, floor levels, and SR values of interest. Nevertheless, the observed conservatism in predicting TAFs in buildings with nominal torsion is acceptable, given the inherent building-to-building uncertainties, modeling assumptions, and the subsequent uncertainties in structural analysis and design.

Chapter 8

Conclusions and Recommendations for Future Work

8.1 Conclusions

Understanding the complex dynamics of buildings with nominal torsion is crucial for developing effective seismic design guidelines. These buildings are particularly vulnerable to earthquake-induced damage due to their pronounced tendency to undergo torsional motions. Such behavior results in uneven distributions of displacement and acceleration demands in the building's floor plan, significantly increasing the risk of failure in both primary and secondary systems during seismic events. This study aims to address existing limitations in the seismic design of secondary systems by introducing torsional amplification factors to accurately capture floor acceleration demands in buildings with nominal torsion.

The research involves an extensive numerical investigation of 24 reinforced-concrete moment-resisting frame (RCMRF) buildings with varying floor plan configurations, heights, nominal torsion, and inelastic response. A total of 14,400 linear and non-linear time history analyses are performed using a far field ground motion suite, both with and without considering rotational ground motions. The study systematically examines the relationships between torsional amplification factors and corresponding elastic floor displacement ratios for rigid, flexible, and very flexible secondary systems. Based on these findings, practice-oriented models are proposed to supplement existing code-prescribed equations, thereby enabling a more accurate representation of nominal torsional effects in the seismic design of the light-weight acceleration-sensitive secondary systems.

To validate the proposed models, an additional set of 1,400 linear and non-linear time history analyses are conducted on two distinct groups of buildings located on flat and sloped terrain conditions. This validation process ensures the robustness and applicability of the proposed modifications in diverse structural and geological conditions, reinforcing their potential integration into seismic design frameworks. From these extensive numerical investigations, the following key conclusions are drawn:

- Current seismic code provisions consistently underestimate the PFA/PGA demands in buildings exhibiting both elastic and moderately inelastic response with nominal torsion. The maximum underestimation of PFA/PGA occurs at the FE (extreme flexible frame) during the elastic response of buildings, with magnitudes reaching 93% according to ASCE 7. In the case of EC 8, the underestimation reached up to 90%, while for IS 16700, it reached up to 137%.

- The torsional amplification factor for the rigid secondary systems, TAF_R, is found to be highest for ETI buildings, followed by WTI and NTI buildings. The maximum (median) TAF_R at the FE occurs under the elastic response of the buildings, and the corresponding values for ETI, WTI, and NTI buildings are 1.76, 1.43, and 1.03, respectively. On the other hand, the maximum (median) TAF_R at the SE occurs under the inelastic response of the buildings, and the corresponding values for ETI, WTI, and NTI buildings are 1.12, 1.00, and 1.00, respectively. These magnitudes of TAF_R suggest their dependency on a building's nominal torsion and strength characteristics. Further, ignoring them, especially at the FE, can significantly underestimate the in-structure acceleration demands for rigid secondary systems.

- For buildings responding elastically, the effects of torsional amplification for rigid secondary systems are more pronounced in the flexible frames, while torsional de-amplification effects are more significant in the stiff frames. The building's inelastic response helps in reducing torsional amplification of accelerations for rigid secondary systems in flexible frames (up to 29%) while increasing it in stiff frames (up to 21%), compared to their elastic counterparts. Hence, the TAF_R are found to be dependent on the extent of nominal torsion

in the building, the location of the frame from the center of rigidity, as well as the extent of inelastic action expected in the building under earthquake excitation.

- The FRS in extreme torsionally irregular buildings exhibits two closely spaced (dual) peaks at the SE, with the effect being most pronounced in 4-story ETI buildings and gradually diminishing for WTI and NTI buildings due to the reduced contribution from the rotational mode of vibration in such buildings. Out of these two peaks, one corresponds to the building's fundamental mode, where a large mass participates primarily in translational motion with a small rotational coupling, while the other peak is associated with the building's rotational mode of vibration, where a significant mass participates in rotational motion, with a small translational coupling.

- Existing seismic design code provisions consistently underestimate component amplification factor, a_p and total amplification, a_t in both torsionally regular and irregular buildings. The highest underestimation of a_p occurs under the elastic response at the FE, reaching 130%, 189%, and 158% for ASCE 7, EC 8, and IS 16700, respectively. For a_t, the highest underestimation also occurs under the elastic response at the FE, reaching 539%, 411%, and 365% for ASCE 7, EC 8, and IS 16700, respectively.

- The extent of nominal torsion has a significant impact on the spectral amplification factor, SAF, and it is maximum for ETI buildings. As the nominal torsion decreases, there is a noticeable reduction in the median SAF, particularly at the FE, and the differences in the SAF values between the FE, the SE, and the CR become almost negligible in NTI buildings.

- The buildings exhibiting inelastic response exhibited elongation in the fundamental period of the building. The effective (elongated) period remains relatively constant across different levels of nominal torsion in buildings, suggesting that the relationship between period elongation and inelasticity is not affected by the extent of nominal torsion in the building.

- The torsional amplification factor for the flexible secondary systems, TAF_F,

is observed to be highest for ETI buildings and the lowest for NTI buildings. The maximum (median) TAF_F at the FE occurs during the buildings' elastic response, with values reaching up to 2.06, 1.69, and 1.08 for ETI, WTI, and NTI buildings, respectively, when the secondary system is tuned within the building's fundamental mode region, and 2.33, 1.83, and 1.04 when the secondary system is tuned within the building's higher mode region. Conversely, the maximum (median) TAF_F at the SE are limited to 1.38, 1.16, and 1.00 for the case when the secondary system is tuned within the building's fundamental mode region, and 1.51, 1.26, and 1.02, when the secondary system is tuned within the building's higher mode region, corresponding to ETI, WTI, and NTI buildings, respectively. These values highlight that torsional amplification effects are more pronounced at the flexible edges and also at short periods (in the vicinity of higher modes).

- The building inelasticity significantly reduces TAF_F. For 4-story buildings exhibiting elastic response, the maximum median TAF_F at the FE for the case, when the secondary system is tuned within the building's fundamental mode region, is 2.06, 1.69, and 1.08 for ETI, WTI, and NTI buildings, respectively. However, in the highly inelastic 4-story buildings, these values decrease to 1.37, 1.15, and 1.03, respectively, highlighting the mitigating effect of the building's inelasticity on TAF_F. Hence, the building inelasticity dependent TAF_F shall be used in the seismic design of flexible secondary systems.

- At very long periods, torsional amplification tends to approach unity due to the reduced degree of dynamic interaction between the secondary system and the building. The presence of nominal torsion has a negligible impact on the very flexible secondary systems, with the median TAF_{VF} values ranging from 1.21 in ETI buildings to 1.02 in NTI buildings at the FE. The TAF_{VF} at the SE remained unaffected, consistently exhibiting the median TAF_{VF} of 1.00, among all analyzed cases. Further, the building inelasticity reduced the maximum median TAF_{VF} at the FE, though the reduction is insignificant. However, at the SE, the median TAF_{VF} remains constant at 1.00, indicating no significant effect of the building inelasticity. Hence, for all practical purposes, TAF_{VF} can be assumed to be independent of the extent of nominal torsion and building

inelasticity.

- The rotational ground motions can significantly increase (or decrease) the floor acceleration demands (PFA and FRS) across all torsional irregularity categories (ETI, WTI, and NTI) and building inelasticity levels, with the SE consistently experiencing the highest increase. The increasing or decreasing effects on floor acceleration demands due to rotational ground motions do not correlate with the degree of torsional irregularity in the building.

- The median increase in PFA/PGA demands due to rotational ground motions is most significant at SE, with a maximum increase of up to 53%. In comparison, the median increase in PFA/PGA due to rotational ground motions at the CR and the FE is 29% and 21%, respectively. On the other hand, the median reduction in PFA/PGA demands due to rotational ground motions is limited to FE, with a maximum reduction of approximately 8%.

- Building inelasticity significantly amplifies the effects of rotational ground motions, with the median PFA/PGA increasing from 20% in elastic buildings to 47% in buildings exhibiting highly inelastic response.

- The rotational ground motions can notably increase SAF values across all torsional irregularity categories (ETI, WTI, and NTI) and levels of building inelasticity, with the SE consistently showing the highest increase, which can be up to 54%. Further, the increase or decrease in SAF values due to rotational ground motions does not correlate with the extent of nominal torsion in the building.

- The rotational ground motions have a greater impact on TAF_R at the SE compared to the FE. The median TAF_R increase at the SE remains relatively consistent, reaching a maximum of 27%, while at the FE, it varies, with a maximum increase limited only up to 4%, and many times even decreases, up to 15%.

- The impact of rotational ground motions on the median peak TAF_F varies with structural configuration and inelasticity levels. The increase in the median peak TAF_F due to rotational ground motions is more significant when the

secondary system is tuned within the building's higher mode region, reaching up to 44%, in contrast to 24% when the secondary system is tuned within the building's fundamental mode region. This observation can be attributed to relatively richer high-frequency content in the rotational ground motions.

- The inclusion of rotational ground motions has no significant impact on TAF_{VF} values. Buildings exhibiting both elastic and inelastic response show consistent trends, with no noticeable amplification at the SE and the FE.

- The torsional amplification factors at the FE show a strong relationship with the torsional irregularity indices ($\Delta_{FF,\,ij}/\Delta_{CR,\,j}$, $\Delta_{max}/\Delta_{avg}$ and $\Delta_{max}/\Delta_{min}$) for both TAFs corresponding to rigid and flexible secondary systems. The findings lead to the proposal of the practice-oriented building's torsional and strength characteristics dependent TAFs. To account for the torsional amplification in regular (NTI) buildings due to rotational ground motions, lower-bound limits are incorporated into the proposed model, ensuring its applicability to regular buildings as well.

- A comparison of the median TAFs obtained for rigid, flexible, and very flexible secondary systems in the validation building set with those predicted by the proposed model demonstrates that the model provides reasonably accurate TAF predictions without requiring extensive time history analyses. This confirms that the elastic displacement ratios ($\Delta_{max}/\Delta_{avg}$, $\Delta_{max}/\Delta_{min}$, and $\Delta_{FF,\,ij}/\Delta_{CR,\,j}$) can effectively estimate the required TAFs with sufficient accuracy.

- The proposed model, while applied in conjunction with the existing provisions of seismic design codes, increased the accuracy of the code proposals for predicting PFA/PGA demands across the floor plan. When applied with ASCE 7 provisions, PFA/PGA demands are reasonably well-predicted, even for buildings with nominal torsion. However, in particular, the underestimation of PFA/PGA demands for elastic buildings is seen mainly for EC 8 and IS 16700. This observation can be attributed to the lack of building-specific characteristics (specifically T_1) in predicting PFA/PGA using EC 8 and IS 16700. The study suggests a need to refine the existing seismic

design provisions of EC 8 and IS 16700 to achieve more precise estimates of the PFA/PGA demands.

- As the inelastic response of the building increases, the detrimental impact of torsional amplification of the PFA/PGA is mitigated by the beneficial effects of the building's inelasticity. As a result, the EC 8 and IS 16700 provide reasonable estimates of PFA/PGA in buildings exhibiting highly inelastic response. In contrast, ASCE 7 explicitly incorporates the effect of building inelasticity in the code prediction equation and hence provides non-conservative estimates of the PFA/PGA, even for buildings exhibiting highly inelastic response with nominal torsion.

- The proposed model also improves the accuracy of total amplification predictions when combined with seismic design codes. However, while the application of TAFs enhances prediction accuracy, underestimation persists, particularly for secondary systems tuned within the building's higher mode region and even for secondary systems tuned within the building's fundamental mode region under the building's elastic response. This limitation stems from the inability of existing code provisions to fully account for higher-mode effects, building inelasticity, and ground motion characteristics. Refining seismic design equations to incorporate these factors is crucial for achieving more precise floor acceleration predictions in buildings with nominal torsion.

- The TAFs predicted using $\Delta_{max}/\Delta_{min}$ are usually more conservative than those predicted using $\Delta_{max}/\Delta_{avg}$ across all buildings, floor levels, and SR values of interest. Nevertheless, the observed conservatism in predicting TAFs in buildings with nominal torsion is acceptable, given the inherent building-to-building uncertainties, modeling assumptions, and the subsequent uncertainties in structural analysis and design.

- The proposed TAFs directly support the fundamental objectives of PBD. By providing more realistic and spatially resolved floor acceleration demands for secondary systems, this work contributes essential input for evaluating component performance under defined seismic hazard levels or ductility

demands. It enables a more nuanced and demand-consistent approach to secondary system design.

8.2 Recommendations for future work

- The present study focused on torsionally rigid RCMRF buildings. The torsionally flexible buildings may display distinct dynamic behavior due to increased displacements at the SE from dominant torsional modes. Future research should investigate TAFs in torsionally flexible buildings, considering both rigid and flexible secondary systems.

- The present study is conducted on torsionally rigid RCMRF buildings without infills. The influence of infill walls and shear walls on TAFs should be explored and integrated into future torsional amplification models.

- The buildings investigated in the present study possess unidirectional eccentricity in the floor plan. Future investigations are required to further understand the effects of bi-directional eccentricity on floor acceleration response and incorporate them into the developed torsional amplification prediction model.

- The present study concentrated on fixed-base buildings on rock sites. Future work should extend the investigations to buildings on medium to soft soils and also to buildings equipped with seismic isolation systems, assessing how isolation impacts TAFs for both rigid and flexible secondary systems.

- The present study evaluated the in-plan distribution of TAFs across the floor plan corresponding to rigid secondary systems; therefore, additional research is necessary to predict the in-plan distribution of TAFs for flexible secondary systems throughout the building floor plan.

- The present study considered ground motions recorded in the far field conditions and mid-rise RCMRF buildings. To comprehensively understand TAFs, further studies should encompass a broader range of building heights, lateral load-resisting systems, and ground motion types (e.g., near-fault records).

- The proposed equations in this study can be tested using shake table experiments on scaled building models subjected to recorded or simulated ground motions.

- The floor acceleration response recorded from instrumented buildings during real earthquakes can be compared with the values predicted by the proposed equations in this study to evaluate their accuracy and practical relevance.

References

[1] SK Jain, CVR Murty, U Dayal, JN Arlekar, and SK Chaubey. The republic day earthquake in the land of M. K. Gandhi, the father of the nation. *Earthquake Engineering Research Institute*, 2001.

[2] HB Kaushik, K Dasgupta, DR Sahoo, and G Kharel. Reconnaissance report Sikkim earthquake of 14 February 2006. *National Information Center of Earthquake Engineering Indian Institute of Technology Kanpur*, 2006.

[3] N Takahashi and H Shiohara. Life cycle economic loss due to seismic damage of nonstructural elements. *13th World Conference on Earthquake Engineering Vancouver, B.C., Canada August 1-6, 2004 Paper No. 203*, 2004.

[4] CVR Murty, R Goswami, AR Vijayanarayanan, and VV Mehta. Some concepts in earthquake behaviour of buildings. *Gujarat State Disaster Management Authority, Government of Gujarat*, 2012.

[5] Bureau of Indian Standards (IS 1893 Part 1). Indian Standard – Criteria for earthquake resistant design of structures, Part 1 – General Provisions and Buildings, New Delhi, India. 2016.

[6] American Society of Civil Engineers (ASCE). Minimum design loads and associated criteria for buildings and other structures, ASCE Standard, ASCE 7-22, Reston, Virginia: American Society of Civil Engineers. 2022.

[7] RP Dhakal. Damage to non-structural components and contents in 2010 Darfield earthquake. *Bulletin of the New Zealand Society for Earthquake Engineering*, 43:404–411, 2010.

[8] J Moehle, J Berger, J Bray, L Dengler, M Greene, J Mitrani-Reiser, and W Siembieda. The 27 February 2010 Central South Chile earthquake: Emerging research needs and opportunities. 2010.

[9] G Magliulo, M Ercolino, C Petrone, O Coppola, and G Manfredi. The Emilia

earthquake: The seismic performance of precast reinforced concrete buildings. *Earthquake Spectra*, 30(2):891–912, 2014.

[10] D Perrone, PM Calvi, R Nascimbene, E Fischer, and G Magliulo. Seismic performance and damage observation of non-structural elements during the 2016 Central Italy earthquake. *Bulletin of Earthquake Engineering*, 17: 5655–5677, 2019.

[11] HB Kaushik and K Dasgupta. Assessment of Seismic Vulnerability of Structures in Sikkim, India, Based on Damage Observation during Two Recent Earthquakes. *Journal of Performance of Constructed Facilities*, 27(6):697–720, 2013.

[12] CVR Murty, STG Raghukanth, A Menon, R Goswami, ARV Narayanan, SR Gandhi, KN Satyanarayana, AR Sheth, DC Rai, and G Mondal. The Mw 6.9 Sikkim-Nepal Border Earthquake of September 18, 2011. *In: EERI Newsletter, EERI Special Earthquake Report*, pages 1–14, 2012.

[13] AW Sadek and WK Tso. Strength eccentricity concept for the inelastic analysis of asymmetrical structures. *Engineering Structures*, 11(3):189–194, 1989.

[14] D Basu and SK Jain. Alternative method to locate the center of rigidity in asymmetric buildings. *Earthquake Engineering and Structural Dynamics*, 36: 965–973, 2007.

[15] MN Fardis. Seismic design, assessment and retrofitting of concrete buildings: based on EN-Eurocode 8. *Springer Sci Business Media*, 2009.

[16] European Committee for Standardization EN 1998-1 (EC-8). Design of structures for earthquake resistance – Part 1: general rules, seismic actions and rules for buildings, Brussels. 2004.

[17] Bureau of Indian Standards (IS 16700). Indian standard – Criteria for structural safety of tall buildings, New Delhi, India. 2017.

[18] R Villaverde. Seismic design of secondary structures: State of the art. *Journal of Structural Engineering*, 123(8):1011–1019, 1997.

[19] RP Dhakal, A Pourali, AS Tasligedik, T Yeow, A Baird, G MacRae, S Pampanin, and A Palermo. Seismic performance of non-structural components and contents in buildings: an overview of NZ research. *Earthquake Engineering and Engineering Vibration*, 15:1–17, 2016.

[20] E Miranda, A Kazantzi, and D Vamvatsikos. Towards a new approach to design acceleration-sensitive non-structural components. *Eleventh U.S. National Conference on Earthquake Engineering Integrating Science, Engineering Policy June 25-29, 2018 Los Angeles, California*, 2018.

[21] A Devin and PJ Fanning. Non-structural elements and the dynamic response of buildings: A review. *Engineering Structures*, 187:242–250, 2019.

[22] E Miranda, G Mosqueda, R Retamales, and G Pekcan. Performance of nonstructural components during the 27 February 2010 Chile earthquake. *Earthquake Spectra*, 28(S1):S453–S471, 2012.

[23] H Varum, R Damaru, A Furtado, AR Barbosa, D Gautam, and H Rodrigues. Seismic Performance of Buildings in Nepal After the Gorkha Earthquake. *In: Impacts and Insights of Gorkha Earthquake*, pages 47–63, 2018.

[24] MK Shrimali and RS Jangid. Seismic analysis of base-isolated liquid storage tanks. *Journal of Sound and Vibration*, 275(1-2):59–75, 2004.

[25] VR Panchal and RS Jangid. Variable friction pendulum system for seismic isolation of liquid storage tanks. *Nuclear Engineering and Design*, 238(6): 1304–1315, 2008.

[26] S Taghavi and E Miranda. Response assessment of non-structural building elements. PEER Report 2003/05, Pacific Earthquake Engineering Research Center, Berkeley, CA, USA. 2003.

[27] American Society of Civil Engineers (ASCE). Minimum design loads and associated criteria for buildings and other structures, ASCE Standard, ASCE 7-16, Reston, Virginia: American Society of Civil Engineers. 2016.

[28] AM Chandler. Building damage in Mexico city earthquake. *Nature*, 320(6062): 497–501, 1986.

[29] AM Chandler, XN Duan, and A Rutenberg. Seismic torsional response: assumptions, controversies and research progress. *European Earthquake Engineering*, 10:37–51, 1996.

[30] C Özmen and Aİ Ünay. Commonly encountered seismic design faults due to the architectural design of residential buildings in Turkey. *Building and Environment*, 42(3):1406–1416, 2007.

[31] Bureau of Indian Standards (Amendment No. 2 to IS 1893 Part 1). Indian Standard – Criteria for earthquake resistant design of structures, Part 1 – General Provisions and Buildings, New Delhi, India. 2020.

[32] Bureau of Indian Standards (IS 456). Indian Standard – Plain and reinforced concrete – Code of practice, New Delhi, India. 2000.

[33] Bureau of Indian Standards (IS 13920). Indian Standard – Ductile design and detailing of reinforced concrete structures subjected to seismic forces – Code of practice, New Delhi, India. 2016.

[34] C Adam, T Furtmüller, and L Moschen. Floor response spectra for moderately heavy nonstructural elements attached to ductile frame structures. *Computational Methods in Earthquake Engineering*, 2:69–89, 2013.

[35] C Adam and T Furtmüller. Response of nonstructural components in ductile load-bearing structures sub- jected to ordinary ground motions. In: Proceedings ofthe 14thworld conference on earthquake engineering, Paper no 05-01-0327, Beijing, China, 12–17 October 2008. 2008.

[36] S Taghavi and E Miranda. Effect of interaction between primary and secondary systems on floor response spectra. *The 14th World Conference on Earthquake Engineering October 12-17, 2008, Beijing, China*, 2008.

[37] Federal Emergency Management Agency (FEMA). Quantification of seismic per- formance factors, FEMA P695, Washington, D.C. 2009.

[38] SC Dutta and PK Das. Inelastic seismic response of code-designed reinforced concrete asymmetric buildings with strength degradation. *Engineering Structures*, 24:1295–1314, 2002.

[39] Y Chen and TT Soong. State of the art: Seismic response of secondary systems. *Engineering Structures*, 10:218–228, 1988.

[40] W Tao, S Qingxue, and L Jichao. Seismic force demands on acceleration-sensitive nonstructural components: a state-of-the-art review. *Earthquake Engineering and Engineering Vibration*, 20:39–62, 2021.

[41] RA Medina, R Sankaranarayanan, and KM Kingston. Floor response spectra for light components mounted on regular moment-resisting frame structures. *Engineering Structures*, 28(14):1927–1940, 2006.

[42] R Sankaranarayanan and RA Medina. Acceleration response modification factors for nonstructural components attached to inelastic moment-resisting frame structures. *Earthquake Engineering and Structural Dynamics*, 36: 2189–2210, 2007.

[43] H Anajafi and RA Medina. Damping modification factor for elastic floor spectra. *Bulletin of Earthquake Engineering*, 17:6079–6108, 2019.

[44] M Surana, M Pisode, Y Singh, and DH Lang. Effect of URM infills on inelastic floor response of RC frame buildings. *Engineering Structures*, 175:861–878, 2018.

[45] D Perrone, E Brunesi, A Filiatrault, and R Nascimbene. Probabilistic estimation of floor response spectra in masonry infilled reinforced concrete building portfolio. *Engineering Structures*, 202:–, 2020.

[46] M Surana, Y Singh, and DH Lang. Effect of structural characteristics on damping modification factors for floor response spectra in RC buildings. *Engineering Structures*, 242, 2021.

[47] AB Aldeka, AHC Chan, and S Dirar. Response of non-structural components mounted on irregular RC buildings: Comparison between FE and EC8 predictions. *Earthquake and Structures*, 6(4):351–373, 2014.

[48] AK Kazantzi, D Vamvatsikos, and E Miranda. The effect of damping on floor spectral accelerations as inferred from instrumented buildings. *Bulletin of Earthquake Engineering*, 18:2149–2164, 2020.

[49] J Lin and SA Mahin. Seismic response of light subsystems on inelastic structures. *Journal of Structural Engineering*, 111(2):400–417, 1985.

[50] M Surana, Y Singh, and DH Lang. Effect of response reduction factor on peak floor acceleration demand in mid-rise RC buildings. *Journal of The Institution of Engineers (India): Series A*, 98:53–65, 2017.

[51] L Berto, M Bovo, I Rocca, A Saetta, and M Savoia. Seismic safety of valuable non-structural elements in RC buildings: Floor Response Spectrum approaches. *Engineering Structures*, 205(110081), 2020.

[52] CG Duff. Simplified method for development of earthquake ground and floor response spectra for nuclear power plant design, Second Canadian Conference on earthquake engineering, Hamilton, Ontario. 1975.

[53] KA Peters, D Schmitz, and U Wagner. Determination of floor response spectra on the basis of the response spectrum method. *Nuclear Engineering and Design*, 44:255–262, 1977.

[54] JL Sackman, AD Kiureghian, and B Nour-omid. Dynamic analysis of light equipment in structures: Modal properties of the combined system. *Journal of Engineering Mechanics*, 109(1):73–89, 1983.

[55] AD Kiureghian, JL Sackman, and B Nour-omid. Dynamic analysis of light equipment in structures: Response to stochastic input. *Journal of Engineering Mechanics*, 109(1):90–110, 1983.

[56] T Igusa and AD Kiureghian. Dynamic characterization of two-degree-of-freedom equipment-structure systems. *Journal of Engineering Mechanics*, 111(1):1–19, 1985a.

[57] T Igusa and AD Kiureghian. Dynamic response of multiply supported secondary systems. *Journal of Engineering Mechanics*, 111(1):20–41, 1985b.

[58] MP Singh and AM Sharma. Seismic floor spectra by mode acceleration approach. *Journal of Engineering Mechanics*, 111(11):1402–1419, 1986.

[59] LE Suarez and MP Singh. Seismic response of SDF Equipment-Structure system. *Journal of Engineering Mechanics*, 113(1):16–30, 1987.

[60] LE Suarez and MP Singh. Floor response spectra with Structure-Equipment interaction effects by a Mode synthesis approach. *Earthquake Engineering and Structural Dynamics*, 15:141–158, 1987.

[61] KJ Elwood and JP Moehle. Shake Table Tests and Analytical Studies on the Gravity Load Collapse of Reinforced Concrete Frames. *Pacific Earthquake Engineering Research Center (PEER 2003/01)*, 2003.

[62] G Magliulo, V Pentangelo, G Maddaloni, V Capozzi, C Petrone, P Lopez, R Talamonti, and G Manfredi. Shake table tests for seismic assessment of suspended continuous ceilings. *Bulletin of Earthquake Engineering*, 10(6): 1819–1832, 2012.

[63] W Duozhi, D Junwu, Q Zhe, and N Xiaoqing. Shake table tests of suspended ceilings to simulate the observed damage in the Ms 7.0 Lushan earthquake, China. *Earthquake Engineering and Engineering Vibration*, 15(2):239–249, 2016.

[64] A Lepage, JM Shoemaker, and AM Memari. Accelerations of Nonstructural Components during Nonlinear Seismic Response of Multistory Structures. *Journal of Architectural Engineering*, 18(4):285–297, 2012.

[65] AE Zaghi, EM Maragakis, A Itani, and E Goodwin. Experimental and Analytical Studies of Hospital Piping Assemblies Subjected to Seismic Loading. *Earthquake Spectra*, 28(1):367–384, 2012.

[66] R Astroza, E Pantoli, F Selva, JI Restrepo, TC Hutchinson, and JP Conte. Experimental Evaluation of the Seismic Response of a Rooftop-Mounted Cooling Tower. *Earthquake Spectra*, 31(3):1567–1589, 2015.

[67] C Shermi and RN Dubey. Performance Evaluation of a Reinforced Masonry Model and an Unreinforced Masonry Model Using a Shake Table Testing Facility. *Journal of Performance of Constructed Facilities*, 32(1), 2017.

[68] S Fathali and B Lizundia. Evaluation of current seismic design equations for nonstructural components in tall buildings using strong motion records. *The Structural Design of Tall and Special Buildings*, 20:S30–S46, 2011.

[69] X Wang, R Astroza, T Huchinson, J Conte, and R Bachman. Seismic demands on acceleration-sensitive nonstructural components using recorded building response data - Case study. *NCEE 2014 - 10th U.S. National Conference on Earthquake Engineering: Frontiers of Earthquake Engineering, July 21-25, 2014 Anchorage, Alaska*, 2014.

[70] H Anajafi and RA Medina. Evaluation of ASCE 7 equations for designing acceleration- sensitive nonstructural components using data from instrumented buildings. *Earthquake Engineering and Structural Dynamics*, 47 (4):1075–1094, 2018.

[71] Y Yasui, J Yoshihara, T Takeda, and A Miyamoto. Direct generation method for floor response spectra. *Transactions of the 12th International Conference on Structural Mechanics in Reactor Technology (SMiRT 12)*, pages 367–372, 1993.

[72] W Jiang, B Li, WC Xie, and MD Pandey. Generate floor response spectra: Part 1. Direct spectra-to-spectra method. *Nuclear Engineering and Design*, 293:525–546, 2015.

[73] E Miranda and S Taghavi. Approximate floor acceleration demands in multistory buildings. I: Formulation. *Journal of Structural Engineering*, 131 (2):203–211, 2005.

[74] E Reinoso and E Miranda. Estimation of floor acceleration demands in high-rise buildings during earthquakes. *Structural Design of Tall and Special Buildings*, 14:107–130, 2005.

[75] V Vukobratović and P Fajfar. A method for the direct determination of approximate floor response spectra for SDOF inelastic structures. *Bulletin of Earthquake Engineering*, 13(5):1405–1424, 2014.

[76] V Vukobratović and P Fajfar. A method for the direct estimation of floor acceleration spectra for elastic and inelastic MDOF structures. *Earthquake Engineering Structural Dynamics*, 45(15):2495–2511, 2016.

[77] V Vukobratović and P Fajfar. Code-oriented floor acceleration spectra for building structures. *Bulletin of Earthquake Engineering*, 15(7):3013–3026, 2017.

[78] X Pan, Z Zheng, and Z Wang. Estimation of Floor response spectra using modified Modal pushover analysis. *Soil Dynamics and Earthquake Engineering*, 92:472–487, 2017.

[79] X Pan, Z Zheng, and Z Wang. A Multi-Mode method for estimation of Floor response spectra. *Journal of Earthquake Engineering*, 22(6):1111–1136, 2018.

[80] TJ Sullivan, PM Calvi, and R Nascimbene. Towards improved floor spectra estimates for seismic design. *Earthquakes and Structures*, 4(1):109–132, 2013.

[81] PM Calvi and TJ Sullivan. Estimating floor spectra in multiple degree of freedom systems. *Earthquakes and Structures*, 7(1):17–38, 2014.

[82] SR Chaudhuri and TC Hutchinson. Distribution of peak horizontal floor acceleration for estimating nonstructural element vulnerability. *13th World Conference on Earthquake Engineering, Vancouver, B.C., Canada August 1-6, 2004 Paper No. 1721*, 2004.

[83] SR Uma, JX Zhao, and AB King. Seismic actions on acceleration sensitive non-structural components in ductile frames. *Bulletin of the New Zealand Society for Earthquake Engineering*, 43(2):110–125, 2010.

[84] AK Chopra and RK Goel. A modal pushover analysis procedure to estimate seismic demands of buildings: theory and preliminary evaluation. Report No. PEER 2001/ 03. Berkeley (CA): Pacific Earthquake Engineering Research Center, University of California. 2001.

[85] AK Chopra and RK Goel. A modal pushover analysis procedure for estimating seismic demands for buildings. *Earthquake Engineering and Structural Dynamics*, 31(3):561–582, 2002.

[86] J Wieser, G Pekcan, AE Zaghi, A Itani, and M Maragakis. Floor accelerations in yielding special moment resisting frame structures. *Earthquake Spectra*, 29 (3):987–1002, 2013.

[87] C Petrone, G Magliulo, and G Manfredi. Floor response spectra in RC frame structures designed according to Eurocode 8. *Bulletin of Earthquake Engineering*, 14(3):747–767, 2016.

[88] Q Shang, J Li, and T Wang. Floor acceleration response spectra of elastic reinforced concrete frames. *Journal of Building Engineering*, 45, 2022.

[89] S Taghavi and E Miranda. Probabilistic study of peak floor acceleration demands in nonlinear structures. *15th World Conference on Earthquake Engineering, September, Lisbon, Portugal*, 2012.

[90] American Society of Civil Engineers (ASCE). Minimum design loads for buildings and other structures, ASCE Standard, ASCE 7-05, Reston, Virginia: American Society of Civil Engineers. 2006.

[91] American Society of Civil Engineers (ASCE). Minimum design loads for buildings and other structures, ASCE Standard, ASCE 7-10, Reston, Virginia: American Society of Civil Engineers. 2011.

[92] An assessment of seismic floor accelerations in wood shear wall buildings. *2nd ATC SEI Conference on Improving the Seismic Performance of Existing Buildings and Other Structures*, 2015.

[93] MP Singh, LM Moreschi, LE Suárez, and EE Matheu. Seismic design forces.II: Flexible nonstructural components. *Journal of Structural Engineering*, 132 (10):1533–1542, 2006.

[94] A Lucchini, F Mollaioli, and P Bazzurro. Floor response spectra for bare and infilled reinforced concrete frames. *Journal of Earthquake Engineering*, 18(7): 1060–1082, 2014.

[95] National Institute of Standards and Technology. Recommendations for improved seismic performance of non-structural components. NIST GCR 18-917-43. Redwood City, CA: Applied Technology Council. 2018.

[96] NZS 1170.5:2004. Structural Design Actions Part 5: Earthquake Actions- New Zealand. Standards New Zealand, New Zealand. 2004.

[97] ME Rodriguez, JI Restrepo, and AJ Carr. Earthquake-induced floor horizontal accelerations in buildings. *Earthquake Engineering and Structural Dynamics*, 31:693–718, 2002.

[98] SR Chaudhuri and TC Hutchinson. Effect of nonlinearity of frame buildings on peak horizontal floor acceleration. *Journal of Earthquake Engineering*, 15 (1):124–142, 2011.

[99] F Mollaioli, A Lucchini, P Bazzurro, S Bruno, and AD Sortis. Floor horizontal acceleration demand in reinforced concrete frames. *FIB Symposium Prague 2011 - Concrete Engineering for Excellence and Efficiency*, 2011.

[100] G Blasi, D Perrone, and MA Aiello. Fragility functions and floor spectra of RC masonry infilled frames : influence of mechanical properties of masonry infills. *Bulletin of Earthquake Engineering*, 16(12):6105–6130, 2018.

[101] Y Bozorgnia, NA Abrahamson, KW Campbell, B Rowshandel, and T Shantz. NGA-West2: A comprehensive research program to update ground motion prediction equations for shallow crustal earthquakes in active tectonic regions. *Proceedings of the 15th World Conference on Earthquake Engineering, Lisbon*, 2012.

[102] MN Fardis. Seismic design, assessment and retrofitting of concrete buildings: based on EN-Eurocode 8. Springer. 2012.

[103] B Poudel, E Özşahin, and G Pekcan. Effect of Torsional Ground Motions on Floor Acceleration Response in Flexible SMRF Buildings. *Journal of Earthquake Engineering*, 26(4):2168–2185, 2022.

[104] A Menon and G Magenes. Definition of seismic input for out-of-plane response of masonry walls: II. Formulation. *Journal of Earthquake Engineering*, 15(2): 195–213, 2011.

[105] M Oropeza, P Favez, and P Lestuzzi. Seismic response of nonstructural components in case of nonlinear structures based on floor response spectra method. *Bulletin of Earthquake Engineering*, 8:387–400, 2010.

[106] C Petrone, G Magliulo, and G Manfredi. Seismic demand on light acceleration-sensitive nonstructural components in European reinforced concrete buildings. *Earthquake Engineering Structural Dynamics*, 44: 1203–1217, 2015.

[107] R Sankaranarayanan and RA Medina. Statistical models for a proposed acceleration-response modification factor for nonstructural components attached to inelastic structures. *14th World Conference on Earthquake Engineering (14WCEE), October 12-17, 2008, Beijing, China*, 2008.

[108] SR Chaudhuri and R Villaverde. Effect of building nonlinearity on seismic response of nonstructural components: A parametric study. *Journal of Structural Engineering*, 134(4):661–670, 2008.

[109] MV Landge and RK Ingle. Comparative study of floor response spectra for regular and irregular buildings subjected to earthquake. *Asian Journal of Civil Engineering*, 22:49–58, 2020.

[110] FX Flores, DL Garcia, and FA Charney. Assessment of floor accelerations in special steel moment frames. *Journal ofConstructional Steel Research*, 106: 154–165, 2015.

[111] C Zhai, Z Zheng, S Li, X Pan, and L Xie. Seismic response of nonstructural components considering the near-fault pulse-like ground motions. *Earthquakes and Structures*, 10(5):1213–1232, 2016.

[112] R Sankaranarayanan. Seismic response of acceleration-sensitive nonstructural components mounted on moment-resisting frame structures. 2007.

[113] RA Medina, J Clayton, R Sankaranarayanan, and M Ferguson. Seismic acceleration demands on nonstructural components attached to elastic and inelastic structures. *ATC SEI 2009 Conference on Improving the Seismic Performance of Existing Buildings and Other Structures*, pages 639–650, 2009.

[114] R Villaverde. Simple method to estimate the seismic nonlinear response of nonstructural components in buildings. *Engineering Structures*, 28:1209–1221, 2006.

[115] AD Angelis, M Pecce, and F Rossi. Linear time history analysis for the out-of-plane seismic demand of infill walls in RC framed buildings. *Bulletin of Earthquake Engineering*, 13:3325–3352, 2015.

[116] A Asgarian and G McClure. Impact of seismic rehabilitation and presence of unreinforced masonry (URM) infill walls on the dynamic characteristics of a hospital building in Montreal. *Canadian Journal of Civil Engineering*, 41: 748–760, 2014.

[117] M Surana, Y Singh, and DH Lang. Effect of irregular structural configuration on floor acceleration demand in hill-side buildings. *Earthquake Engineering and Structural Dynamics*, 47(10):2032–2054, 2018.

[118] M Surana. Evaluation of Seismic Design Provisions for Acceleration-Sensitive Non-Structural Components. *Earthquakes and Structures*, 16(5):611–623, 2019.

[119] Y Yang and W Huang. Seismic response of light equipment in torsional buildings. *Earthquake Engineering Structural Dynamics*, 22:113–128, 1993.

[120] AK Agrawal and TK Datta. Seismic response of a secondary system mounted on a torsionally coupled non-linear primary system. *Journal of Earthquake Engineering*, 2(3):339–356, 1998.

[121] B Qu, RK Goel, and CB Chadwell. Evaluation of ASCE/SEI 7 provisions for determination of seismic demands on nonstructural components. *Proceedings of the 10th National Conference in Earthquake Engineering, Earthquake Engineering Research Institute, Anchorage, Alaska*, 2014.

[122] AB Aldeka, S Dirar, AHC Chan, and P Martinez-Vazquez. Seismic response of non-structural components attached to reinforced concrete structures with different eccentricity ratios. *Earthquake and Structures*, 8(5):1069–1089, 2015.

[123] H Anajafi and RA Medina. Lessons learned from evaluating the responses of instrumented buildings in the United States: The effects of supporting building characteristics on floor response spectra. *Earthquake Spectra*, 35(1):159–191, 2019.

[124] S Ruggieri and V Vukobratović. The influence of torsion on acceleration demands in low-rise RC buildings. *Bulletin of Earthquake Engineering*, 22 (5):2433—2468, 2024.

[125] A Lucchini, P Franchin, and F Mollaioli. Probabilistic seismic demand model for nonstructural components. *Earthquake Engineering Structural Dynamics*, 45:599–617, 2016.

[126] M Surana, Y Singh, and DH Lang. Floor Spectra of Inelastic RC Frame Buildings Considering Ground Motion Characteristics. *Journal of Earthquake Engineering*, 22(3):488–519, 2018.

[127] R Sisman and E Taciroglu. Characteristics of torsional ground motions obtained for Turkey and their appraisal against Eurocode 8. *Bulletin of Earthquake Engineering*, 22(5):2353–2373, 2024.

[128] SR Dahmardeh, M Motamedi, and A Aziminejad. A study on the effects of torsional component of ground motions on seismic response of low- and mid-rise buildings. *Structural Design of Tall and Special Buildings*, 29(4): 1–25, 2020.

[129] H Anajafi, RA Medina, and E Santini-Bell. Inelastic floor spectra for designing anchored acceleration - sensitive nonstructural components. *Bulletin of Earthquake Engineering*, 18:2115–2147, 2020.

[130] R Astroza, E Pantoli, F Selva, JI Restrepo, TC Hutchinson, and JP Conte. Experimental evaluation of the seismic response of a rooftop-mounted cooling tower. *Earthquake Spectra*, 31(3):1567–1589, 2015.

[131] LF Aragaw and PM Calvi. Earthquake-induced floor accelerations in base-rocking wall buildings. *Journal of Earthquake Engineering*, 25(5): 941–969, 2018.

[132] RJ Merino, D Perrone, and A Filiatrault. Consistent floor response spectra for performance- based design of nonstructural elements. *Earthquake Engineering Structural Dynamics*, 49(3):261–284, 2020.

[133] M Shooshtari, M Saatcioglu, N Naumoski, and S Foo. Floor response spectra for seismic design of operational and functional components of concrete buildings in Canada. *Canadian Journal of Civil Engineering*, 37 (12):1590–1599, 2010.

[134] RA Medina. Seismic design horizontal accelerations for non-structural components. *Vienna Congress on Recent Advances in Earthquake Engineering and Structural Dynamics 2013 (VEESD 2013), Vienna, Austria*, 2013.

[135] H Hou, W Fu, W Wang, B Qu, Y Chen, Y Chen, and C Qiu. Horizontal seismic force demands on nonstructural components in low-rise steel building frames with tension-only braces. *Engineering Structures*, 168:852–864, 2018.

[136] CSI (Computers and Structures Inc.). Integrated Building Analysis and Design Software (ETABS 2016). Computers and Structures Inc. 2016.

[137] Bureau of Indian Standards (IS 875 Part 1). Code of practice for design loads (other than earthquake) for buildings and structures (Dead loads), New Delhi, India. 1987.

[138] Bureau of Indian Standards (IS 875 Part 2). Code of practice for design loads (other than earthquake) for buildings and structures (Live loads), New Delhi, India. 1987.

[139] F McKenna, G Fenves, M Scott, and B Jeremic. Open System for Earthquake Engineering Simulation (OpenSees). Pacific Earthquake Engineering Research Center, University of California. 2000.

[140] R Bhaskar and A Menon. Torsional irregularity indices for the seismic demand assessment of RC moment resisting frame buildings. *Structures*, 26:888–900, 2020.

[141] P Bisch, E Carvalho, H Degee, P Fajfar, M Fardis, P Franchin, M Kreslin, A Pecker, P Pinto, A Plumier, H Somja, and G Tsionis. Seismic Design of

Buildings - Worked examples. EUR 25204 EN. Luxembourg (Luxembourg): Publications Office of the European Union. 2012.

[142] E Spacone, V Ciampi, and FC Filippou. Mixed formulation of nonlinear beam finite element. *Computers and Structures*, 58(1):71–83, 1996.

[143] JB Mander, MJN Priestley, and R Park. Theoretical stress-strain model for confined concrete. *Journal of Structural Engineering*, 114(8):1804–1826, 1988.

[144] MM Karthik and JB Mander. Stress-block parameters for unconfined and confined concrete based on a Unified Stress-Strain Model. *Journal of Structural Engineering*, 137(2):270–273, 2011.

[145] FC Filippou, EP Popov, and VV Bertero. Effects of Bond Deterioration on Hysteretic Behavior of Reinforced Concrete Joints. Earthquake Engineering Research Center, University of California (Report EERC 83-19). 1983.

[146] D Basu, AS Whittaker, and MC Constantinou. Characterizing the rotational components of earthquake ground motion. *Technical Report MCEER-12-0005*, 2012.

[147] LP Suwal and R Kuwano. Statically and dynamically measured poisson's ratio of granular soils on triaxial laboratory specimens. *Geotechnical Testing Journal*, 36(4):493–505, 2013.

[148] DL Wells and KJ Coppersmith. New Empirical Relationships among Magnitude, Rupture Length, Rupture Width, Rupture Area, and Surface Displacement. *Bulletin of the Seismological Society of America*, 84(4): 974–1002, 1994.

[149] TS Breusch and AR Pagan. A simple test for heteroscedasticity and random coefficient variation. *Econometrica*, 47(5):1287–1294, 1979.

[150] WH Greene. Econometric Analysis (5th edition) 2003; Prentice Hall, Upper Saddle River, New Jersey 07458. 2003.

[151] DEQ. Seismic vulnerability of multi-storey buildings in Noida. Tech. Rep. Department of earthquake engineering, Indian Institute of Technology Roorkee, Roorkee, India. pages 1–118, 2009.

[152] M Surana, Y Singh, and DH Lang. Seismic characterization and vulnerability of building stock in hilly regions. *Natural Hazards Review*, 19(1), 2017.

[153] KJ Elwood. Modelling failures in existing reinforced concrete columns. *Canadian Journal of Civil Engineering*, 31(5):846–859, 2004.

[154] KJ Elwood and JP Moehle. Drift Capacity of Reinforced Concrete Columns with Light Transverse Reinforcement. *Earthquake Spectra*, 21(1):71–89, 2005.

[155] H Sezen and JP Moehle. Shear Strength Model for Lightly Reinforced Concrete Columns. *Journal of Structural Engineering*, 130(11):1692–1703, 2004.

Appendix A

Peak Floor Acceleration

A.1 Peak floor acceleration response

Figures A.1–A.6 illustrates the comparison of peak floor acceleration responses at the CS, CR, SE, and FE, obtained from time history analyses with and without considering rotational ground motions, against the values predicted by code equations [6, 16, 17]. The observed trend follows the same pattern as discussed in Chapter 4.

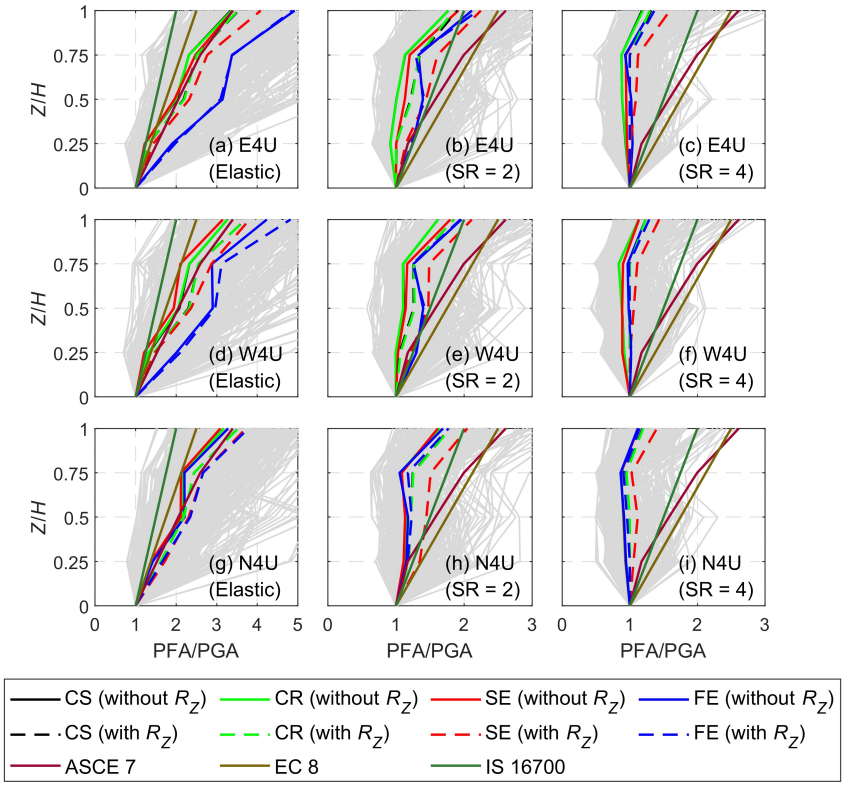

Figure A.1: PFA/PGA at various locations on the floor plan of the 'E4U', 'W4U', and 'N4U' buildings.

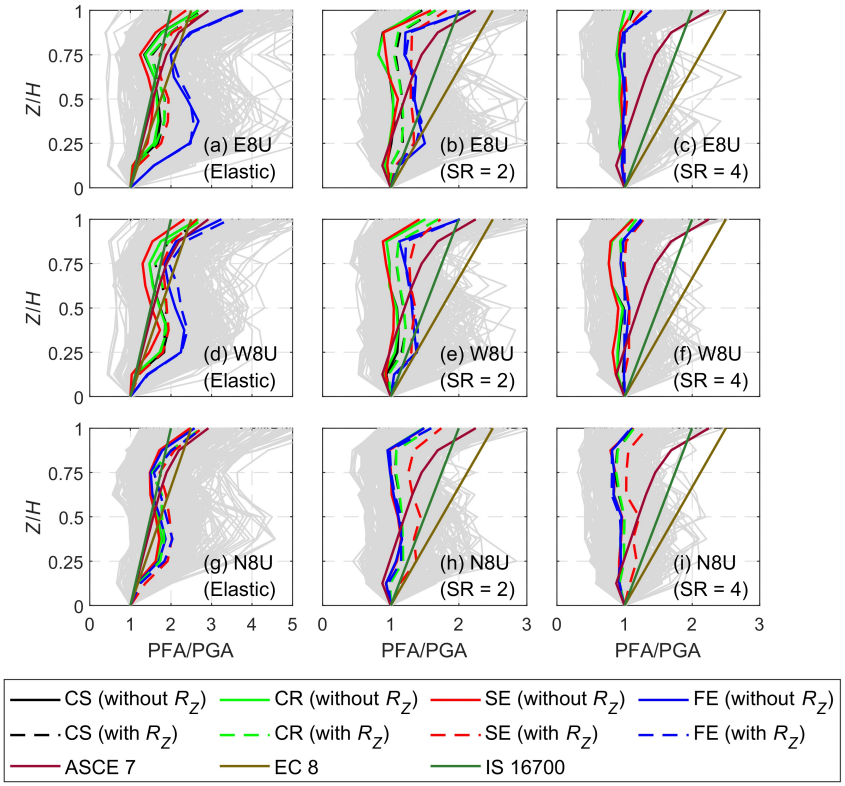

Figure A.2: PFA/PGA at various locations on the floor plan of the 'E8U', 'W8U', and 'N8U' buildings.

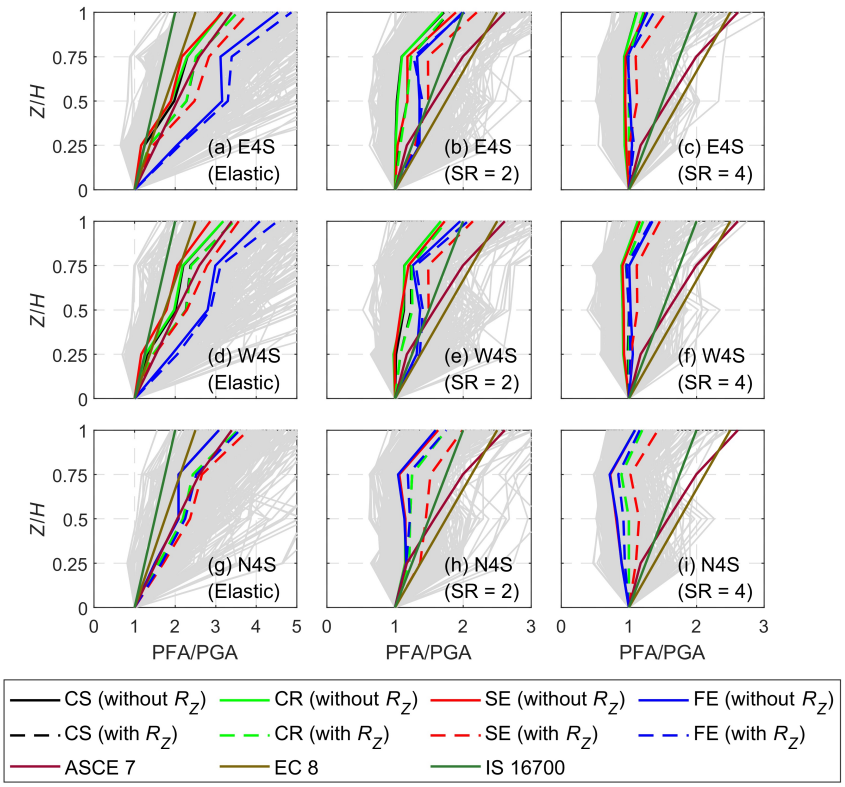

Figure A.3: PFA/PGA at various locations on the floor plan of the 'E4S', 'W4S', and 'N4S' buildings.

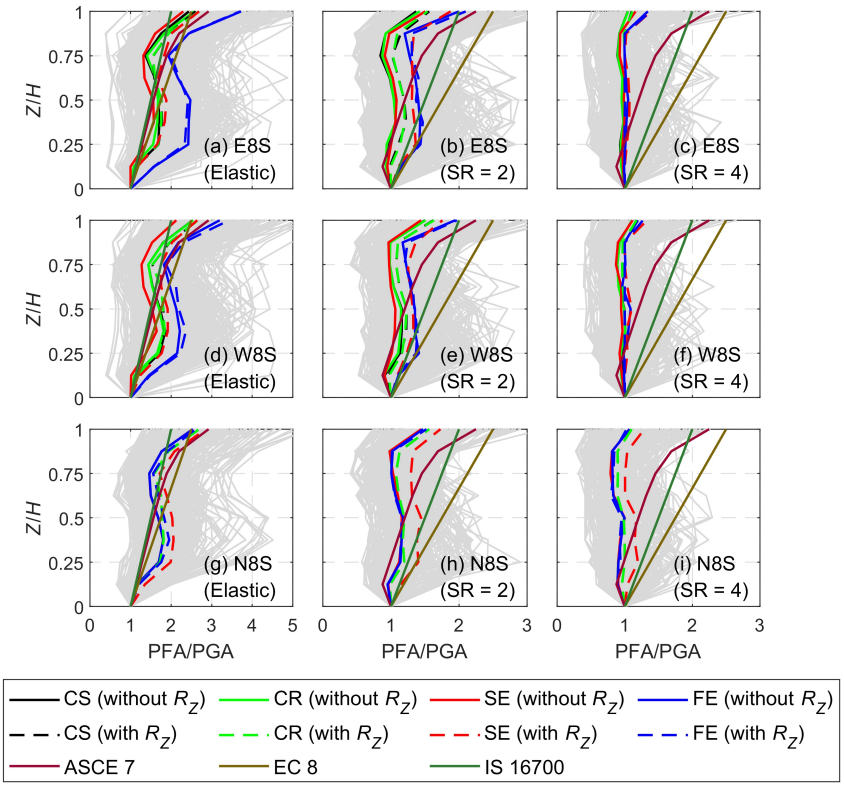

Figure A.4: PFA/PGA at various locations on the floor plan of the 'E8S', 'W8S', and 'N8S' buildings.

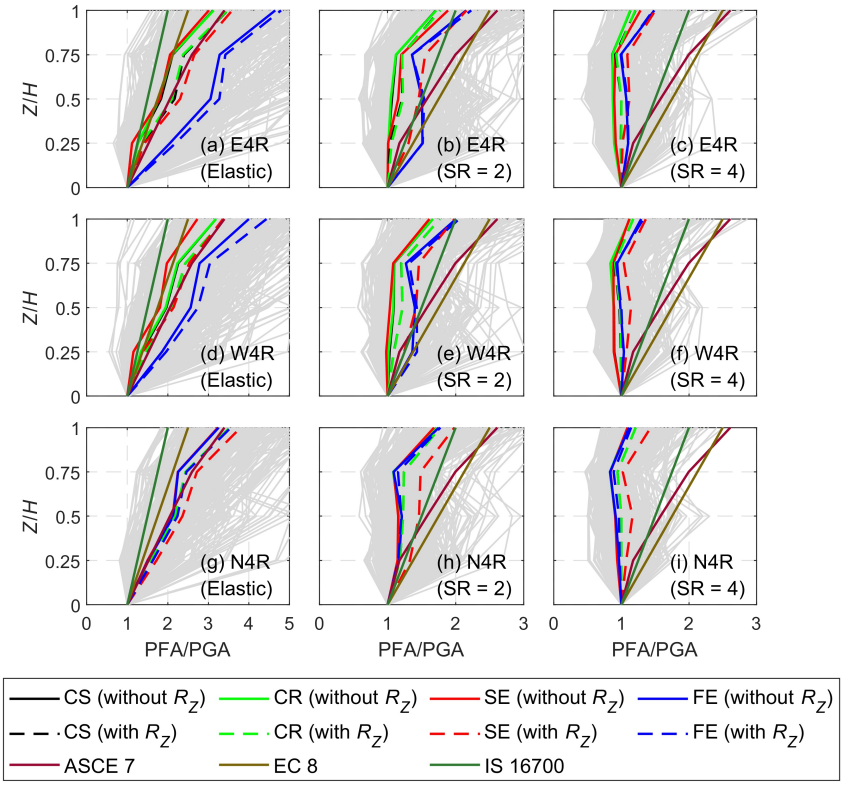

Figure A.5: PFA/PGA at various locations on the floor plan of the 'E4R', 'W4R', and 'N4R' buildings.

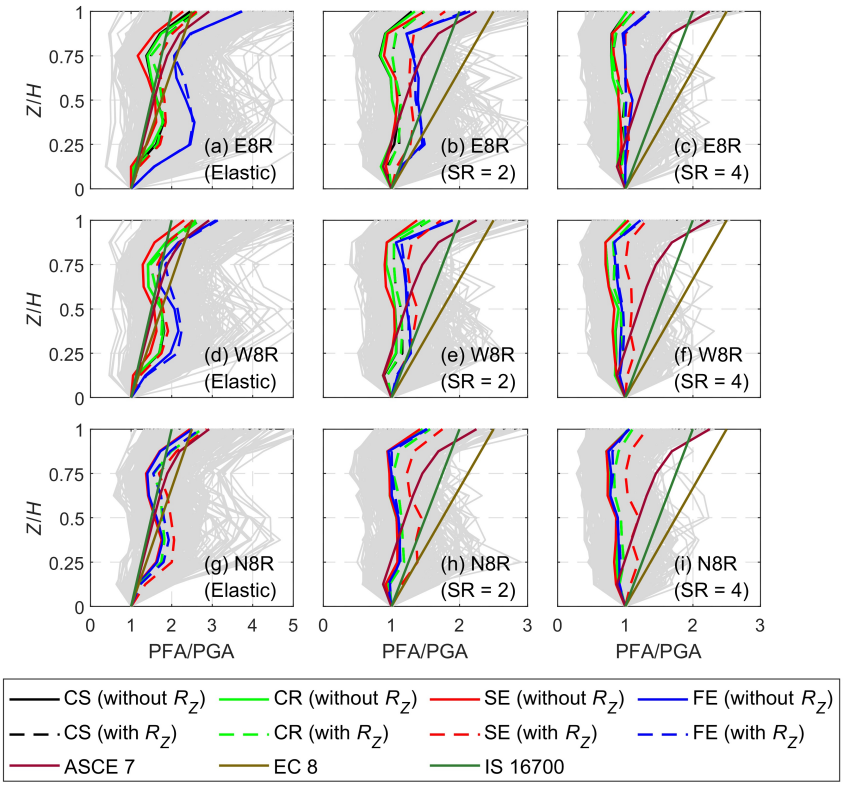

Figure A.6: PFA/PGA at various locations on the floor plan of the 'E8R', 'W8R', and 'N8R' buildings.

A.2 In-plan distribution of the peak floor acceleration response

Figures A.7–A.24 present a comparison of peak floor acceleration responses across the floor plan, estimated from the time history analyses with and without considering rotational ground motions, against the values predicted by code equations [6, 16, 17]. The observed trend follows the same pattern as discussed in Chapter 4.

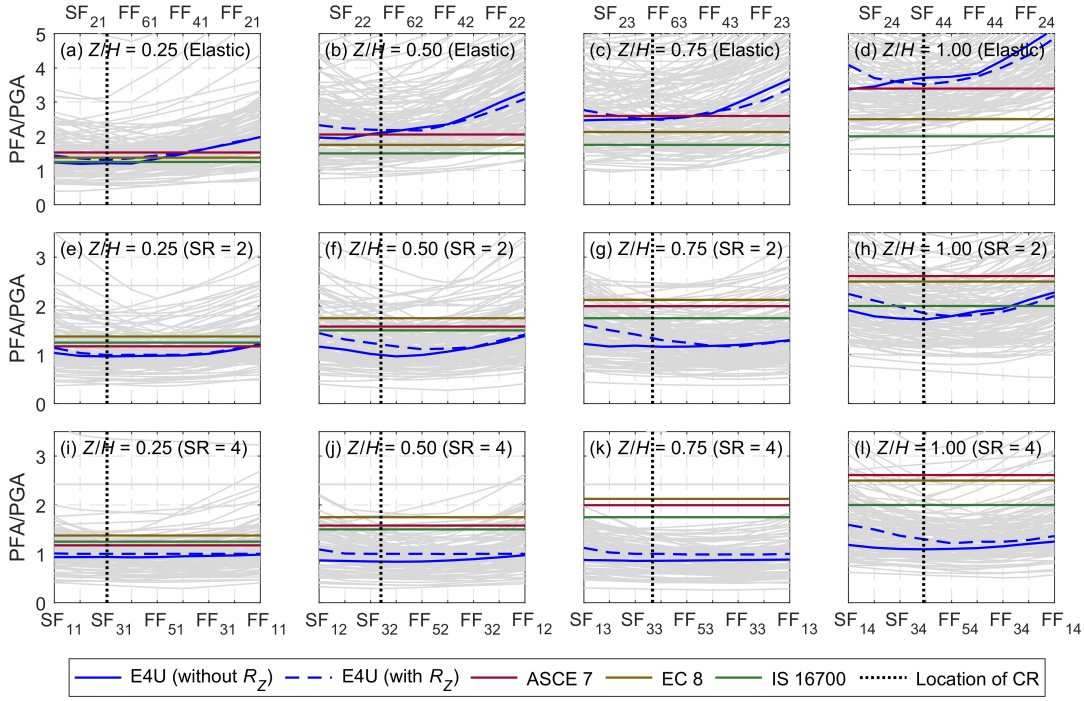

Figure A.7: In-plan distribution of PFA/PGA at different floors of the 'E4U' building.

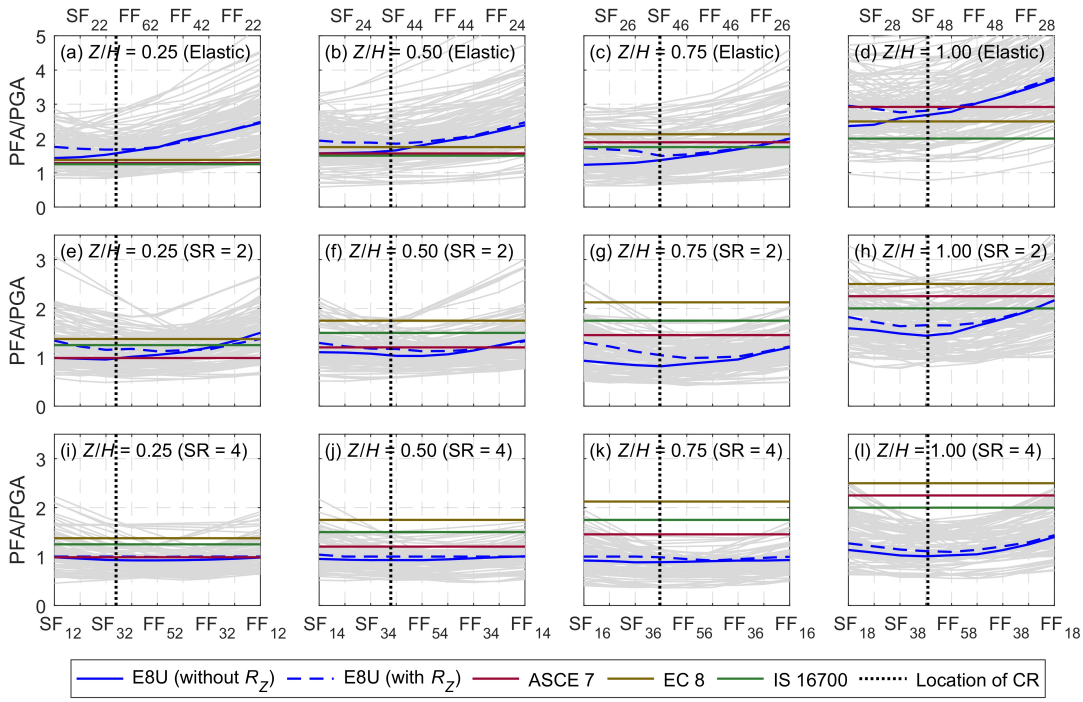

Figure A.8: In-plan distribution of PFA/PGA at different floors of the 'E8U' building.

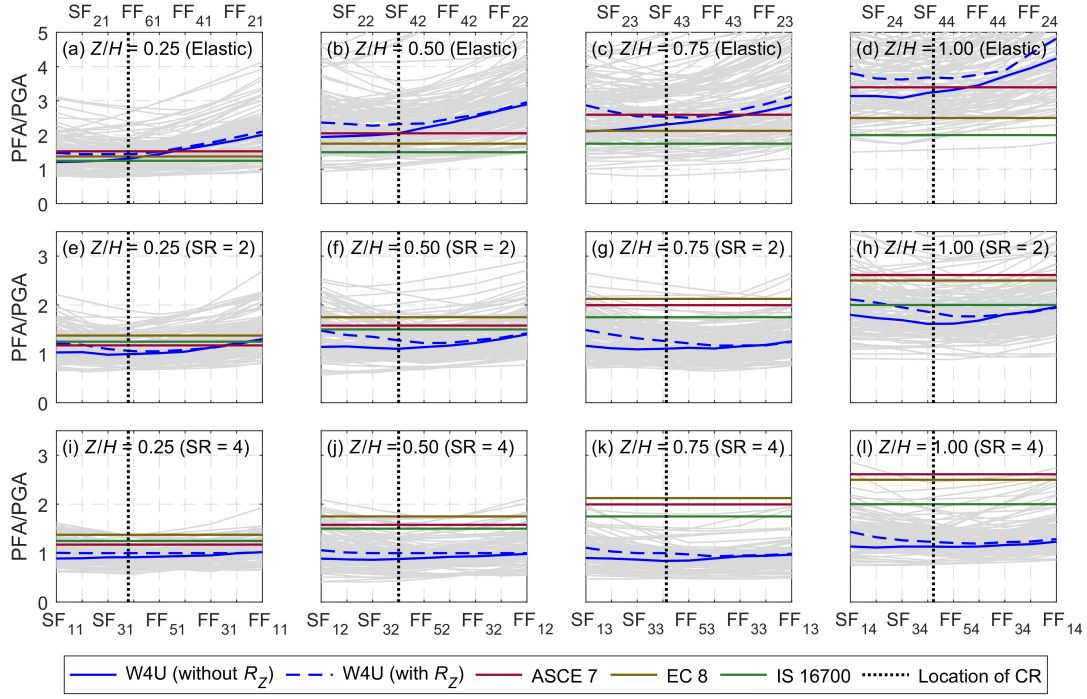

Figure A.9: In-plan distribution of PFA/PGA at different floors of the 'W4U' building.

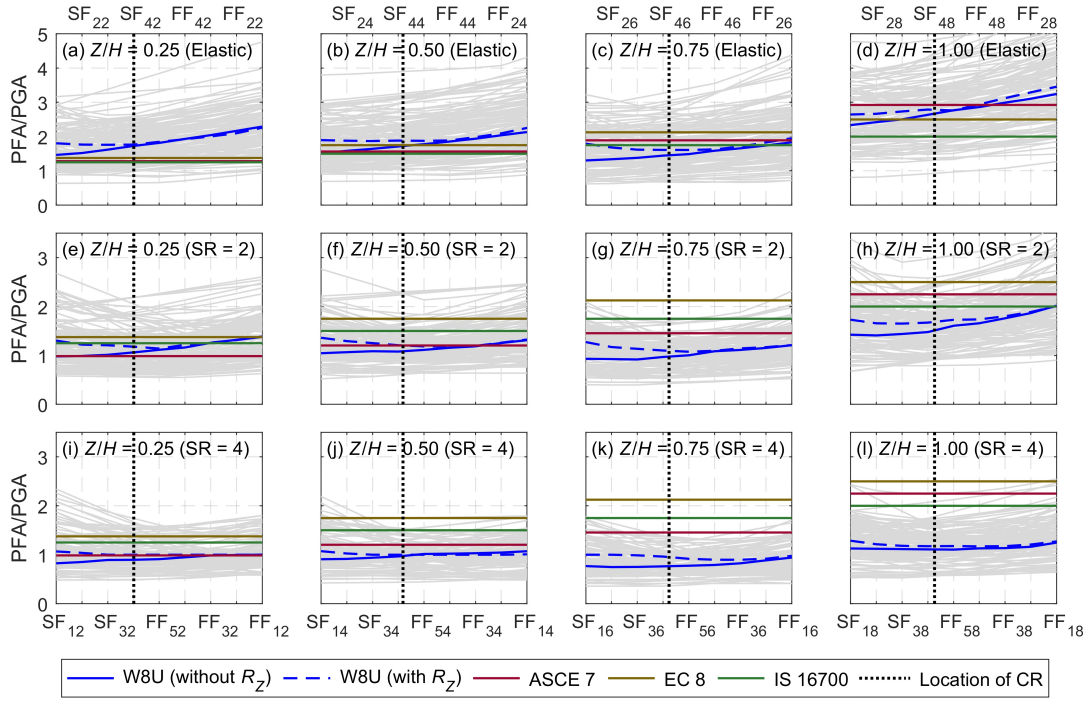

Figure A.10: In-plan distribution of PFA/PGA at different floors of the 'W8U' building.

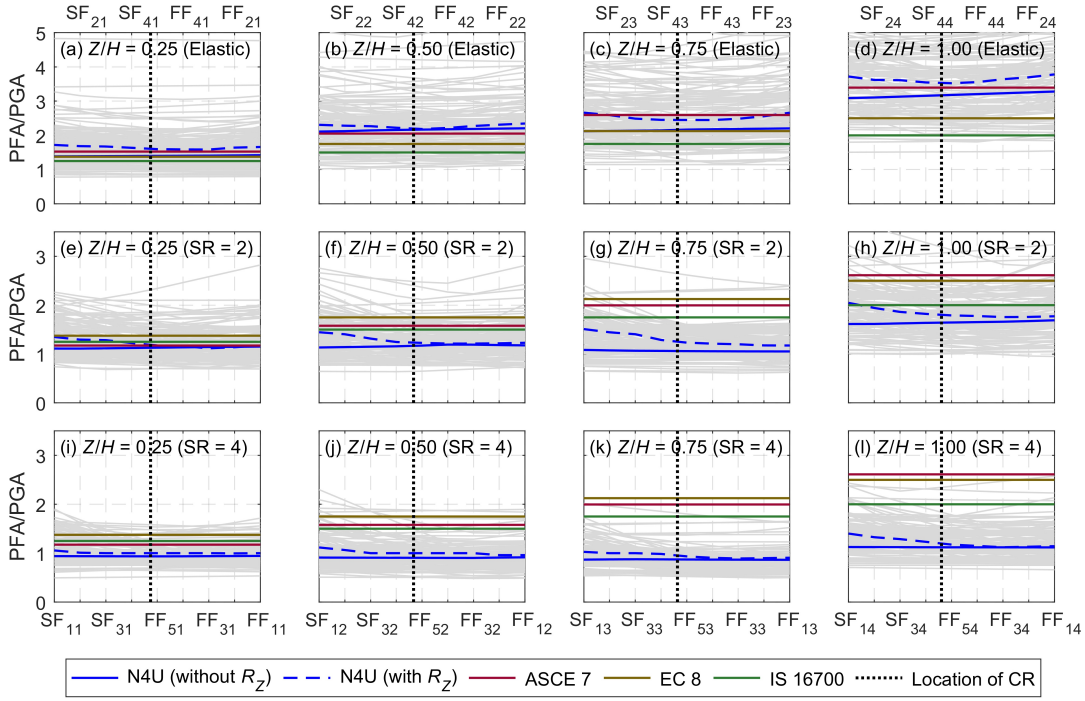

Figure A.11: In-plan distribution of PFA/PGA at different floors of the 'N4U' building.

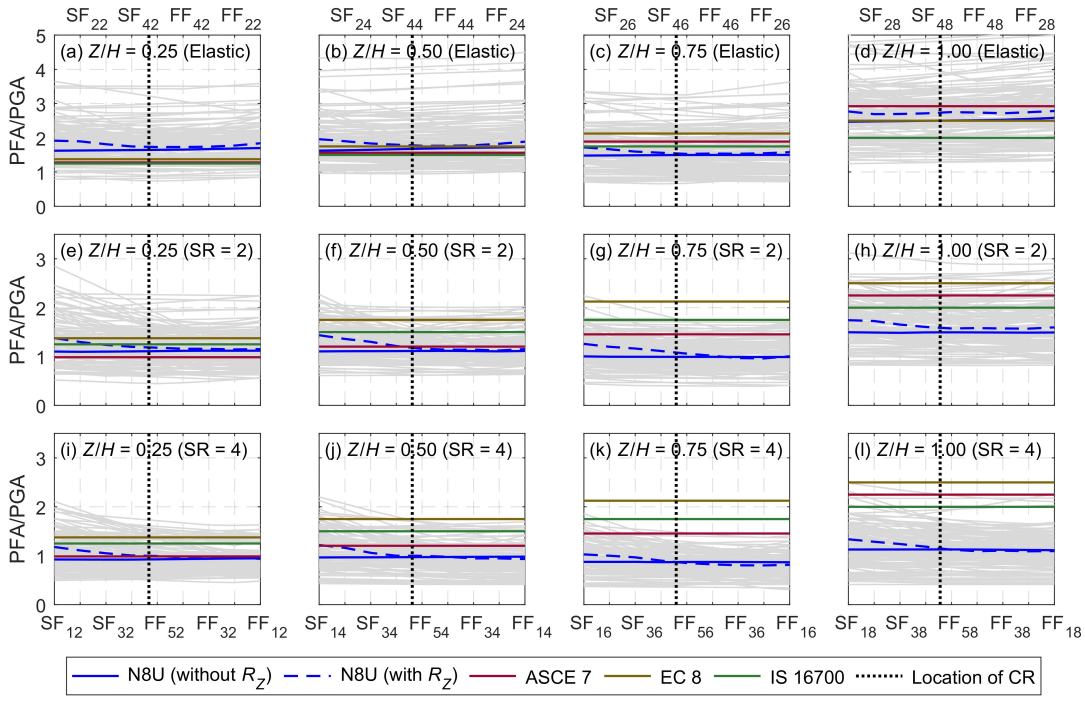

Figure A.12: In-plan distribution of PFA/PGA at different floors of the 'N8U' building.

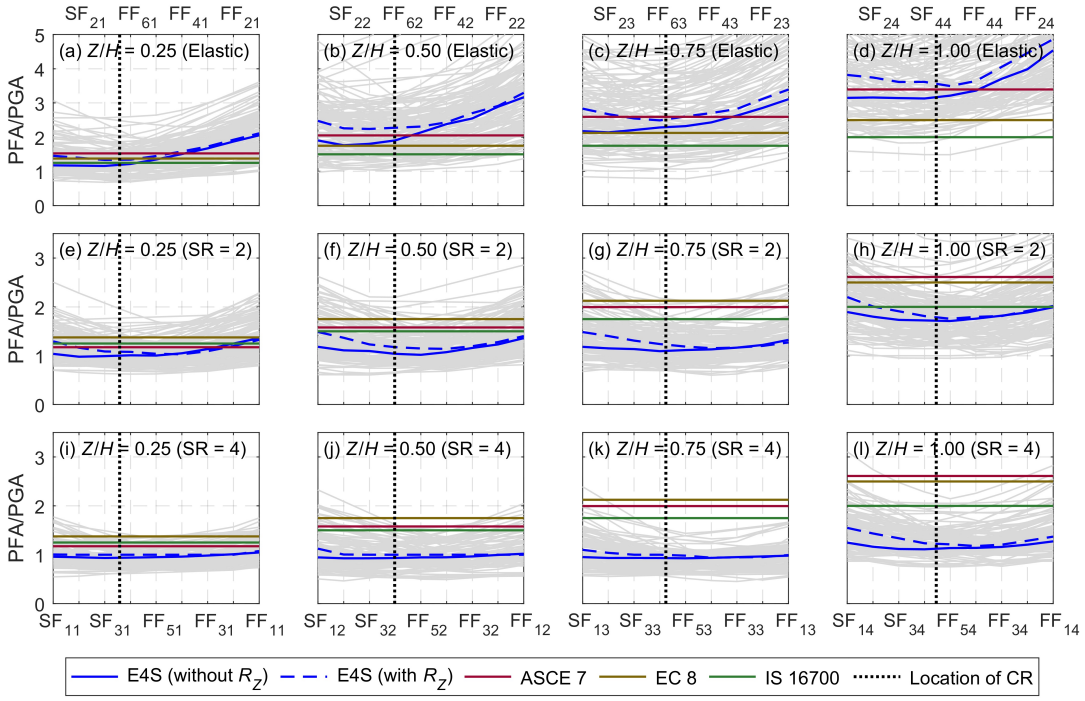

Figure A.13: In-plan distribution of PFA/PGA at different floors of the 'E4S' building.

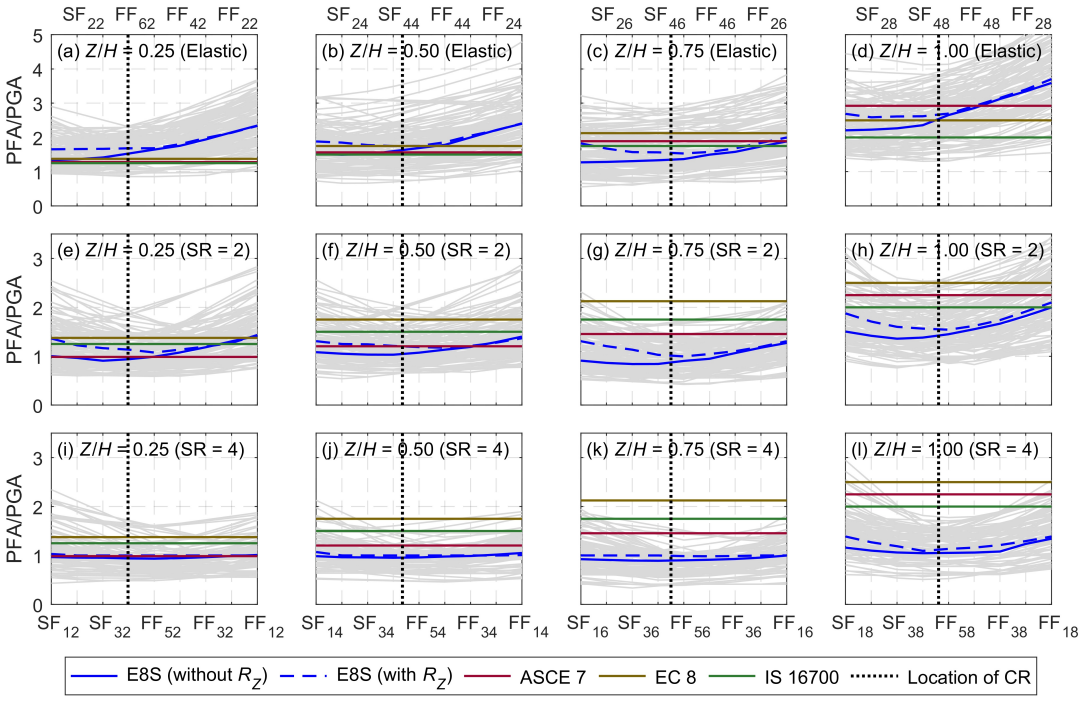

Figure A.14: In-plan distribution of PFA/PGA at different floors of the 'E8S' building.

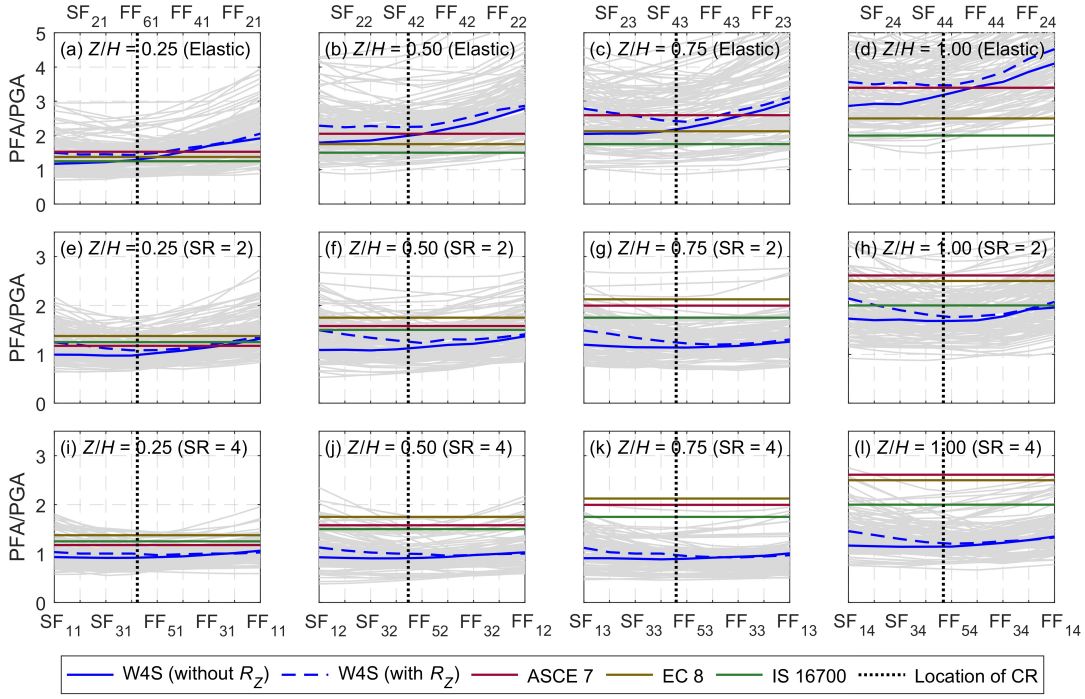

Figure A.15: In-plan distribution of PFA/PGA at different floors of the 'W4S' building.

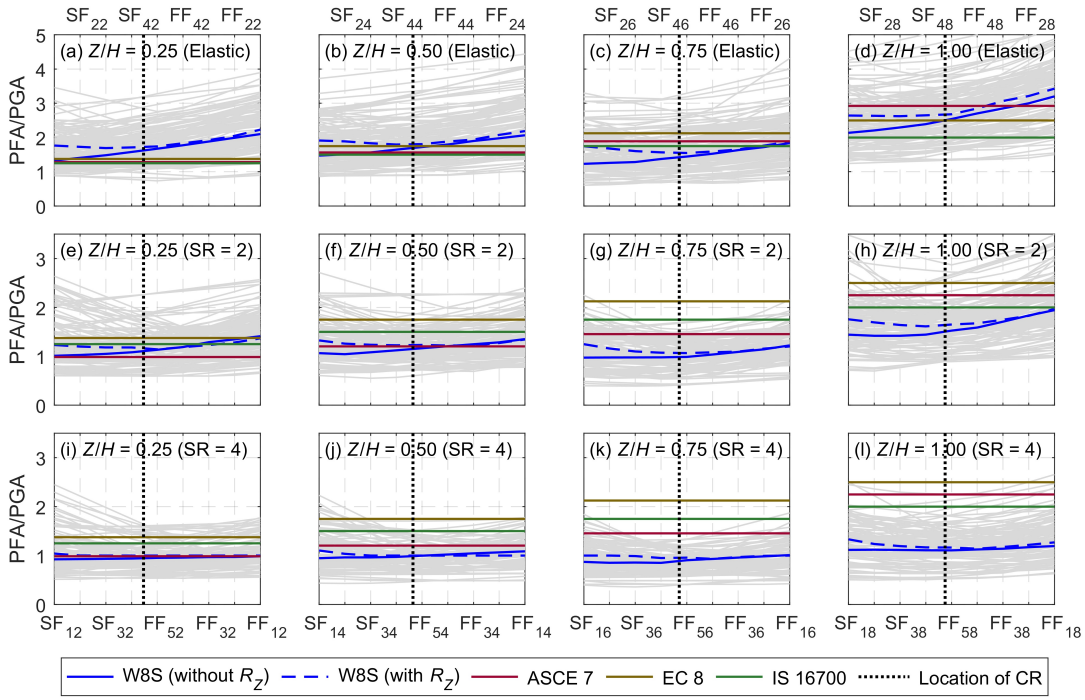

Figure A.16: In-plan distribution of PFA/PGA at different floors of the 'W8S' building.

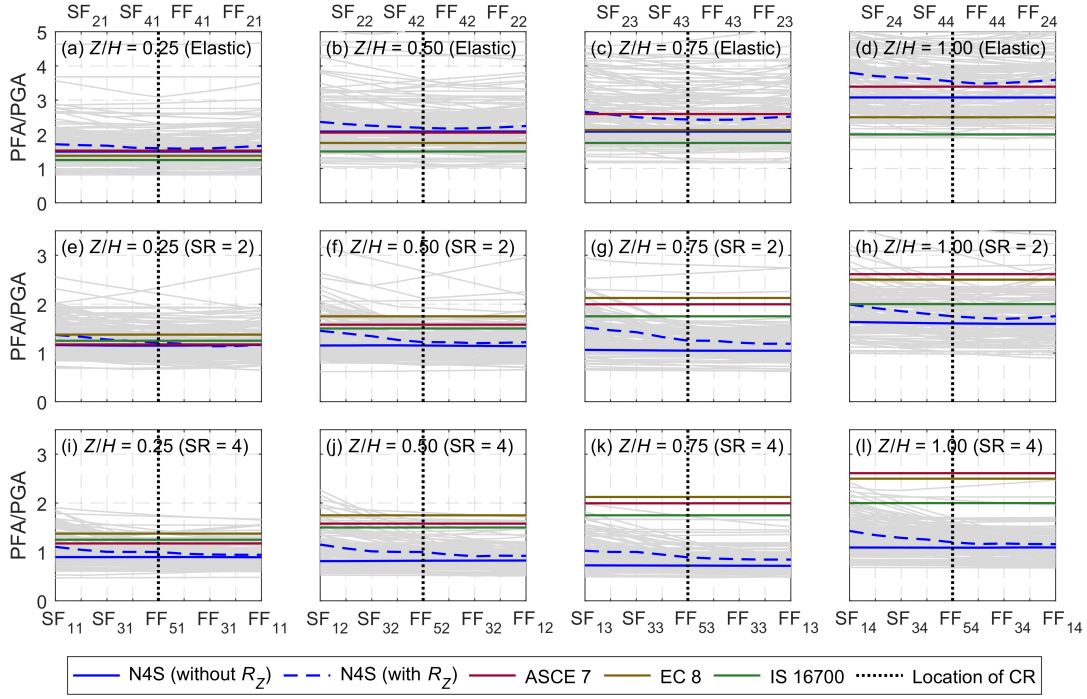

Figure A.17: In-plan distribution of PFA/PGA at different floors of the 'N4S' building.

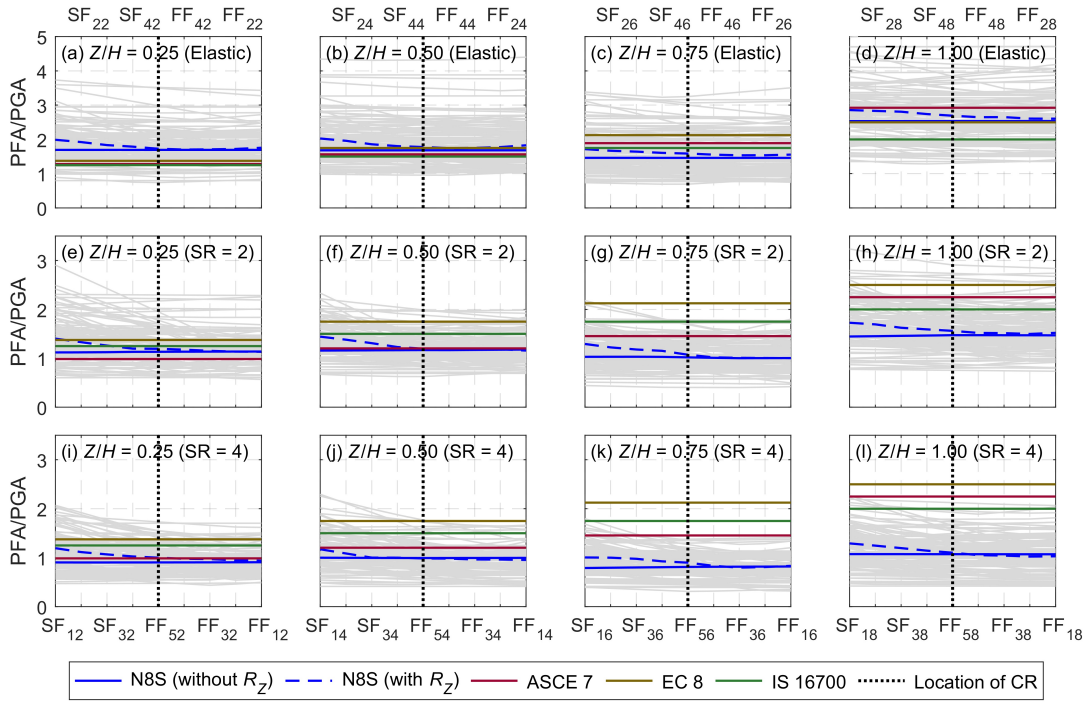

Figure A.18: In-plan distribution of PFA/PGA at different floors of the 'N8S' building.

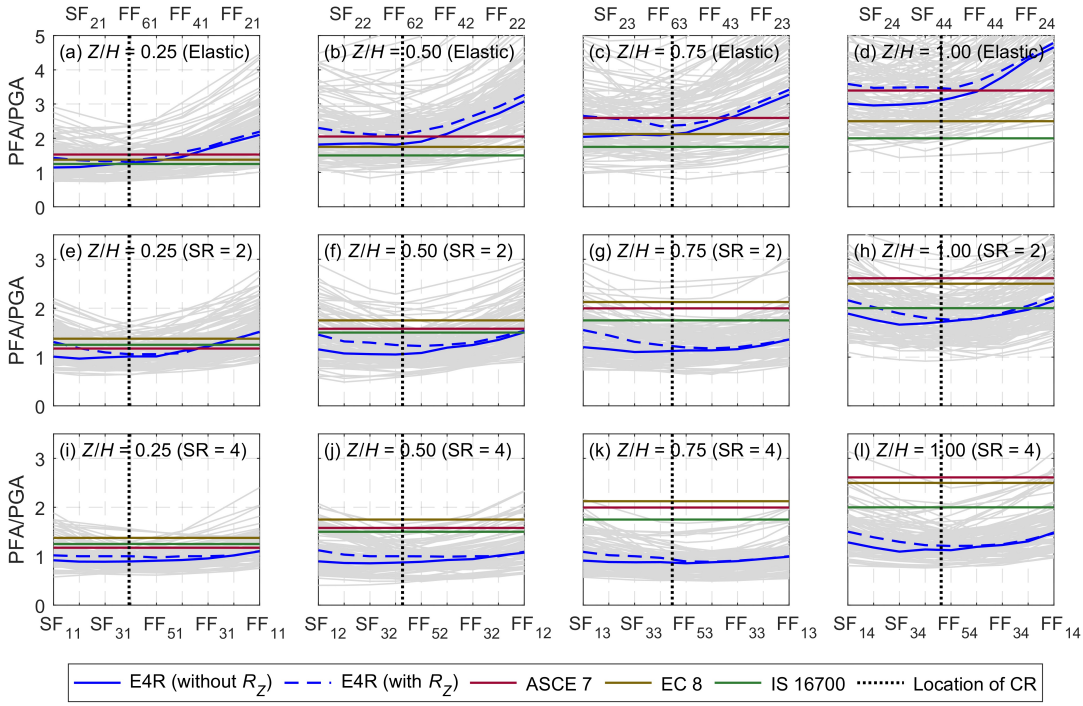

Figure A.19: In-plan distribution of PFA/PGA at different floors of the 'E4R' building.

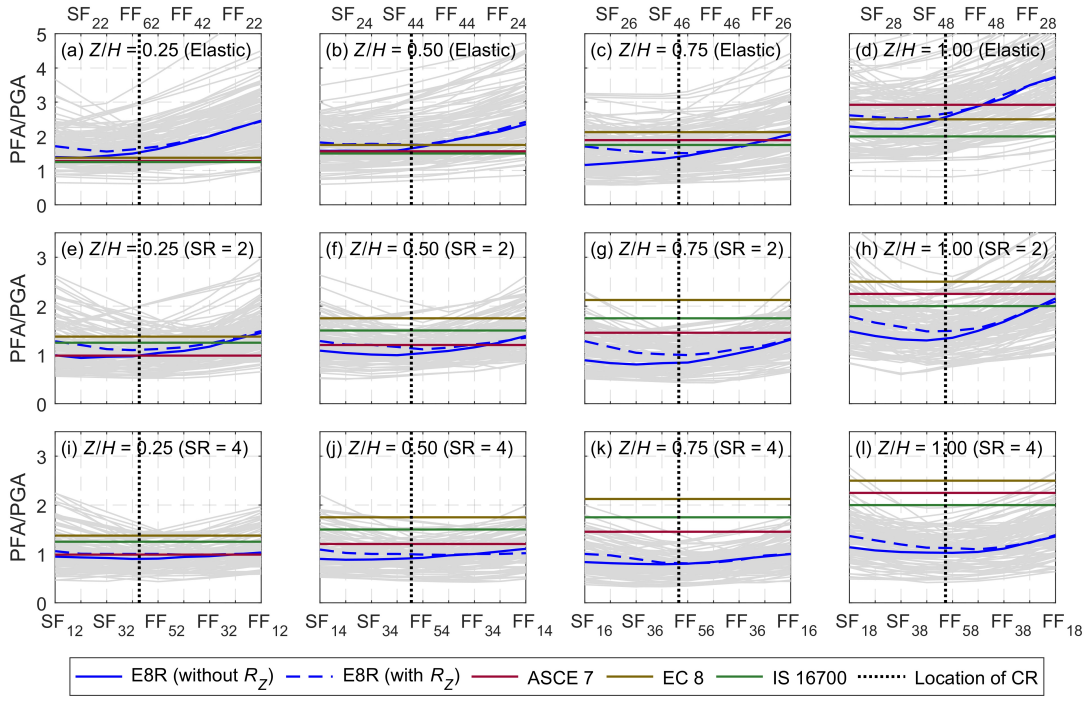

Figure A.20: In-plan distribution of PFA/PGA at different floors of the 'E8R' building.

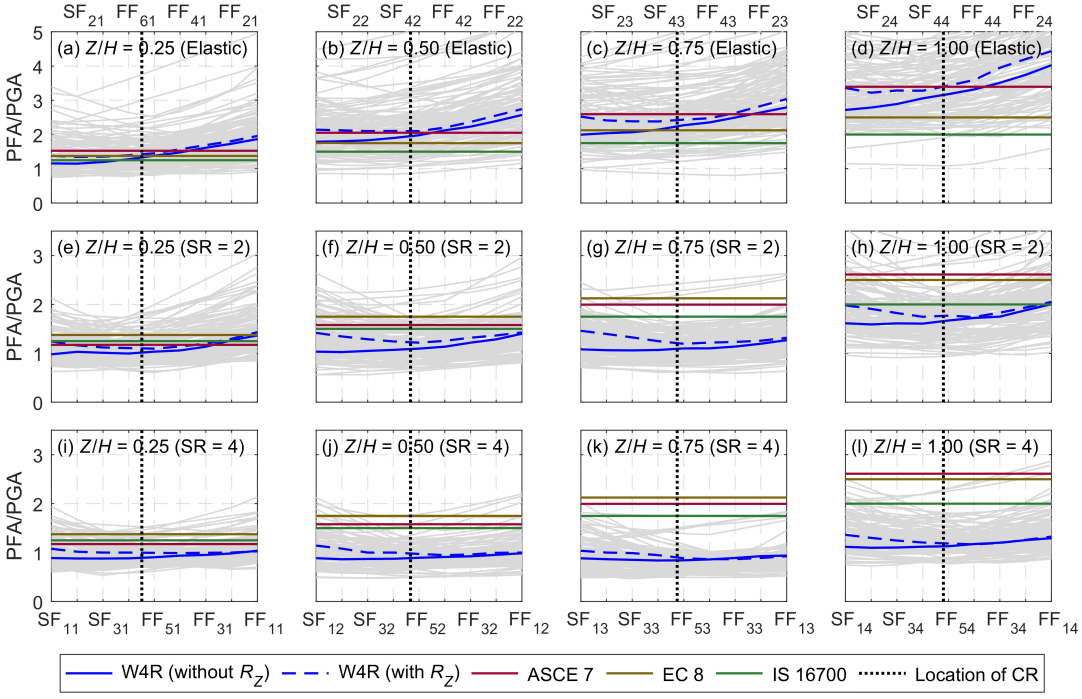

Figure A.21: In-plan distribution of PFA/PGA at different floors of the 'W4R' building.

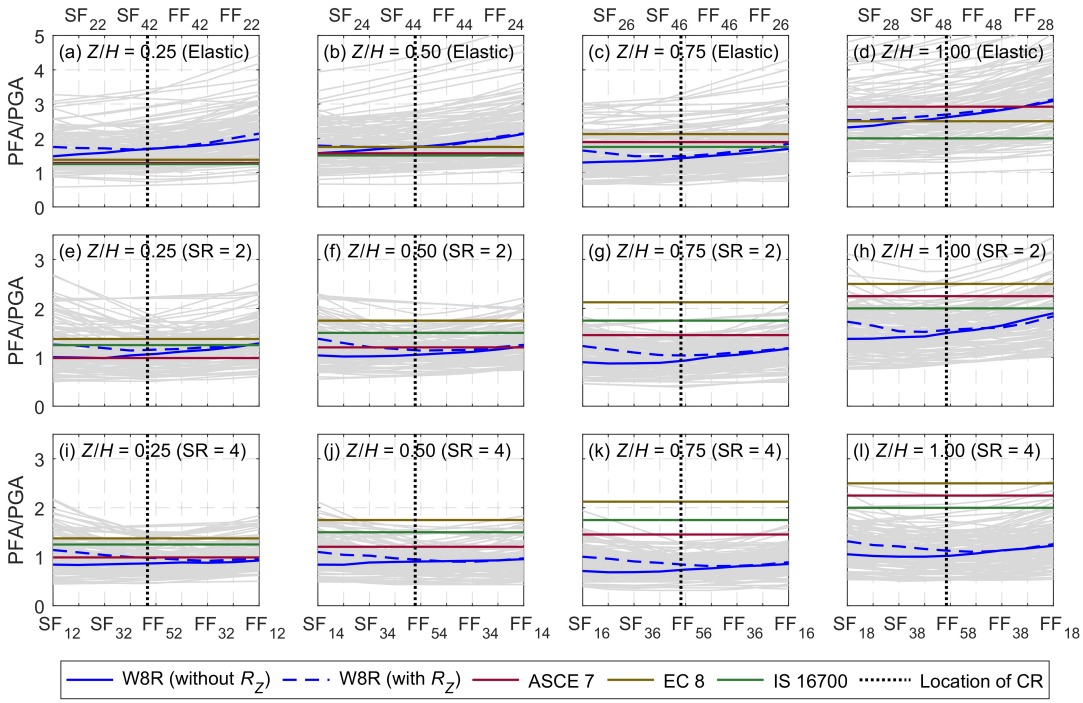

Figure A.22: In-plan distribution of PFA/PGA at different floors of the 'W8R' building.

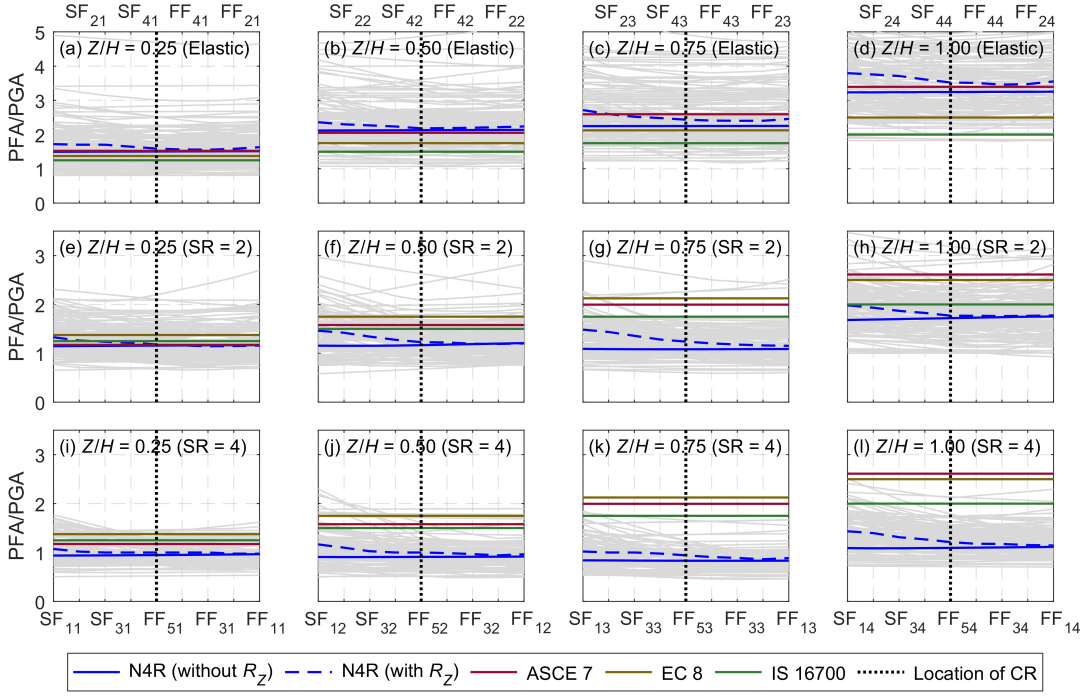

Figure A.23: In-plan distribution of PFA/PGA at different floors of the 'N4R' building.

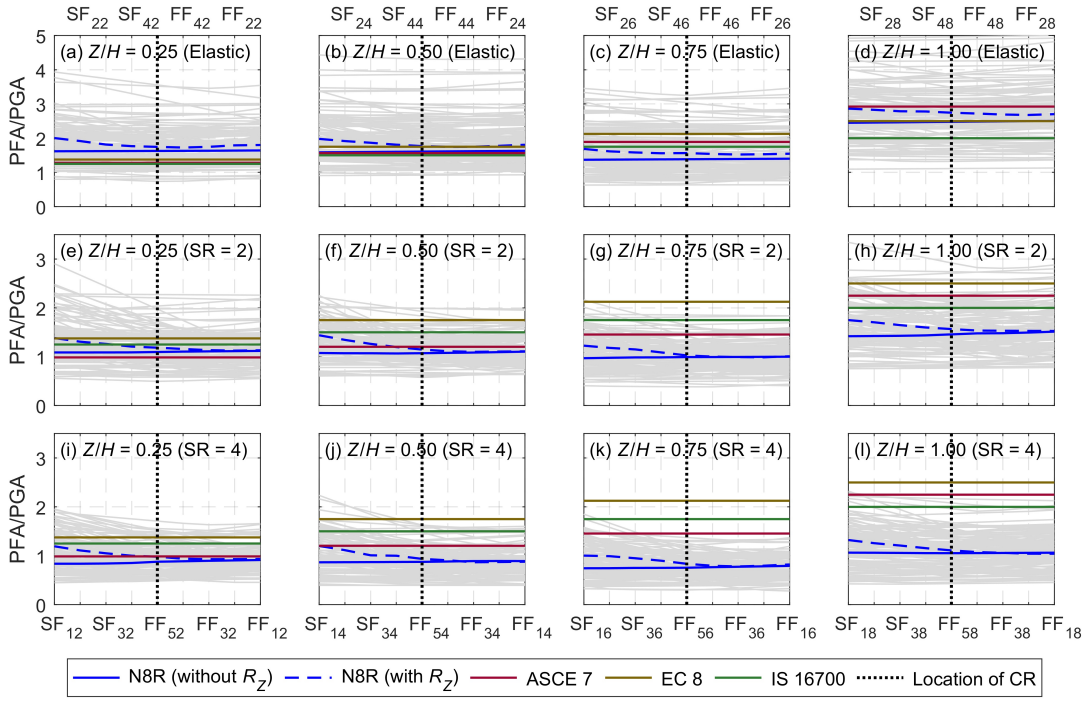

Figure A.24: In-plan distribution of PFA/PGA at different floors of the 'N8R' building.

Appendix B

Floor Response Spectra

B.1 Component amplification factor

Figures B.1–B.18 illustrate the comparison of Component amplification factors (a_p) at the CS, CR, SE, and FE, obtained from bi-directional time history analyses, against the values predicted by code equations [6, 16, 17]. The observed trend follows the same pattern as discussed in Chapter 5.

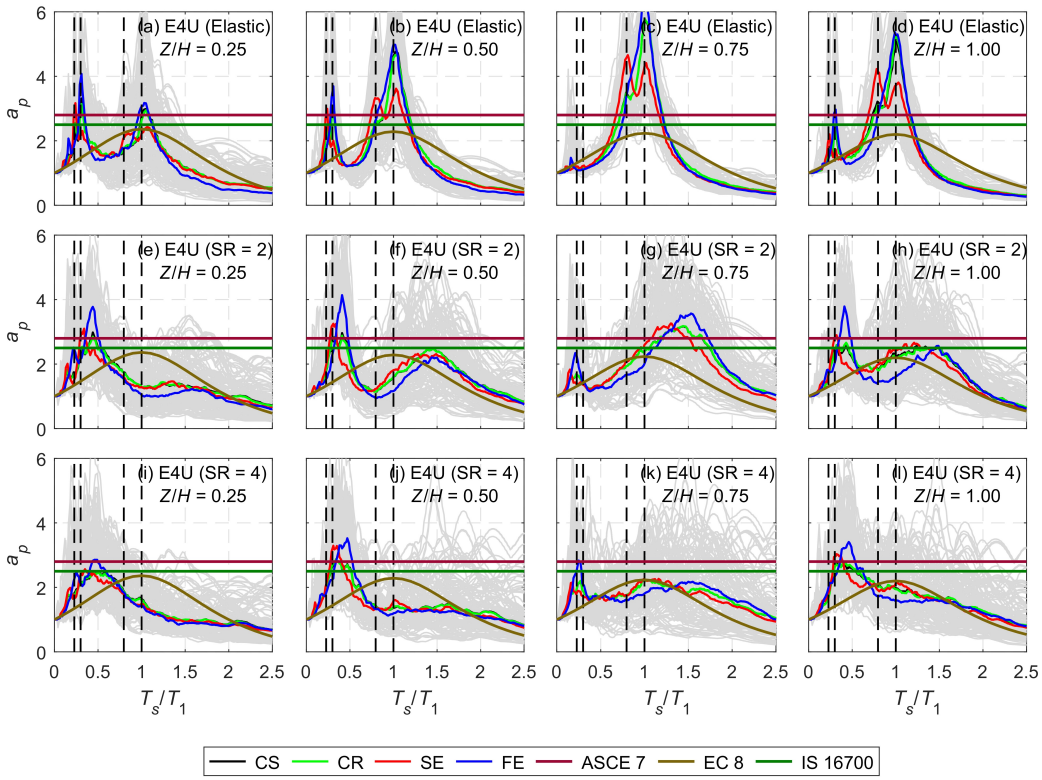

Figure B.1: Component amplification factors for the 'E4U' building obtained using bi-directional time history analyses. Dashed vertical lines indicate the elastic modal periods in the direction under consideration.

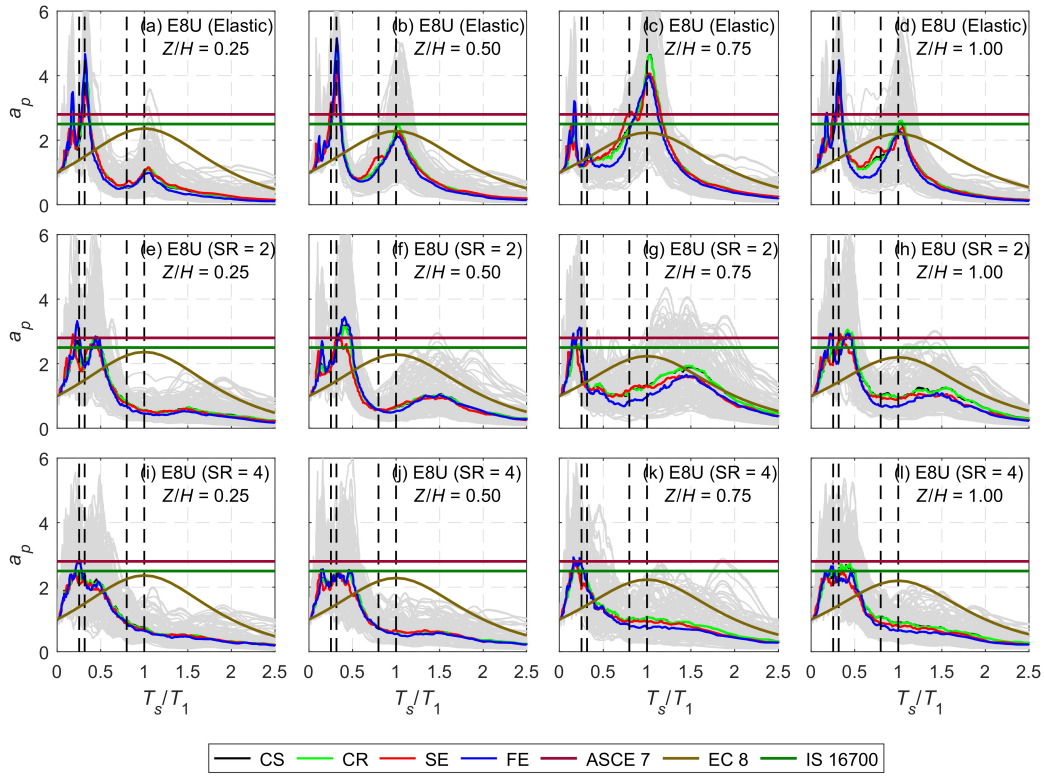

Figure B.2: Component amplification factors for the 'E8U' building obtained using bi-directional time history analyses. Dashed vertical lines indicate the elastic modal periods in the direction under consideration.

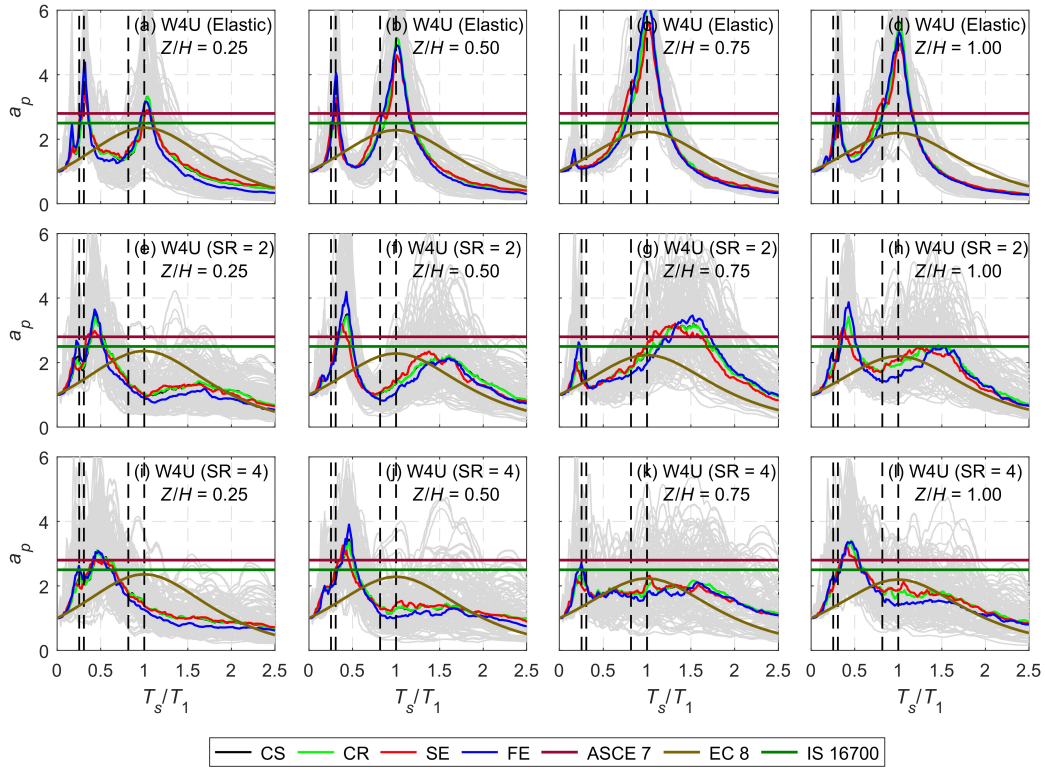

Figure B.3: Component amplification factors for the 'W4U' building obtained using bi-directional time history analyses. Dashed vertical lines indicate the elastic modal periods in the direction under consideration.

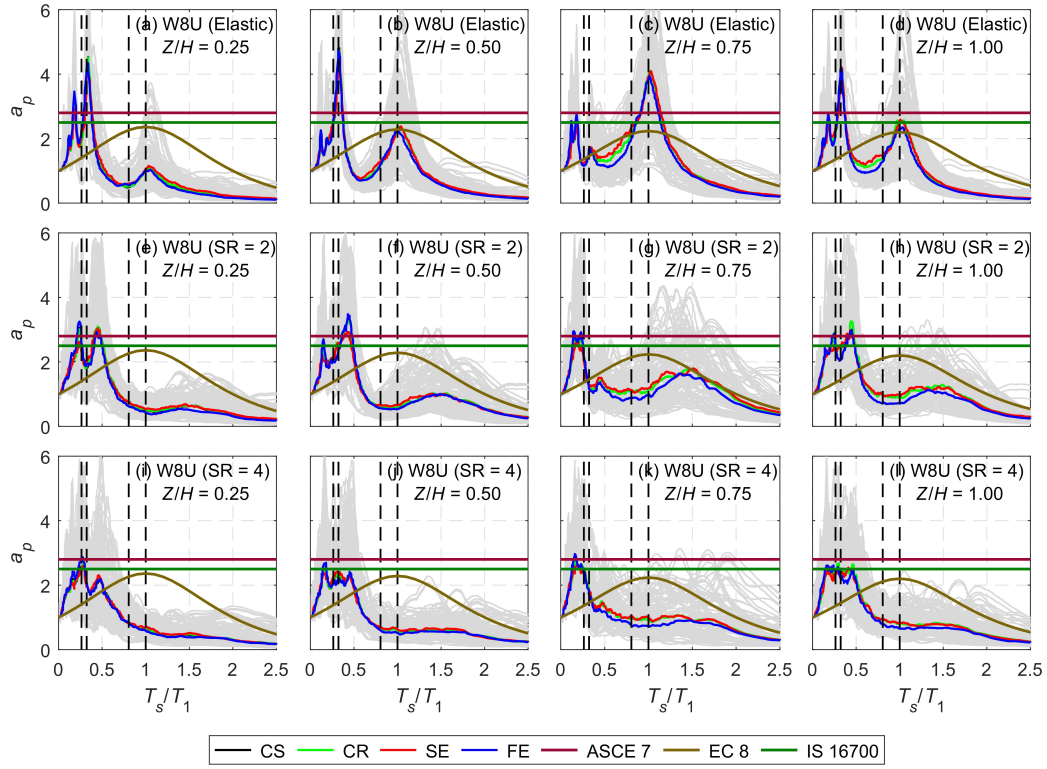

Figure B.4: Component amplification factors for the 'W8U' building obtained using bi-directional time history analyses. Dashed vertical lines indicate the elastic modal periods in the direction under consideration.

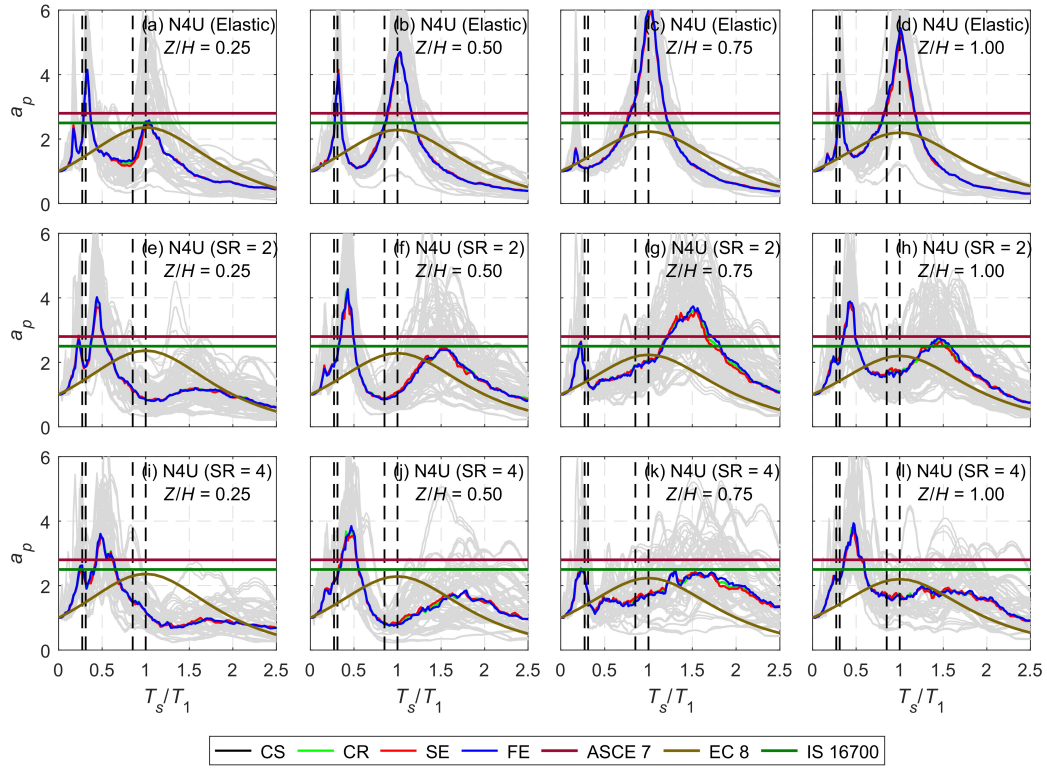

Figure B.5: Component amplification factors for the 'N4U' building obtained using bi-directional time history analyses. Dashed vertical lines indicate the elastic modal periods in the direction under consideration.

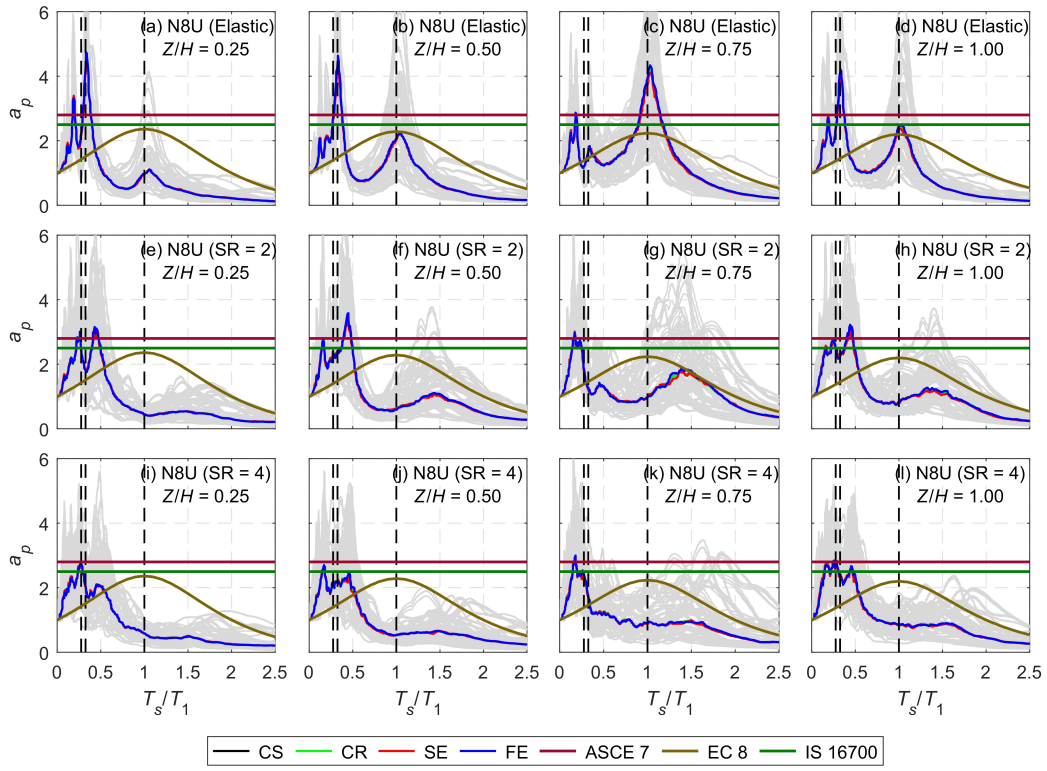

Figure B.6: Component amplification factors for the 'N8U' building obtained using bi-directional time history analyses. Dashed vertical lines indicate the elastic modal periods in the direction under consideration.

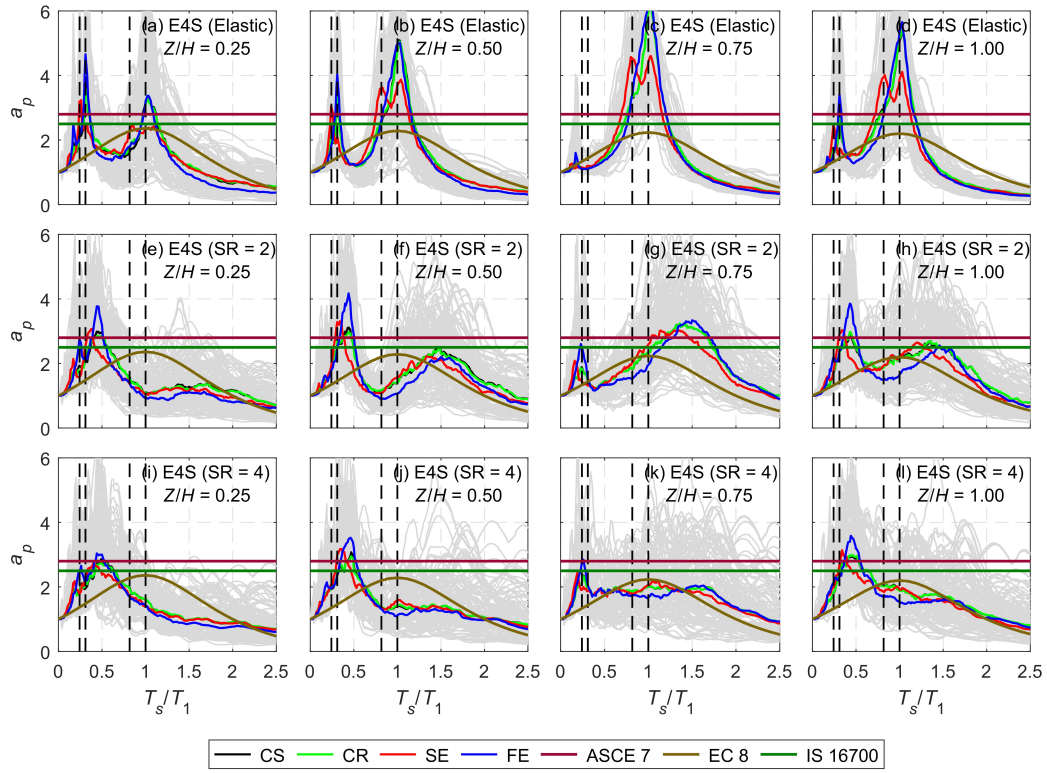

Figure B.7: Component amplification factors for the 'E4S' building obtained using bi-directional time history analyses. Dashed vertical lines indicate the elastic modal periods in the direction under consideration.

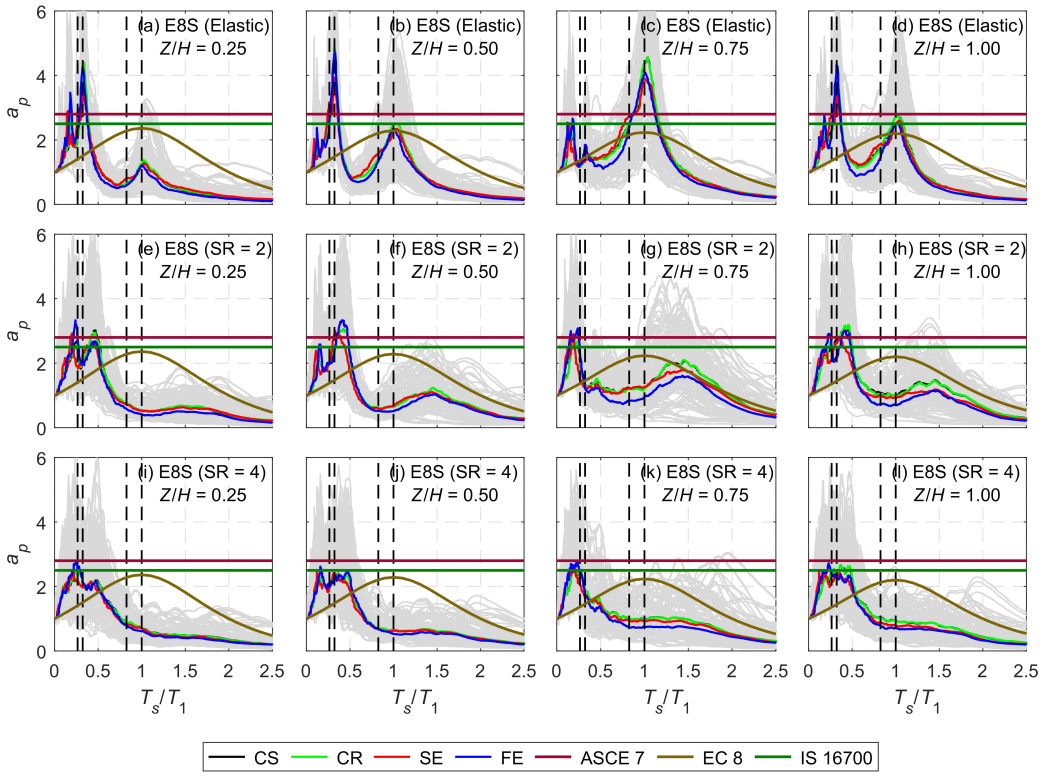

Figure B.8: Component amplification factors for the 'E8S' building obtained using bi-directional time history analyses. Dashed vertical lines indicate the elastic modal periods in the direction under consideration.

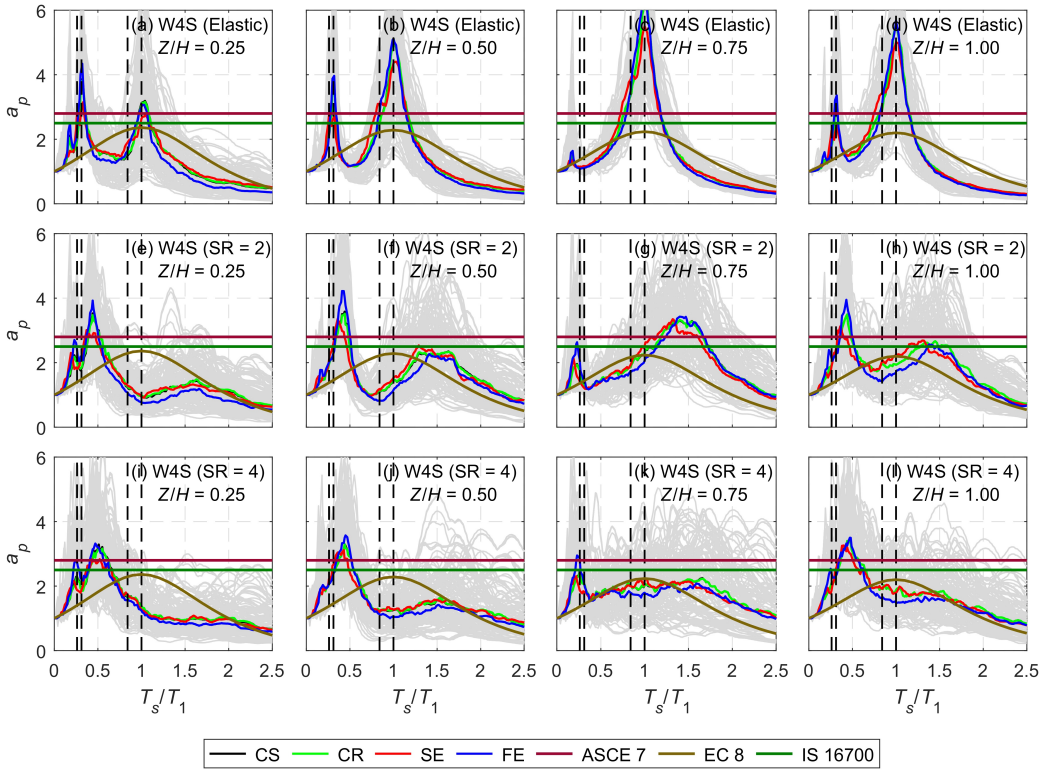

Figure B.9: Component amplification factors for the 'W4S' building obtained using bi-directional time history analyses. Dashed vertical lines indicate the elastic modal periods in the direction under consideration.

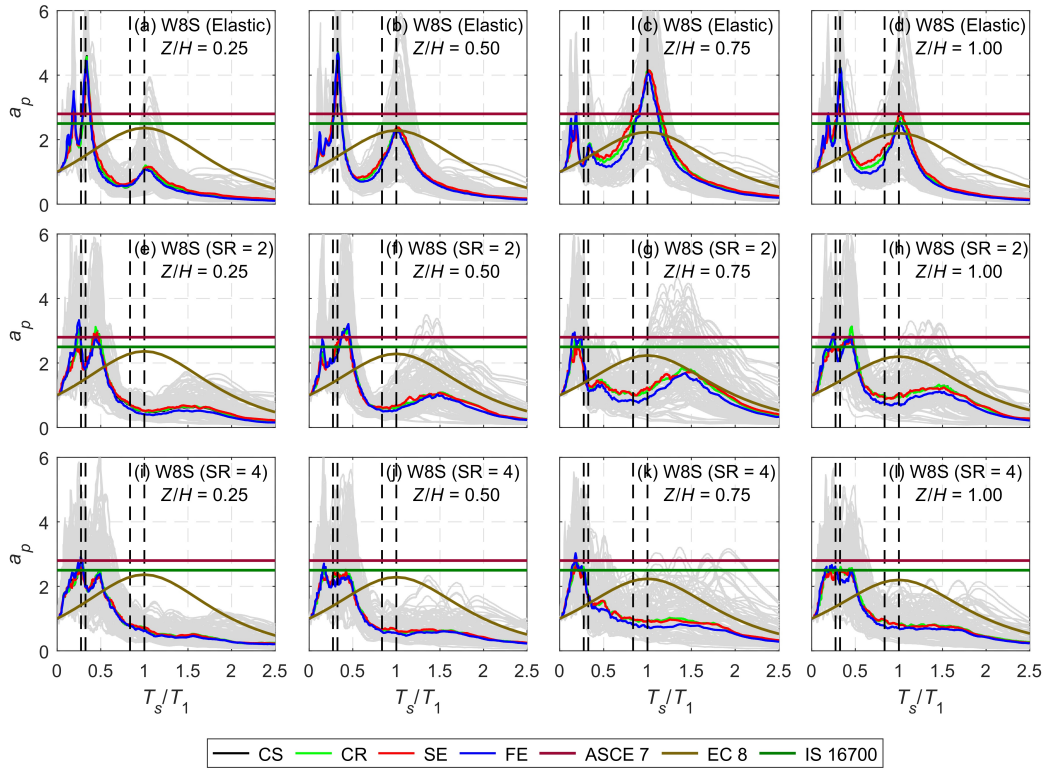

Figure B.10: Component amplification factors for the 'W8S' building obtained using bi-directional time history analyses. Dashed vertical lines indicate the elastic modal periods in the direction under consideration.

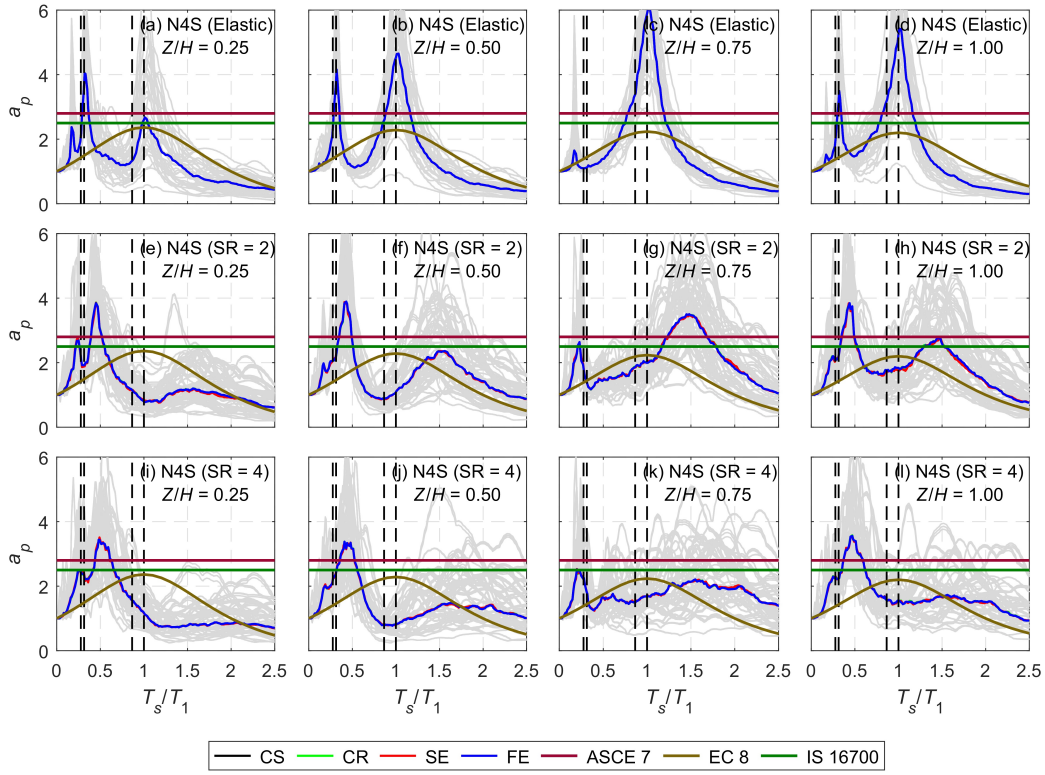

Figure B.11: Component amplification factors for the 'N4S' building obtained using bi-directional time history analyses. Dashed vertical lines indicate the elastic modal periods in the direction under consideration.

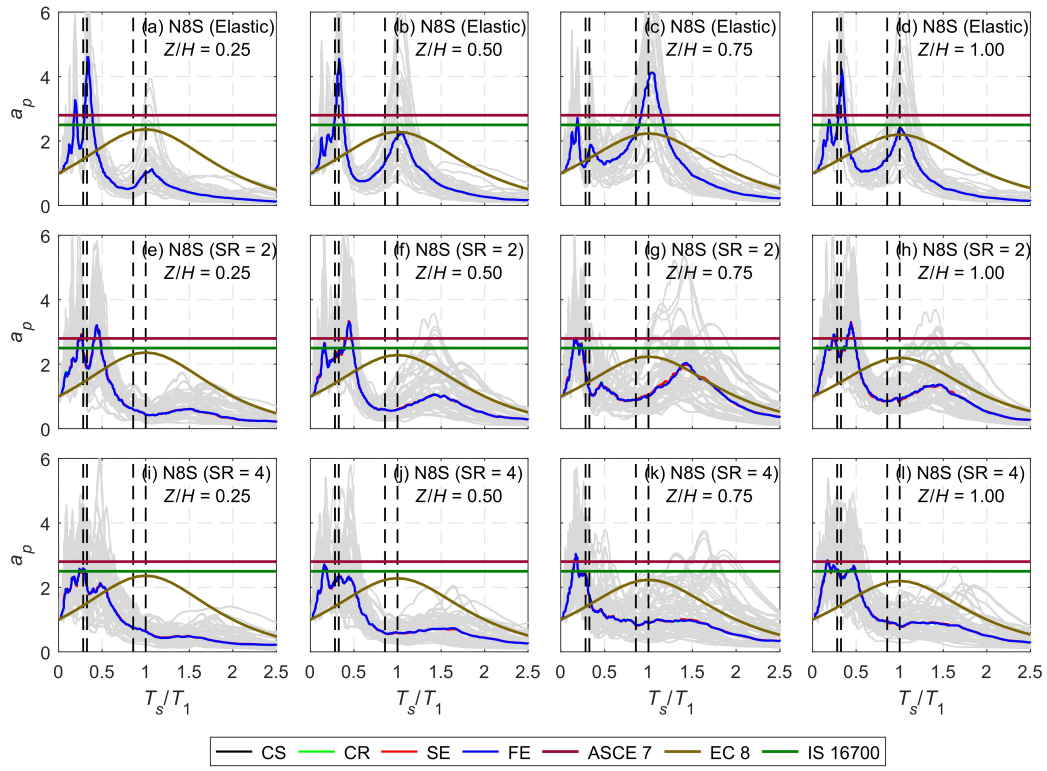

Figure B.12: Component amplification factors for the 'N8S' building obtained using bi-directional time history analyses. Dashed vertical lines indicate the elastic modal periods in the direction under consideration.

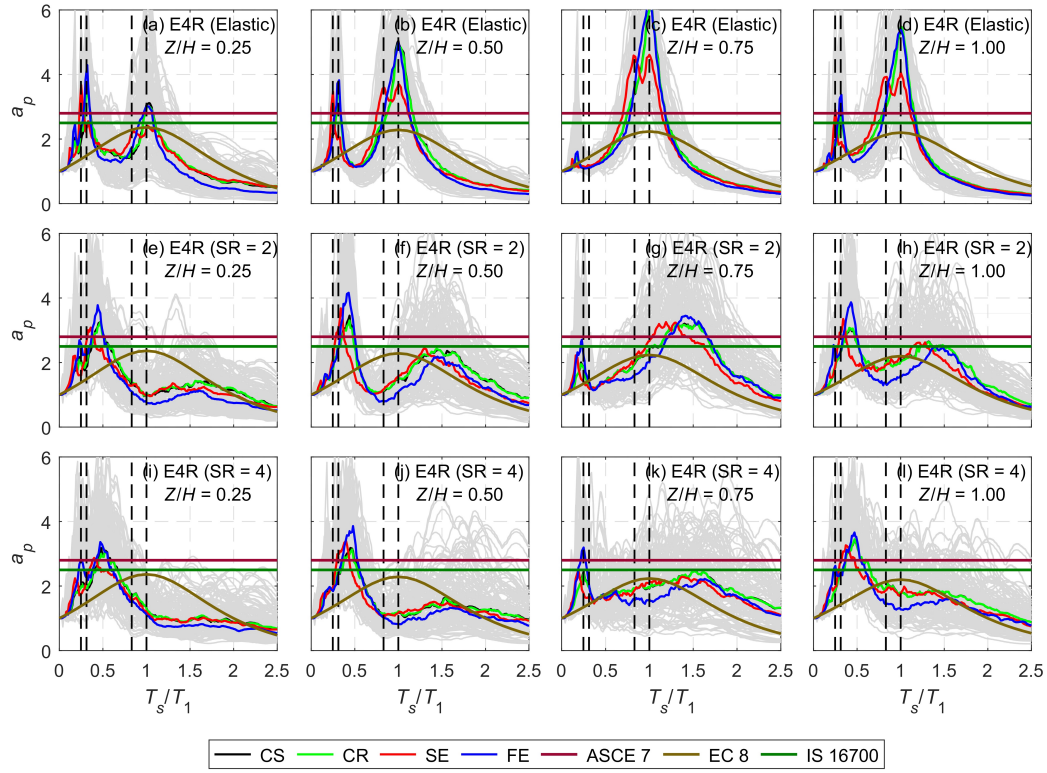

Figure B.13: Component amplification factors for the 'E4R' building obtained using bi-directional time history analyses. Dashed vertical lines indicate the elastic modal periods in the direction under consideration.

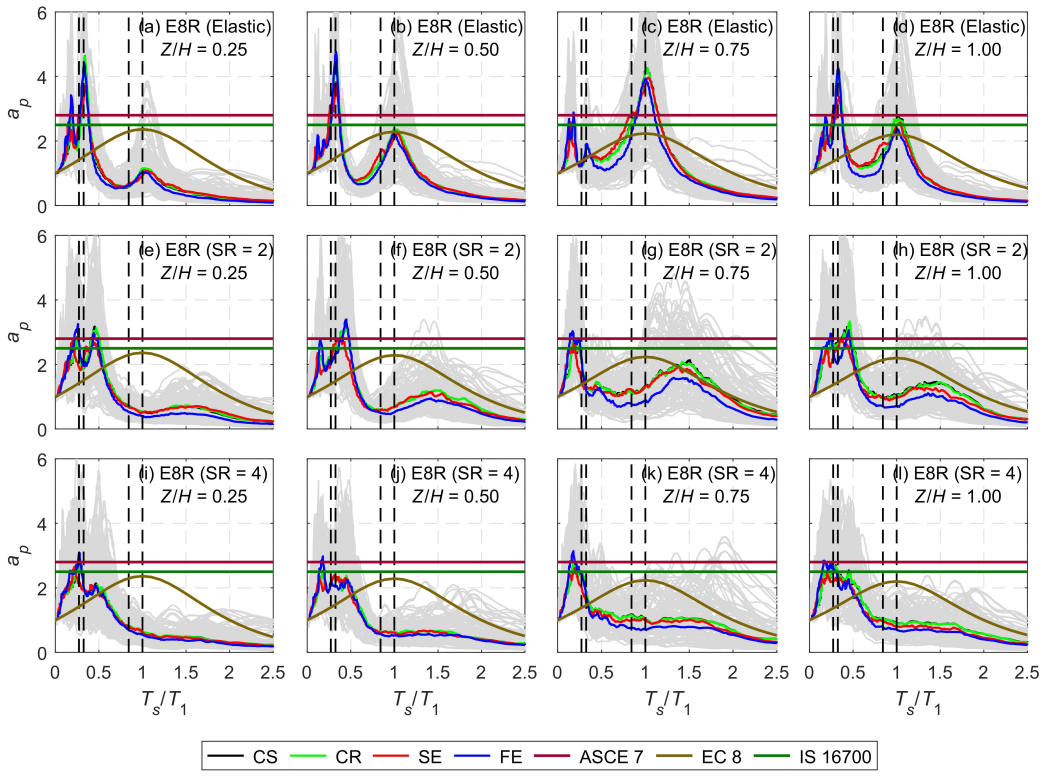

Figure B.14: Component amplification factors for the 'E8R' building obtained using bi-directional time history analyses. Dashed vertical lines indicate the elastic modal periods in the direction under consideration.

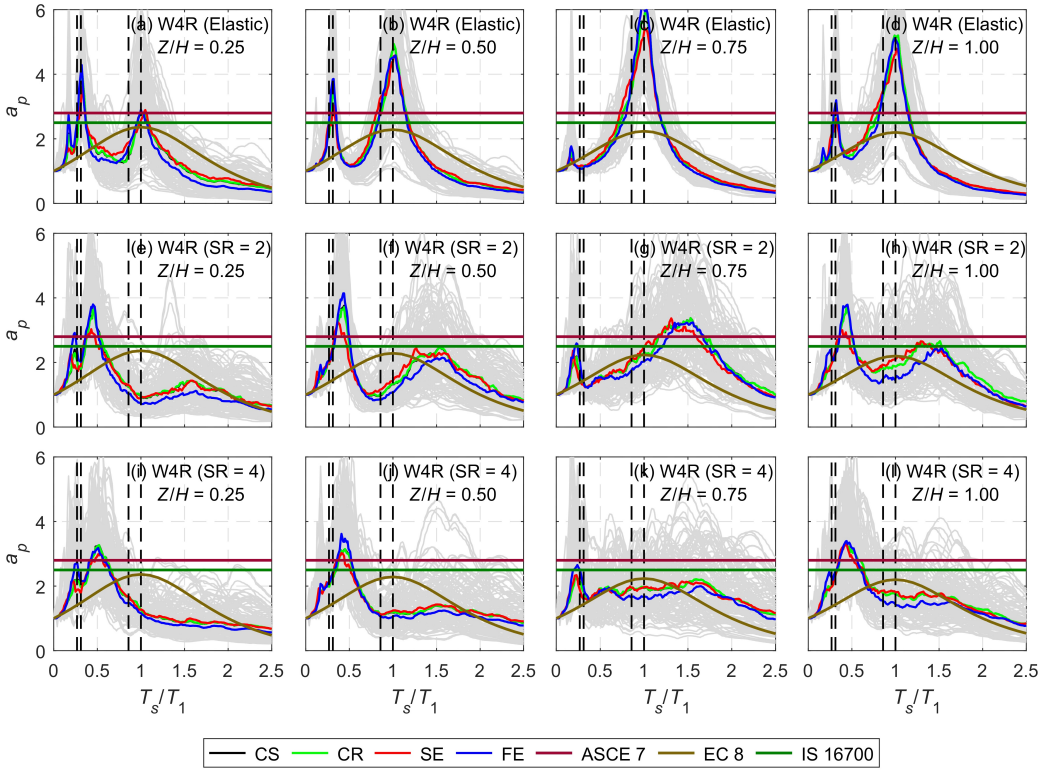

Figure B.15: Component amplification factors for the 'W4R' building obtained using bi-directional time history analyses. Dashed vertical lines indicate the elastic modal periods in the direction under consideration.

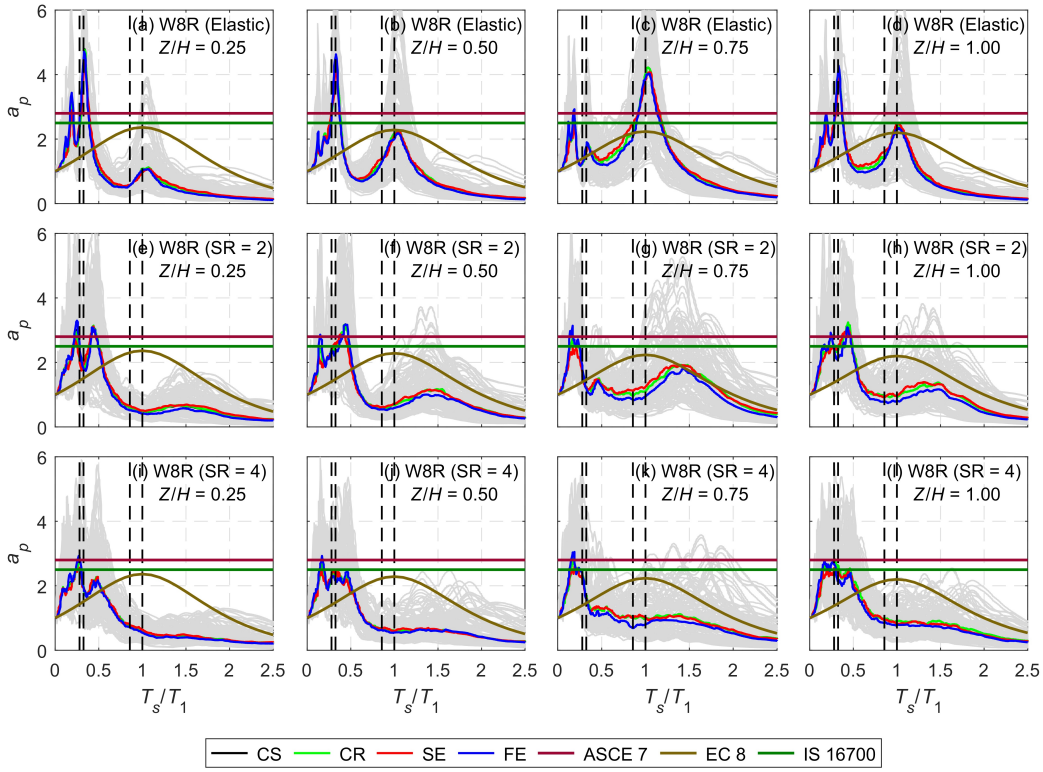

Figure B.16: Component amplification factors for the 'W8R' building obtained using bi-directional time history analyses. Dashed vertical lines indicate the elastic modal periods in the direction under consideration.

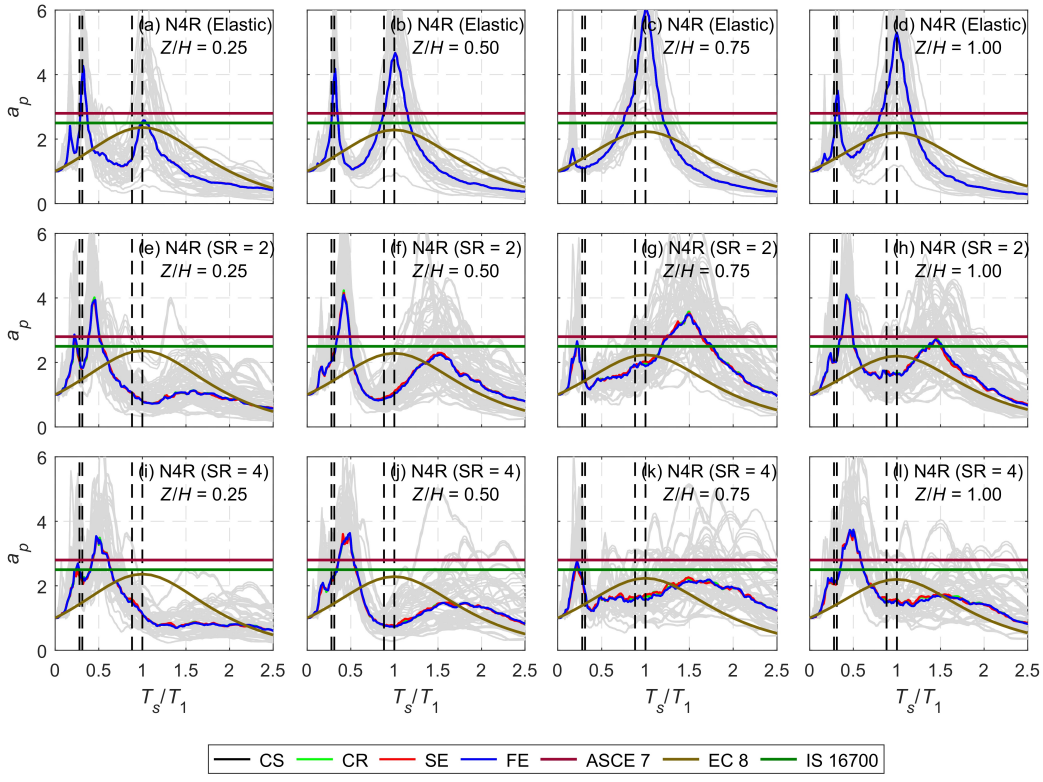

Figure B.17: Component amplification factors for the 'N4R' building obtained using bi-directional time history analyses. Dashed vertical lines indicate the elastic modal periods in the direction under consideration.

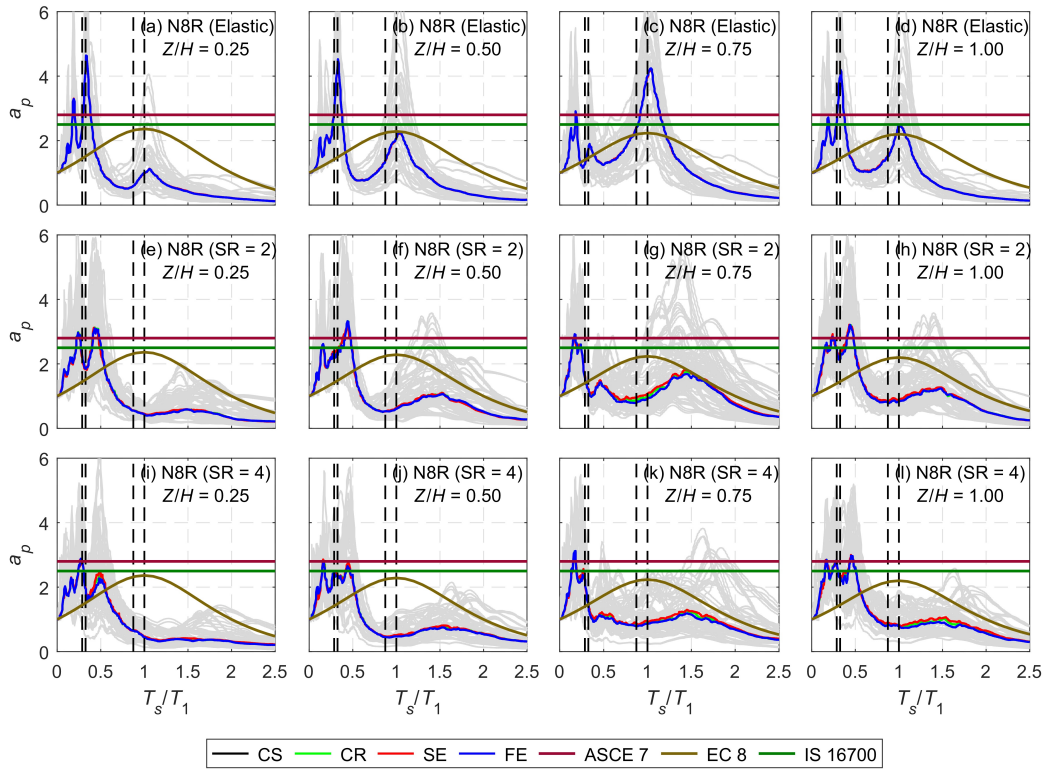

Figure B.18: Component amplification factors for the 'N8R' building obtained using bi-directional time history analyses. Dashed vertical lines indicate the elastic modal periods in the direction under consideration.

B.2 Total amplification factor

Figures B.19–B.36 illustrate the comparison of Total amplification factors (a_t) at the CS, CR, SE, and FE, obtained from bi-directional time history analyses, against the values predicted by code equations [6, 16, 17]. The observed trend follows the same pattern as discussed in Chapter 5.

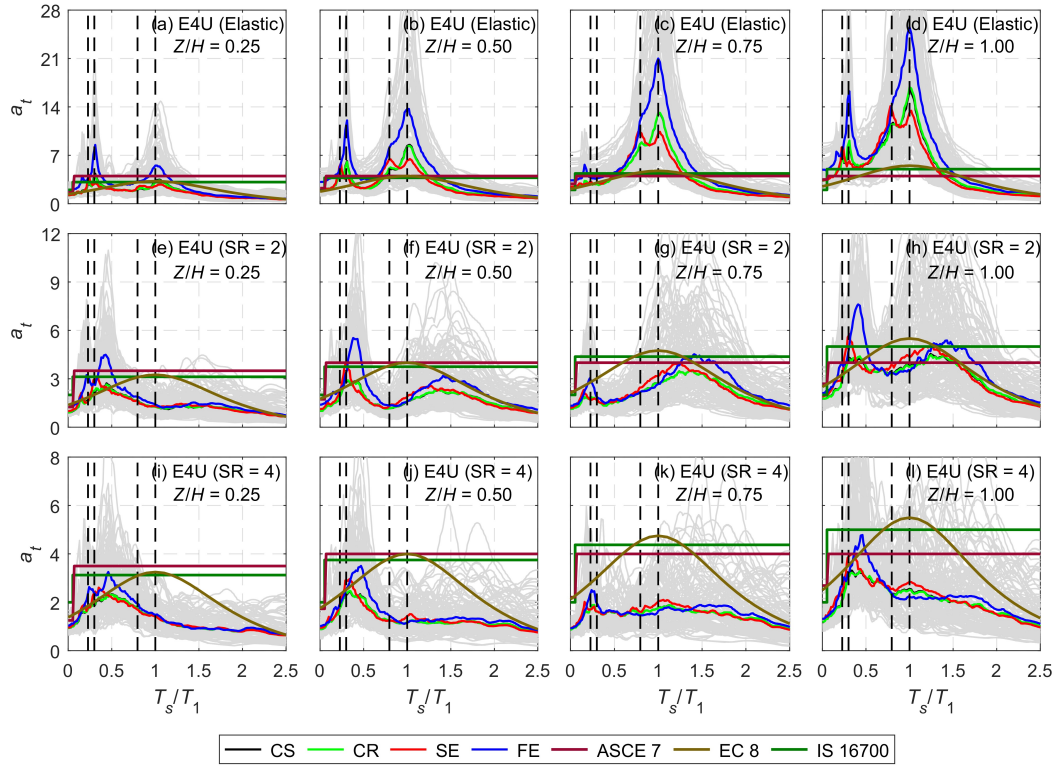

Figure B.19: Total amplification factors for the 'E4U' building obtained using bi-directional time history analyses. Dashed vertical lines indicate the elastic modal periods in the direction under consideration.

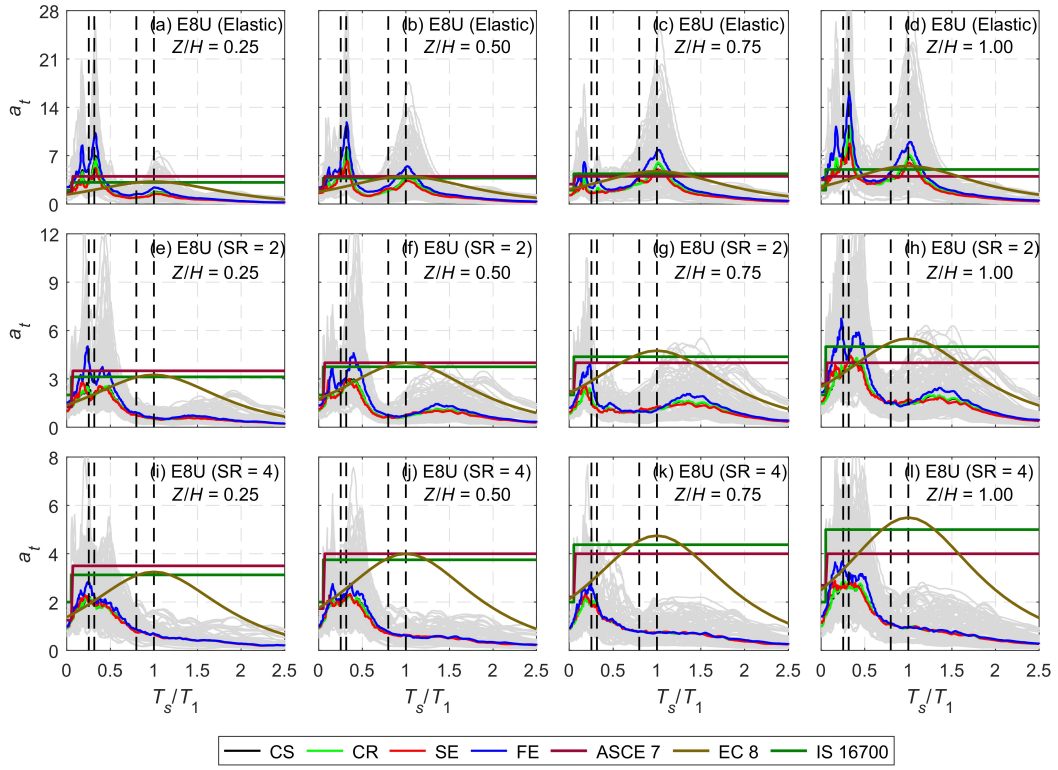

Figure B.20: Total amplification factors for the 'E8U' building obtained using bi-directional time history analyses. Dashed vertical lines indicate the elastic modal periods in the direction under consideration.

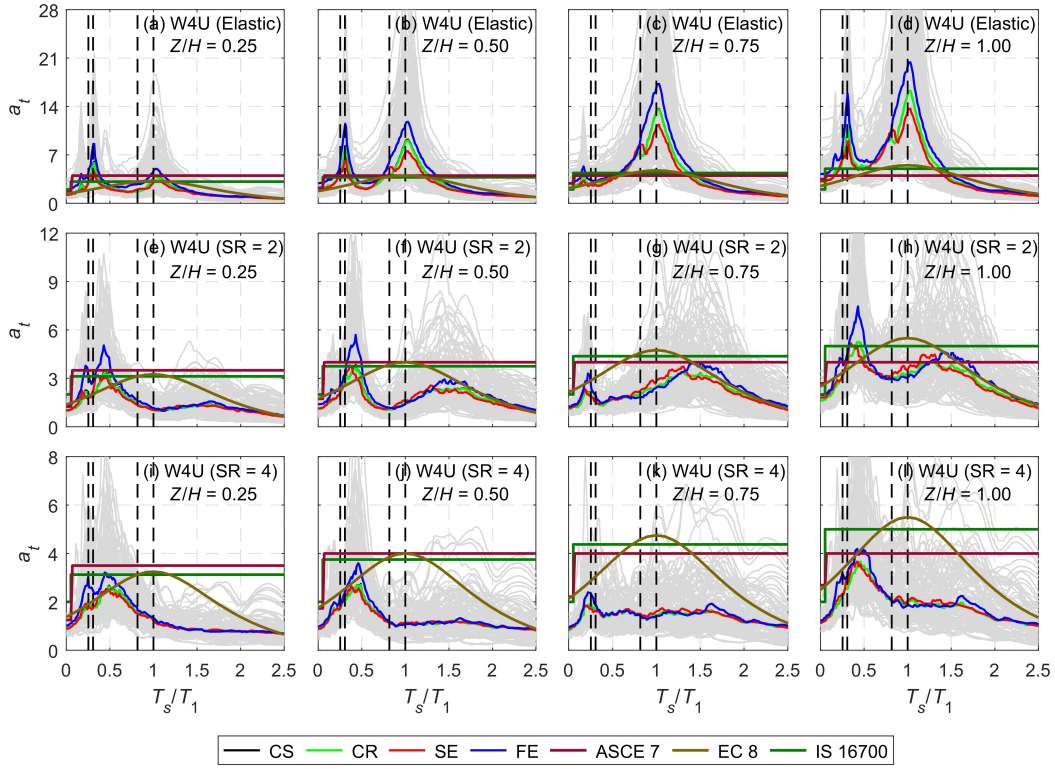

Figure B.21: Total amplification factors for the 'W4U' building obtained using bi-directional time history analyses. Dashed vertical lines indicate the elastic modal periods in the direction under consideration.

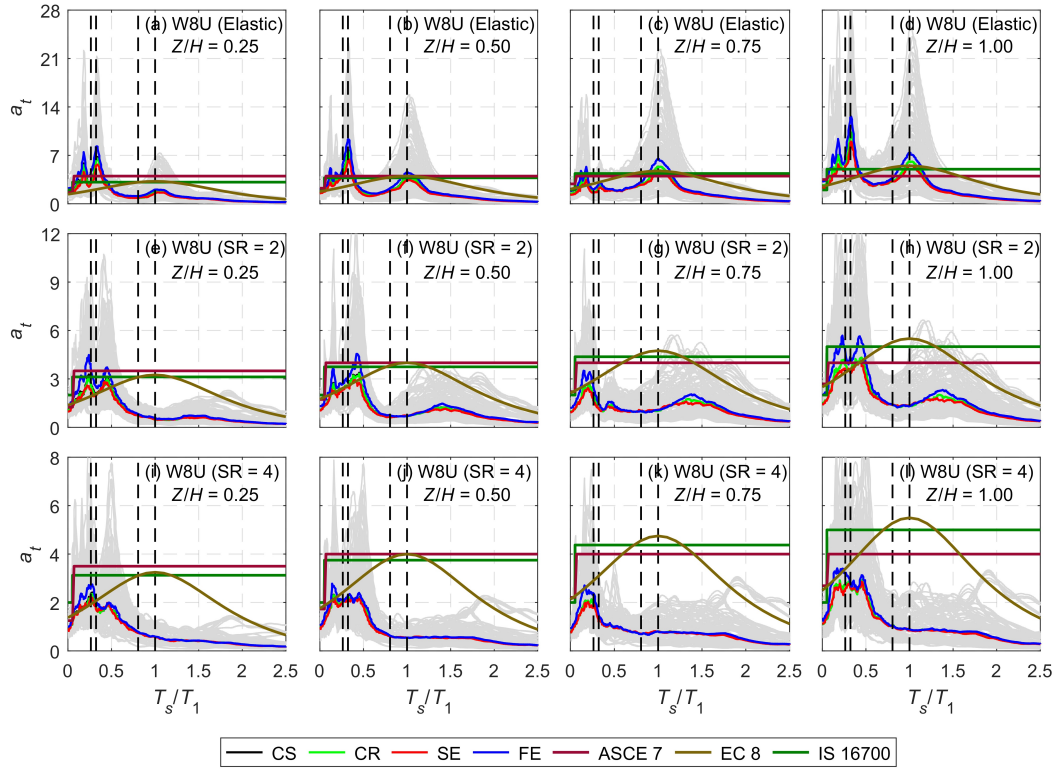

Figure B.22: Total amplification factors for the 'W8U' building obtained using bi-directional time history analyses. Dashed vertical lines indicate the elastic modal periods in the direction under consideration.

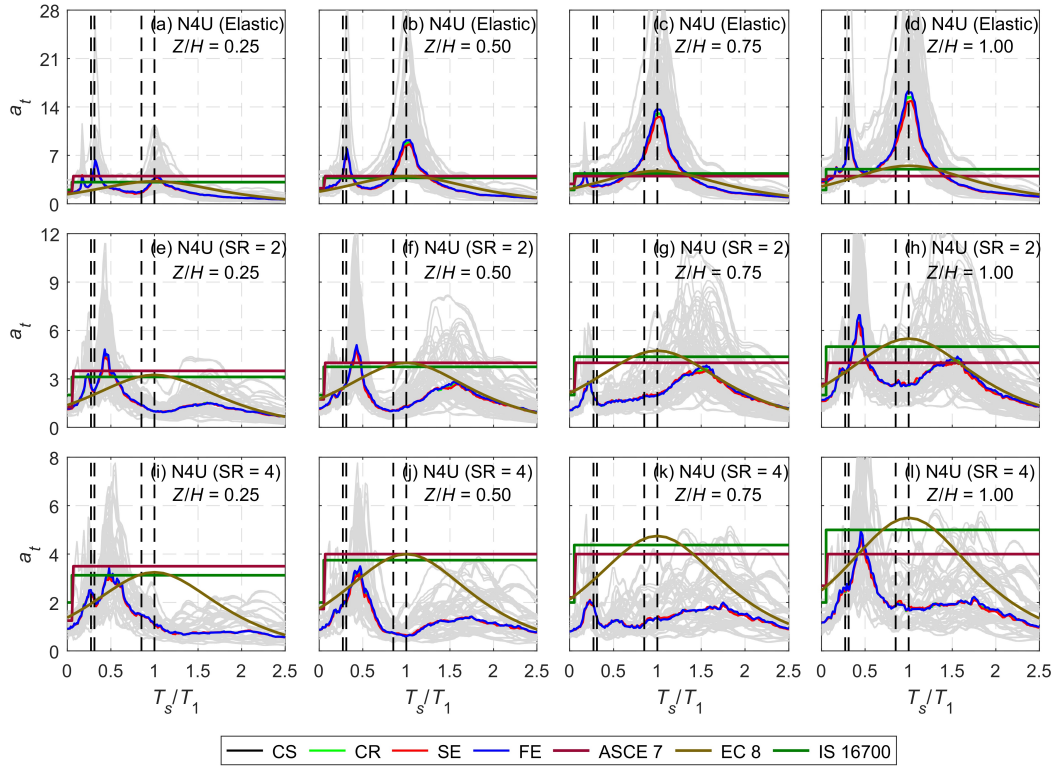

Figure B.23: Total amplification factors for the 'N4U' building obtained using bi-directional time history analyses. Dashed vertical lines indicate the elastic modal periods in the direction under consideration.

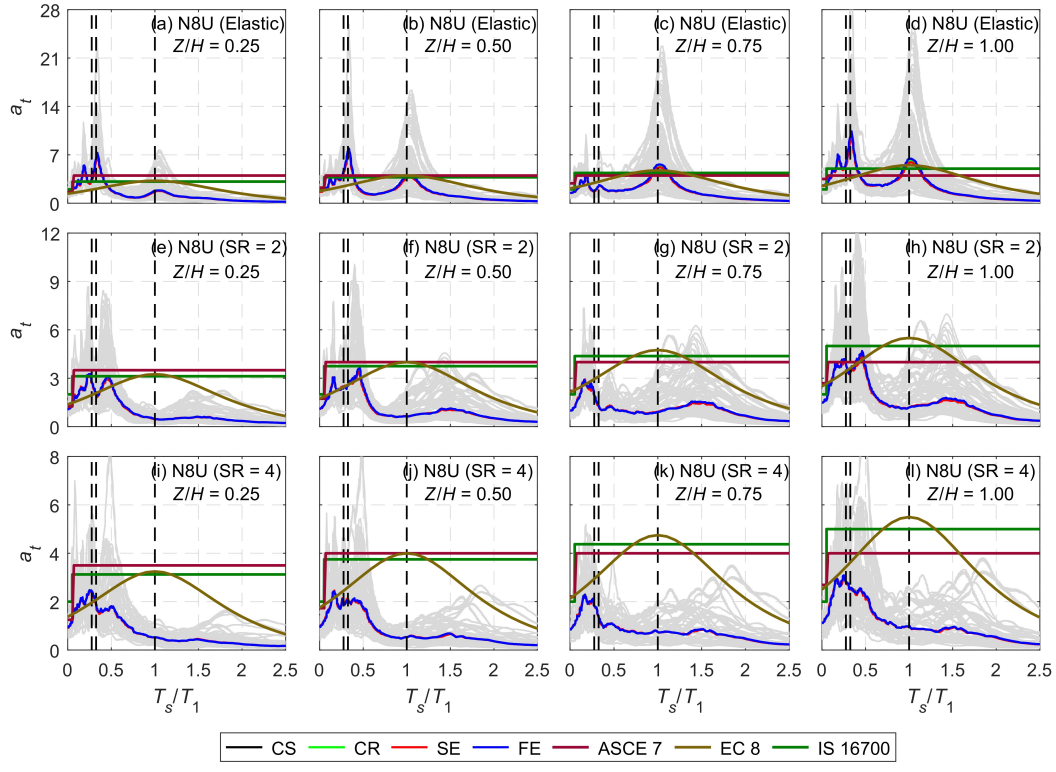

Figure B.24: Total amplification factors for the 'N8U' building obtained using bi-directional time history analyses. Dashed vertical lines indicate the elastic modal periods in the direction under consideration.

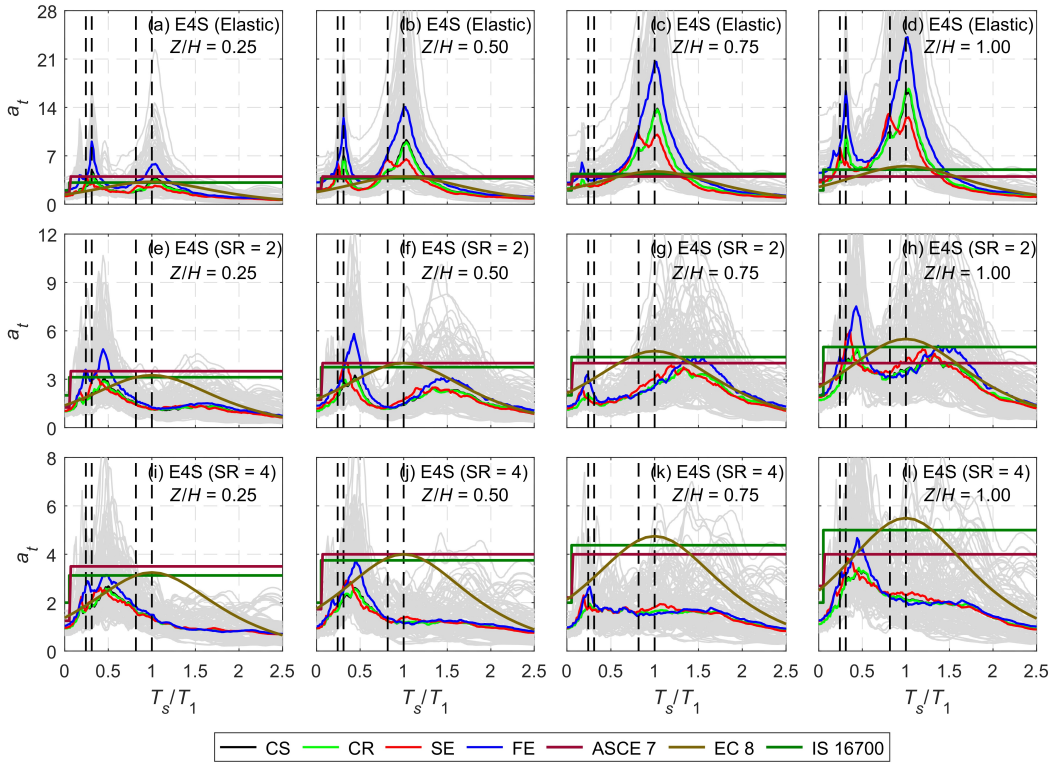

Figure B.25: Total amplification factors for the 'E4S' building obtained using bi-directional time history analyses. Dashed vertical lines indicate the elastic modal periods in the direction under consideration.

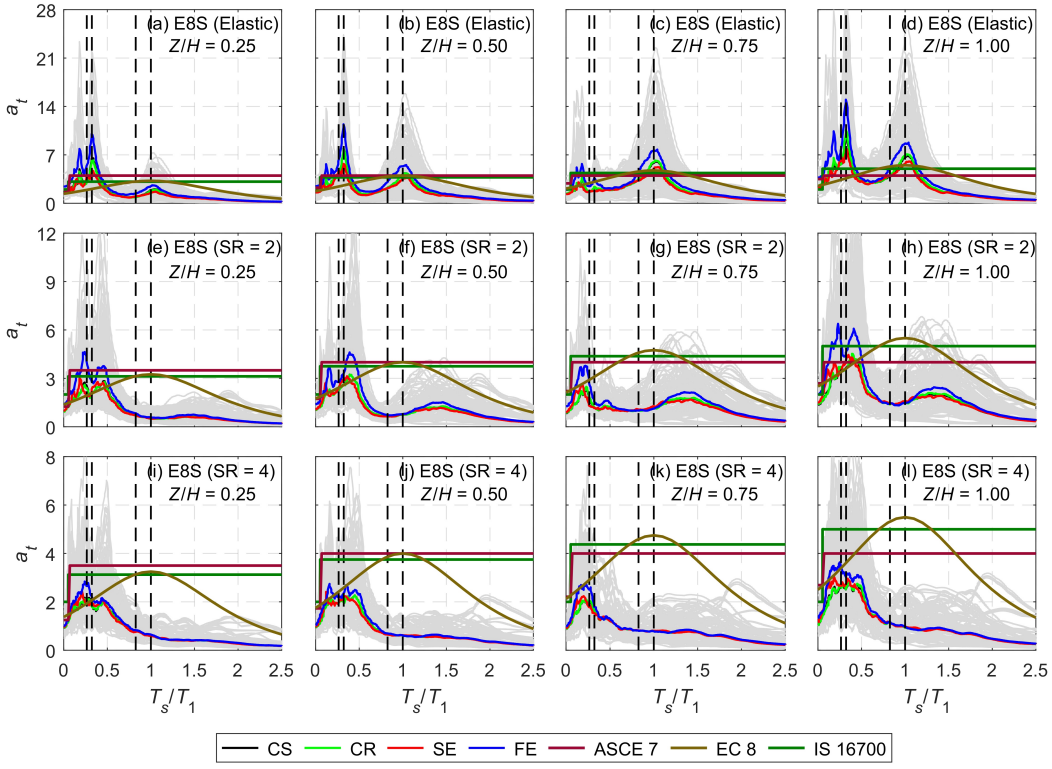

Figure B.26: Total amplification factors for the 'E8S' building obtained using bi-directional time history analyses. Dashed vertical lines indicate the elastic modal periods in the direction under consideration.

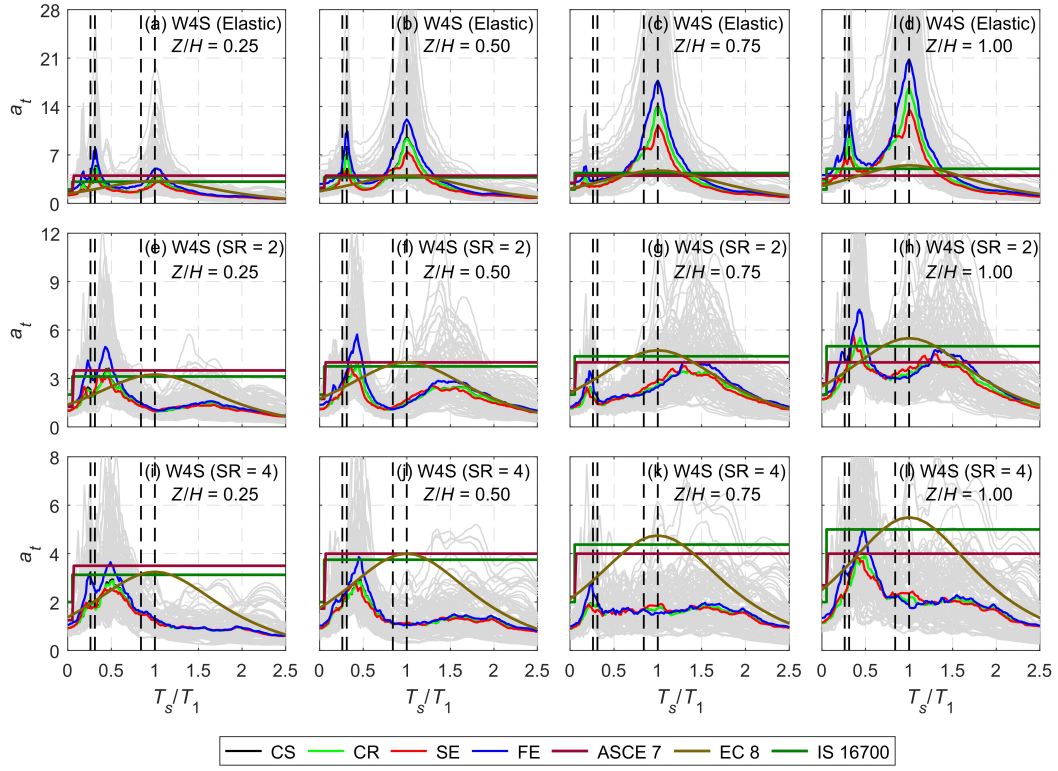

Figure B.27: Total amplification factors for the 'W4S' building obtained using bi-directional time history analyses. Dashed vertical lines indicate the elastic modal periods in the direction under consideration.

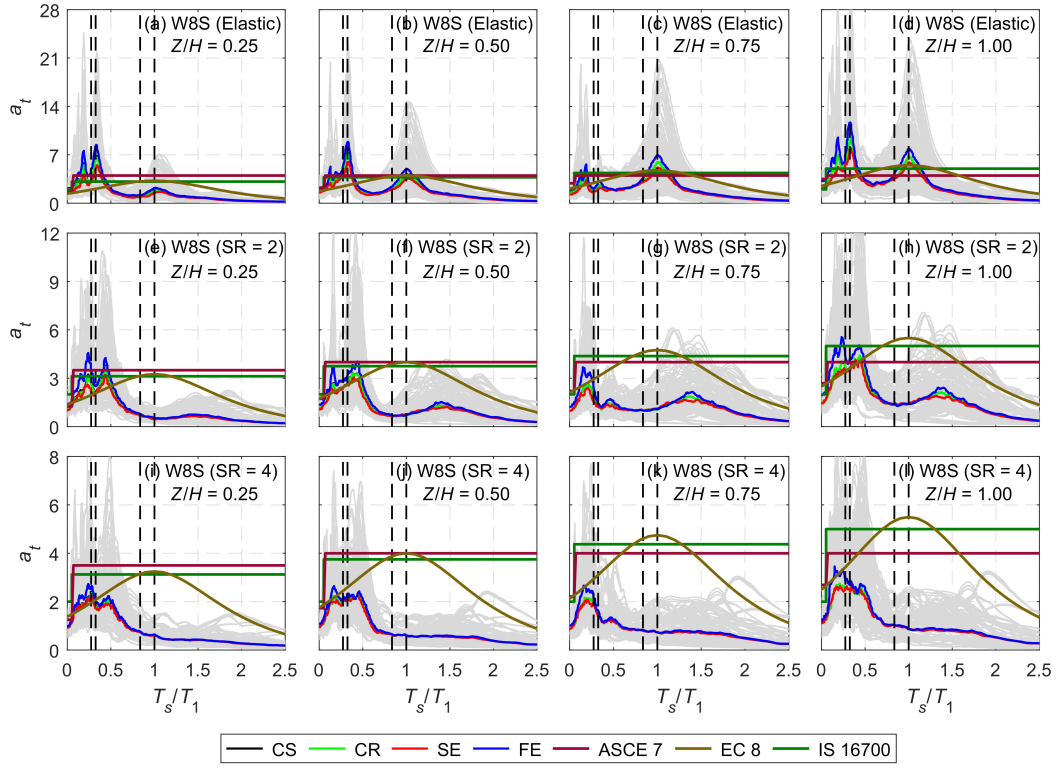

Figure B.28: Total amplification factors for the 'W8S' building obtained using bi-directional time history analyses. Dashed vertical lines indicate the elastic modal periods in the direction under consideration.

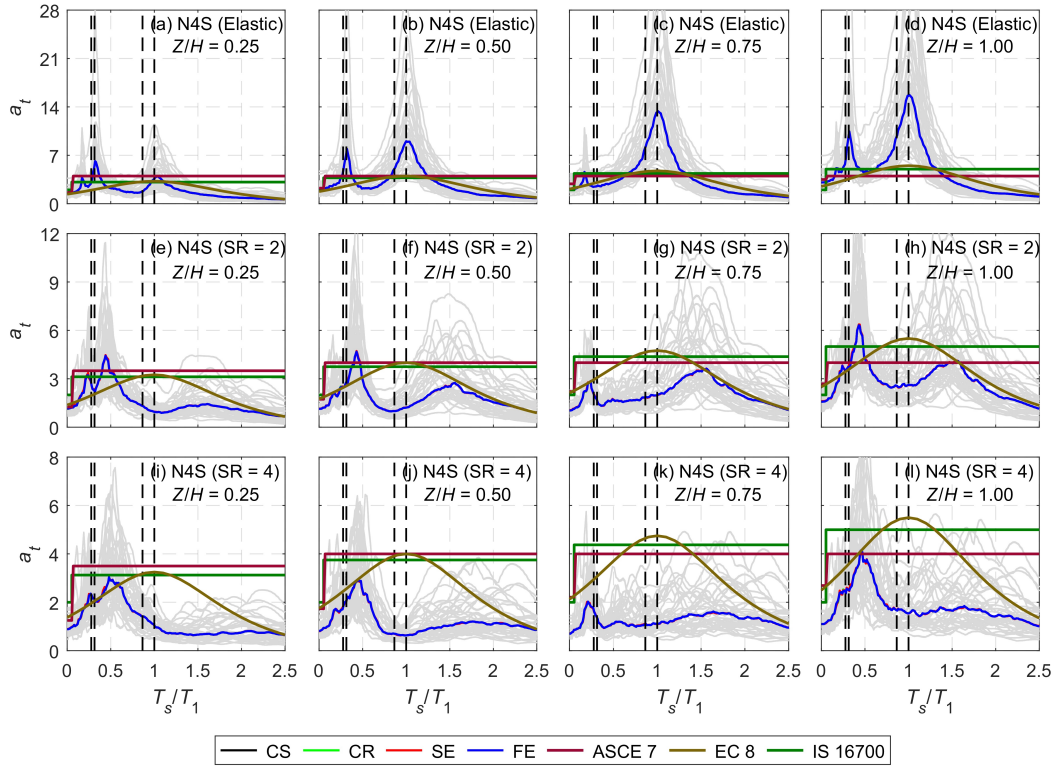

Figure B.29: Total amplification factors for the 'N4S' building obtained using bi-directional time history analyses. Dashed vertical lines indicate the elastic modal periods in the direction under consideration.

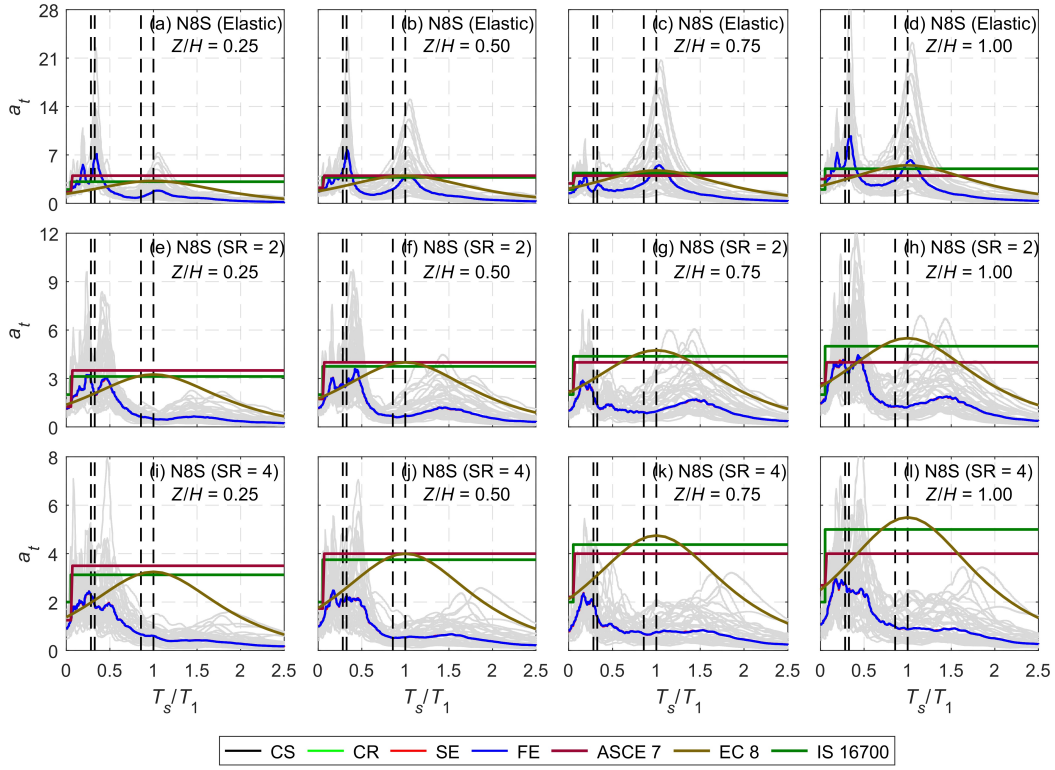

Figure B.30: Total amplification factors for the 'N8S' building obtained using bi-directional time history analyses. Dashed vertical lines indicate the elastic modal periods in the direction under consideration.

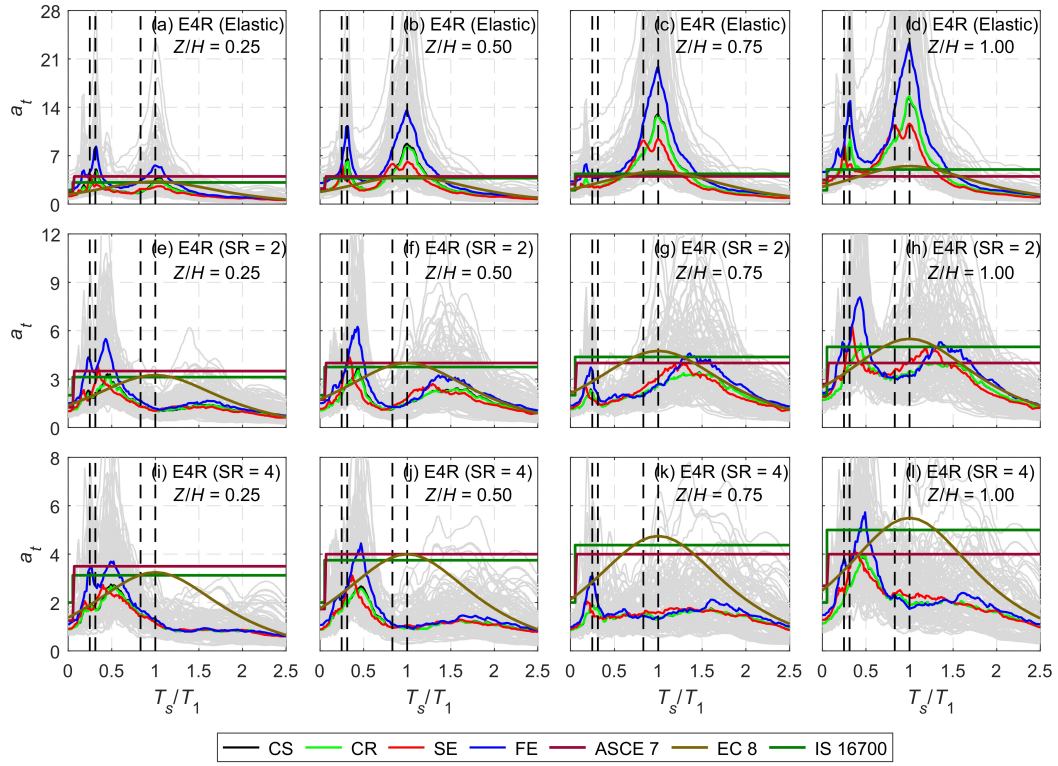

Figure B.31: Total amplification factors for the 'E4R' building obtained using bi-directional time history analyses. Dashed vertical lines indicate the elastic modal periods in the direction under consideration.

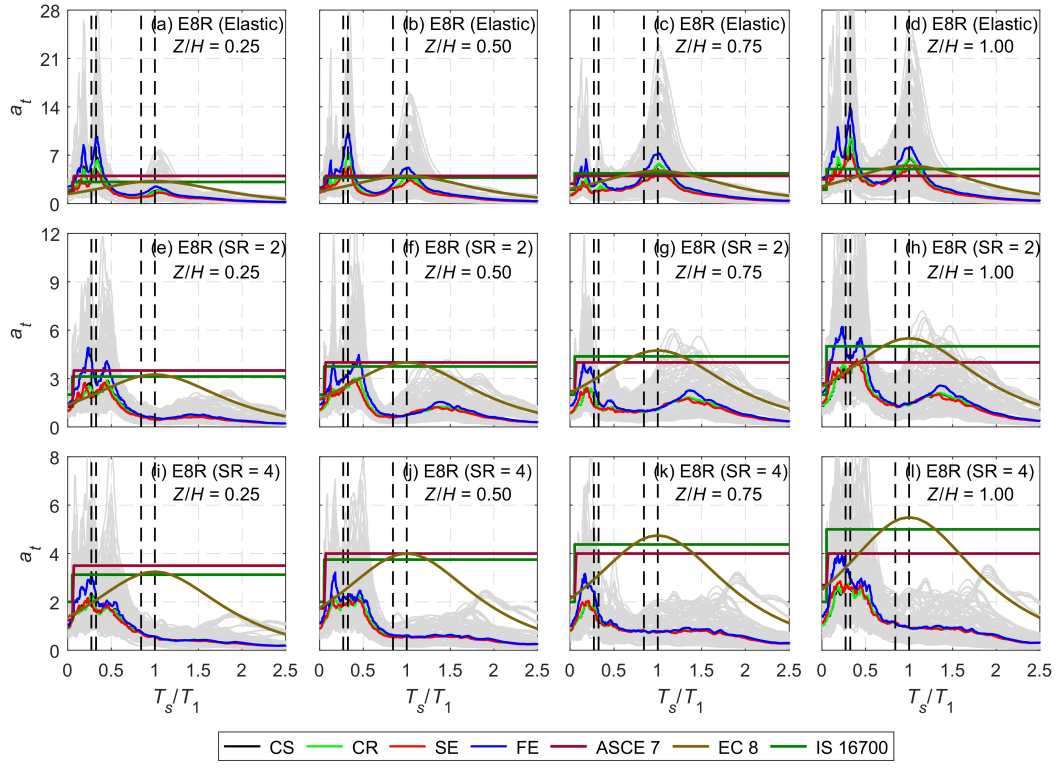

Figure B.32: Total amplification factors for the 'E8R' building obtained using bi-directional time history analyses. Dashed vertical lines indicate the elastic modal periods in the direction under consideration.

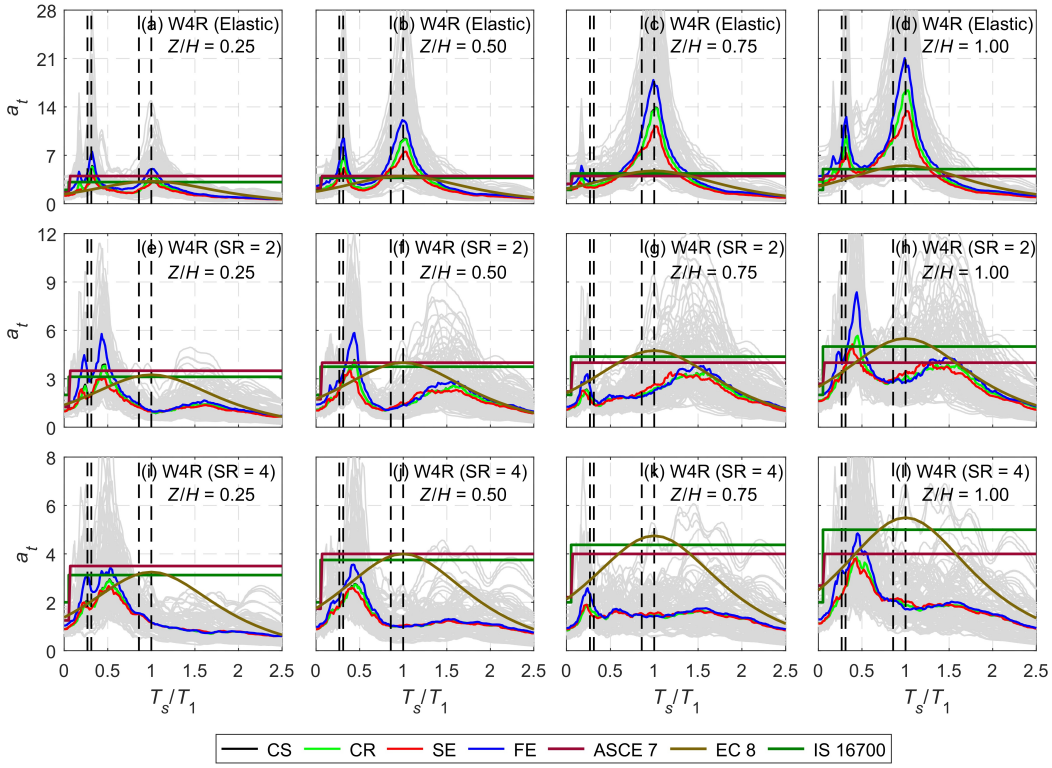

Figure B.33: Total amplification factors for the 'W4R' building obtained using bi-directional time history analyses. Dashed vertical lines indicate the elastic modal periods in the direction under consideration.

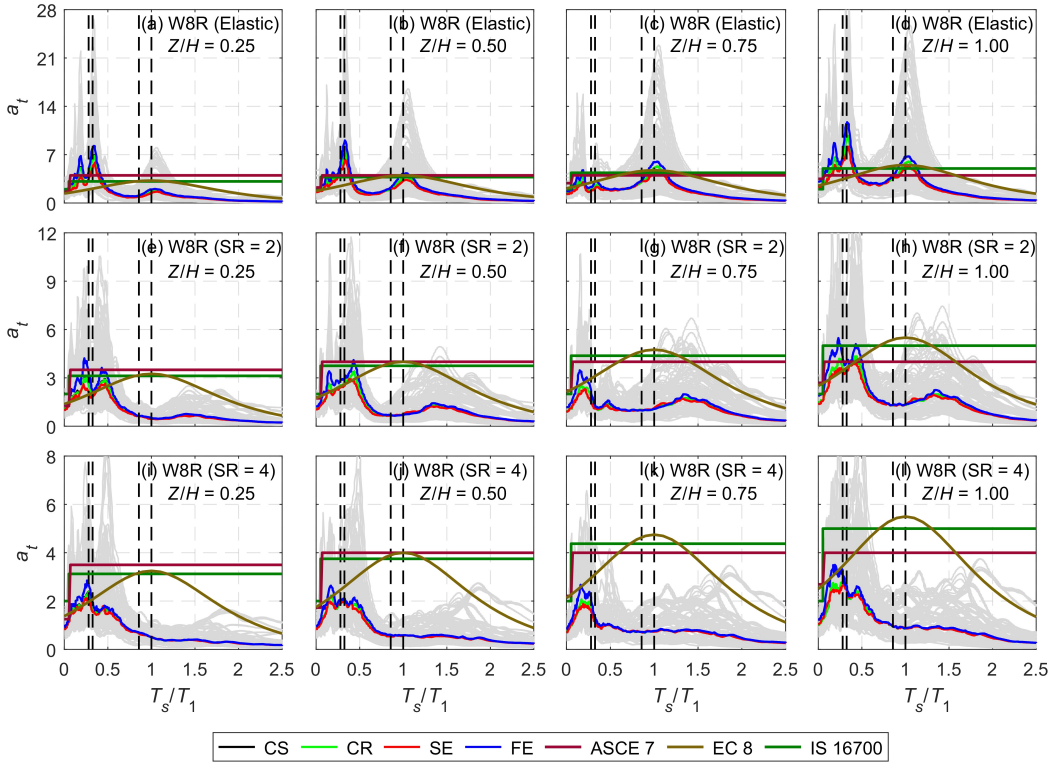

Figure B.34: Total amplification factors for the 'W8R' building obtained using bi-directional time history analyses. Dashed vertical lines indicate the elastic modal periods in the direction under consideration.

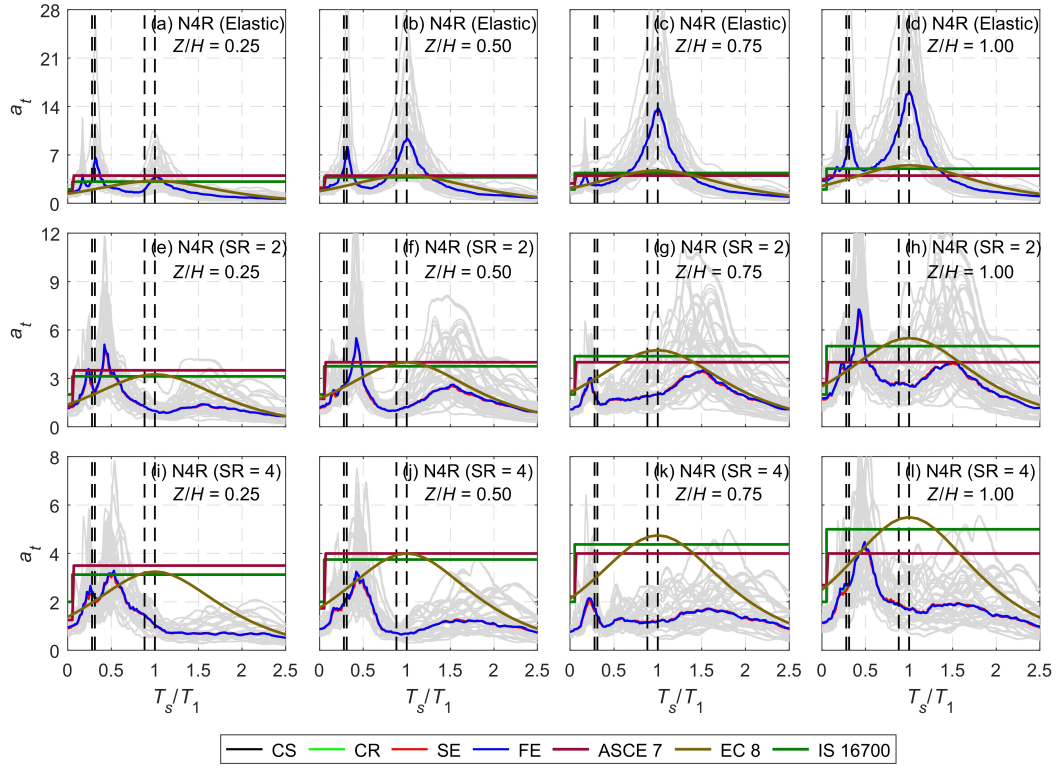

Figure B.35: Total amplification factors for the 'N4R' building obtained using bi-directional time history analyses. Dashed vertical lines indicate the elastic modal periods in the direction under consideration.

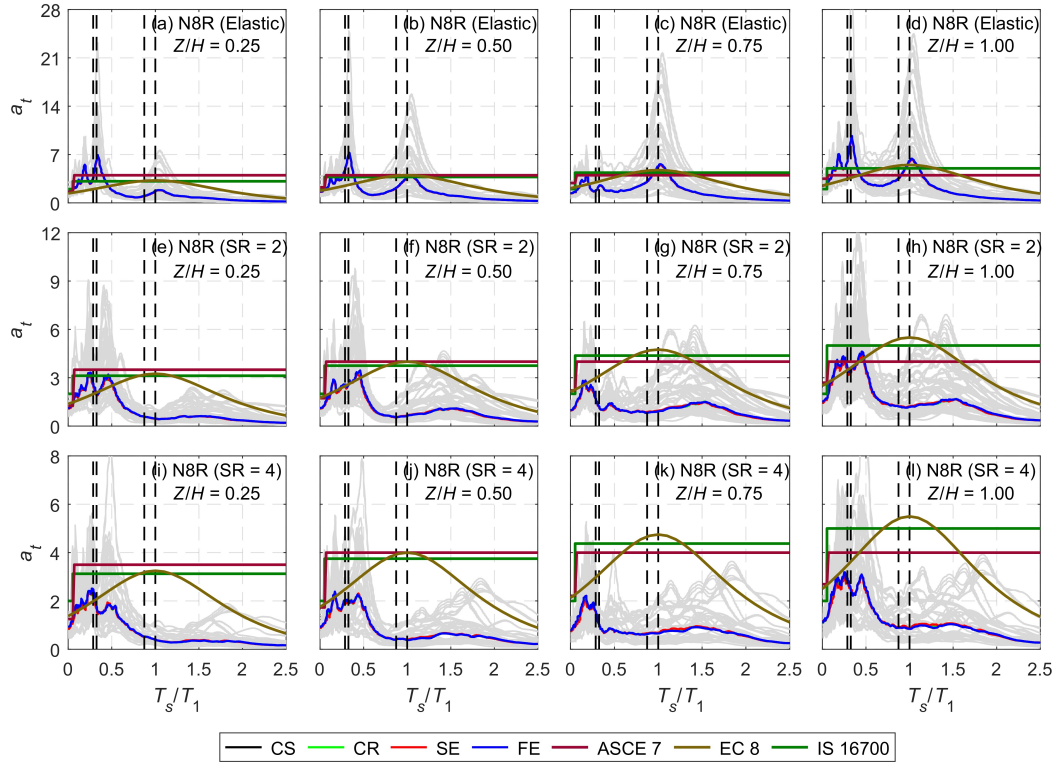

Figure B.36: Total amplification factors for the 'N8R' building obtained using bi-directional time history analyses. Dashed vertical lines indicate the elastic modal periods in the direction under consideration.

B.3 Spectral amplification factor

Figures B.37–B.54 present the spectral amplification factors (SAF) at the CS, CR, SE, and FE, as derived from time history analyses. The results are shown for cases both with and without rotational ground motions. The observed trend follows the same pattern as discussed in Chapter 5.

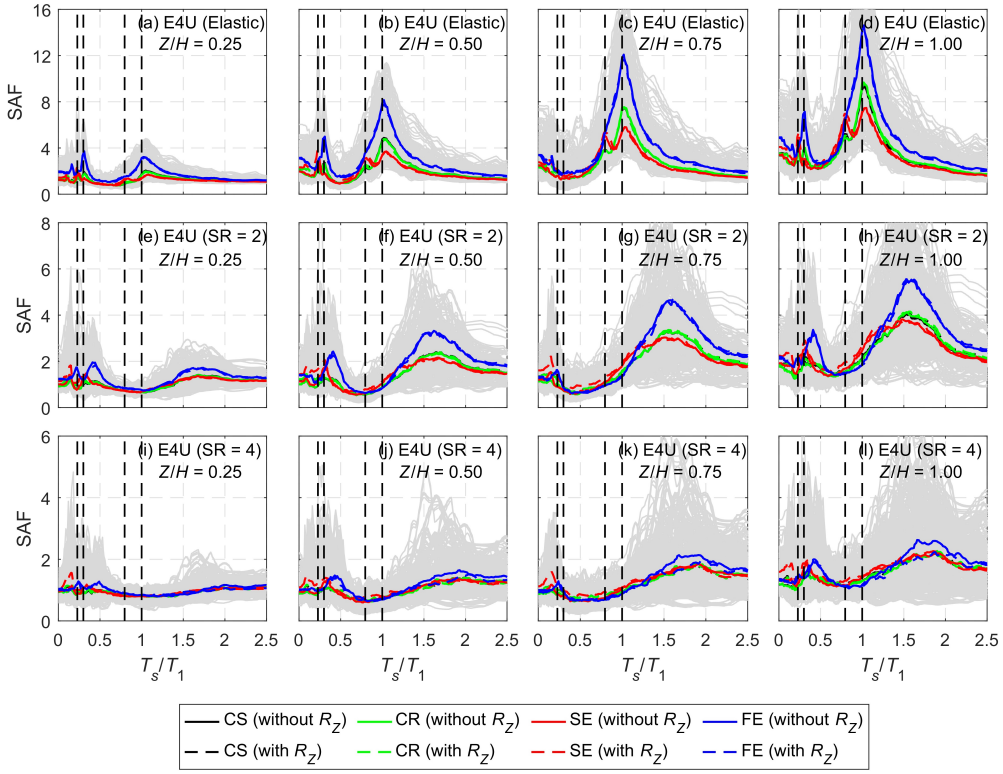

Figure B.37: Spectral amplification factors for the 'E4U' building, with and without the rotational ground motions. Dashed vertical lines indicate the elastic modal periods in the direction under consideration.

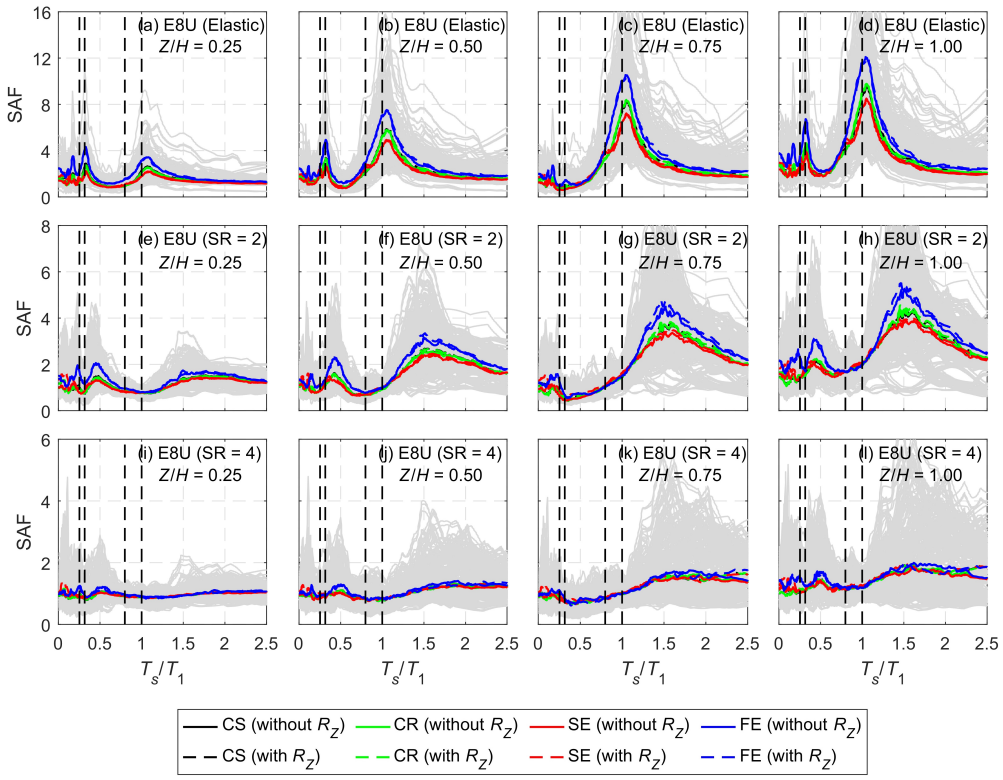

Figure B.38: Spectral amplification factors for the 'E8U' building, with and without the rotational ground motions. Dashed vertical lines indicate the elastic modal periods in the direction under consideration.

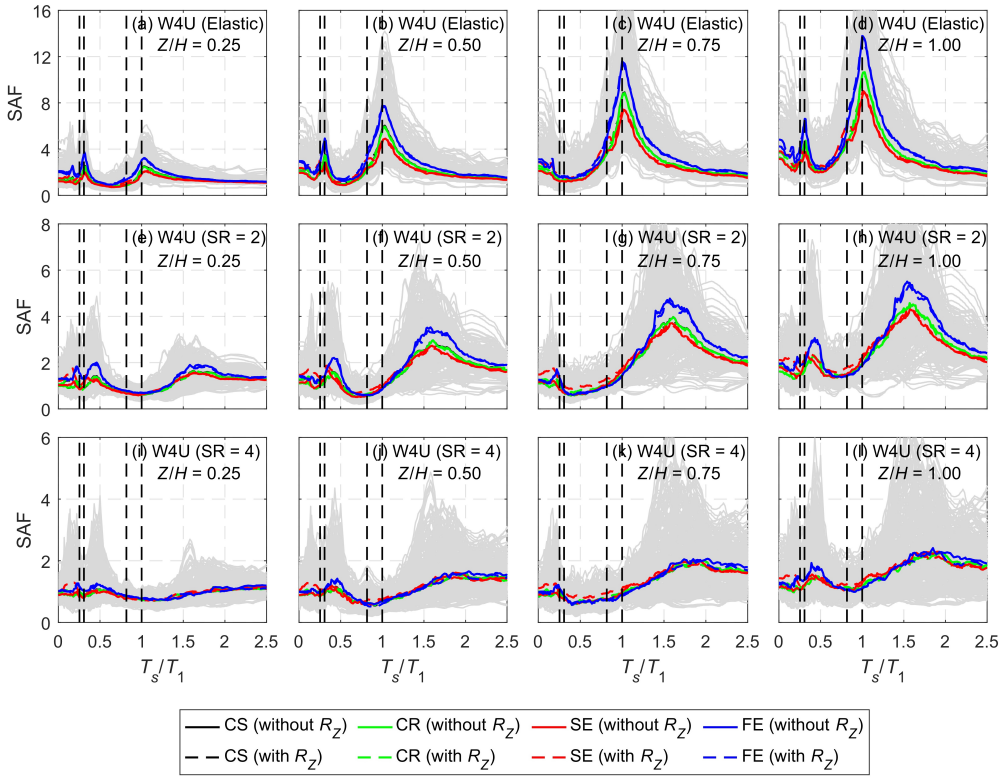

Figure B.39: Spectral amplification factors for the 'W4U' building, with and without the rotational ground motions. Dashed vertical lines indicate the elastic modal periods in the direction under consideration.

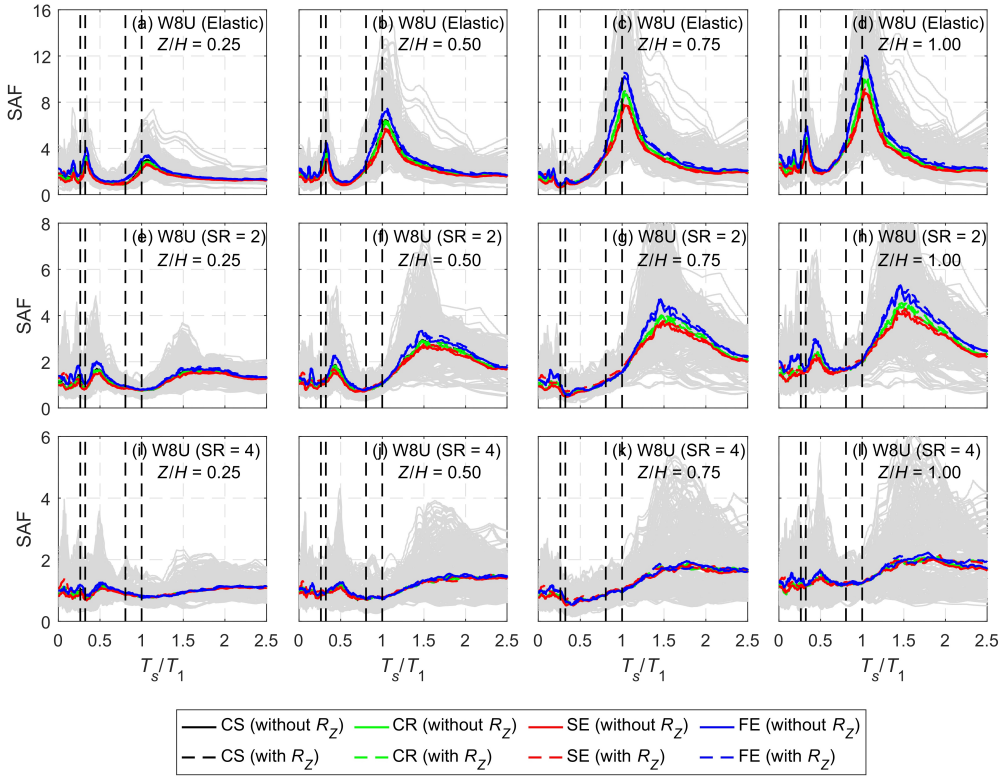

Figure B.40: Spectral amplification factors for the 'W8U' building, with and without the rotational ground motions. Dashed vertical lines indicate the elastic modal periods in the direction under consideration.

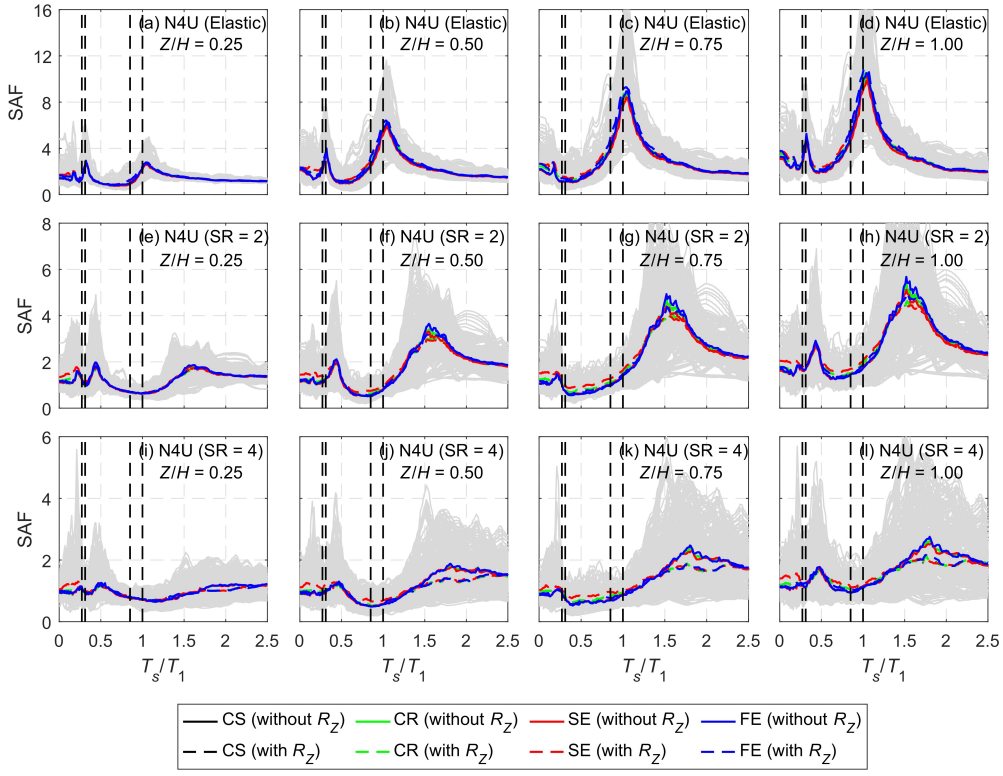

Figure B.41: Spectral amplification factors for the 'N4U' building, with and without the rotational ground motions. Dashed vertical lines indicate the elastic modal periods in the direction under consideration.

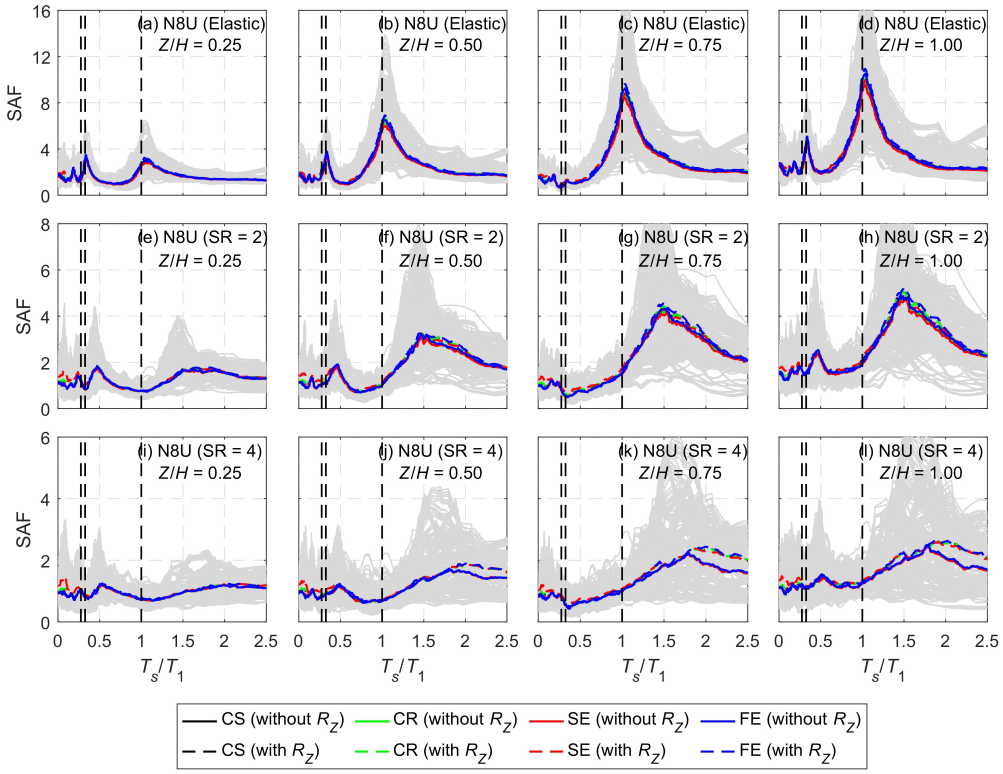

Figure B.42: Spectral amplification factors for the 'N8U' building, with and without the rotational ground motions. Dashed vertical lines indicate the elastic modal periods in the direction under consideration.

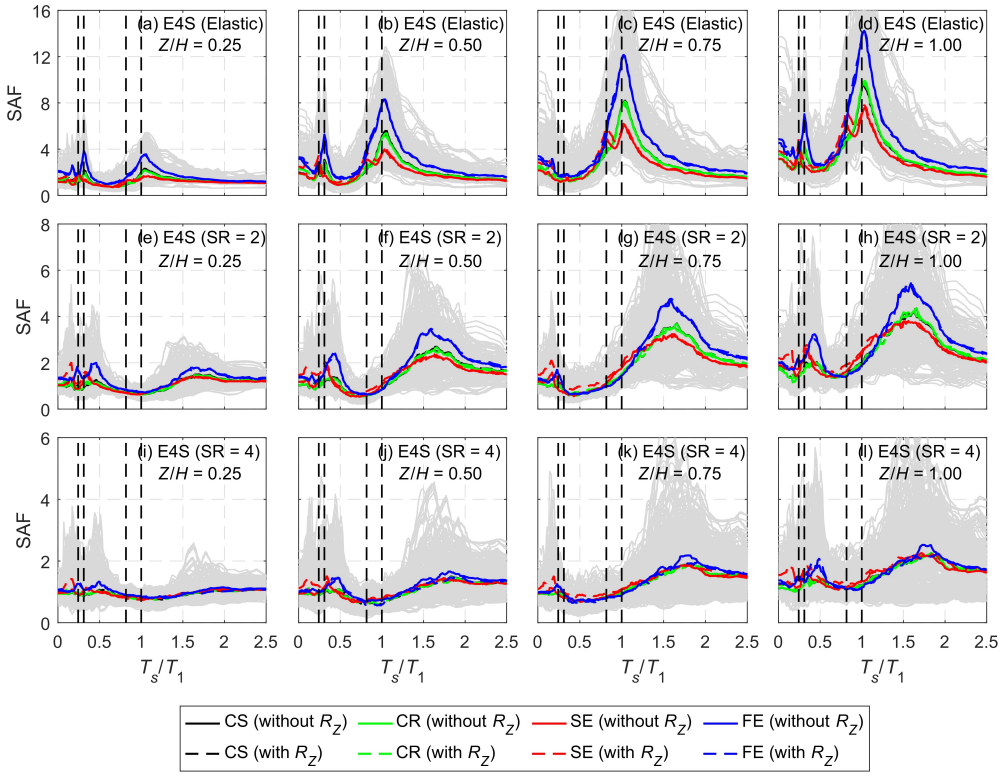

Figure B.43: Spectral amplification factors for the 'E4S' building, with and without the rotational ground motions. Dashed vertical lines indicate the elastic modal periods in the direction under consideration.

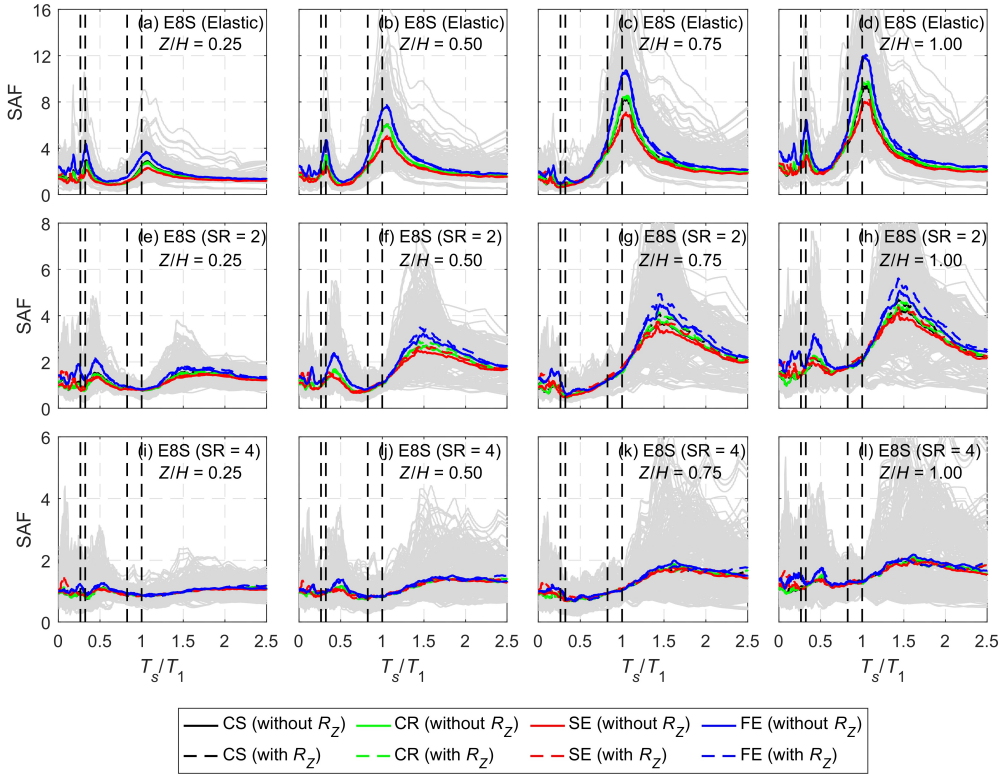

Figure B.44: Spectral amplification factors for the 'E8S' building, with and without the rotational ground motions. Dashed vertical lines indicate the elastic modal periods in the direction under consideration.

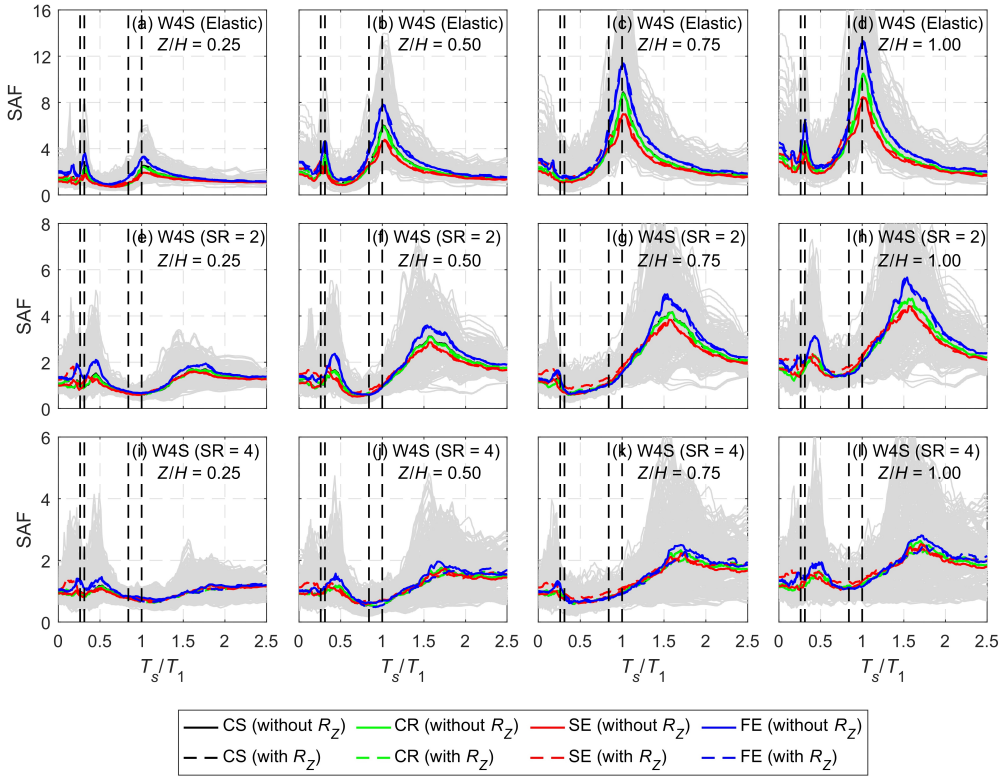

Figure B.45: Spectral amplification factors for the 'W4S' building, with and without the rotational ground motions. Dashed vertical lines indicate the elastic modal periods in the direction under consideration.

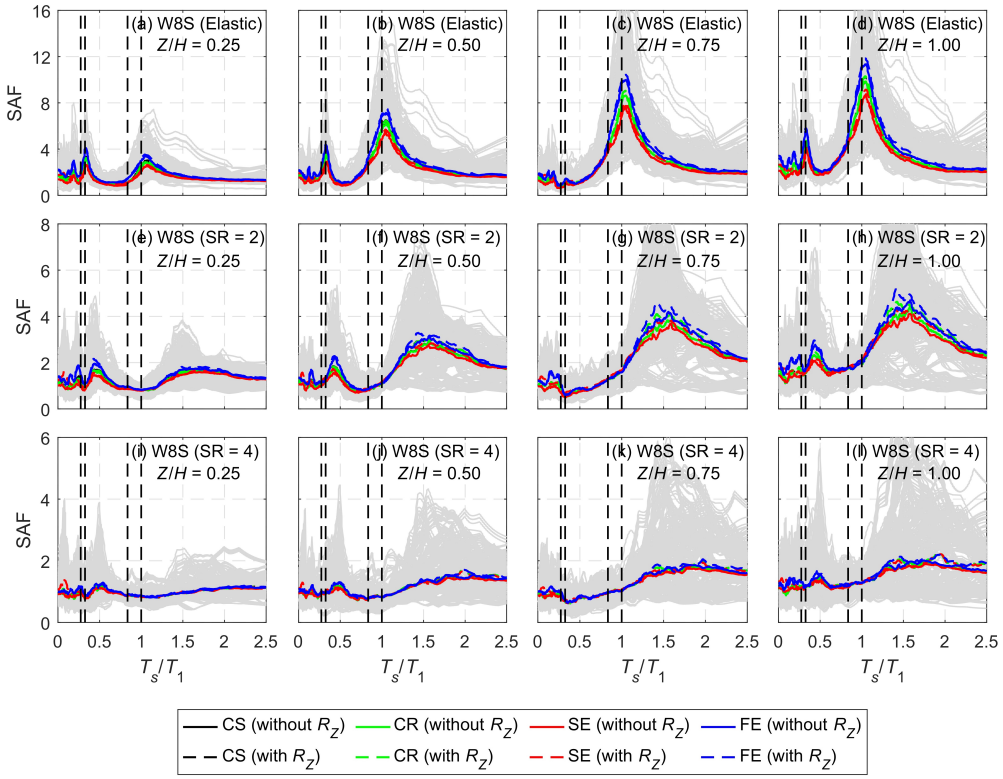

Figure B.46: Spectral amplification factors for the 'W8S' building, with and without the rotational ground motions. Dashed vertical lines indicate the elastic modal periods in the direction under consideration.

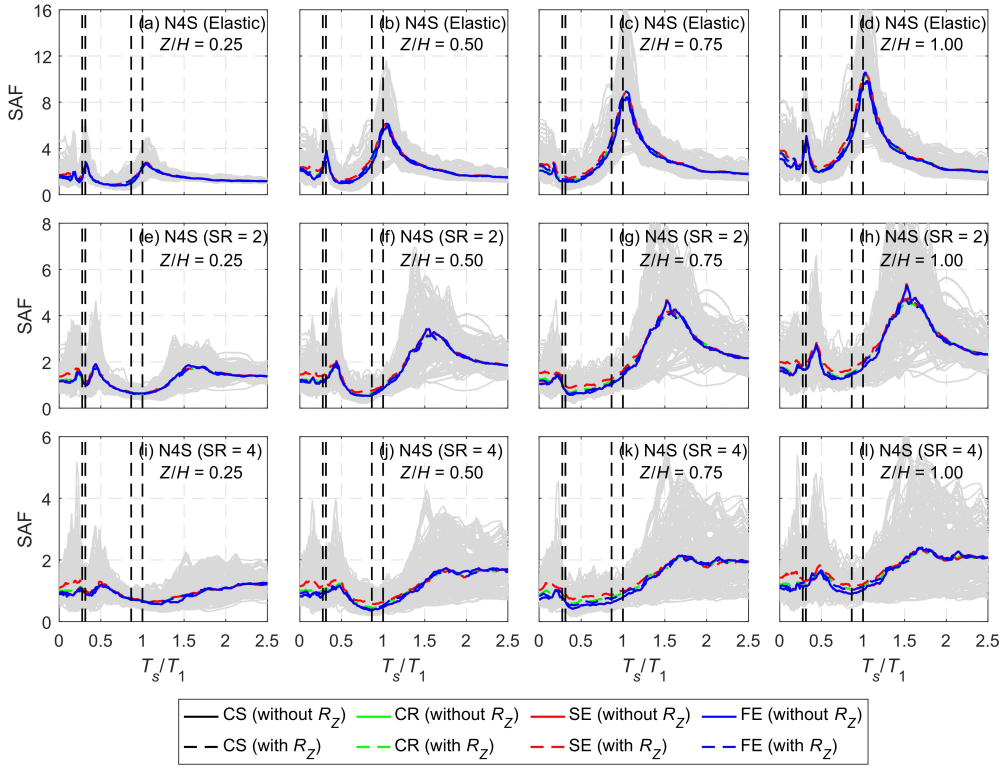

Figure B.47: Spectral amplification factors for the 'N4S' building, with and without the rotational ground motions. Dashed vertical lines indicate the elastic modal periods in the direction under consideration.

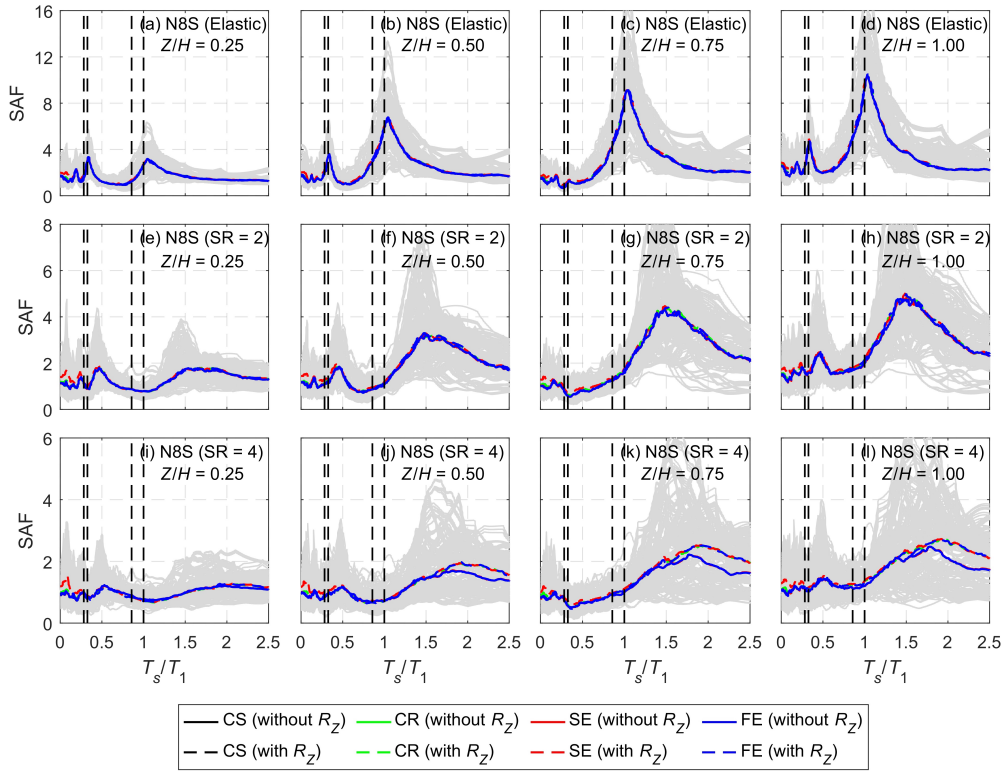

Figure B.48: Spectral amplification factors for the 'N8S' building, with and without the rotational ground motions. Dashed vertical lines indicate the elastic modal periods in the direction under consideration.

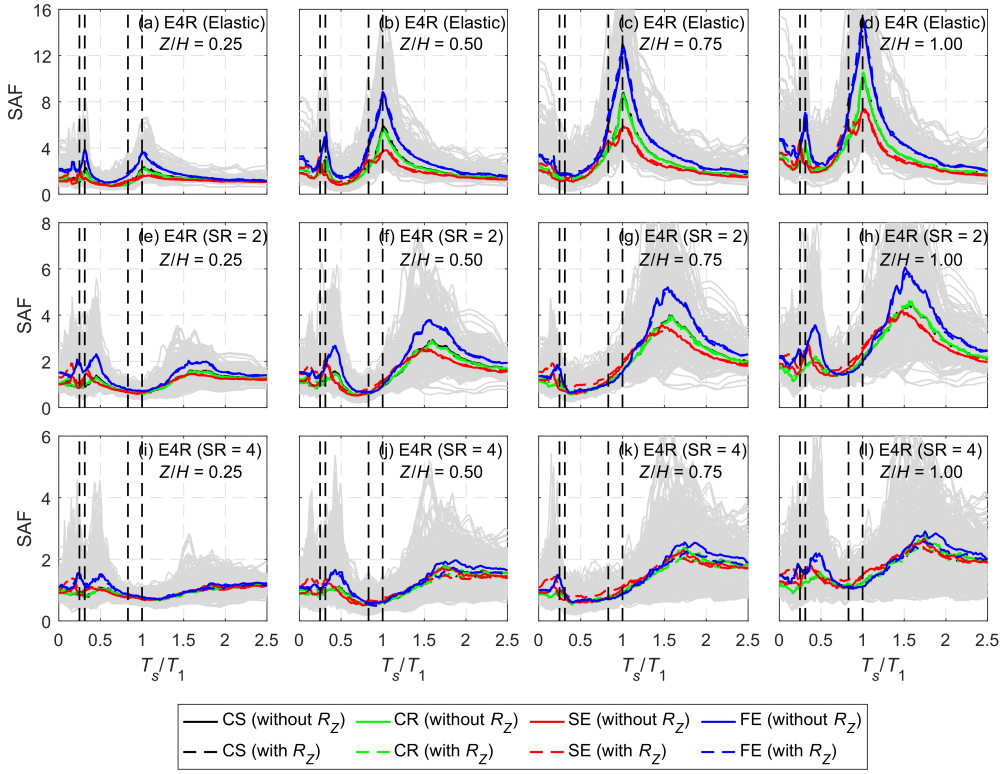

Figure B.49: Spectral amplification factors for the 'E4R' building, with and without the rotational ground motions. Dashed vertical lines indicate the elastic modal periods in the direction under consideration.

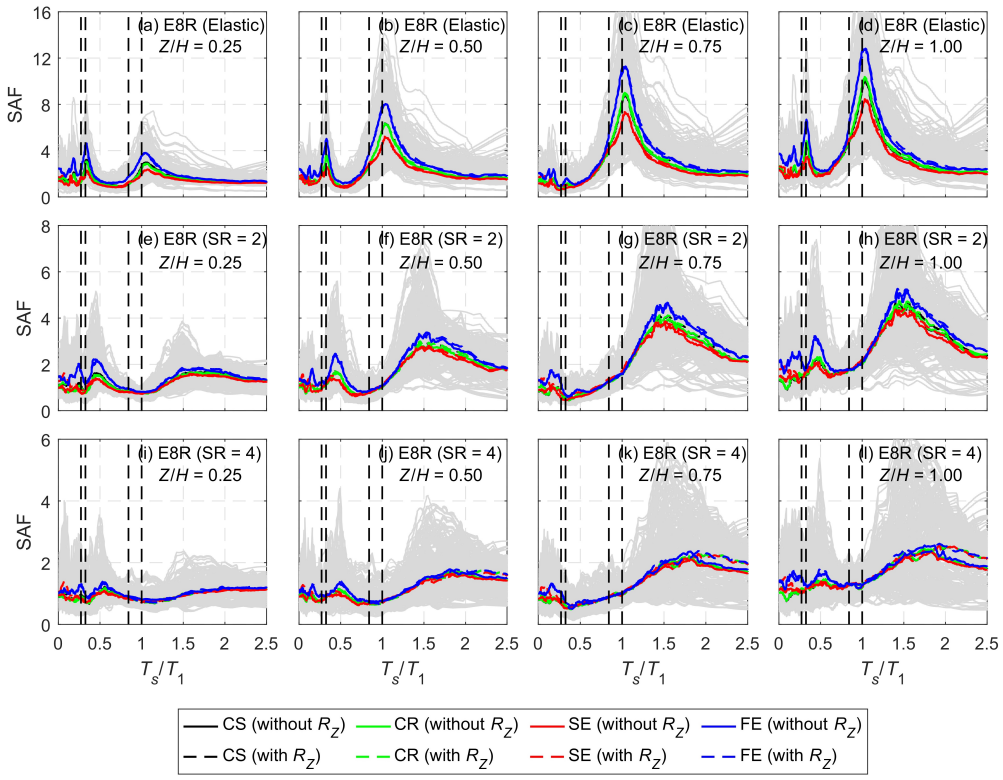

Figure B.50: Spectral amplification factors for the 'E8R' building, with and without the rotational ground motions. Dashed vertical lines indicate the elastic modal periods in the direction under consideration.

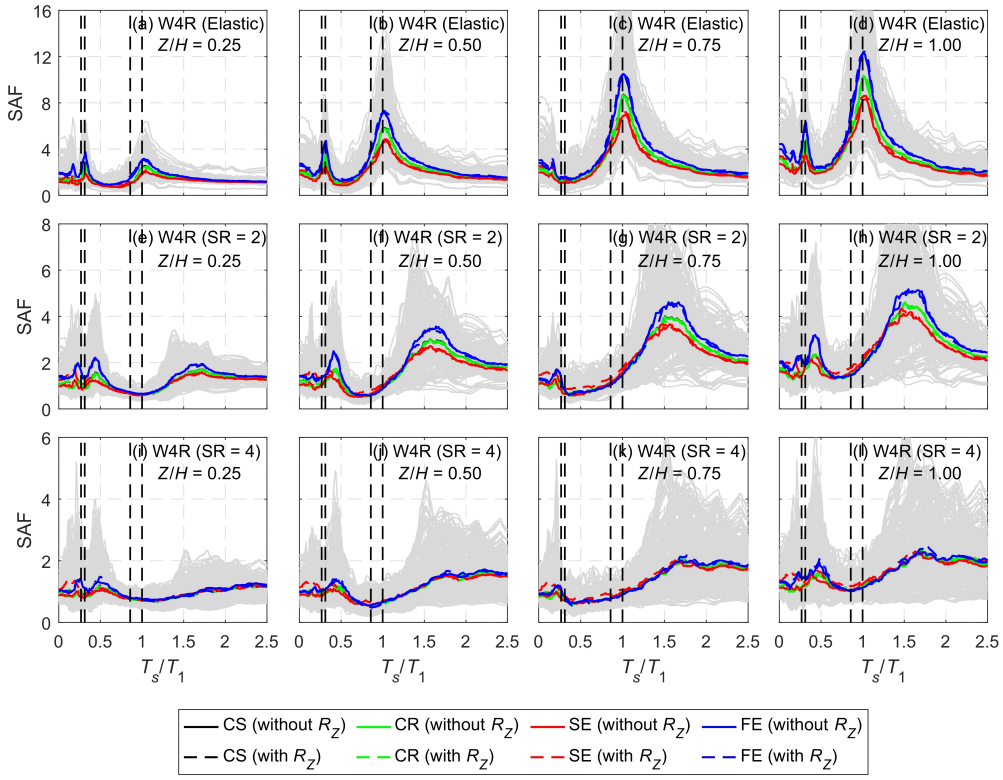

Figure B.51: Spectral amplification factors for the 'W4R' building, with and without the rotational ground motions. Dashed vertical lines indicate the elastic modal periods in the direction under consideration.

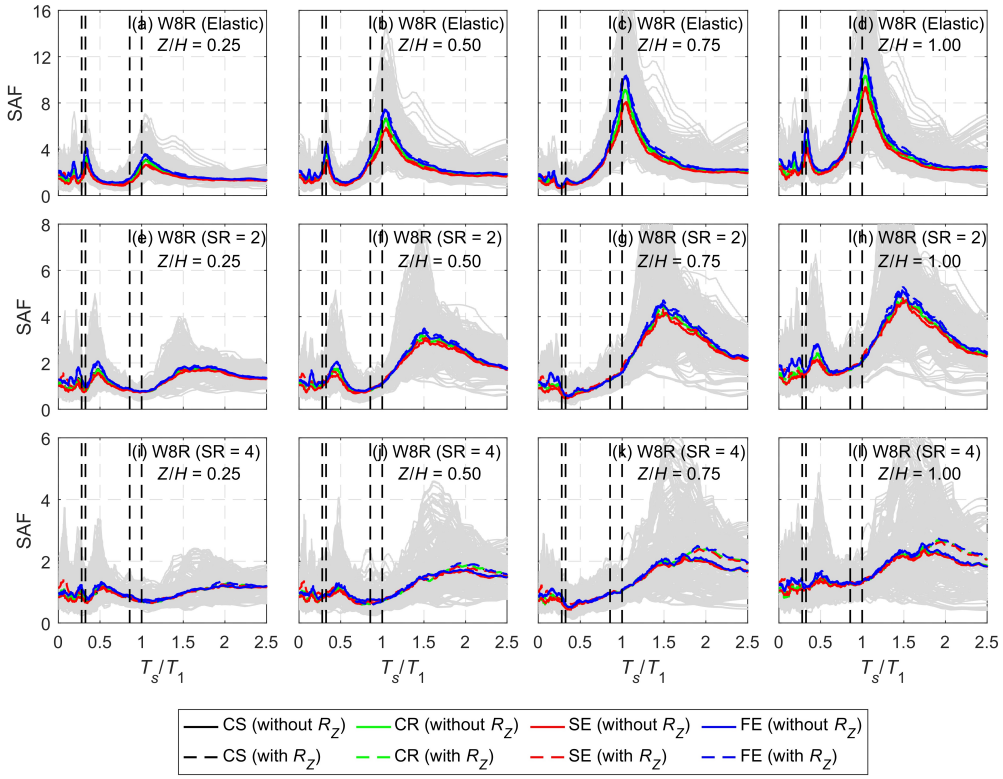

Figure B.52: Spectral amplification factors for the 'W8R' building, with and without the rotational ground motions. Dashed vertical lines indicate the elastic modal periods in the direction under consideration.

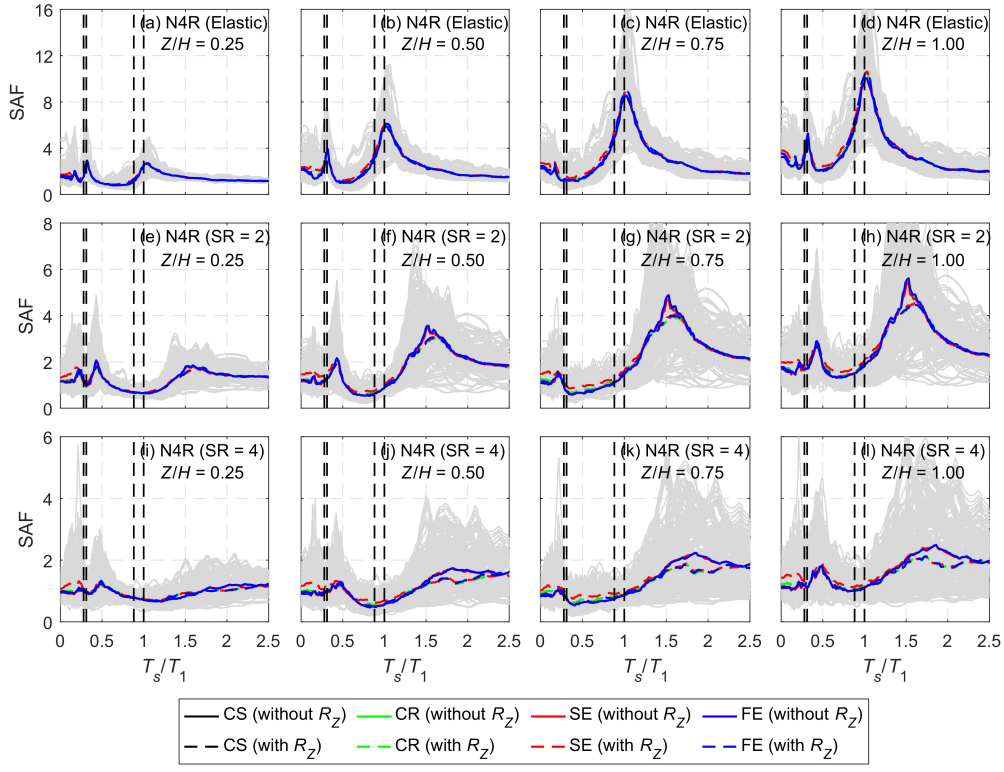

Figure B.53: Spectral amplification factors for the 'N4R' building, with and without the rotational ground motions. Dashed vertical lines indicate the elastic modal periods in the direction under consideration.

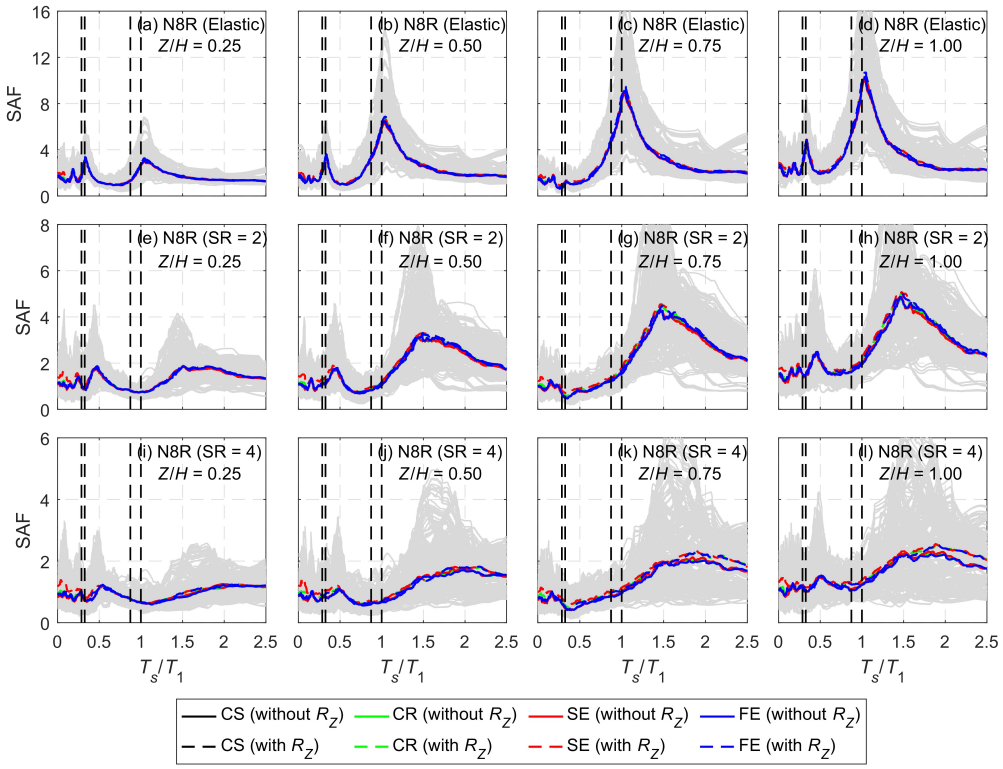

Figure B.54: Spectral amplification factors for the 'N8R' building, with and without the rotational ground motions. Dashed vertical lines indicate the elastic modal periods in the direction under consideration.

Appendix C

Torsional Amplification Factors

C.1 Torsional amplification factors for the rigid secondary systems

C.1.1 At the extreme edges

Figures C.1–C.6 present the estimated torsional amplification factors for rigid secondary systems at the SE and FE along the building height, relative to the CS and CR, based on time history analyses conducted with and without considering rotational ground motions. The observed trend follows the same pattern as discussed in Chapter 6.

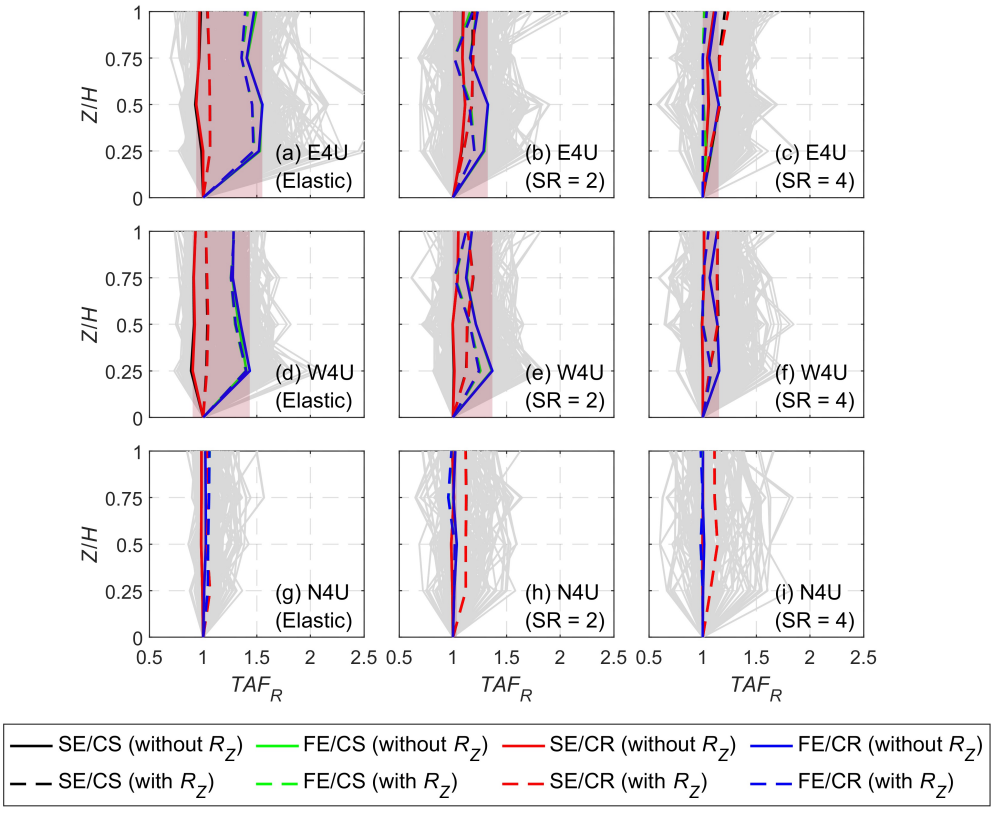

Figure C.1: Variations of torsional amplification factor for the rigid secondary systems along the height of the 'E4U', 'W4U', and 'N4U' buildings.

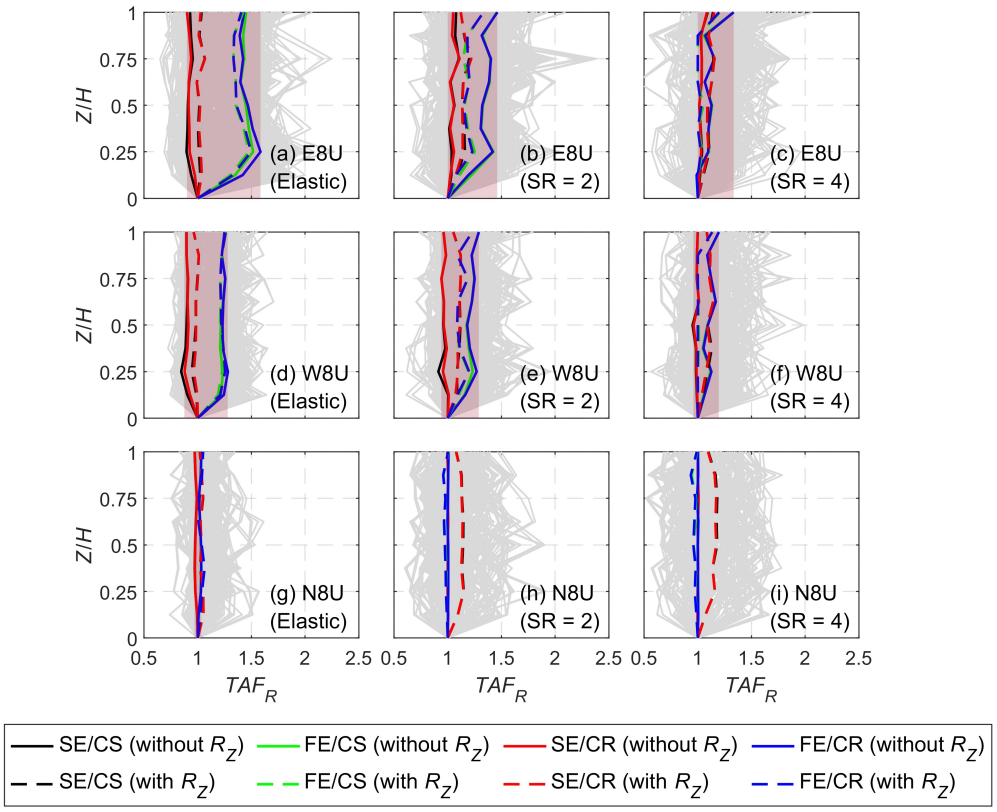

Figure C.2: Variations of torsional amplification factor for the rigid secondary systems along the height of the 'E8U', 'W8U', and 'N8U' buildings.

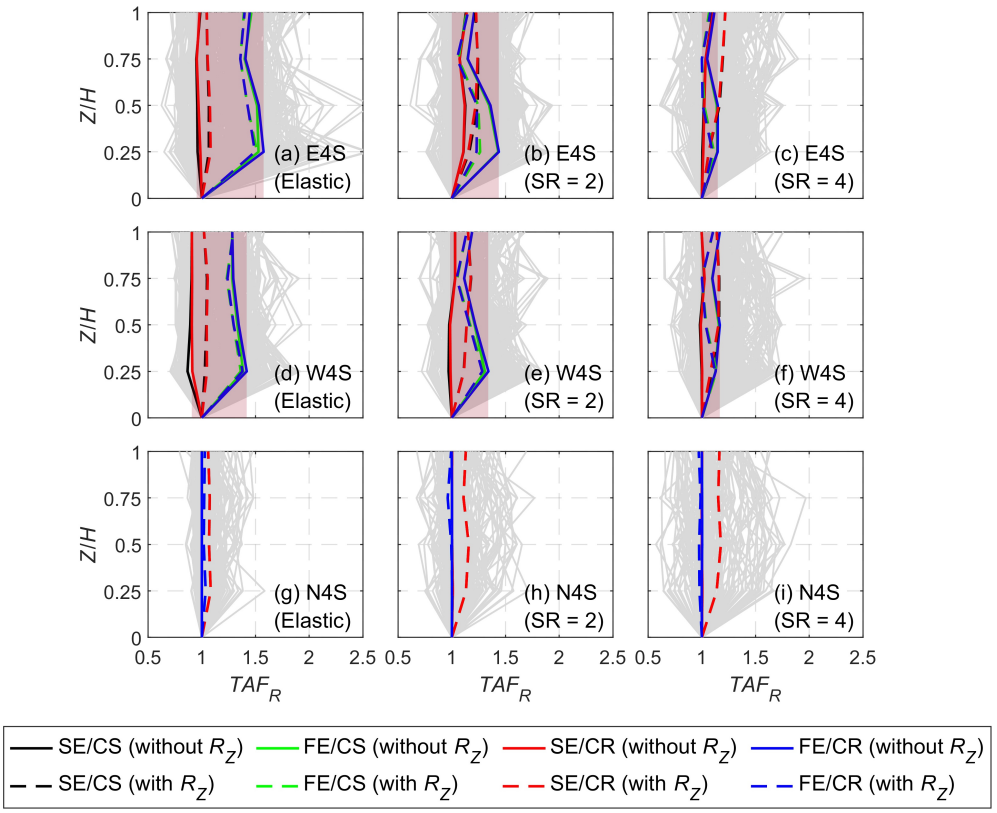

Figure C.3: Variations of torsional amplification factor for the rigid secondary systems along the height of the 'E4S', 'W4S', and 'N4S' buildings.

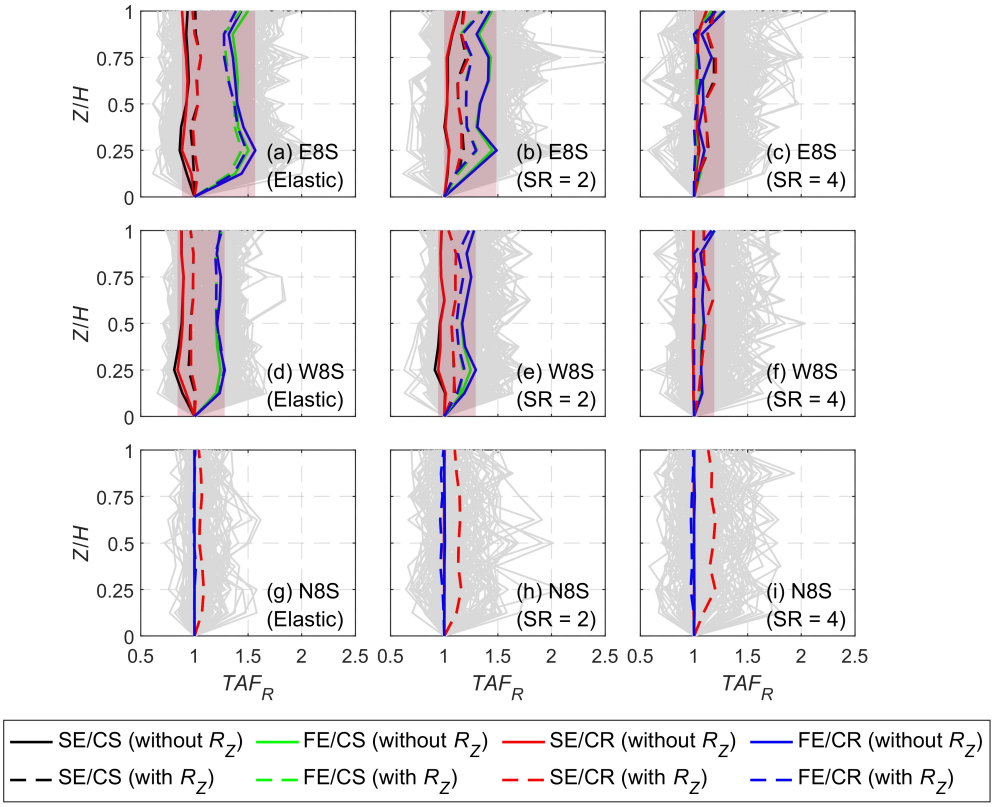

Figure C.4: Variations of torsional amplification factor for the rigid secondary systems along the height of the 'E8S', 'W8S', and 'N8S' buildings.

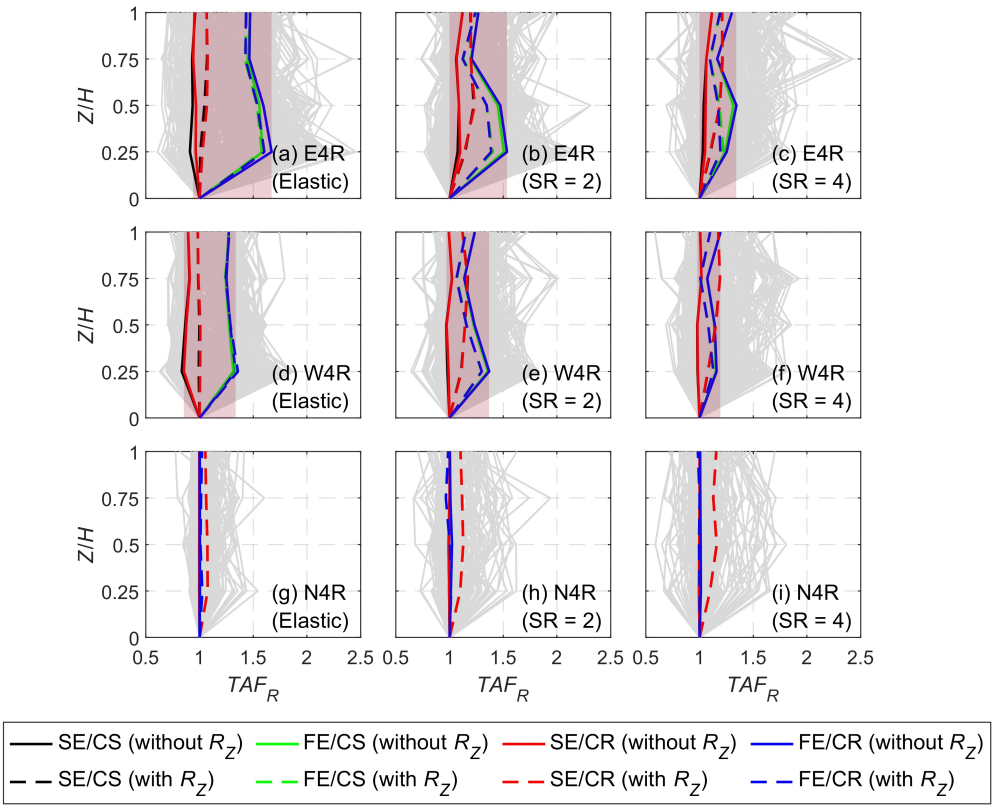

Figure C.5: Variations of torsional amplification factor for the rigid secondary systems along the height of the 'E4R', 'W4R', and 'N4R' buildings.

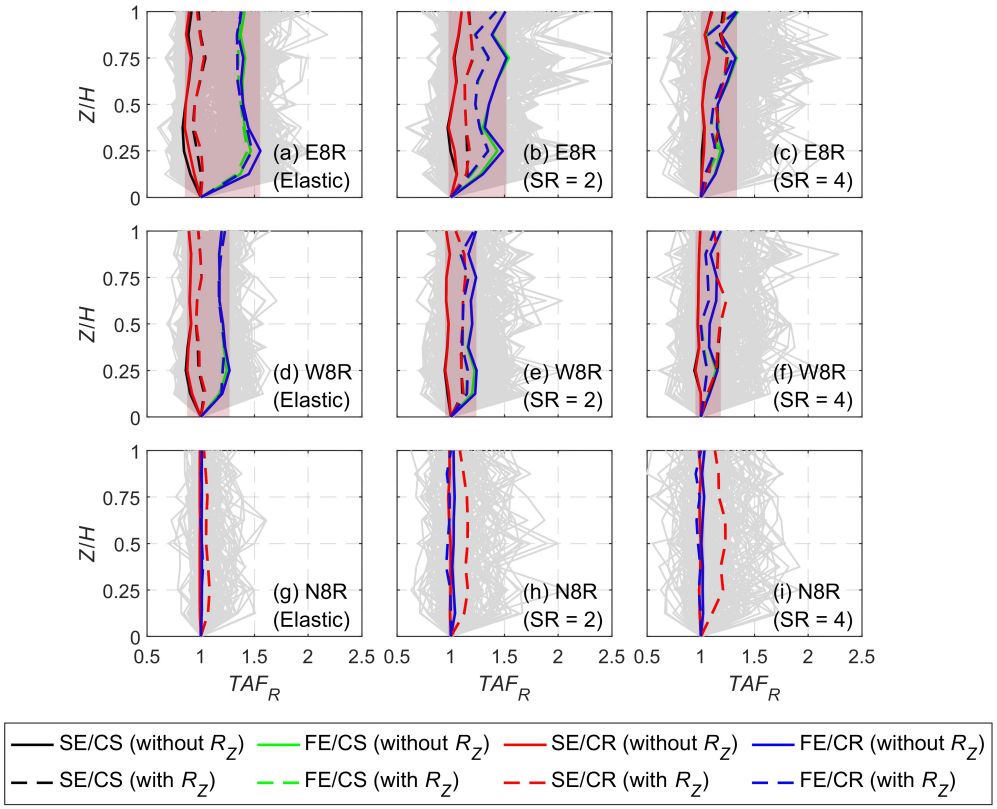

Figure C.6: Variations of torsional amplification factor for the rigid secondary systems along the height of the 'E8R', 'W8R', and 'N8R' buildings.

C.1.2 Across the floor plan

Figures C.7–C.24 illustrate the estimated torsional amplification factors for rigid secondary systems across the floor plan, relative to the CS and CR, using time history analyses performed with and without considering rotational ground motions. The observed trend follows the same pattern as discussed in Chapter 6.

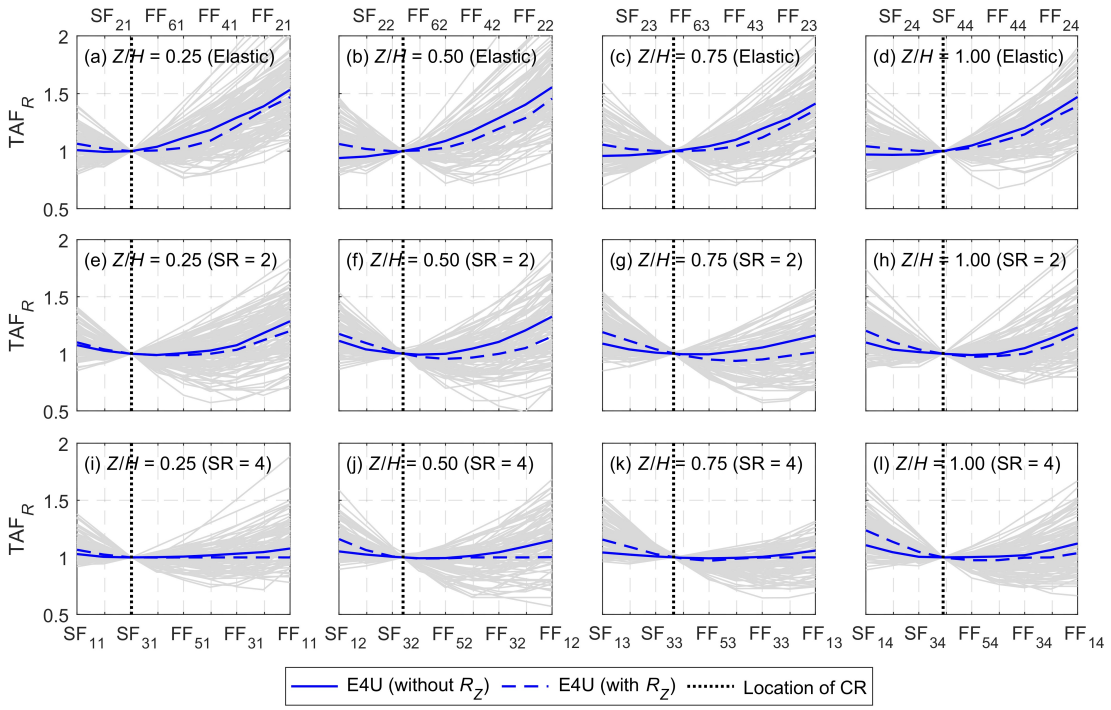

Figure C.7: In-plan distribution of torsional amplification factor for rigid secondary systems at different floors of the 'E4U' building.

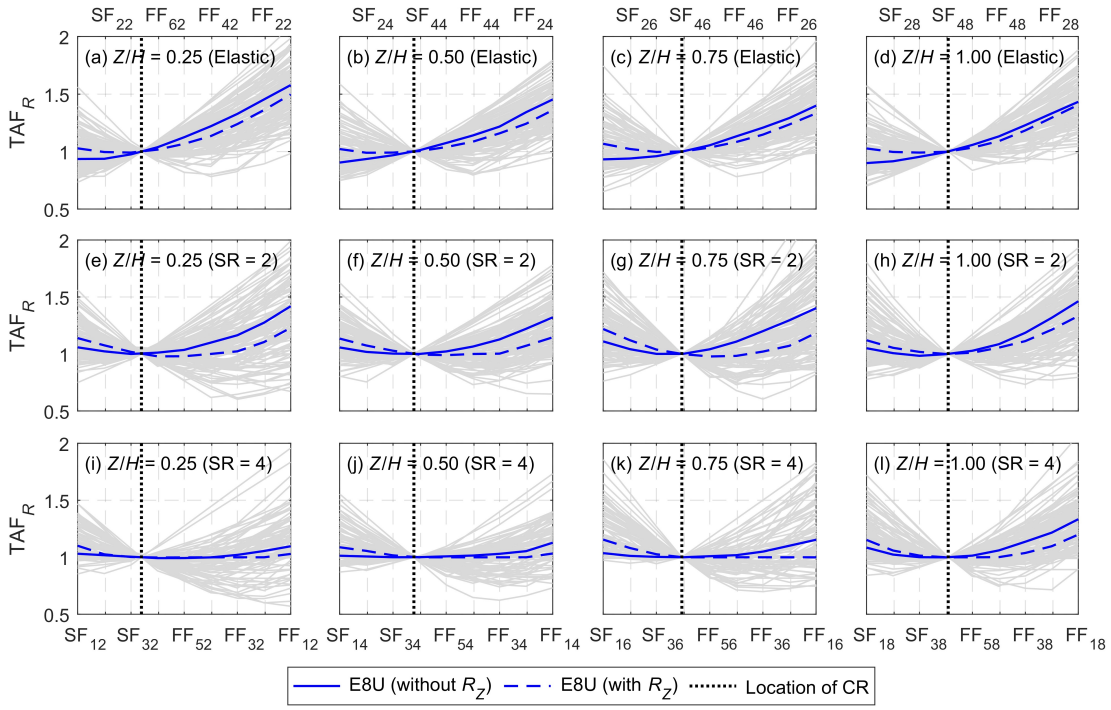

Figure C.8: In-plan distribution of torsional amplification factor for rigid secondary systems at different floors of the 'E8U' building.

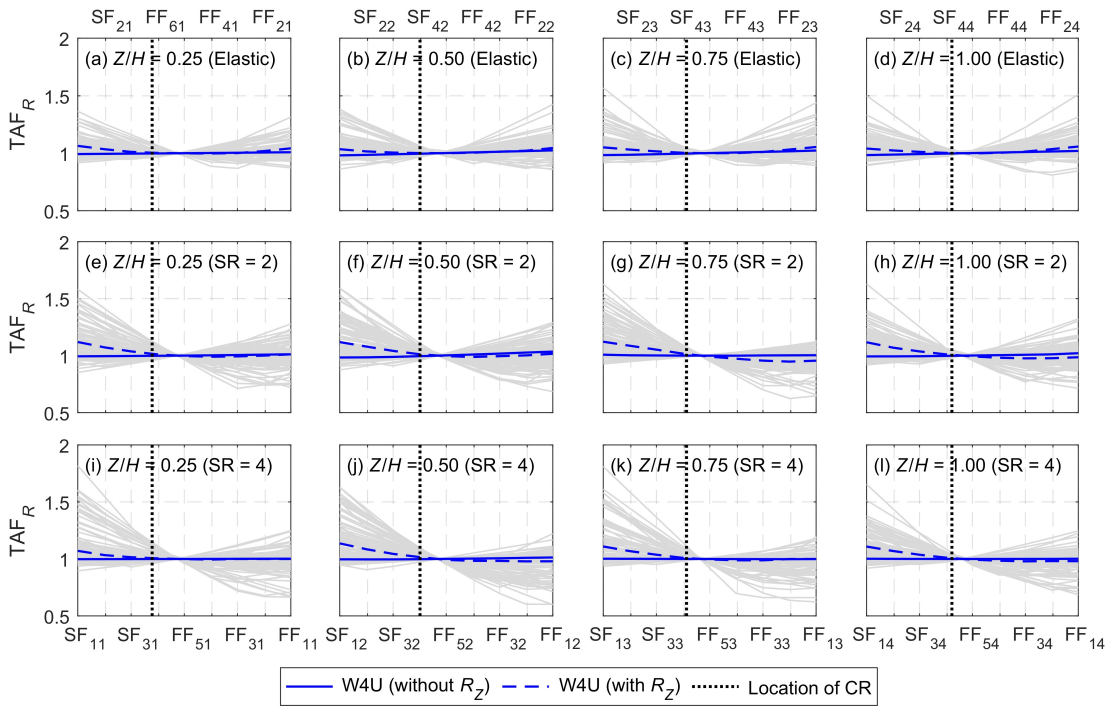

Figure C.9: In-plan distribution of torsional amplification factor for rigid secondary systems at different floors of the 'W4U' building.

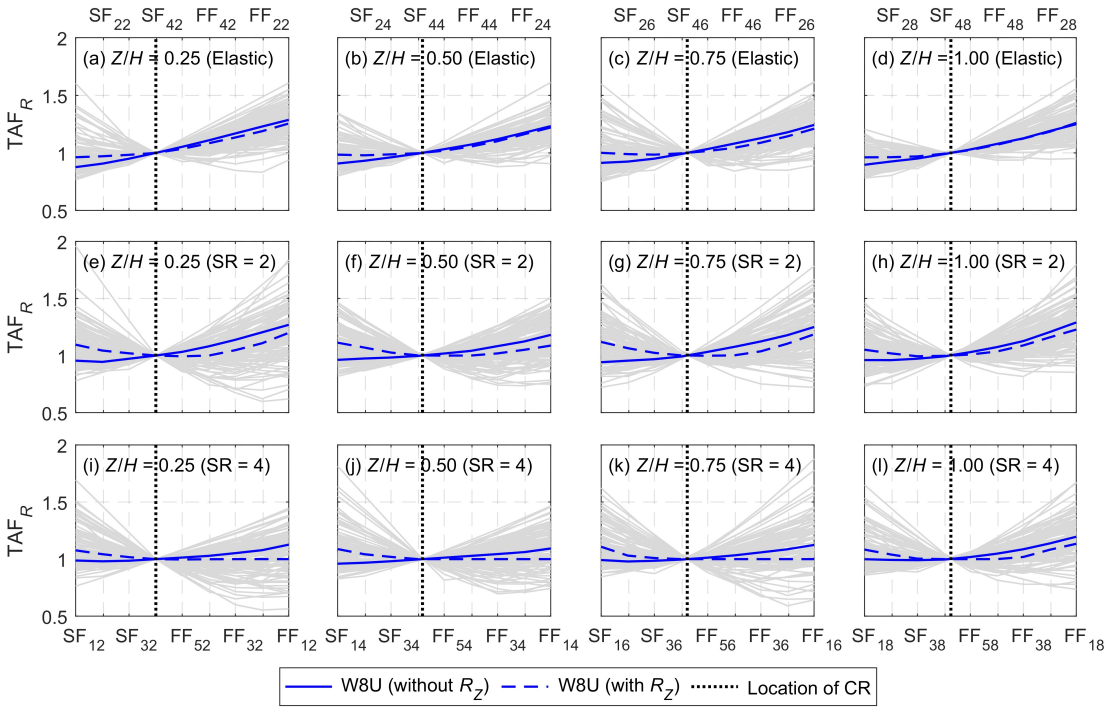

Figure C.10: In-plan distribution of torsional amplification factor for rigid secondary systems at different floors of the 'W8U' building.

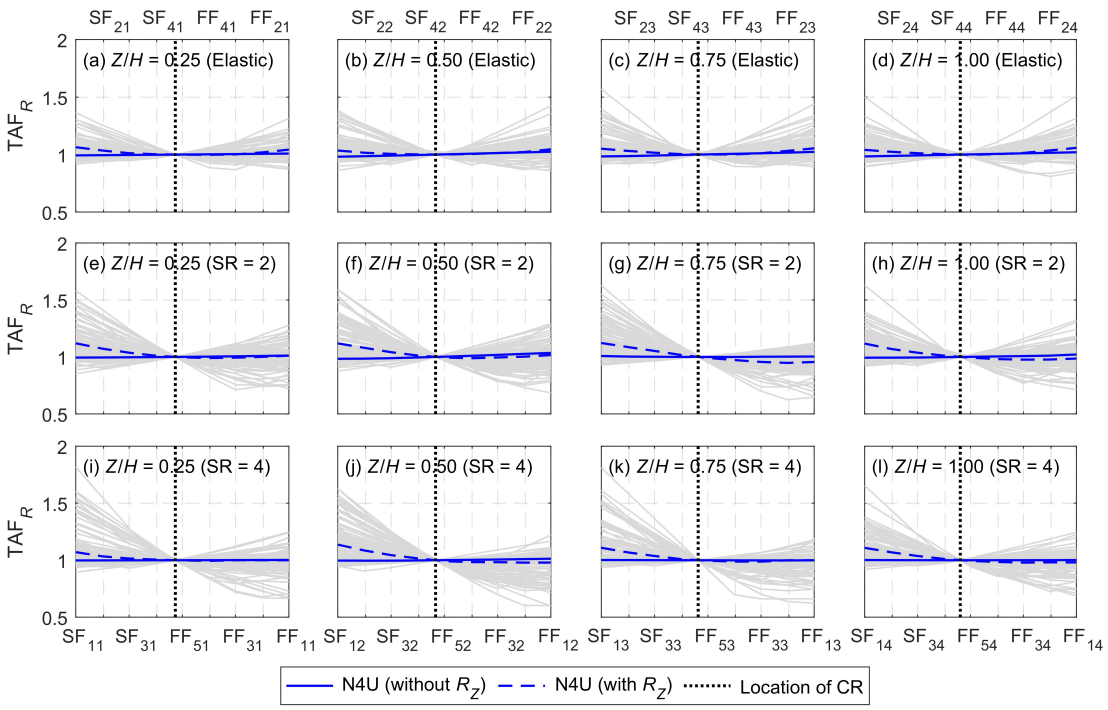

Figure C.11: In-plan distribution of torsional amplification factor for rigid secondary systems at different floors of the 'N4U' building.

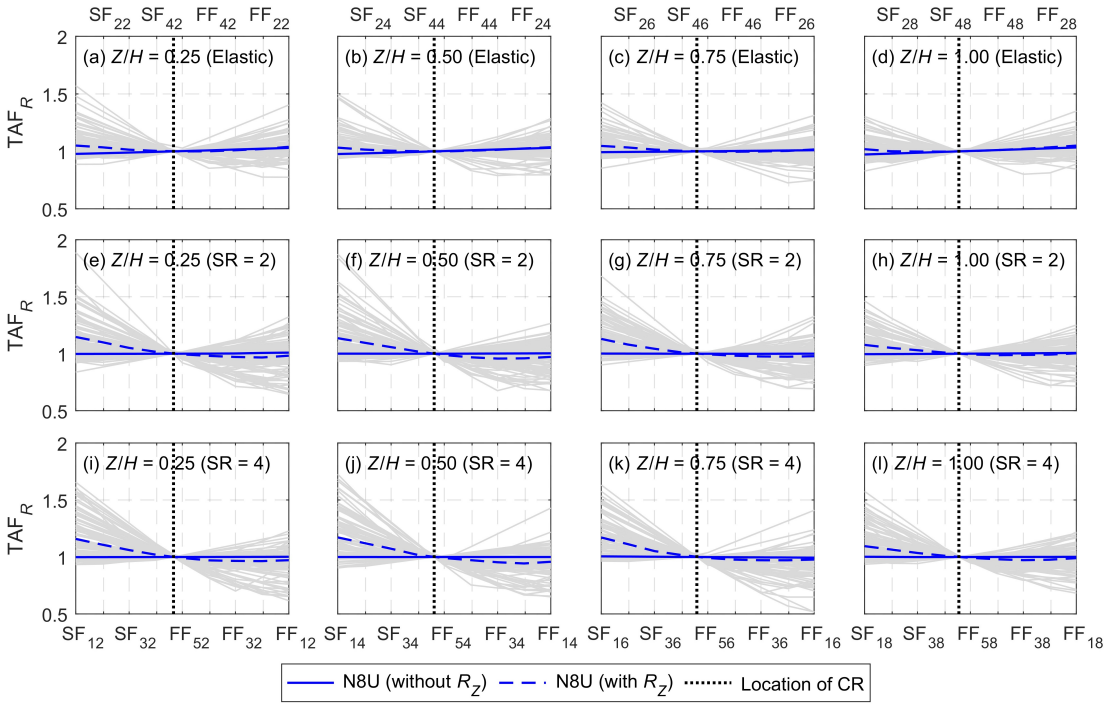

Figure C.12: In-plan distribution of torsional amplification factor for rigid secondary systems at different floors of the 'N8U' building.

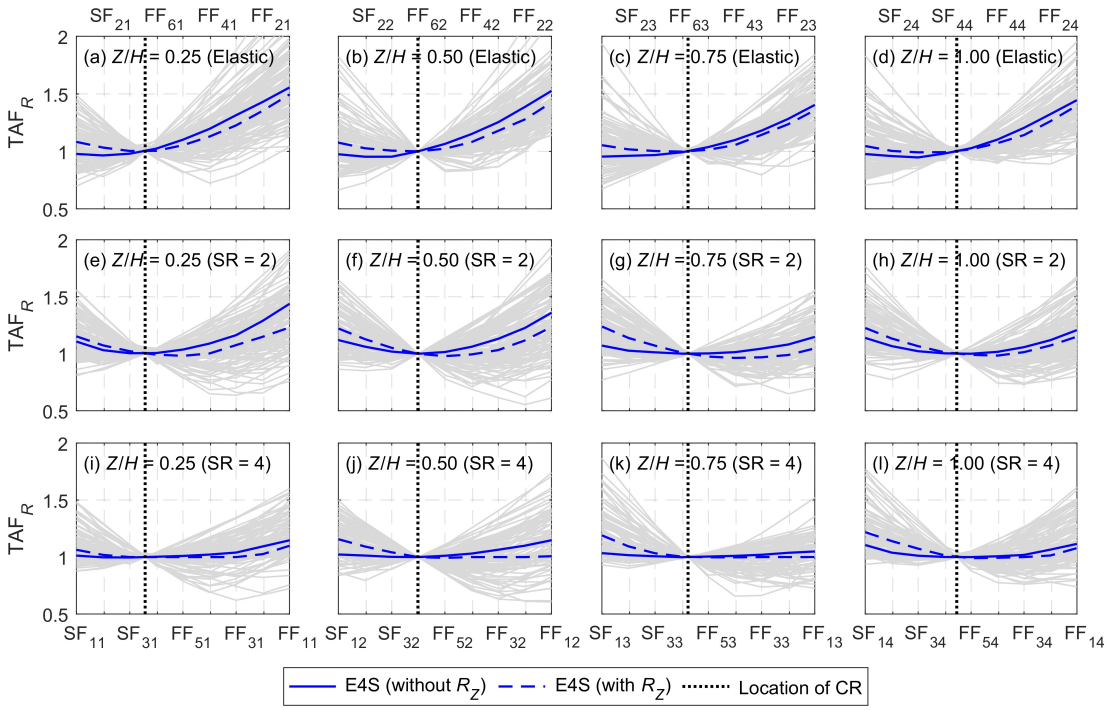

Figure C.13: In-plan distribution of torsional amplification factor for rigid secondary systems at different floors of the 'E4S' building.

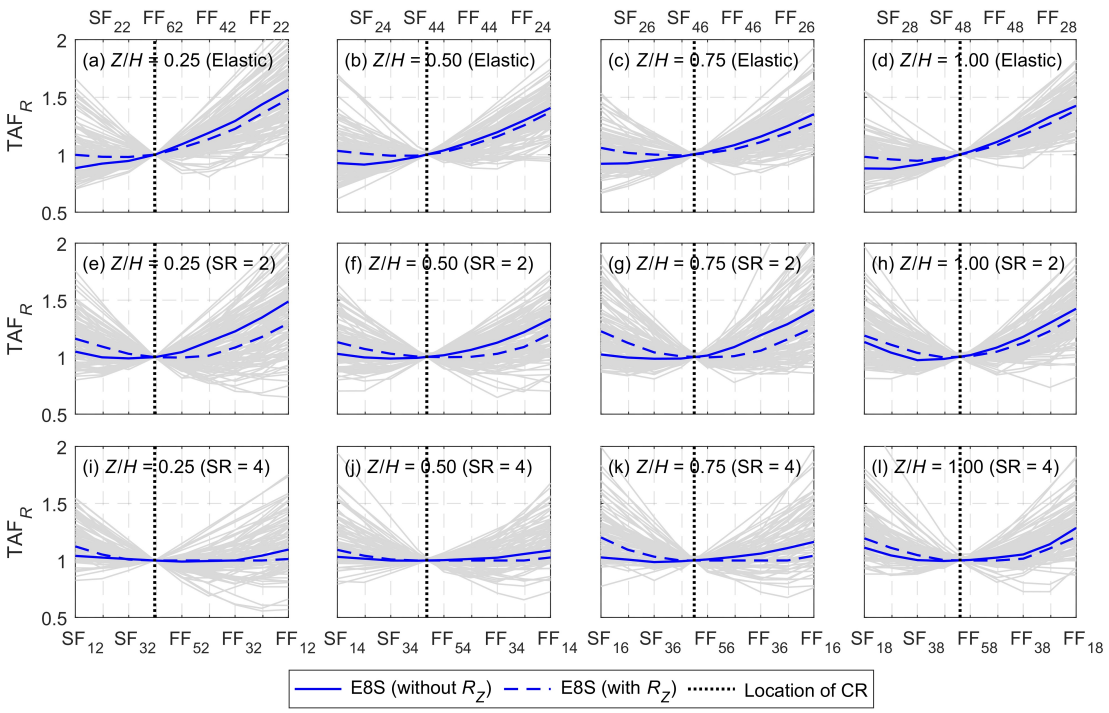

Figure C.14: In-plan distribution of torsional amplification factor for rigid secondary systems at different floors of the 'E8S' building.

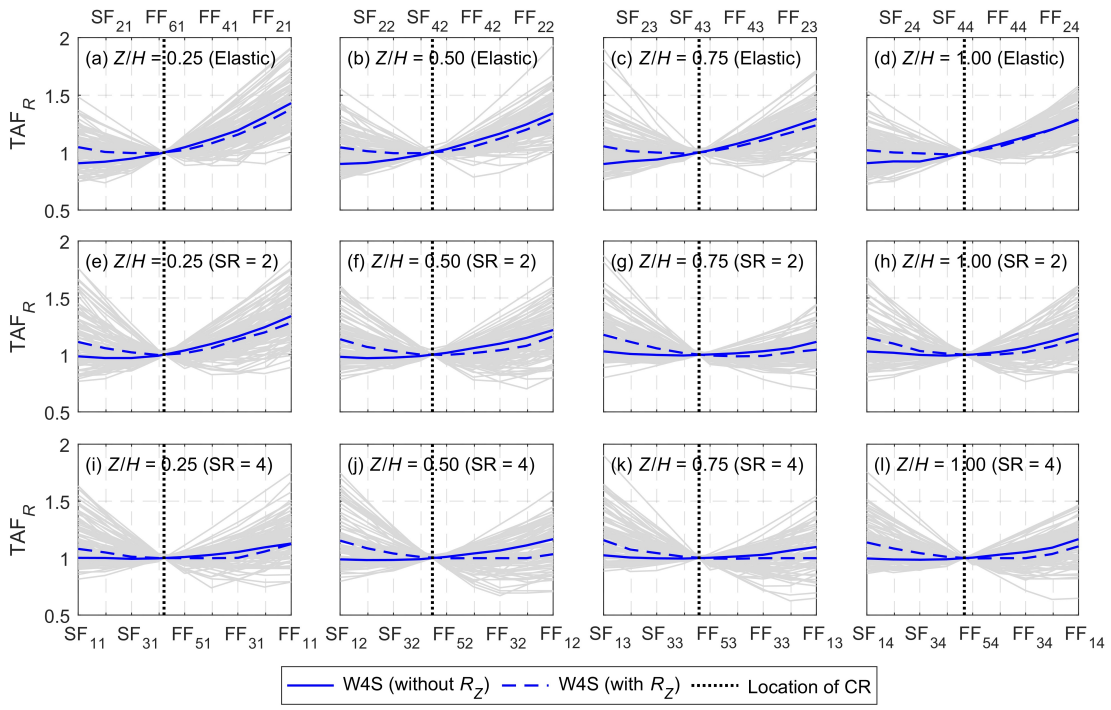

Figure C.15: In-plan distribution of torsional amplification factor for rigid secondary systems at different floors of the 'W4S' building.

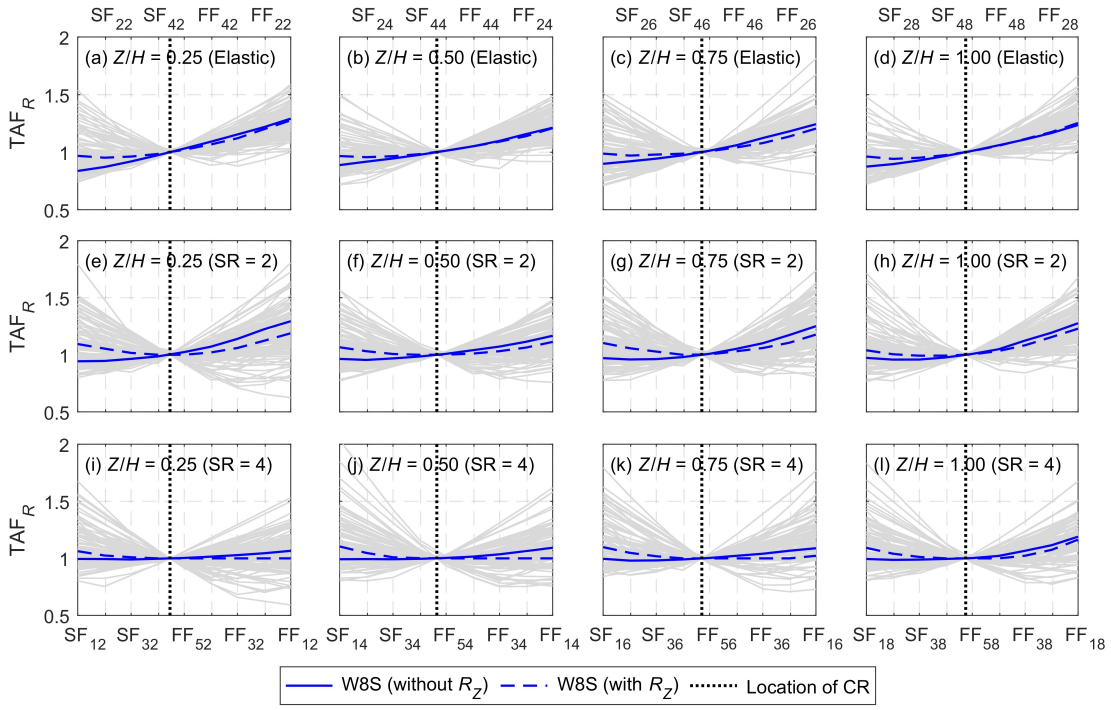

Figure C.16: In-plan distribution of torsional amplification factor for rigid secondary systems at different floors of the 'W8S' building.

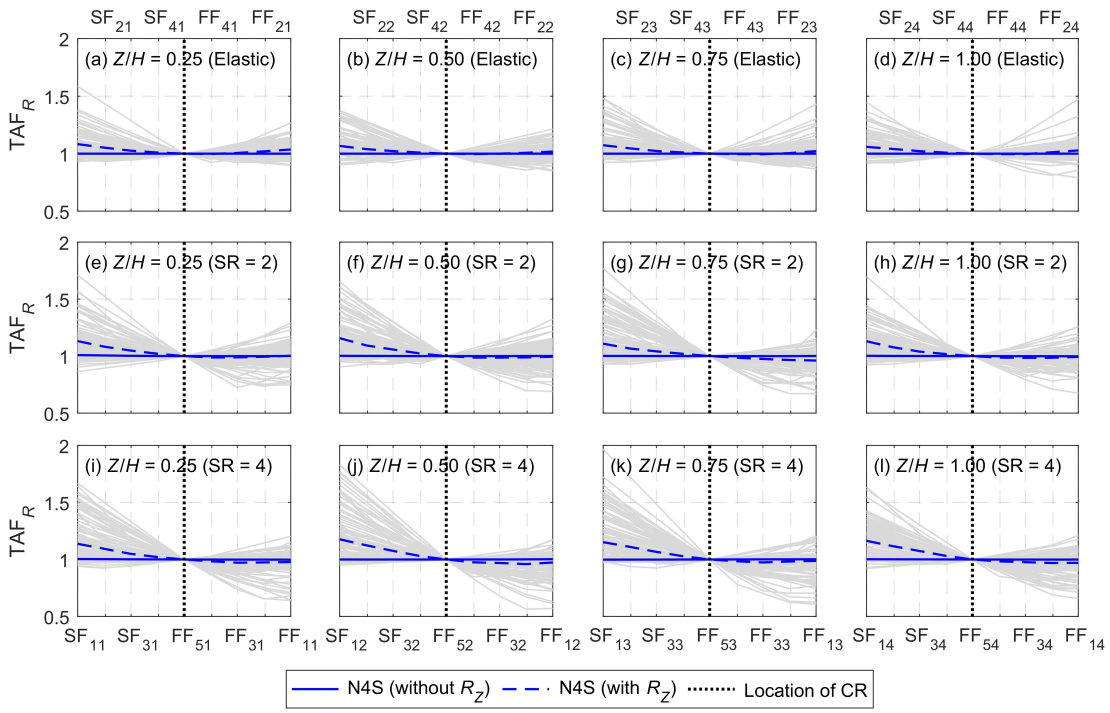

Figure C.17: In-plan distribution of torsional amplification factor for rigid secondary systems at different floors of the 'N4S' building.

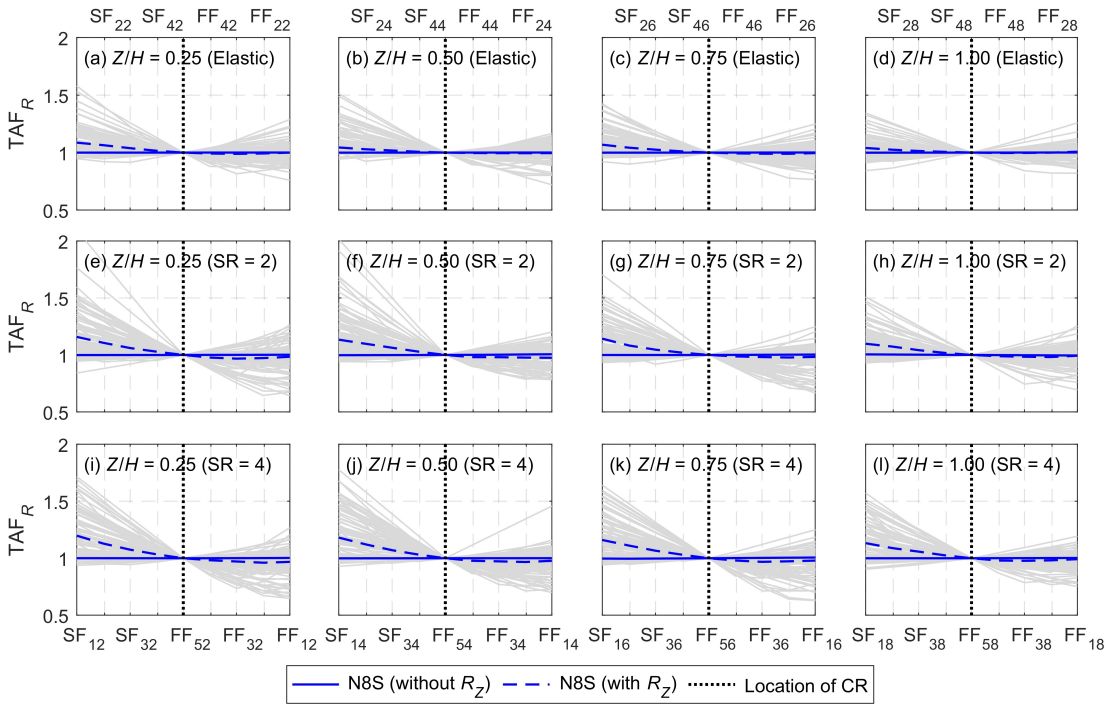

Figure C.18: In-plan distribution of torsional amplification factor for rigid secondary systems at different floors of the 'N8S' building.

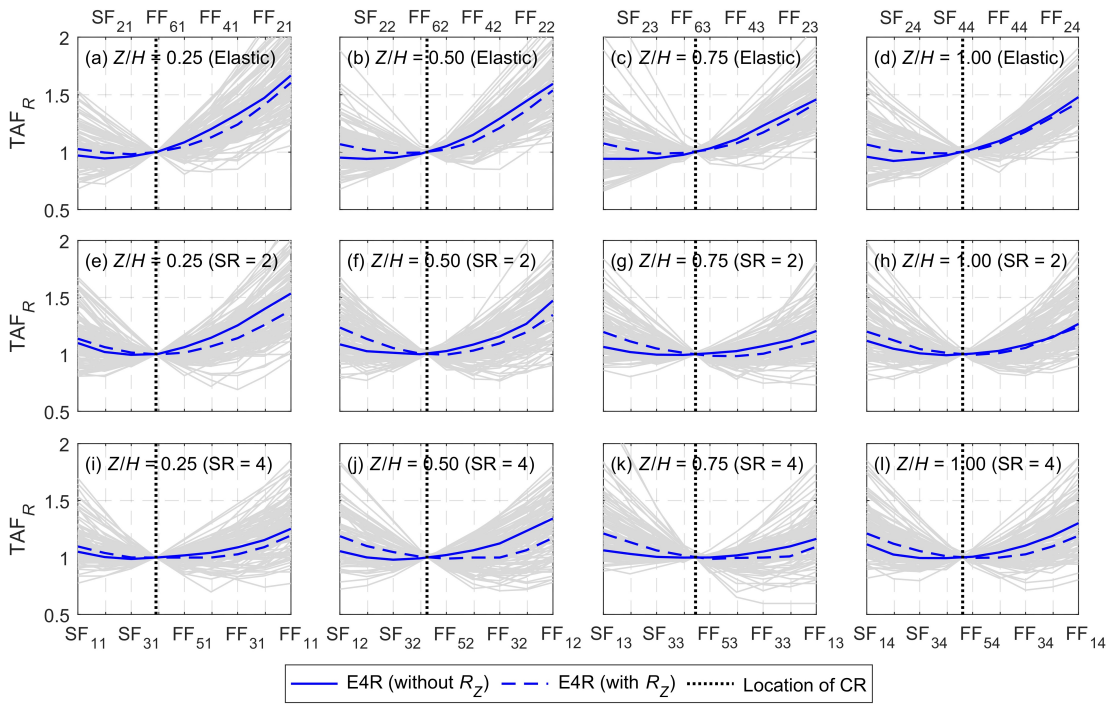

Figure C.19: In-plan distribution of torsional amplification factor for rigid secondary systems at different floors of the 'E4R' building.

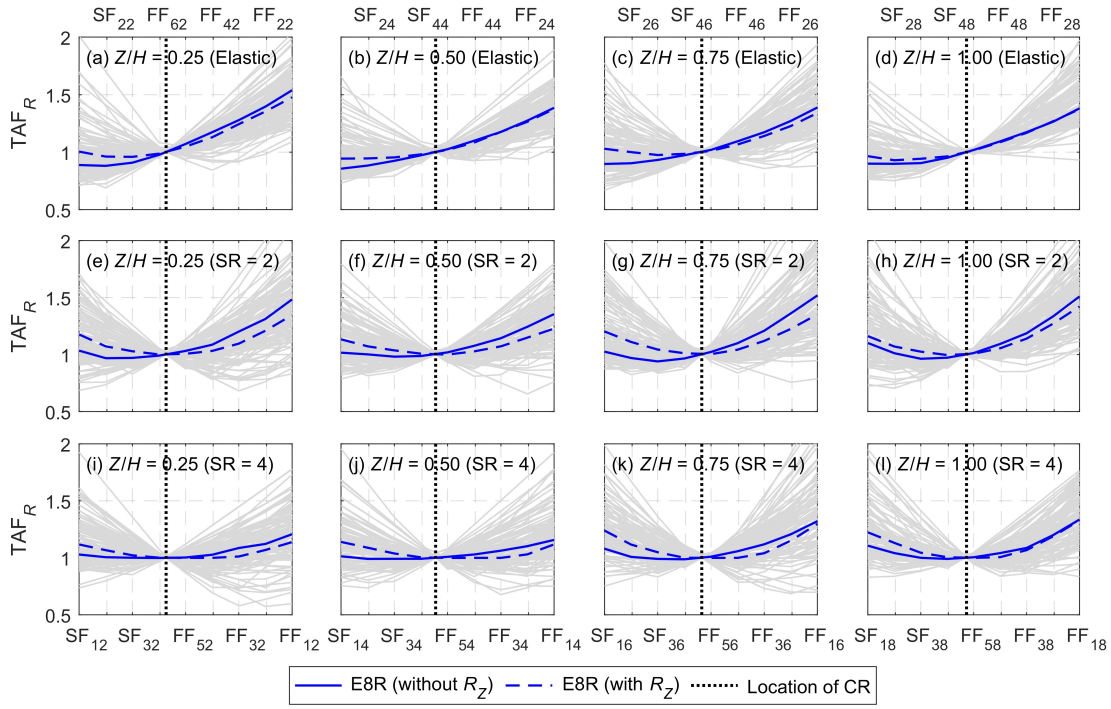

Figure C.20: In-plan distribution of torsional amplification factor for rigid secondary systems at different floors of the 'E8R' building.

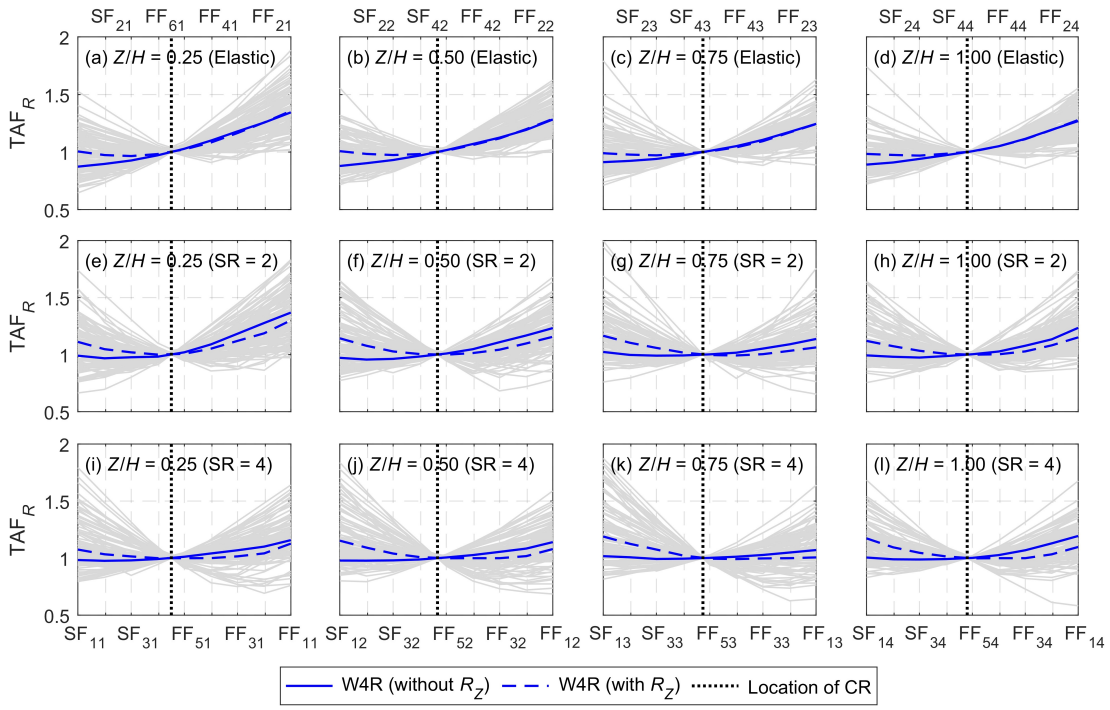

Figure C.21: In-plan distribution of torsional amplification factor for rigid secondary systems at different floors of the 'W4R' building.

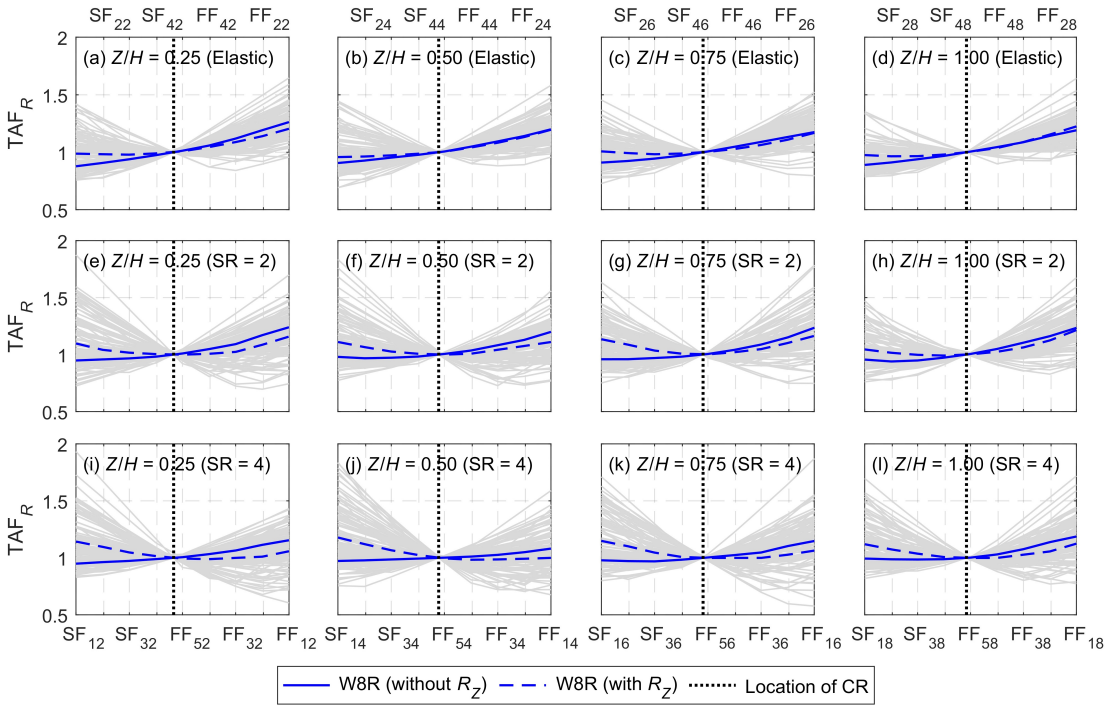

Figure C.22: In-plan distribution of torsional amplification factor for rigid secondary systems at different floors of the 'W8R' building.

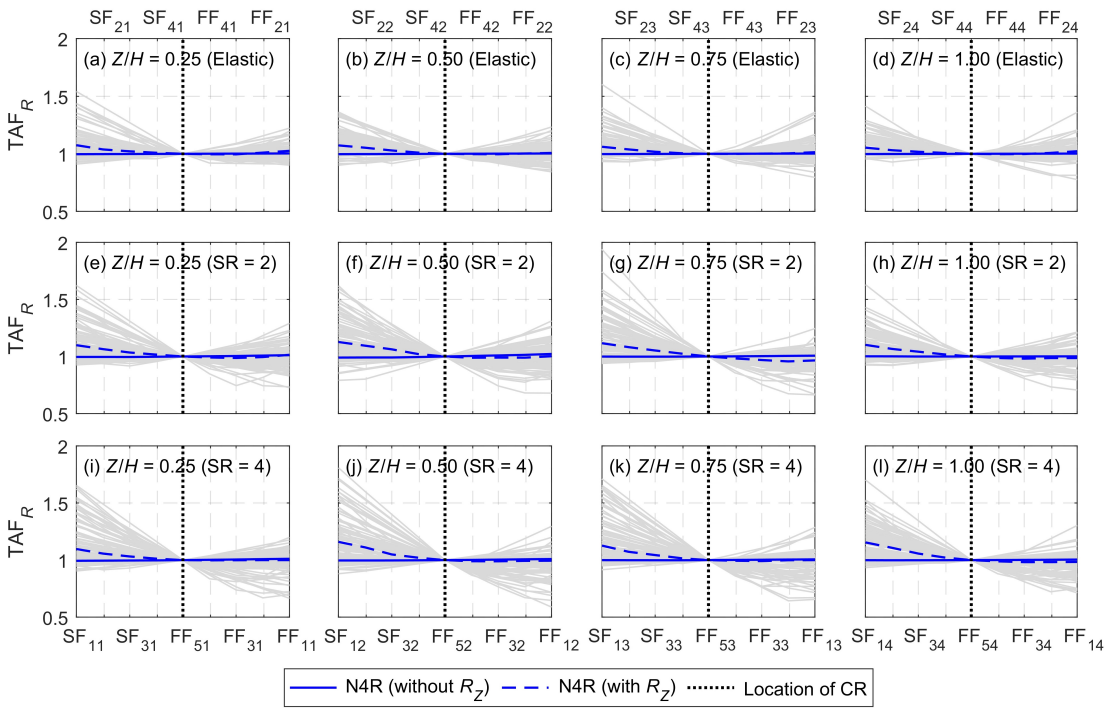

Figure C.23: In-plan distribution of torsional amplification factor for rigid secondary systems at different floors of the 'N4R' building.

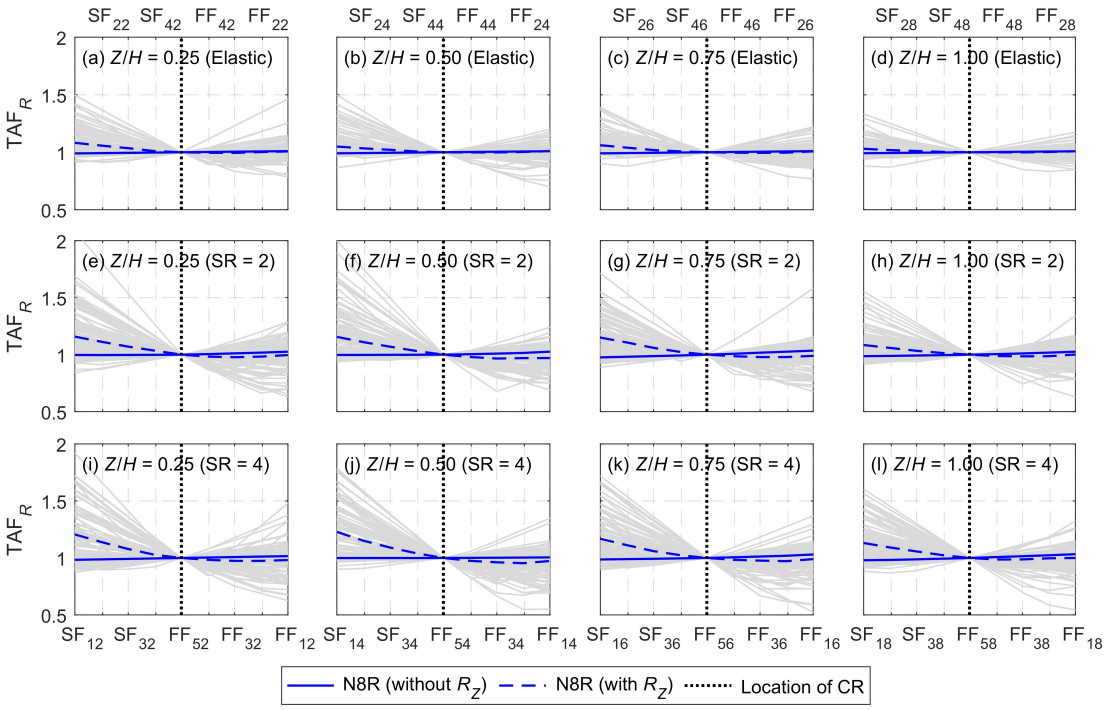

Figure C.24: In-plan distribution of torsional amplification factor for rigid secondary systems at different floors of the 'N8R' building.

C.2 Torsional amplification factors for the rigid, flexible, and very flexible secondary systems

Figures C.25–C.42 present the estimated torsional amplification spectra, representing the TAFs for rigid, flexible, and very flexible secondary systems at the SE and FE, relative to the CS and CR. These spectra are derived from time history analyses conducted with and without considering rotational ground motions. The observed trend follows the same pattern as discussed in Chapter 6.

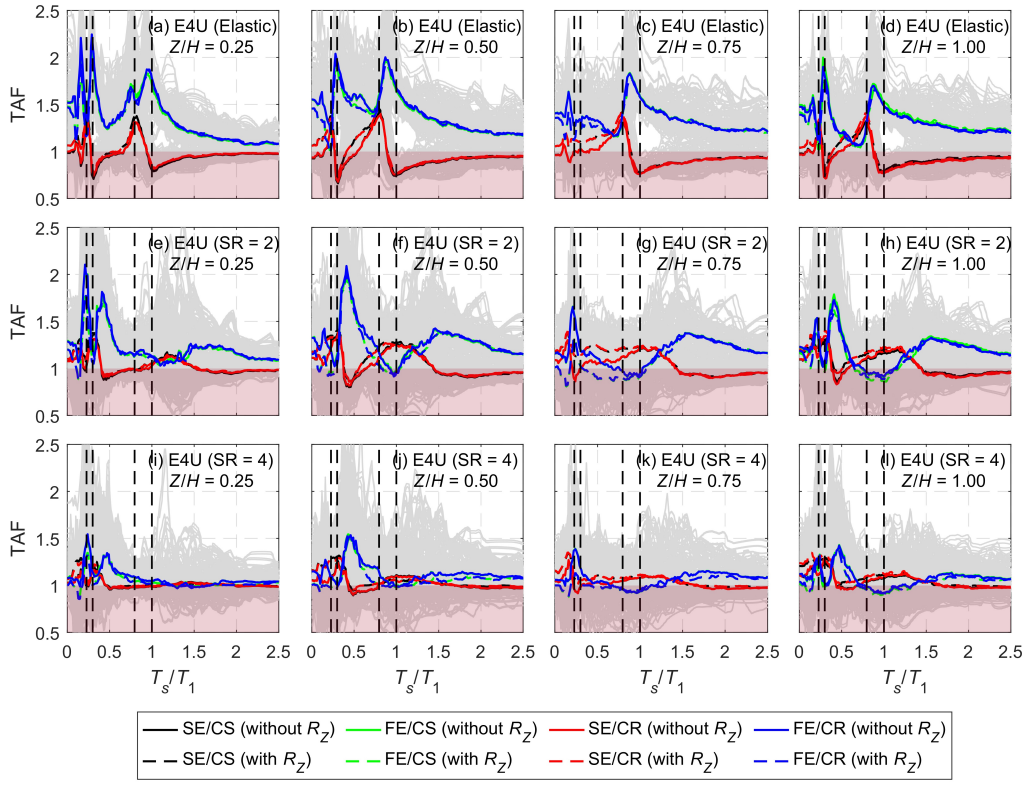

Figure C.25: Torsional amplification factors for the 'E4U' building estimated using time history analyses with and without rotational ground motions. Dashed vertical lines indicate the elastic modal periods in the direction under consideration.

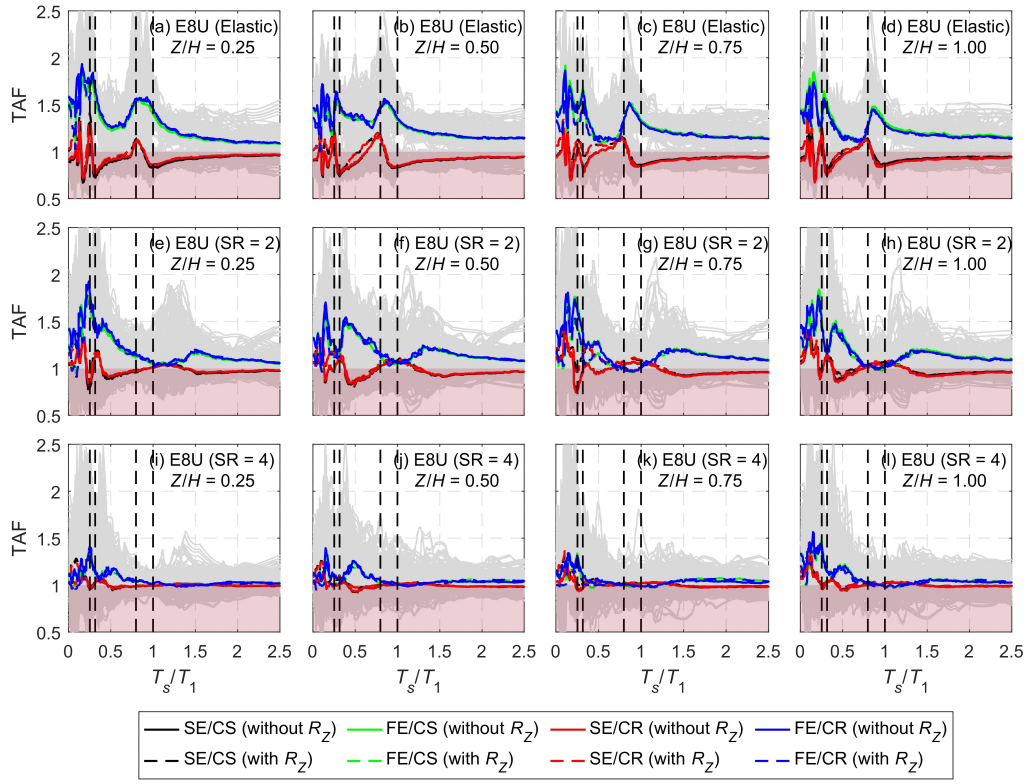

Figure C.26: Torsional amplification factors for the 'E8U' building estimated using time history analyses with and without rotational ground motions. Dashed vertical lines indicate the elastic modal periods in the direction under consideration.

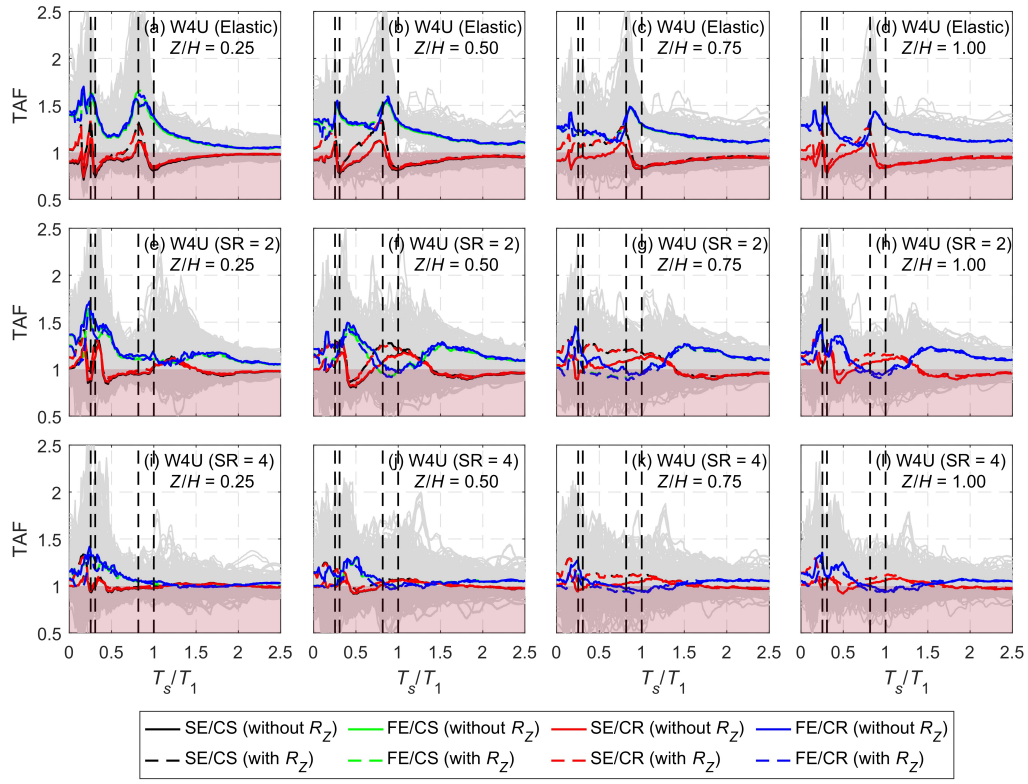

Figure C.27: Torsional amplification factors for the 'W4U' building estimated using time history analyses with and without rotational ground motions. Dashed vertical lines indicate the elastic modal periods in the direction under consideration.

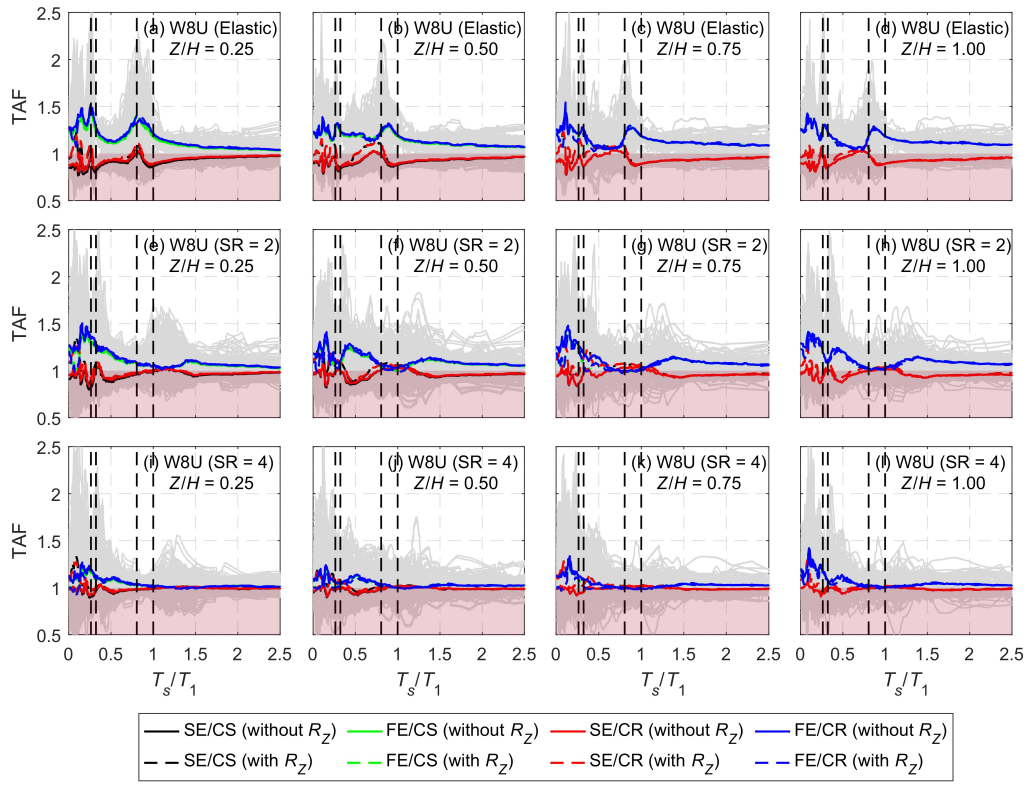

Figure C.28: Torsional amplification factors for the 'W8U' building estimated using time history analyses with and without rotational ground motions. Dashed vertical lines indicate the elastic modal periods in the direction under consideration.

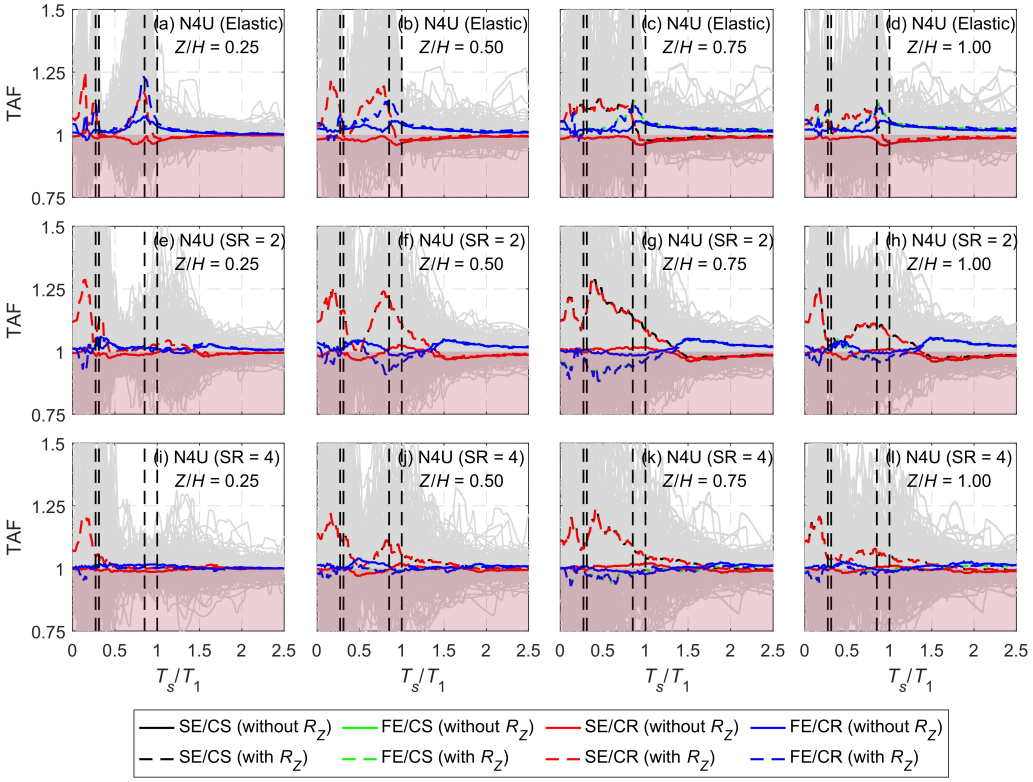

Figure C.29: Torsional amplification factors for the 'N4U' building estimated using time history analyses with and without rotational ground motions. Dashed vertical lines indicate the elastic modal periods in the direction under consideration.

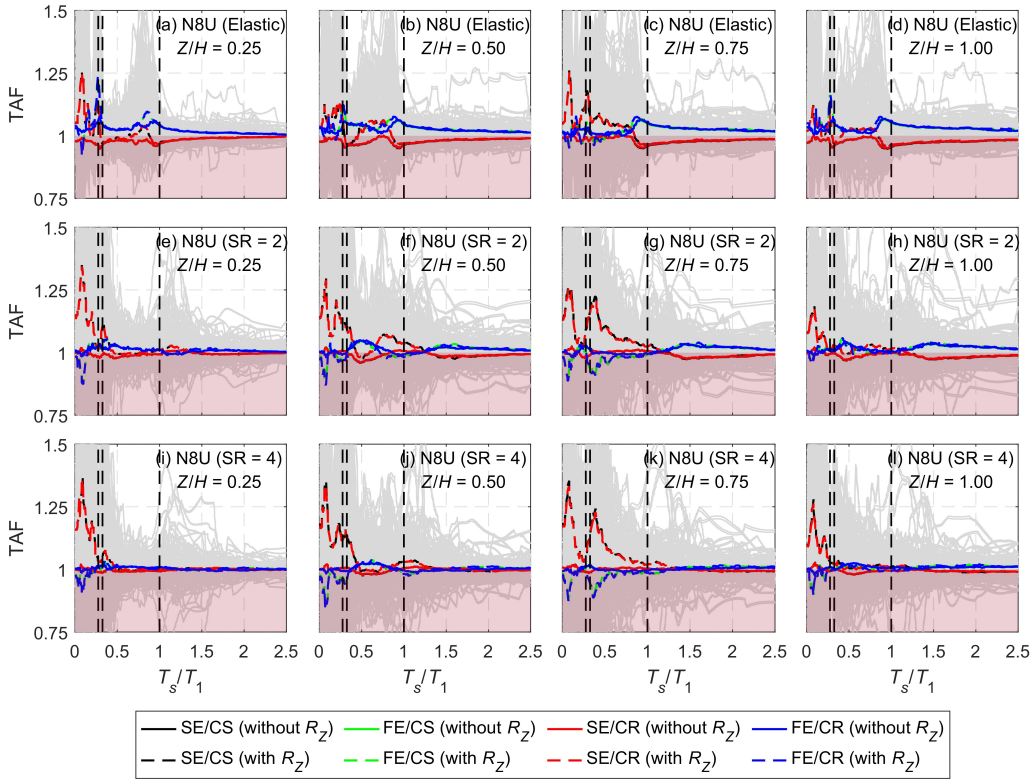

Figure C.30: Torsional amplification factors for the 'N8U' building estimated using time history analyses with and without rotational ground motions. Dashed vertical lines indicate the elastic modal periods in the direction under consideration.

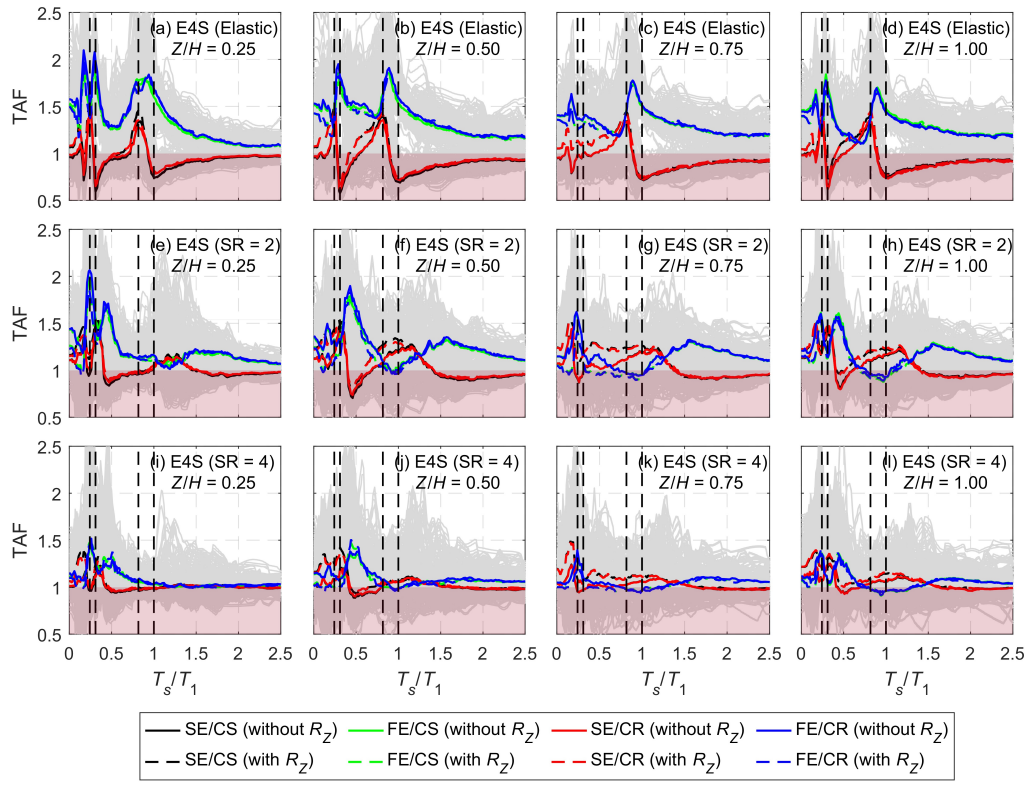

Figure C.31: Torsional amplification factors for the 'E4S' building estimated using time history analyses with and without rotational ground motions. Dashed vertical lines indicate the elastic modal periods in the direction under consideration.

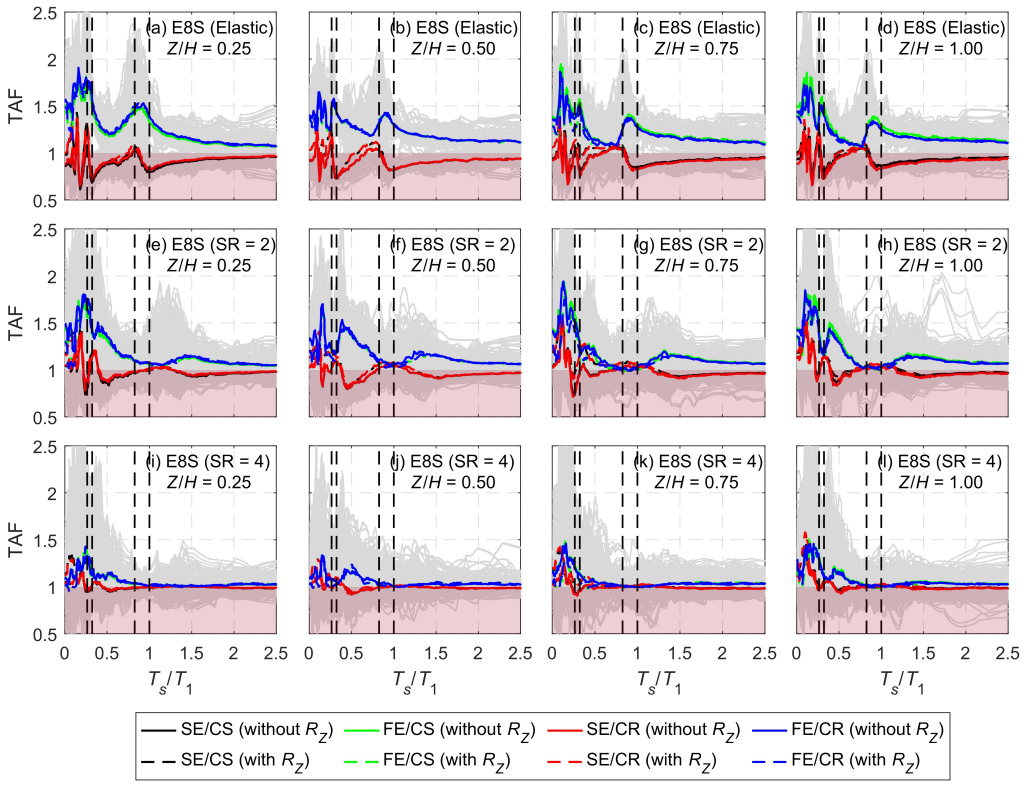

Figure C.32: Torsional amplification factors for the 'E8S' building estimated using time history analyses with and without rotational ground motions. Dashed vertical lines indicate the elastic modal periods in the direction under consideration.

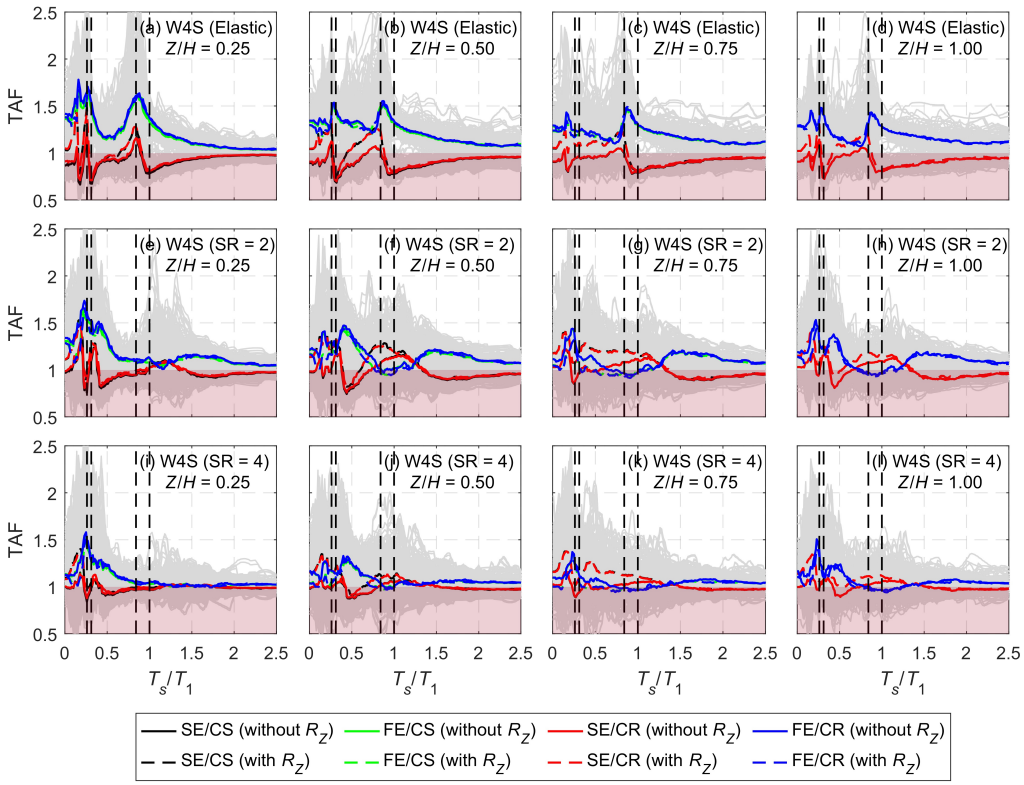

Figure C.33: Torsional amplification factors for the 'W4S' building estimated using time history analyses with and without rotational ground motions. Dashed vertical lines indicate the elastic modal periods in the direction under consideration.

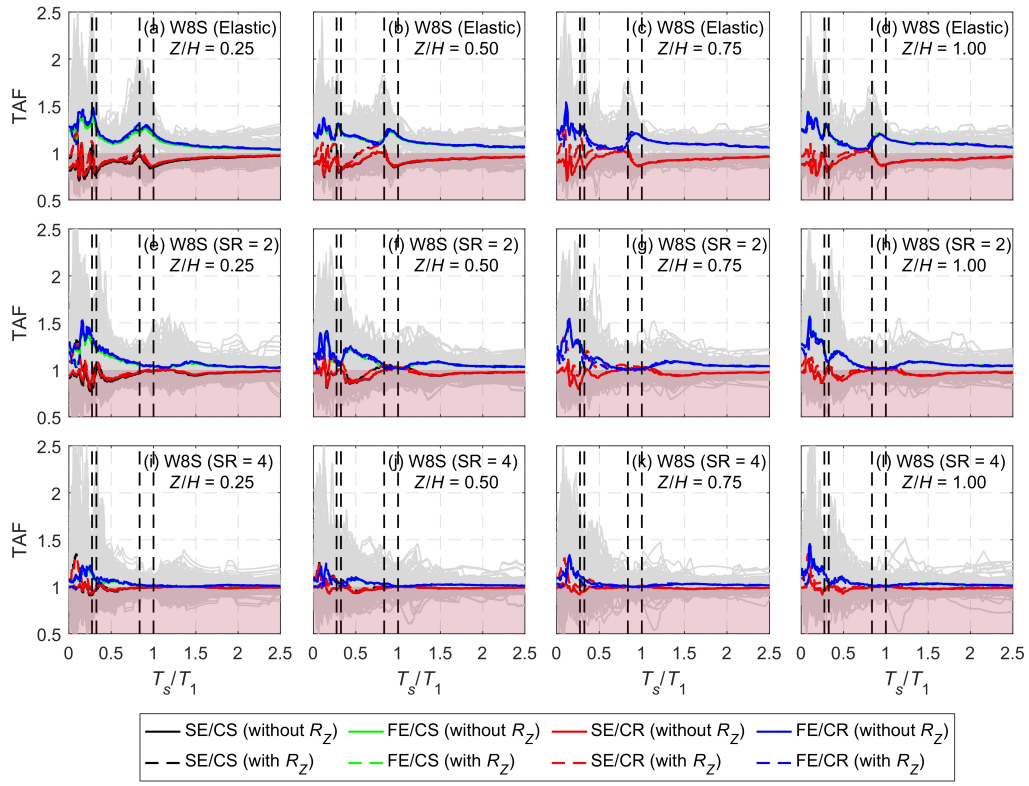

Figure C.34: Torsional amplification factors for the 'W8S' building estimated using time history analyses with and without rotational ground motions. Dashed vertical lines indicate the elastic modal periods in the direction under consideration.

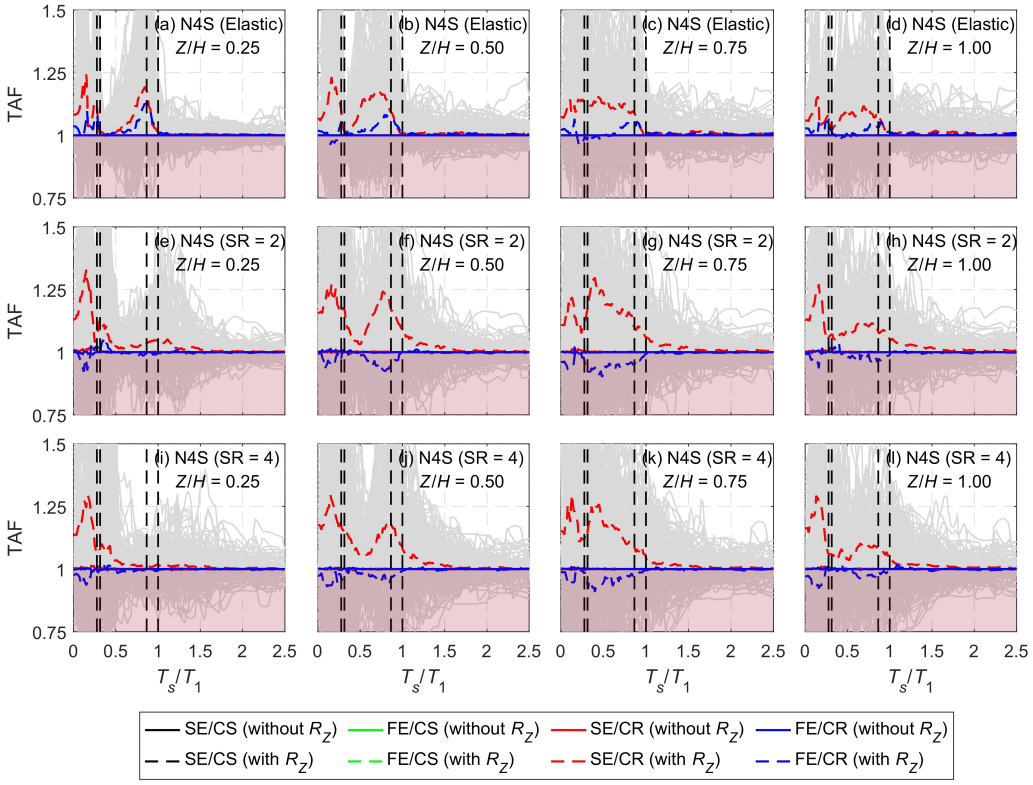

Figure C.35: Torsional amplification factors for the 'N4S' building estimated using time history analyses with and without rotational ground motions. Dashed vertical lines indicate the elastic modal periods in the direction under consideration.

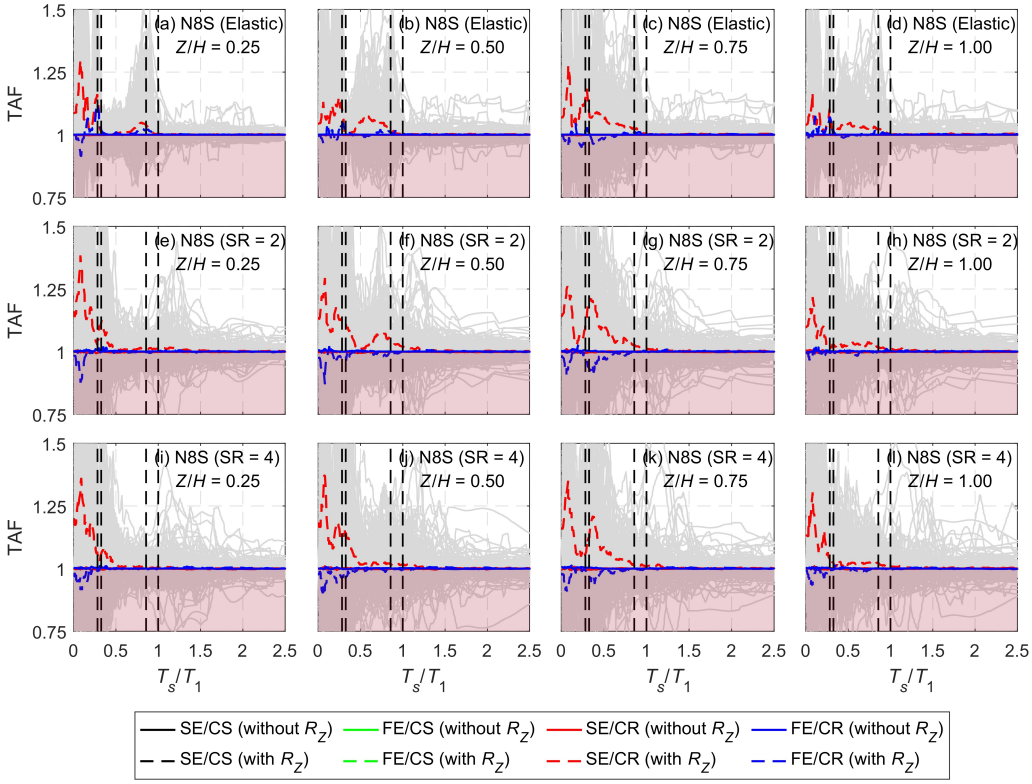

Figure C.36: Torsional amplification factors for the 'N8S' building estimated using time history analyses with and without rotational ground motions. Dashed vertical lines indicate the elastic modal periods in the direction under consideration.

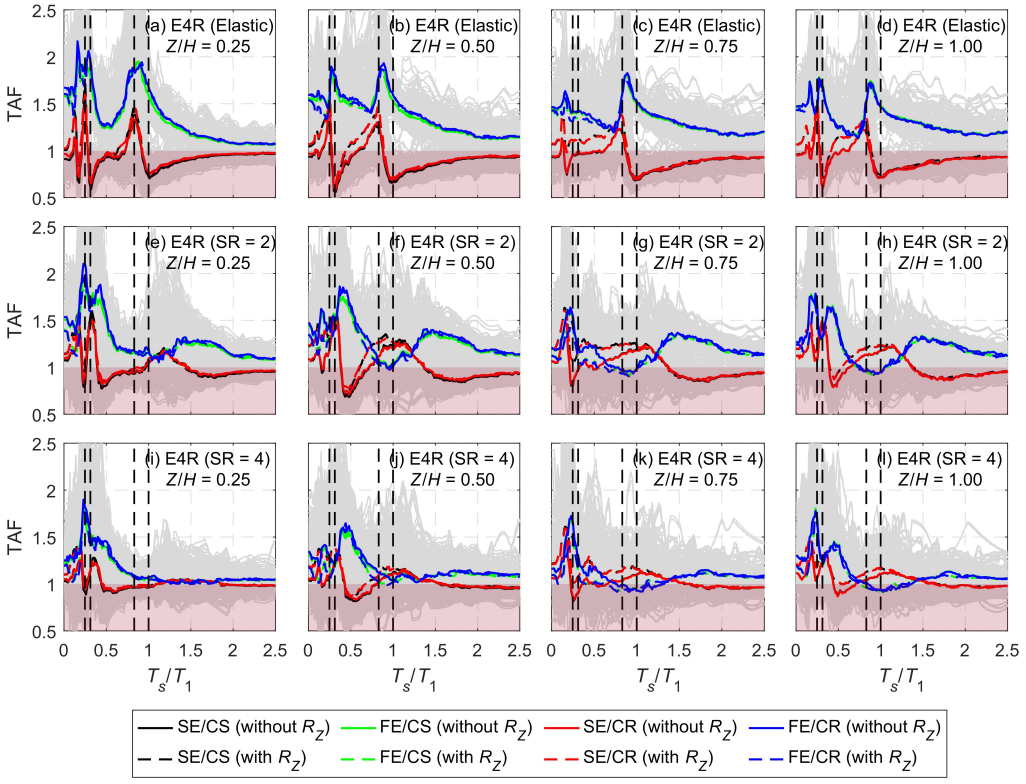

Figure C.37: Torsional amplification factors for the 'E4R' building estimated using time history analyses with and without rotational ground motions. Dashed vertical lines indicate the elastic modal periods in the direction under consideration.

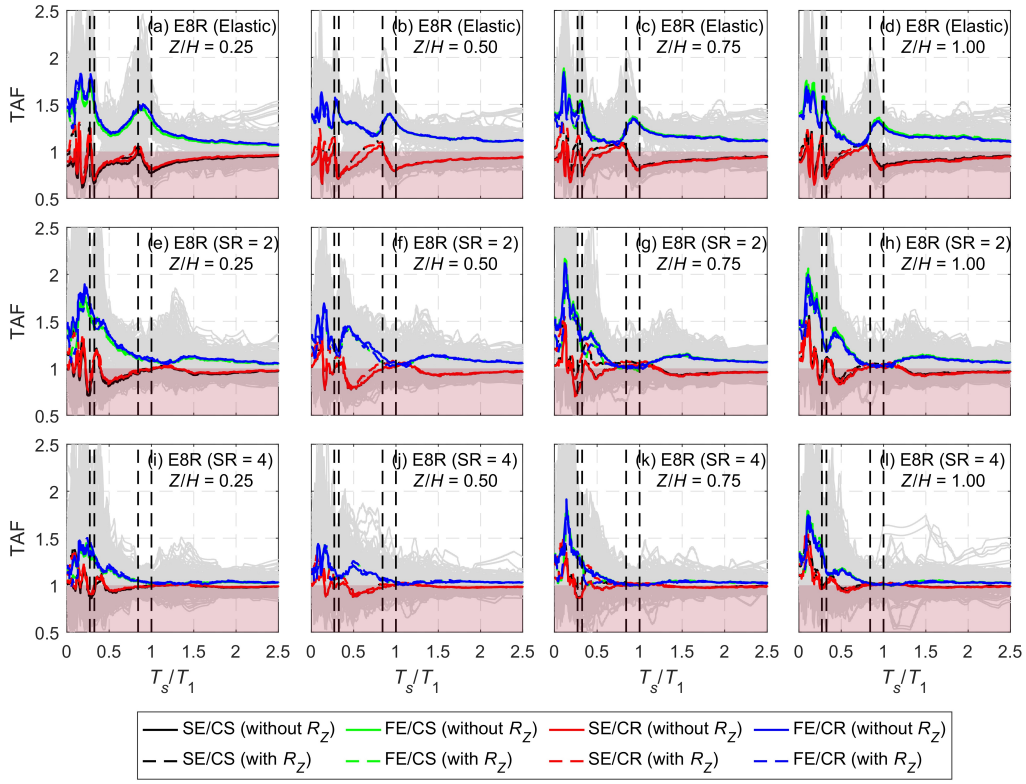

Figure C.38: Torsional amplification factors for the 'E8R' building estimated using time history analyses with and without rotational ground motions. Dashed vertical lines indicate the elastic modal periods in the direction under consideration.

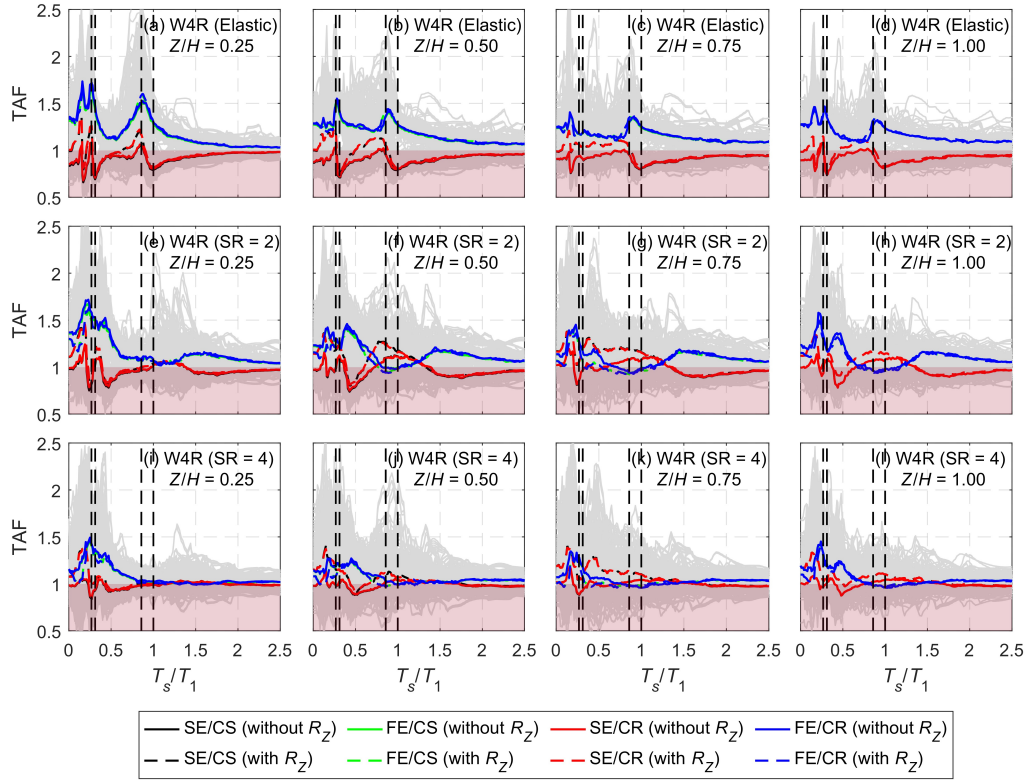

Figure C.39: Torsional amplification factors for the 'W4R' building estimated using time history analyses with and without rotational ground motions. Dashed vertical lines indicate the elastic modal periods in the direction under consideration.

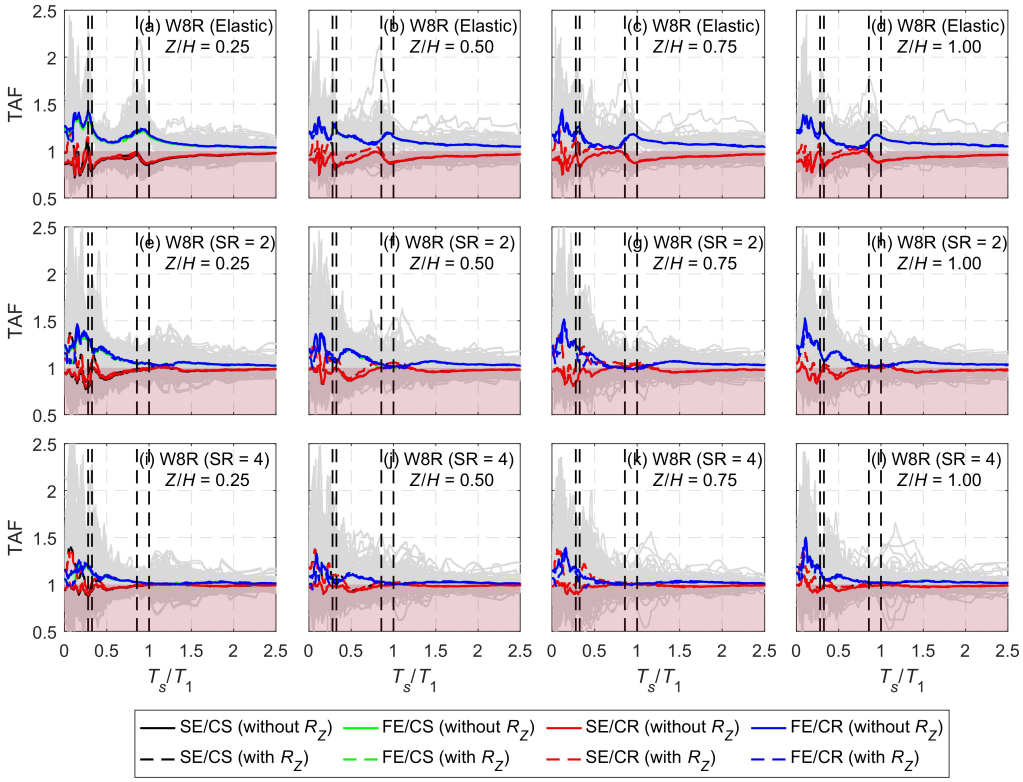

Figure C.40: Torsional amplification factors for the 'W8R' building estimated using time history analyses with and without rotational ground motions. Dashed vertical lines indicate the elastic modal periods in the direction under consideration.

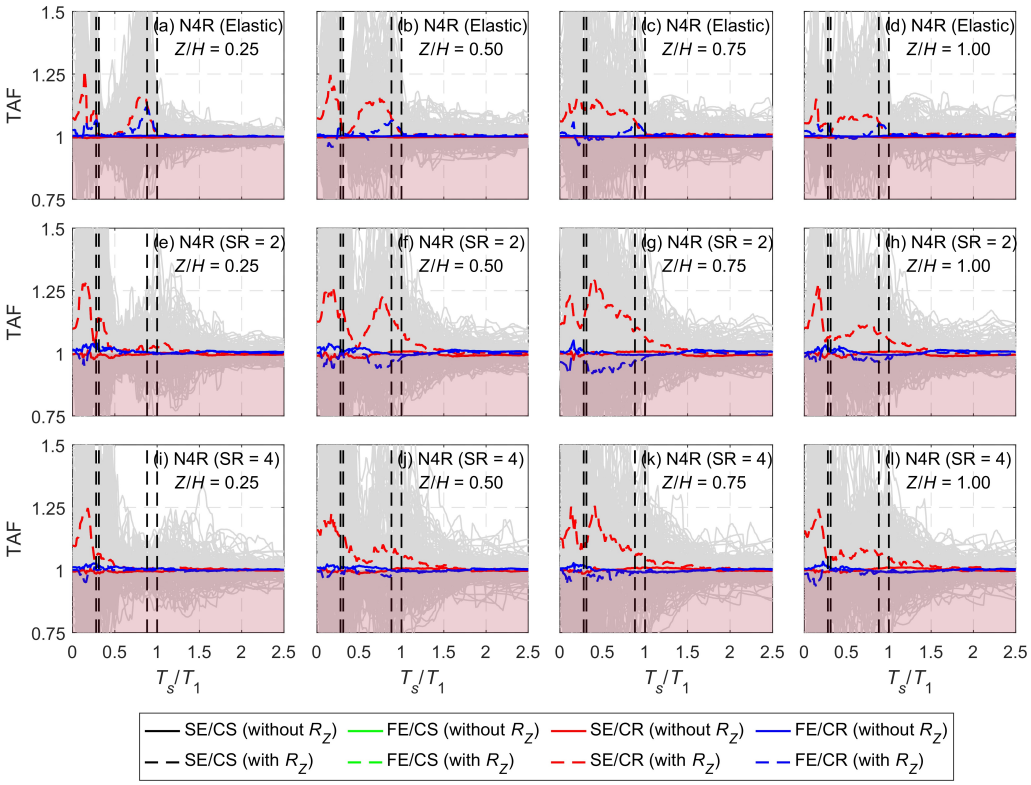

Figure C.41: Torsional amplification factors for the 'N4R' building estimated using time history analyses with and without rotational ground motions. Dashed vertical lines indicate the elastic modal periods in the direction under consideration.

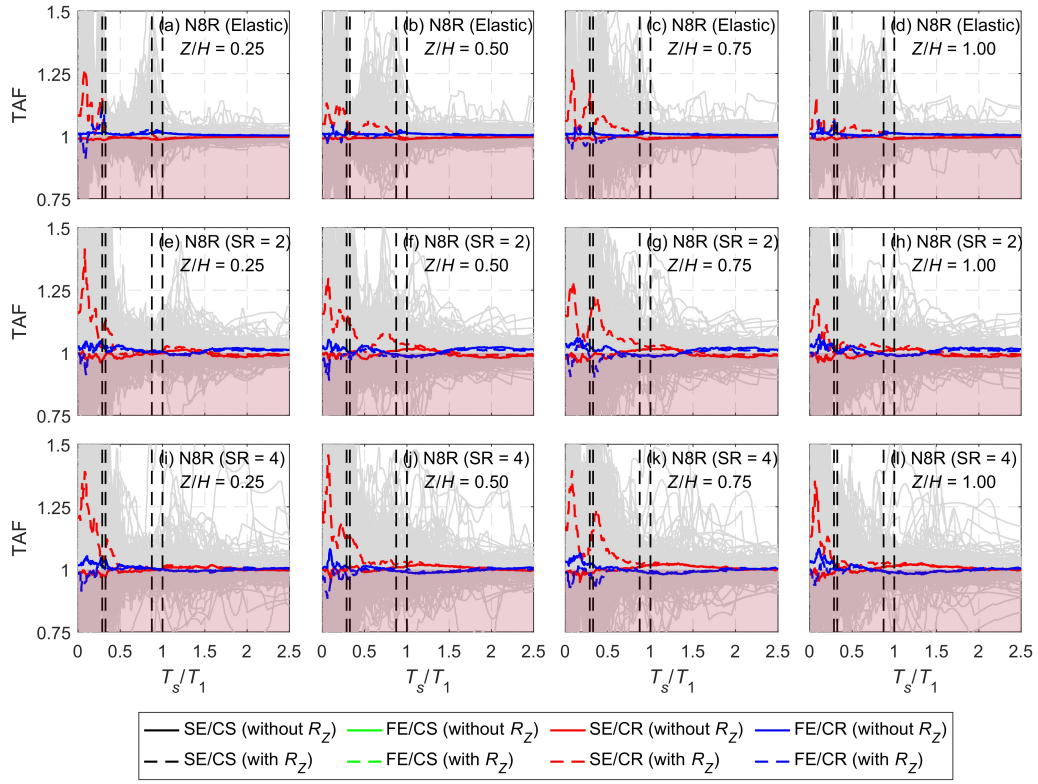

Figure C.42: Torsional amplification factors for the 'N8R' building estimated using time history analyses with and without rotational ground motions. Dashed vertical lines indicate the elastic modal periods in the direction under consideration.

C.3 Regression analysis parameters

C.3.1 For rigid secondary systems

Tables C.1–C.2 present the regression analysis parameters obtained when analyzing TAF_R using $\Delta_{max}/\Delta_{avg}$ and $\Delta_{max}/\Delta_{min}$. A detailed discussion of these trends is provided in Chapter 6.

Table C.1: Regression analysis parameters for $\Delta_{max}/\Delta_{avg}$ versus torsional amplification factor for rigid secondary systems at the FE.

SR	Building	Exponent 'a'	t-value	Pr(>|t|)	R^2	Adjusted R^2	F-statistic	p-value
Elastic	W4T	1.62	27.21	0.00	0.82	0.81	740.32	0.00
Elastic	W8T	1.77	36.84	0.00	0.80	0.80	1357.00	0.00
Elastic	W4U	1.64	35.74	0.00	0.88	0.88	1277.30	0.00
Elastic	W8U	1.65	34.87	0.00	0.78	0.78	1216.20	0.00
Elastic	W4S	1.52	32.59	0.00	0.86	0.86	1062.30	0.00
Elastic	W4R	1.48	26.56	0.00	0.81	0.81	705.63	0.00
Elastic	E4T	1.79	37.45	0.00	0.89	0.89	1402.20	0.00
Elastic	E8T	1.97	42.98	0.00	0.85	0.85	1847.10	0.00
Elastic	E4U	1.59	32.08	0.00	0.86	0.86	1029.00	0.00
Elastic	E8U	1.86	39.74	0.00	0.82	0.82	1579.10	0.00
Elastic	E4S	1.56	34.57	0.00	0.88	0.88	1195.20	0.00
Elastic	E8S	1.83	39.02	0.00	0.82	0.82	1522.20	0.00
Elastic	E4R	1.65	37.16	0.00	0.89	0.89	1381.10	0.00
2	W4T	1.43	20.53	0.00	0.72	0.72	421.64	0.00
2	W8T	1.54	26.31	0.00	0.69	0.69	691.93	0.00
2	W4U	1.45	24.99	0.00	0.80	0.80	624.72	0.00
2	W8U	1.53	25.61	0.00	0.68	0.68	655.60	0.00
2	W4S	1.37	25.04	0.00	0.80	0.80	627.13	0.00
2	W4R	1.54	22.14	0.00	0.75	0.74	489.94	0.00
2	W8R	1.70	25.25	0.00	0.67	0.67	637.56	0.00
2	E4T	1.53	25.32	0.00	0.80	0.80	641.19	0.00
2	E8T	1.71	26.01	0.00	0.69	0.69	676.41	0.00
2	E4U	1.21	24.01	0.00	0.79	0.79	576.44	0.00
2	E8U	1.59	26.57	0.00	0.70	0.70	705.71	0.00
2	E4S	1.24	23.23	0.00	0.77	0.77	539.84	0.00
2	E8S	1.67	25.38	0.00	0.68	0.68	644.10	0.00
2	E4R	1.41	25.16	0.00	0.81	0.81	632.99	0.00
2	E8R	1.77	26.38	0.00	0.69	0.69	695.71	0.00
4	W8T	1.14	15.91	0.00	0.60	0.60	253.01	0.00
4	W4U	1.36	20.81	0.00	0.80	0.80	433.24	0.00
4	W8U	1.23	16.05	0.00	0.64	0.64	257.54	0.00
4	W4S	1.17	16.75	0.00	0.72	0.71	280.48	0.00
4	W8S	1.21	12.64	0.00	0.65	0.64	159.87	0.00
4	W4R	1.28	17.36	0.00	0.69	0.69	301.38	0.00
4	W8R	1.45	20.61	0.00	0.66	0.66	424.77	0.00
4	E4T	1.20	15.22	0.00	0.73	0.72	231.60	0.00
4	E8T	1.48	15.09	0.00	0.64	0.64	227.60	0.00
4	E4U	1.14	14.71	0.00	0.74	0.74	216.29	0.00
4	E8U	1.23	09.15	0.00	0.51	0.51	83.79	0.00
4	E4S	1.16	17.74	0.00	0.79	0.79	314.78	0.00
4	E8S	1.39	11.82	0.00	0.60	0.59	139.59	0.00
4	E4R	1.26	20.21	0.00	0.79	0.78	408.44	0.00
4	E8R	1.53	17.47	0.00	0.61	0.60	305.22	0.00

Table C.2: Regression analysis parameters for $\Delta_{max}/\Delta_{min}$ versus torsional amplification factor for rigid secondary systems at the FE.

SR	Building	Exponent 'a'	t-value	Pr(>|t|)	R^2	Adjusted R^2	F-statistic	p-value
Elastic	W4T	0.71	26.28	0.00	0.81	0.80	690.85	0.00
Elastic	W8T	0.81	35.94	0.00	0.79	0.79	1291.50	0.00
Elastic	W4U	0.73	34.55	0.00	0.88	0.88	1193.60	0.00
Elastic	W8U	0.75	33.87	0.00	0.77	0.77	1147.30	0.00
Elastic	W4S	0.66	31.25	0.00	0.85	0.85	976.29	0.00
Elastic	W4R	0.66	25.87	0.00	0.80	0.80	669.37	0.00
Elastic	E4T	0.73	35.05	0.00	0.88	0.88	1228.70	0.00
Elastic	E8T	0.85	40.61	0.00	0.83	0.83	1649.40	0.00
Elastic	E4U	0.66	30.30	0.00	0.85	0.85	917.79	0.00
Elastic	E8U	0.80	37.23	0.00	0.81	0.80	1386.30	0.00
Elastic	E4S	0.64	32.34	0.00	0.86	0.86	1046.00	0.00
Elastic	E8S	0.79	36.70	0.00	0.80	0.80	1347.20	0.00
Elastic	E4R	0.67	34.66	0.00	0.88	0.88	1201.60	0.00
2	W4T	0.63	20.04	0.00	0.71	0.71	401.71	0.00
2	W8T	0.70	25.79	0.00	0.68	0.68	664.99	0.00
2	W4U	0.64	24.25	0.00	0.79	0.79	587.83	0.00
2	W8U	0.70	25.03	0.00	0.67	0.67	626.64	0.00
2	W4S	0.60	24.22	0.00	0.79	0.79	586.77	0.00
2	W4R	0.69	21.70	0.00	0.74	0.74	471.03	0.00
2	W8R	0.79	24.78	0.00	0.66	0.66	614.07	0.00
2	E4T	0.62	23.85	0.00	0.78	0.78	568.89	0.00
2	E8T	0.73	24.77	0.00	0.67	0.67	613.35	0.00
2	E4U	0.50	23.00	0.00	0.77	0.77	529.05	0.00
2	E8U	0.68	25.10	0.00	0.68	0.67	629.97	0.00
2	E4S	0.51	21.90	0.00	0.75	0.74	479.60	0.00
2	E8S	0.71	23.92	0.00	0.65	0.65	572.30	0.00
2	E4R	0.57	23.61	0.00	0.79	0.79	557.37	0.00
2	E8R	0.76	25.09	0.00	0.67	0.67	629.57	0.00
4	W8T	0.52	15.50	0.00	0.59	0.59	240.14	0.00
4	W4U	0.60	20.38	0.00	0.80	0.79	415.17	0.00
4	W8U	0.56	15.71	0.00	0.63	0.63	246.63	0.00
4	W4S	0.51	16.23	0.00	0.70	0.70	263.31	0.00
4	W8S	0.55	12.26	0.00	0.63	0.63	150.21	0.00
4	W4R	0.57	17.01	0.00	0.68	0.68	289.40	0.00
4	W8R	0.67	20.06	0.00	0.65	0.65	402.19	0.00
4	E4T	0.49	14.48	0.00	0.71	0.70	209.74	0.00
4	E8T	0.63	14.38	0.00	0.62	0.62	206.76	0.00
4	E4U	0.47	14.03	0.00	0.72	0.72	196.88	0.00
4	E8U	0.52	8.69	0.00	0.49	0.48	75.53	0.00
4	E4S	0.48	16.94	0.00	0.78	0.77	286.82	0.00
4	E8S	0.59	11.20	0.00	0.57	0.56	125.36	0.00
4	E4R	0.51	19.20	0.00	0.77	0.77	368.70	0.00
4	E8R	0.65	16.63	0.00	0.58	0.58	276.61	0.00

C.3.2 For flexible secondary systems

Tables C.3–C.4 present the regression parameters derived from the analysis of $TAF_{F,max}$, considering $\Delta_{max}/\Delta_{avg}$ and $\Delta_{max}/\Delta_{min}$. A detailed discussion of these trends is provided in Chapter 6.

Table C.3: Regression analysis parameters for $\Delta_{max}/\Delta_{avg}$ versus peak torsional amplification factor for flexible secondary systems at the FE.

SR	Building	Exponent '*c*'	t-value	Pr(>|t|)	R^2	Adjusted R^2	F-statistic	*p*-value
Elastic	E4T	2.62	37.36	0.00	0.89	0.89	1395.70	0.00
Elastic	E4U	2.53	43.57	0.00	0.92	0.92	1897.90	0.00
Elastic	E4S	2.46	45.96	0.00	0.93	0.93	2112.20	0.00
Elastic	W4T	2.49	26.92	0.00	0.81	0.81	724.60	0.00
Elastic	W4U	2.62	39.92	0.00	0.91	0.90	1593.30	0.00
Elastic	W4R	2.23	26.53	0.00	0.81	0.81	703.61	0.00
Elastic	E8T	2.01	37.77	0.00	0.81	0.81	1426.60	0.00
Elastic	E8S	1.87	36.11	0.00	0.80	0.79	1303.60	0.00
Elastic	W8U	2.14	32.56	0.00	0.76	0.76	1060.10	0.00
Elastic	W8S	1.77	32.35	0.00	0.76	0.76	1046.60	0.00
2	E4T	1.66	31.34	0.00	0.85	0.85	982.02	0.00
2	E4U	1.68	30.13	0.00	0.84	0.84	907.83	0.00
2	E4R	1.53	30.50	0.00	0.85	0.85	930.52	0.00
2	W4U	1.72	26.38	0.00	0.81	0.81	695.89	0.00
2	W4S	1.41	27.25	0.00	0.82	0.82	742.38	0.00
2	E8T	0.93	28.09	0.00	0.70	0.70	789.18	0.00
2	W8T	0.90	26.58	0.00	0.68	0.68	706.64	0.00
2	W8U	1.12	24.75	0.00	0.65	0.65	612.40	0.00
2	W8S	0.89	26.37	0.00	0.67	0.67	695.40	0.00
2	W8R	1.00	25.79	0.00	0.67	0.66	665.15	0.00
4	E4T	1.09	20.40	0.00	0.71	0.71	416.18	0.00
4	E4U	1.04	19.90	0.00	0.70	0.70	395.85	0.00
4	E4S	1.00	19.43	0.00	0.69	0.69	377.56	0.00
4	E4R	0.99	19.25	0.00	0.69	0.69	370.66	0.00
4	W4T	0.86	16.48	0.00	0.62	0.62	271.70	0.00
4	W4U	1.04	19.19	0.00	0.69	0.69	368.25	0.00
4	W4S	0.93	20.27	0.00	0.71	0.71	410.69	0.00
4	E8T	0.55	22.13	0.00	0.59	0.59	489.78	0.00
4	E8U	0.55	18.42	0.00	0.50	0.50	339.26	0.00
4	E8S	0.56	18.19	0.00	0.50	0.50	330.81	0.00
4	E8R	0.65	23.22	0.00	0.62	0.62	539.27	0.00
4	W8T	0.52	22.26	0.00	0.60	0.60	495.63	0.00
4	W8U	0.57	20.30	0.00	0.55	0.55	411.92	0.00
4	W8S	0.50	20.71	0.00	0.56	0.56	428.85	0.00
4	W8R	0.64	21.55	0.00	0.58	0.58	464.38	0.00

Table C.4: Regression analysis parameters for $\Delta_{max}/\Delta_{min}$ versus peak torsional amplification factor for flexible secondary systems at the FE.

SR	Building	Exponent 'c'	t-value	Pr(>|t|)	R^2	Adjusted R^2	F-statistic	p-value
Elastic	E4T	1.07	33.77	0.00	0.87	0.87	1140.30	0.00
Elastic	E4U	1.04	38.28	0.00	0.90	0.90	1465.20	0.00
Elastic	E4S	1.01	40.26	0.00	0.91	0.91	1620.50	0.00
Elastic	W4T	1.09	25.88	0.00	0.80	0.80	669.80	0.00
Elastic	W4U	1.16	37.78	0.00	0.90	0.89	1427.70	0.00
Elastic	W4R	0.99	25.77	0.00	0.80	0.80	663.97	0.00
Elastic	E8T	0.86	35.52	0.00	0.79	0.79	1261.50	0.00
Elastic	E8S	0.80	33.56	0.00	0.77	0.77	1126.60	0.00
Elastic	W8U	0.98	31.53	0.00	0.75	0.75	994.13	0.00
Elastic	W8S	0.80	31.35	0.00	0.75	0.75	983.05	0.00
2	E4T	0.68	28.82	0.00	0.83	0.83	830.50	0.00
2	E4U	0.69	27.90	0.00	0.82	0.82	778.48	0.00
2	E4R	0.62	28.27	0.00	0.83	0.83	799.06	0.00
2	W4U	0.76	25.30	0.00	0.79	0.79	639.96	0.00
2	W4S	0.61	25.87	0.00	0.80	0.80	669.43	0.00
2	E8T	0.40	26.84	0.00	0.68	0.68	720.59	0.00
2	E8S	0.44	27.65	0.00	0.70	0.69	764.33	0.00
2	W8T	0.41	25.97	0.00	0.67	0.67	674.19	0.00
2	W8U	0.51	24.07	0.00	0.63	0.63	579.26	0.00
2	W8S	0.41	25.66	0.00	0.66	0.66	658.62	0.00
2	W8R	0.46	25.23	0.00	0.66	0.65	636.69	0.00
4	E4T	0.44	19.56	0.00	0.70	0.69	382.58	0.00
4	E4U	0.43	19.18	0.00	0.69	0.69	367.90	0.00
4	E4S	0.41	18.62	0.00	0.67	0.67	346.69	0.00
4	E4R	0.40	18.17	0.00	0.66	0.66	330.30	0.00
4	W4T	0.38	16.06	0.00	0.61	0.60	257.86	0.00
4	W4U	0.46	18.72	0.00	0.68	0.68	350.58	0.00
4	W4S	0.40	19.58	0.00	0.70	0.69	383.44	0.00
4	E8T	0.24	21.34	0.00	0.58	0.57	455.53	0.00
4	E8U	0.23	17.71	0.00	0.48	0.48	313.48	0.00
4	E8S	0.24	17.53	0.00	0.48	0.48	307.39	0.00
4	E8R	0.28	22.37	0.00	0.60	0.60	500.35	0.00
4	W8T	0.24	21.75	0.00	0.59	0.58	473.25	0.00
4	W8U	0.26	19.86	0.00	0.54	0.54	394.28	0.00
4	W8S	0.23	20.27	0.00	0.55	0.55	410.70	0.00
4	W8R	0.30	21.10	0.00	0.57	0.57	445.18	0.00